



Light-Driven Syntheses of Monophosphorus Compounds

Dissertation

Zur Erlangung des Doktorgrades der Naturwissenschaften

Dr. rer. nat.

am Institut für Anorganische Chemie
an der Fakultät Chemie und Pharmazie
der Universität Regensburg

vorgelegt von

Marion Till

aus Thürnthenning

Regensburg, November 2022

Der experimentelle Teil der vorliegenden Arbeit wurde in der Zeit zwischen November 2018 und Juni 2022 unter Anleitung von Prof. Dr. Robert Wolf am Institut für Anorganische Chemie der Universität Regensburg angefertigt.

Die Arbeit wurde angeleitet von:		Prof. Dr. Robert Wolf
Promotionsgesuch eingereicht am:		30.11.2022
Tag der mündlichen Prüfung:		26.01.2023
Promotionsausschuss:	Vorsitz	Prof. Dr. Rainer Müller
	Erstgutachter	Prof. Dr. Robert Wolf
	Zweitgutachter	Prof. Dr. Manfred Scheer
	Dritte Prüferin	Prof. Dr. Ruth M. Gschwind

Prologue

This thesis primarily reports on the synthesis of valuable organic phosphorus compounds (OPCs) such as phosphines and phosphonium salts. Chapter 1 reviews the industrial state-of-the-art procedure to transform P_4 into monophosphorus compounds and recently reported developments in the organofunctionalization of inorganic phosphorus compounds are presented. Chapter 2 describes the *photochemical* synthesis of OPCs such as arylated phosphines and phosphonium salts directly from P_4 , using carbon-centered radicals provided by reduction of chlorobenzene in presence of super-photoreductant tetrakis(dimethylamino)ethylene (TDAE) with UV-light irradiation. In chapter 3 a simple *photocatalytic* method for the stannylation of P_4 using a cheap, commercially-available distannane $(Bu_3Sn)_2$ and anthraquinone as a simple photocatalyst is described. Subsequent ‘one-pot’ transformation of the resulting stannylated monophosphine intermediate $(Bu_3Sn)_3P$ provides direct access to valuable OPCs. The *photoelectrocatalytic* arylation of diphenylphosphine (PPh_2H) into phosphines and phosphonium salts *via* reductive activation of organic halides by electrochemically mediated photoredox catalysts (e-PRCat) is reported in chapter 4. Chapter 5 covers a distinct project and describes the synthesis and characterization of bidentate isonitrile iron complexes. Finally, chapter 6 gives a summary of the results described in this thesis and provides a short outlook.

Prolog

Diese Dissertation behandelt hauptsächlich die Darstellung von organischen Phosphorverbindungen, wie beispielsweise Phosphanen und Phosphoniumsalzen. Kapitel 1 gibt zunächst einen Überblick über die industrielle Darstellung von Monophosphorverbindungen durch die Funktionalisierung von weißem Phosphor (P_4) und stellt aktuelle akademische Forschungsergebnisse in Bereich der Organofunktionalisierung von anorganischen Phosphorverbindungen dar. In Kapitel 2 wird die photochemische Synthese von arylierten Phosphanen und Phosphoniumsalzen aus P_4 beschrieben, indem die eingesetzten Chlorbenzole mithilfe des Photoreduktionsmittels Tetrakis(dimethylamino)ethylen (TDAE) unter Bestrahlung von UV-Licht zu Arylradikalen reduziert werden. Kapitel 3 befasst sich mit der photokatalytischen Stannylierung von P_4 und der Darstellung des Intermediates $(Bu_3Sn)_3P$ durch Verwendung von Bis-(tributylzinn) und Photokatalysator Anthrachinon. Durch Umsetzung des Intermediats $P(SnBu_3)_3$ kann eine Vielzahl an wertvollen Organophosphorverbindungen synthetisiert werden. Die photoelektrokatalytische Arylierung von Diphenylphosphan (PPh_2H) durch Arylhalogenide wird in Kapitel 4 beschrieben. Für die reduktive Aktivierung der Substrate wurden elektrochemisch vermittelte Photoredoxkatalysatoren verwendet. Kapitel 5 beschreibt mit der Synthese und Charakterisierung von bidentaten Isonitrileisenkomplexen ein weiteres, thematisch abgegrenztes Projekt. Das letzte Kapitel fasst die Ergebnisse dieser Arbeit zusammen und gibt einen kurzen Ausblick.

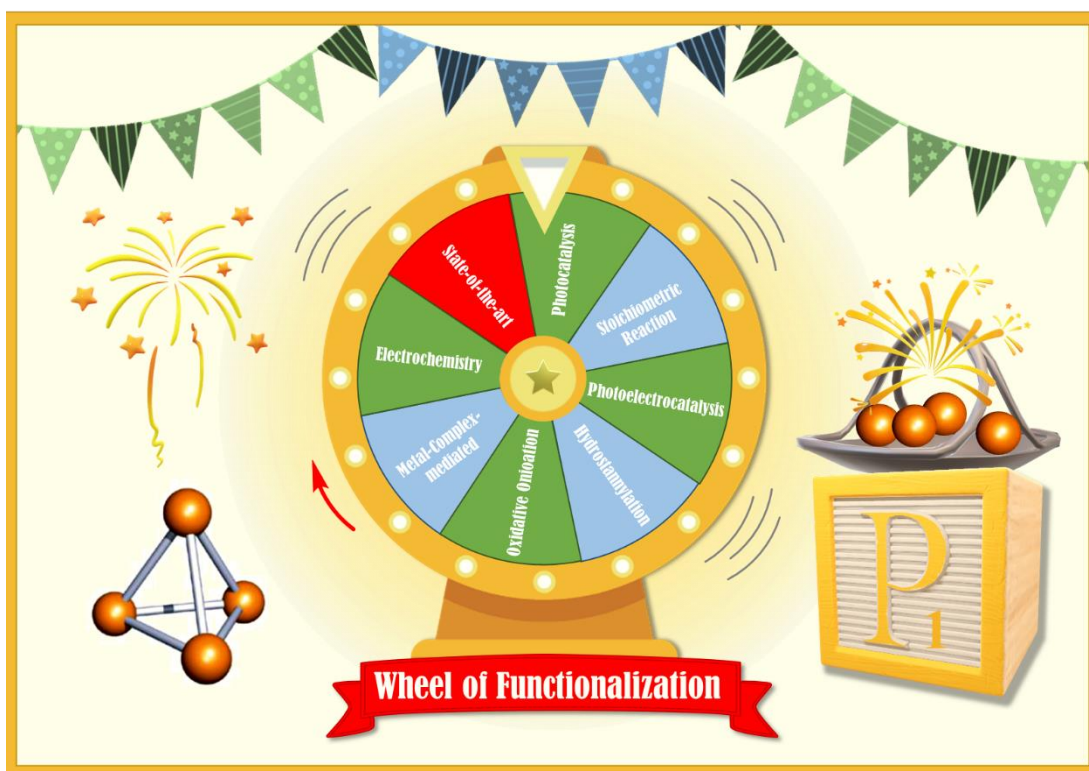
Table of Contents

1	Recent Developments in the Organofunctionalization of Inorganic Phosphorus Compounds	1
1.1	Direct functionalization of white phosphorus: State-of-the-art.....	3
1.2	Functionalization of white phosphorus with carbon-centered radicals	5
1.3	Functionalization of white phosphorus with stannyl radicals	13
1.4	Electrochemical functionalization of white phosphorus	15
1.5	Direct functionalization of white phosphorus into versatile phosphorus transfer reagents via oxidative onioation	19
1.6	Metal complex mediated functionalization of P ₄	21
1.7	Functionalization of phosphites and H-phosphonates with carbon-centered radicals....	24
1.8	Phosphoric acid as a precursor to chemicals traditionally synthesized from white phosphorus	30
1.9	Conclusion and Outlook.....	32
1.10	References	33
2	Photochemical Transformation of Chlorobenzenes and White Phosphorus into Arylphosphines and Phosphonium salts	39
2.1	Introduction	41
2.2	Results and Discussion.....	43
2.3	Conclusion.....	49
2.4	Supporting Information	50
2.5	References	83
3	Photocatalytic Stannylation of White Phosphorus	85
3.1	Introduction	87
3.2	Results and Discussion.....	87
3.3	Conclusion.....	93
3.4	Supporting Information	94
3.5	References	139
4	Reductive Photoelectrocatalytic Activation of Organic Halides and Diphenylphosphine into Arylphosphines and Phosphonium Salts	143
4.1	Introduction	145
4.2	Results and Discussion.....	152
4.3	Conclusion.....	161
4.4	Supporting Information	162
4.5	References	219
5	Synthesis and Characterization of Bidentate Isonitrile Iron Complexes	221
5.1	Introduction	223
5.2	Results and Discussion.....	225
5.3	Conclusion.....	234

5.4	Supporting Information.....	235
5.5	References.....	274
6	Summary and Outlook	279
7	Acknowledgements.....	286
8	Curriculum Vitae	288
9	List of Publications.....	290
10	Eidesstattliche Erklärung.....	291

1 Recent Developments in the Organofunctionalization of Inorganic Phosphorus Compounds^[a]

Abstract: Organophosphorus compounds (OPCs) are an important and industrially relevant class of molecules with numerous applications, e.g., as flame retardants, photoinitiators, herbi-/pesticides, pharmaceuticals, and as reagents in organic synthesis and catalysis. Current state-of-the-art methods used in industry for the synthesis of these valuable compounds rely on hazardous, multistep procedures converting white phosphorus (P_4) into toxic chlorinated monophosphorus intermediates (PCl_3 and PCl_5). Direct functionalization protocols are rare and the development of new methods avoiding these chlorinated P intermediates by directly converting P_4 into OPCs is a challenging yet highly desirable objective. Developing chlorine-free procedures for the synthesis of useful OPCs directly from P_4 or other P sources has been an active area of research for the last several decades. A variety of mechanistically diverse functionalization methods of P_4 and other P sources, such as stoichiometric reactions, photo- and electrocatalysis, hydrostannylation or metal-mediated activation were reported over the last few years. These current developments are described in this chapter.



^[a] Marion Till wrote the manuscript with input from Thomas Horsley Downie and Robert Wolf.

1.1 Direct functionalization of white phosphorus: State-of-the-art

Since its discovery in the 17th century, elemental phosphorus is a fascinating, essential element for life, existing in different allotropic modifications.^[1] White phosphorus (P₄) – the most reactive elemental form – is produced on a >900,000 t scale annually *via* the electrothermal reduction of phosphate minerals in an electric arc furnace.^[2] While most of the P₄ produced worldwide is used for high-purity phosphate fertilizer, a significant proportion (ca. 18%) is converted into a large variety industrially relevant organophosphorus compounds (OPCs).^[2] These OPCs have an important impact on daily life through their numerous applications, e.g., in pharmaceuticals, fertilizers, flame retardants and surfactants. Figure 1 illustrates the key role of white phosphorus as a key precursor for a broad range of phosphorus-based chemicals used in technical applications.^{[2],[3]}

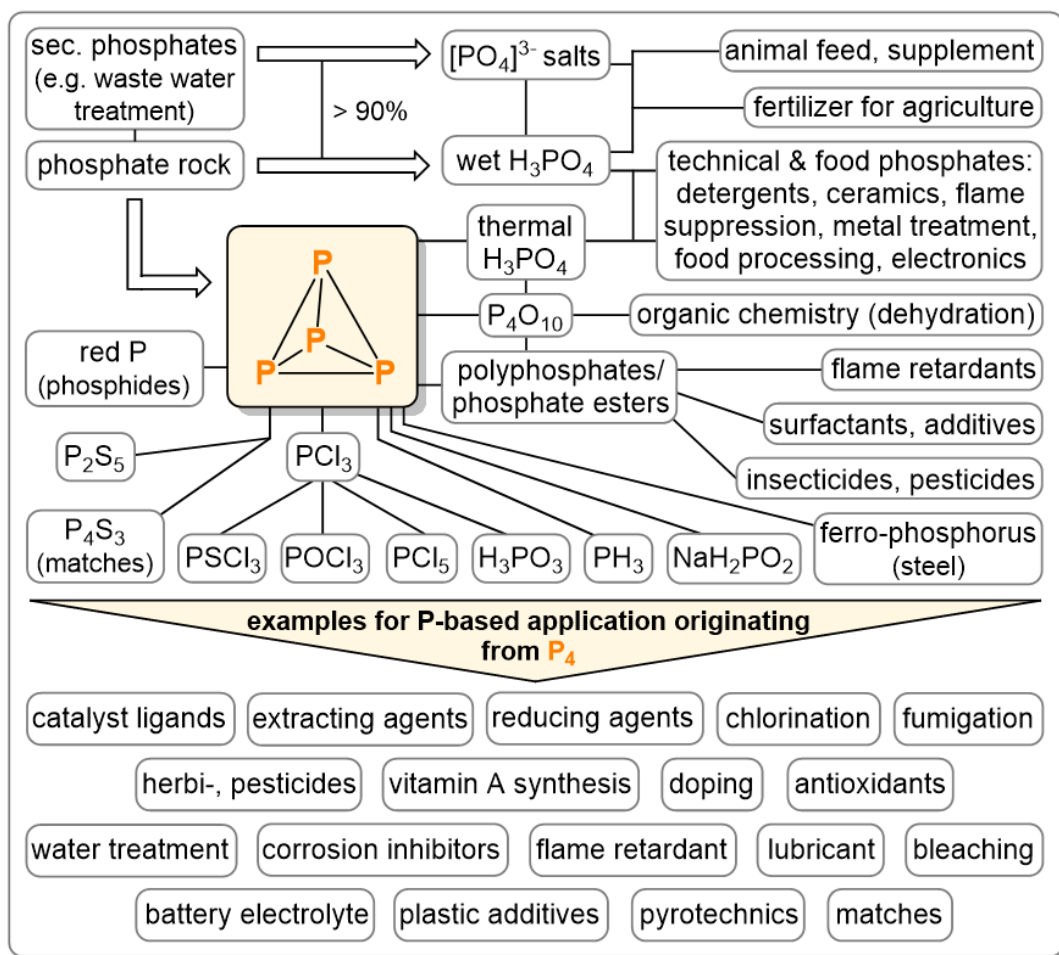


Figure 1. Overview of technical applications of P-based compounds originating from white phosphorus (adapted from ref. [3]).

Unfortunately, the current industrial state-of-the-art method for accessing these myriad, valuable organophosphorus compounds (OPCs) rely on an atom-inefficient, multistep procedure involving the initial chlorination or oxychlorination of P₄ with toxic chlorine

gas to generate PCl_3 , PCl_5 , and POCl_3 (Figure 2).^{[2],[3]} These chlorinated intermediates can subsequently be transformed into a variety of P_1 products by reaction with nucleophiles, such as organolithium or Grignard reagents. Alongside reliance on extremely toxic and hazardous starting materials and intermediates (Cl_2 gas, PCl_3 and sodium) these procedures for synthesizing OPCs cause large amounts of chloride-containing waste.^[2] An alternative route is provided by the generation of flammable and highly toxic PH_3 gas, *via* either acid- or base-mediated disproportionation of P_4 , which can be subsequently employed in the hydrophosphination of unsaturated organic substrates (Figure 2).^[2]

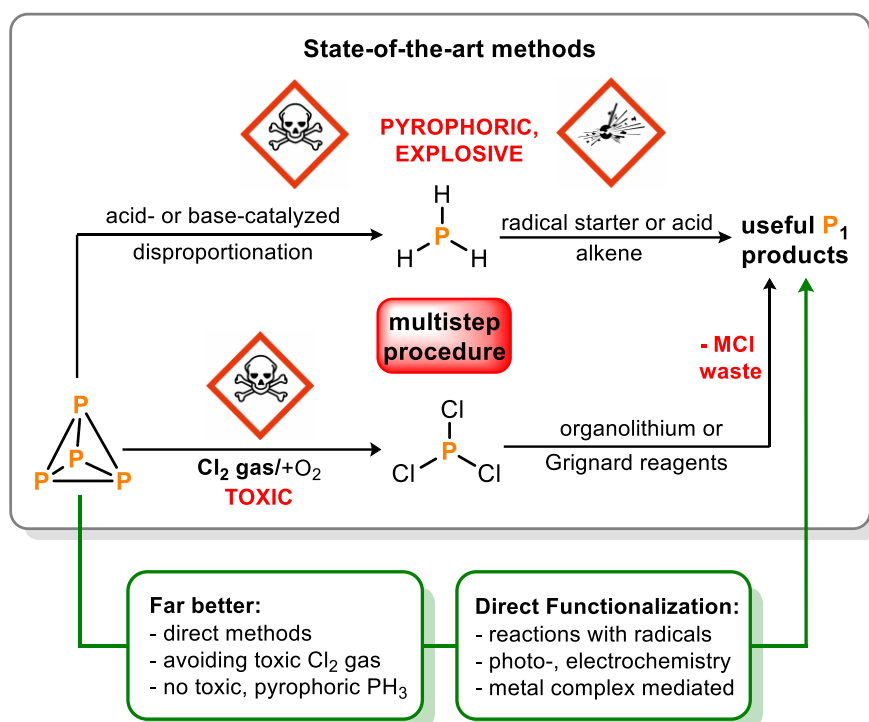


Figure 2. Hazardous and multistep state-of-the-art methods for the synthesis of organophosphorus compounds (OPCs) directly from white phosphorus and suggestions for direct functionalization methods.

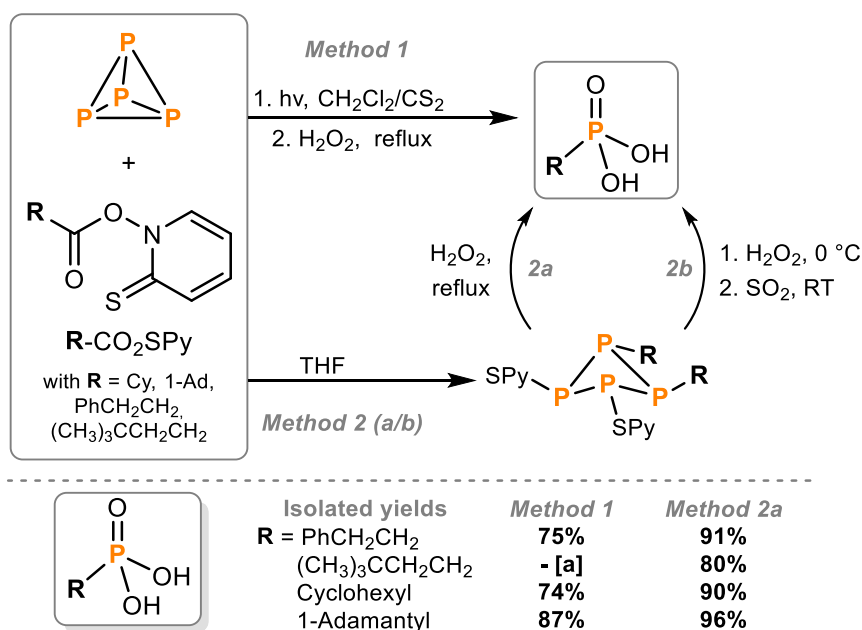
Developing alternative procedures for the synthesis of useful OPCs by direct functionalization of P_4 or other P sources is a challenging yet highly desirable objective. Over the last several decades the development of alternative routes which avoid chlorine gas and circumvent the toxic intermediates PCl_3 or PH_3 has received significant academic interest. In pursuit of this challenging objective, a variety of mechanistically diverse methods for direct functionalization of P_4 into important OPCs have been developed, which utilize stoichiometric reactions, photo- and electrocatalysis with carbon-centered radicals, hydrostannylation and metal-mediated activation. These routes for the functionalization of P_4 and other organic phosphorus sources will be examined in detail in the following section.

1.2 Functionalization of white phosphorus with carbon-centered radicals

1.2.1 Stoichiometric functionalization

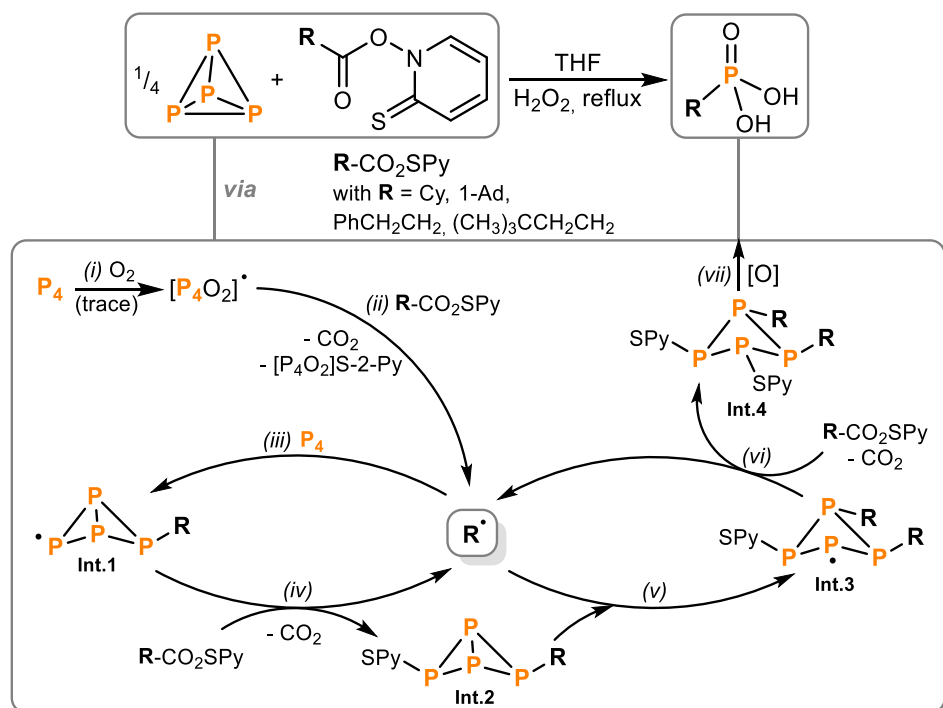
1.2.1.1. Functionalization with Barton PTOC esters

In 1992, Barton and Zhu reported a new procedure to convert carboxylic acids into the corresponding phosphonic acids using the notable ability of P_4 to efficiently trap carbon-centered radicals.^[4] Irradiation of P_4 with white light in a CH_2Cl_2/CS_2 solvent mixture in the presence of *N*-hydroxy-2-thiopyridone (Barton PTOC ester, $R-CO_2SPy$) and subsequent oxidation with excess H_2O_2 yielded up to 87% of the phosphonic acid (Scheme 1, Method 1). Some years later, in 1998 Barton and Vonder Embse described a modified method for the synthesis of phosphonic acids directly from P_4 with improved yields.^[5] The new procedure replaced the binary solvent mixture CH_2Cl_2/CS_2 with THF and the radical chain functionalization of P_4 was found to be complete in less than a minute in darkness (Scheme 1, Method 2). Addition of the Barton PTOC ester to the solution of P_4 in THF led to spontaneous CO_2 evolution and after oxidation with H_2O_2 the targeted phosphonic acid was generated. Further investigations showed that addition of sulfur dioxide (SO_2) improved the oxidation step to phosphonic acids with sensitive functional groups, including vinyl groups (Scheme 1, Method 2b). The two-step oxidation process uses first H_2O_2 at 0 °C and subsequently SO_2 at room temperature.^[5] Natural carboxylic acids are transformed effectively into the corresponding phosphonic acids *via* this procedure.



Scheme 1. Synthesis of phosphonic acids by reaction of white phosphorus with carbon-centered radicals derived from Barton PTOC esters.^{[4],[5]}

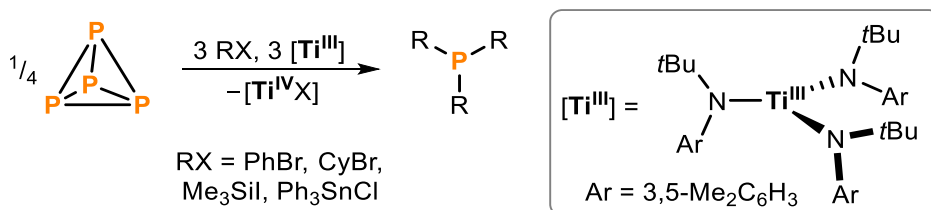
Deeper investigation (e.g., radical chain inhibition by TEMPO (2,2,6,6-tetramethylpiperidin-1-oxyl) or screening different stoichiometries of P_4 and Barton esters) into the mechanistic details of the functionalization of P_4 with carbon-centered radicals derived by Barton PTOC esters ($R-CO_2SPy$ with $R = Cy, 1-Ad, PhCH_2CH_2$ and $(CH_3)_3CCH_2CH_2$) revealed that traces of O_2 are essential to initiate the radical chain reactions through attack on the P_4 tetrahedron. A likely mechanism is displayed in Scheme 2. The resulting $[P_4O_2]^\bullet$ radicals react with the Barton PTOC ester with evolution of CO_2 and generation of alkyl radicals (R^\bullet) (step ii). These carbon-centered radicals are trapped by P_4 to form a $[RP_4]^\bullet$ radical intermediate (**Int.1**, step iii) which further propagates the radical chain mechanism by attacking a second Barton ester molecule (step iv). Bicyclo[1.1.0]tetraphosphabutane $[RP_4SPy]$ (**Int.2**), showing a well-known “butterfly structure”, is presumably formed as the next intermediate. Repetition of the same sequence (steps v and vi) by reaction of an alkyl radical (R^\bullet) with the $[RP_4SPy]$ intermediate (**Int.2**) and subsequent consumption of another Barton ester affords the $[R_2P_4(SP_2)_2]$ tetraphosphetane (**Int.4**), which yields the corresponding phosphonic acid after oxidation (step vii).^[5]



Scheme 2. Mechanism of the direct functionalization of P_4 with Barton PTOC esters.^[5]

1.2.1.2. Ti(III)-mediated functionalization

Pioneering studies by Barton and co-workers identified P₄ as a good radical trapping agent and found that this property can be used to generate OPCs directly from P₄. Building on this, in 2010 Cossairt and Cummins reported a stoichiometric functionalization reaction of P₄ in which the generation of reactive carbon-centered radicals was achieved by reacting organic iodides or bromides with a titanium(III) complex which functions as a halogen atom abstractor (Scheme 3).^[6]

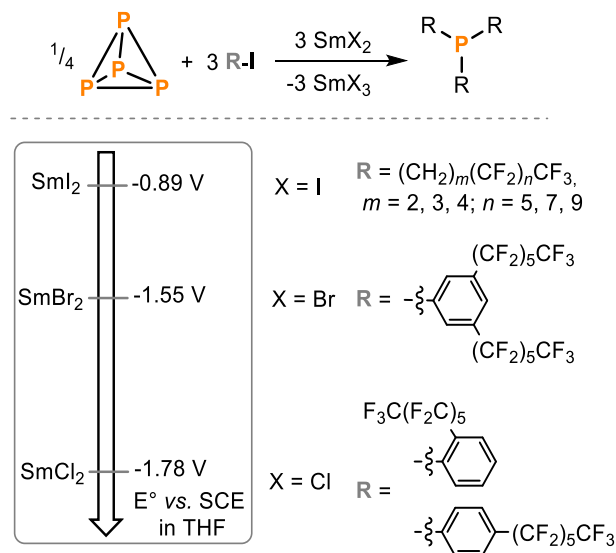


Scheme 3. Radical synthesis of trialkyl, triaryl, trisilyl and tristannyl phosphines from P₄.^[6]

The three-coordinate complex Ti(N(*t*Bu)Ar)₃ ([Ti^{III}], with Ar = 3,5-C₆H₃Me₂) is able to abstract the halogen atom from the organic halide used (RX = CyBr, PhBr, Me₃SiI, Ph₃SnCl) to generate the corresponding alkyl-, aryl-, silyl- or stannyl radical. These radicals are trapped by P₄ and break down the P₄ tetrahedron to synthesize valuable tertiary phosphines. For example, the stoichiometric reaction of bromobenzene (PhBr), [Ti^{III}] (3 equiv.) and P₄ (0.25 equiv.) affords a product mixture of triphenylphosphine (Ph₃P, 71%) and tetraphenyldiphosphine (Ph₄P₂, 21%), with the latter being a stable intermediate of the stoichiometric arylation reaction. By increasing the amount of PhBr and [Ti^{III}] (5 equiv.) used, complete conversion of P₄ (0.25 equiv.) to Ph₃P was achieved (95% NMR yield, 72% isolated yield). The aryl- and alkylation mediated by the titanium complex is limited to organic bromides and iodides, whereas the use of organic chlorides led to no product formation. Treatment of P₄ (0.25 equiv.) with a stoichiometric amount of Me₃SiI or Ph₃SnCl (3 equiv.) in the presence of [Ti^{III}] (3 equiv.) resulted in the selective formation of (Me₃Si)₃P or (Ph₃Sn)₃P, respectively, with excellent yields of up to 97%.^[6]

1.2.1.3. Sm(II)-mediated functionalization

While developing and investigating the [Ti^{III}]-mediated functionalization of P₄, other typical one-electron reducing agents such as CoCl(Ph₃P)₃, SmI₂ or Cp₂TiCl were tested for their ability to abstract the halogen atom, but no reaction was observed when using PhBr as a substrate.^[6] Nevertheless, a report by Gosh, Cummins and Gladysz shows that the stronger reductants SmBr₂ (E° = -1.55 V vs. SCE)^[7] or SmCl₂ (E° = -1.78 V vs. SCE)^[7] can be successfully used for the synthesis of triaryl- and trialkylphosphines directly from P₄ and fluororous aryl/alkyl iodides (Scheme 4).^[8] The formation of trialkylphosphines could also be achieved using the milder reductant SmI₂ for more easily reduced fluororous alkyl iodides. This transformation is postulated to occur *via* the addition to the P₄ molecule from radicals generated using a modest excess of substrate and the samarium(II) reducing agent. As mentioned by Gladysz, Budnikova and co-workers already reported related studies a few years earlier. By an electrochemically mediated functionalization of P₄ with fluororous alkyl iodides as the same substrate class the corresponding phosphines were formed using a nickel catalyst precursor.^[9] Later Budnikova et al. reported that electrochemically generated SmCl₂ can be used in catalytic quantities for the non-fluororous P₄ activation.^[10]

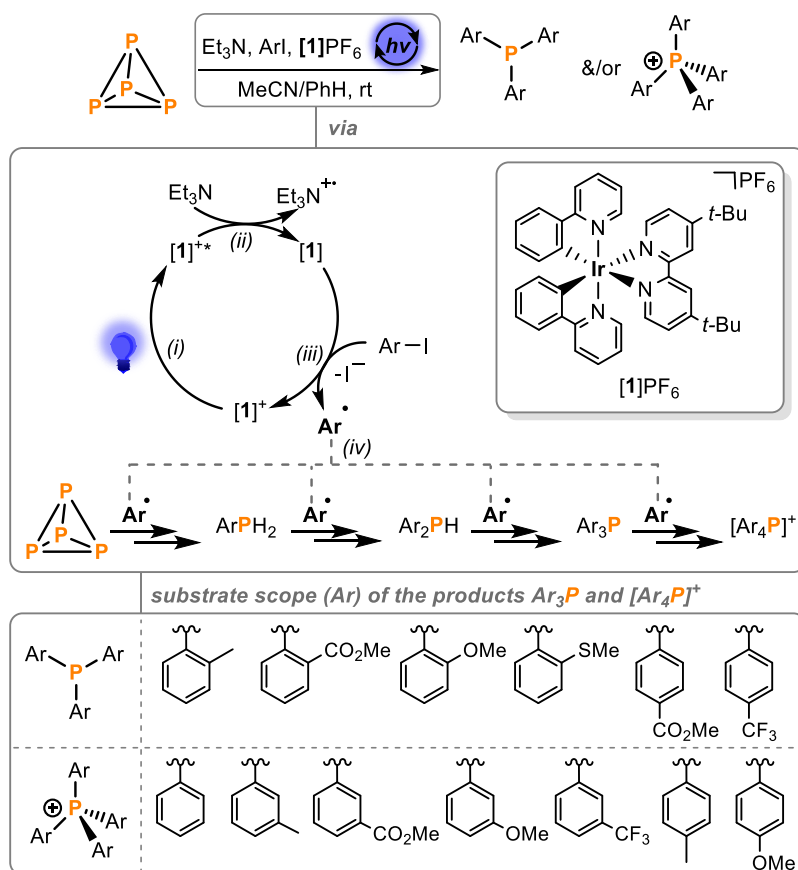


Scheme 4. A direct route from white phosphorus and fluororous alkyl and aryl iodides to the corresponding trialkyl- and triarylphosphines.^{[7],[8]}

1.2.2 Photocatalytic generation of P₁ compounds

1.2.2.1. Photocatalytic functionalization of P₄

In late 2019, Wolf and co-workers described the first example of a photocatalytic functionalization of P₄ directly into useful organophosphorus compounds (OPCs).^[11] Triarylphosphines and tetraarylphosphonium salts were obtained from P₄ and aryl iodides (ArI) mediated by an iridium photoredox-catalyst and blue light irradiation in the presence of triethylamine (Et₃N). This method for the catalytic functionalization of P₄ relies on the ability of P₄ to trap carbon-centered radicals (Ar[•]) (*vide supra*). The proposed mechanism starts with blue-light (455 nm) irradiation of the photoredox catalyst [Ir(dtbbpy)(ppy)₂PF₆] ([1]PF₆, dtbbpy = 4,4'-di-*tert*-butyl-2,2'-bipyridine, ppy = 2-(2-pyridyl)phenyl, see Scheme 5, step i). Absorption of a blue photon generates the excited form [1]^{+*} which is reduced in its (triplet) excited state by Et₃N (step ii). The reduced photoredox catalyst [1] exhibits the perfect redox potential (Ir(III)/Ir(II) E° = -1.51 V vs. SCE)^[12] to reduce aryl iodides (E° = -1.16 V vs. SCE)^[13] in a single-electron transfer step, generating aryl radicals Ar[•] (step iii). These carbon-centered radicals then attack and break down the P₄ tetrahedron, producing in sequence ArPH₂, Ar₂PH, Ar₃P and finally the phosphonium salt [Ar₄P]⁺ (step iv).

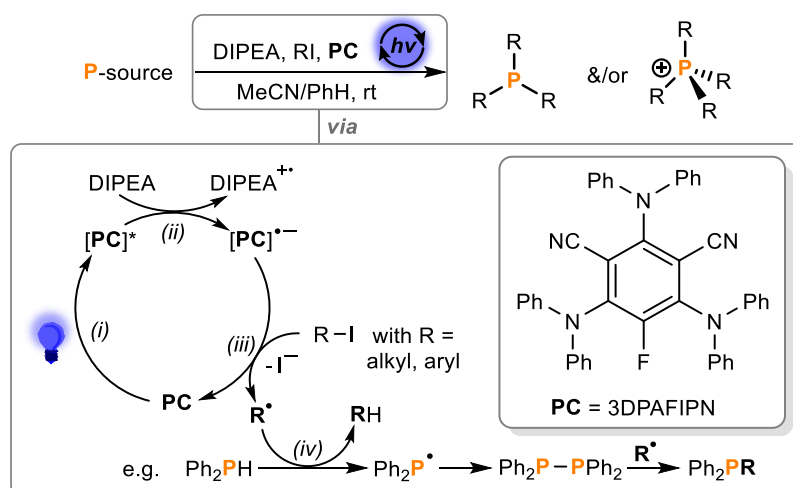


Scheme 5. Direct photocatalytic transformation of white phosphorus into arylphosphines and phosphonium salts.^[11]

The catalytic arylation of P_4 was shown to be limited to the use of organic iodides as substrates while attempts to switch from ArI to the more chemically inert $PhBr$ or $PhCl$ led to no product formation in both cases. A variety of substituted organic iodides were successfully employed, including substrates bearing electron-withdrawing ($COOMe$, CF_3) and electron-donating (Me , OMe) groups. In contrast to the model substrate PhI , which selectively yielded the tetraphenylphosphonium iodide $[Ph_4P]I$, other substituted iodobenzenes resulted in a mixture of phosphine and phosphonium salt. Depending on the steric properties of the substrate the phosphine was exclusively formed, e.g., the reaction with (*ortho*- Tol) I (*ortho*- Tol = 2-methylphenyl) selectively yielded the tertiary phosphine (*ortho*- Tol) $_3P$, because with the additional bulk of the *ortho*- Me groups the maximum coordination number at the phosphorus is limited.^[11]

1.2.2.2. Photocatalytic functionalization of Ph_2PH

Wolf and co-workers subsequently reported a modified photocatalytic arylation of P_4 using the simple and cheap organo-photocatalyst, 3DPAFIPN (**PC**, see Scheme 6) instead of the costly $[1]PF_6$. In the same reaction protocol 3DPAFIPN can be used to generate aryl and alkyl radicals from the corresponding organic iodides to functionalize P_4 into tertiary phosphines and quaternary phosphonium salts.^[14] For the synthesis of asymmetric phosphines and phosphonium salts other P sources, namely mono- and diphenylphosphine ($PhPH_2$, Ph_2PH), could be used instead of P_4 for the stepwise photocatalytic arylation. Initial irradiation (455 nm) of the photoredox catalyst **PC** (Scheme 6, step i) and subsequent reduction of the photoexcited species $[PC]^*$ by the sacrificial reducing agent DIPEA (*N,N*-diisopropylethylamine, step ii) results in the corresponding radical anion $[PC]^{*-}$, which generates aryl or alkyl radicals *via* SET with the organic iodide.



Scheme 6. Versatile visible-light driven synthesis of asymmetrical phosphines and phosphonium salts.^[14]

Depending on the starting material (P_4 vs. primary or secondary phosphine), the transformation with the photocatalytically generated carbon-centered radicals provides access to either symmetric or asymmetric OPCs in moderate to good yields by using a range of aryl iodides bearing electron-donating (Me, OMe) and electron-withdrawing (COOMe, CF_3) groups, as well as alkyl iodides (see Figure 3). For *ortho*-substituted substrates the preferential formation of the triarylphosphine product was observed. Employing tetraphenyldiphosphine (Ph_4P_2), another interesting ligand class – PCP pincer ligands – was synthesized by using 1,3-bis(bromomethyl)benzene as a substrate. In scope and selectivity, the photocatalytic arylation of P_4 using 3DPAFIPN (**PC**) mirrors the previously observed results when using **[1]PF₆** as the catalyst.^[14]

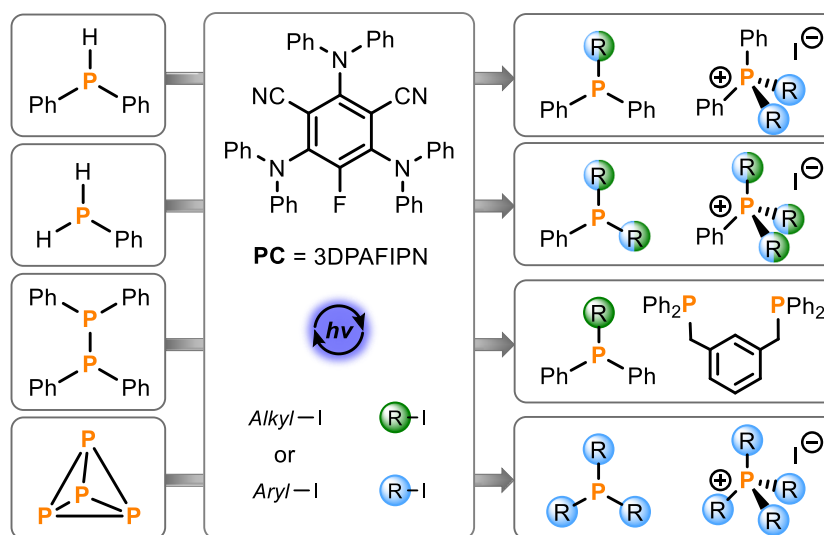
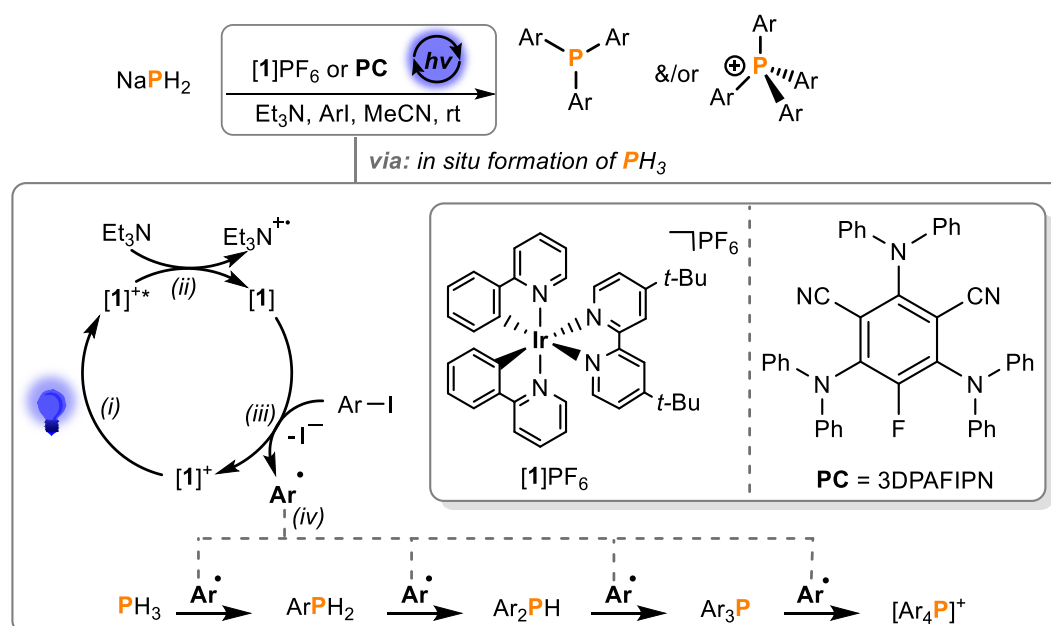


Figure 3. Photocatalytic synthesis of asymmetrical phosphines and phosphonium salts using different P sources.^[14]

In both photocatalytic systems replacing the organic iodide with Ph_3SnCl leads to the stannylated phosphine $(Ph_3Sn)_3P$, rendering catalytic the synthesis of $(Ph_3Sn)_3P$ directly from P_4 , compared to the stoichiometric $[Ti^{III}]$ -mediated synthesis previously reported by Cossairt and Cummins.^[6] This mild and versatile, visible-light-mediated system provided access to a broad scope of asymmetrical aryl/aryl and aryl/alkyl OPCs. The mechanistic approach of using radicals for the transformation of P_4 and other P sources offers huge potential for further development in this research field.

1.2.2.3. Photocatalytic functionalization of PH₃

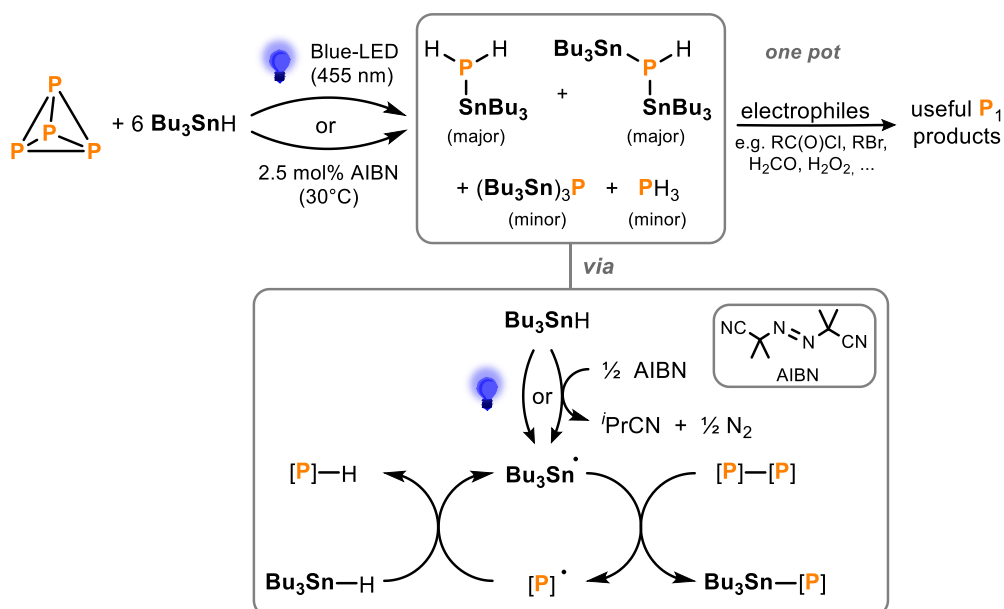
Extensive ³¹P{¹H} NMR spectroscopic investigations reported by Gschwind and Wolf allowed a deeper insight into the radical mechanism and the degradation of P₄ in the photocatalytic functionalization procedure.^[15] With these mechanistic investigations a few so far unrecognized intermediates and side products could be identified, which support the proposed mechanism mediated by the iridium catalyst [1]PF₆ and the organic photoredox catalyst 3DPAFIPN (PC) discussed in the previous sections (see 1.2.2.1 and 1.2.2.2, also Scheme 7, steps i-iv). The specific observation of phosphane (PH₃) being a minor intermediate in the light-driven phenylation of P₄ led to the consideration of functionalizing this key industrial compound in the same manner. Therefore, the Wolf group developed the first photocatalytic functionalization of PH₃ which provided access to triarylphosphines and tetraarylphosphonium salts similar to the P₄ arylation method (Scheme 7). However, to avoid the direct handling of PH₃ gas, a combination of metal phosphides Zn₃P₂ or NaPH₂ and HCl were employed as PH₃ surrogates. Initial set up limitations using a two-chambered system, which caused an inefficient concentration of the *in situ* generated PH₃ gas in the photocatalytic reaction mixture, were improved by generating PH₃ from NaPH₂ in the absence of HCl in a single-chambered apparatus directly in the reaction mixture, containing Et₃N, aryl iodides and photocatalyst ([1]PF₆ or PC) upon irradiation with blue light. After optimization of the reaction conditions and investigation of several substituted aryl iodides, both photocatalysts were successfully employed to provide the targeted phosphines and phosphonium salts in similar conversions and selectivity.



Scheme 7. Photocatalytic functionalization of NaPH₂ as a surrogate for PH₃.^[15]

1.3 Functionalization of white phosphorus with stannyl radicals

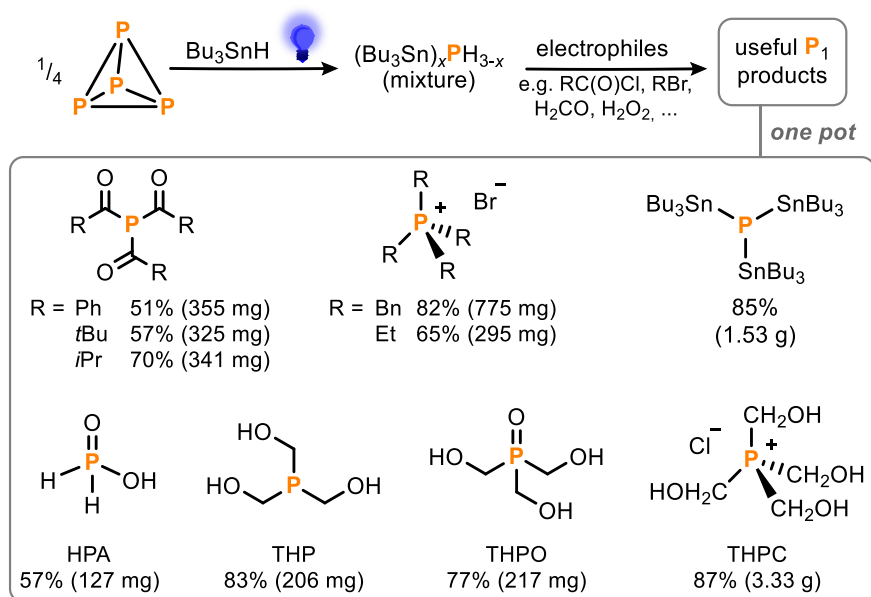
Beside the extensive investigation of the past several years to generate OPCs directly from P_4 or from other P sources in stoichiometric^{[4]-[8]} or photocatalytic manner^{[11],[14],[15]} by using organic carbon-centered radicals, Scott and Wolf recently reported a new procedure to transform P_4 into valuable P_1 products employing inorganic stannyl radicals (R_3Sn^\bullet ; $R = nBu, Ph$).^[16] Initial Bu_3Sn^\bullet radical formation from the radical agent Bu_3SnH is mediated by visible light (blue-LED, 455 nm) or a chemical radical initiator such as azabis(isobutyronitrile) (AIBN, 2.5 mol%) (Scheme 8). The hydrostannylation then proceeds by the efficient attack of the stannyl radicals on the P–P bonds, breaking down the P_4 tetrahedron in a radical chain reaction which results in a mixture of hydrostannylated phosphines $(Bu_3Sn)_xPH_{3-x}$ ($x = 0-3$).^[16]



Scheme 8. Hydrostannylation of white phosphorus and subsequent 'one-pot' transformation into useful P_1 products with electrophiles.^[16]

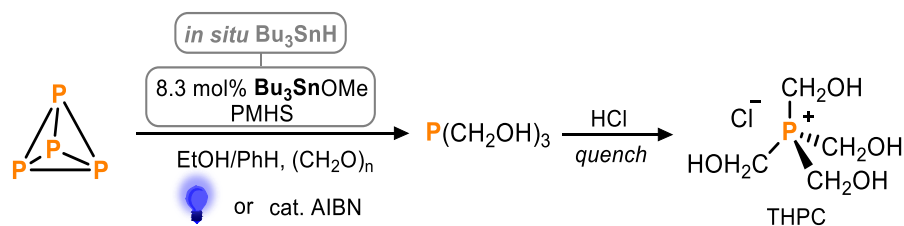
Stoichiometric amounts of Bu_3SnH (6 equiv. per P_4 molecule) were sufficient to convert P_4 into the mixture of stannylated phosphines $(Bu_3Sn)_xPH_{3-x}$ ($x = 0-3$), yielding the primary and secondary stannyl phosphine Bu_3SnPH_2 ^[17] and $(Bu_3Sn)_2PH$ ^[18] in a combined conversion of 75% (with PH_3 and tristannylphosphine $(Bu_3Sn)_3P$ present in minor amounts). The resulting $(Bu_3Sn)_xPH_{3-x}$ mixture – acting as a ' P^{3-} ' synthon – can then be converted into P_1 products by reaction with a variety of electrophiles in a one-pot fashion (Scheme 9).^[16] This further transformation provides access to valuable OPCs such as tetrakis(hydroxymethyl) phosphonium salt (THPC)^[18] which is used as a flame-retardant precursor or tetrabenzyl phosphonium salt $[Bn_4P]Br$ used as a precursor for the Wittig

reaction.^[17] Very recently, Scott and Wolf additionally reported the hydrostannylation of red phosphorus, similarly by irradiation in the presence of Bu_3SnH , providing access to the same selection of P_1 products.^[21]



Scheme 9. Synthesis of monophosphines directly from white phosphorus.^[16]

During the workup of THPC in a gram scale synthesis (Scheme 9, 87%, 3.33 g isolated yield) the byproduct of the type Bu_3SnX ($\text{X} = \text{halide}$) was separated and recovered in almost quantitative yield. Treatment of the recovered Bu_3SnX with Na_2CO_3 and PMHS (polymethylhydrosiloxane) successfully provided the initial stannyl radical source Bu_3SnH and allowed the construction of a ‘one-pot’ closed loop procedure (first cycle: 80% THPC, second cycle: 66% THPC). Further investigation into improving the recycling of tin compounds showed that it is possible to perform the hydrostannylation of P_4 and subsequent transformation into the THPC in a fully catalytic manner (Scheme 10) by *in situ* generation of Bu_3SnH via Bu_3SnOMe and PMHS. Irradiation with blue light gave a turnover number (TON) of 10.7 per P–P bond of P_4 corresponding to 60% conversion of P_4 . Similar results were obtained using AIBN as an initiator (TON = 10.7 59% conversion).^[16]



Scheme 10. Synthesis of THPC in catalytic manner. Catalyst loading in mol% is defined per P atom.^[16]

1.4 Electrochemical functionalization of white phosphorus

1.4.1 Electrochemical generation of phosphines directly from P₄

The electrochemical behavior of P₄ was first studied more than fifty years ago by the Tomilov group.^[22] Polarography studies showed that white phosphorus can be reduced at a potential of $E^\circ = -1.55$ V (vs. Hg in dimethylformamide (DMF)) and forms the radical anion [P₄]^{•-} in an irreversible process.^[22] However, it was not until nearly 30 years later that the potential for functionalization of P₄ via electrochemical approaches was investigated by Sinyashin and Yakhvarov.^[23] They examined a combination of metal complex catalysis and organic electrosynthesis because of its high selectivity and efficiency for the formation of new element-carbon bonds.^[23] This approach provided access to the preparation of OPCs directly from P₄ using organonickel and organozinc complexes in an electrochemical procedure. The proposed mechanism is displayed in Figure 4. For the electrochemical functionalization of P₄ a single compartment cell and an electrode set of a platinum cathode and an electrochemically soluble metal (Zn, Al, Mg), which serves as the sacrificial anode (Figure 4, step i). Reduction of the nickel complex [Ni^{II}(bpy)]Br₂ (bpy = 2,2'-bipyridine) with a platinum cathode (in combination with a zinc anode) generates the catalyst complex [Ni⁰(bpy)] (step ii). After subsequent oxidative addition of the substrate ArBr to [Ni⁰(bpy)] (step iii), the resulting nickel(II) species [Ni^{II}Br(Ar)(bpy)] transfers the aryl moiety to the P₄ molecule (step iv). Following stepwise arylation, triarylphosphine PAr₃ is formed as a final product. By changing the sacrificial anode from zinc to magnesium, the pentaphospholane P₅Ph₅ was formed as the main product. When using an aluminum anode, selective formation of triphenylphosphine oxide (OPPh₃) was observed.

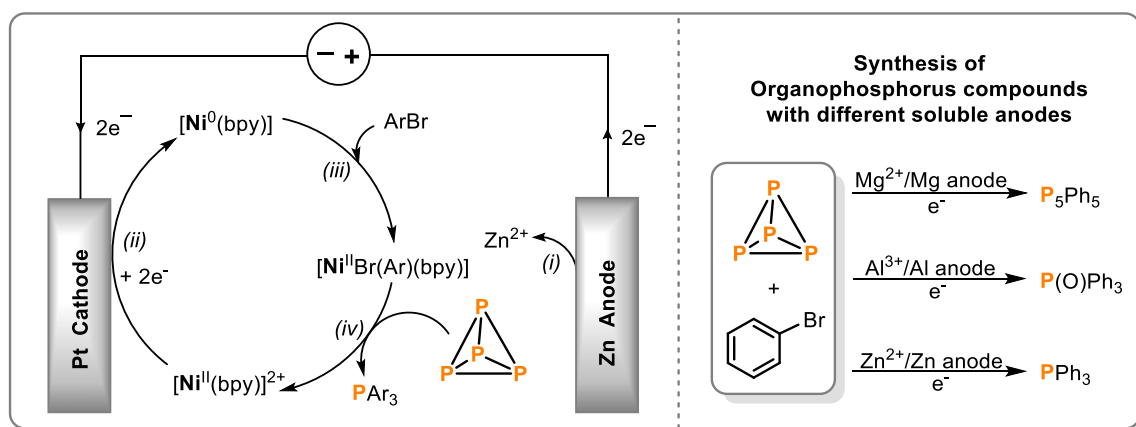


Figure 4. Electrochemical functionalization of P₄ using an electrogenerated Ni(0) complex.^[23]

The Budnikova group reported a conceptionally similar electrochemically-mediated functionalization of P_4 with fluororous alkyls, using the same nickel pre-catalyst, to generate the corresponding phosphines.^{[9],[10]} More recently, Budnikova and co-workers developed a route to synthesize triphenylphosphine directly from P_4 without an additional catalyst, using an electrochemically generated zinc(0) species from the used zinc electrode (Figure 5).^[24] This simple synthesis is performed in an undivided cell, using DMF as solvent and an electrode set combining Pt(+)/Zn(-). Initially, anodically generated Zn^{2+} ions (Figure 5, step i) are subsequent electrochemically reduced to form the active Zn^0 species (step ii), which reacts with the organic halide PhX (X = Br, I) to generate organozinc reagents $[PhZnX]$ (step iii). The organozinc reagent cleaves one of the P–P bonds of the P_4 tetrahedron forming organophosphorus derivatives containing a P–C bond and zinc phosphides (step iv). The resulting zinc phosphides are further transformed with another organic halide, affording a new P–C bond in the bis-arylated P_4 butterfly complex $[P_4Ph_2]$. The Zn^{2+} ion is regenerated and is then reduced again to the Zn^0 species as part of the electrochemical loop. Repetition of the arylation step (step iv) by transformation with organozinc compound $[PhZnX]$ and cleavage of all P–P bonds results in the formation of triphenylphosphine (PPh_3) as the final product. This simple electrochemical procedure selectively affords widely-used PPh_3 in up to 82% yield (relative to P_4).^[24]

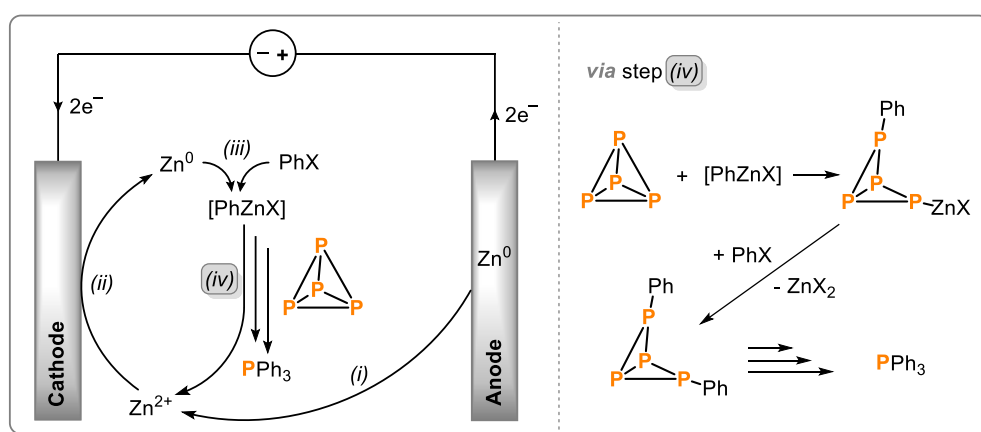


Figure 5. Electrochemical functionalization of P_4 using active zinc(0) species.^[24]

1.4.2 Electrochemical generation of a dicyanophosphide anion directly from P₄

Complementing the work of Sinyashin, Yakhvarov and Budnikova,^{[23],[24]} who focused on the reductive electrochemical functionalization of P₄, the Liu group developed a new procedure to OPCs *via* the dicyanophosphide anion salt Li[P(CN)₂], accessed by electrochemical activation of P₄ by using hydrogen cyanide (HCN) as an oxidant.^[25] Although the dicyanophosphide anion [P(CN)₂]⁻ had been previously reported by Schmidpeter in 1977,^[26] all existing synthetic routes towards this anion suffer from very poor P atom economy.^{[26],[27]} Liu and co-workers reported a facile electrochemical synthesis of [P(CN)₂]⁻ with excellent conversions of 92% (reduced conversion of 55% (1.96 g) on preparative scale of 5.0 mmol P₄) by reacting P₄ with a mixture of Me₃SiCN and LiOH in an undivided electrochemical cell using an electrode combination of Pt(+)/C(-) (Figure 6). It is proposed that HCN and LiCN are generated *in situ* by reaction of Me₃SiCN and LiOH. In an undivided cell a potential of 4 V was applied to a THF solution of P₄, Me₃SiCN and LiOH. The generated HCN is reduced to H₂ at the platinum cathode, providing the cyanide anion which reacts with the P₄ yielding the P₁ product Li[P(CN)₂].^[25]

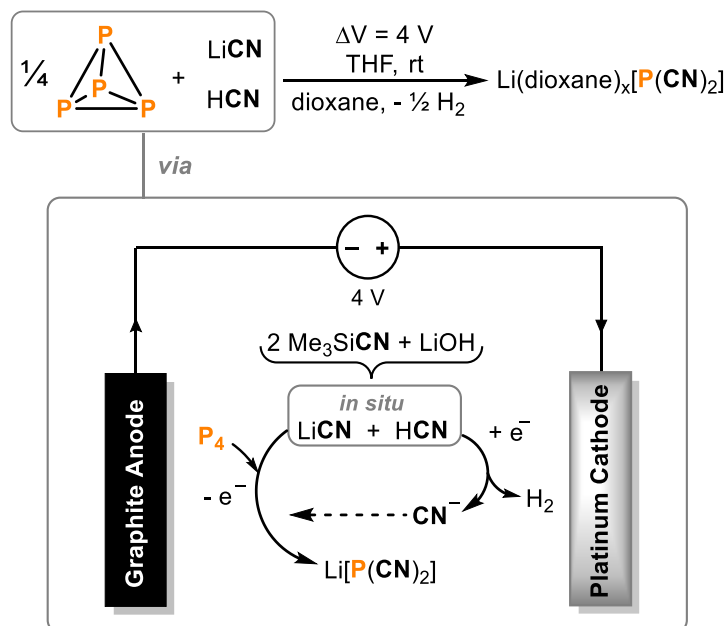


Figure 6. Facile synthesis of [Li(dioxane)_x][P(CN)₂] *via* electro-oxidation of white phosphorus.^[25]

Further reactivity studies of the dicyanophosphide anion [P(CN)₂]⁻ towards neutral and anionic carbon-based nucleophiles provided access to a variety of OPCs involving phosphinidenes, cyclophosphanes, and phospholides (Figure 7).^[25] Treatment of the precursor Li(dioxane)_x[P(CN)₂] with organolithium reagents showed good conversion

into cyclophosphanes (Figure 7, step i), whereas organo-dilithium reagents yielded substituted phospholides, another useful P containing product class (step iii). Reaction of $[\text{P}(\text{CN})_2]^-$ with neutral carbon nucleophiles, such as *N*-heterocyclic carbenes (NHC) or cyclic(alkyl)(amino)carbenes (CAAC) provided access to various base-stabilized phosphinidenes (step ii).^[25]

This simple synthetic route using electrochemistry for the direct functionalization of P_4 and further transformation of the electrochemically generated precursor $[\text{P}(\text{CN})_2]^-$ into numerous P_1 products shows that not only the established reductive pathway, but also the electrochemical activation of P_4 by using oxidants offers great potential in further development of this research area.

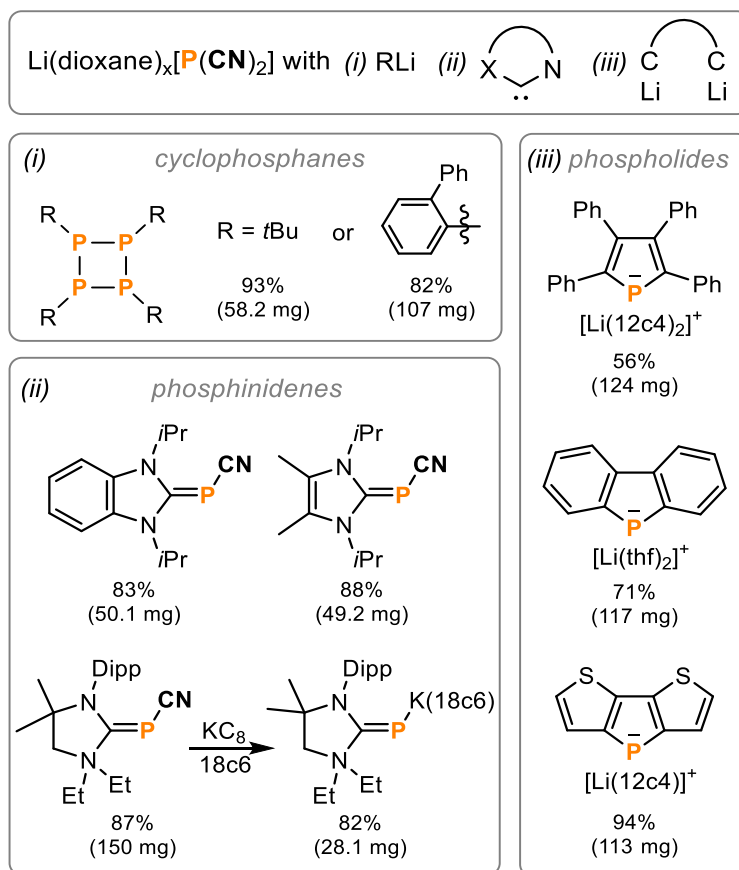
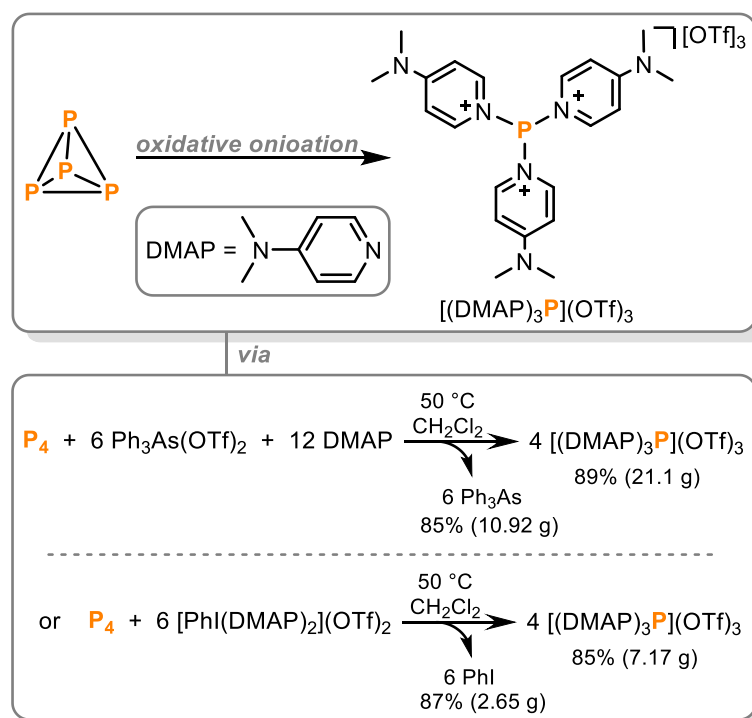


Figure 7. Overview of products generated from $[\text{Li}(\text{dioxane})_x][\text{P}(\text{CN})_2]$.^[25]

1.5 Direct functionalization of white phosphorus into versatile phosphorus transfer reagents via oxidative onioation

Very recently, Weigand and co-workers reported a mechanistically unique method for the synthesis of versatile phosphorus transfer reagents (Scheme 11).^[28] The key to their procedure is the facile and selective synthesis of viable tricationic P(III) transfer reagents $[P(L_N)](OTf)_3$ by reaction of an oxidant and a suitable N-based donor (L_N) with P_4 . This process was termed *oxidative onioation*. The Weigand group had previously reported that the highly Lewis-acidic compound $Ph_3As(OTf)_2$, prepared from Ph_3AsO and Tf_2O (trifluoromethanesulfonic anhydride), can be used to form polyphosphorus frameworks by reaction with PCl_3 .^[29] Oxidative treatment of a dichloromethane solution of P_4 with $Ph_3As(OTf)_2$ and 4-dimethylaminopyridin (DMAP) yielded the P(III) species $[(DMAP)_3P](OTf)_3$, featuring three onio-ligands ($DMAP^+$), in excellent yield on a multigram scale (89%, 21.1 g, see Scheme 11). An alternative route to this highly electrophilic trication $[(DMAP)_3P]^{3+}$ is the reaction of P_4 with $[PhI(DMAP)_2](OTf)_2$ which also delivers an excellent yield of 85%. The side products of the oxidative onioation reaction are Ph_3As or PhI , which can be conveniently recycled in yields of up to 87% (Scheme 11).^[28]



Scheme 11. Selective oxidative onioation of white phosphorus into the P_1 transfer reagent $[(DMAP)_3P](OTf)_3$ (DMAP = 4-dimethylaminopyridine).^[28]

Investigation into the reactivity of the base-stabilized P₁ transfer reagent [(DMAP)₃P](OTf)₃ towards pronucleophiles (NuH) revealed that it exhibited similar behavior to the analogous P(III) intermediate PCl₃. Thus, access is provided to trialkyl- and triarylphosphites P(OR)₃ via the formation of new P–O bonds (Figure 8, P(OR)₃ with R = Ph, Cy, 2-ethylhexyl and 2,4-*t*Bu₂-C₆H₃). The implementation of P–C and P–N bonds yields a variety of industrially relevant phosphines (e.g., Ph₃P) in good yields (Figure 8).^[28]

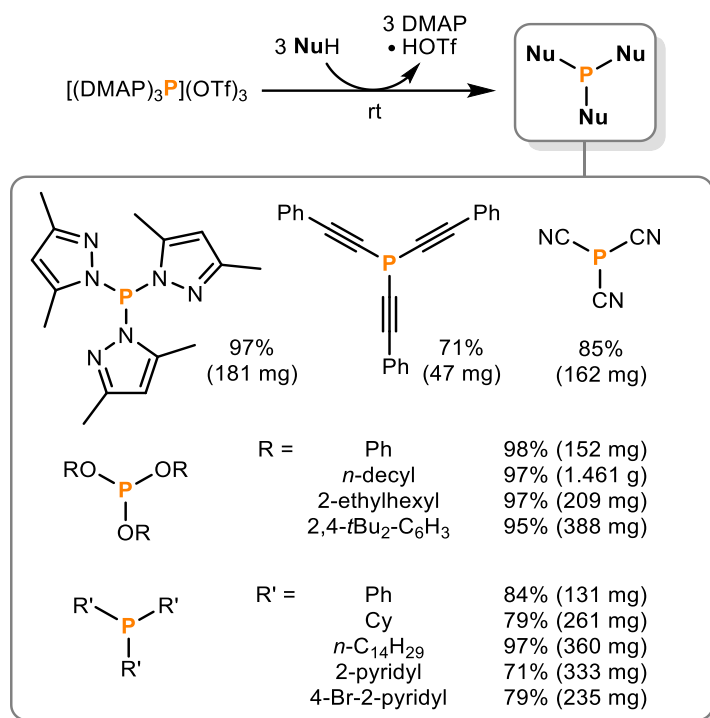
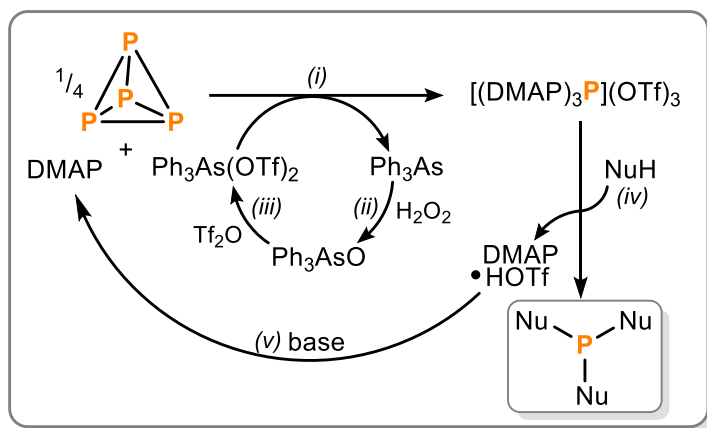


Figure 8. Application of [(DMAP)₃P](OTf)₃ as an alternative to PCl₃ for the formation of P–C, P–N and P–O bonds.^[28]

Scheme 12 presents a closed loop strategy devised by Weigand and co-workers for the oxidative onioation of P₄ into [(DMAP)₃P](OTf)₃ (step i) using Ph₃As(OTf)₂, which is generated by the oxidation of Ph₃As with H₂O₂ (step ii) and subsequent reaction of the arsane oxide Ph₃AsO with Tf₂O (step iii). Thus, the byproduct Ph₃As can be isolated and used in a closed loop. Subsequent conversion of [(DMAP)₃P](OTf)₃ into OPCs with (pro)nucleophiles (NuH) (step iv) affords the desired P₁ products and the pyridinium salt DMAP·HOTf, which can be recovered by treatment with base (step v). Thus, both the oxidant and base used during this P₄ functionalization are recycled in a closed loop.^[29] The oxidative onioation of P₄ represents a mechanistically new method for the synthesis of valuable OPCs through transformation of the ‘P³⁺’ synthon [(DMAP)₃P](OTf)₃, which is generated directly from P₄ and presents a viable alternative to the use of toxic PCl₃ as an intermediate.^[28]

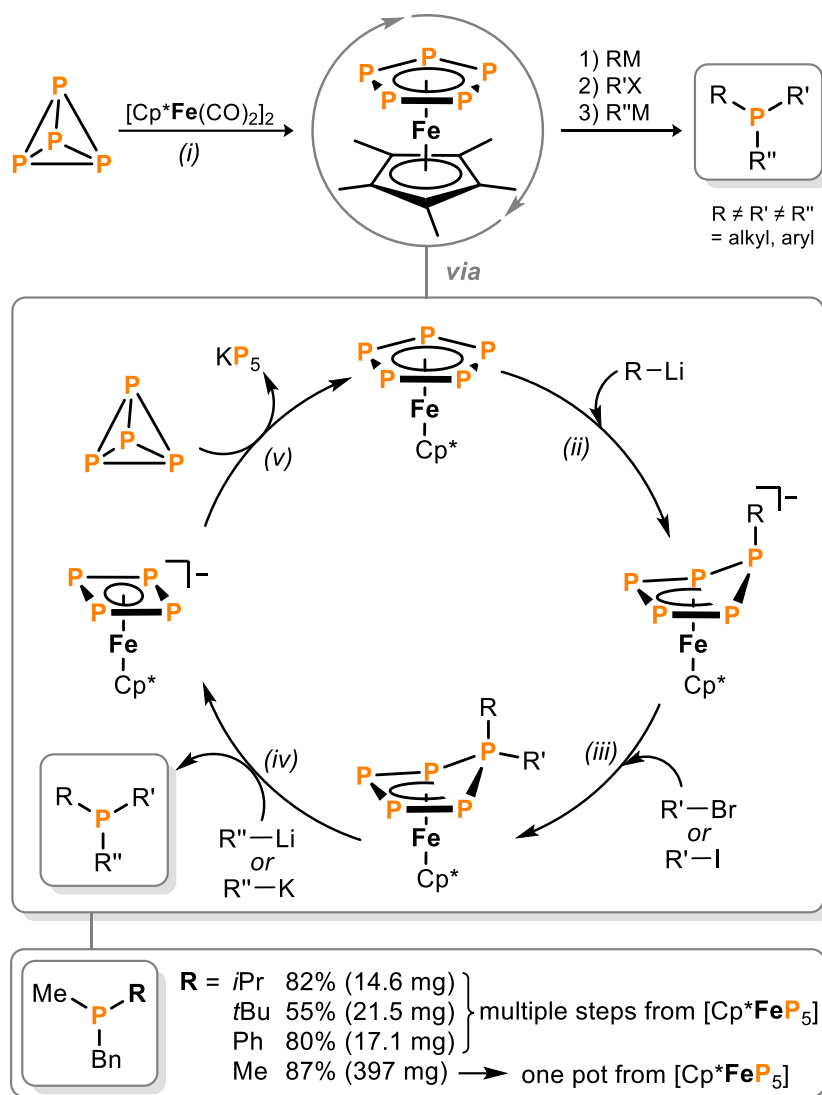


Scheme 12. Closed loop strategy of the oxidative functionalization of P_4 into P_1 transfer reagent $[(\text{DMAP})_3\text{P}](\text{OTf})_3$ and subsequent transformation into P_1 products by recycling of base and oxidant. Tf_2O = trifluoromethanesulfonic anhydride.^[28]

1.6 Metal complex mediated functionalization of P_4

1.6.1 Pentaphosphaferrocene mediated synthesis of phosphines $\text{P}(\text{RR}'\text{R}'')$

Metal-mediated activation of white phosphorus is a well-studied research area with a plethora of examples using transition-metal (TM) and main group elements and compounds as precursors for the activation and further functionalization of P_4 .^[30] One widely explored transition-metal-mediated P_4 activation product is the oligophospholide-containing ferrocene analogue η^5 -pentaphosphaferrocene ($[\text{Cp}^*\text{FeP}_5]$, with $\text{Cp}^* = \eta^5\text{-C}_5(\text{CH}_3)_5$), which was first synthesized by Scherer in 1987 by reaction of the dimeric iron-carbonyl compound $[\text{Cp}^*\text{Fe}(\text{CO})_2]_2$ with P_4 .^[31] Recently, Scheer and co-workers described a conceptionally innovative method for the direct synthesis of asymmetrically substituted phosphines (Scheme 13).^[32] Based on previous work, treatment of $[\text{Cp}^*\text{Fe}(\eta^5\text{-P}_5)]$ (step i) with an organolithium reagent RLi ($\text{R} = \text{Me}, t\text{Bu}, \text{Ph}$) results in a selective nucleophilic addition to the *cyclo*- P_5 ring (step ii).^[33] Treatment of the resulting $[\text{Cp}^*\text{Fe}(\eta^4\text{-P}_5\text{R})]^-$ species with an alkyl halide $\text{R}'\text{X}$ ($\text{R}' = \text{Me}, i\text{Pr}; \text{X} = \text{Br}, \text{I}$) selectively affords the 1,1-diorgano-substituted complex $[\text{Cp}^*\text{Fe}(\eta^4\text{-P}_5\text{RR}')]$ (step iii). Further addition of a second organometallic reagent $\text{R}''\text{M}$ ($\text{KBn}, n\text{BuLi}, \text{MeLi}$) releases the asymmetric phosphine ($\text{PRR}'\text{R}''$, with $\text{R} \neq \text{R}' \neq \text{R}'' = \text{alkyl, aryl}$) by nucleophilic attack (step iv).^[32] The phosphine is isolated by distillation and the residual organometallic byproduct $[\text{Cp}^*\text{Fe}(\eta^4\text{-P}_4)]^-$ can be converted back to the starting material $[\text{Cp}^*\text{FeP}_5]$ by addition of P_4 and heating at $275\text{ }^\circ\text{C}$ (step v). This strategy provided access to asymmetric phosphines in good yields up to 82%. Additionally, PMe_2Bn was prepared in a one pot manner from $[\text{Cp}^*\text{FeP}_5]$ in 87% yield (Scheme 13).



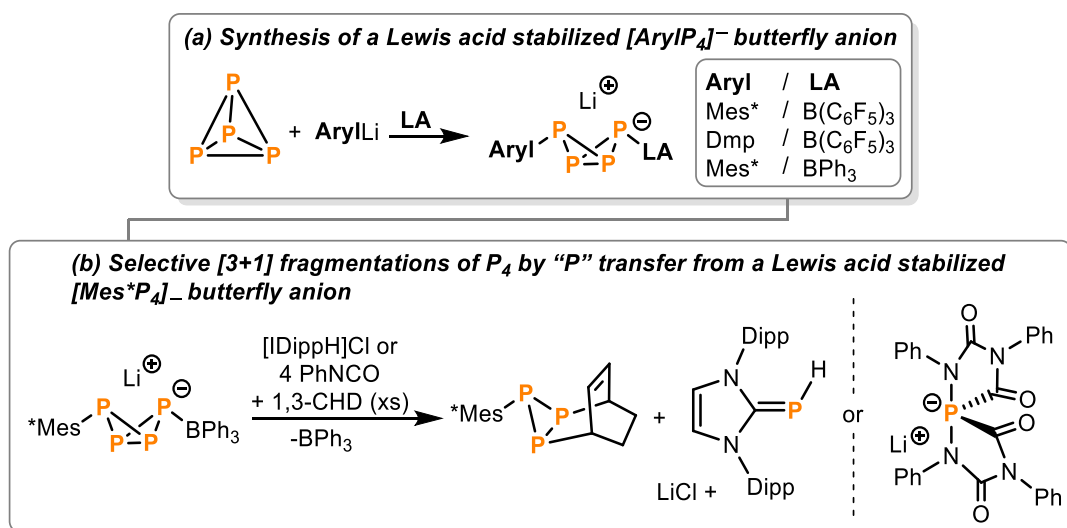
Scheme 13. Pentaphosphaferrocene-mediated synthesis of asymmetric organo-phosphines starting from white phosphorus.^[32]

Recycling studies showed that the regenerated starting material [Cp*FeP₅] can be reused in multiple reaction cycles (up to three cycles) to generate a variety of asymmetric phosphines.^[32] The resulting side product, KP₅, can in principle be used to generate new pentaphosphaferrocene (though in completely). Thus, the P atom efficiency of the method currently still suffers from some practical limitations.

1.6.2 Selective [3+1] fragmentation of P₄ and formation of P₁ products

Functionalization of white phosphorus using main group metal organyls, such as organolithium or Grignard reagents, are well-known reactions which were first reported in 1963 by Rauhut and co-workers.^[34] They demonstrated the formation of P–C bonds by reaction of organolithium reagents (PhLi, *n*BuLi, or Grignard salts (MgBr)) with P₄. This yielded, besides undesirable organopolyphosphines, the primary or tertiary phosphines

only in low conversion. Fluck and co-workers isolated the first example of a butterfly shaped bicyclo[1.1.0]tetraphosphabutane ($\text{Mes}^*\text{P}_4\text{Mes}^*$, with $\text{Mes}^* = 2,4,6\text{-}t\text{Bu}_3\text{C}_6\text{H}_2$) by reaction of P_4 with the sterically encumbered Mes^*Li .^[35] In 2014, the Lammertsma group confirmed that this bicyclo[1.1.0]tetraphosphabutane compound is formed through a highly reactive transient $[\text{ArylP}_4]^-$ butterfly anion, which is generated through a single P–P bond cleavage.^{[36],[37]} This butterfly anion $[\text{ArylP}_4]^-$ was stabilized by use of sterically encumbered ArylLi reagents (Aryl = Mes^* , Dmp (= 2,6-dimesitylphenyl)) and triarylborane Lewis acids (LA, $\text{B}(\text{C}_6\text{F}_5)_3$ or BPh_3) (Scheme 14a). Reactivity studies of the Lewis acid stabilized bicyclo[1.1.0]tetraphosphabutane $\text{Li}[\text{Mes}^*\text{P}_4 \cdot \text{BPh}_3]$ showed a [3+1] fragmentation by reaction with an imidazolium salt ($[\text{IDippH}]\text{Cl}$; IDipp = 1,3-bis(2,6-diisopropylphenyl)-imidazol-2-ylidene) or phenylisocyanate (PhNCO) (Scheme 14b).



Scheme 14. Selective [3+1] fragmentations of P_4 by “P” transfer from a Lewis acid stabilized $[\text{ArylP}_4]^-$ butterfly anion. $\text{Mes}^* = 2,4,6\text{-}t\text{Bu}_3\text{C}_6\text{H}_2$; Dmp = 2,6-dimesitylphenyl; 1,3-CHD = cyclohexadiene; IDipp = 1,3-bis(2,6-diisopropylphenyl)-imidazol-2-ylidene.^{[36],[37]}

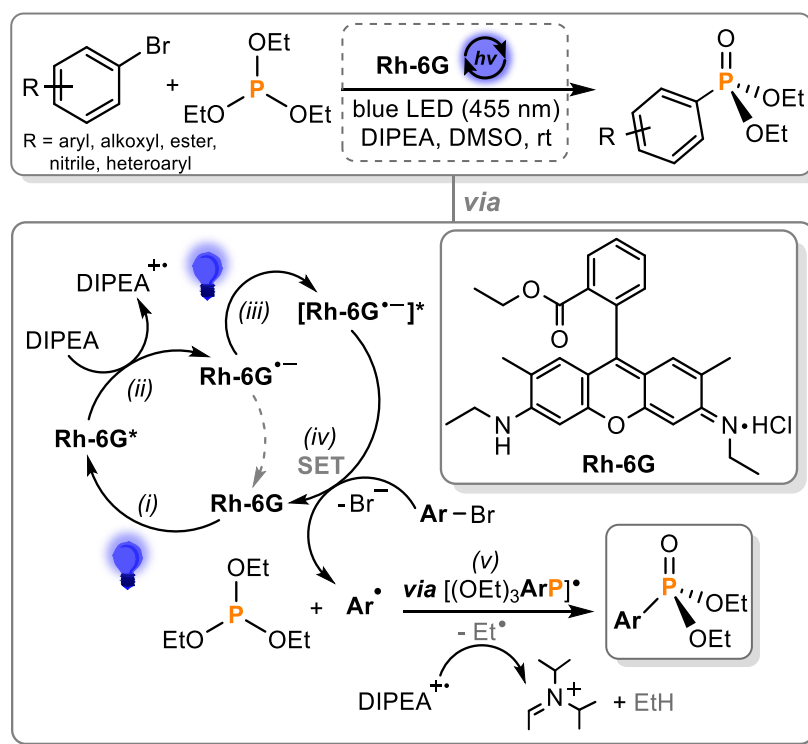
Reaction with the *N*-heterocyclic carbene precursor $[\text{IDippH}]\text{Cl}$ formed a carbene-phosphinidene adduct through “P” transfer from the BPh_3 -stabilized butterfly anion. The [3+1] fragmentation induced by phenylisocyanate PhNCO led to a spirophosphoranide as the product. The [3+1] fragmentation of the $\text{Li}[\text{Mes}^*\text{P}_4 \cdot \text{BPh}_3]$ butterfly anion released the triphosphirene Mes^*P_3 as a side product regardless of the substrate ($[\text{IDippH}]\text{Cl}$ or PhNCO). The triphosphirene was isolated as a dimer or could be trapped by 1,3-cyclohexadiene (1,3-CHD) as a Diels-Alder adduct (see Scheme 14b). This unprecedented [3+1] fragmentation of the Lewis acid stabilized $[\text{ArylP}_4]^-$ butterfly anion provided access to interesting P_1 - and P_3 -containing moieties directly from white phosphorus.^{[36]-[38]}

1.7 Functionalization of phosphites and H-phosphonates with carbon-centered radicals

1.7.1 Photocatalytic functionalization

1.7.1.1. Visible-light photo-Arbusov reaction of triethyl phosphite and aryl bromides

Aryl phosphonates and phosphine oxides are important structural motifs which find their application in many pharmaceutically active molecules.^[39] These kind of valuable OPCs are usually prepared by transition-metal-catalysis, e.g., palladium-, nickel- or copper-catalyzed cross-coupling of diarylphosphine oxides ($R_2P(O)H$) with a coupling partner *via* P–H bond activation.^[40] In 2016, König and co-workers reported an efficient, mild and metal-free synthesis of those aryl phosphonates relying on visible-light photoredox catalysis (photo-Arbusov reaction) using Rhodamin-6G (Rh-6G) as a photocatalyst (Scheme 15).^[41]



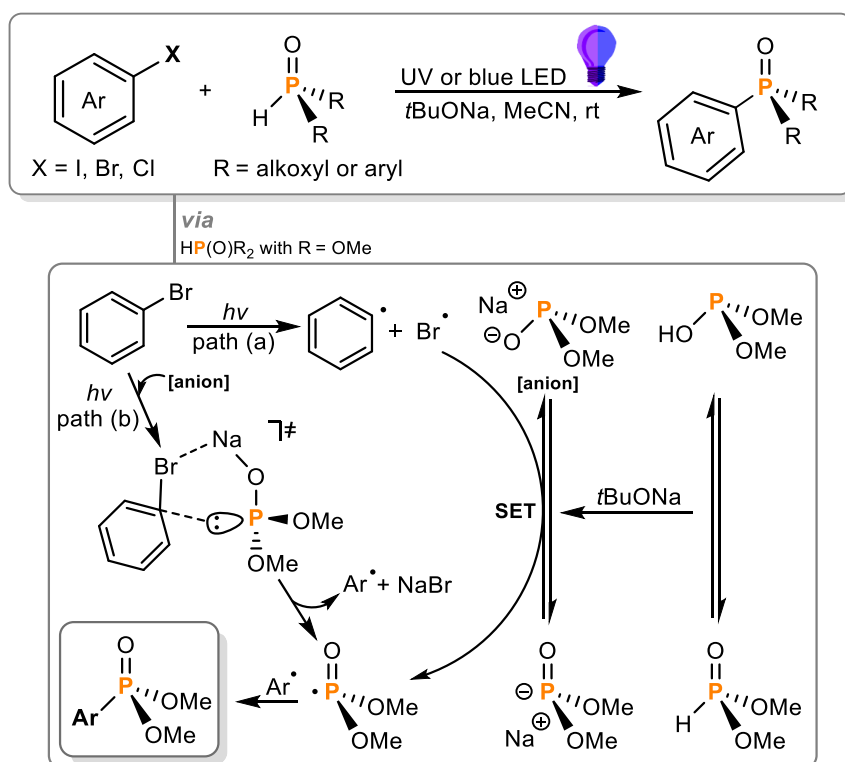
Scheme 15. Visible-light Photo-Arbusov reaction of aryl bromides and trialkyl phosphites yielding aryl phosphonates.^[41]

Through C–H bond activation *via* photoinduced electron transfer (PET) reactive aryl radicals are generated which are the key intermediates for the P–C bond formation. The proposed mechanism is displayed in Scheme 15. Upon blue light irradiation the photoexcited Rh-6G is reduced by sacrificial reducing agent *N,N*-diisopropylethylamine

(DIPEA) (steps i and ii). Photoexcitation of the resulting radical anion $[\text{Rh-6G}^{\bullet-}]$ ($E^\circ = -2.4 \text{ V vs. SCE}$)^[42] forms the excited species $[\text{Rh-6G}^{\bullet-}]^*$ (step iii) which reduces the aryl halide ArX ($\text{X} = \text{Br, Cl}$) used as a substrate by a single electron transfer (SET) (step iv). The generated carbon-centered radicals Ar^\bullet react with the trialkyl phosphite ($\text{P}(\text{OEt})_3$) used as a P source, forming a new P–C bond and the corresponding unstable phosphoranyl radical $[(\text{OEt})_3\text{ArP}]^\bullet$ (step v).^[43] After release of an ethyl radical (Et^\bullet), which is quenched by the photo-oxidized $\text{DIPEA}^{+\bullet}$, rearrangement of the arylated P species yields the targeted aryl phosphonate. This visible-light-driven phosphonylation of aryl halides, especially biologically active ones, provides access to a variety of phosphonates in moderate to good yields using a broad scope of trialkyl phosphites and halogenated heteroarenes.^[41]

1.7.1.2. Photoinduced transition-metal-free cross-coupling of aryl halides with H-phosphonates

Three years later, Li and Zeng developed a photoinduced transition-metal- and photosensitizer-free cross-coupling of aryl halides ArX ($\text{X} = \text{Cl, Br}$ and I) with H-phosphonates to provide arylphosphine oxides (Scheme 16).^[44]



Scheme 16. Photoinduced transition-metal-free cross coupling of aryl halides with H-phosphonates.^[44]

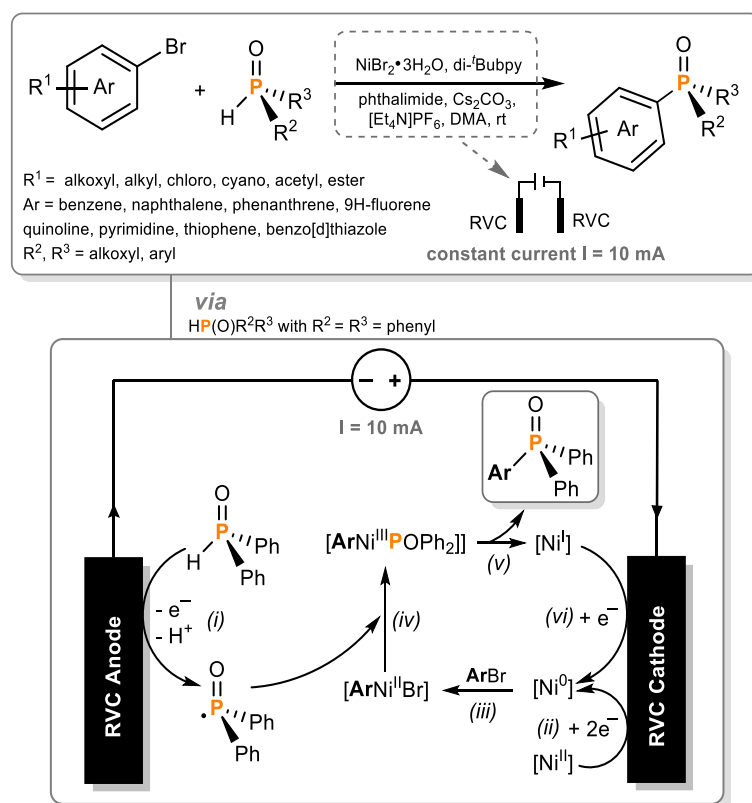
For example, UV light irradiation (254 nm) of dimethyl phosphonate with organic halides in the presence of an excess of strong base sodium *tert*-butoxide (*t*BuONa) and tetrabutylammonium iodide (TBAI, [*n*Bu₄N]I) as an additive yielded good conversions of the arylated phosphonates. Using ArI as a substrate, irradiation with 405 nm light was sufficient in the absence of additives to perform the reaction. In the case of the more chemically inert substrates ArBr and ArCl the additive TBAI and a higher energy irradiation source with 254 nm were needed to ensure complete conversion to the targeted OPCs. All the organic halides used as substrates gave moderate to good isolated yields of the corresponding products (ArCl: 56%, ArBr: 70% and ArI: 78%). The arylation was performed using a variety of aryl halides bearing different functional groups, which can have electron-withdrawing and electron-donating properties.^[44]

Two different mechanistic pathways for this photoinduced P–C cross coupling reaction were postulated (Scheme 16, paths (a) and (b)), both of which rely on the irradiation of bromobenzene. In path (a) homolytic cleavage of the C–Br bond affords a free aryl radical Ar• and a bromine radical Br•. The Br• radical oxidizes sodium dimethyl phosphite generated by tautomerization of dimethyl phosphonate after treatment with a strong base (*t*BuONa) *via* SET. This process generates a phosphonate radical which recombines with Ar•, forming the aryl phosphonate product. In path (b) a five-membered-ring transition state is proposed, which forms Ar• by intramolecular electron transfer from the lone pair of the phosphorus to the carbon-halide bond. As in path (a), the aryl radical and the concurrently generated phosphonate radical recombine to yield the product.^[44]

1.7.2 (Photo)-Electrochemical functionalization

1.7.2.1. Nickel-catalyzed electrochemical phosphorylation of aryl bromides

Beside the electrochemical functionalization of P₄ (section 1.4), different studies reported electrochemical cross-coupling reactions of aryl bromides with dialkyl phosphites, ethyl phenylphosphinate and diphenylphosphine oxide mediated by a metal precursor.^{[45]-[47]} State-of-the-art synthesis of arylated phosphonates, phosphinates and phosphine oxides uses transition-metal-catalyzed phosphorylation of aryl halides.^[40] Cross-coupling reactions of H-phosphonates with aryl halides catalyzed by nickel complexes require harsh temperatures and, for the recently reported photoinduced phosphinylation of organic halides, a strong base, such as *t*BuONa, is necessary for the reaction to proceed.^[44] A more environmentally friendly route to these arylated P₁ products is organic electrosynthesis. In 2018, the Léonel group reported the nickel-catalyzed electrochemical cross-coupling reaction of dialkyl phosphites with aryl bromides, applying high current (200 mA) and using a sacrificial iron anode.^[45] One year later, Cui and Xiang reported an improved nickel-catalyzed electrochemical procedure for the synthesis of OPCs from aryl bromide and dialkyl phosphite by using a nonsacrificial anode (reticulated vitreous carbon electrode, RVC) in an undivided cell (Scheme 17).^[46]

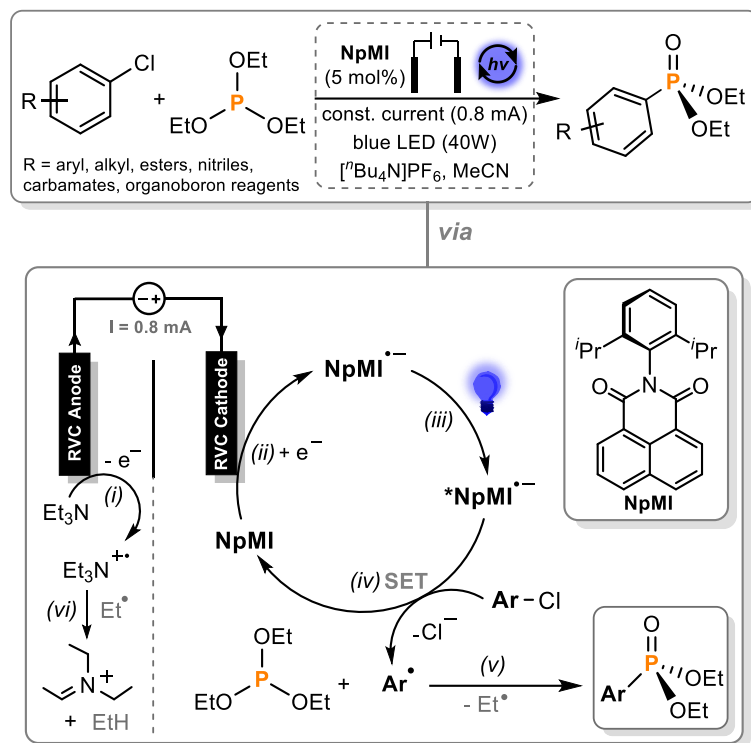


Scheme 17. Nickel-catalyzed electrochemical phosphorylation of aryl bromides.^[46]

Constant-current electrolysis (10 mA, RVC electrodes) of a *N,N'*-dimethylacetamide (DMA) solution containing the substrate, diphenylphosphine oxide (HP(O)Ph₂), NiBr₂·3H₂O as a precatalyst, di-*t*bubpy (ligand), phthalimide (additive), Cs₂CO₃ (base) and [Et₄N]PF₆ (electrolyte) yielded the corresponding triarylphosphine oxide. The control experiment of TEMPO inhibiting product formation indicates a radical process is involved in this arylation of HP(O)Ph₂. As shown in Scheme 17, the proposed mechanism is initiated by deprotonation of HP(O)Ph₂ and oxidation on the RVC anode (step i). Thereby, the radical •P(O)Ph₂ is generated. In a separate process, two-electron-reduction of the Ni^{II} salt on the RVC cathode (step ii) to Ni⁰ species which oxidatively adds ArBr, forming [ArNi^{II}Br] (step iii). Through subsequent trapping of the phosphorus-centered radical •P(O)Ph₂, the intermediate [ArNi^{II}Br] is converted to the [Ni^{III}] complex ([ArNi^{III}P(O)Ph₂]) (step iv). Reductive elimination yields the corresponding triarylphosphine oxide and an Ni^I intermediate (step v) which is reduced at the cathode to regenerate the Ni⁰ species (step vi). This method provides an efficient route for oxidative P–C bond formation and offers access to a variety of OPCs.^[46] Concurrent with Cui and Xiang's report, the Wang group described related work involving the catalyst-free electrochemical cross-coupling reaction of aryl halides with trialkyl phosphite, performed in an undivided cell with a Ni-anode and a graphite cathode.^[47]

1.7.2.2. Electron-primed photoredox catalysis for aryl chloride phosphorylation

Recently, Wickens and co-workers described a new catalytic strategy to combine electrochemistry with common photoredox-catalysis for the dehalogenation of organic halides and subsequent synthesis of useful OPCs.^{[48]–[52]} That the reduction step of the photoredox catalyst, usually performed by reducing agents such as triethylamine (Et₃N),^[48] can be facilitated electrochemically was successfully demonstrated and embodies a mechanistically new approach. This electrochemically mediated photoredox catalysis (e-PRC), using organocatalyst *N*-2,6-diisopropylphenyl naphthalene monoimide (**NpMI**), showed efficient dehalogenation of relatively inert organic chlorides ($E^\circ = -3.4$ V vs. SCE), and following SET-induced radical phosphorylation a variety of arylated phosphine oxides were accessed (Scheme 18).^[52] The photoelectro-catalytic reaction was performed in a divided cell equipped with a set of two RVC electrodes and using [nBu₄N]PF₆ as the electrolyte. On the anodic cell, oxidation of Et₃N to Et₃N⁺⁺ was chosen as the counter reaction while applying constant current (0.8 mA) to the system (Scheme 18, step i).



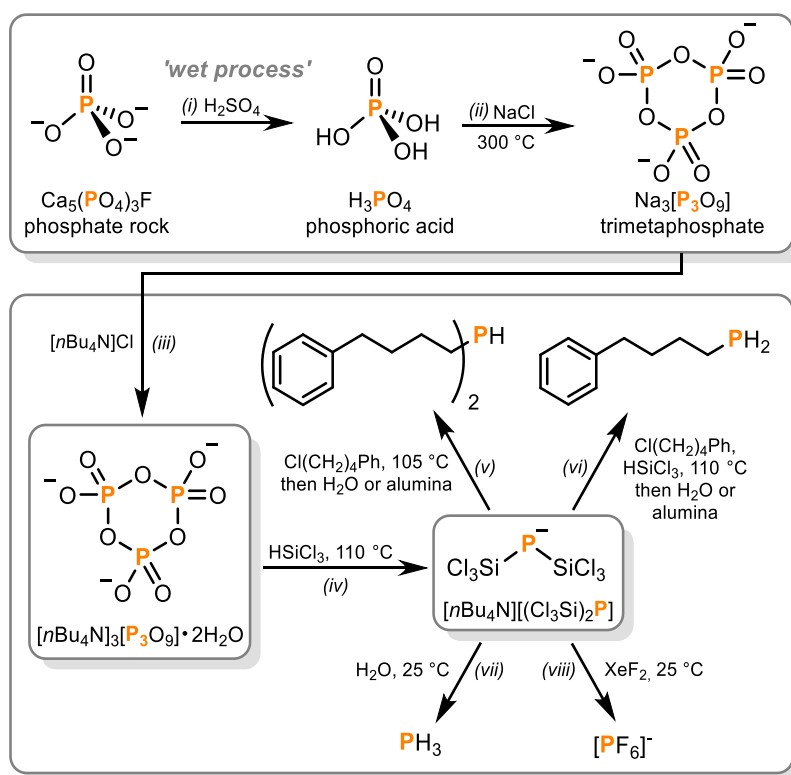
Scheme 18. Electron-primed photoredox catalysis for the dehalogenation of aryl chlorides and subsequent arylation of trialkyl phosphite ($\text{P}(\text{OEt})_3$) using organocatalyst *N*-2,6-diisopropylphenyl naphthalene monoimide (**NpMI**).^[52]

In the cathodic chamber containing substrate ArCl , trialkyl phosphite ($\text{P}(\text{OEt})_3$) and electrochemically mediated photoredox catalyst (e-PRCat) **NpMI**, the dehalogenation and subsequent phosphorylation takes place under irradiation with blue LED light (455 nm, 40W). **NpMI** is electrochemically reduced at the RVC cathode to form **NpMI**^{•-} which is subsequently excited by irradiation (step ii, step iii). The resulting photo-excited reduced species, ***NpMI**^{•-}, possesses a reduction potential comparable to that of lithium ($E^\circ = -3.3 \text{ V vs. SCE}$)^{[12],[52]} and is able to dehalogenate the substrate ArCl *via* SET to form aryl radicals (Ar^\bullet) (step iv). Subsequent reaction of these highly reactive radicals with $\text{P}(\text{OEt})_3$ leads to the formation of a new P–C bond and, after rearrangement and elimination of an ethyl radical, yields the corresponding aryl phosphonate (step v). The ethyl radical is quenched through deprotonation of Et_3N^+ , previously formed in the anodic counter reaction (step vi).

The arylation of triethyl phosphite developed by Wickens and co-workers presents an interesting, mechanistically innovative route to valuable aryl phosphonates.

1.8 Phosphoric acid as a precursor to chemicals traditionally synthesized from white phosphorus

White phosphorus (P_4) is generated by the direct reduction of phosphate minerals in a ‘thermal process’. P_4 is the key industrial starting material for the synthesis of OPCs, such as flame-retardants, pharmaceuticals, and herbicides.^{[2],[3]} In the so-called ‘wet-process’, raw phosphate rock is treated with sulfuric acid to generate high purity phosphoric acid, which is used for the production of fertilizers (see Scheme 19, step i).^[2] Recently, Cummins and co-worker reported a simple method avoiding the use of P_4 for the synthesis of OPCs, instead converting phosphoric acid into the bis(trichlorosilyl)phosphide anion ($[(Cl_3Si)_2P]^-$) which is readily transformed into valuable monophosphorus compounds (Scheme 19).^{[53],[54]} Dehydration of phosphoric acid with sodium chloride (NaCl) at elevated temperature was previously reported by Pham Minh to form the oligomeric compound trimetaphosphate $Na_3[P_3O_9]$ (Scheme 19, step ii).^[55] Cummins converted the sodium salt of the trimetaphosphate into the tetrabutylammonium salt $[nBu_4N]_3[P_3O_9] \cdot 2H_2O$ (step iii) to improve its solubility in organic solvents and investigated its reactivity, positing an analogy between the monomeric metaphosphate ion unit (PO_3^-) and carbon dioxide.^[53]



Scheme 19. Formation of bis(trichlorosilyl)phosphide $[(Cl_3Si)_2P]^-$ from tetrabutylammonium trimetaphosphate $[nBu_4N]_3[P_3O_9] \cdot 2H_2O$ and its subsequent transformation into P_1 products by formation of P–H, P–C and P–F bonds.^{[53],[54]}

Reductive treatment of trimetaphosphate in neat trichlorosilane (HSiCl_3) at $110\text{ }^\circ\text{C}$ yielded the tetrabutylammonium bis(trichlorosilyl)phosphide ($[\text{nBu}_4\text{N}][(\text{Cl}_3\text{Si})_2\text{P}]$) in 65% conversion (step iv). The stability of the $[(\text{Cl}_3\text{Si})_2\text{P}]^-$ anion is presumed to be increased by the electron-withdrawing trichlorosilyl groups.^[53] Bis(trichlorosilyl)phosphide exhibits similar reactivity to trisilylphosphines (e.g., $\text{P}(\text{SiMe}_3)_3$).^[56] Reaction of $[(\text{Cl}_3\text{Si})_2\text{P}]^-$ with $\text{Ph}(\text{CH}_2)_4\text{Cl}$ yielded the dialkylsilylphosphine $[\text{Ph}(\text{CH}_2)_4]_2\text{PSiCl}_3$. This was not isolated, but directly converted *via* aqueous workup (or with alumina) to the secondary alkyl phosphine $[\text{Ph}(\text{CH}_2)_4]_2\text{PH}$ (step v). By addition of trichlorosilane HSiCl_3 to a mixture of $[(\text{Cl}_3\text{Si})_2\text{P}]^-$ and $\text{Ph}(\text{CH}_2)_4\text{Cl}$ the alkylsilylphosphine $\text{Ph}(\text{CH}_2)_4\text{P}(\text{SiCl}_3)\text{H}$ was generated. Aqueous workup or the use of basic alumina provided access to the corresponding primary phosphine $\text{Ph}(\text{CH}_2)_4\text{PH}_2$ by cleavage of the P–Si bond (step vi). Simple hydrolytic cleavage of the P–Si bonds by treatment with water cleanly converted $[(\text{Cl}_3\text{Si})_2\text{P}]^-$ to phosphine (PH_3) (step vii).^[53] Finally, the hexafluorophosphate anion ($[\text{PF}_6]^-$), which is used in lithium ion batteries as an electrolyte, was synthesized by reaction of $[(\text{Cl}_3\text{Si})_2\text{P}]^-$ with xenon difluoride (XeF_2) (step viii).^{[53],[54]}

The work by Cummins and Geeson is important because it showed for the first time that the use of P_4 as an intermediate for the synthesis of OPCs can be circumvented. Key to the success of this method is the transformation of H_3PO_4 into trimetaphosphate and its subsequent conversion into the monophosphorus intermediate $[\text{nBu}_4\text{N}][(\text{Cl}_3\text{Si})_2\text{P}]$.

1.9 Conclusion and Outlook

Over the last decades the phosphorus research area was extended by developing new organofunctionalization methods of inorganic phosphorus compounds and the synthesis of valuable P₁ products. Ultimately, the methods that have been described in this overview show that P₄ functionalization is a very versatile research field and possesses great potential for further development. These reports discuss interesting routes for the synthesis of OPCs, but they all remain proof of principles and cannot replace the state-of-the-art procedure.^{[57],[58]}

Metal-mediated functionalization methods of P₄ into P₁ products demonstrate interesting reactivity of P-containing moieties, however, they usually lack high yield and atom economy due to extensive multistep procedures. The most promising strategies are direct, catalytic P₄ functionalization processes, which remain exceedingly rare. Though photocatalytic methods have given access to a fairly efficient route to OPCs, free of chlorinated intermediates, they still require several other reagents which generate waste products. Judged from the perspective of green chemistry, the use of renewable phosphorus sources^[54] and sustainable approaches, e.g., electrochemical applications, are additional considerations beside simply circumventing chlorinated intermediates. Electrochemically functionalization of white phosphorus can be used as versatile alternative synthesis procedure accessing a variety of distinct organophosphorus moieties. The advanced photoelectrocatalytic strategy, which combines electrochemistry with common photoredox catalysis for the dehalogenation of organic halides and the generation of carbon-centered radicals mediated by highly reducing photoredox catalysts, is up to now only utilizable for the functionalization of phosphites. However, applying this photoelectrocatalytic manner for the functionalization of P₄ into tertiary phosphines and quaternary phosphonium salts, which has not been reported to date, features an interesting opportunity for further development.

As previously discussed, OPCs have numerous applications throughout industry and academia and are necessary in daily life of society. Thus, the development of new direct functionalization protocols for their synthesis remains a highly desirable objective.

The primary focus of the work presented in this doctoral thesis is the development of chlorine-free functionalization procedures for the synthesis of valuable OPCs. Related mechanistic methods, such as photochemistry, photocatalysis and photoelectrocatalysis starting from P₄ and diphenyl phosphine (Ph₂PH) as P source are described.

1.10 References

- [1] a) F. Bachhuber, J. von Appen, R. Dronskowski, P. Schmidt, T. Nilges, A. Pfitzner and R. Wehrich, *Angew. Chem. Int. Ed.*, 2014, **53**, 11629–11633; b) A. F. Holleman, E. Wiberg and N. Wiberg, *Anorganische Chemie, Band 1, Grundlagen und Hauptgruppenelemente* (de Gruyter), Berlin, 2017, p. 846.
- [2] a) W. Gleason, *JOM*, 2007, **59**, 17-19; b) G. Bettermann, W. Krause, G. Riess and T. Hofmann, *Ullmann's Encyclopedia of Industrial Chemistry* (Wiley), 2000; c) D. E. C. Corbridge, *Chemistry, Biochemistry and Technology* (Elsevier), 2000.
- [3] O. Ganter, W. Schipper, and J. J. Weigand, *Sustainable Phosphorus Management*, (Springer), 2014, Spotlight 8, 237–242.
- [4] D. H. R. Barton and J. Zhu, *J. Am. Chem. Soc.*, 1993, **115**, 2071–2072.
- [5] D. H. R. Barton and R. A. Vonder Embse, *Tetrahedron*, 1998, **54**, 12475–12496.
- [6] B. M. Cossairt and C. C. Cummins, *New. J. Chem.*, 2010, **34**, 1533–1536.
- [7] M. Szostak, M. Spain and D. J. Procter, *J. Org. Chem.*, 2014, **79**, 2522–2537.
- [8] S. K. Ghosh, C. C. Cummins and J. A. Gladysz, *Org. Chem. Front.*, 2018, **5**, 3421–3429.
- [9] Y. G. Budnikova, D. G. Yakhvarov and Yu. M. Kargin, *Mendeleev Commun.*, 1997, **7**, 67–68.
- [10] a) Y. G. Budnikova, D. G. Yakhvarov and Y. M. Kargin, *Russ. J. Gen. Chem.*, 1998, **68**, 566–569 (*Zh. Obshch. Khim.*, 1998, **68**, 603–606); b) D. Y. Mikhaylov, T. V. Gryaznova, Y. B. Dudkina, F. M. Polyancev, S. K. Latypov, O. G. Sinyashin and Y. H. Budnikova, *J. Fluorine Chem.*, 2013, **153**, 178–182.
- [11] U. Lennert, P. B. Arockiam, V. Streitferdt, D. J. Scott, C. Rödl, R. M. Gschwind and R. Wolf, *Nat. Catal.*, 2019, **2**, 1101–1106.
- [12] D. DiRocco, *Electrochemical Series of Photocatalysts and Common Organic Compounds*, Merck, 2014.
- [13] C. J. Zeman, IV, S. Kim, F. Zhang and K. S. Schanze, *J. Am. Chem. Soc.*, 2020, **142**, 2204–2207.
- [14] P. B. Arockiam, U. Lennert, C. Graf, R. Rothfelder, D. J. Scott, T. G. Fischer, K. Zeitler and R. Wolf, *Chem. Eur. J.*, 2020, **26**, 16374–16382.
- [15] R. Rothfelder, V. Streitferdt, U. Lennert, J. Cammarata, D. J. Scott, K. Zeitler, R. M. Gschwind and R. Wolf, *Angew. Chem. Int. Ed.*, 2021, **60**, 24650–24658.
- [16] D. J. Scott, J. Cammarata, M. Schimpf and R. Wolf, *Nat. Chem.*, 2021, **13**, 458–464.
- [17] A. D. Norman, *J. Organomet. Chem.*, 1971, **28**, 81–86.
- [18] H. Schumann, *Angew. Chem. Int. Ed.*, 1969, **8**, 937–950.

- [19] a) K. V. Katti, H. Gali, C. J. Smith and D. E. Berning, *Chem. Res.*, 1999, **32**, 9–17; b) M. J. Chen, C. R. Chen, Y. Tan, J. Q. Huang, X.L. Wang, L. Chen and Y. Z. Wang, *Ind. Eng. Chem. Res.*, 2014, **53**, 1160–1171; c) W. J. Vullo, *Ind. Eng. Chem. Proc. Res. Dev.*, 1966, **5**, 346–349; d) W. J. Vullo, *J. Org. Chem.*, 1968, **33**, 3665–3667.
- [20] H. Schmidbaur, U. Deschler, B. Milewski-Mahrla and B. Zimmer-Gasser, *Chem. Ber.*, 1981, **114**, 608–619.
- [21] J. Cammarata, D. J. Scott and R. Wolf, *Chem. Eur. J.*, 2022, e202202456.
- [22] I. N. Brago and A. P. Tomilov, *Elektrokhimiya*, 1968, **4**, 697 [Sov. Electrochem. (Engl Transl.), 1968, **4**, No. 6).
- [23] a) D. G. Yakhvarov, Yu. S. Ganushevich, E. A. Trofimova and O. G. Sinyashin, *Russian Pat.*, No. 2396375, 2010; b) D.G. Yakhvarov, E. A. Trofimova and O. G. Sinyashin, *Russian Pat.*, No. 85903, 2009; c) D. G. Yakhvarov, Y. H. Budnikova, D. I. Tazeev and O. G. Sinyashin, *Russ. Chem. Bull.*, 2002, **51**, 2059–2064; d) Y. H. Budnikova, D. G. Yakhvarov and O. G. Sinyashin, *J. Organomet. Chem.*, 2005, **690**, 2416–2425; e) Y. G. Budnikova, D. I. Tazeev, A. G. Kafiyatullina, D. G. Yakhvarov, V. I. Morozov, N. K. Gusarova, B. A. Trofimov and O. G. Sinyashin, *Russ. Chem. Bull.*, 2005, **54**, 942–947; f) D. G. Yakhvarov, E. V. Gorbachuk, R. M. Kagiroy and O. G. Sinyashin, *Russ. Chem. Bull.*, 2012, **61**, 1300–1312; g) D. G. Yakhvarov, E. V. Gorbachuk and O. G. Sinyashin, *Eur. J. Inorg. Chem.*, 2013, **27**, 4709–4726.
- [24] a) D. G. Yakhvarov, Y. G. Budnikova and O. G. Sinyashin, *Russ. J. Electrochem.*, 2003, **39**, 1261–1270; b) Y. H. Budnikova, T. V. Gryaznova, V. V. Grinenko, Y. B. Dudkina and M. N. Khrizanforov, *Pure Appl. Chem.*, 2017, **89**, 311–330.
- [25] Y. Mei, Z. Yan and L. L. Liu, *J. Am. Chem. Soc.*, 2022, **144**, 1517–1522.
- [26] a) A. Schmidpeter and F. Zwaschka, *Angew. Chem. Int. Ed. Engl.*, 1977, **16**, 704–705; b) W. S. Sheldrick, J. Kroner, F. Zwaschka and A. Schmidpeter, *Angew. Chem. Int. Ed. Engl.*, 1979, **18**, 934–935.
- [27] a) J. F. Binder, S. C. Kosnik, P. B. J. St Onge and C. L. B. Macdonald, *Chem. Eur. J.*, 2018, **24**, 14644–14648; b) A. Schmidpeter, G. Burget, D. J. Chandler and R. A. Jones, *Inorg. Synth.*, 1989, **25**, 126–129; c) A. Schmidpeter, G. Burget, F. Zwaschka and W. S. Sheldrick, *Z. Anorg. Allg. Chem.*, 1985, **527**, 17–32.
- [28] M. Donath, K. Schwedtmann, T. Schneider, F. Hennersdorf, A. Bauzá, A. Frontera and J. J. Weigand, *Nat. Chem.*, 2022, **14**, 384–391.
- [29] M. Donath, M. Bodensteiner and J. J. Weigand, *Chem. Eur. J.*, 2014, **20**, 17306–17310.

- [30] a) B. M. Cossairt, N. A. Piro and C. C. Cummins, *Chem. Rev.*, 2010, **110**, 4164–4177; b) M. Caporali, L. Gonsalvi, A. Rossin and M. Peruzzini, *Chem. Rev.*, 2010, **110**, 4178–4235; c) M. Scheer, G. Balázs and A. Seitz, *Chem. Rev.*, 2010, **110**, 4236–4256; d) C. M. Hoidn, D. J. Scott and R. Wolf, *Chem. Eur. J.*, 2021, **27**, 1886–1902; e) L. Giusti, V. R. Landaeta, M. Vanni, J. A. Kelly, R. Wolf and M. Caporali, *Coord. Chem. Rev.*, 2021, **441**, 2139276–2139375.
- [31] O. J. Scherer and T. Brück, *Angew. Chem. Int. Ed. Engl.*, 1987, **26**, 59; *Angew. Chem.*, 1987, **99**, 59.
- [32] S. Reichl, E. Mädl, F. Riedelberger, M. Piesch, G. Balázs, M. Seidl and M. Scheer, *Nat. Commun.*, 2021, **12**, 5774–5783.
- [33] E. Mädl, M. V. Butovskii, G. Balázs, E. V. Peresyphkina, A. V. Virovets, M. Seidl and M. Scheer, *Angew. Chem. Int. Ed.*, 2014, **53**, 7643–7646.
- [34] a) M. M. Rauhut and A. M. Semsel, *J. Org. Chem.*, 1963, **28**, 471–473; b) M. M. Rauhut and A. M. Semsel, *J. Org. Chem.*, 1963, **28**, 473–477.
- [35] R. Riedel, H.-D. Hausen and E. Fluck, *Angew. Chem. Int. Ed. Engl.*, 1985, **24**, 1056–1057; *Angew. Chem.*, 1985, **97**, 1050–1050.
- [36] J. E. Borger, A. W. Ehlers, M. Lutz, J. C. Slootweg and K. Lammertsma, *Angew. Chem. Int. Ed.*, 2017, **56**, 285–290.
- [37] J. E. Borger, A. W. Ehlers, M. Lutz, J. C. Slootweg and K. Lammertsma, *Chem. Eur. J.*, 2017, **23**, 11738–11746.
- [38] For selected examples of metal-mediated P₄ functionalization focusing on the formation of P₁ products, see: a) G. Luo, S. Du, P. Wang, F. Liu, W.-X. Zhang and Y. Luo, *Chem. Eur. J.*, 2020, **26**, 13282–13287; b) L. Xu, Y. Chi, S. Du, W.-X. Zhang and Z. Xi, *Angew. Chem. Int. Ed.*, 2016, **55**, 9187–9190; c) M. Cicač-Hudi, J. Bender, S. H. Schlindwein, M. Bispinghoff, M. Nieger, H. Grützmacher and D. Gudat, *Eur. J. Inorg. Chem.*, 2016, 649–658.
- [39] a) C. S. Demmer, N. K. Larsen and L. Bunch, *Chem. Rev.*, 2011, **111**, 7981–8006; b) K. Luo, Y. Z. Chen, W. C. Zhu and L. Wu, *L. Org. Lett.*, 2016, **18**, 452–455; c) K. Moonen, I. Laureyn and C. V. Stevens, *Chem. Rev.*, 2004, **104**, 6177–6216; d) P. Guga, *Curr. Top. Med. Chem.*, 2007, **7**, 695–713.
- [40] a) J. L. Montchamp and Y. R. Dumond, *J. Am. Chem. Soc.*, 2001, **123**, 510–511; b) A. L. Schwan, *Chem. Soc. Rev.*, 2004, **33**, 218–224; c) T. Chen, J. S. Zhang and L. B. Han, *Dalton Trans.*, 2016, **45**, 1843–1849; d) Y. H. Budnikova and O. G. Sinyashin, *Russ. Chem. Rev.*, 2015, **84**, 917–951; e) A. J. Bloomfield and S. B. Herzon, *Org. Lett.*, 2012, **14**, 4370–4373; f) E. L. Deal, C. Petit and J. L. Montchamp, *Org. Lett.*, 2011, **13**, 3270–3273; g) K. Xu, H. Hu, F. Yang and Y. Wu, *Eur. J. Org. Chem.*, 2013, **2013**, 319–325; h) M. Kalek, M. Jerowska and J.

- Stawinski, *Adv. Synth. Catal.*, 2009, **351**, 3207–3216; i) J. Ke, Y. Tang, H. Yi, Y. Li, Y. Cheng, C. Liu and A. Li, *Angew. Chem. Int. Ed.*, 2015, **54**, 6604–6607; j) R. Zhuang, J. Xu, Z. Cai, G. Tang, M. Fang and Y. Zhao, *Org. Lett.*, 2011, **13**, 2110–2113; k) G. Hu, W. Chen, T. Fu, Z. Peng, H. Qiao, Y. Gao and Y. Zhao, *Org. Lett.*, 2013, **15**, 5362–5365; l) J. Yang, T. Chen, L. B. Han, *J. Am. Chem. Soc.*, 2015, **137**, 1782–1785; m) Y. L. Zhao, G. J. Wu, Y. Li, L. X. Gao and F. S. Han, *Chem. Eur. J.*, 2012, **18**, 9622–9627; n) H. Zhang, X. Y. Zhang, D. Q. Dong and Z. L. Wang, *RSC Adv.*, 2015, **5**, 52824–52831; o) E. Jablonkai and G. Keglevich, *Curr. Org. Synth.*, 2014, **11**, 429–453; p) Y. M. Li and S. D. Yang, *Synlett*, 2013, **24**, 1739–1744; q) C. Shen, G. Yang and W. Zhang, *Org. Biomol. Chem.*, 2012, **10**, 3500–3505; r) Q. Yao and S. Levchik, *Tetrahedron Lett.*, 2006, **47**, 277–281.
- [41] R. S. Shaikh, S. J. S. Düsel and B. König, *ACS Catal.*, 2016, **6**, 8410–8414.
- [42] I. Ghosh and B. König, *Angew. Chem. Int. Ed.*, 2016, **55**, 7676–7679.
- [43] J. J. L. Fu, W. G. Bentrude and C. E. Griffin, *J. Am. Chem. Soc.*, 1972, **94**, 7717–7722.
- [44] H. Zeng, Q. Dou and C.-J. Li, *Org. Lett.*, 2019, **21**, 1301–1305.
- [45] S. Sengmany, A. Ollivier, E. Le Gall and E. Léonel, *Org. Biomol. Chem.*, 2018, **16**, 4495–4500.
- [46] Y. Bai, N. Liu, S. Wang, S. Wang, S. Ning, L. Shi, L. Cui, Z. Zhang and J. Xiang, *Org. Lett.*, 2019, **21**, 6835–6838.
- [47] S. Wang, C. Yang, S. Sun and J. Wang, *Chem. Commun.*, 2019, **55**, 14035–14038.
- [48] For general reviews of electroorganic synthesis, see: a) M. Yan, Y. Kawamata and P. S. Baran, *Chem. Rev.*, 2017, **117**, 13230–13319; b) J. Yoshida, K. Kataoka, R. Horcajada and A. Nagaki, *Chem. Rev.*, 2008, **108**, 2265–2299; c) A. Wiebe, T. Gieshoff, S. Möhle, E. Rodrigo, M. Zirbes and S. R. Waldvogel, *Angew. Chem. Int. Ed.*, 2018, **57**, 5594–5619; d) K. D. Moeller, *Chem. Rev.*, 2018, **118**, 4817–4833.
- [49] For reviews specifically focused on electrocatalysis, see: a) R. Francke and R. D. Little, *Chem. Soc. Rev.*, 2014, **43**, 2492–2521; b) T. H. Meyer, L. H. Finger, P. Gandeepan and L. Ackermann, *Trends Chem.*, 2019, **1**, 63–76.
- [50] For selected reviews of visible-light photoredox catalysis, see: a) C. K. Prier, D. A. Rankic and D. W. C. MacMillan, *Chem. Rev.*, 2013, **113**, 5322–5363; b) M. H. Shaw, J. Twilton and D. W. C. MacMillan, *J. Org. Chem.*, 2016, **81**, 6898–6926; c) N. A. Romero and D. A. Nicewicz, *Chem. Rev.*, 2016, **116**, 10075–10166; d) K. L. Skubi, T. R. Blum and T. P. Yoon, *Chem. Rev.*, 2016, **116**, 10035–10074; e) D. A. DiRocco, K. Dykstra, S. Krska, P. Vachal, D. V.

- Conway and M. Tudge, *Angew. Chem., Int. Ed.*, 2014, **53**, 4802–4806; f) J. M. R. Narayanam and C. R. Stephenson, *Chem. Soc. Rev.*, 2011, **40**, 102–113.
- [51] For a special issue on photoredox catalysis in organic chemistry, see: *Accounts of Chemical Research* 2016, Vol. **49**, Issue 10.
- [52] N. G. W. Cowper, C. P. Chernowsky, O. P. Williams and Z. K. Wickens, *J. Am. Chem. Soc.*, 2020, **142**, 2093–2099.
- [53] M. B. Geeson and C. C. Cummins, *Science*, 2018, **359**, 1383–1385.
- [54] M. B. Geeson and C. C. Cummins, *ACS Cent. Sci.*, 2020, **6**, 848–860.
- [55] D. Pham Minh, J. Ramaroson, A. Nzihou and P. Sharrock, *Ind. Eng. Chem. Res.*, 2012, **51**, 3851–3854.
- [56] D. C. Gary and B. M. Cossairt, *Chem. Mater.*, 2013, **25**, 2463–2469.
- [57] D. J. Scott, *Angew. Chem. Int. Ed.*, 2022, **61**, e202205019.
- [58] H. Grützmacher, *Nat. Chem.*, 2022, **14**, 362–364.

2 Photochemical Transformation of Chlorobenzenes and White Phosphorus into Arylphosphines and Phosphonium salts^[a]

Abstract: Chlorobenzenes are important starting materials for the preparation of commercially valuable triarylphosphines and tetraarylphosphonium salts, but their use for the direct arylation of elemental phosphorus has been elusive. Here we describe a simple photochemical route toward such products. UV-LED irradiation (365 nm) of chlorobenzenes, white phosphorus (P₄) and the organic superphotoreductant tetrakis(dimethylamino)ethylene (TDAE) affords the desired arylphosphorus compounds in a single reaction step.



Reproduced with permission from: M. Till, V. Streitferdt, D. J. Scott, M. Mende, R. M. Gschwind and R. Wolf, *Chem. Commun.*, 2022, **58**, 1100–1103. (Front cover)

^[a] M. Till performed the reactions and the isolation and characterization of selected compounds. M. Mende assisted with the substrate screening as part of a practical course. V. Streitferdt performed the *in situ* NMR experiments and NMR investigations of the intermediate **Int1**. R. M. Gschwind analyzed the results of the NMR spectroscopic studies with V. Streitferd. R. Wolf and D. J. Scott supervised and directed the project. M. Till wrote the manuscript with input from R. M. Gschwind, D. J. Scott and R. Wolf. The image for the front cover was designed by M. Till.

2.1 Introduction

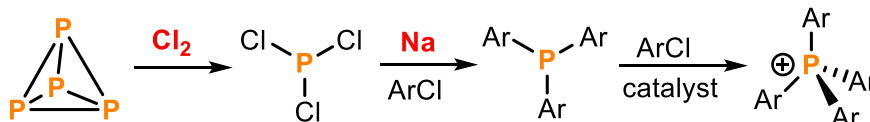
Commercially valuable and academically interesting organo-phosphorus compounds (OPCs) such as arylated phosphines (Ar_3P) and phosphonium salts ($[\text{Ar}_4\text{P}]^+$) are currently prepared by a wasteful and inefficient multi-step procedure which relies on the initial oxidation of white phosphorus (P_4) using toxic Cl_2 gas to give highly reactive PCl_3 which is further converted into the desired monophosphorus species (Figure 1a).^{[1],[2]} Given the numerous drawbacks of this method the direct transformation of P_4 into OPCs and other P-containing compounds, avoiding potentially hazardous intermediates, has long been an exceedingly important yet challenging objective.^[3]

Pioneering studies by Barton and co-workers demonstrated the excellent ability of P_4 to trap carbon-centered radicals, and that this can provide the basis for subsequent transformation of white phosphorus into valuable OPCs.^{[4],[5]} Subsequently, stoichiometric functionalization reactions were reported by Cummins and co-workers in which the generation of reactive organoradicals by reacting organic bromides and iodides with a titanium(III) complex (or more recently samarium(II) halides) is again the fundamental first step in converting P_4 into the corresponding tertiary phosphines (Figure 1b).^{[6],[7]} Expanding on these stoichiometric methodologies in which organic halides are reduced by metal-containing reductants in the presence of P_4 , recently, we reported the first catalytic procedure to obtain OPCs directly from P_4 (Figure 1c).^{[8]–[10]} The reduced form of a photoexcited iridium photocatalyst or, alternatively, an organophotocatalyst is able to reduce aryl iodides (ArI) to generate carbon-centered aryl radicals which are again trapped by P_4 to directly form arylated phosphines and phosphonium salts.

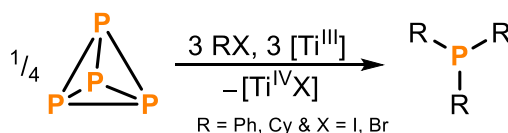
All these efforts to prepare OPCs directly from P_4 through the use of carbon-centered radicals were realized only by using organic bromides and iodides.^{[11]–[13]} However, from an economic point of view the use of bromo- and iodobenzenes for the preparation of tertiary phosphines is infeasible, with these substrates often even being more expensive than the target phosphines. In contrast, organic chlorides are cheap and abundant substrates which comprise over two-thirds of commercially available aryl halides,^{[14],[15]} but their use as substrates and radical precursors in photocatalysis and photochemistry is challenging because of their chemical inertness.^{[16]–[19]} Herein, we describe a simple photochemical method for the

preparation of various valuable triarylphosphines and tetraarylphosphonium salts directly from P_4 by using only readily and cheaply commercially available aryl chlorides.

(a) State-of-the-art: indirect industrial routes to Ar_3P and $[Ar_4P]^+$



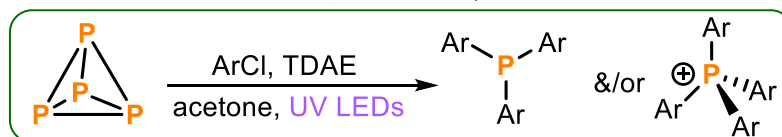
(b) Stoichiometric functionalization of P_4 using **organic bromides / iodides**



(c) Direct, photocatalytic arylation of P_4 using **iodobenzenes**



(d) This work: photochemical arylation of P_4 using **chlorobenzenes**



✓ **mild reagents and conditions**

- ✓ **organic chlorides** as cheap and readily available substrates
- ✓ **metal free** procedure by using organic super-photoreductant

Figure 1. (a) Indirect methods for the synthesis of triarylphosphines Ar_3P and tetraarylphosphonium salts $[Ar_4P]^+$ (Ar = aryl substituent) employed industrially^{[1],[2]}, (b) stoichiometric transformation of P_4 into tertiary phosphines R_3P ($[Ti^{III}] = Ti(N[tBu]Ar)_3$),^[6] (c) recently reported direct photocatalytic transformation of P_4 into Ar_3P and $[Ar_4P]^+$,^{[8]-[10]} and (d) photochemical arylation of P_4 using chlorobenzenes and an organic super-photoreductant (TDAE = tetrakis(dimethylamino)ethylene).

2.2 Results and Discussion

Recently, Wenger and co-workers reported on a remarkably simple light-driven reductive hydrodehalogenation of organic chlorides *via* aryl radicals mediated by tetrakis(dimethylamino)ethylene (TDAE) as a photoreductant.^[20] We anticipated that radicals generated in the same manner could be trapped to functionalize P₄. And, indeed, UV light irradiation (365 nm) of a solution of P₄ (added as a stock solution in benzene), PhCl (as a simple model substrate) and TDAE in acetone for 20 hours yielded the phosphonium salt [Ph₄P]Cl (53% yield determined by NMR) and tertiary phosphine Ph₃P (9% NMR yield) (Table 1, entry 1). To our knowledge, this represents the first example of an aryl chloride successfully being reacted with P₄ to provide such products directly. Further variations of solvent, light source, temperature, stoichiometry and reaction time (see ESI, S3, Tables 1–7) indicated that the reaction parameters given in Table 1 (entry 1) are optimal.

Table 1. Photochemical functionalization of P₄ to Ph₃P and [Ph₄P]Cl: screening of radical sources and control experiments.

$$\text{P}_4 \xrightarrow[\text{acetone/benzene, N}_2 \text{ atmosphere, } -[\text{TDAE}]\text{Cl}_2 \downarrow]{\text{PhCl, TDAE, UV-LEDs}}$$

$$[\text{Ph}_4\text{P}]^+\text{Cl}^- + \text{Ph}_3\text{P}$$

Entry	Conditions	Full conv. of P ₄ ?	Conv. to [Ph ₄ P]Cl / %	Conv. to Ph ₃ P / %
1	Standard ^[a]	✓	53	9
2	No light	✗	0	0
3	No TDAE	✗	0	0
4	No PhCl	✗	0	0
5	PhF instead of PhCl	✗	0	0
6	PhBr instead of PhCl	✓	43	10
7	PhI instead of PhCl	✓	14	10
8	P _{red} instead of P ₄	—	0	0

[a] Reactions were performed with 40.7 μL chlorobenzene (10 equiv. based on phosphorus atoms, 40 equiv. based on P₄), 46.5 μL TDAE (5 equiv. based on phosphorus atoms) and P₄ (0.01 mmol, as a stock solution in 71.3 μL benzene) in 0.5 mL acetone as solvent. Samples were prepared under N₂ atmosphere in a sealed tube and placed in a water-cooled block during irradiation (20h) with UV light (365 nm). Conversions were determined by quantitative ³¹P{¹H} NMR experiments with subsequently added Ph₃PO as an internal standard.

For the transformation of one P₄ molecule into four [Ph₄P]Cl at least 16 PhCl have to be reduced to form the needed 16 P–C bonds. For a clean stoichiometric functionalization, a stoichiometric ratio of TDAE to PhCl of 8:16 (equiv. based on P₄) should suffice to efficiently generate the final phosphonium salt (assuming TDAE acts as a two-electron donor; *vide infra*). Nevertheless, adapting the reaction stoichiometry to this level was found to result in appreciably reduced conversion (see ESI, S3, Table S5). In part this is likely due to side reactions such as forming benzene from an aryl radical/anion or generating biphenyl by recombination of two radicals (confirmed by GC-MS). Although all P₄ is consumed quantitative product formation is not observed, even after an increase of the reaction time (40 h) as shown by quantitative ³¹P{¹H} NMR spectroscopy (see ESI, S3, Table S6). The loss of phosphorus intensity is possibly caused by formation of polymerized phosphorus species, which was also a limiting factor in our recently reported photocatalytic procedure.^[8]

Control experiments confirmed that all reaction components (P₄, PhCl, TDAE and UV light) are necessary to observe product formation (Table 1, entries 2–4). Switching from PhCl to the less reactive PhF or the more easily reducible substrates PhBr or PhI was found to be detrimental (Table 1, entries 5–7). In the case of PhF no reaction occurred at all. Also replacing P₄ with red phosphorus yielded no product (Table 1, entry 8).

Various other substituted aryl chlorides could also successfully be employed under identical reaction conditions, albeit with somewhat lower conversions than for chlorobenzene (see ESI, Table S8 and Figure S22). The investigated substrate scope shows that the method is more suitable for substrates bearing electron-donating (Me, OMe) groups than for chloroarenes with electron-withdrawing groups (EWGs, such as CF₃, COOMe), which generally gave poor conversions. Gratifyingly, not only aryl radicals led to product formation. For benzyl chloride 27% conversion to tribenzylphosphine was achieved. Even more impressively, employing (2-chloroethyl)benzene as substrate the product tris(phenylethyl)phosphine was formed selectively in 75% NMR yield. Selected products (tetraphenylphosphonium chloride and tris(phenylethyl)phosphine) were synthesized by performing reactions on a preparative (0.8 mmol) scale and isolated in modest yields by precipitation from dichloromethane/*n*-hexane (for the

phosphonium salt) or fractional distillation (for the phosphine). See the ESI for details of the purification and isolation of these products.

The chemical inertness of these chlorobenzenes (e.g. PhCl; -2.78 V *vs.* SCE in DMF,^[21] Figure 2) is due to the high energetic barrier for C–Cl bond activation. To overcome this a strong (photo)reductant is needed. TDAE as a single-electron reducing agent with an oxidation potential of -0.78 V *vs.* SCE (CH₃CN)^[22] is not strong enough to split off a chloride anion to generate aryl radicals. By contrast the photoactive excited state of TDAE (*TDAE) offers an extraordinary reducing power of -3.4 V *vs.* SCE^[20] (Figure 2) which makes it a super-photoreductant. Luminescence lifetime measurements showed that the excited state of TDAE is quenched by acetone.^[20] Thus, instead of a direct single electron transfer (SET) from photoexcited TDAE to the substrate, acetone (-2.84 V *vs.* SCE)^[23] is reduced and forms an acetone radical anion which subsequently undergoes SET to the organic chlorides and generates carbon-centered radicals. Using a solvent which cannot be reduced by photoexcited TDAE such as acetonitrile or benzene (-3.42 V *vs.* SCE),^[24] or employing the substrate PhCl as solvent decreased the yield of phosphonium salt and phosphine (see ESI, S3, Table S4).

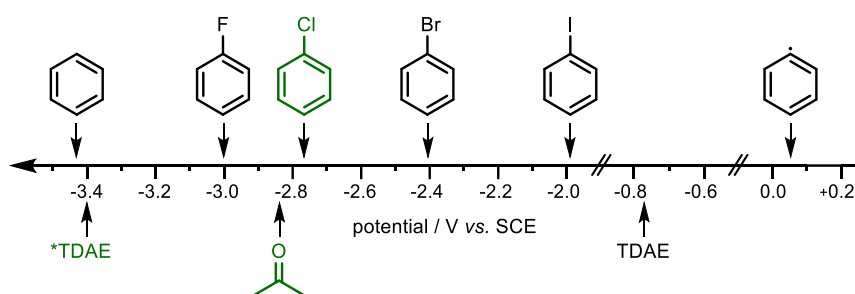


Figure 2. Reducing power of ground-state and excited-state organic photoreductant TDAE^[20] and reduction potentials of used solvents (acetone and benzene)^{[23],[24]}, aryl halides (fluoro-, chloro-,^[21] bromo- and iodobenzene)^[25] and the corresponding aryl radical.^[26]

Usually, organic chlorides are more inactive substrates than the corresponding bromides and iodides because of their high bond dissociation energy (PhCl 327 kJ·mol⁻¹).^[16] As mentioned above, however, using substrates such as bromobenzene or iodobenzene (PhBr -2.44 V *vs.* SCE, PhI -1.93 V *vs.* SCE)^[25] for this photochemical procedure reduced the product formation. While the reasons for this are not entirely clear, it is presumably related to the fact that the bromide and iodide can more easily be reduced than aryl chlorides, leading to more rapid accumulation of aryl radicals, that may then be more prone to unwanted side-

reactions such as dimerization or over-reduction (+0.05 V vs. SCE).^{[26],[27]} In contrast, using aryl fluorides as radical source yielded no product at all, presumably because PhF is outcompeted by the solvent as an oxidative quencher of ^{*}TDAE, and the resulting acetone radical anion is incapable of reducing PhF (see Figure 2).

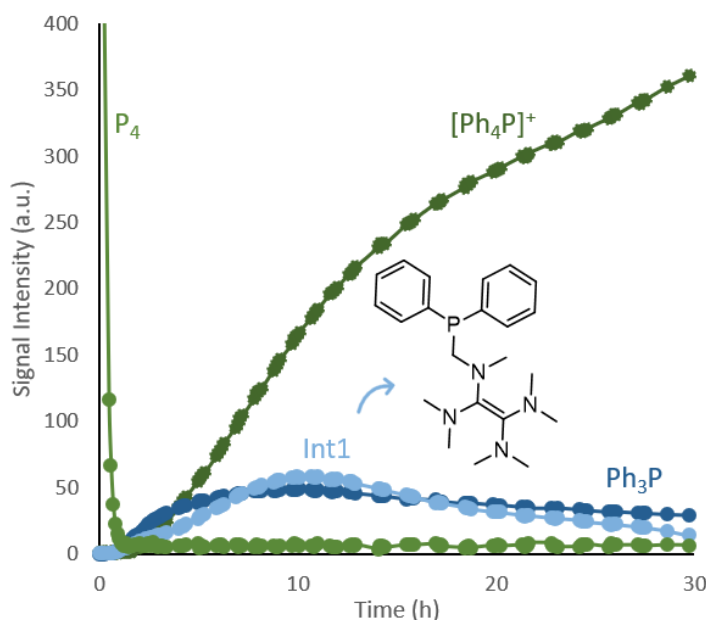


Figure 3. *In situ* ³¹P{¹H} NMR monitoring of phosphorus speciation during photochemical functionalization of white phosphorus using chlorobenzene and TDAE (see ESI, S6 for full reaction details and qualitative kinetics). The diagram is cut off at the x (30 h) and y axis (400). Overall the reaction was monitored for 90 h and the initial P₄ intensity is defined as 1000. The relatively long reaction time can be attributed to the reduced irradiation power of the *in situ* light source and lack of stirring.

Time-resolved ³¹P{¹H} NMR spectroscopic investigation of the model reaction using chlorobenzene showed rapid consumption of P₄ (Figure 3, completely consumed within one hour under *in situ* NMR conditions, see also ESI, S3, Table S6) and the formation of Ph₃P, [Ph₄P]Cl and another intermediate (**Int1**). The structure of **Int1** could be assigned based on a combination of its ³¹P chemical shift, ¹H–³¹P HMQC experiments and comparison with literature data,^[28] which suggest a TDAE skeleton that is coordinated to a Ph₂P moiety *via* one of its methyl groups (Figure 3, see also ESI, S6, Figure S36).

On the basis of the results mentioned above, the light-driven functionalization of P₄ in the presence of chlorobenzene and TDAE in acetone is proposed to proceed by the mechanism summarized in Figure 4. First, irradiation of TDAE with UV light provides a super-photoreductant (TDAE^{*}) (see Figure 4 (i)) which is then able to reduce the solvent acetone by a SET generating TDAE^{•+} and acetone^{•-} (Figure 4 (ii)). Next, the acetone radical anion reduces the substrate PhCl (Figure

4 (iii)) which can then provide phenyl radicals after elimination of Cl^- (Figure 4 (iv)). We denote steps (ii) to (iv) as the solvent radical mechanism. The aryl radicals thus generated then sequentially functionalize P_4 by controlled cleavage of all six P–P bonds of the P_4 tetrahedron (Figure 4 (v)), producing a sequence of different arylated intermediates analogous to that observed in our previous photocatalytic method,^{[8]–[10]} such as the primary phosphine (PhPH_2), the secondary phosphine (Ph_2PH), the diphosphine (Ph_4P_2), Ph_3P and finally $[\text{Ph}_4\text{P}]\text{Cl}$. The first arylation step to the primary phosphine (PhPH_2) is presumably too rapid to be tracked by $^{31}\text{P}\{^1\text{H}\}$ NMR, but small amounts of Ph_2PH were observable during NMR monitoring (ESI, S6.1, Figure S32). For the formation of the intermediates PhPH_2 and Ph_2PH the required H-atoms could potentially be transferred from the oxidized radical cation $\text{TDAE}^{+\bullet}$ (see Figure 4) which is an effective H-atom donor.^{[29],[30]} Nevertheless, mechanistic investigations and *in situ* NMR experiments^{[31],[32]} (see ESI, S6) using deuterated acetone- d_6 showed clear deuterium incorporation into these intermediates, suggesting that acetone is involved in the mechanism. It should be noted, however, that P_4 arylation also proceeds in the absence of acetone with 30–40% total conversion to a mixture of $[\text{Ph}_4\text{P}]\text{Cl}$ and Ph_3P (^{31}P NMR spectroscopic monitoring, see the ESI, Table S4). Hence, the direct, non-acetone mediated reduction may be an additional, significant pathway.

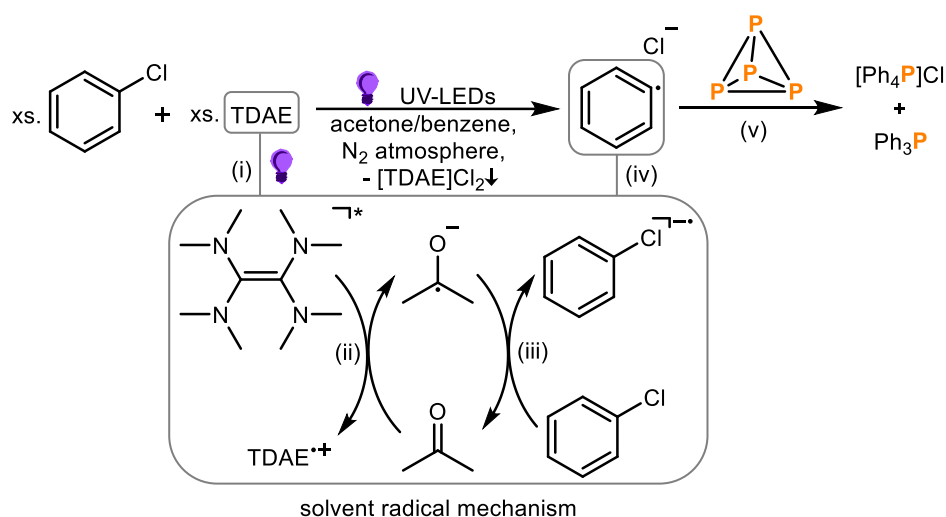


Figure 4. Proposed mechanism for the light-driven photochemical arylation of P_4 in the presence of aryl chloride and TDAE.

To validate their intermediacy, the photochemical arylation was also analyzed starting from the different arylated phosphorus compounds PhPH₂, Ph₂PH, Ph₄P₂ and Ph₃P (see ESI, S7). By using Ph₂PH as a starting material a mixture of [Ph₄P]Cl (76%) and Ph₃P (15%) could be obtained in good yields. PhPH₂ also showed good conversion to the phosphonium salt (68%) and using Ph₄P₂ as the P-containing species yielded a mixture of 55% [Ph₄P]Cl and 28% Ph₃P. Interestingly, further investigations of the stability of the phosphonium salt under the applied photochemical conditions confirmed some decomposition of the product (loss of [Ph₄P]Cl intensity dependent on amount of TDAE, see ESI, S7, Table S13) which is probably a factor behind the consistently sub-quantitative yields of the P₄ arylation reaction.

Finally, it was noted that during the photochemical reaction [TDAE]Cl₂^[33] is formed as a side product (see ESI, S8) which is almost completely insoluble in acetone and precipitates as a white solid over the course of the reaction and can be recovered by simple filtration. Since it is known that [TDAE]Cl₂ can be used to regenerate TDAE using simple reductants such as Zn,^[34] this recovery suggests the possibility of using the organic photoreductant as part of a closed loop, in which a much cheaper reagent acts as the effective terminal reductant. Synthetic efforts in this direction are currently underway.

2.3 Conclusion

In conclusion, we have described herein the direct photochemical arylation of white phosphorus using inexpensive, commercially available aryl chlorides for the first time, which has long been an important yet challenging objective. The simple light-driven procedure is mediated by TDAE and acetone under irradiation with UV light. The remarkable reducing power of photoexcited TDAE enables the reduction of different substituted organic chlorides to generate the corresponding aryl radicals which can be trapped by P₄ to form new P–C bonds and ultimately valuable aryl phosphines and phosphonium salts. While these observations represent an important proof-of-principle, the present method still suffers from several practical disadvantages, e.g., the need for an excess of aryl chloride and TDAE, poor selectivity toward the formation of either phosphonium salt or phosphine and our current inability to recycle the TDAE photoreductant effectively. Solutions to these limitations are the subject of ongoing investigations, alongside further studies into the activation of chloro- and bromobenzenes for (catalytic) P₄ functionalization.

2.4 Supporting Information

S1. General Information

All reactions and manipulations were performed under an N₂ atmosphere (< 0.1 ppm O₂, H₂O) through use of a GS Glovebox (GS117717). All glassware was oven-dried (160 °C) overnight prior to use. Acetonitrile, dimethyl sulfoxide and dimethylformamide were distilled from CaH₂ and stored over molecular sieves (3 Å). Benzene was distilled from Na/benzophenone and stored over molecular sieves (3 Å). Acetone was stirred over CaSO₄ (3 h) and distilled after dynamically drying over molecular sieves (3 Å). THF and toluene were purified using an MBraun SPS-800 system and stored over molecular sieves (3 Å). C₆D₆ was distilled from K and stored over molecular sieves (3 Å). All other chemicals were purchased from major suppliers (Aldrich, ABCR); liquids were purified by Kugelrohr distillation and freeze-pump-thaw degassed three times prior to use; P₄, Ph₃P and Ph₃PO were purified by sublimation; all others were used as received.

With the exception of *in situ* experiments (for details of which, see section S6), qualitative NMR spectra were recorded at room temperature on Bruker Avance III HD 400 (400 MHz) spectrometers and were processed using Topspin 3.2. Chemical shifts δ , are reported in parts per million (ppm); ¹H and ¹³C shifts are reported relative to SiMe₄ and were calibrated internally to residual solvent peaks, while ³¹P shifts were referenced externally to 85 % H₃PO₄ (aq.).

NMR samples were prepared in the glovebox using NMR tubes fitted with screw caps. Optimization reactions (see S3) and photochemical phenylation reactions of PhPH₂, Ph₂PH, Ph₄P₂ and Ph₃P (see S7) were analyzed by ³¹P{¹H} spectra using only a single scan (DS = 0, D1 = 2 s). The accuracy of this method was confirmed by preparing solutions of (*o*-tol)₃P or [Ph₄P]Cl and 0.05 mmol Ph₃PO in MeCN/PhH (1.5 mL, 0.5 mL, respectively), and comparing the measured and expected relative integrations (Figure S1).

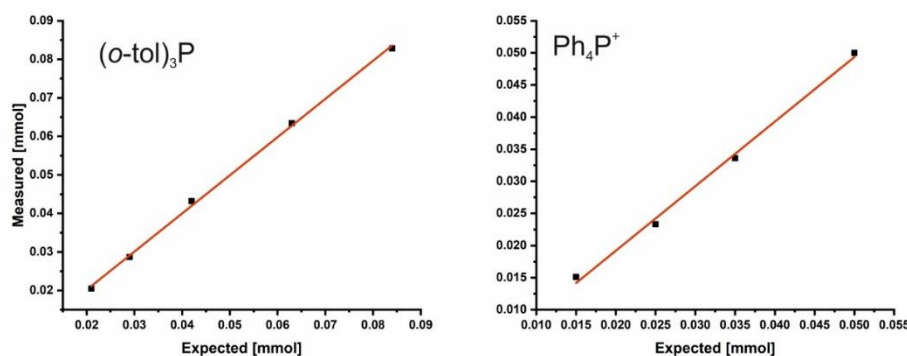


Figure S1. Plots showing the consistency between measured (by integration against 0.05 mmol Ph₃PO using a ³¹P{¹H} experiment (zgif) with a single scan) and expected (based on mass added) molar quantities of (*o*-tol)₃P (left) or [Ph₄P]Cl (right) in MeCN/PhH (3:1) solutions.

Quantitative measurements for the substrate screening were conducted on *Bruker Avance HD III 400* (400 MHz) spectrometers. Yields were determined by 1D $^{31}\text{P}\{^1\text{H}\}$ NMR spectroscopy. In order to meet quantitative conditions special attention was paid to the following aspects:

- Pulse lengths were calibrated. The O1P of the spectrum was set close to the frequencies of interest to enable maximum excitation. In cases where the distance between signals of interest was greater than 21000 Hz, one spectrum was recorded for each signal of interest, having its O1P close to the respective frequency.
- T_1 relaxation times were determined for all peaks of interest and a D1 of $\geq 5 \times T_1$ was used to ensure full relaxation between scans.
- The NS was adjusted so that the S/N-ratio (signal to noise ratio) was higher than 100/1. In order to reduce measurement time and to increase the S/N-ratio compared to a standard 1D experiment using only a 90° pulse (zg experiment), the zgig pulse program (inverse gated decoupled) was used, applying proton decoupling during the acquisition time. Since the zgig pulse program uses decoupling, it had to be ensured that any signal enhancement due to NOE (nuclear Overhauser effect) is negligible. Therefore, zg and zgig experiments were conducted and the integrals of the signals of interest were compared. For all reaction mixtures investigated, the integrals corresponding to both the internal standard (Ph_3PO) and the product stayed constant.
- After acquisition, the spectra were processed and integrated, and the yields were determined by referencing the integral of the product to that of the standard Ph_3PO .
- The quantitative spectra of the substrate screening are shown in S4.

S2. General procedure for photochemical functionalization of P₄

(0.04 mmol scale)

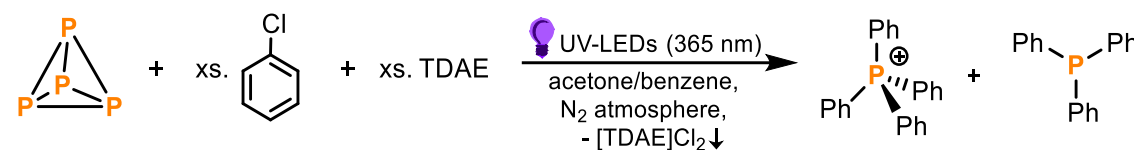
To a 10 mL stoppered tube equipped with a stirring bar were added the appropriate chlorobenzene derivative (0.4 mmol, 10 equiv. based on the phosphorus atom), organic photoreductant TDAE^[20] (0.2 mmol, 5 equiv. based on the phosphorus atom), and P₄ (0.01 mmol, 1 equiv., as a stock solution in 71.3 μ L benzene). The mixture was dissolved in acetone (0.5 mL). The tube was sealed, placed in a water-cooled block (to ensure a near-ambient temperature was maintained, Figure S2), and irradiated with UV light (365 nm, 4.3 V, 700 mA, Osram OSOLON SSL 80) for 20 h (unless stated otherwise). Ph₃PO (0.02 mmol, stock solution in benzene) was subsequently added to act as an internal standard. The resulting mixture was subjected to NMR analysis.



Figure S2. Illustration of the equipment setup used for photochemical reactions at 0.04 mmol scale.

S3. Optimization of reaction conditions

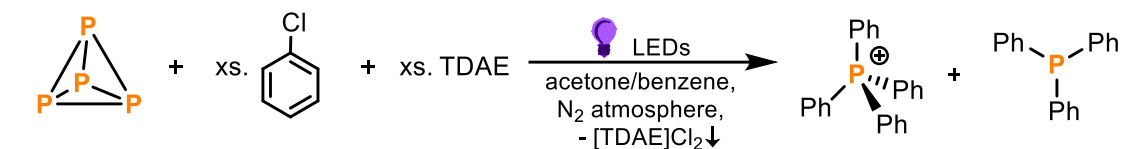
Table S1. Photochemical functionalization of P₄ to [Ph₄P]Cl and Ph₃P: screening of **control** experiments.^[a]



Entry	Conditions	Full conv. of P ₄ ?	Conv. to [Ph ₄ P]Cl / %	Conv. to Ph ₃ P / %
1	Standard ^[a]	✓	53	9
2	No light	✗	0	0
3	No TDAE	✗	0	0
4	No PhCl	✗	0	0
5	PhF instead of PhCl	✗	0	0
6	PhBr instead of PhCl	✓	43	10
7	PhI instead of PhCl	✓	14	10
8	P _{red} instead of P ₄	—	0	0

[a] For the general procedure, see section S2.

Table S2. Photochemical functionalization of P₄ to [Ph₄P]Cl and Ph₃P: screening of **LEDs** at different temperatures.^[a]

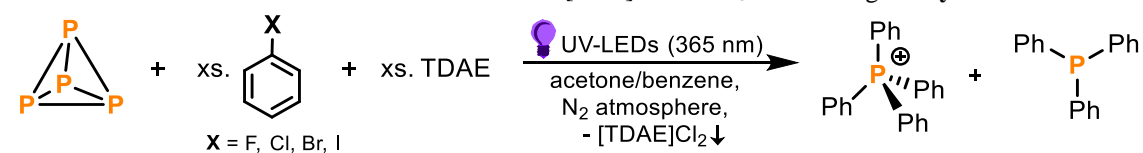


Entry	LEDs	Full conv. of P ₄ ?	Conv. to [Ph ₄ P]Cl / %	Conv. to Ph ₃ P / %	Conv. to Ph ₄ P ₂ / %	Conv. to Int1 / %
1	455 nm	✓	21	8	3	3
2	455 nm ^[b]	✓	17	11	3	0 ^[~]
3	420 nm	✓	52	15	0 ^[~]	0 ^[~]
4	420 nm ^[c]	✓	37	12	0 ^[~]	4
5	400 nm	✓	43	15	0 ^[~]	4
6	385 nm	✓	38	9	0 ^[~]	0 ^[~]
7	365 nm ^[a]	✓	53	9	1	
8	365 nm ^[d]	✓	43	11	2	0 ^[~]
9	365 nm ^[c]	✓	39	10	0 ^[~]	2

[a] The general procedure (section S2) was modified to use the LEDs indicated. For the general procedure, see section S2. [b] Photoreactor 7W, 36 °C. [c] Cooling with cryostat to -5 °C. [d] Cooling with cryostat to 0 °C. [~] Signal in the ³¹P{¹H} NMR (NS 256), but too small to determine the yield in the quantitative ³¹P{¹H} NMR (NS 1).

Chapter 2. Photochemical Transformation of Chlorobenzenes and White Phosphorus into Arylphosphines and Phosphonium salts

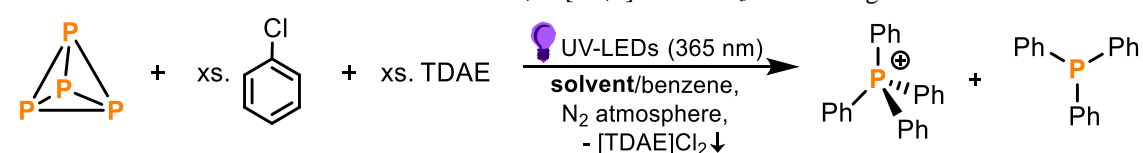
Table S3. Photochemical functionalization of P_4 to $[Ph_4P]Cl$ and Ph_3P : screening of **aryl halides**.^[a]



Entry	Aryl halide	Full conv. of P_4 ?	Conv. to $[Ph_4P]X$ / %	Conv. to Ph_3P / %	Conv. to Ph_4P_2 / %	Conv. to Int1 / %
1	Fluorobenzene	X	0	0	0	0
2	Chlorobenzene ^[a]	✓	53	9	1	0
3	Bromobenzene	✓	43	10	0 ^[~]	4
4	Iodobenzene	✓	14	10	0 ^[~]	4

[a] For the general procedure, see section S2. [~] Signal in the $^{31}P\{^1H\}$ NMR (NS 256), but too small to determine the yield in the quantitative $^{31}P\{^1H\}$ NMR (NS 1).

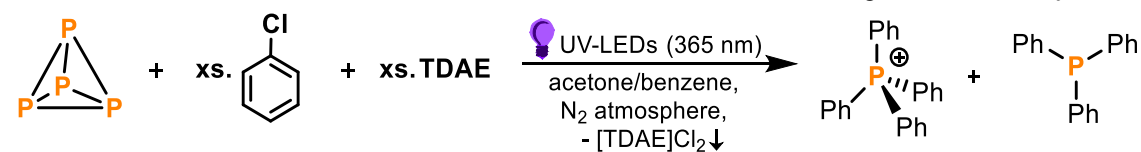
Table S4. Photochemical functionalization of P_4 to $[Ph_4P]Cl$ and Ph_3P : screening of **solvents**.^[a]



Entry	Solvent	Full conv. of P_4 ?	Conv. to $[Ph_4P]Cl$ / %	Conv. to Ph_3P / %	Conv. to Ph_4P_2 / %	Conv. to Int1 / %
1	Acetone ^[a]	✓	53	9	1	0
2	Acetone ^[b]	✓	47	4	0 ^[~]	0
3	Acetone ^[c]	✓	41	10	0 ^[~]	0 ^[~]
4	Acetone ^[d]	✓	31	13	0 ^[~]	0 ^[~]
5	Benzene	✓	27	11	0 ^[~]	5
6	Acetonitrile	✓	31	11	2	0
7	THF	✓	0 ^[~]	2	11	0
8	Toluene	✓	19	7	0 ^[~]	2
9	DMSO	✓	6	0	0	0
10	DMF	✓	11	11	0 ^[~]	0
11	Chlorobenzene	✓	23	12	0 ^[~]	7

[a] The general procedure (section S2) was modified to use the solvent system indicated (identical solvent volume). [b] 0.25 mL solvent volume. [c] 1.0 mL solvent volume. [d] 2.0 mL solvent volume. [~] Signal in the $^{31}P\{^1H\}$ NMR (NS 256), but too small to determine the yield in the quantitative $^{31}P\{^1H\}$ NMR (NS 1).

Table S5. Photochemical functionalization of P₄ to [Ph₄P]Cl and Ph₃P: screening of stoichiometry.^{[a][b]}



Entry	Stoichiometry ^[b] TDAE:PhCl	Full conv. of P ₄ ?	Conv. to [Ph ₄ P]Cl / %	Conv. to Ph ₃ P / %	Conv. to Ph ₄ P ₂ / %	Conv. to Int1 / %
1	8:16	✓	8	17	0	8
2	12:24	✓	23	16	0 ^[~]	6
3	16:16	✓	40	12	3	0 ^[~]
4	16:16 ^[c]	✓	12	14	1	10
5	16:16 ^[d]	✓	19	16	0 ^[~]	11
6	16:16 ^[e]	✓	11	14	0	9
7	16:16 ^[f]	✓	11	12	0	13
8	16:16 ^[g]	✓	8	10	0 ^[~]	12
9	32:16	✓	3	9	0	7
10	20:20	✓	12	14	0 ^[~]	11
11	20:40 ^[a]	✓	53	9	1	0
12	20:40 ^[c]	✓	48	10	0 ^[~]	0
13	(2 · 20):40 ^[h]	✓	50	8	0 ^[~]	0
14	20:40 ^[i]	✓	42	11	0	0 ^[~]
15	20:40 ^[j]	✓	43	9	0 ^[~]	0 ^[~]
16	40:20	✓	5	10	0 ^[~]	9
17	40:20 ^[c]	✓	4	9	0 ^[~]	8
18	40:40	✓	26	12	5	0 ^[~]
19	40:40 ^[d]	✓	30	15	0 ^[~]	1

[a] For the general procedure, see section S2. [b] Listed equivalents are defined per P₄ molecule. [c] 0.25 mL solvent volume. [d] Cooling with cryostat to 0 °C. [e] Cooling with cryostat to -5 °C. [f] 400 nm LED. [g] 420 nm LED. [h] To a reaction with standard conditions (Entry 10, 20:40, UV, 20h) another 20 equiv. TDAE were added and irradiated for additional 20h. [i] modified P₄ concentration (0.005 mmol). [j] modified P₄ concentration (0.02 mmol). [~] Signal in the ³¹P{¹H} NMR (NS 256), but too small to determine the yield in the quantitative ³¹P{¹H} NMR (NS 1).

Table S6. Photochemical functionalization of P₄ to [Ph₄P]Cl and Ph₃P: **kinetic investigations.**^[a]

P4 + xs. c1ccccc1Cl + xs. TDAE $\xrightarrow[\text{acetone/benzene, N}_2 \text{ atmosphere, } - [\text{TDAE}]\text{Cl}_2 \downarrow]{\text{UV-LEDs (365 nm)}}$ [Ph]4P+ + Ph3P

Entry	Time	Full conv. of P ₄ ?	Conv. to [Ph ₄ P]Cl / %	Conv. to Ph ₃ P / %	Conv. to Ph ₂ PH / %	Conv. to Ph ₄ P ₂ / %	Conv. to Int1 / %
1	5 min	X	0[~]	0[~]	0[~]	0[~]	0[~]
2	10 min	✓	0[~]	0[~]	0[~]	0[~]	0[~]
3	30 min	✓	0[~]	2	2	2	2
4	1 h	✓	17	19	0	0[~]	11
5	3 h	✓	30	11	0	0	8
6	5 h	✓	35	11	0	0	6
7	7 h	✓	34	10	0	0	8
8	20 h ^[a]	✓	53	9	0	1	0
9	40 h	✓	48	8	0	1	0

[a] For the general procedure, see section S2. [~] Signal in the ³¹P{¹H} NMR (NS 256), but too small to determine the yield in the quantitative ³¹P{¹H} NMR (NS 1).

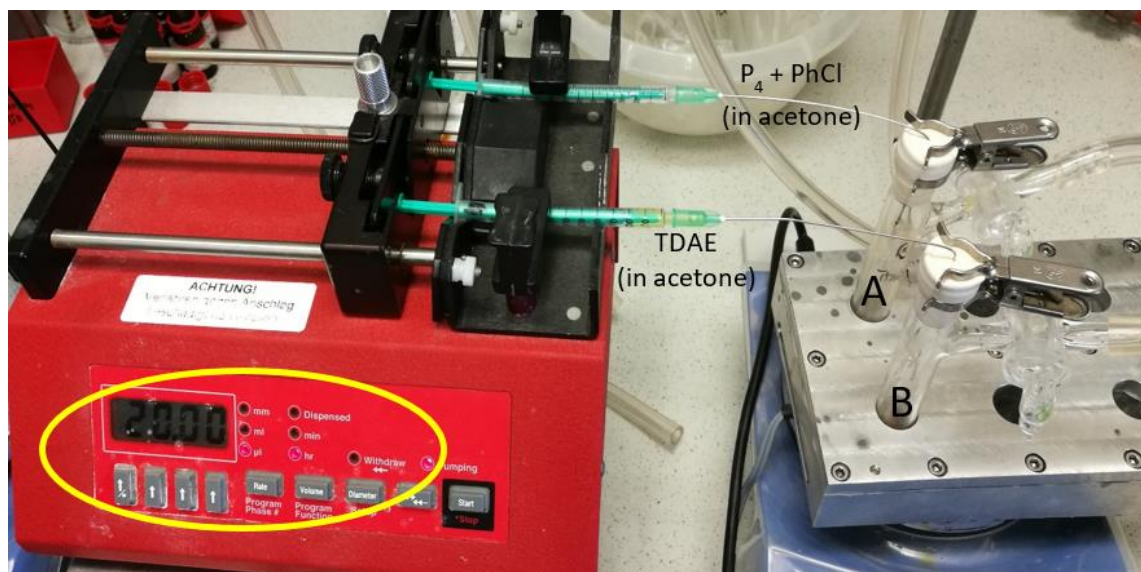
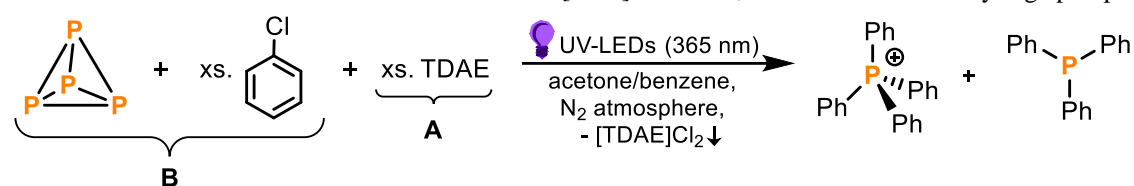


Figure S3. Illustration of the equipment setup used for slow addition *via* syringe pump for the photochemical reactions at 0.04 mmol scale. Standard reaction conditions: Chlorobenzene (0.4 mmol), TDAE (0.2 mmol) and P₄ (0.01 mmol) in acetone (0.5 mL). Reaction 1: slow addition of a P₄/PhCl mixture in acetone to TDAE/acetone solution (A). Reaction 2: slow addition of TDAE in acetone to a P₄/PhCl/acetone mixture (B). Syringe pump conditions: injected syringe volume 250 μ L (syringe dead volume 100 μ L), injection rate 20 μ L/hour, injection period 12.5 hours, irradiation period 20h.

Table S7. Photochemical functionalization of P₄ to [Ph₄P]Cl and Ph₃P: **slow addition** *via* syringe pump.^[a]

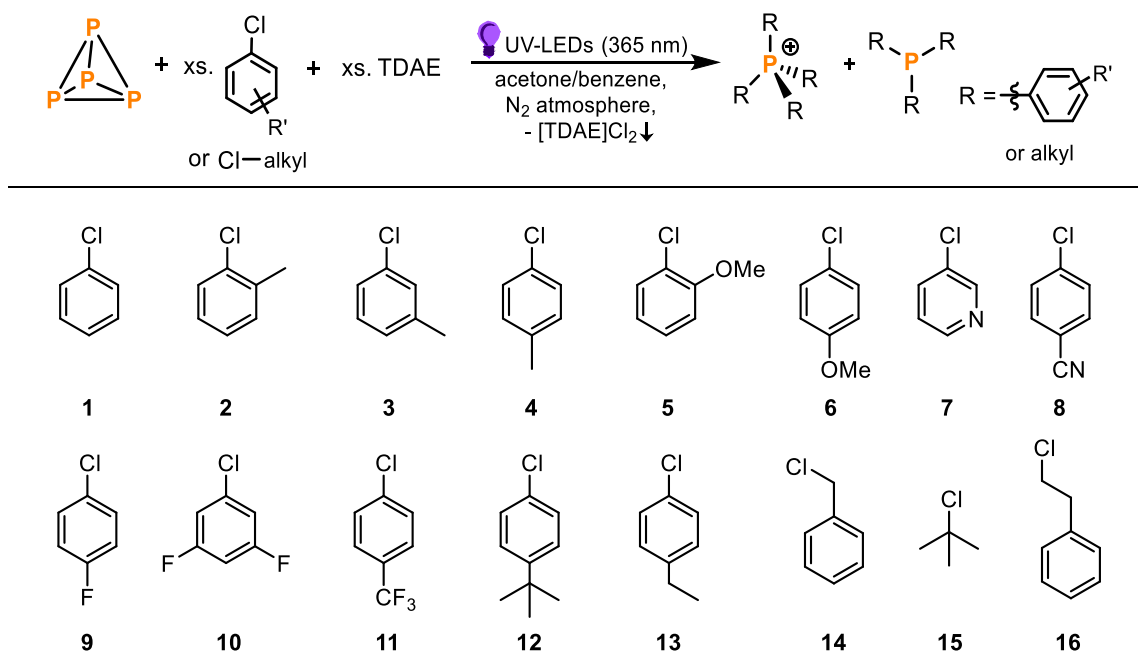


Entry	Schlenk	Slow addition	Full conv. of P ₄ ?	Conv. to [Ph ₄ P]Cl / %	Conv. to Ph ₃ P / %	Conv. to Ph ₄ P ₂ / %	Conv. to Int1 / %
1	A (TDAE)	P ₄ /PhCl	X	11	6	0[~]	2
2	B (P ₄ + PhCl)	TDAE	✓	37	0[~]	0[~]	0[~]

[a] For the general procedure, see section S2. [~] Signal in the ³¹P{¹H} NMR (NS 256), but too small to determine the yield in the quantitative ³¹P{¹H} NMR (NS 1).

S4. Characterization of optimized 0.04 mmol scale reactions

Table S8. Substrate scope for photochemical P₄ functionalization.



Substrate ^[a]	R'	Conv. to [R ₄ P]Cl / %	Conv. to R ₃ P / %
1	R' = H	53	9
2	R' = 2-Me	0	10
3	R' = 3-Me	39	16
4	R' = 4-Me	35	10
5	R' = 2-OMe	0	3
6	R' = 4-OMe	20	6
7	3-PyrCl	27	7
8	R' = 4-CN	0	7
9	R' = 4-F	9	11
10	R' = 3,5-F	0	8
11	R' = 4-CF ₃	0	9
12	R' = 4- ^t Bu	17	14
13	R' = 4-Et	24	9
14	BnCl	0	27
15	^t BuCl	0	5
16	(2-chloroethyl) benzene	0	75

[a] The general procedure for reactions at 0.04 mmol scale (section S2) was modified by replacing chlorobenzene (Entry 1) with chlorobenzene derivatives.

The conversions were determined by quantitative $^{31}\text{P}\{^1\text{H}\}$ (zgig) NMR experiments (161.98 MHz, 300 K, C_6D_6) as mentioned in the text (Ph_3PO (0.02 mmol) as internal standard, see S1 for further information).

S4.1 Tetraphenylphosphonium chloride & Triphenylphosphine

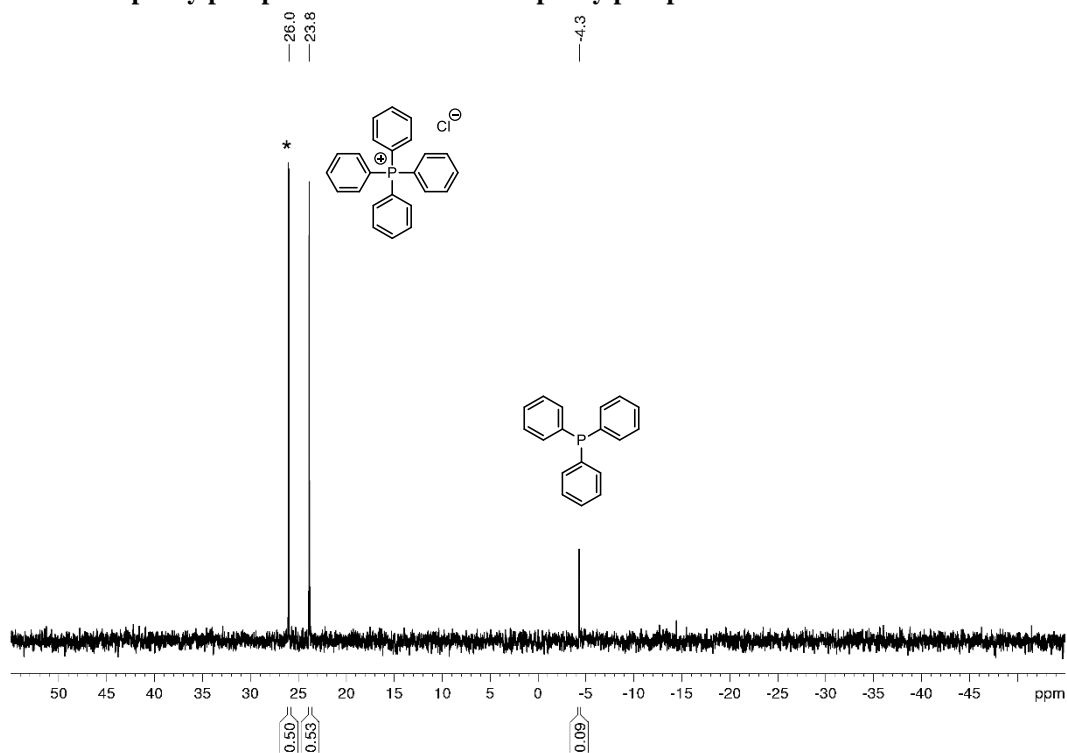


Figure S4. Quantitative single scan $^{31}\text{P}\{^1\text{H}\}$ (zgig) NMR spectrum for the photochemical functionalization of P_4 using chlorobenzene (Table S8, Entry 1). * marks the internal standard Ph_3PO (0.02 mmol).

S4.2 Tri(*o*-tolyl)phosphine

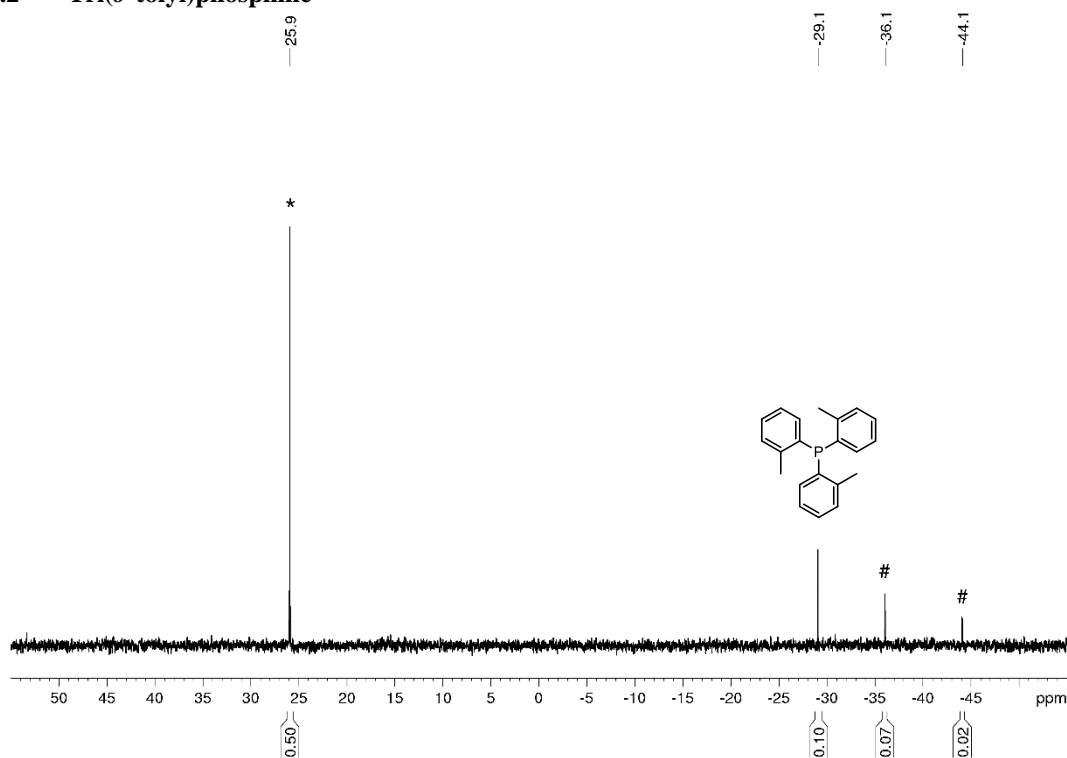


Figure S5. Quantitative single scan $^{31}\text{P}\{^1\text{H}\}$ (zgig) NMR spectrum for the photochemical functionalization of P_4 using 2-chlorotoluene (Table S8, Entry 2). * marks the internal standard Ph_3PO (0.02 mmol). # marks the signals of unknown by-products.

S4.3 Tetra(*m*-tolyl)phosphonium chloride & Tri(*m*-tolyl)phosphine

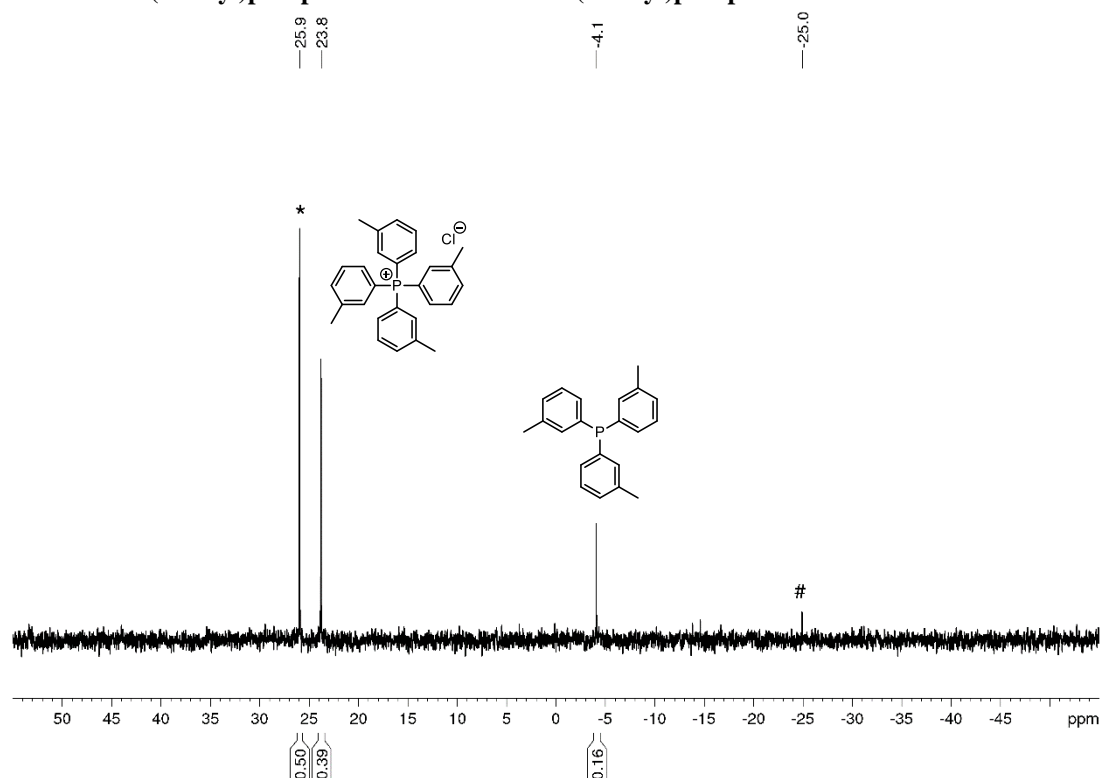


Figure S6. Quantitative single scan $^{31}\text{P}\{^1\text{H}\}$ (zgig) NMR spectrum for the photochemical functionalization of P_4 using 3-chlorotoluene (Table S8, Entry 3). * marks the internal standard Ph_3PO (0.02 mmol). # marks the signal of an unknown by-product.

S4.4 Tetra(*p*-tolyl)phosphonium chloride & Tri(*p*-tolyl)phosphine

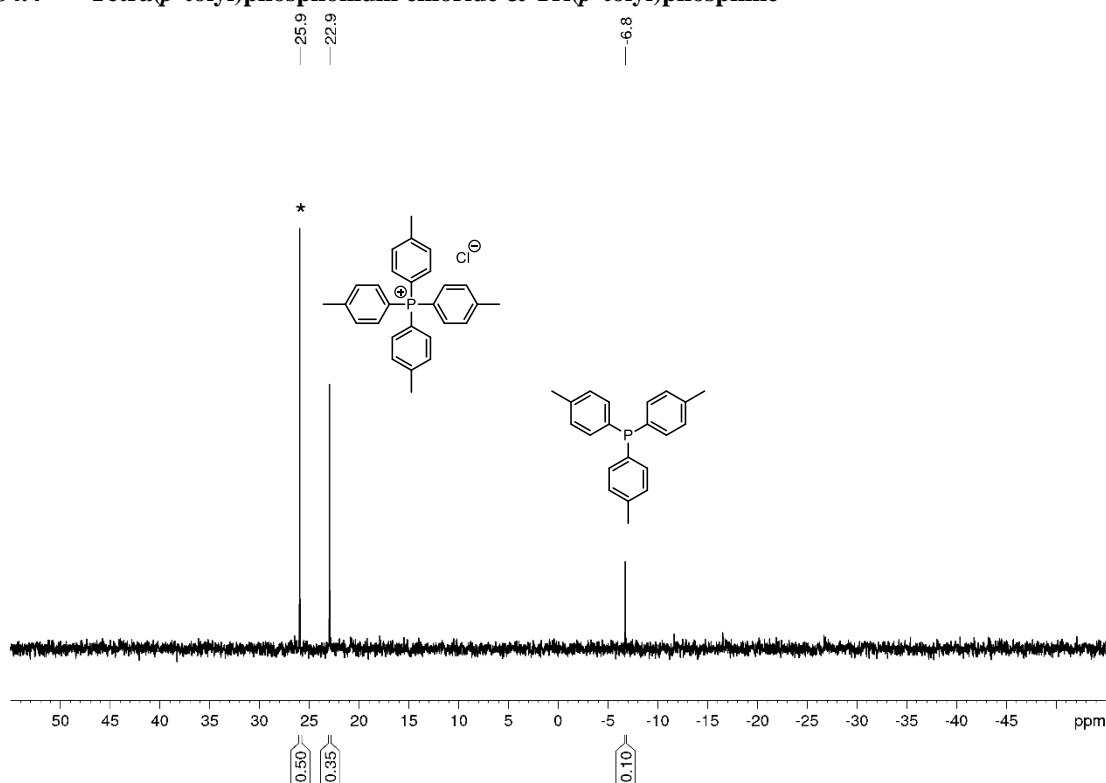


Figure S7. Quantitative single scan $^{31}\text{P}\{^1\text{H}\}$ (zgig) NMR spectrum for the photochemical functionalization of P_4 using 4-chlorotoluene (Table S8, Entry 4). * marks the internal standard Ph_3PO (0.02 mmol).

S4.5 Tris(2-methoxyphenyl)phosphine

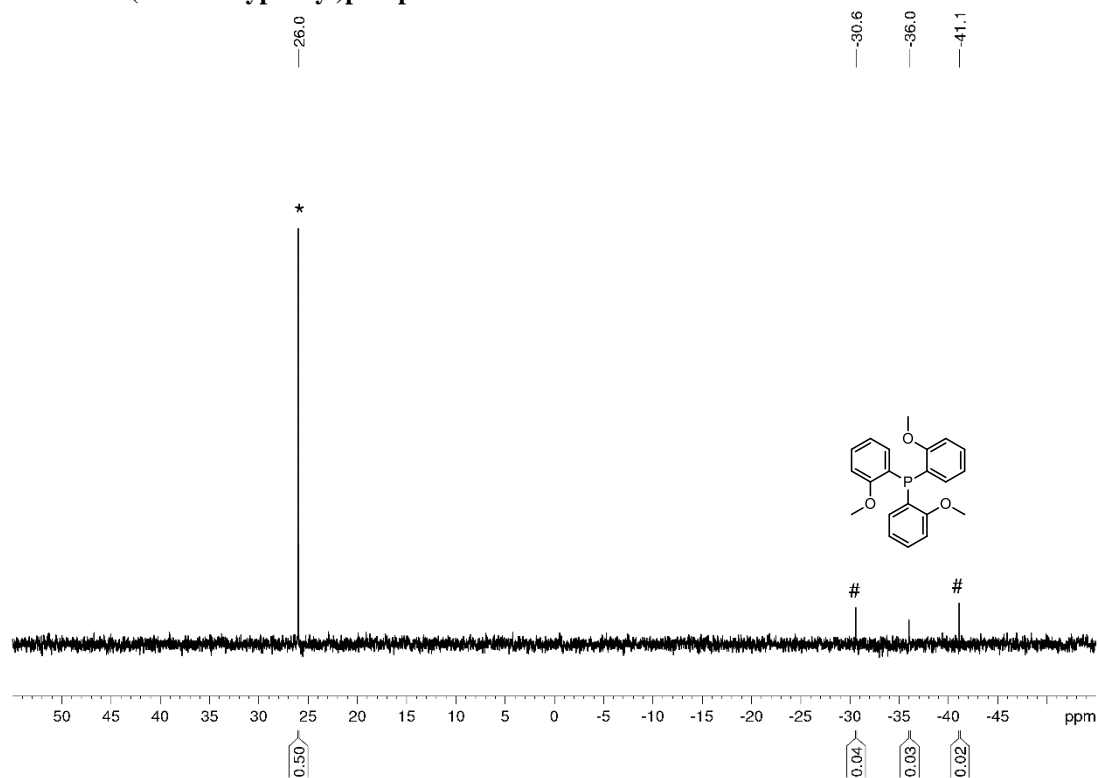


Figure S8. Quantitative single scan $^{31}\text{P}\{^1\text{H}\}$ (zgig) NMR spectrum for the photochemical functionalization of P_4 using 2-chloroanisole (Table S8, Entry 5). * marks the internal standard Ph_3PO (0.02 mmol). # marks the signals of unknown by-products.

S4.6 Tetrakis(4-methoxyphenyl)phosphonium chloride & Tris(4-methoxyphenyl)phosphine

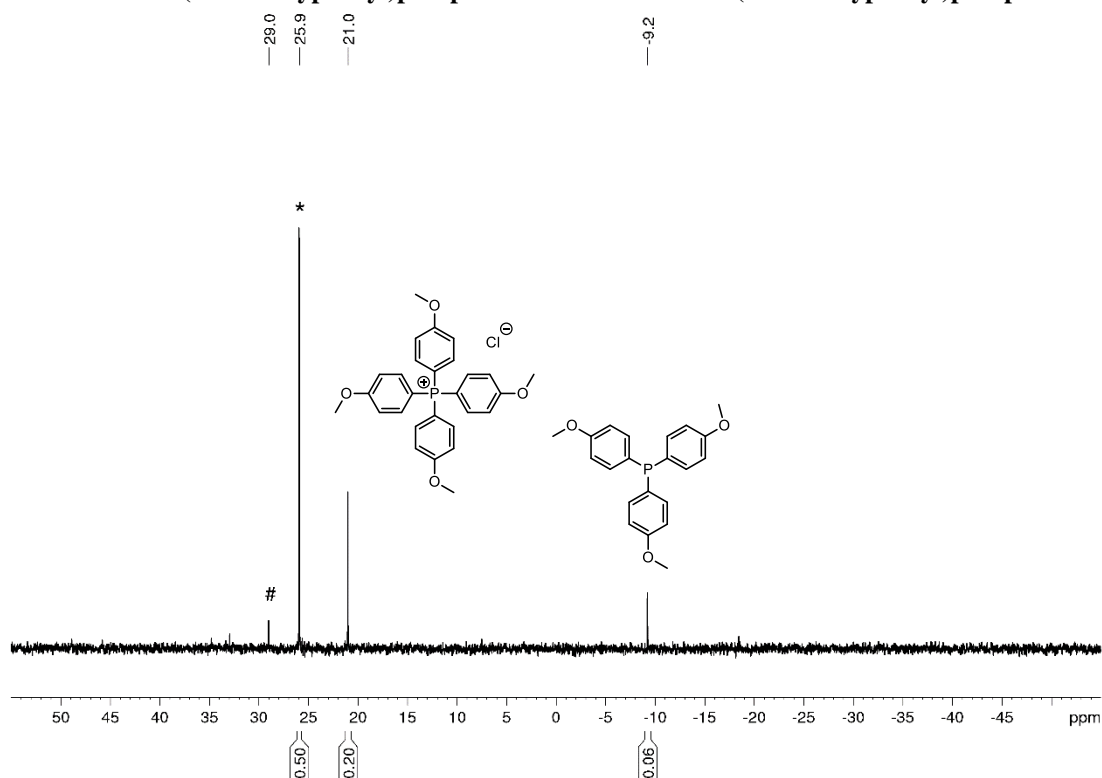


Figure S9. Quantitative single scan $^{31}\text{P}\{^1\text{H}\}$ (zgig) NMR spectrum for the photochemical functionalization of P_4 using 4-chloroanisole (Table S8, Entry 6). * marks the internal standard Ph_3PO (0.02 mmol). # marks the signal of an unknown by-product.

S4.7 Tetrakis(pyridin-3-yl)phosphonium chloride & Tris(pyridine-3-yl)phosphine

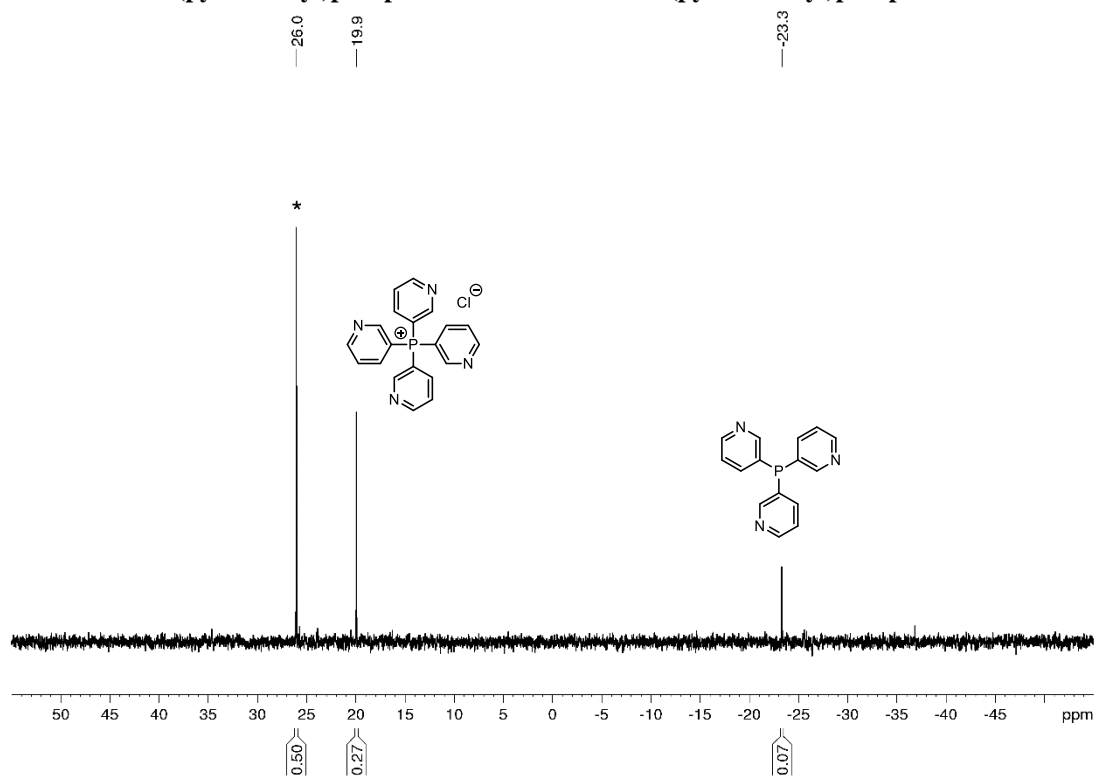


Figure S10. Quantitative single scan $^{31}\text{P}\{^1\text{H}\}$ (zgif) NMR spectrum for the photochemical functionalization of P_4 using 3-chloropyridine (Table S8, Entry 7). * marks the internal standard Ph_3PO (0.02 mmol).

S4.8 Tris(4-benzonitrile)phosphine

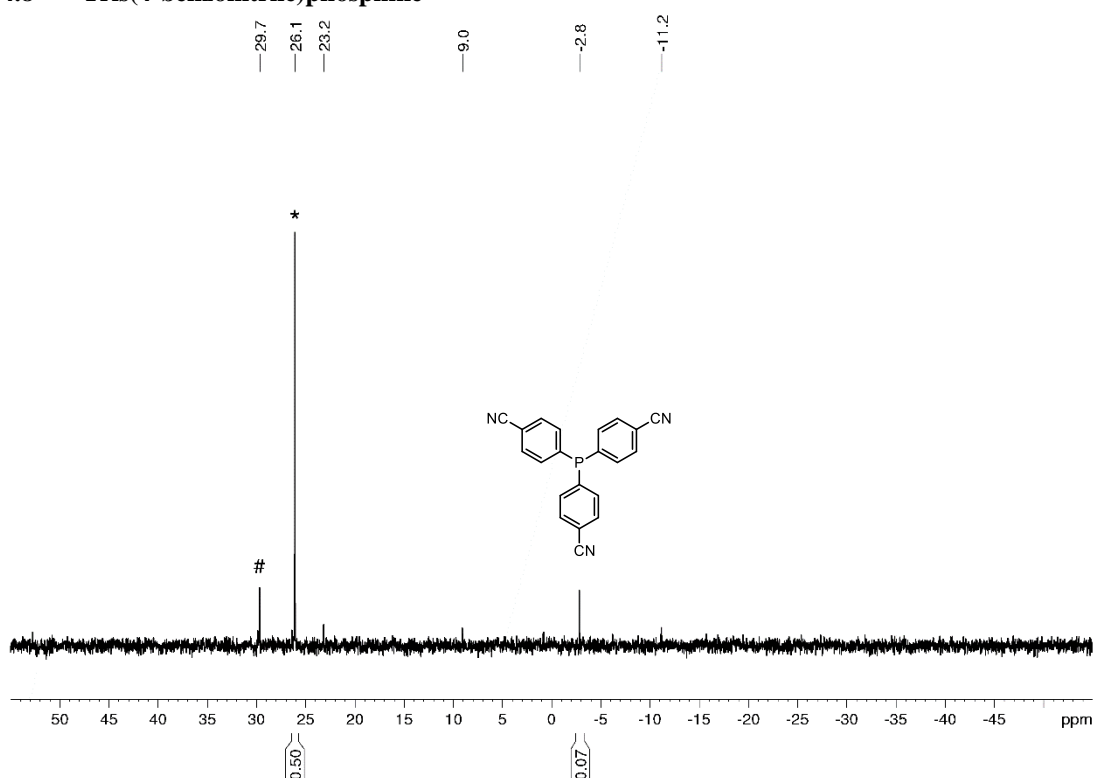


Figure S11. Quantitative single scan $^{31}\text{P}\{^1\text{H}\}$ (zgif) NMR spectrum for the photochemical functionalization of P_4 using 4-chlorobenzonitrile (Table S8, Entry 8). * marks the internal standard Ph_3PO (0.02 mmol). # marks the signal of an unknown by-product.

S4.9 Tetrakis(4-fluorophenyl)phosphonium chloride & Tris(4-fluorophenyl)phosphine

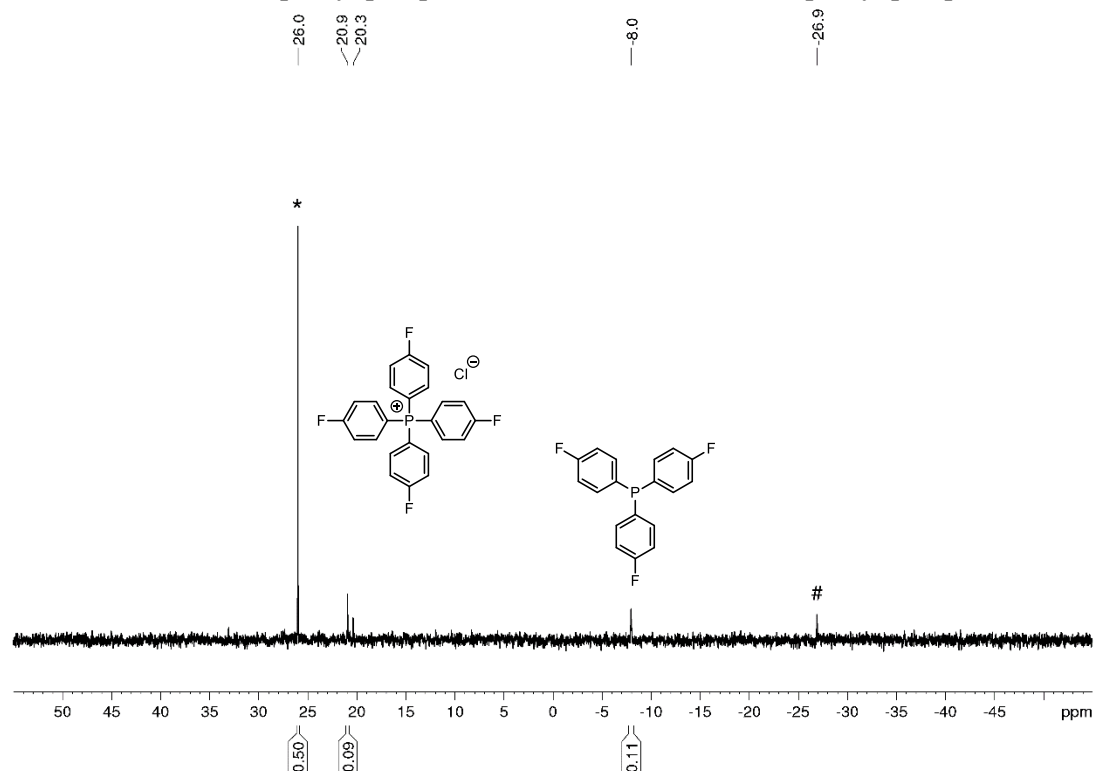


Figure S12. Quantitative single scan $^{31}\text{P}\{^1\text{H}\}$ (zgif) NMR spectrum for the photochemical functionalization of P_4 using 1-chloro-4-fluorobenzene (Table S8, Entry 9). * marks the internal standard Ph_3PO (0.02 mmol). # marks the signal of an unknown by-product.

S4.10 Tris(3,5-difluorophenyl)phosphine

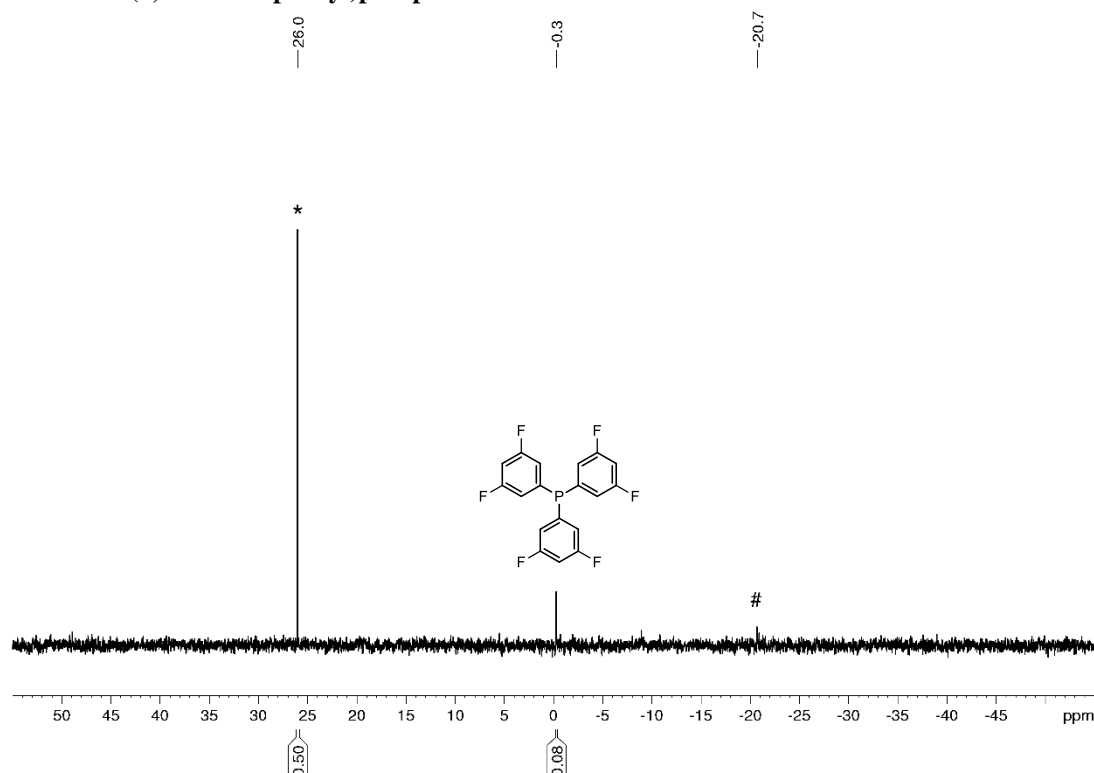


Figure S13. Quantitative single scan $^{31}\text{P}\{^1\text{H}\}$ (zgif) NMR spectrum for the photochemical functionalization of P_4 using 1-chloro-3,5-difluorobenzene (Table S8, Entry 10). * marks the internal standard Ph_3PO (0.02 mmol). # marks the signal of an unknown by-product.

S4.11 Tris(4-(trifluoromethyl)phenyl)phosphine

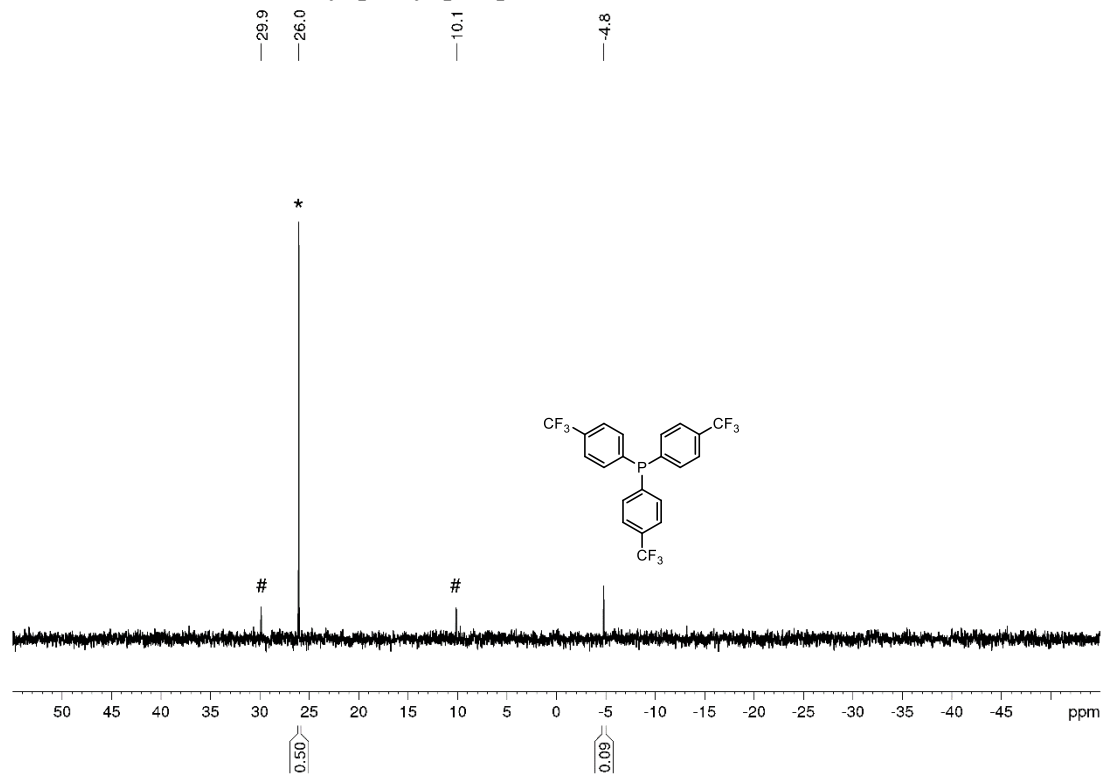


Figure S14. Quantitative single scan $^{31}\text{P}\{^1\text{H}\}$ (zgig) NMR spectrum for the photochemical functionalization of P_4 using 1-chloro-4-(trifluoromethyl)benzene (Table S8, Entry 11). * marks the internal standard Ph_3PO (0.02 mmol). # marks the signals of unknown by-product.

S4.12 Tetrakis(4-(*tert*-butyl)phenyl)phosphonium chloride & Tris(4-(*tert*-butyl)phenyl)phosphine

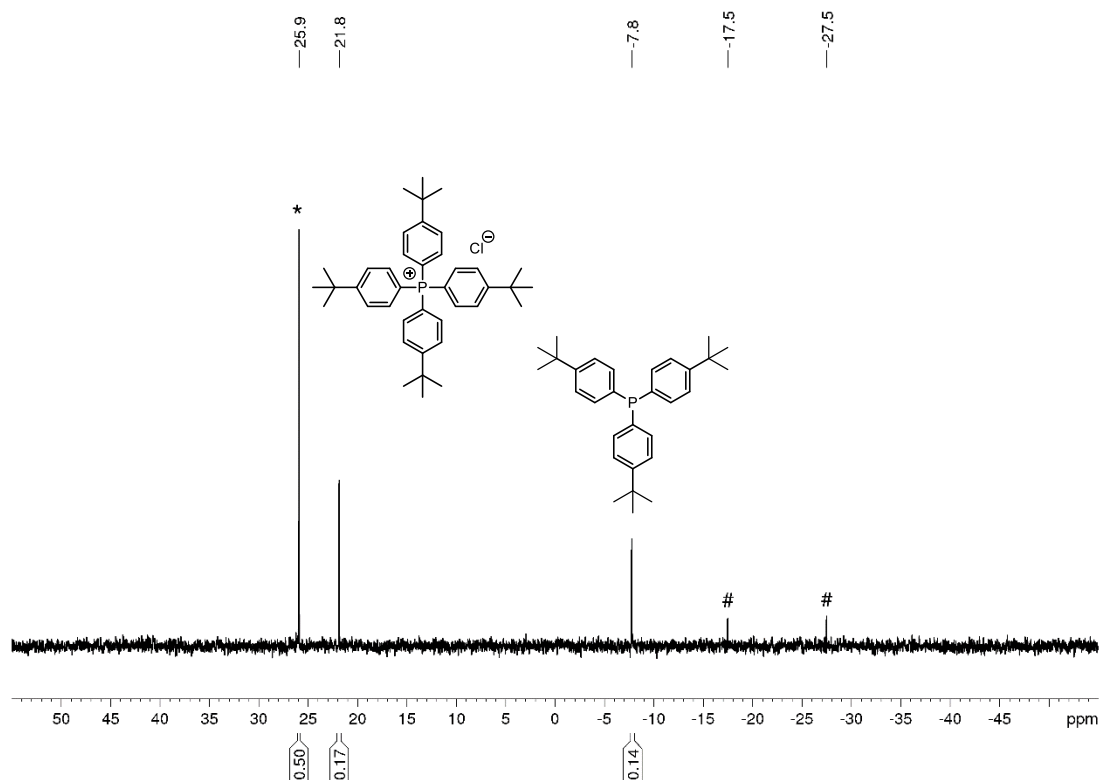


Figure S15. Quantitative single scan $^{31}\text{P}\{^1\text{H}\}$ (zgig) NMR spectrum for the photochemical functionalization of P_4 using 1-(*tert*-butyl)-4-chlorobenzene (Table S8, Entry 12). * marks the internal standard Ph_3PO (0.02 mmol). # marks the signals of unknown by-products.

S4.13 Tetrakis(4-ethylphenyl)phosphonium chloride & Tris(4-ethylphenyl)phosphine

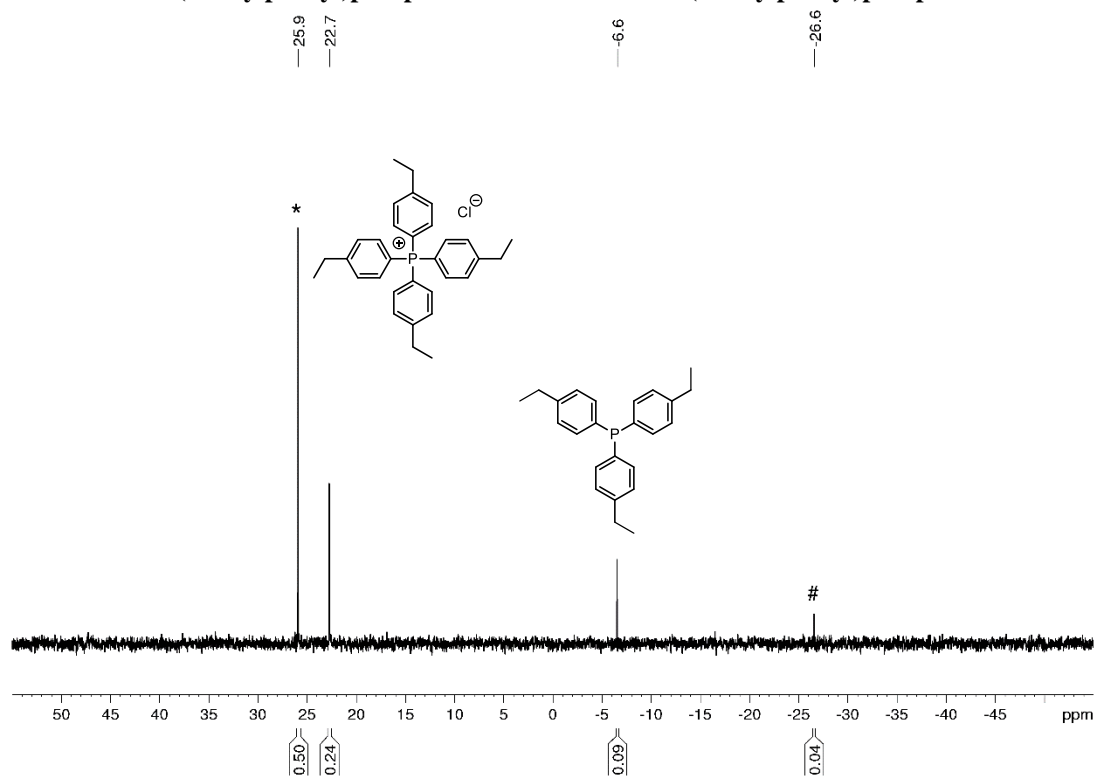


Figure S16. Quantitative single scan $^{31}\text{P}\{^1\text{H}\}$ (zgig) NMR spectrum for the photochemical functionalization of P_4 using 1-chloro-4-ethylbenzene (Table S8, Entry 13). * marks the internal standard Ph_3PO (0.02 mmol). # marks the signal of an unknown by-product.

S4.14 Tribenzylphosphine

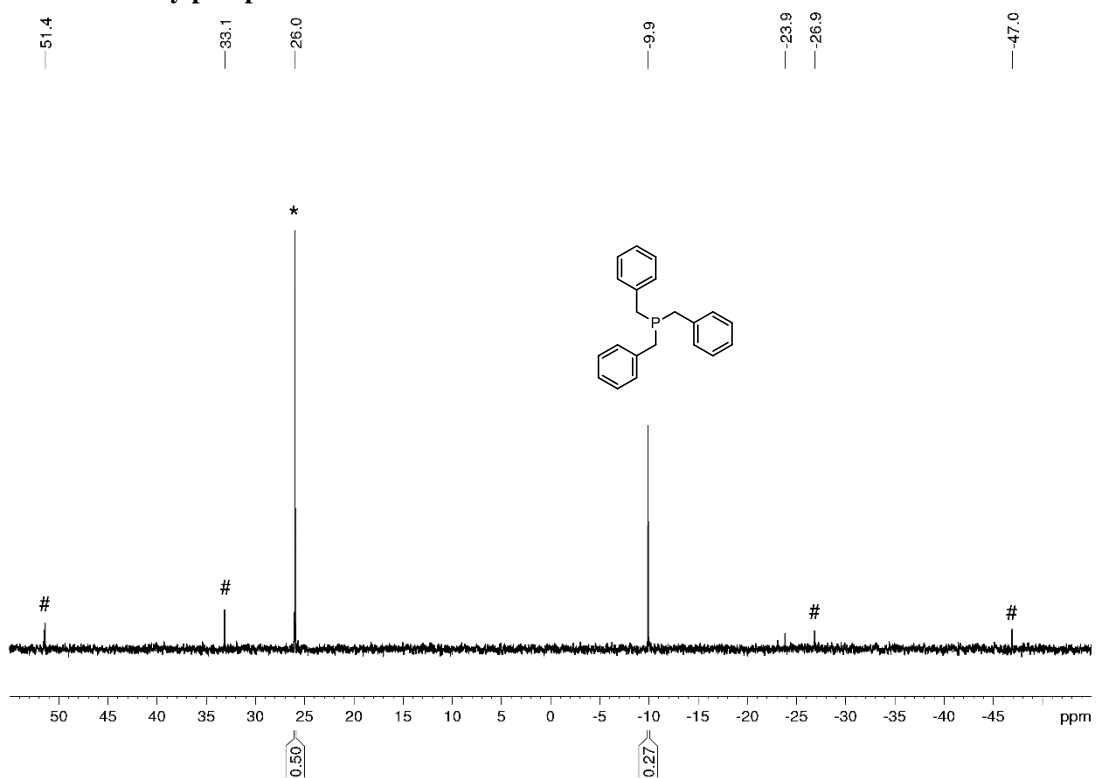


Figure S17. Quantitative single scan $^{31}\text{P}\{^1\text{H}\}$ (zgig) NMR spectrum for the photochemical functionalization of P_4 using benzyl chloride (Table S8, Entry 14). * marks the internal standard Ph_3PO (0.02 mmol). # marks the signals of unknown by-products.

S4.15 Tri(*tert*-butyl)phosphine

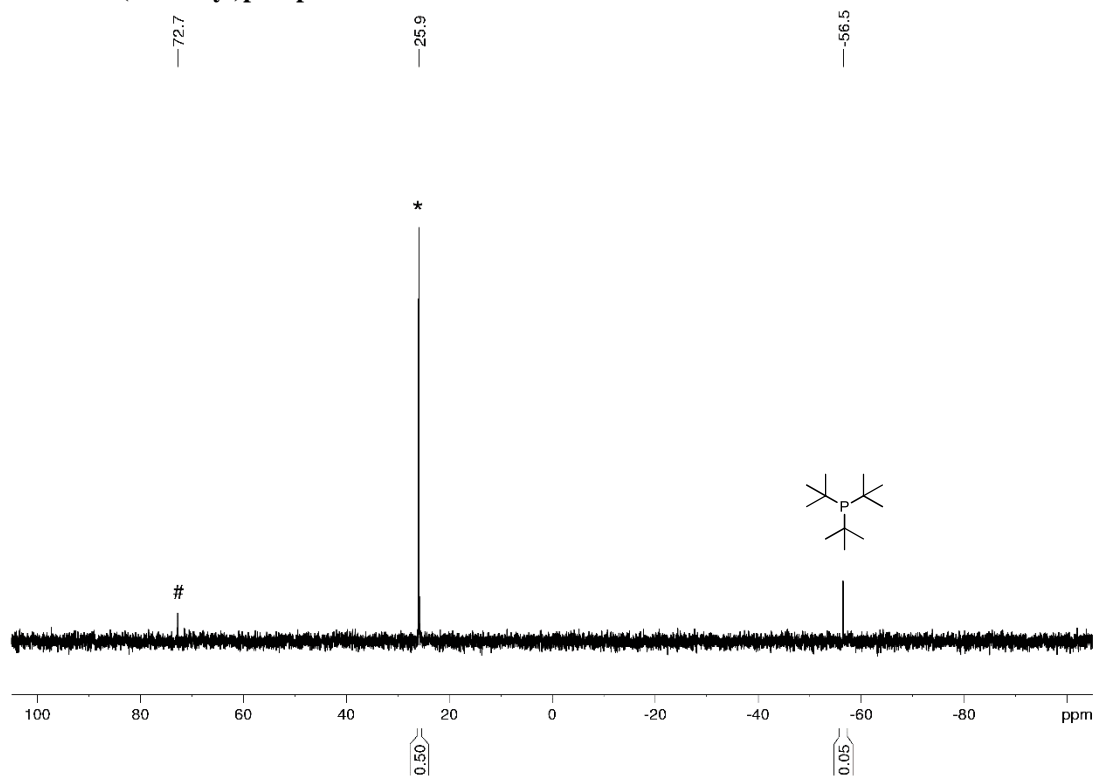


Figure S18. Quantitative single scan $^{31}\text{P}\{^1\text{H}\}$ (zgig) NMR spectrum for the photochemical functionalization of P_4 using *tert*-butyl chloride (Table S8, Entry 15). * marks the internal standard Ph_3PO (0.02 mmol). # marks the signal of an unknown by-product.

S4.16 Tris(phenylethyl)phosphine

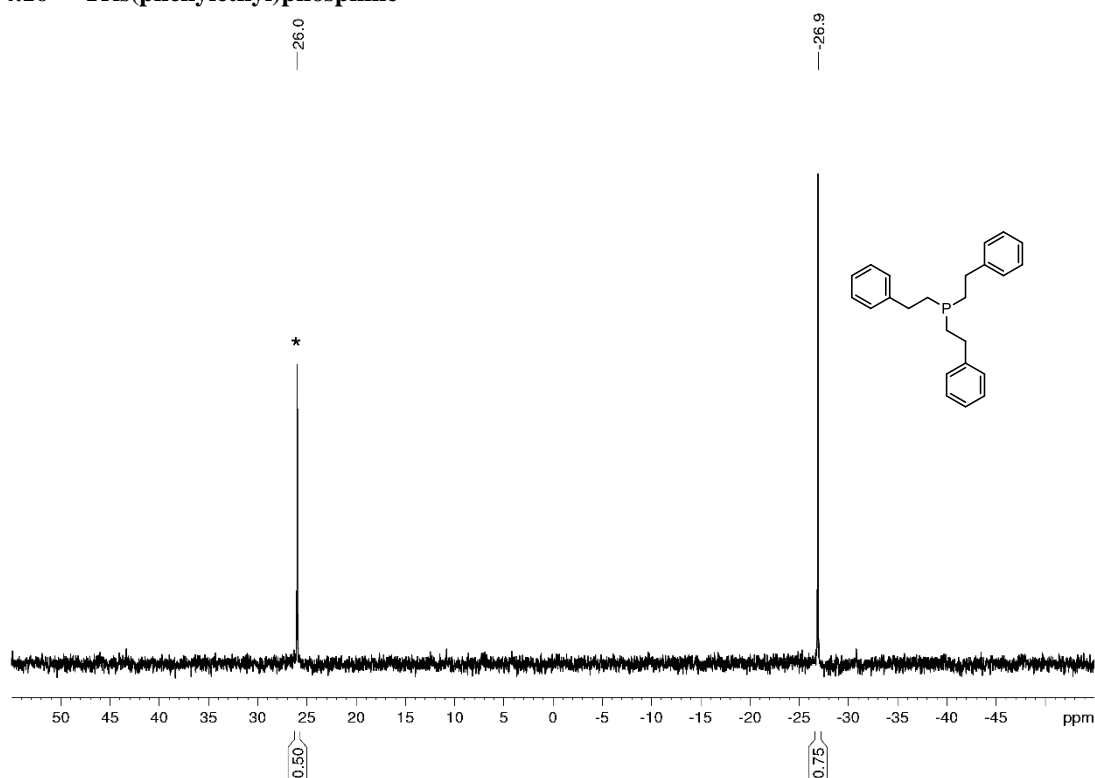


Figure S19. Quantitative single scan $^{31}\text{P}\{^1\text{H}\}$ (zgig) NMR spectrum for the photochemical functionalization of P_4 using (2-chloroethyl)benzene (Table S8, Entry 16). * marks the internal standard Ph_3PO (0.02 mmol).

S4.17 Reactivity of 1,4-hetero-halogenated benzene derivatives

S4.17.1 Tetrakis(4-chlorophenyl)phosphonium iodide & Tris(4-chlorophenyl)phosphine^[35]

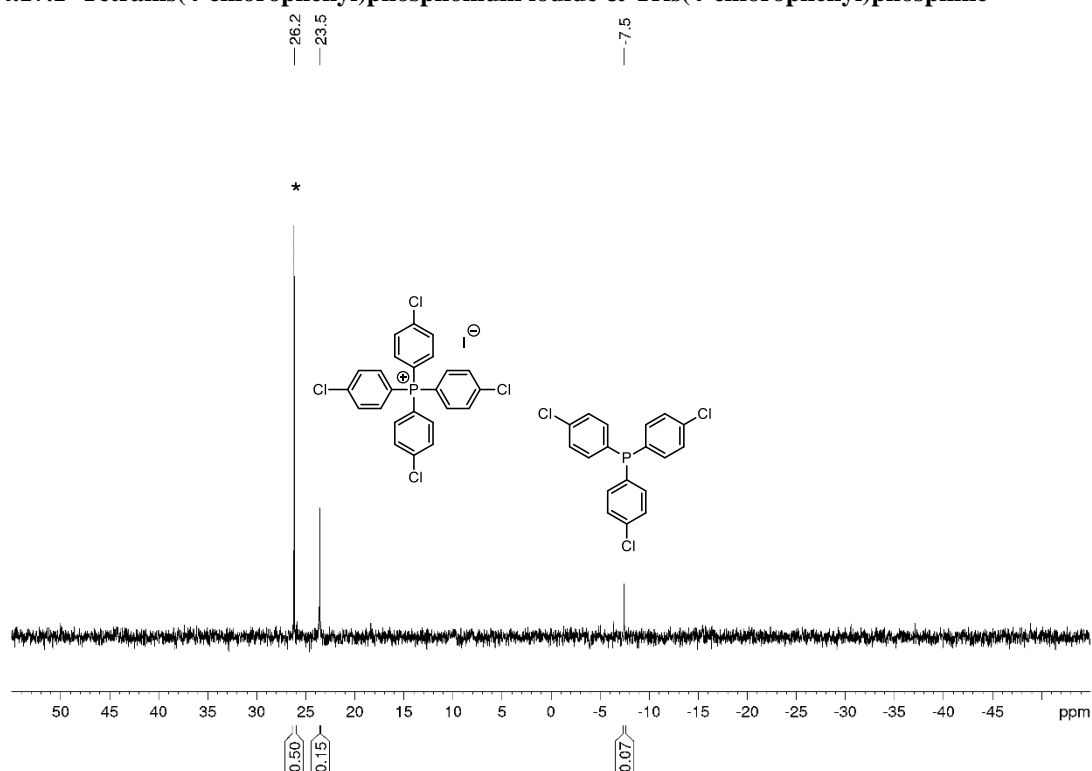


Figure S20. Quantitative single scan ³¹P{¹H} (zgif) NMR spectrum for the photochemical functionalization of P₄ using 1-chloro-4-iodobenzene. * marks the internal standard Ph₃PO (0.02 mmol). The signals were assigned to the stated products based on the chemical shifts found in the literature.^[35]

S4.17.2 Mixed activation of the C-X bonds by using 1-bromo-4-chlorobenzene

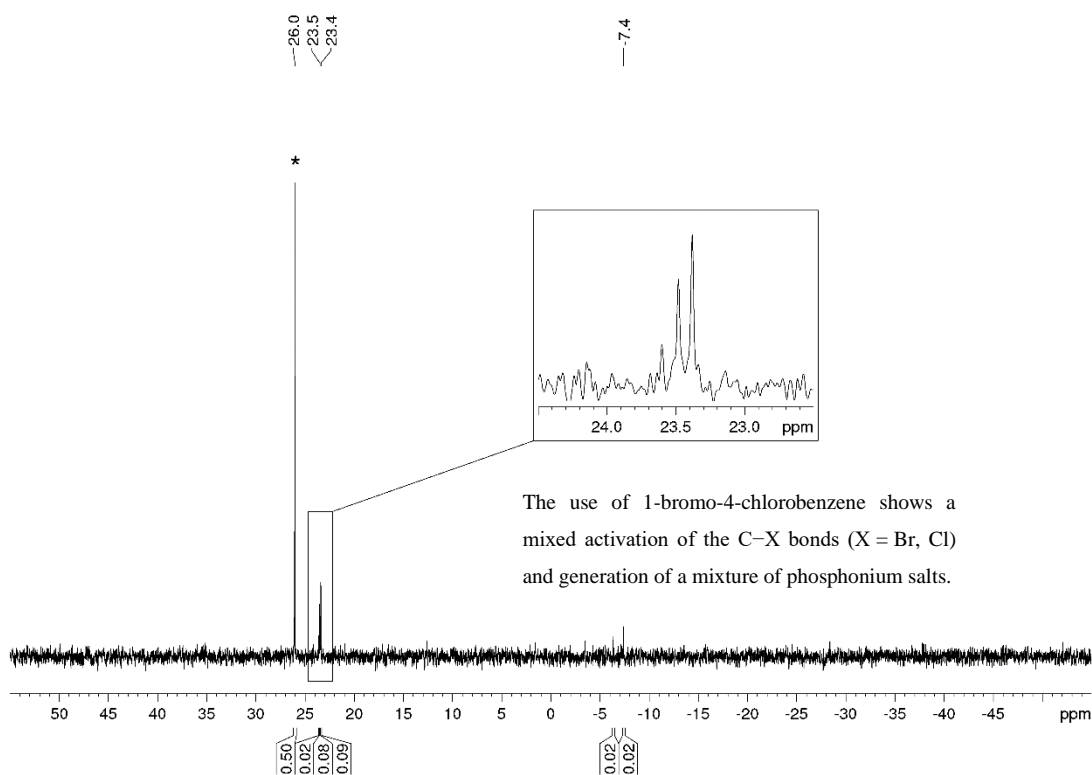


Figure S21. Quantitative single scan ³¹P{¹H} (zgif) NMR spectrum for the photochemical functionalization of P₄ using 1-bromo-4-chlorobenzene. * marks the internal standard Ph₃PO (0.02 mmol).

S4.18 Unsuccessful substrate scope

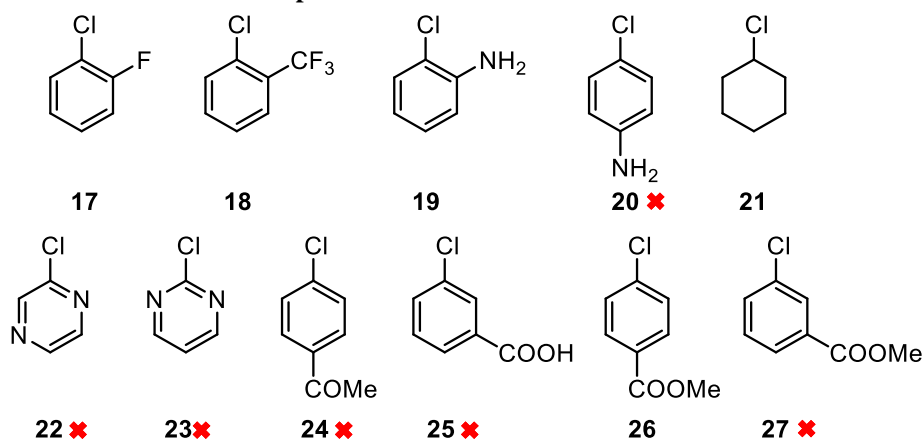


Figure S22. Further substrate scope for photochemical P_4 functionalization. These substrates were not able to generate the corresponding phosphonium salts and phosphines. The reactions with the substrates highlighted with a red sign did not show full conversion of P_4 by $^{31}P\{^1H\}$ NMR. Substrates **17**, **19**, **20** and **22-25** showed no signal beside the internal standard PPh_3O and P_4 (see red signs above, no P_4 in the reactions with **17** and **19**). Using substrates **18**, **21**, **26** and **27** (P_4 still left) the $^{31}P\{^1H\}$ NMR showed very unselective reactions with a lot of unknown side-products, but no product formation.

S5. Isolation and characterization of selected products

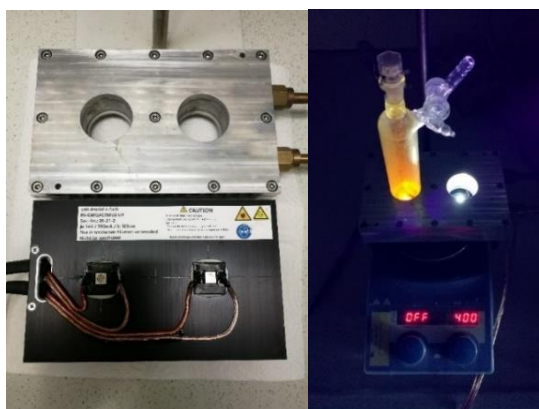


Figure S23. Illustration of the equipment setup used for photochemical reactions at 0.8 mmol scale.

S5.1 Photochemical preparation of tetraphenylphosphonium chloride from P₄ (0.8 mmol scale)

To a 100 mL stoppered tube equipped with a stirring bar were added chlorobenzene (8.0 mmol, 10 equiv. based on the phosphorus atom), organic photoreductant TDAE^[20] (4.0 mmol, 5 equiv. based on the phosphorus atom), and P₄ (0.2 mmol, 1 equiv., as a stock solution in 1.426 mL benzene). The mixture was dissolved in acetone (5 mL). The tube was sealed, placed in a water-cooled block (to ensure a near-ambient temperature was maintained, Figure S21), and irradiated with UV light (365 nm, 14 V, 700 mA, Osram OSOLON SSL 80) for 20 h. Quantitative ³¹P{¹H} (zgig) NMR spectroscopy (Ph₃PO as internal standard) showed 54% tetraphenylphosphonium chloride and 8% triphenylphosphine (see Figure S24).

The reaction mixture was filtered to remove the side product [TDAE]Cl₂ which was formed during the reaction. The solvent was evaporated *in vacuo* and the red orange waxy residue was washed with diethyl ether (4 x 3 mL) to separate the unreacted chlorobenzene, TDAE and the intermediate triphenylphosphine (Ph₃P) and tetraphenyldiphosphine (Ph₄P₂) from the tetraphenylphosphonium chloride. The residue was dissolved in H₂O (8 mL) and filtered. Subsequently, aqueous HCl (1 M, 10 mL) was added to the filtrate, and the solution was extracted with DCM (3 x 15 mL). The combined organic phases were dried over anhydrous Na₂SO₄, and the solvent was removed under reduced pressure. Subsequently, the light-yellow residue was redissolved in DCM. Addition of *n*-hexane to the DCM solution afforded NMR-spectroscopically pure tetraphenylphosphonium chloride as a white solid after filtration (57.2 mg, 19%).

The characterization data of the product are consistent with the data found in the literature.^[36]

¹H NMR (400 MHz, CDCl₃): δ[ppm] 7.94-7.90 (m, 4H), 7.81 (dt, *J* = 7.8, 3.5 Hz, 8H), 7.64 (dd, *J* = 12.9, 7.6 Hz, 8H).

¹³C{¹H} NMR (100 MHz, CDCl₃): δ[ppm] 135.8 (d, *J* = 3.0 Hz), 134.5 (d, *J* = 10.3 Hz), 130.9 (d, *J* = 12.9 Hz), 117.5 (d, *J* = 89.5 Hz).

³¹P{¹H} NMR (162 MHz, CDCl₃): δ[ppm] 23.8.

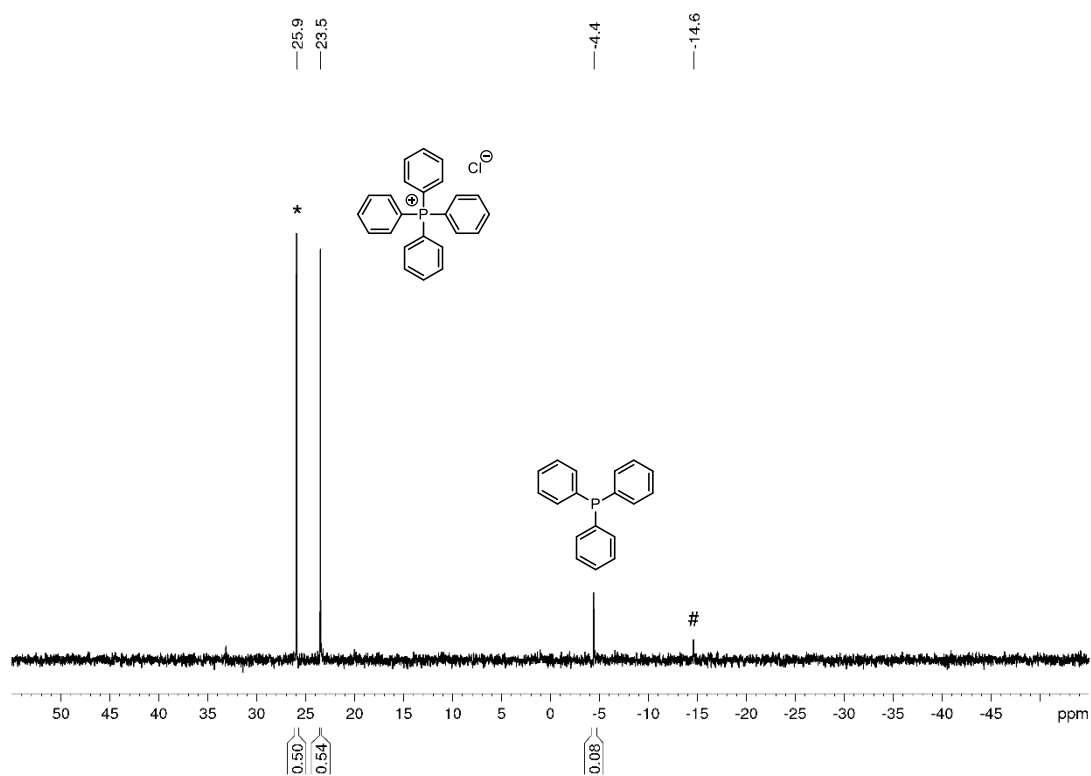


Figure S24. Quantitative single scan ³¹P{¹H} (zgig) NMR spectrum for the scale-up photochemical functionalization of P₄ using chlorobenzene. * marks the internal standard Ph₃PO. # marks the intermediate Ph₄P₂.

Chapter 2. Photochemical Transformation of Chlorobenzenes and White Phosphorus into Arylphosphines and Phosphonium salts

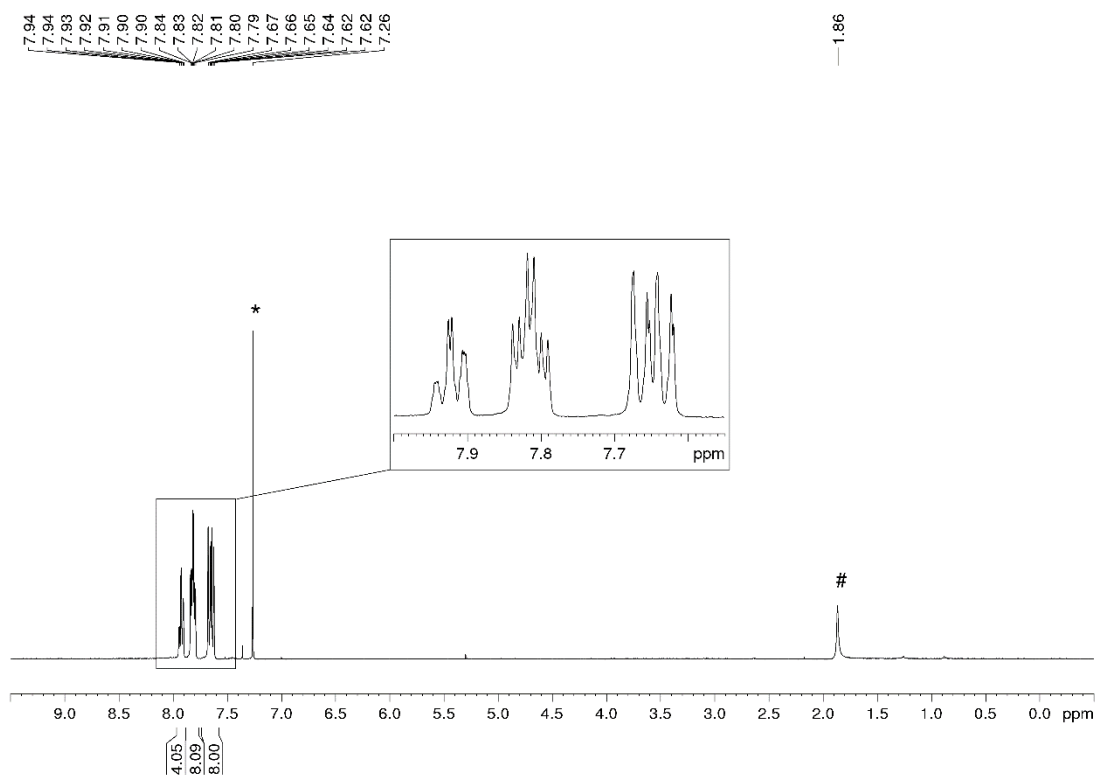


Figure S25. ^1H NMR spectrum of tetraphenylphosphonium chloride prepared photochemically from P_4 at 0.8 mmol scale. * marks CDCl_3 . # marks adventitious H_2O .

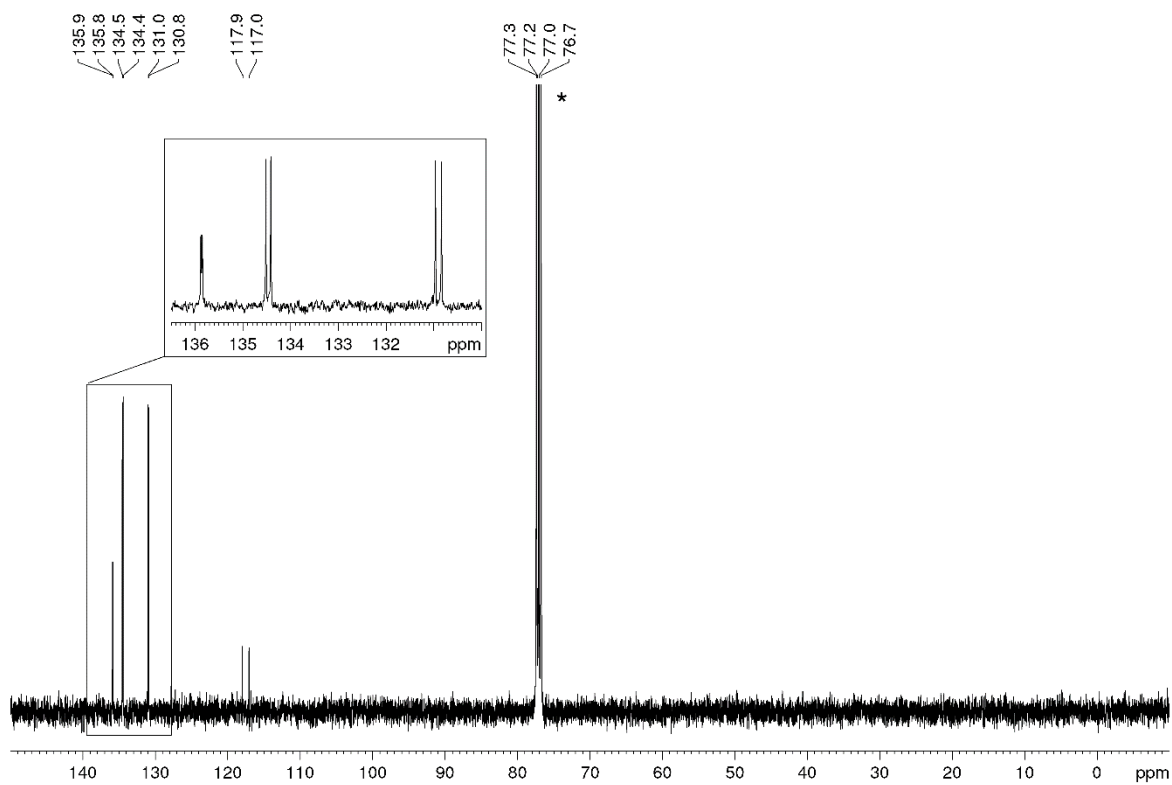


Figure S26. ^{13}C NMR spectrum of tetraphenylphosphonium chloride prepared photochemically from P_4 at 0.8 mmol scale. * marks CDCl_3 .

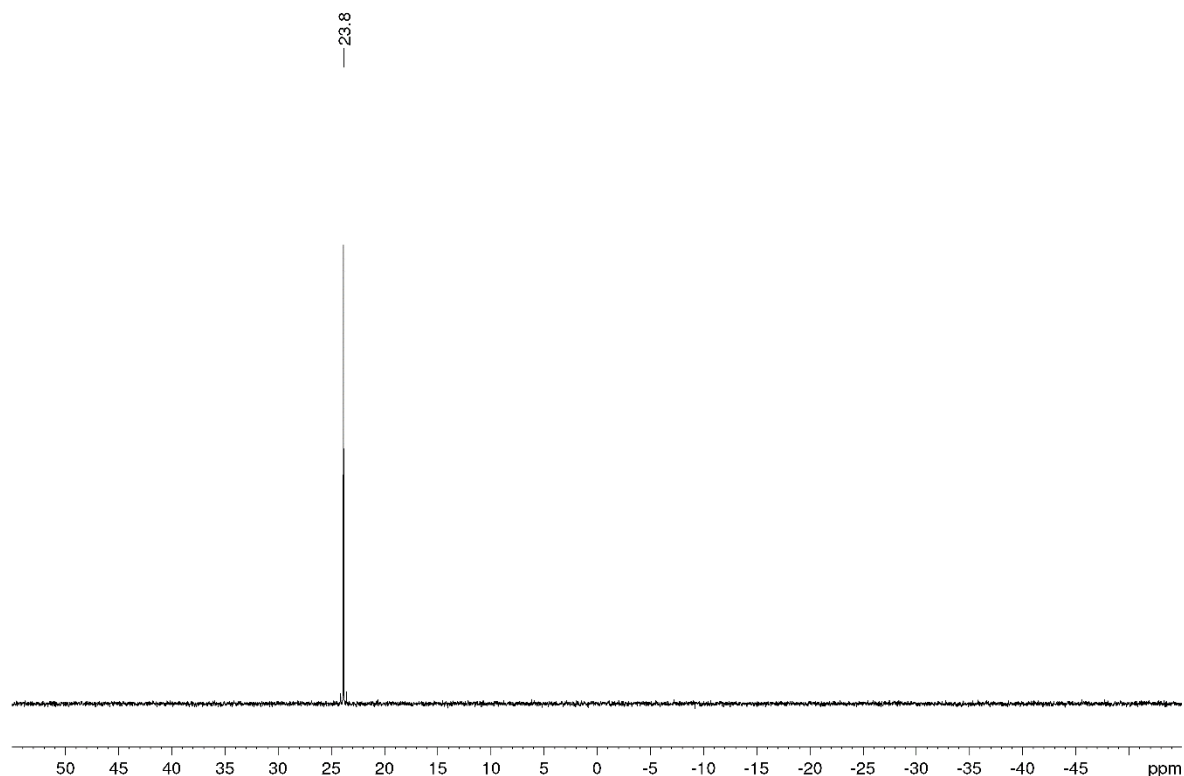


Figure S27. $^{31}\text{P}\{^1\text{H}\}$ NMR spectrum of tetraphenylphosphonium chloride prepared photochemically from P_4 at 0.8 mmol scale.

S5.2 Photochemical preparation of tris(phenylethyl)phosphine from P_4 (0.8 mmol scale)

All operations were carried out under inert gas atmosphere. To a 100 mL stoppered tube equipped with a stirring bar were added (2-chloroethyl)benzene (8.0 mmol, 10 equiv. based on the phosphorus atom), organic photoreductant TDAE^[20] (4.0 mmol, 5 equiv. based on the phosphorus atom), and P_4 (0.2 mmol, 1 equiv., as a stock solution in 1.426 mL benzene). The mixture was dissolved in acetone (5 mL). The tube was sealed, placed in a water-cooled block (to ensure a near-ambient temperature was maintained, Figure S21), and irradiated with UV light (365 nm, 14 V, 700 mA, Osram OSRON SSL 80) for 20 h. The reaction mixture was filtered to remove the side product $[\text{TDAE}]\text{Cl}_2$. The solvent, unreacted (2-chloroethyl)benzene and TDAE were evaporated *in vacuo* at 80 °C (ca. $2 \cdot 10^{-2}$ mbar). The side product 1,4-diphenylbutane was removed by distillation at low pressure (ca $1 \cdot 10^{-2}$ mbar) by warming the flask with a heat gun. The product tris(phenylethyl)phosphine was distilled from the remaining orange oil on a high vacuum pump ($1 \cdot 10^{-5}$ mbar) while heating with a heat gun to 300 °C (40.1 mg, 14%).

The characterization data of the product are consistent with the data found in the literature.^[37]

^1H NMR (400 MHz, C_6D_6): δ [ppm] 7.19-7.05 (m, 15H & C_6D_6), 2.66-2.60 (m, 6H), 1.59-1.55 (m, 6H).

$^{13}\text{C}\{^1\text{H}\}$ NMR (100 MHz, C_6D_6): δ [ppm] 142.9 (d, $J = 10.1$ Hz), 128.4 (s), 128.2 (s), 125.9 (s), 32.4 (d, $J = 15.2$ Hz), 29.3 (d, $J = 15.9$ Hz).

$^{31}\text{P}\{^1\text{H}\}$ NMR (162 MHz, C_6D_6): δ [ppm] -27.7.

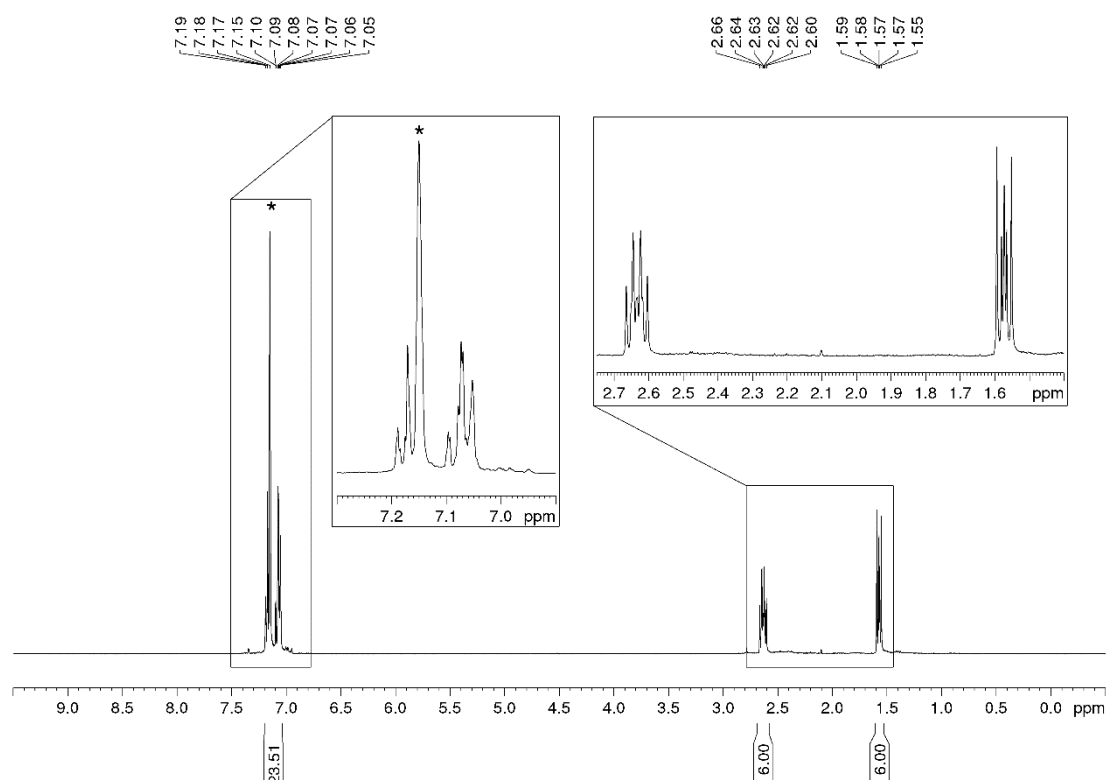


Figure S28. ^1H NMR spectrum of tris(phenylethyl)phosphine prepared photochemically from P_4 at 0.8 mmol scale. * marks C_6D_6 .

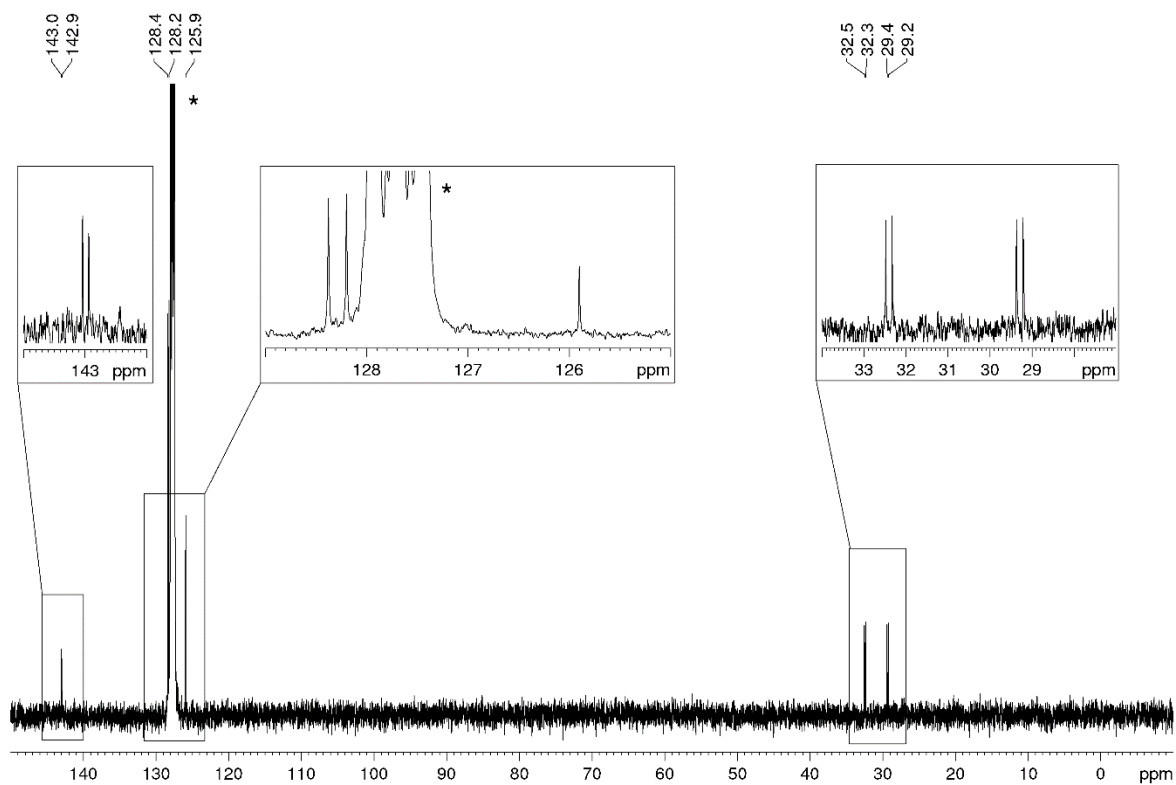


Figure S29. ^{13}C NMR spectrum of tris(phenylethyl)phosphine prepared photochemically from P_4 at 0.8 mmol scale. * marks C_6D_6 .

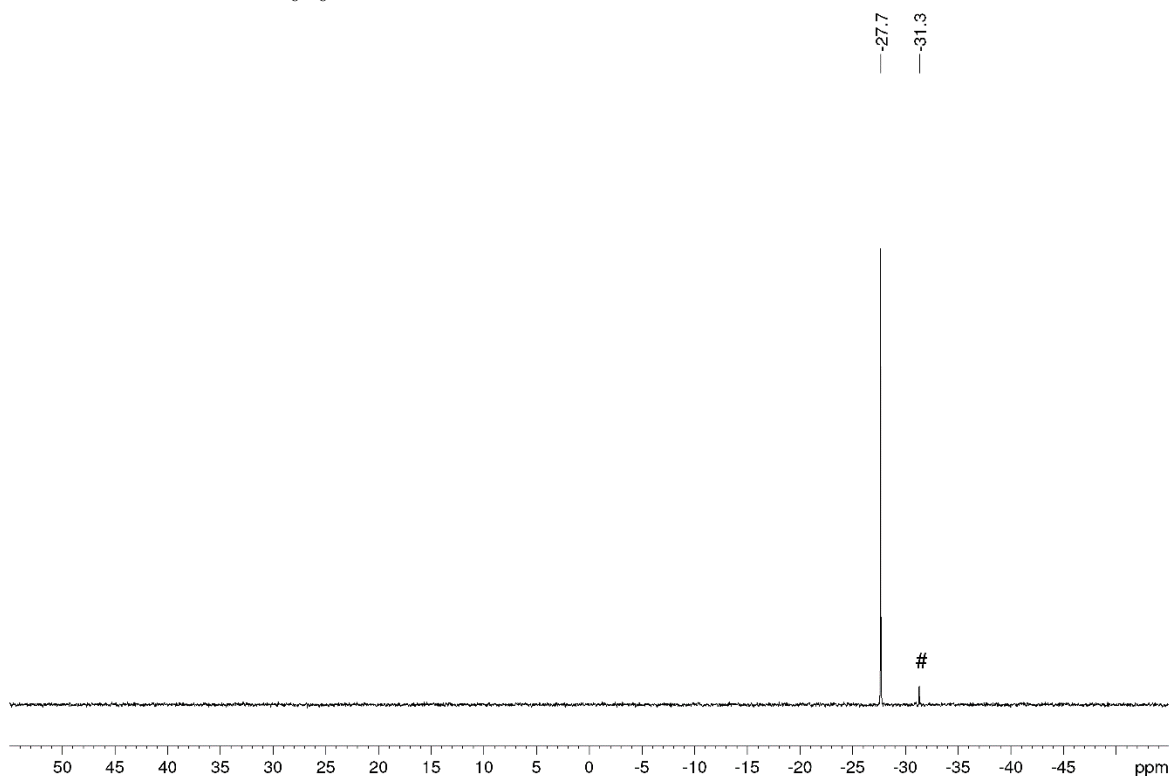


Figure S30. $^{31}\text{P}\{^1\text{H}\}$ NMR spectrum of tris(phenylethyl)phosphine prepared photochemically from P_4 at 0.8 mmol scale. # marks an unknown impurity.

S6. *In situ* NMR experiments

The apparatus used for *in situ* NMR reaction monitoring with *in situ* illumination has been reported previously.^[31] The insert and the NMR tube were connected with the screw cap of a recently published UVNMR-illumination device to enable measurements under inert conditions.^[32] Two FEP (fluorinated ethylene propylene) coated rubber septa increased the attachment between the insert and the tube. (Figure S31). The same illumination apparatus was used for *in situ* NMR reaction monitoring with *in situ* illumination that was used in previous investigations of the light-driven arylation of P₄.^{[8],[10]}

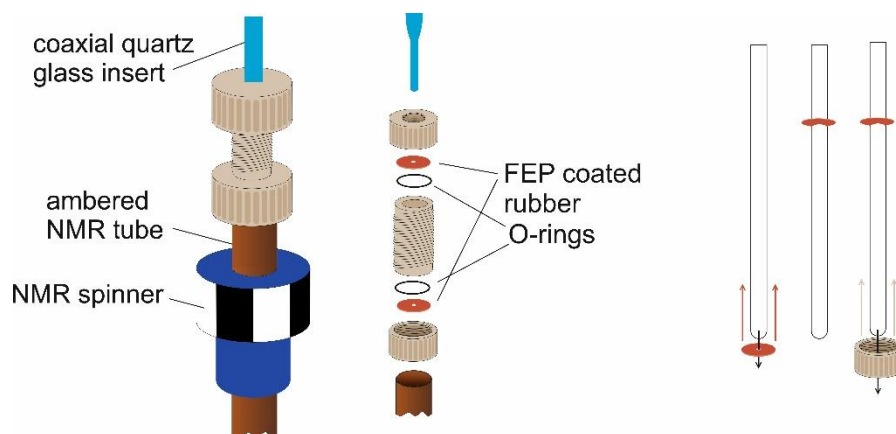


Figure S31. Schematic representation showing connection between the ambered NMR tube and illuminating insert used for *in situ* NMR reaction monitoring.

A 365 nm LED (LEUVA66 from Lasercomponents) was employed for sample illumination inside the NMR spectrometer. The spectra were recorded at 298 K and processed with *Bruker TopSpin 4.0.3*.

In order to cover the full chemical shift range of the ³¹P-NMR signals occurring during the reaction monitoring within a single spectrum, the spectra were recorded with broadband excitation using the broadband pulse shapes “xyBEBOP” (excitation window of 500 kHz with a pulse duration of 500 ms) kindly provided to us by Prof. Dr. Burkhard Luy.^[38]

The spectra were recorded with ¹H-decoupling (power gated decoupling) to increase the signal-to-noise ratio of potential intermediates. Therefore, the reaction monitoring gives no quantitative but qualitative information about the kind and sequence of phosphorus species. For integration, these spectra were processed with magnitude calculation (*mc*) and the baseline was corrected automatically with the command *absn*.

Measurements were conducted on a *Bruker Avance NEO 600* (600 MHz) spectrometer equipped with a double resonance broad band probe (BBO). NMR frequencies were referenced externally and are given in parts per million (ppm). ¹H and ¹³C frequencies are referenced to TMS (tetramethylsilane) and ³¹P to H₃PO₄ (85 wt. % in H₂O). ¹H-NMR

spectra were calibrated on the solvent residual peak of acetone- d_6 (2.05 ppm). In case non-deuterated acetone was used as solvent, the ^1H -NMR of acetone was calibrated to 2.08 ppm (due to isotopic shift between acetone- d_2 to acetone- d_1 and probably further to acetone- d_0 of 10 Hz each on the 600 MHz spectrometer; see Figure S32). Heteronuclear spectra (^{13}C and ^{31}P) were then calibrated using the unified scaling procedure recommended by IUPAC.^[39]

S6.1 Procedure for ^{31}P and ^1H monitoring of the model reaction

The reaction mixture was prepared in accordance with the general procedure for photochemical functionalization of P_4 in a 0.01 mmol scale (section S2) using chlorobenzene as the substrate, with the exception that deuterated acetone- d_6 (CD_3) $_2\text{CO}$ was used as solvent. A 300 μL aliquot of this reaction mixture was then taken for NMR reaction monitoring. The reaction mixture was prepared under inert atmosphere (N_2) in an ambered NMR-tube. The *in situ* illumination device was inserted into the tube and fastened with the screw cap.

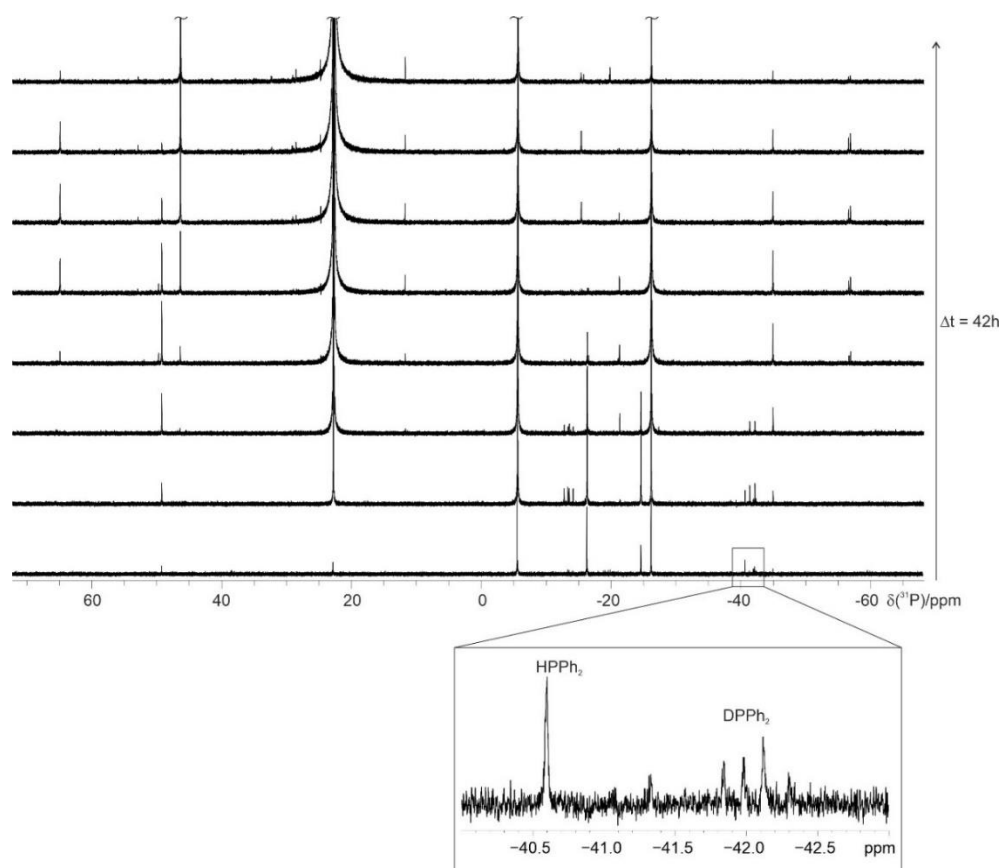


Figure 32. *In situ* $^{31}\text{P}\{^1\text{H}\}$ NMR monitoring of the model reaction (time = 42 h). Deuterium incorporation of deuterated acetone- d_6 into the arylated HPPh_2 forming a mixture of deuterated and non-deuterated intermediates.

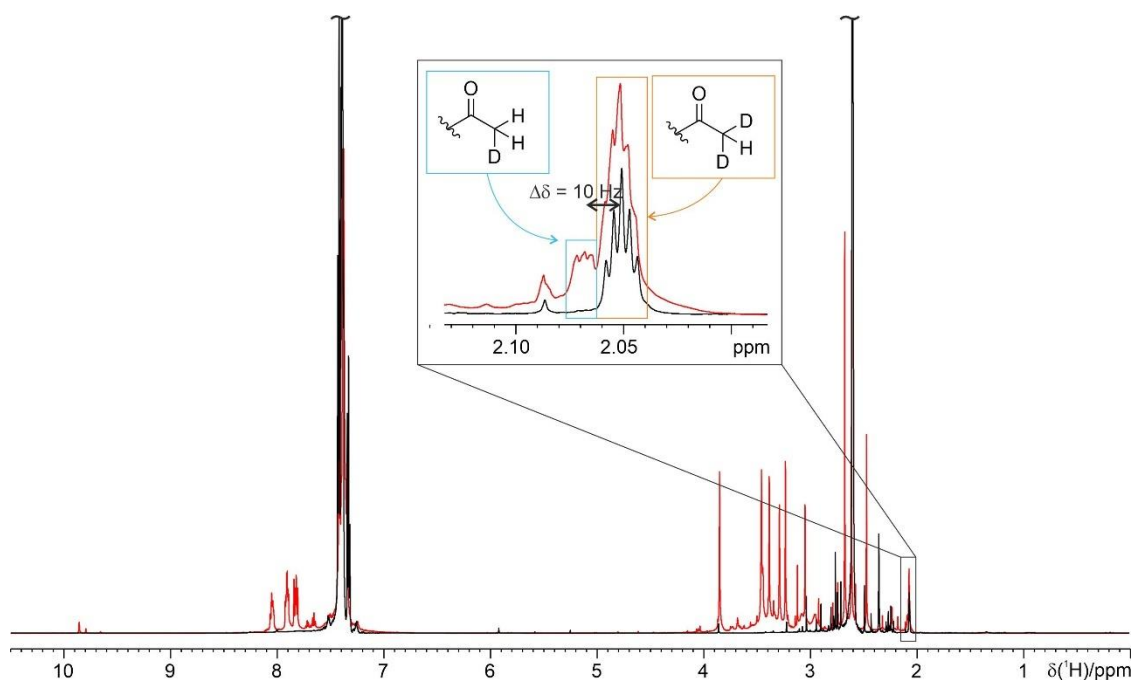


Figure S33. *In situ* ^1H NMR monitoring of the model reaction showed that monodeuterated acetone is generated indicating the presence of H/D exchange processes during the reaction.

S6.2 NMR Investigations of the Intermediate Int1

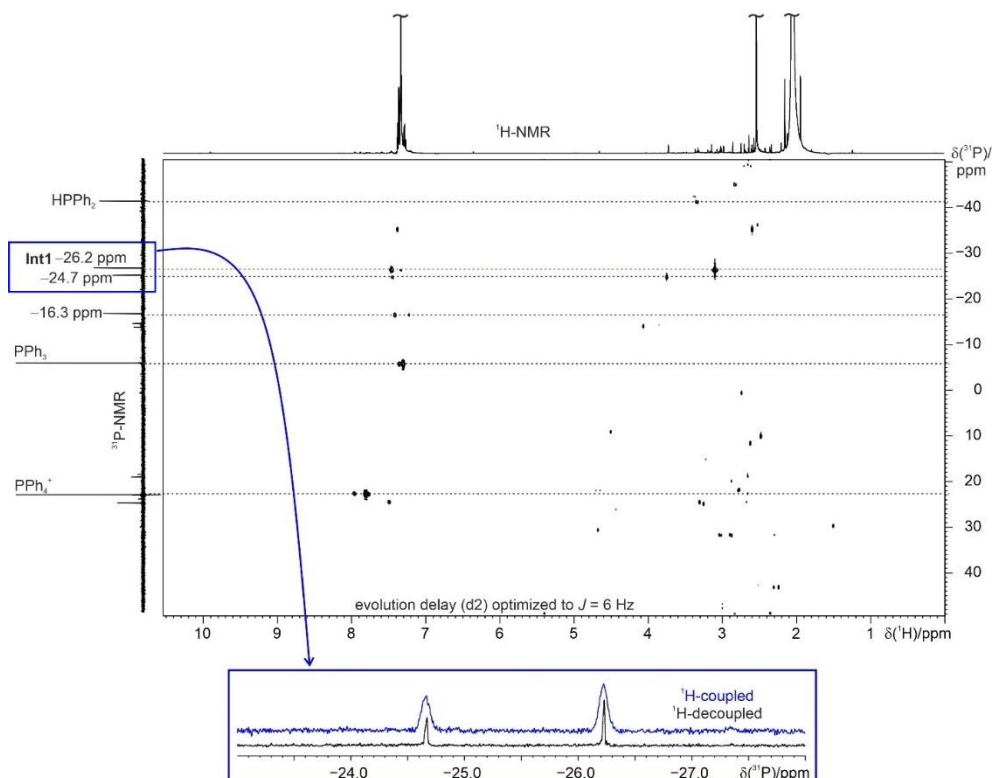


Figure S34. 2D ^1H - ^{31}P -HMOC experiment recorded of the model reaction after irradiation for one hour. $^{31}\text{P}\{^1\text{H}\}$ -NMR experiments indicated only small couplings between ^1H and ^{31}P for the intermediate **Int1**.

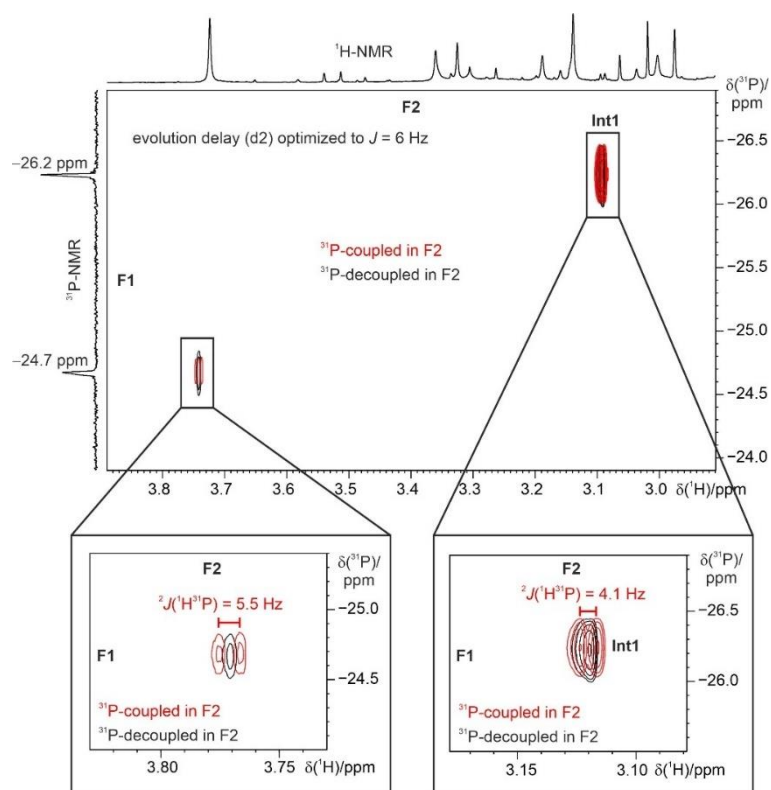


Figure S35. 2D ^1H - ^{31}P -HMQC experiment recorded of the model reaction after irradiation for one hour.

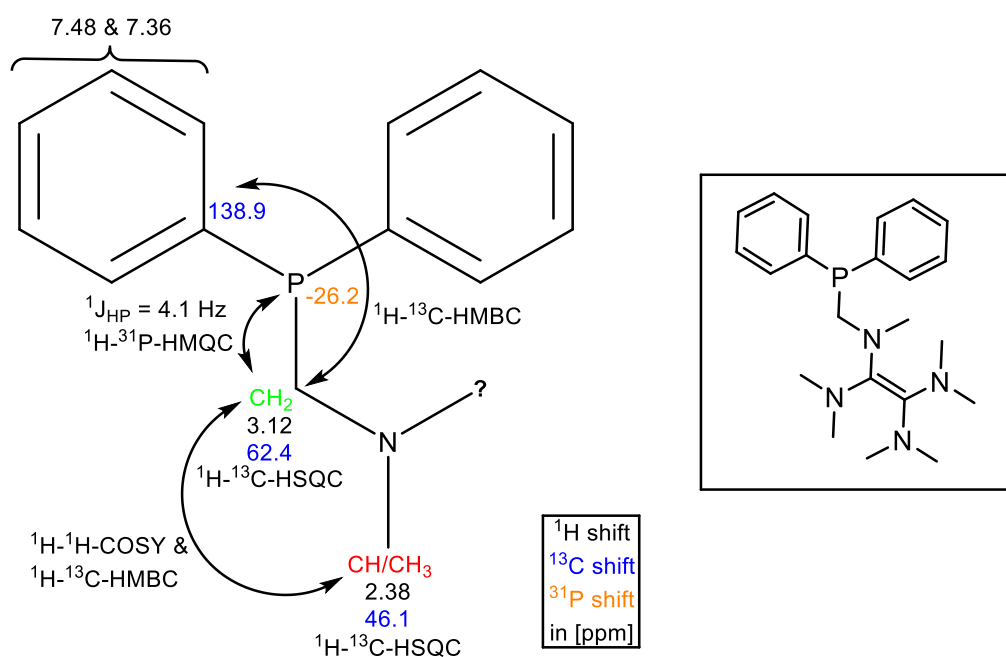
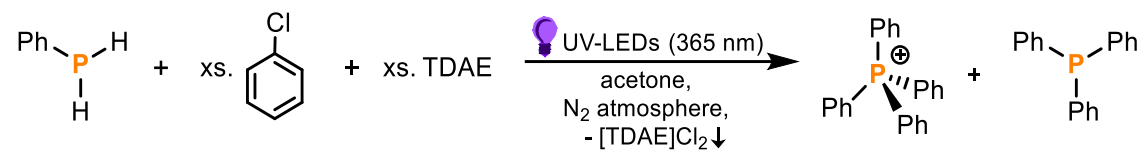


Figure S36. Left: Proposed structural core of the intermediate **Int1** based on combination of its ^{31}P chemical shift, ^1H - ^{31}P -HMQC, ^1H - ^{13}C -HSQC and -HMBC, ^1H - ^1H -COSY experiments and comparison with literature data.^[28] Right: Proposed structure fitting to the chemical context of the here investigated reactions.

S7. Photochemical phenylation of PhPH₂, Ph₂PH, Ph₄P₂ and Ph₃P

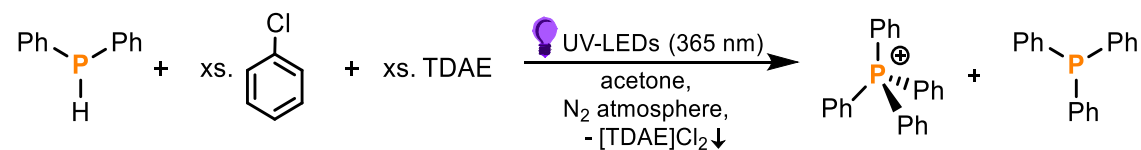
Table S9. Photochemical functionalization of PhPH₂ to [Ph₄P]Cl.^{[a][b]}



Entry	Conditions ^{[a][b]} TDAE:PhCl	Conv. to [Ph ₄ P]Cl / %	Conv. to Ph ₃ P / %	Intermediates	Consumption of PhPH ₂ / %
1	3:6	52	24	Ph ₄ P ₂ (4), Int1 (5)	100
2	TDAE (3 equiv.) no PhCl	–	–	unselective	92
3	5:10	68%	9	–	100

[a] The general procedure for reactions at 0.04 mmol scale (section S2) was modified by replacing P₄ with PhPH₂ (4.4 μL, 0.04 mmol). [b] Listed equivalents are defined per P atom.

Table S10. Photochemical functionalization of Ph₂PH to [Ph₄P]Cl.^{[a][b]}

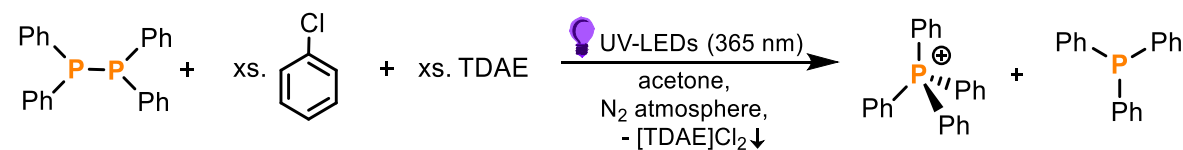


Entry	Conditions ^{[a][b]} TDAE:PhCl	Conv. to [Ph ₄ P]Cl / %	Conv. to Ph ₃ P / %	Intermediates	Consumption of Ph ₂ PH / %
1	3:6	76	15	Int1 (16)	100
2	TDAE (3 equiv.) no PhCl	0	5	P ₂ Ph ₄ (40)	78
3	5:10	41	4	3	100

[a] The general procedure for reactions at 0.04 mmol scale (section S2) was modified by replacing P₄ with Ph₂PH (7.0 μL, 0.04 mmol). [b] Listed equivalents are defined per P atom.

Chapter 2. Photochemical Transformation of Chlorobenzenes and White Phosphorus into Arylphosphines and Phosphonium salts

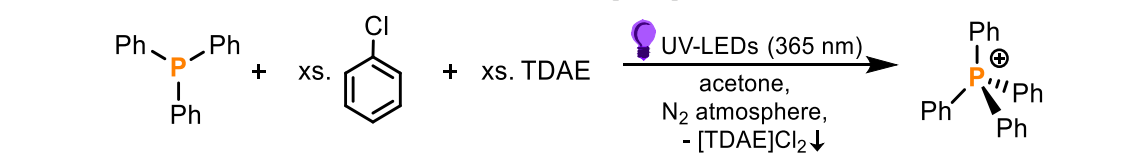
Table S11. Photochemical functionalization of **Ph₄P₂** to [Ph₄P]Cl.^{[a][b]}



Entry	Conditions ^{[a][b]} TDAE:PhCl	Conv. to [Ph ₄ P]Cl / %	Conv. to Ph ₃ P / %	Intermediates	Consumption of Ph ₄ P ₂ / %
1	1.5:3	55	28	Int1 (8)	100
2	TDAE (2 equiv.) no PhCl	0	6	PPh ₂ H (6)	68
3	3:3	39	28	Int1 (8), PPh ₂ H (3)	100
4	3:6	55	5	Int1	100
5	5:10	44	6	Int1	100

[a] The general procedure for reactions at 0.04 mmol scale (section S2) was modified by replacing P₄ with Ph₄P₂ (7.4 mg, 0.02 mmol). [b] Listed equivalents are defined per P atom.

Table S12. Photochemical functionalization of **Ph₃P** to [Ph₄P]Cl.^{[a][b]}

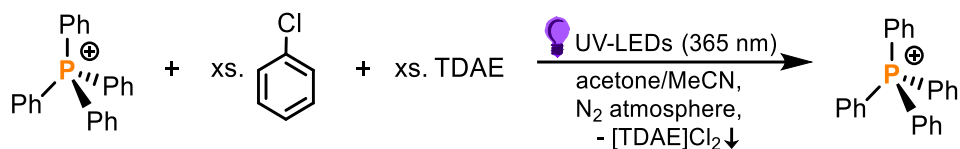


Entry	Conditions ^{[a][b]} TDAE:PhCl	Conv. to [Ph ₄ P]Cl / %	Leftover Ph ₃ P / %	Consumption of PPh ₃ / %
1	1.5:3	36	5	95
2	TDAE (1.5 equiv.) no PhCl	–	92	8
3	3:6	55	0 ^[~]	100
4	5:10	43	0 ^[~]	100

[a] The general procedure for reactions at 0.04 mmol scale (section S2) was modified by replacing P₄ with Ph₃P (10.5 mg, 0.04 mmol). [b] Listed equivalents are defined per P atom.). [~] Signal in the ³¹P{¹H} NMR (NS 256), but too small to determine the yield in the quantitative ³¹P{¹H} NMR (NS 1).

Chapter 2. Photochemical Transformation of Chlorobenzenes and White Phosphorus into Arylphosphines and Phosphonium salts

Table S13. Stability test of phosphonium salt $[\text{Ph}_4\text{P}]\text{Cl}$ toward photochemical conditions.^{[a][b]}



Entry	Conditions ^{[a][b]} TDAE:PhCl	Leftover [Ph ₄ P]Cl / %	Decomposition ^[c] of [Ph ₄ P]Cl / %
1	1.5:3	56	44 ^[c]
2	TDAE (1.5 equiv) no PhCl	80	12 (8) ^[d]
3	5:10	37	63 ^[c]

[a] The general procedure for reactions at 0.04 mmol scale (section S2) was modified by replacing P_4 with $[\text{Ph}_4\text{P}]\text{Cl}$ (15.0 mg, 0.04 mmol) for stability check of the phosphonium salt under the photochemical conditions. For better solubility of the phosphonium salt a mixture of acetone (0.5 mL) and MeCN (0.2 mL) was used. [b] Listed equivalents are defined per P atom. [c] No decomposition or other signals appear in the $^{31}\text{P}\{^1\text{H}\}$ NMR. [d] Decomposition to the triphenylphosphine Ph_3P .

S8. Side product [TDAE]Cl₂

The side product [TDAE]Cl₂^[33] can be recovered by simple filtration of the reaction mixture and recrystallization by slow diffusion of acetone into a DMSO solution which resulted in colorless crystals.

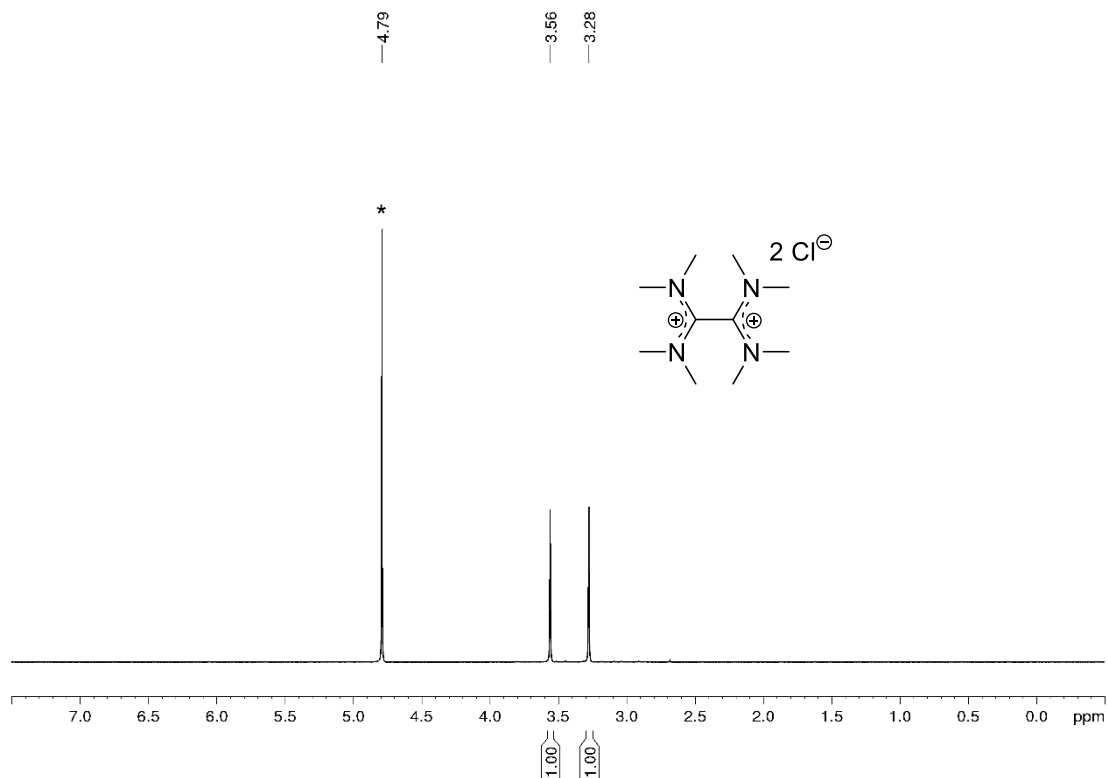


Figure S37. ¹H NMR spectrum (400.13 MHz, 300 K, D₂O) of byproduct [TDAE]Cl₂. * marks D₂O.

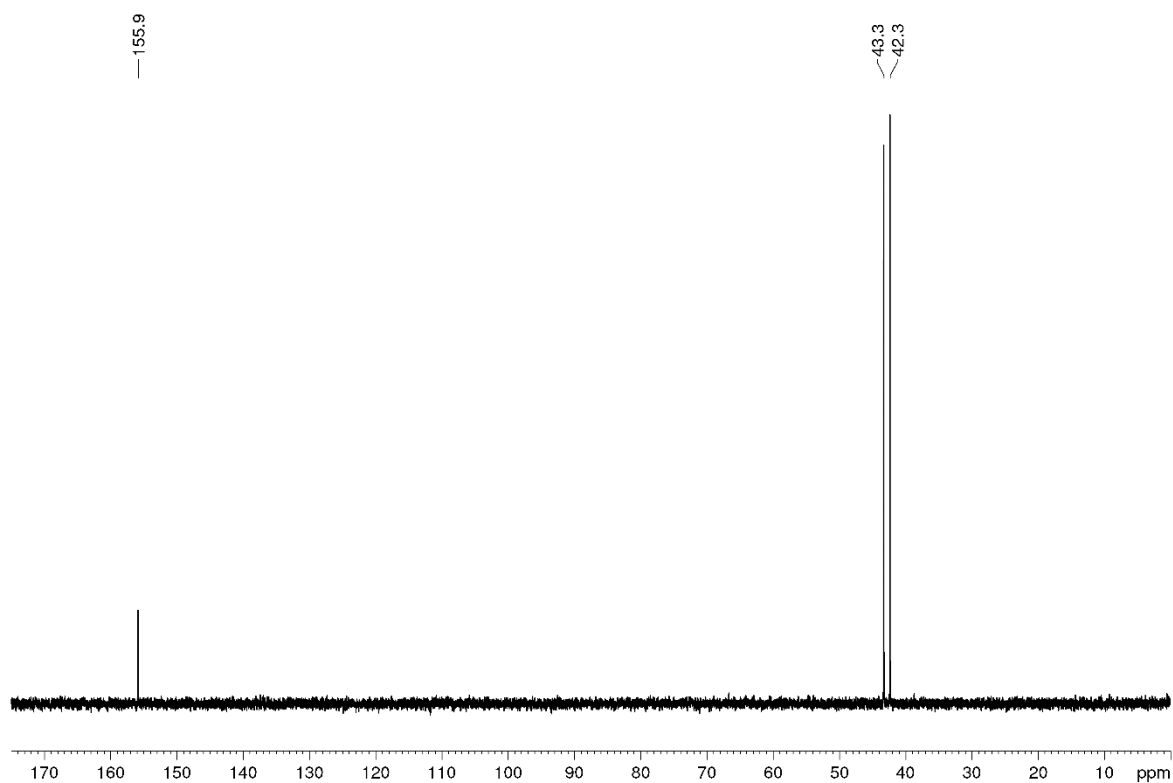


Figure S38. ¹³C{¹H} NMR spectrum (100.61 MHz, 300 K, D₂O) of byproduct [TDAE]Cl₂.

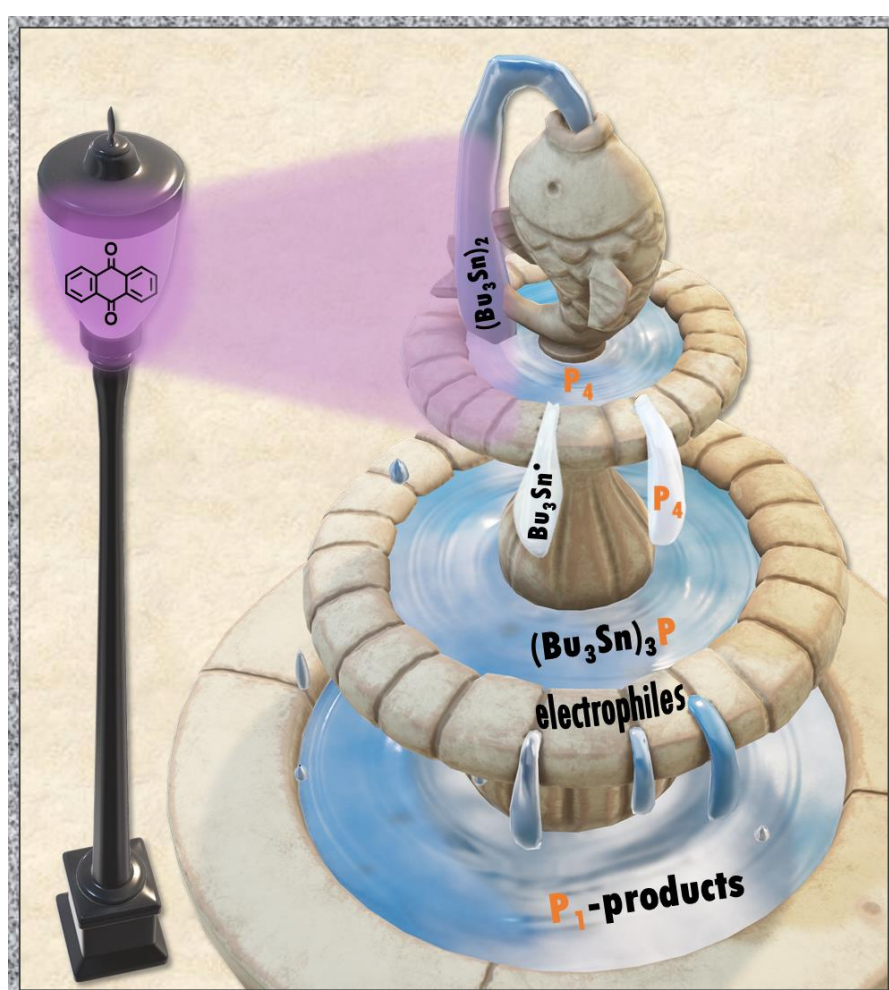
2.5 References

- [1] G. Bettermann, W. Krause, G. Riess and T. Hofmann, *Ullmann's Encyclopedia of Industrial Chemistry* (Wiley), 2000.
- [2] D. E. C. Corbridge, *Chemistry, Biochemistry and Technology* (Elsevier), 2000.
- [3] C. M. Hoidn, D. J. Scott and R. Wolf, *Chem. Eur. J.*, 2021, **27**, 1886–1902.
- [4] D. H. R. Barton and J. Zhu, *J. Am. Chem. Soc.*, 1993, **115**, 2071–2072.
- [5] D. H. R. Barton and R. A. Vonder Embse, *Tetrahedron*, 1998, **54**, 12475–12496
- [6] B. M. Cossairt and C. C. Cummins, *J. Chem.*, 2010, **34**, 1533–1536.
- [7] S. K. Ghosh, C. C. Cummins and J. A. Gladysz, *Org. Chem. Front.*, 2018, **5**, 3421–3429.
- [8] U. Lennert, P. B. Arockiam, V. Streitferdt, D. J. Scott, C. Rödl, R. M. Gschwind and R. Wolf, *Nat. Catal.*, 2019, **2**, 1101–1106.
- [9] P. B. Arockiam, U. Lennert, C. Graf, R. Rothfelder, D. J. Scott, T. G. Fischer, K. Zeitler and R. Wolf, *Chem. Eur. J.*, 2020, **26**, 16374–16382.
- [10] R. Rothfelder, V. Streitferdt, U. Lennert, J. Cammarata, D. J. Scott, K. Zeitler, R. M. Gschwind and R. Wolf, *Angew. Chem. Int. Ed.*, 2021, **60**, 24650–24658.
- [11] N. G. W. Cowper, C. P. Chernowsky, O. P. Williams and Z. K. Wickens, *J. Am. Chem. Soc.*, 2020, **142**, 2093–2099.
- [12] For direct organofunctionalization of P₄ using Sn-based radicals: D. J. Scott, J. Cammarata, M. Schimpf and R. Wolf, *Nat. Chem.*, 2021, **13**, 458–464.
- [13] a) D. G. Yakhvarov, E. V. Gorbachuk, R. M. Kagirov and O. G. Sinyashin, *Russ. Chem. Bull.*, 2012, **61**, 1300–1312; b) D. G. Yakhvarov, E. V. Gorbachuk and O. G. Sinyashin, *Eur. J. Inorg. Chem.*, 2013, 4709–4726; c) Y. H. Budnikova, T. V. Gryaznova, V. V. Grinenko, Y. B. Dudkina and M. N. Khrizanforov, *Pure Appl. Chem.*, 2017, **89**, 311–330.
- [14] L. Huang, L. K. G. Ackerman, K. Kang, A. M. Parsons and D. J. Weix, *J. Am. Chem. Soc.*, 2019, **141**, 10978–10983.
- [15] A. F. Chmiel, O. P. Williams, C. P. Chernowsky, C. S. Yeung and Z. K. Wickens, *J. Am. Chem. Soc.*, 2021, **143**, 10882–10889.
- [16] M. Cybularczyk-Cecotka, J. Szczepanik and M. Giedyk, *Nat. Catal.*, 2020, **3**, 872–886.
- [17] I. Ghosh, T. Ghosh, J. I. Bardagi and B. König, *Science*, 2014, **346**, 725–728.
- [18] H. Kim, H. Kim, T. H. Lambert and S. Lin, *J. Am. Chem. Soc.*, 2020, **142**, 2087–2092.
- [19] N. Kvasovs and V. Gevorgyan, *Chem. Soc. Rev.*, 2021, **50**, 2244–2259.
- [20] F. Glaser, C. B. Larsen, C. Kerzig and O. S. Wenger, *Photochem. Photobiol. Sci.*, 2020, **19**, 1035–1041.
- [21] L. Pause, M. Robert and J. M. Savéant, *J. Am. Chem. Soc.*, 1999, **121**, 7158–7159.
- [22] C. Burkholder, W. R. Dolbier Jr. and M. Médebielle, *J. Org. Chem.*, 1998, **63**, 5385–5394.

- [23] T. Fuchigami, M. Atobe and S. Inagi, *Fundamentals and Applications of Organic Electrochemistry: Synthesis, Materials, Devices* (John Wiley & Sons, Chichester, West Sussex, U. K.), 2015.
- [24] J. Mortensen and J. Heinze, *Angew. Chem., Int. Ed. Engl.*, 1984, **23**, 84–85.
- [25] C. J. Zeman, IV, S. Kim, F. Zhang and K. S. Schanze, *J. Am. Chem. Soc.*, 2020, **142**, 2204–2207.
- [26] C. P. Andrieux and J. Pinson, *J. Am. Chem. Soc.*, 2003, **125**, 14801–14806.
- [27] M. Mahesh, J. A. Murphy, F. LeStrat and H. P. Wessel, *Beilstein J. Org. Chem.*, 2009, **5**.
- [28] E. G. Bowes, D. D. Beattie and J. A. Love, *Inorg. Chem.*, 2019, **58**, 5, 2925–2929.
- [29] P. J. Delaive, T. K. Foreman, C. Giannotti and D. G. Whitten, *J. Am. Chem. Soc.*, 1980, **102**, 5627–5631.
- [30] Y. Pellegrin and F. Odobel, *C. R. Chim.*, 2017, **20**, 283–295.
- [31] C. Feldmeier, H. Bartling, E. Riedle and R. M. Gschwind, *J. Magn. Reson.*, 2013, **232**, 39–44.
- [32] A. Seegerer, P. Nitschke, and R. M. Gschwind, *Angew. Chem. Int. Ed.*, 2018, **57**, 7493–7497.
- [33] C. Knopf, U. Herzog, G. Roewer, E. Brendler. G. Rheinwald and H. Lang, *J. Organomet. Chem.*, 2002, **662**, 14–22.
- [34] N. Wiberg and J. W. Buchler, *Chem. Ber.*, 1963, **96**, 3223–3229.
- [35] Q. Zhang, S. Zhang and S. Li, *Macromolecules*, 2012, **45**, 2981–2988.
- [36] D. Marcoux and A. B. Charrette, *J. Org. Chem.*, 2008, **73**, 590–593.
- [37] a) T. Bartik, B. Bartik, B. E. Hanson, I. Guo and I. Tóth, *Organometallics*, 1992, **12**, 164–170; b) L. Brandsma, S. Arbuzova, R. J. De Lang, N. Gusarova and B. Trofimov, *Phosphorus, Sulfur and Silicon*, 1997, **126**, 125–128.
- [38] C. Koch, *NMR Spectroscopic Investigations on Copper-Catalyzed Reactions and Zintl Anions*, University of Regensburg, 2015.
- [39] IUPAC, *Pure and Applied Chemistry*, **73**, 1795–1818.

3 Photocatalytic Stannylation of White Phosphorus^[a]

Abstract: Organophosphorus compounds (OPCs) are highly important chemicals, finding numerous applications in both academia and industry. Herein we describe a simple photocatalytic method for the stannylation of white phosphorus (P_4) using a cheap, commercially-available distannane, $(Bu_3Sn)_2$, and anthraquinone as a simple photocatalyst. Subsequent ‘one pot’ transformation of the resulting stannylated monophosphine intermediate $(Bu_3Sn)_3P$ provides direct, convenient and versatile access to valuable OPCs such as acylated phosphines and tetraalkylphosphonium salts.



Reproduced with permission from: M. Till, J. Cammarata, R. Wolf and D. J. Scott, *Chem. Commun.*, 2022, **58**, 8986–8989.

^[a] M. Till performed the reactions and the isolation and characterization of selected compounds. D. J. Scott and R. Wolf supervised and directed the project. M. Till and D. J. Scott wrote the manuscript with input from R. Wolf.

3.1 Introduction

White phosphorus (P_4) – the most chemically important allotrope of this ubiquitous and abundant element – acts as the common precursor from which all commercially valuable and academically important organophosphorus compounds (OPCs) are prepared. The current methods used for the industrial synthesis of these myriad useful P_1 products include the oxidation of P_4 with toxic Cl_2 gas to generate PCl_3 which can subsequently be transformed into a variety of OPCs by reaction with nucleophiles (Scheme 1a). As an alternative route, initial acid- or base-mediated disproportionation of P_4 can be used to generate highly toxic PH_3 gas which is then employed for the hydrophosphination of unsaturated organic substrates.^[1]

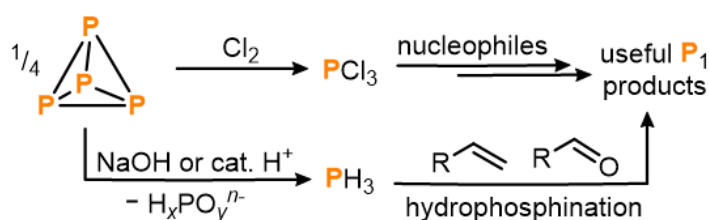
Given the drawbacks of these methods, a highly prominent aim has long been to find ways of bypassing these multi-step procedures. In particular, there is a longstanding desire to develop more step-efficient *direct* – and, ideally, *catalytic* – methods to functionalize P_4 and generate OPCs in a single reaction.

As a result, for several decades comprehensive efforts have been made to better understand the fundamental reactivity of P_4 .^[2] However, it is only very recently that it has finally become possible to successfully transform P_4 directly into a variety of useful P_1 products.^[3] Moreover, and despite these extensive investigations, the number of successful examples remains extremely low, and those that do exist still suffer from substantial limitations.^[4] As such, there remains a clear need to expand the range of strategies available for direct, productive P_4 activation, with new catalytic methods being particularly desirable.^[4a]

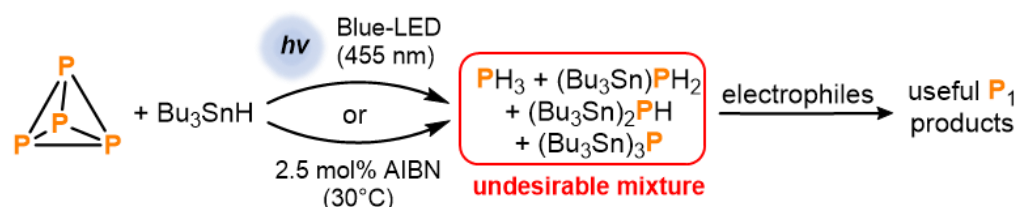
3.2 Results and Discussion

In one of our own contributions to this area, we recently reported a simple ‘one pot’ method in which the classical radical reagent tri-*n*-butyltin hydride (Bu_3SnH) is used for initial hydrostannylation of P_4 (Scheme 1b).^[5] This reductive P_4 activation is mediated either by light or by a chemical radical initiator such as AIBN (azobis(isobutyronitrile)) which can initiate a radical chain reaction that breaks down the P_4 tetrahedron, yielding a mixture of hydrostannylated phosphines $(Bu_3Sn)_xPH_{3-x}$ ($x = 0-3$). Key to this mechanism is the attack of stannyl radicals (Bu_3Sn^\bullet) on the P–P bonds of P_4 . The resulting $(Bu_3Sn)_xPH_{3-x}$ mixture can then be converted into a number of important and useful OPCs by reaction with electrophiles.^[5]

(a) State-of-the-art: indirect industrial routes to P_1 products

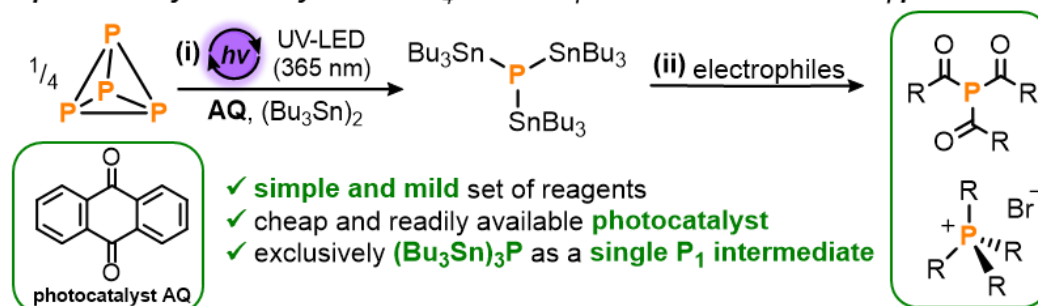


(b) Hydrostannylation of P_4 and "one pot" transformation into P_1 products



(c) This work:

photocatalytic stannylation of P_4 and "one pot" transformation into P_1 products



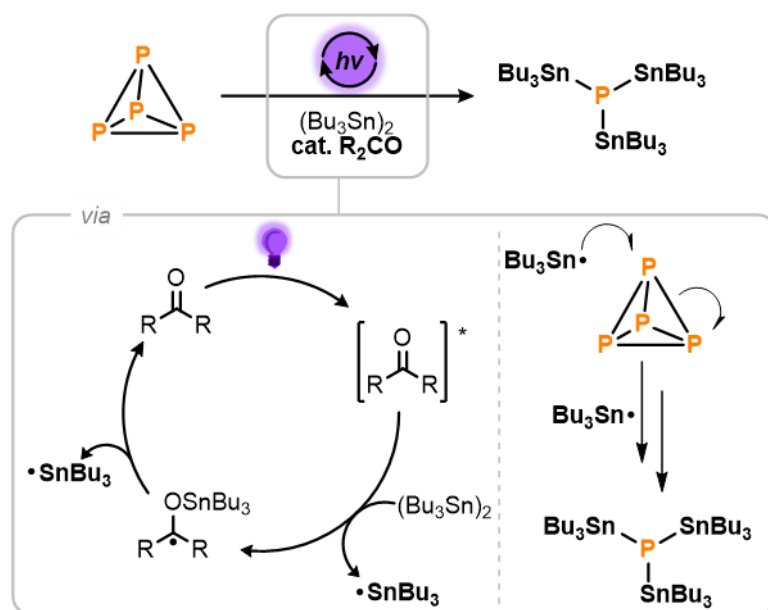
Scheme 1. (a) Current state-of-the-art industrial methods for the synthesis of valuable P_1 products.^[1] (b) Recently reported hydrostannylation of white phosphorus (P_4) using Bu_3SnH followed by reaction with electrophiles to generate useful P_1 products in a 'one-pot' fashion.^[5] (c) This work: (i) photocatalytic stannylation of P_4 using the photocatalyst anthraquinone (AQ) and hexabutyl-distannane (Bu_3Sn)₂; and (ii) subsequent functionalization of the intermediate $(Bu_3Sn)_3P$ with electrophiles into products such as triacylphosphines and tetraalkylphosphonium salts.

Unfortunately, one significant disadvantage of this hydrostannylation strategy is the complexity of the $(Bu_3Sn)_xPH_{3-x}$ mixture, which complicates 'downstream' reaction development by requiring functionalization of two different types of bond (P–Sn and P–H), both of which are distributed over four distinct molecules. Moreover, the presence of gaseous PH_3 as a component of this mixture has been suggested to have a limiting effect on overall yields as it can easily be lost during subsequent manipulations,^[4a] and it is also problematic from a safety perspective.

These drawbacks would be overcome if the initial P_4 reduction step could instead furnish a single species with just one functionalizable motif, but with reactivity otherwise similar to $(Bu_3Sn)_xPH_{3-x}$. To achieve this, we describe herein a simple photocatalytic strategy for the atom-precise stannylation of P_4 using the cheap, commercially-available distannane $(Bu_3Sn)_2$ and simple benzophenone derivatives as photocatalysts (Scheme 1c). This new procedure generates exclusively the stannylated monophosphine $(Bu_3Sn)_3P$ and

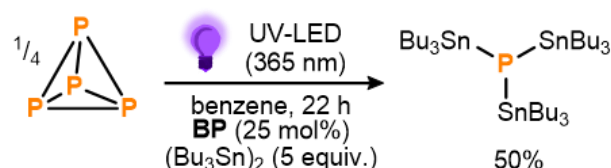
subsequent, simplified ‘one pot’ transformations with electrophiles afford valuable OPCs including acylated phosphines and alkylated phosphonium salts.

Based on the analysis above, we sought to develop a new method by which P_4 could be selectively transformed into $(Bu_3Sn)_3P$ as the sole product.^[6] It is worth noting that the closely related product $(Ph_3Sn)_3P$ has previously been prepared from P_4 using Ph_3SnCl as the stannylating reagent, but this required use of a relatively elaborate Ti(III) reagent as a halogen atom abstractor.^[3f] Instead, we imagined that an ideal reagent for such a reaction would be the distannane $(Bu_3Sn)_2$, which is cheap to purchase and could in principle provide the target phosphine with perfect atom economy.^[7] Indeed, Sn–Sn homolysis of $(Bu_3Sn)_2$ is known to furnish Bu_3Sn^\bullet radicals, which previous work has shown are capable of adding to P_4 .^{[3f],[5]} However, achieving this homolysis directly requires extreme temperatures or very high energy UV light irradiation that is known to lead to unselective reactivity, and is also unlikely to be compatible with P_4 .^{[8],[9],[10]} Fortunately, it has been reported that simple ketones can be used as photocatalysts to access Bu_3Sn^\bullet radicals by Sn–Sn bond cleavage under much lower energy irradiation.^[11] The light-driven photocatalytic stannylation of P_4 was therefore targeted, based on the mechanistic proposal outlined in Scheme 2.^[9] It was anticipated that photoirradiation of the ketone R_2CO would first provide an excited state, $[R_2CO]^*$,^[12] capable of reacting with $(Bu_3Sn)_2$ to generate a stannylated ketyl radical and a free Bu_3Sn^\bullet radical.^[11] The former could then thermally release a second Bu_3Sn^\bullet radical to close the catalytic cycle. Once formed, these Bu_3Sn^\bullet radicals would then add to the P–P bonds of P_4 , ultimately breaking it down to generate $(Bu_3Sn)_3P$ as the only P_1 product.^[13]



Scheme 2. Proposed mechanism for the light-driven, photocatalytic stannylation of P_4 in the presence of hexabutyldistannane, $(Bu_3Sn)_2$, and a ketone photocatalyst, R_2CO .

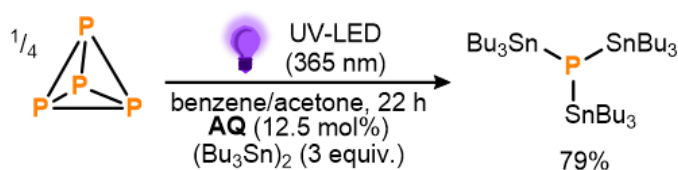
To begin, benzophenone (**BP**) was chosen as a proof-of-principle photocatalyst due to both its simplicity and the fact that its photoreactivity towards hexaalkyldistannanes has been studied previously.^[11d] Gratifyingly, after an initial optimization the photocatalytic stannylation of P_4 could successfully be achieved, with use of 25 mol% **BP** (all stoichiometries, in both equiv. and mol%, are defined per P atom) and a 3.3-fold excess (5 equiv.) of $(Bu_3Sn)_2$ providing 50% conversion to the target stannylated phosphine $(Bu_3Sn)_3P$ after stirring under near UV LEDs overnight (Scheme 3; see also ESI, S3). Control experiments confirmed that all reaction components (P_4 , $(Bu_3Sn)_2$, **BP**, irradiation) were necessary for the reaction to proceed productively (see ESI, S3, Table S1).



Scheme 3. Initial conditions for the direct, photocatalytic stannylation of P_4 into $(Bu_3Sn)_3P$ optimized using benzophenone (**BP**) as photocatalyst. Stoichiometries in equiv. and mol% are defined by P atom.

These initial results provided a clear proof-of-principle for the proposed mechanistic strategy. Notably, the observed conversion indicates the activation of at least three Sn–Sn bonds per available equivalent of **BP**,^[14] making this a rare example of a system where P_4 activation has been achieved catalytically, using an otherwise inert substrate.^{[5],[9a],[9b],[9c],[15]} Nevertheless, in order to improve the reaction outcome further,

a broader range of benzophenone derivatives was subsequently screened, with several found to provide markedly improved performance (see ESI, S5). Particularly impressive results were achieved using anthraquinone (**AQ**) and following brief further optimization (see ESI, S5 and S7) 79% conversion to $(\text{Bu}_3\text{Sn})_3\text{P}$ could be achieved using significantly reduced loadings of both **AQ** (12.5 mol%) and $(\text{Bu}_3\text{Sn})_2$ (3 equiv.) over the same timeframe (Scheme 4; see also ESI, S7). Based on the catalytic cycle proposed in Scheme 2, this would correspond to a turnover number (TON) of 10.0 for **AQ**. Further reductions in catalyst loading to 6.3 mol% or 2.5 mol% were found to lead to even higher TONs (16.8 and 28.2, respectively), albeit at the cost of lower overall conversions (see ESI, S7, Table S11).

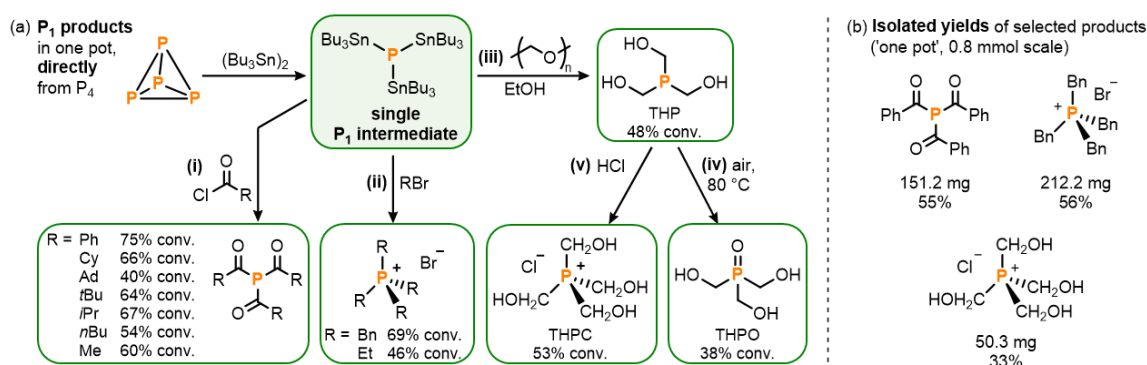


Scheme 4. Optimized conditions for the direct, photocatalytic stannylation of P_4 into $(\text{Bu}_3\text{Sn})_3\text{P}$ using anthraquinone (**AQ**) as photocatalyst. Stoichiometries in equiv. and mol% are defined by P atom.

With the stannylation of P_4 optimized, attention was then shifted to its subsequent, ‘one pot’ transformation into other useful P_1 products. Having previously developed procedures for the analogous transformation of the phosphine mixture $(\text{Bu}_3\text{Sn})_x\text{PH}_{3-x}$, which includes $(\text{Bu}_3\text{Sn})_3\text{P}$ as a minor component, it was anticipated that addition of electrophiles to photocatalytically-generated $(\text{Bu}_3\text{Sn})_3\text{P}$ should be similarly productive,^{[4],[5]} especially since neither the **AQ** photocatalyst nor the $(\text{Bu}_3\text{Sn})_2$ starting material is expected to show appreciable reactivity towards such substrates. And, indeed, *in situ* addition of a variety of acid chlorides yielded the corresponding triacylphosphines $(\text{R}(\text{O})\text{C})_3\text{P}$ ($\text{R} = \text{Ph}, \text{Cy}, \text{Ad}, i\text{Bu}, i\text{Pr}, n\text{Bu}, \text{Me}$) with good conversions of up to 75% (Scheme 5a,(i)).^{[5],[16]} Notably, and in comparison to our previously-reported hydrostannylation system, no exclusion of light and no additional base were required for this step, highlighting both the robustness and simplicity of $(\text{Bu}_3\text{Sn})_3\text{P}$ as a “ P^3 ” synthon, relative to $(\text{Bu}_3\text{Sn})_x\text{PH}_{3-x}$.

Similarly, reaction of $(\text{Bu}_3\text{Sn})_3\text{P}$ with alkyl bromides RBr ($\text{R} = \text{Bn}, \text{Et}$) under moderate heating successfully provided ‘one pot’ access to the corresponding phosphonium salts, $[\text{R}_4\text{P}]\text{Br}$, including tetrabenzylphosphonium bromide, $[\text{Bn}_4\text{P}]\text{Br}$, which is a known precursor for useful Wittig chemistry (Scheme 5a,(ii)).^[17] Again, no auxiliary base was required for these reactions, in contrast to the analogous procedures *via* $(\text{Bu}_3\text{Sn})_x\text{PH}_{3-x}$ where the absence of base leads to a 50% reduction in yield.^[5]

Finally, another industrially important class of P_1 products was targeted. Hydroxymethyl-substituted phosphine derivatives are used as flame-retardant materials (among a number of other applications),^[18] and could be accessed by reacting the stannylated monophosphine $(\text{Bu}_3\text{Sn})_3\text{P}$ with paraformaldehyde in EtOH to furnish tris(hydroxymethyl)phosphine, $(\text{HOCH}_2)_3\text{P}$ (THP; Scheme 5a,(iii)).^[18a] Subsequent exposure to air then yielded the corresponding phosphine oxide, $(\text{HOCH}_2)_3\text{PO}$ (THPO; Scheme 5a,(iv)),^[18b] while the phosphonium salt tetrakis(hydroxymethyl)phosphonium chloride, $[(\text{HOCH}_2)_4\text{P}]\text{Cl}$ (THPC),^{[18c],[18d]} could be accessed by quenching the *in situ* generated THP with HCl, all in one pot (Scheme 5a,(v)).



Scheme 5. a) One-pot synthesis directly from P_4 , via photocatalytically generated P_1 intermediate $(\text{Bu}_3\text{Sn})_3\text{P}$, of (i) triacylphosphines $(\text{R}(\text{O})\text{C})_3\text{P}$ (4 equiv. $\text{RC}(\text{O})\text{Cl}$, $\text{R} = t\text{Bu}$, Ph, Me, *n*Bu, Cy, *i*Pr, Ad), (ii) phosphonium salts $[\text{R}_4\text{P}]\text{Br}$ (5 equiv. RBr , $\text{R} = \text{Bn}$, Et, 60–80 °C), (iii) tris(hydroxymethyl)phosphine, THP (EtOH, 3 equiv. paraformaldehyde), (iv) tris(hydroxymethyl)phosphine oxide, THPO (as for (iii) then air, 80 °C), and (v) tetrakis(hydroxymethyl)phosphonium chloride, THPC (as for (iii) using 12.5 equiv. paraformaldehyde, then 10 equiv. HCl); and b) Isolated yields for the reactions on preparative scale (0.8 mmol). Stoichiometries in equiv. are defined per P atom.

To demonstrate the viability of these reactions on a preparative scale the triacylphosphine $(\text{Ph}(\text{O})\text{C})_3\text{P}$ and the phosphonium salts $[\text{Bn}_4\text{P}]\text{Br}$ and THPC were selected as representative examples for isolation (Scheme 5b; see ESI S9). At 0.8 mmol scale $(\text{Ph}(\text{O})\text{C})_3\text{P}$ could be isolated in 55% yield,^[19] which compares well with our previously-reported hydrostannylation method (51%). $[\text{Bn}_4\text{P}]\text{Br}$ could also be isolated in good 56% yield, and THPC in a more modest yield of 33%.^[19] For this last reaction, efforts were also made to recover the Sn-containing compounds present at the end of the reaction. We have previously shown that for the analogous synthesis of THPC *via* $(\text{Bu}_3\text{Sn})_x\text{PH}_{3-x}$ recovery of the Bu_3SnCl byproduct allows for convenient regeneration and recycling of the Bu_3SnH starting material, thus minimizing the formation of organotin-containing waste. Bu_3SnCl can also be used to regenerate $(\text{Bu}_3\text{Sn})_2$ through a net one-electron reduction,^[8]

meaning similar recycling should be feasible for this newer system, provided Bu_3SnCl can again be cleanly recovered. Satisfyingly, Bu_3SnCl could indeed be recovered during THPC workup through simple washing with diethyl ether, being isolated as part of an otherwise clean mixture with unreacted $(\text{Bu}_3\text{Sn})_2$ in an excellent overall yield of 92% (1.3:1 molar ratio, see ESI S9).

3.3 Conclusion

In conclusion, we have developed a simple, new method for the direct transformation of P_4 into a variety of commercially and academically interesting OPCs. The reaction proceeds through a photocatalytic stannylation of white phosphorus, which generates $(\text{Bu}_3\text{Sn})_3\text{P}$ with perfect atom economy as a single, convenient P_1 intermediate using an inexpensive, commercially available distannane and a simple photocatalyst. This method can be used to prepare a variety of different products through inclusion of a range of different electrophilic substrates, and we have demonstrated that the Sn-containing byproducts of the reaction can in principle be recovered and recycled. These results expand the currently very limited range of strategies that are available for the direct functionalization of P_4 , and suggest the intriguing possibility that P_4 activation might also be achievable by reaction with other weak E–E bonds under similar photocatalytic conditions.

3.4 Supporting Information

S1. General Information

All reactions and manipulations were performed under an N₂ atmosphere (< 0.1 ppm O₂, H₂O) through use of a GS Glovebox (GS117717). All glassware was oven-dried (160 °C) overnight prior to use. Benzene was distilled from Na/benzophenone and stored over molecular sieves (3 Å). Acetonitrile was distilled from CaH₂ and stored over molecular sieves (3 Å). Acetone was stirred over CaSO₄ (30 min) and dynamically dried by passing over molecular sieves (3 Å). THF was purified using an MBraun SPS-800 system and stored over molecular sieves (3 Å). C₆D₆ was distilled from K and stored over molecular sieves (3 Å). Hexabutyldistannane (Bu₃Sn)₂ was purchased from ABCR or Thermo Scientific (97% purity). The photocatalysts benzophenone, 4-benzoylpyridine, xanthone, thioxanthone, anthraquinone and DDQ (2,3-dichloro-5,6-dicyano-1,4-benzochinone) were ordered from major chemical suppliers (Sigma, ABCR) and used as received. All other chemicals were also purchased from major suppliers (Aldrich, ABCR); liquids were purified by Kugelrohr distillation and freeze-pump-thaw degassed three times prior to use; P₄ and Ph₃PO were purified by sublimation; all others were used as received.

Qualitative NMR spectra were recorded at room temperature on Bruker Avance III HD 400 (400 MHz) spectrometers and were processed using Topspin 3.2. Chemical shifts δ , are reported in parts per million (ppm); ¹H and ¹³C shifts are reported relative to SiMe₄ and were calibrated internally to residual solvent peaks, while ³¹P shifts and ¹¹⁹Sn shifts were referenced externally to 85 % H₃PO₄ (aq.) and Me₄Sn, respectively. NMR samples were prepared in the glovebox using NMR tubes fitted with screw caps. Optimization reactions (see sections S5, S6 and S7) and photocatalytic stannylation of P₄ to (Bu₃Sn)₃P and subsequent functionalization to P₁ products were analyzed by ³¹P{¹H} spectra using triphenylphosphine, Ph₃PO, as a standard.

For determining the conversion of the P₁ products, the following **quantitative ³¹P{¹H} NMR pulse programs** were used:

- Triacylphosphines^[5] → **T1_{IS} < T1_{Prod} = 10s, D1 = 40 s, zgig30, inverse gated decoupled, LB = 10**
- Phosphonium salts^{[9a],[9d]} → **single scan, DS = 0, D1 = 2 s, D1 ≥ 5 x T1, zgig90, inverse gated decoupled, LB = 1.**

LEDs used for the optimization reactions of the photocatalytic stannylation of P_4 to $(Bu_3Sn)_3P$ were:

- Green LED: 528 nm, 3.5 V, 700 mA, Osram OSOLON SSL 80
- Blue LED: 455 nm (± 15 nm), 3.2 V, 700 mA, Osram OSOLON SSL 80
- Violet/Blue LED: 415 nm (± 5 nm), 3.5 V, 700 mA, Intelligent LED Solutions ILH-XC01-5410-SC211-WIR200
- Violet LED: 405 nm (± 10 nm), 4.0 V, 700 mA, Edixeon EDEV-SLC1-03
- UV LED: 385nm (± 15 nm), 3,4 V, 350 mA LST1-01G01-UV02-00
- UV LED: 365 nm, 4.3 V, 700 mA, Osram OSOLON SSL 80
- UV LED: 365 nm, 14 V, 700 mA, Osram OSOLON SSL 80 (scale-up reactions)

S2. Supplementary mechanistic discussion

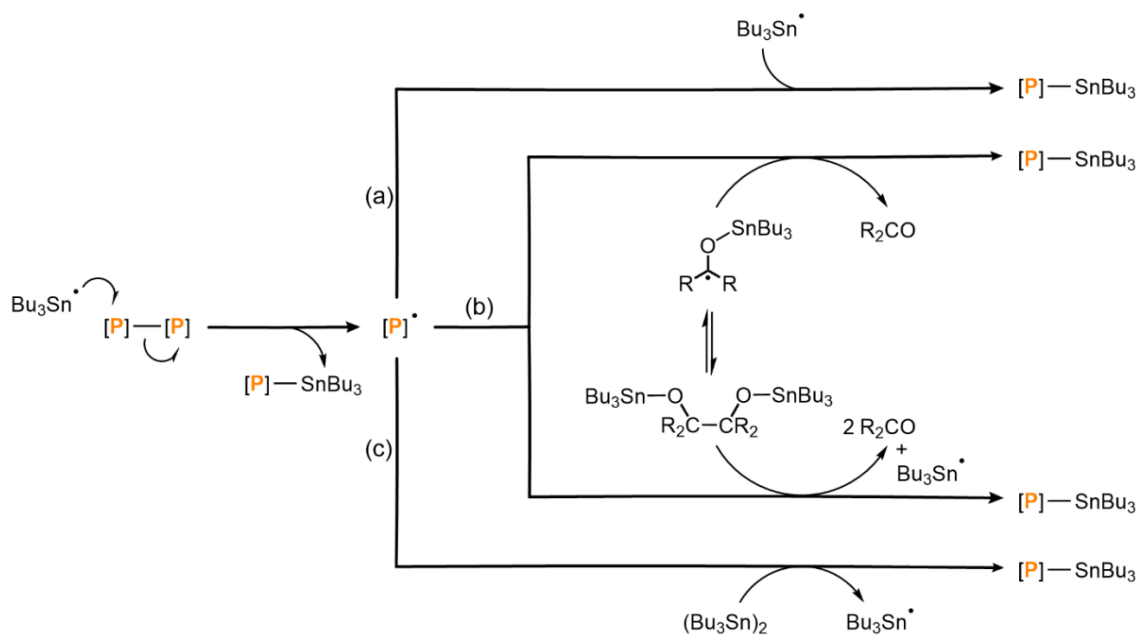
The proposed mechanism for the photocatalytic stannylation of P₄ by (Bu₃Sn)₂ catalyzed by simple ketones is outlined in Scheme 2 of the primary manuscript. However, it should be noted that in the absence of more comprehensive mechanistic studies it is currently not possible to exclude the involvement of several alternative elementary reaction steps. For example, while the formation of an intermediate stannylated ketyl radical [R₂COSnBu₃][•] is supported by the prior literature,^[11] an alternative energy transfer from [R₂CO]^{*} to (Bu₃Sn)₂ resulting in cleavage to Bu₃Sn[•] by a purely outer sphere mechanism has not yet been definitively excluded.

One key question left unanswered at present relates to the precise mechanism by which radical breakdown of the P₄ tetrahedron is achieved. Based on our previous studies it can be confidently proposed that each P–P bond cleavage step is likely to begin with attack of a photocatalytically-generated Bu₃Sn[•] radical (Scheme S1).^[5] The simplest subsequent step would be recombination of the resulting P-centered radical with a second Bu₃Sn[•] radical, thus completing the stannylation of the original P–P moiety (Scheme S1a). Note, however, that this requires bimolecular recombination of two transient radicals whose concentrations are expected to be low.

Alternatively, stannylation of this P-centered radical could be achieved through S_H2-type attack on the proposed intermediate [R₂COSnBu₃][•] and/or its pinacol-type dimer, examples of which are known from the literature to exist in equilibrium (Scheme S1b).^[11] In this scenario, this equilibrium would act as a stabilized and hence more persistent reservoir of chemically-accessible “Bu₃Sn”.

A third scenario is that S_H2-type attack could occur directly on the (Bu₃Sn)₂ substrate, which should be present in high concentrations throughout the reaction. This scenario would result in a radical chain mechanism analogous to that proposed previously for P₄ hydrostannylation (Scheme S1c).^[5] In this case the R₂CO photocatalyst would formally act as a photosensitizing initiator for the chain reaction, rather than as a strict catalyst *per se*. However, we currently consider this to be a less likely option, due to several qualitative experimental observations. Firstly, attempts to achieve an analogous chain reaction mechanism using “standard” chemical initiators such as AIBN under thermal conditions (instead of R₂CO under photochemical conditions) have thus far been unsuccessful, not leading to any identifiable change by ³¹P{¹H} NMR spectroscopy (for example, see Figure S1).

Secondly, attempts to initiate the same radical chain under thermal conditions by using catalytic quantities of both AIBN and Bu₃SnH, which should definitely result in formation of Bu₃Sn[•], have also been unsuccessful. These led only to trace hydrostannylation, consistent with the amount of Bu₃SnH present and similar to the outcome when no distannane is present, which argues against any efficient radical interception by (Bu₃Sn)₂ (for example, see Figure S2).



Scheme S1. Illustration of the equipment setup used for photocatalytic reactions at 0.04 mmol scale.

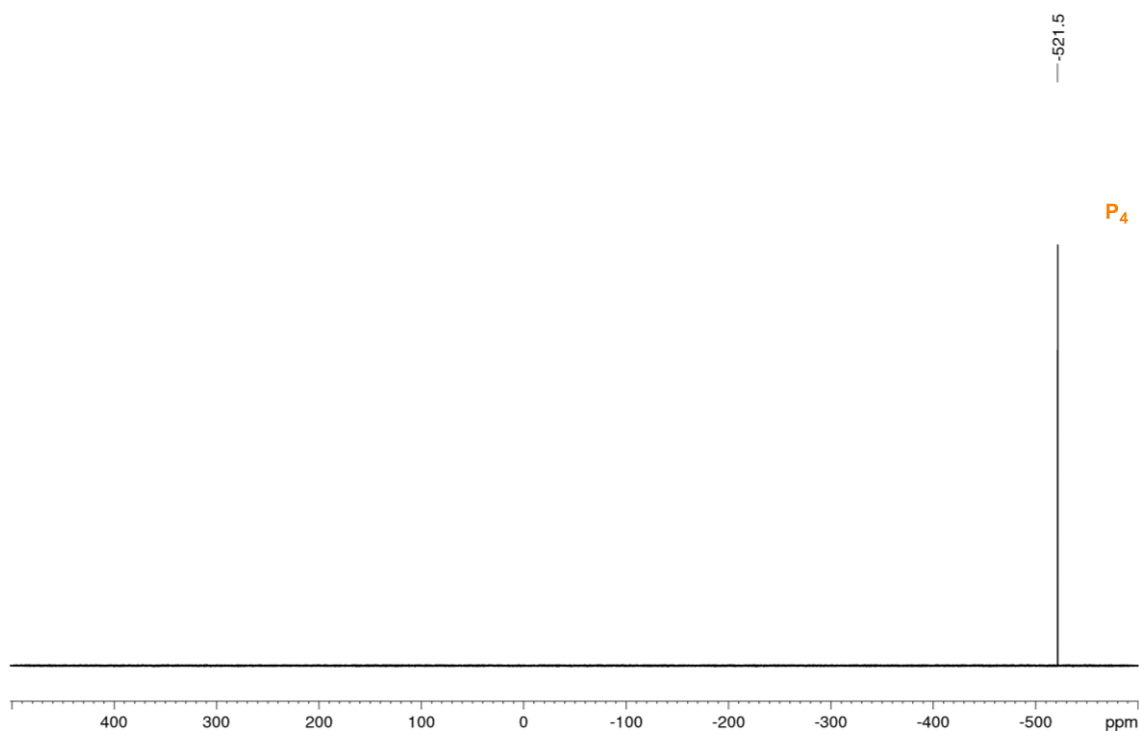


Figure S1. Representative $^{31}\text{P}\{^1\text{H}\}$ NMR spectrum for the attempted stannylation of P_4 using $(\text{Bu}_3\text{Sn})_2$ and 12.5 mol% AIBN in toluene, after heating to 80 °C for 16 h.

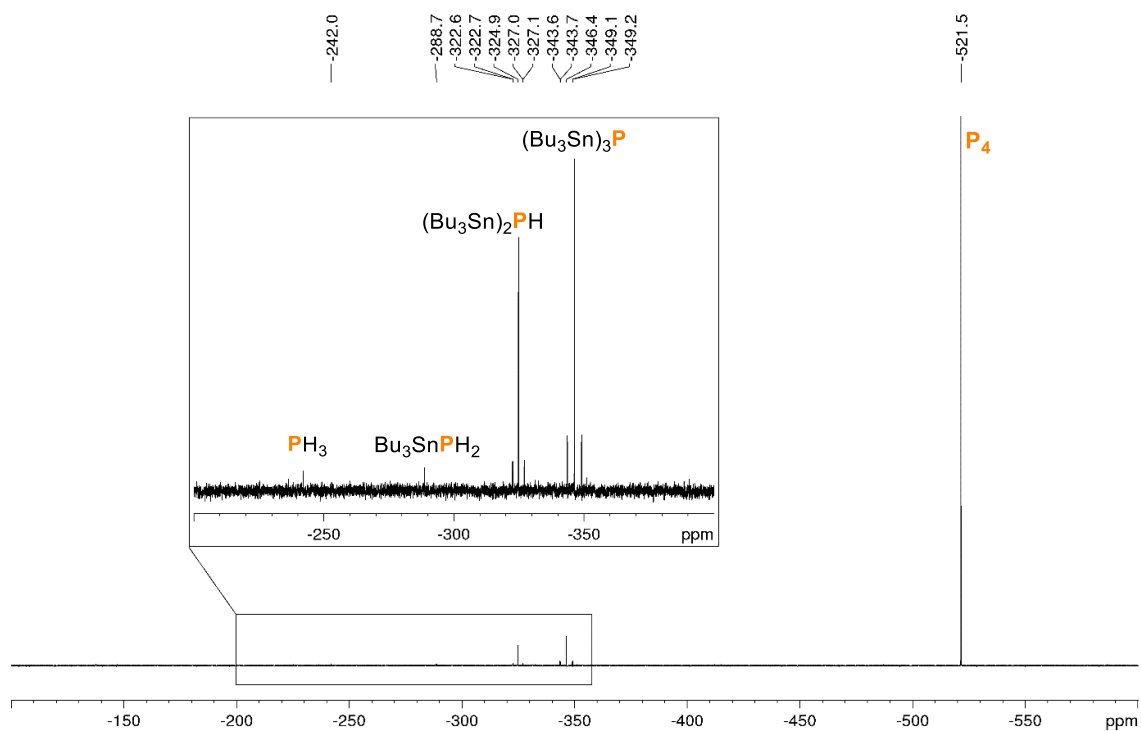


Figure S2. Representative $^{31}\text{P}\{^1\text{H}\}$ NMR spectrum for the attempted stannylation of P_4 using $(\text{Bu}_3\text{Sn})_2$ and 12.5 mol% of both AIBN and Bu_3SnH in toluene, after heating to 80°C for 18 h. The relatively high proportion of $(\text{Bu}_3\text{Sn})_2\text{PH}$ and $(\text{Bu}_3\text{Sn})_3\text{P}$ relative to Bu_3SnPH_2 (*c.f.* ref. [5]) can likely be attributed to $\text{Bu}_3\text{Sn}/\text{H}$ ligand scrambling at the elevated reaction temperature and/or the high loading of AIBN relative to Bu_3SnH which reduces the number of available H atoms. This is supported by the observation that when the reaction is repeated in the absence of $(\text{Bu}_3\text{Sn})_2$ the resulting $(\text{Bu}_3\text{Sn})_x\text{PH}_{3-x}$ mixture is also heavily weighted towards $(\text{Bu}_3\text{Sn})_2\text{PH}$ and $(\text{Bu}_3\text{Sn})_3\text{P}$.

S3. General procedure for photocatalytic functionalization of P₄ (0.04 mmol scale) into stannylated phosphine (Bu₃Sn)₃P using benzophenone

At the start of this project, benzophenone (**BP**) was chosen as a photocatalyst for the initial reaction optimization due to both its simplicity and the fact that its (photo)reactivity towards hexaalkyldistannanes has been studied previously.^[11]

To a 10 mL stoppered tube equipped with a stirring bar were added (Bu₃Sn)₂ (101.1 μL, 5 equiv. based on phosphorus atoms, 20 equiv. based on P₄), **BP** (0.01 mmol, as a stock solution in 149.2 μL benzene, 1 equiv. based on P₄) and P₄ (0.01 mmol, as a stock solution in 71.3 μL benzene) in benzene as solvent (in total 0.5 mL). The tube was sealed, placed in a water-cooled block (to ensure a near-ambient temperature was maintained, Figure S3),^[9] and irradiated with UV light (365 nm, 4.3 V, 700 mA, Osram OSOLON SSL 80) for 22 h (unless stated otherwise). Ph₃PO (0.02 mmol, stock solution in benzene) was subsequently added to act as an internal standard. The resulting mixture was subjected to ³¹P{¹H} NMR analysis (Figure S4). Formation of (Bu₃Sn)₃P was indicated by the characteristic ^{117/119}Sn-satellited resonance at -346.5 ppm.^[5]

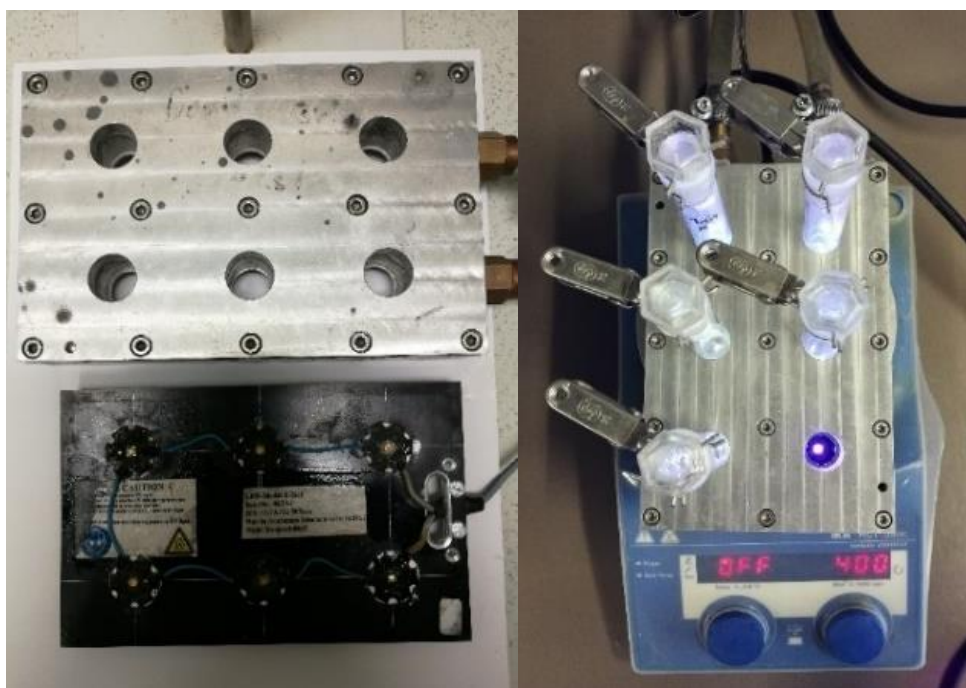


Figure S3. Illustration of the equipment setup used for photocatalytic reactions at 0.04 mmol scale.

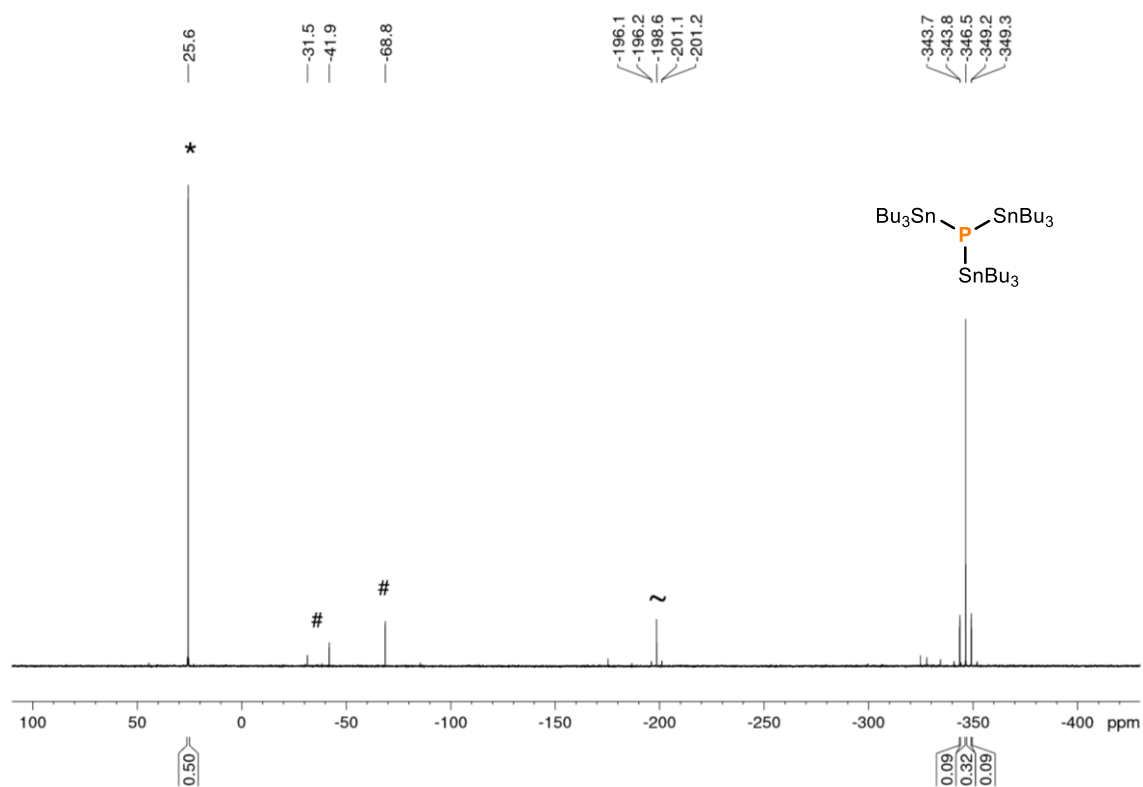
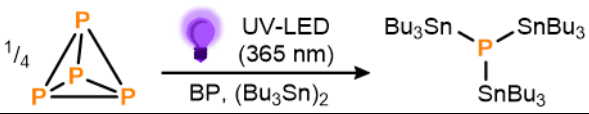


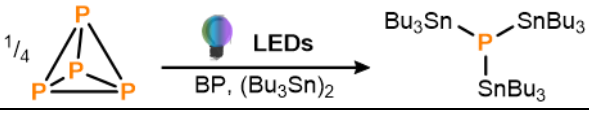
Figure S4. Representative $^{31}\text{P}\{^1\text{H}\}$ NMR spectrum for the photocatalytic functionalization of P_4 using **benzophenone** (BP) as a photocatalyst (Table 1, Entry 1). * marks the internal standard Ph_3PO (0.02 mmol). ~ marks an unknown Sn-containing side product. # marks unknown side products.

S4. Optimization of photocatalytic reaction conditions using benzophenone

Table S1. Photocatalytic functionalization of P₄ to (Bu₃Sn)₃P: screening of control experiments.^[a]


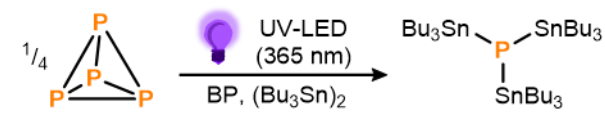
Entry	Conditions	Full conv. of P ₄ ?	Conv. to (Bu ₃ Sn) ₃ P / %
1	Standard ^[a]	✓	50
2	No light	X	0
3	No benzophenone	✓	0
4	No (Bu ₃ Sn) ₂	X	0
5	Blue LEDs (455 nm)	X	0
6	Violet LEDs (405nm)	✓	26
7	P _{red} instead of P ₄	—	1

[a] For the general procedure, see section S3.

Table S2. Photocatalytic functionalization of P₄ to (Bu₃Sn)₃P: screening of different radiation sources (LEDs).^[a]


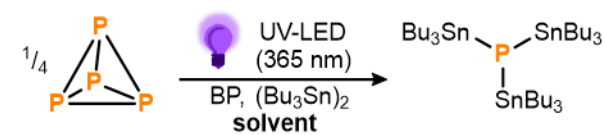
Entry	LEDs	Full conv. of P ₄ ?	Conv. to (Bu ₃ Sn) ₃ P / %
1	365 nm ^[a] (UV LED)	✓	50
2	385 nm (UV LED)	✓	40
3	405 nm (violet LED)	✓	26
4	420 nm (violet blue LED)	✓	21
5	455 nm (blue LED)	X	0
6	528 nm (green LED)	X	0

[a] The general procedure (see section S3) was modified to use the LEDs indicated.

Table S3. Photocatalytic functionalization of P₄ to (Bu₃Sn)₃P: screening of **irradiation period**.^[a]


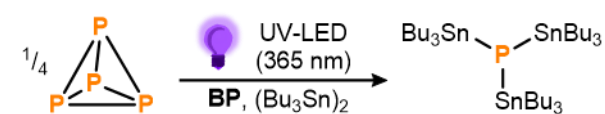
Entry	Irradiation period	Full conv. of P ₄ ?	Conv. to (Bu ₃ Sn) ₃ P / %
1	16 h	✓	41
2	18 h	✓	43
3	20 h	✓	45
4	22 h	✓	50

[a] The general procedure (see section S3) was modified in the period of irradiation with UV light (365 nm).

Table S4. Photocatalytic functionalization of P₄ to (Bu₃Sn)₃P: screening of **solvents**.^[a]


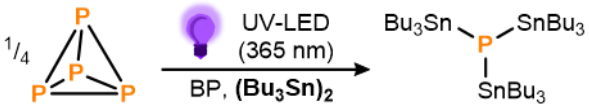
Entry	Solvent	Full conv. of P ₄ ?	Conv. to (Bu ₃ Sn) ₃ P / %
1	Benzene ^[a]	✓	50
2	Benzene ^[b]	✓	47
3	Acetone	✓	50
4	Acetonitrile	✓	35
5	THF	✓	11
6	Toluene	✓	48

[a] The general procedure (see section S3) was modified to use a solvent mixture (P₄ and **BP** stock solutions still in benzene, total solvent volume of 0.5 mL). [b] 0.22 mL solvent volume.

Table S5. Photocatalytic functionalization of P₄ to (Bu₃Sn)₃P: screening of **amounts of benzophenone**.^{[a][b]}


Entry	BP / equiv. ^[b]	Full conv. of P ₄ ?	Conv. to (Bu ₃ Sn) ₃ P / %
1	0.5	✓	45
2	1	✓	50
3	4	✓	60
4	10	✓	59

[a] For the general procedure, see section S3. [b] Listed equivalents are defined per P₄ molecule.

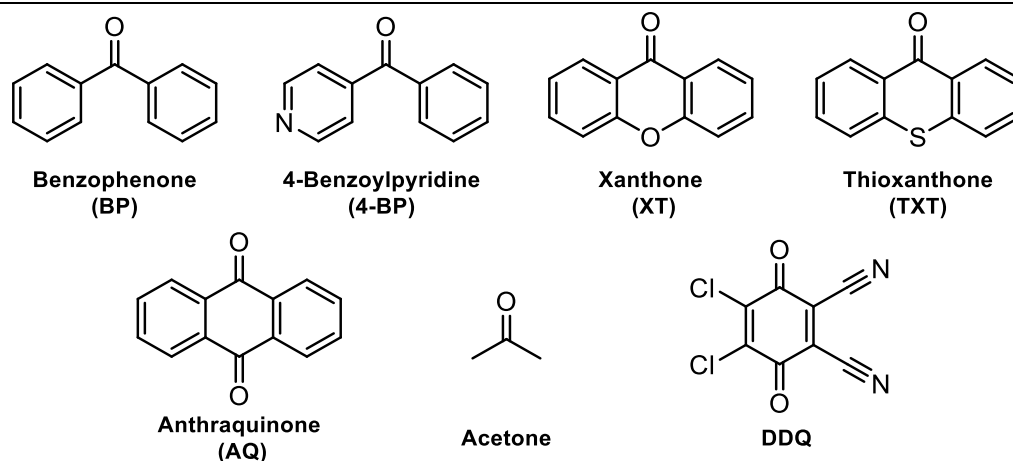
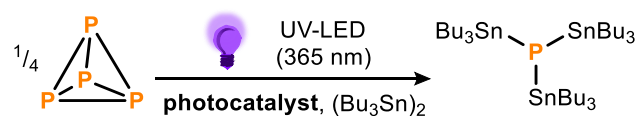
Table S6. Photocatalytic functionalization of P₄ to (Bu₃Sn)₃P: screening of amounts of (Bu₃Sn)₂.^{[a][b]}


Entry	(Bu ₃ Sn) ₂ / equiv. ^[a]	Full conv. of P ₄ ?	Conv. to (Bu ₃ Sn) ₃ P / %
1	30	✓	58
2	20	✓	51
3	15	✓	49
4	12	✓	45
5	6	✓	35

[a] For the general procedure, see section S3. [b] Listed equivalents are defined per P₄ molecule.

S5. Benzophenone derivatives used as photocatalysts for the photocatalytic functionalization of P₄ to (Bu₃Sn)₃P

Table S7. Photocatalytic functionalization of P₄ to (Bu₃Sn)₃P: screening of benzophenone derivatives.^{[12a],[a]}



Entry	Photoinitiator (PI)	Full conv. of P ₄ ?	Conv. to (Bu ₃ Sn) ₃ P / %
1	Benzophenone ^[a] (BP)	✓	50
2	Benzophenone ^[b] (BP)	✓	50
3	4-Benzoylpyridine (4-BP)	✓	73
4	Xanthone (XT)	✓	39
5	Thioxanthone (TXT)	✓	70
6	Thioxanthone ^[b] (TXT)	✓	66
7	Anthraquinone (AQ)	✓	62
8	Anthraquinone ^[b] (AQ)	✓	75
9	Anthraquinone ^{[b][c]} (AQ)	✓	83
10	Acetone	✓	2
11	DDQ	✓	8

[a] For the general procedure, see section S3. [b] A solvent mixture of benzene (71.3 μL of the P₄ stock solution) and acetone (429 μL) was used. [c] Instead of the usual 1 equiv. of the photocatalyst only 0.5 equiv. of the anthraquinone (AQ) was used.

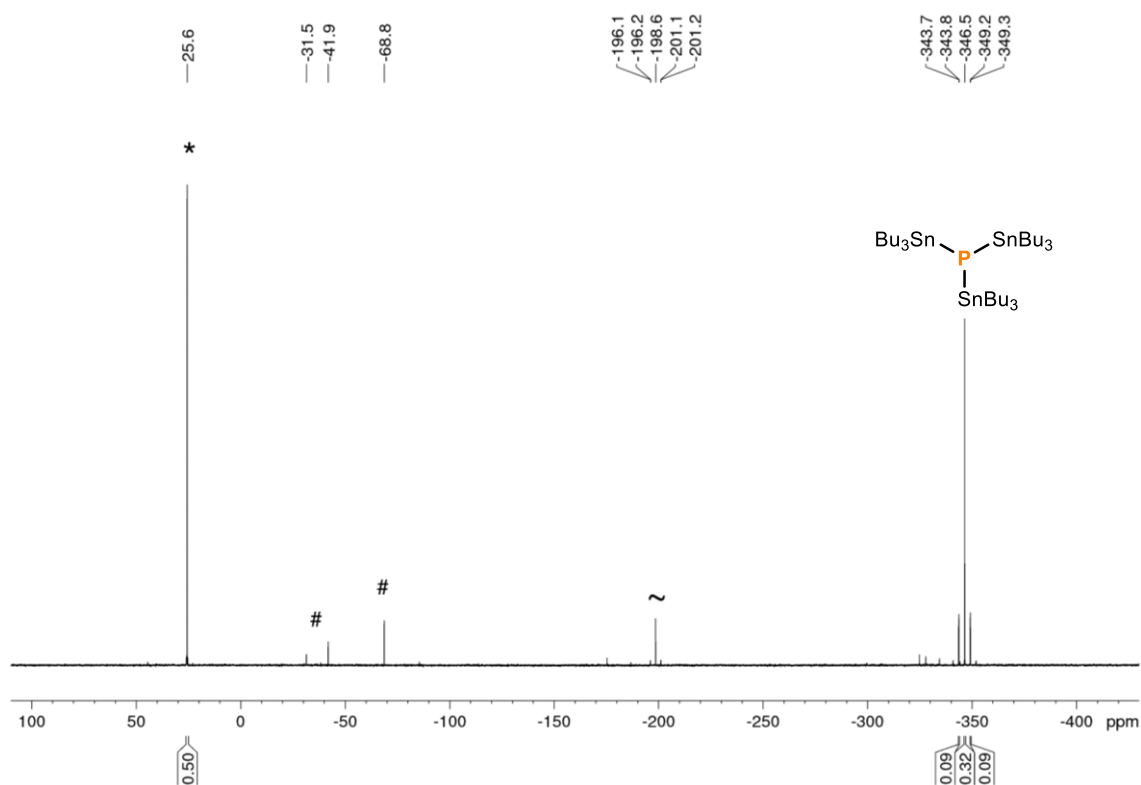


Figure S5. $^{31}\text{P}\{^1\text{H}\}$ NMR spectrum for the photocatalytic functionalization of P_4 using **benzophenone (BP)** as a photocatalyst (Table 7, Entry 1). * marks the internal standard Ph_3PO (0.02 mmol). ~ marks an unknown Sn-containing side product. # marks unknown side products.

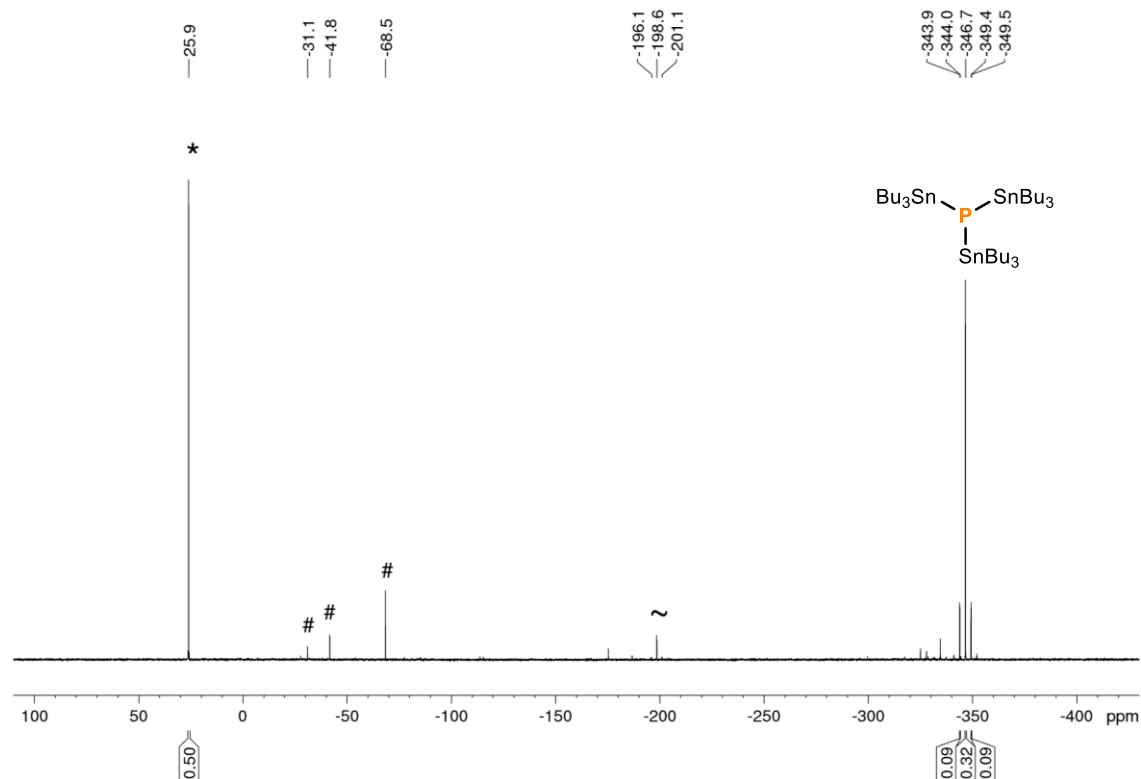


Figure S6. $^{31}\text{P}\{^1\text{H}\}$ NMR spectrum for the photocatalytic functionalization of P_4 using **benzophenone (BP)** as a photocatalyst (Table 7, Entry 2, **PhH/acetone**). * marks the internal standard Ph_3PO (0.02 mmol). ~ marks an unknown Sn-containing side product. # marks unknown side products.

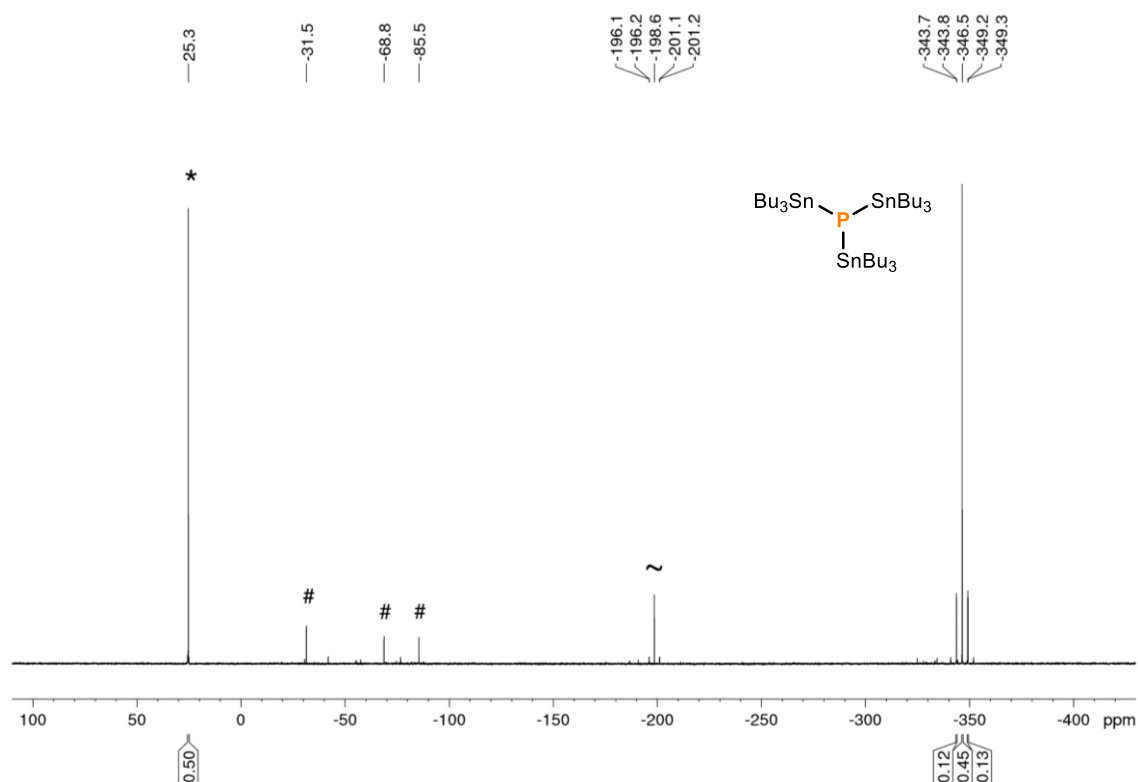


Figure S7. $^{31}\text{P}\{^1\text{H}\}$ NMR spectrum for the photocatalytic functionalization of P_4 using **4-benzoylpyridine (4-BP)** as a photocatalyst (Table S7, Entry 3). * marks the internal standard Ph_3PO (0.02 mmol). ~ marks an unknown Sn-containing side product. # marks unknown side products.

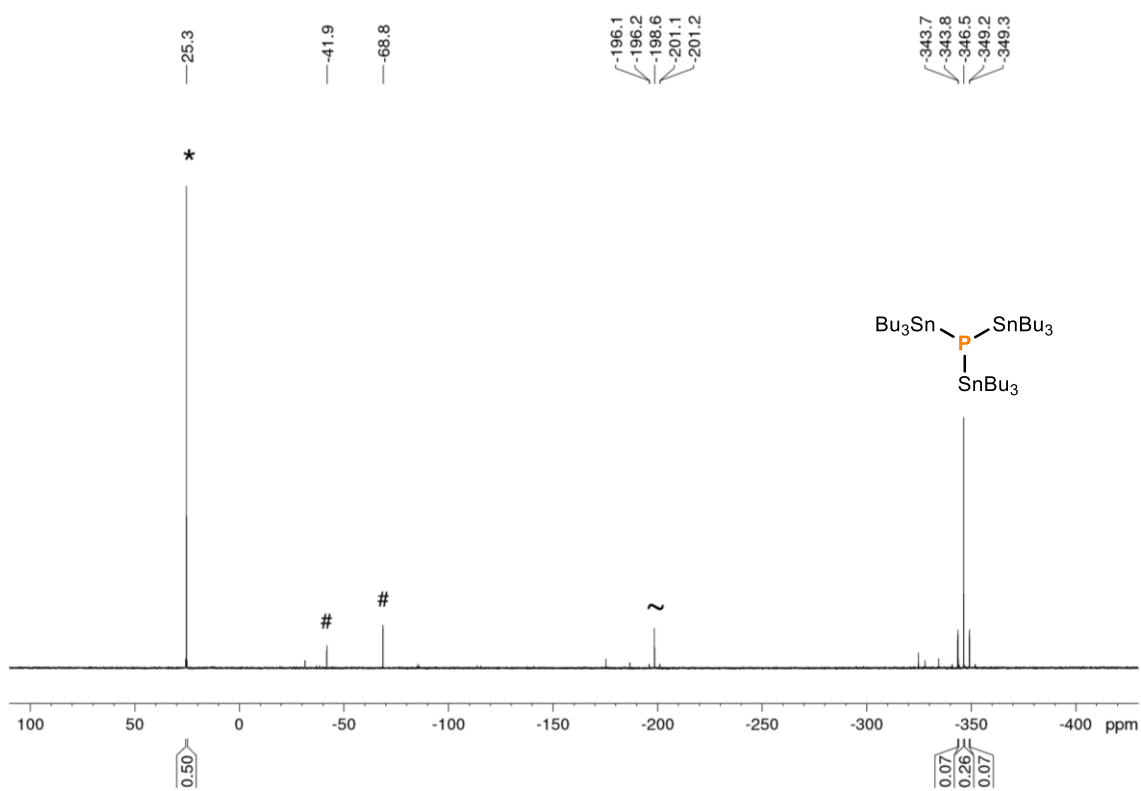


Figure S8. $^{31}\text{P}\{^1\text{H}\}$ NMR spectrum for the photocatalytic functionalization of P_4 using **xanthone (XT)** as a photocatalyst (Table S7, Entry 4). * marks the internal standard Ph_3PO (0.02 mmol). ~ marks an unknown Sn-containing side product. # marks unknown side products.

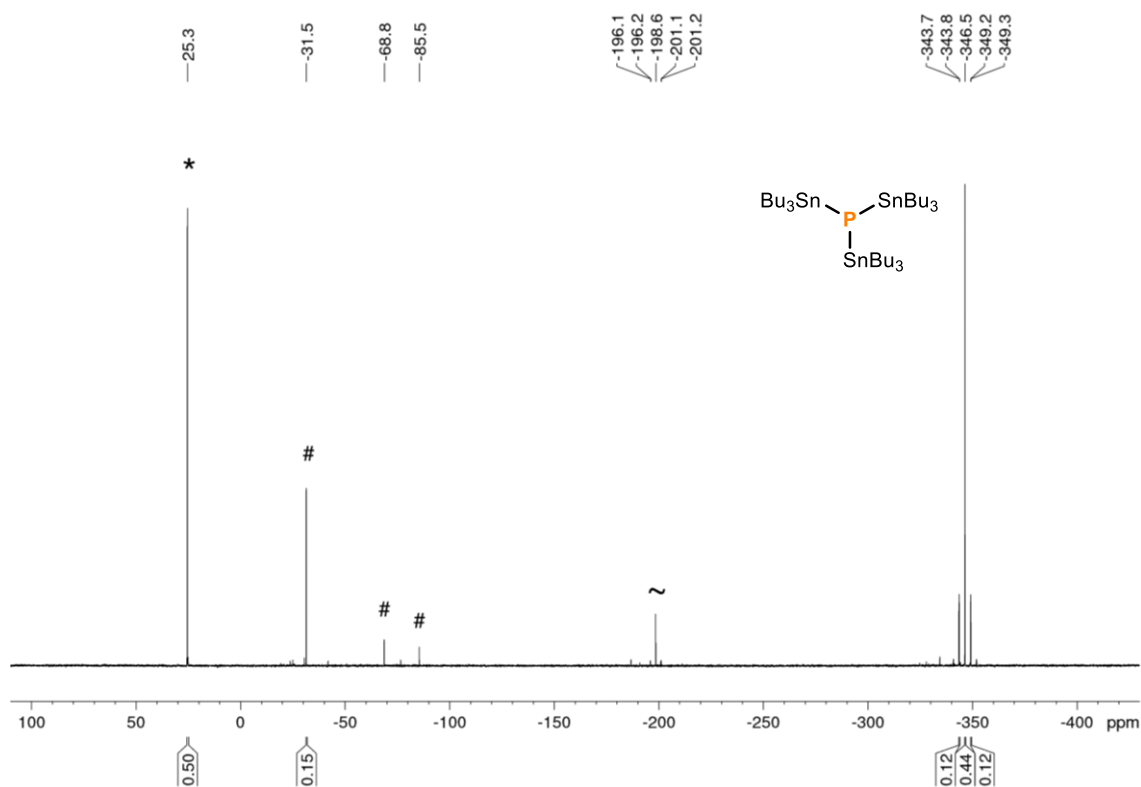


Figure S9. $^{31}\text{P}\{^1\text{H}\}$ NMR spectrum for the photocatalytic functionalization of P_4 using **thioxanthone (TXT)** as a photocatalyst (Table S7, Entry 5). * marks the internal standard Ph_3PO (0.02 mmol). ~ marks an unknown Sn-containing side product. # marks unknown side products.

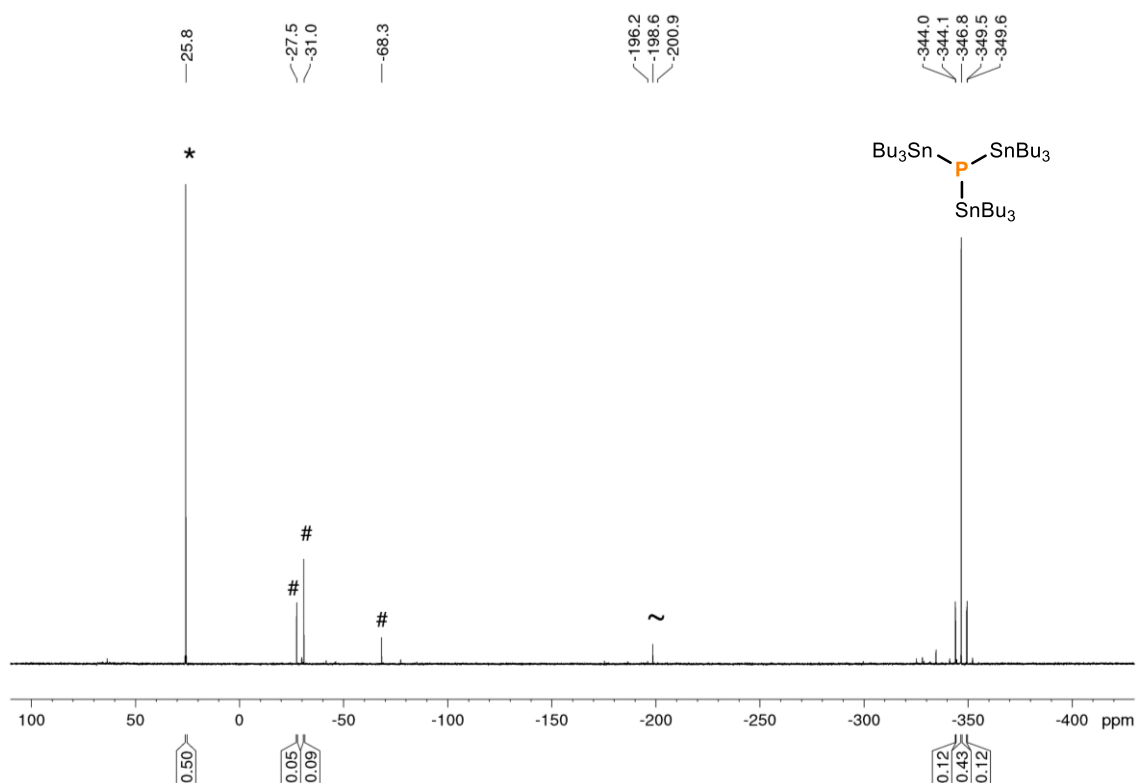


Figure S10. $^{31}\text{P}\{^1\text{H}\}$ NMR spectrum for the photocatalytic functionalization of P_4 using **thioxanthone (TXT)** as a photocatalyst (Table S7, Entry 6, **PhH/acetone**). * marks the internal standard Ph_3PO (0.02 mmol). ~ marks an unknown Sn-containing side product. # marks unknown side products.

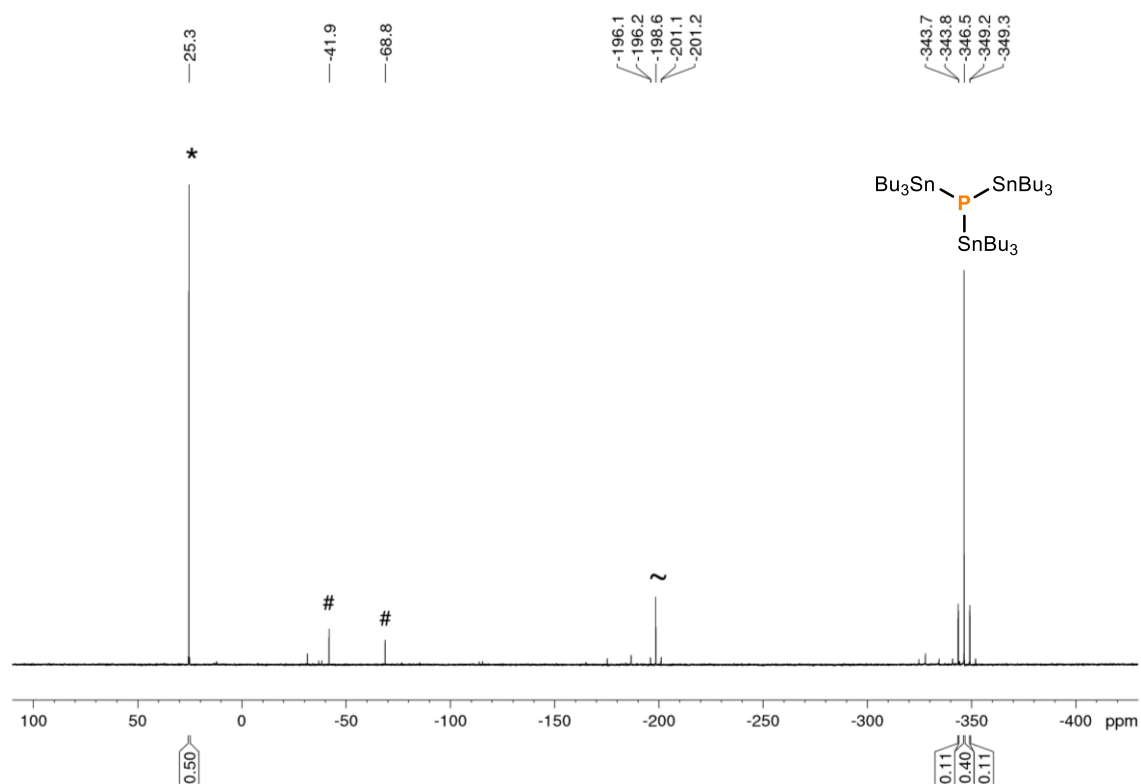


Figure S11. $^{31}\text{P}\{^1\text{H}\}$ NMR spectrum for the photocatalytic functionalization of P_4 using **anthraquinone (AQ)** as a photocatalyst (Table S7, Entry 7). * marks the internal standard Ph_3PO (0.02 mmol). ~ marks an unknown Sn-containing side product. # marks unknown side products.

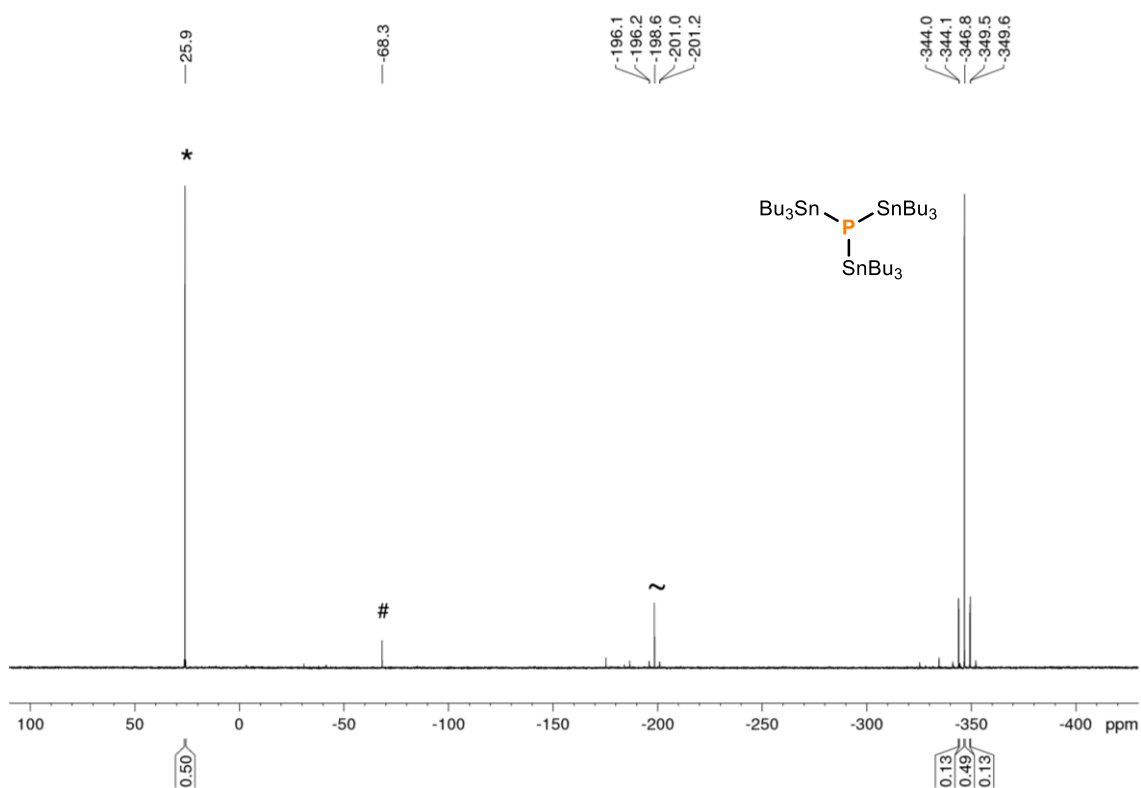


Figure S12. $^{31}\text{P}\{^1\text{H}\}$ NMR spectrum for the photocatalytic functionalization of P_4 using **anthraquinone (AQ)** as a photocatalyst (Table S7, Entry 8, **PhI/acetone**). * marks the internal standard Ph_3PO (0.02 mmol). ~ marks an unknown Sn-containing side product. # marks unknown side products.

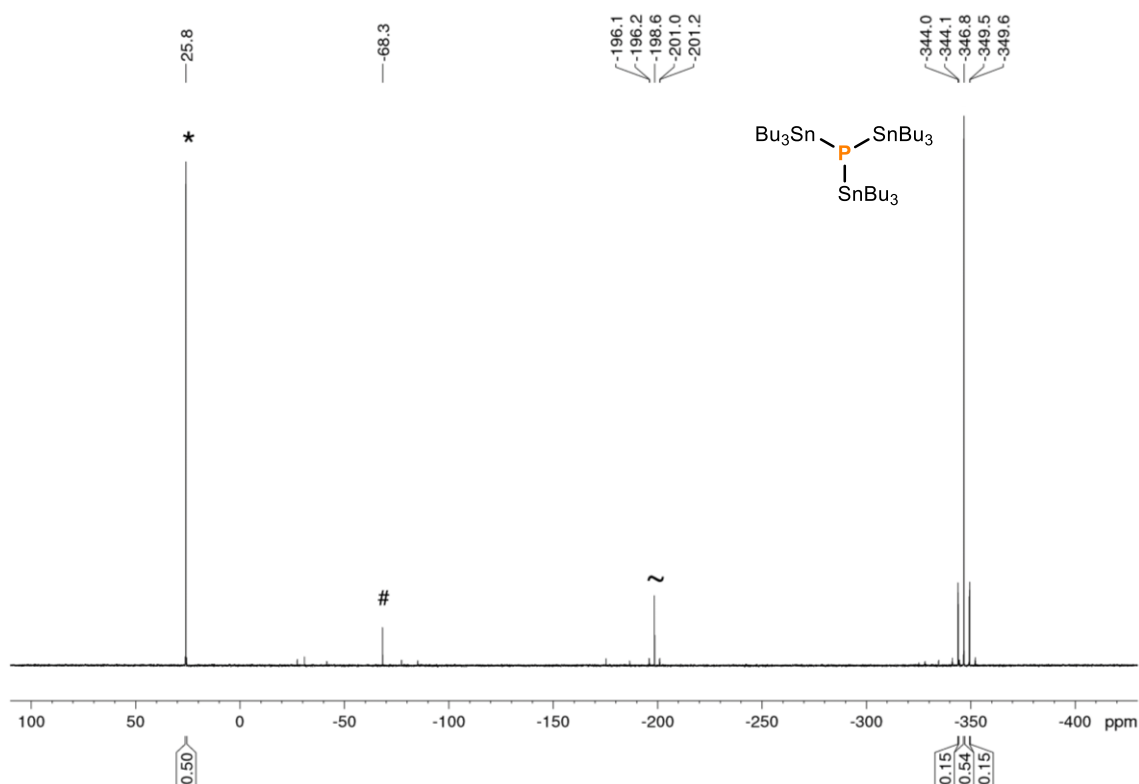


Figure S13. $^{31}\text{P}\{^1\text{H}\}$ NMR spectrum for the photocatalytic functionalization of P_4 using **anthraquinone (AQ)** as a photocatalyst (Table S7, Entry 9, **0.5 equiv. anthraquinone** in **PhH/acetone**). * marks the internal standard Ph_3PO (0.02 mmol). ~ marks an unknown Sn-containing side product. # marks unknown side products.

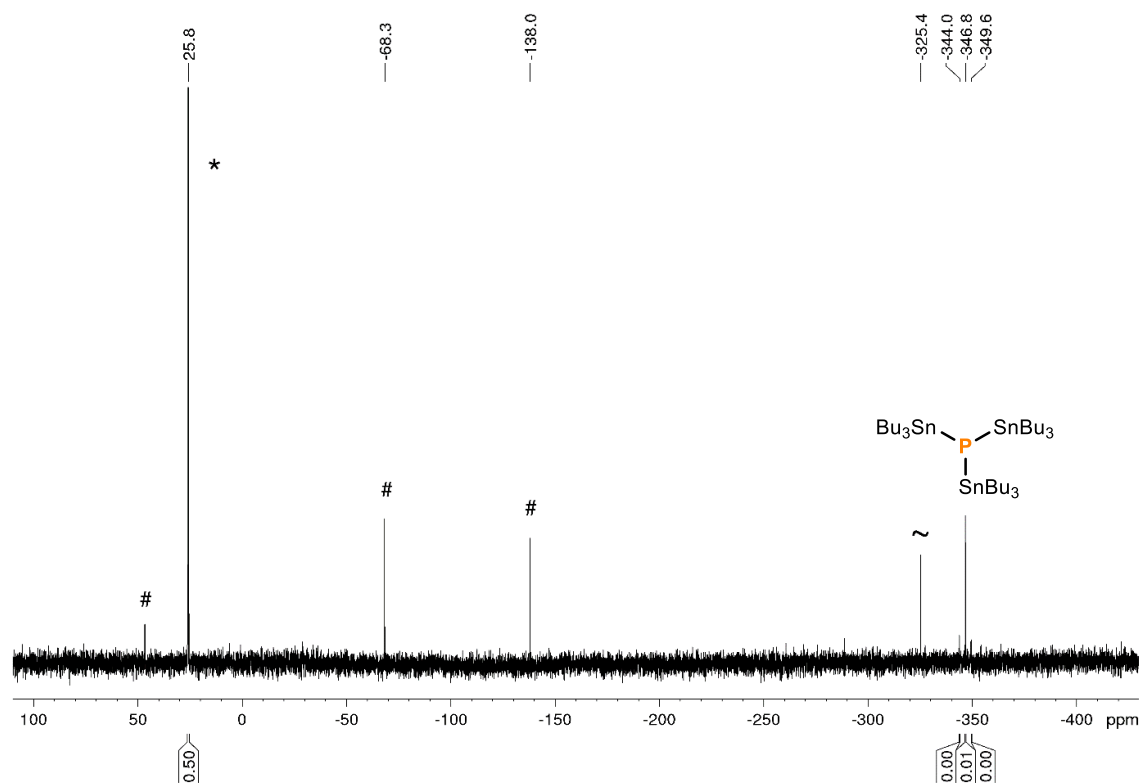


Figure S14. $^{31}\text{P}\{^1\text{H}\}$ NMR spectrum for the photocatalytic functionalization of P_4 using **acetone** as a photocatalyst (Table S7, Entry 10). * marks the internal standard Ph_3PO (0.02 mmol). ~ marks an unknown Sn-containing side product. # marks unknown side products.

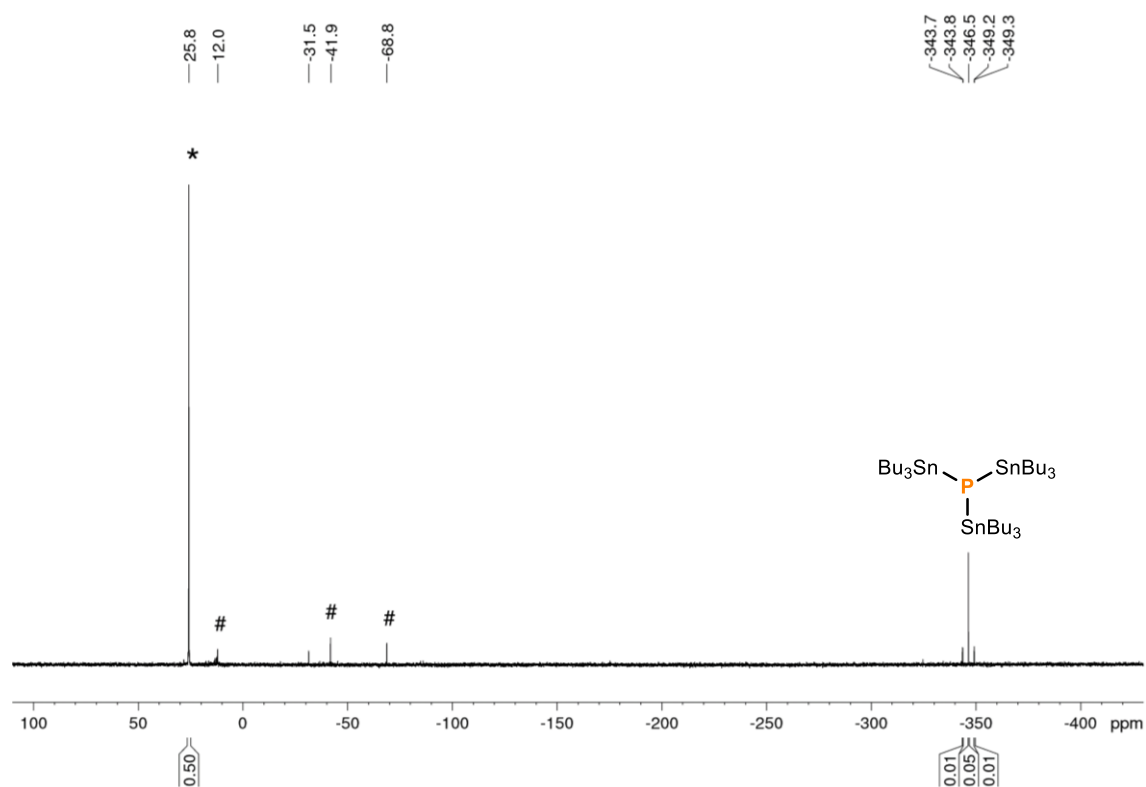


Figure S15. $^{31}\text{P}\{^1\text{H}\}$ NMR spectrum for the photocatalytic functionalization of P_4 using **DDQ** as a photocatalyst (Table S7, Entry 11). * marks the internal standard Ph_3PO (0.02 mmol). # marks unknown side products.

S6. General procedure for photocatalytic functionalization of P₄ (0.04 mmol scale) into stannylated phosphine (Bu₃Sn)₃P using anthraquinone

To a 10 mL stoppered tube equipped with a stirring bar were added (Bu₃Sn)₂ (101.1 μL, 5 equiv. based on phosphorus atoms, 20 equiv. based on P₄), anthraquinone (AQ) (1.0 mg, 0.5 equiv. based on P₄) and P₄ (0.01 mmol, as a stock solution in 71.3 μL benzene) in acetone as solvent (429 μL, in total 0.5 mL PhH/acetone mixture). The tube was sealed, placed in a water-cooled block (to ensure a near-ambient temperature was maintained, Figure S16), and irradiated with UV light (365 nm, 4.3 V, 700 mA, Osram OSOLON SSL 80) for 22 h (unless stated otherwise). Ph₃PO (0.02 mmol, stock solution in benzene) was subsequently added to act as an internal standard. The resulting mixture was subjected to ³¹P{¹H} NMR analysis and showed 83% conversion to the product (Bu₃Sn)₃P^[5] (Figure S17).

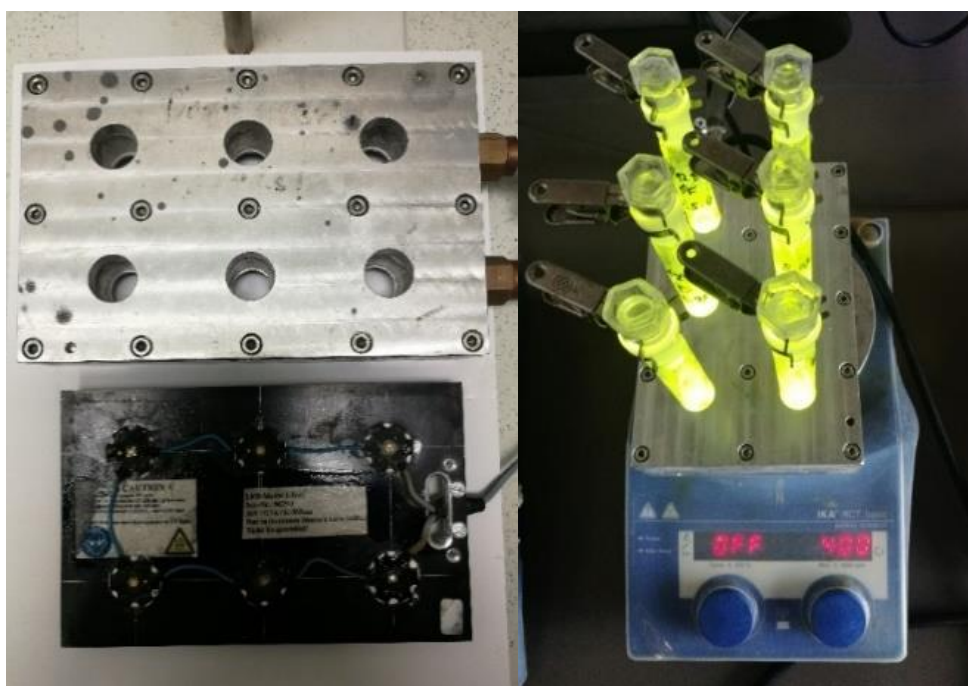


Figure S16. Illustration of the equipment setup used for photocatalytic reactions at 0.04 mmol scale.

Spectroscopic data of (Bu₃Sn)₃P:

³¹P{¹H} and ¹¹⁹Sn{¹H} NMR data of the photocatalytically generated (Bu₃Sn)₃P were extracted from spectra of the crude reaction mixture (see Figure S17 and S18), and are consistent with previous reports.^[5] Note that isolation of (Bu₃Sn)₃P was not pursued due to separation from unreacted (Bu₃Sn)₂ being complicated by very similar solubilities as well as the high boiling point of both compounds.

³¹P{¹H} NMR (161.98 MHz, 300 K, C₆D₆): δ = -346.8 ppm (s).

¹¹⁹Sn{¹H} NMR (149.21 MHz, 300 K, C₆D₆): δ = 38.0 ppm (d, ¹J(³¹P-¹¹⁹Sn) = 912.5 Hz, ²J(¹¹⁹Sn-¹¹⁷Sn) = 278.2 Hz).

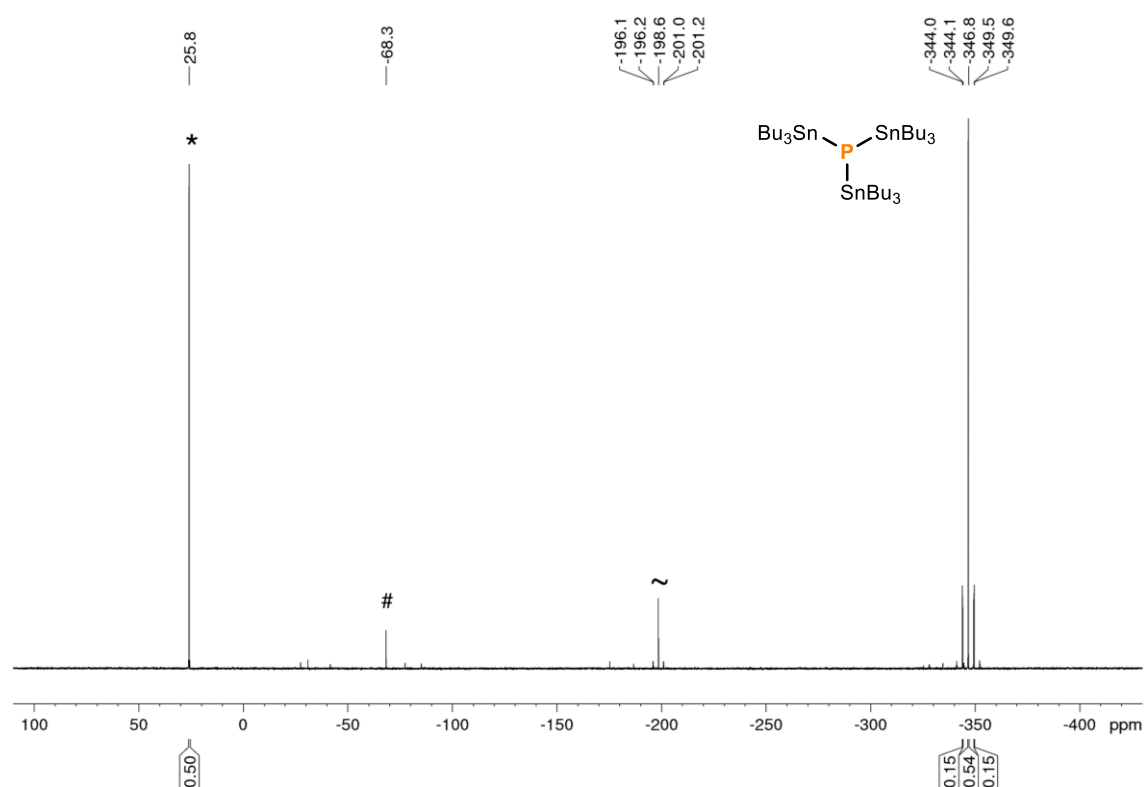


Figure S17. Representative $^{31}\text{P}\{^1\text{H}\}$ NMR spectrum for the photocatalytic functionalization of P_4 using **anthraquinone (AQ)** as a photoinitiator (section S5, Table S8, Entry 1). * marks the internal standard Ph_3PO (0.02 mmol). ~ marks an unknown Sn-containing side product. # marks unknown side products.

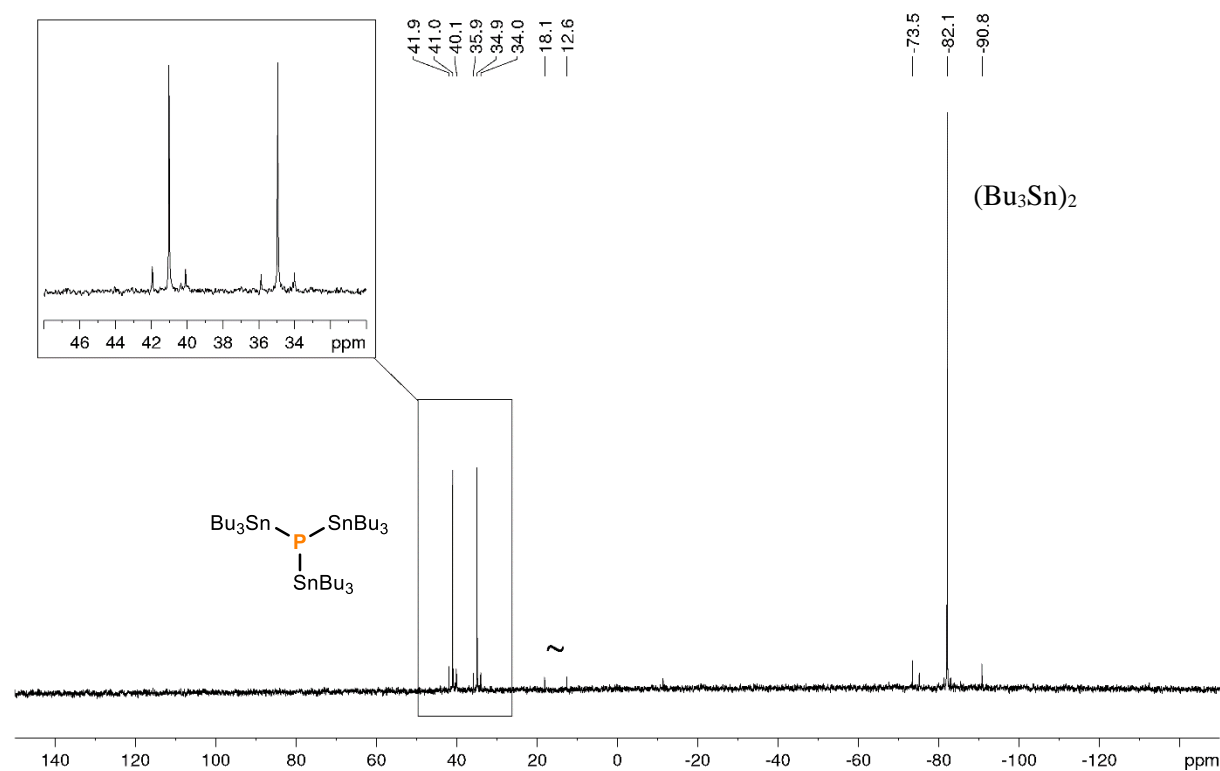


Figure S18. $^{119}\text{Sn}\{^1\text{H}\}$ NMR spectrum for the photocatalytic functionalization of P_4 using **anthraquinone (AQ)** as a photoinitiator (**0.5 equiv. anthraquinone** and **12 equiv. $(\text{Bu}_3\text{Sn})_2$** in **PhH/acetone**). ~ marks an unknown side product (see Figure S15, $^{31}\text{P}\{^1\text{H}\}$ NMR $\delta = -198.6$ ppm).

S7. Optimization of photocatalytic reaction conditions using anthraquinone

Table S8. Photocatalytic functionalization of P₄ to (Bu₃Sn)₃P: screening of control experiments.^[a]

Reaction scheme showing the photocatalytic functionalization of P₄ to (Bu₃Sn)₃P. The reactant is 1/4 P₄ (represented as a tetrahedron with one vertex highlighted). The reaction conditions are UV-LED (365 nm) and AQ, (Bu₃Sn)₂. The product is (Bu₃Sn)₃P (represented as a central P atom bonded to three SnBu₃ groups).

Entry	Conditions	Full conv. of P ₄ ?	Conv. to (Bu ₃ Sn) ₃ P / %
1	Standard ^[a]	✓	83
2	No light	✗	0
3	No AQ ^[b]	✓	2
4	No (Bu ₃ Sn) ₂	✗	0
5	Blue LEDs (455 nm)	✗	15
6	Violet/Blue LEDs (420 nm)	✓	76
7	P _{red} instead of P ₄	—	0

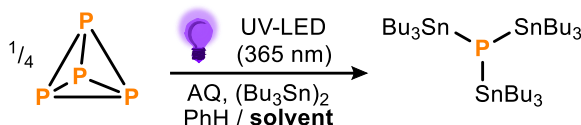
[a] For the general procedure, see section S6. [b] The reaction without anthraquinone (AQ) as a photoinitiator shows small conversion to (Bu₃Sn)₃P presumably because acetone used as a solvent can act as an alternative but less efficient photocatalyst (see section S5, Table S7, Entry 10).

Table S9. Photocatalytic functionalization of P₄ to (Bu₃Sn)₃P: screening of different radiation sources (LEDs).^[a]

Reaction scheme showing the photocatalytic functionalization of P₄ to (Bu₃Sn)₃P. The reactant is 1/4 P₄ (represented as a tetrahedron with one vertex highlighted). The reaction conditions are LEDs and AQ, (Bu₃Sn)₂. The product is (Bu₃Sn)₃P (represented as a central P atom bonded to three SnBu₃ groups).

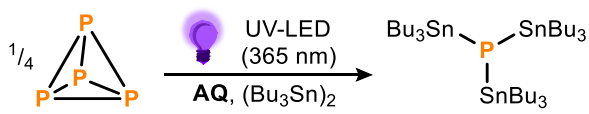
Entry	LEDs	Full conv. of P ₄ ?	Conv. to (Bu ₃ Sn) ₃ P / %
1	365 nm ^[a] (UV LED)	✓	83
2	385 nm (UV LED)	✓	66
3	405 nm (violet LED)	✓	21
4	420 nm (violet blue LED)	✓	76
5	455 nm (blue LED)	✓	15
6	528 nm (green LED)	✗	0

[a] The general procedure (section S6) was modified to use the LEDs indicated.

Table S10. Photocatalytic functionalization of P_4 to $(Bu_3Sn)_3P$: screening of **solvents**.^[a]


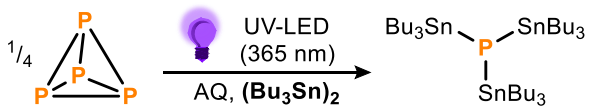
Entry	Solvent	Full conv. of P_4 ?	Conv. to $(Bu_3Sn)_3P$ / %
1	Benzene ^[a]	✓	58
2	Acetone	✓	83
3	Acetone ^[b]	✓	79
4	Acetonitrile	✓	5
5	THF	✓	35
6	Toluene	✓	60
7	Ethanol	✓	3

[a] The general procedure (section S6) was modified to use a solvent mixture (P_4 stock solutions in benzene). [b] 0.22 mL solvent volume.

Table S11. Photocatalytic functionalization of P_4 to $(Bu_3Sn)_3P$: screening of **amounts of anthraquinone**.^{[a][b]}


Entry	AQ / equiv. ^[b]	Full conv. of P_4 ?	Conv. to $(Bu_3Sn)_3P$ / %
1	0.01 ^[c]	✓	4
2	0.1 ^[c]	✓	47 ^[d]
3	0.25	✓	70 ^[e]
4	0.5	✓	83
5	1	✓	73
6	4	✓	45

[a] For the general procedure, see section S6. [b] Listed equivalents are defined per P_4 molecule. [c] For catalytic use of photoinitiator anthraquinone (**AQ**) a stock solution (1 mg **AQ** in 1 mL benzene) was prepared for screening 0.01 equiv. **AQ** (20.8 μ L, Entry 1) and 0.1 mmol **AQ** (208 μ L, Entry 2). [d] This catalyst loading corresponds to a TON of 28.2. [e] This catalyst loading corresponds to a TON of 16.8.

Table S12. Photocatalytic functionalization of P_4 to $(Bu_3Sn)_3P$: screening of amounts of $(Bu_3Sn)_2$.^{[a][b]}


Entry	AQ / equiv.	$(Bu_3Sn)_2$ / equiv. ^[a]	Full conv. of P_4 ?	Conv. to $(Bu_3Sn)_3P$ / %
1	1	30	✓	82
2	1	20	✓	75
3	1	12	✓	82
4	1	6	✓	61
5	0.5	30	✓	84
6	0.5	20	✓	83
7	0.5	12	✓	79
8	0.5	6	✓	64

[a] For the general procedure, see section S6. [b] Listed equivalents are defined per P_4 molecule (0.01 mmol).

Note:

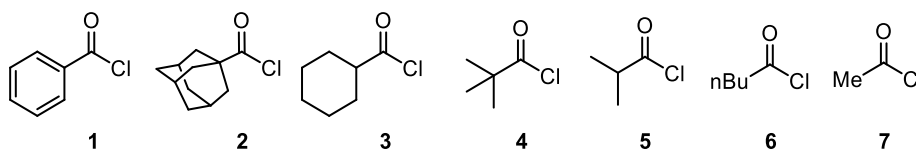
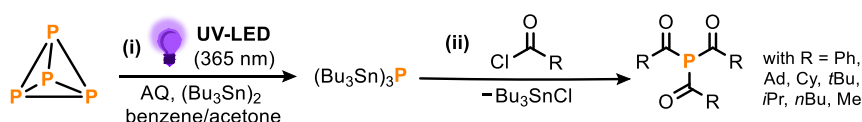
In the final stage of optimization, it was found that reducing the $(Bu_3Sn)_2$ loading from 20 equiv. to 12 equiv. had only a very minor impact on conversion to $(Bu_3Sn)_3P$ (from 83% to 79%). Thus, while the reaction with 20 equiv. formally gave the best conversion, the reaction with 12 equiv. was chosen as being optimal for further elaboration into ‘one pot’ reactions, as it should reduce the formation of stoichiometric, Sn-containing waste.

S8. Characterization of optimized reactions using anthraquinone

S8.1 Synthesis of triacylphosphines $(R(O)C)_3P$ ($R = Ph, Ad, Cy, tBu, iPr, nBu, Me$)^[5] (0.04 mmol scale)

To a 10 mL stoppered tube equipped with a stirring bar were added $(Bu_3Sn)_2$ (60.6 μ L, 3 equiv. based on phosphorus atoms, 12 equiv. based on P_4), anthraquinone (**AQ**) (1.0 mg, 0.5 equiv. based on P_4) and P_4 (0.01 mmol, as a stock solution in 71.3 μ L benzene) in acetone as solvent (429 μ L, in total 0.5 mL PhH/acetone mixture). The tube was sealed, placed in a water-cooled block (to ensure a near-ambient temperature was maintained, Figure S14), and irradiated with UV light (365 nm, 4.3 V, 700 mA, Osram OSOLON SSL 80) for 22 h. To further functionalize the P_1 intermediate $(Bu_3Sn)_3P$ into triacylphosphines $(R(O)C)_3P$ in an ‘one-pot’ manner, different acyl chlorides $RC(O)Cl$ (0.16 mmol, 16 equiv. based on P_4 , 4 equiv. based on phosphorus atoms, with $R = Ph, Ad, Cy, tBu, iPr, nBu$ and Me , see Table S13) were added to the photocatalytic reaction mixture, which each showed a color change from an orange to a yellow solution while stirring overnight.

Table S13. Substrate scope for functionalization of $(Bu_3Sn)_3P$ generated photocatalytically using anthraquinone into **triacyl phosphines**.



Substrate	R	Full conv. of $(Bu_3Sn)_3P$?	Conv. ^[a] to $(R(O)C)_3P$ / %
1	R = Phenyl (Ph)	✓	75
2	R = Adamantyl (Ad)	✓	40
3	R = Cyclohexyl (Cy)	✓	66
4	R = <i>tert</i> -Butyl (<i>t</i> Bu)	✓	64
5	R = <i>iso</i> -Propyl (<i>i</i> Pr)	✓	67
6	R = <i>n</i> -Butyl (<i>n</i> Bu)	✓	54
7	R = Methyl (Me)	✓	60

‘One-pot’ synthesis of triacyl phosphines: (i) For the general procedure of the photocatalytic stannylation of P_4 into $(Bu_3Sn)_3P$ (0.04 mmol scale) see section S6. (ii) Subsequent functionalization of $(Bu_3Sn)_3P$ using acyl chlorides to generate triacyl phosphines $(R(O)C)_3P$. The conversions were determined by $^{31}P\{^1H\}$ NMR experiments (161.98 MHz, 300 K, C_6D_6) (0.02 mmol Ph_3PO as internal standard). [a] The conversions were determined by quantitative $^{31}P\{^1H\}$ NMR ($T_{1S} < T_{1Prod} = 10s$, $D1 = 40s$, (zgif30, inverse gated decoupled).

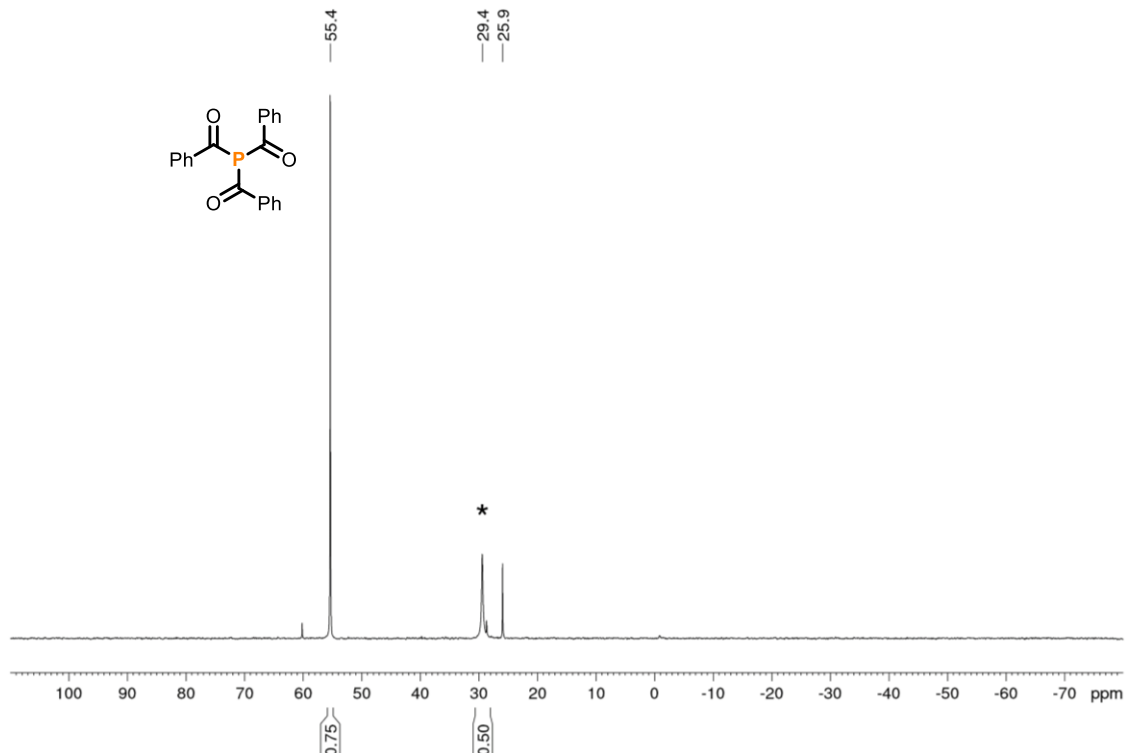
S8.1.1 Synthesis and quantification of (Ph(O)C)₃P

Figure S19. Quantitative $^{31}\text{P}\{^1\text{H}\}$ NMR spectrum of (Ph(O)C)₃P generated *via* photocatalytic stannylation of P₄ in benzene/acetone followed by acylation with benzoyl chloride PhC(O)Cl (**1**) (Table S13, **12 equiv.** (Bu₃Sn)₂, T_{1IS} < T_{1Prod} = 10s, D1 = 40 s, zig30, inverse gated decoupled, LB = 10). * marks the internal standard Ph₃PO (0.02 mmol).

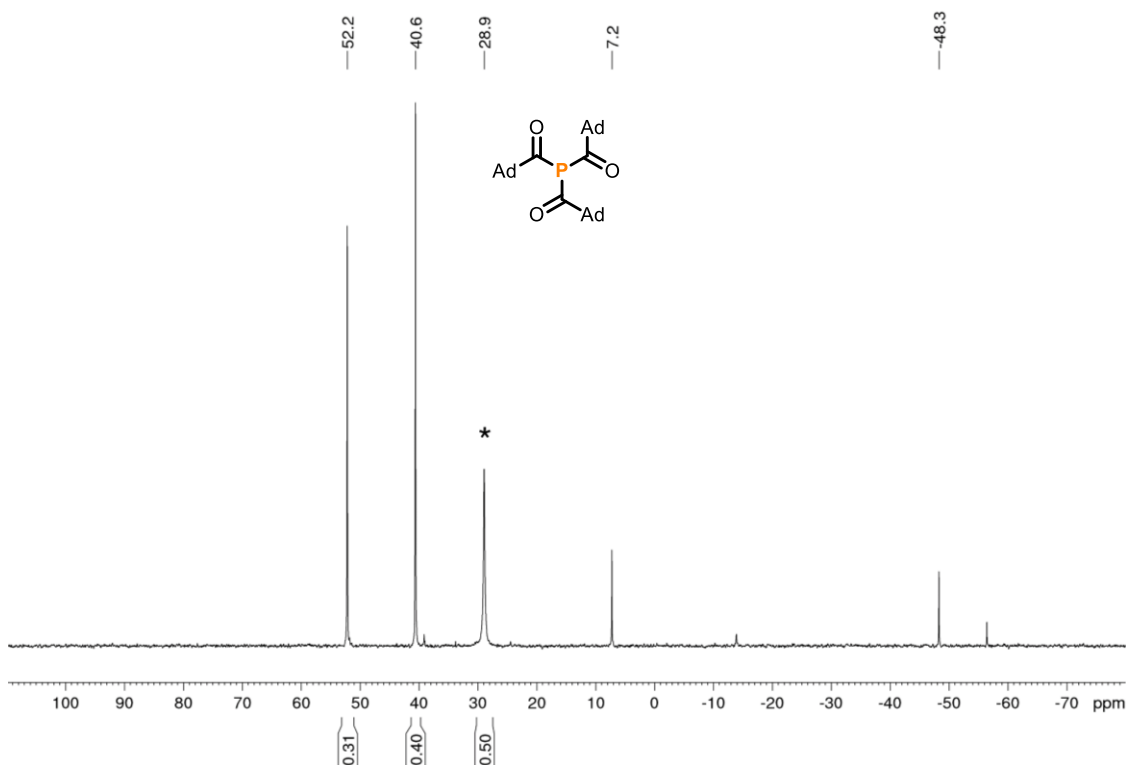
S8.1.2 Synthesis and quantification of (Ad(O)C)₃P

Figure S20. Quantitative $^{31}\text{P}\{^1\text{H}\}$ NMR spectrum of (Ad(O)C)₃P generated *via* photocatalytic stannylation of P₄ in benzene/acetone followed by acylation with 1-adamantanecarbonyl chloride AdC(O)Cl (**2**) (Table S13, **12 equiv.** (Bu₃Sn)₂, T_{1IS} < T_{1Prod} = 10s, D1 = 40 s, zig30, inverse gated decoupled, LB = 10). * marks the internal standard Ph₃PO (0.02 mmol).

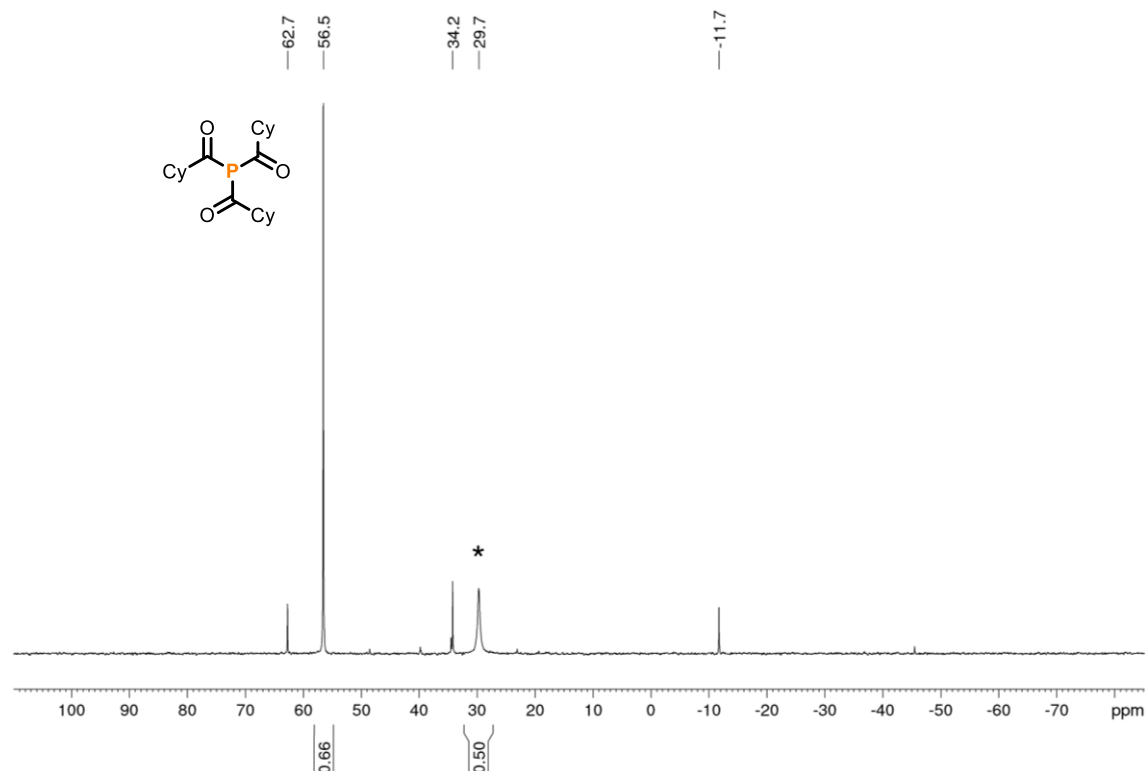
S8.1.3 Synthesis and quantification of (Cy(O)C)₃P

Figure S21. Quantitative $^{31}\text{P}\{^1\text{H}\}$ NMR spectrum of (Cy(O)C)₃P generated *via* photocatalytic stannylation of P₄ in benzene/acetone followed by acylation with cyclohexanecarbonyl chloride CyC(O)Cl (**3**) (Table S13, **12 equiv.** (Bu₃Sn)₂, T_{1IS} < T_{1Prod} = 10s, D1 = 40 s, **zgif30**, **inverse gated decoupled**, LB = 10). * marks the internal standard Ph₃PO (0.02 mmol).

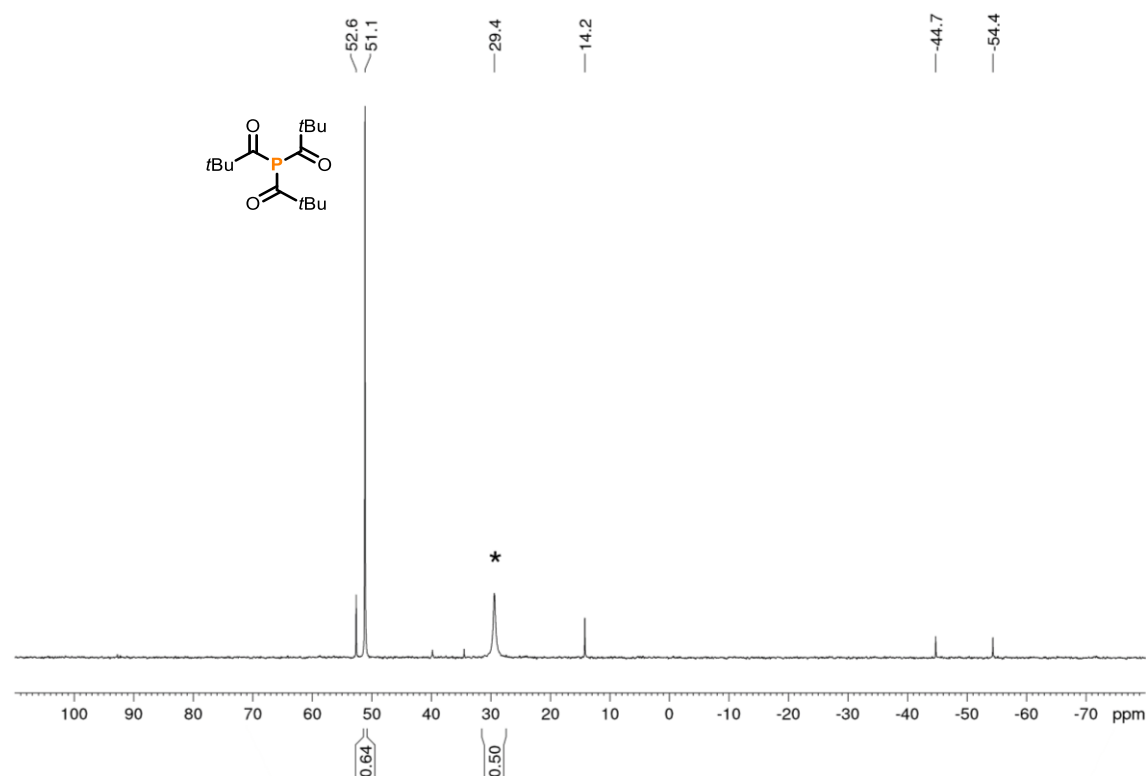
S8.1.4 Synthesis and quantification of (tBu(O)C)₃P

Figure S22. Quantitative $^{31}\text{P}\{^1\text{H}\}$ NMR spectrum of (tBu(O)C)₃P generated *via* photocatalytic stannylation of P₄ in benzene/acetone followed by acylation with pivaloyl chloride tBuC(O)Cl (**4**). (Table S13, **12 equiv.** (Bu₃Sn)₂, T_{1IS} < T_{1Prod} = 10s, D1 = 40 s, **zgif30**, **inverse gated decoupled**, LB = 10) * marks the internal standard Ph₃PO (0.02 mmol).

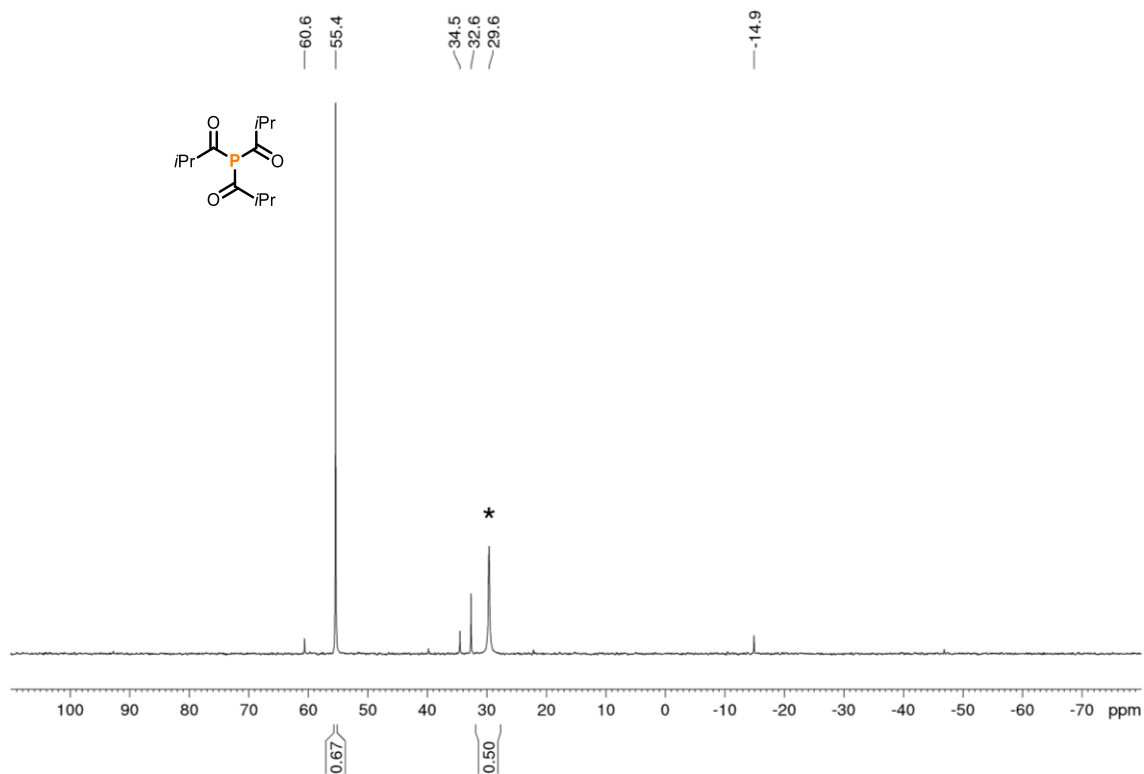
S8.1.5 Synthesis and quantification of (*i*Pr(O)C)₃P

Figure S23. Quantitative $^{31}\text{P}\{^1\text{H}\}$ NMR spectrum of (*i*Pr(O)C)₃P generated *via* photocatalytic stannylation of P₄ in benzene/acetone followed by acylation with isobutyryl chloride *i*PrC(O)Cl (**5**). (Table S13, **12 equiv.** (Bu₃Sn)₂, T1_S < T1_{Prod} = 10s, D1 = 40 s, **zgig30, inverse gated decoupled, LB = 10**) * marks the internal standard Ph₃PO (0.02 mmol).

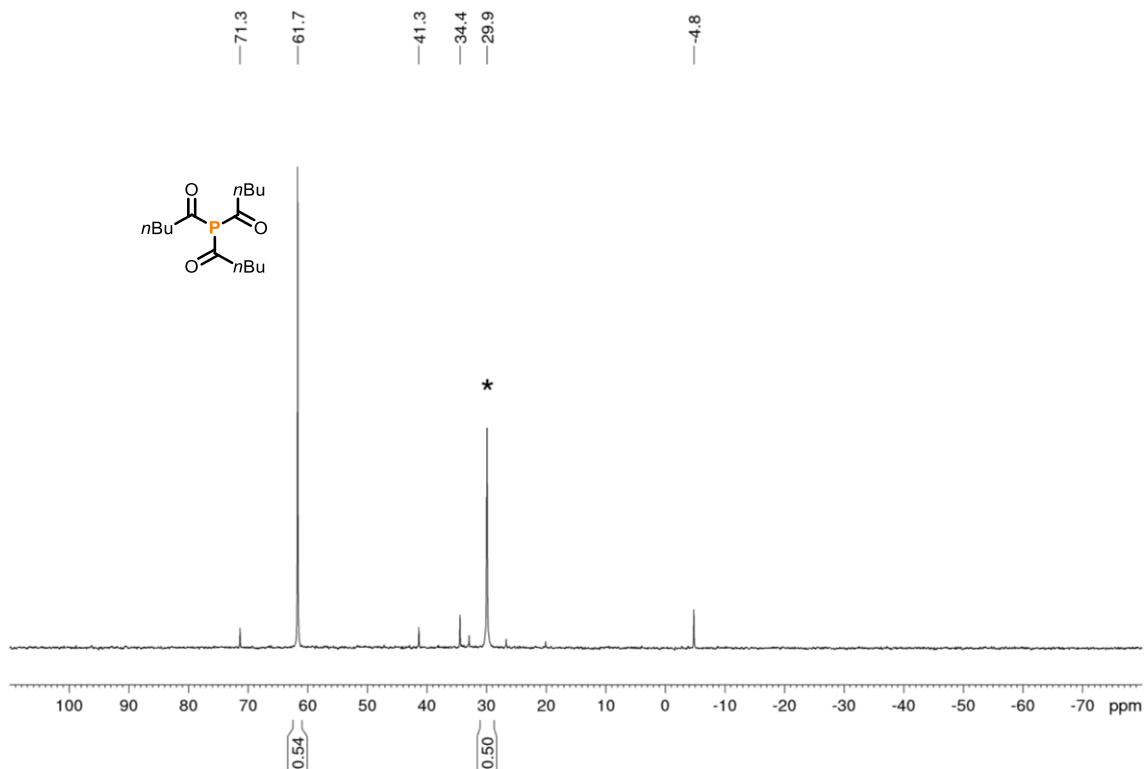
S8.1.6 Synthesis and quantification of (*n*Bu(O)C)₃P

Figure S24. Quantitative $^{31}\text{P}\{^1\text{H}\}$ NMR spectrum of (*n*Bu(O)C)₃P generated *via* photocatalytic stannylation of P₄ in benzene/acetone followed by acylation with valeroyl chloride *n*BuC(O)Cl (**6**). (Table S13, **12 equiv.** (Bu₃Sn)₂, T1_S < T1_{Prod} = 10s, D1 = 40 s, **zgig30, inverse gated decoupled, LB = 10**). * marks the internal standard Ph₃PO (0.02 mmol).

S8.1.7 Synthesis and quantification of (Me(O)C)₃P

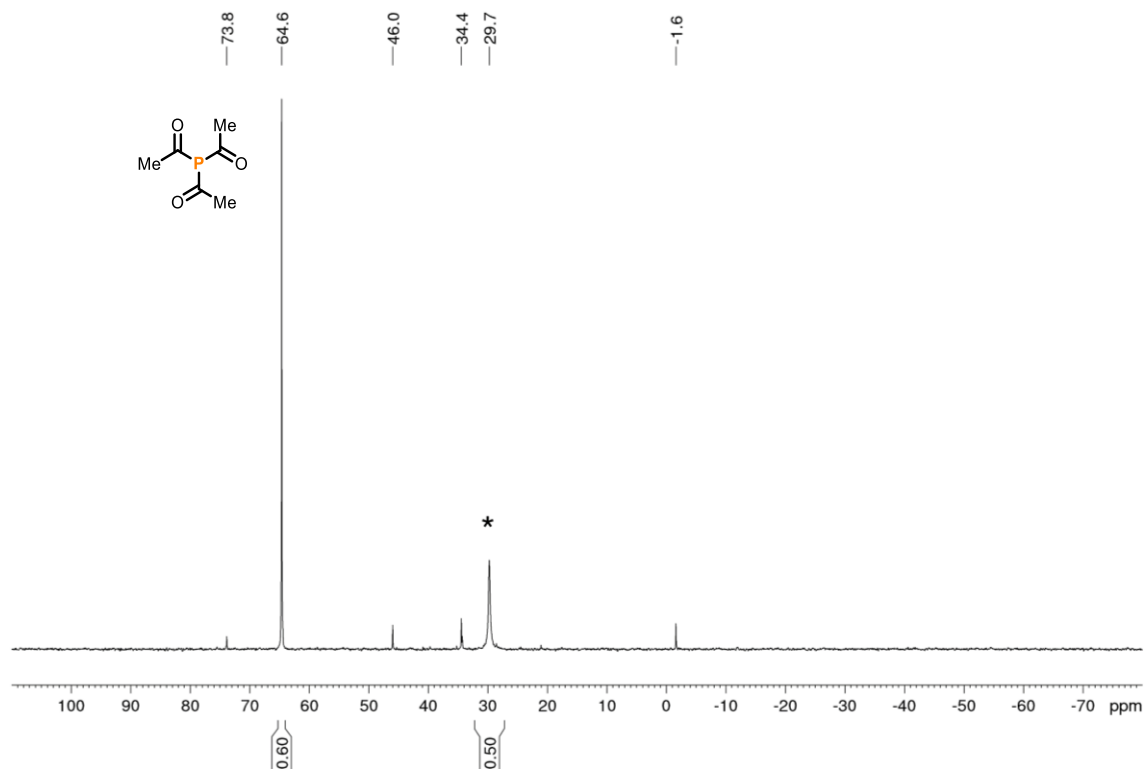


Figure S25. Quantitative ³¹P{¹H} NMR spectrum of (Me(O)C)₃P generated *via* photocatalytic stannylation of P₄ in benzene/acetone followed by acylation with acetyl chloride MeC(O)Cl (**7**). (Table S13, **12 equiv.** (Bu₃Sn)₂, **T1_{IS}** < **T1_{Prod}** = **10s**, **D1** = **40 s**, **zgig30**, **inverse gated decoupled**, **LB** = **10**). * marks the internal standard Ph₃PO (0.02 mmol).

S8.2 Synthesis of the phosphonium salts $[\text{R}_4\text{P}]\text{Br}^{[5]}$

To a 10 mL stoppered tube equipped with a stirring bar were added $(\text{Bu}_3\text{Sn})_2$ (60.6 μL , 3 equiv. based on phosphorus atoms, 12 equiv. based on P_4), anthraquinone (**AQ**) (1.0 mg, 0.5 equiv. based on P_4) and P_4 (0.01 mmol, as a stock solution in 71.3 μL benzene) in acetone as solvent (429 μL , in total 0.5 mL PhH/acetone mixture). The tube was sealed, placed in a water-cooled block (to ensure a near-ambient temperature was maintained, Figure S14), and irradiated with UV light (365 nm, 4.3 V, 700 mA, Osram OSOLON SSL 80) for 22 h. After photocatalytic generation of the stannylated phosphine $(\text{Bu}_3\text{Sn})_3\text{P}$ directly from P_4 this P_1 intermediate was further converted into phosphonium salts in an ‘one-pot’ manner. Alkyl bromides such as benzyl bromide or ethyl bromide (0.2 mmol, 20 equiv. based on P_4 , 5 equiv. based on phosphorus atoms) were added to the photocatalytic reaction mixture. While heating the reaction mixture (for $[\text{Bn}_4\text{P}]\text{Br}$: overnight at 60 $^\circ\text{C}$, for $[\text{Et}_4\text{P}]\text{Br}$: 2d at 80 $^\circ\text{C}$) a color change from an orange to a yellow solution was obtained. Ph_3PO (0.02 mmol, stock solution in benzene) was subsequently added to act as an internal standard. The resulting mixture was subjected to $^{31}\text{P}\{^1\text{H}\}$ NMR analysis (Figure S26 and S27).

Table S14. Substrates for functionalization of photocatalytic generated $(\text{Bu}_3\text{Sn})_3\text{P}$ into **phosphonium salts**.

Entry	Substrate	Full conv. of $(\text{Bu}_3\text{Sn})_3\text{P}$?	Conv. to $[\text{R}_4\text{P}]^+$ / %
1	Benzyl bromide (BnBr)	✓	69%
2	Ethyl bromide (EtBr)	✓	46%

One-pot’ synthesis of phosphonium salts: (i) For the general procedure of the photocatalytic stannylation of P_4 into $(\text{Bu}_3\text{Sn})_3\text{P}$ (0.04 mmol scale) see section S6. (ii) Subsequent functionalization of $(\text{Bu}_3\text{Sn})_3\text{P}$ using alkyl bromides (RBr) to generate phosphonium salts $[\text{R}_4\text{P}]\text{Br}$.

S8.2.1 Synthesis and quantification of [Bn₄P]Br

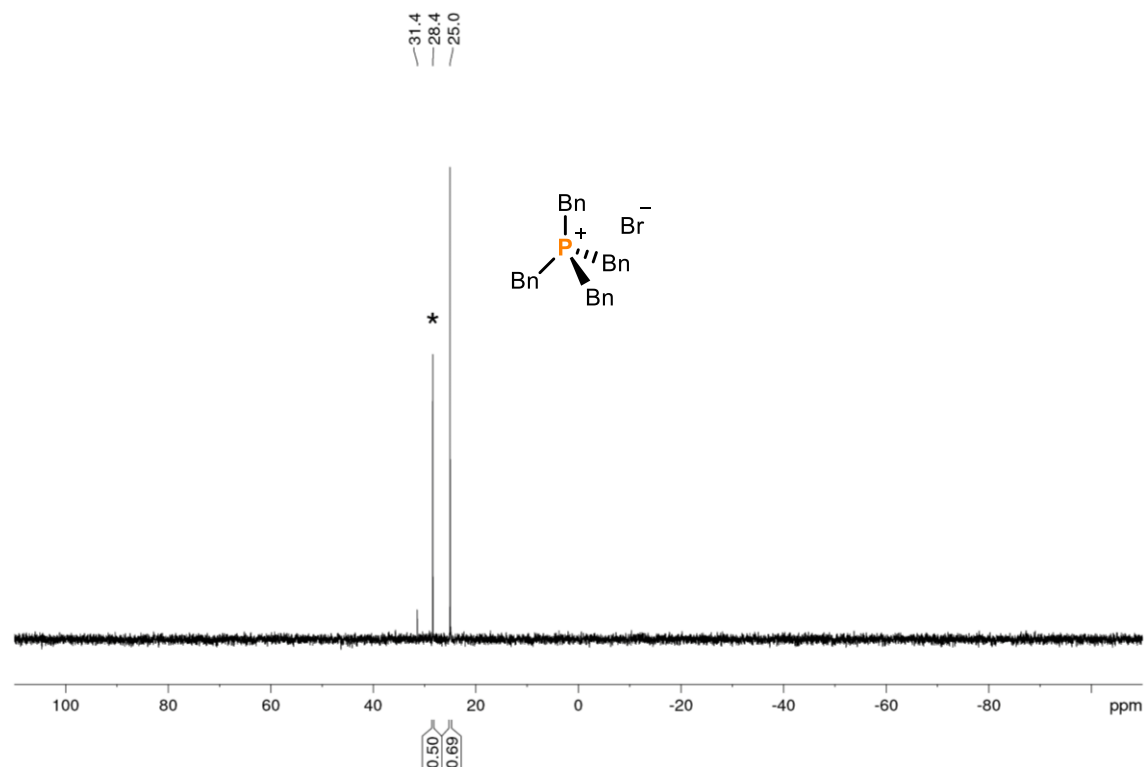


Figure S26. Quantitative $^{31}\text{P}\{^1\text{H}\}$ NMR (zgig) spectrum of [Bn₄P]Br generated *via* photocatalytic stannylation of P₄ in benzene/acetone followed by alkylation with benzyl bromide (BnBr, Table S14, Entry 1). * marks the internal standard Ph₃PO (0.02 mmol).

S8.2.2 Synthesis and quantification of [Et₄P]Br

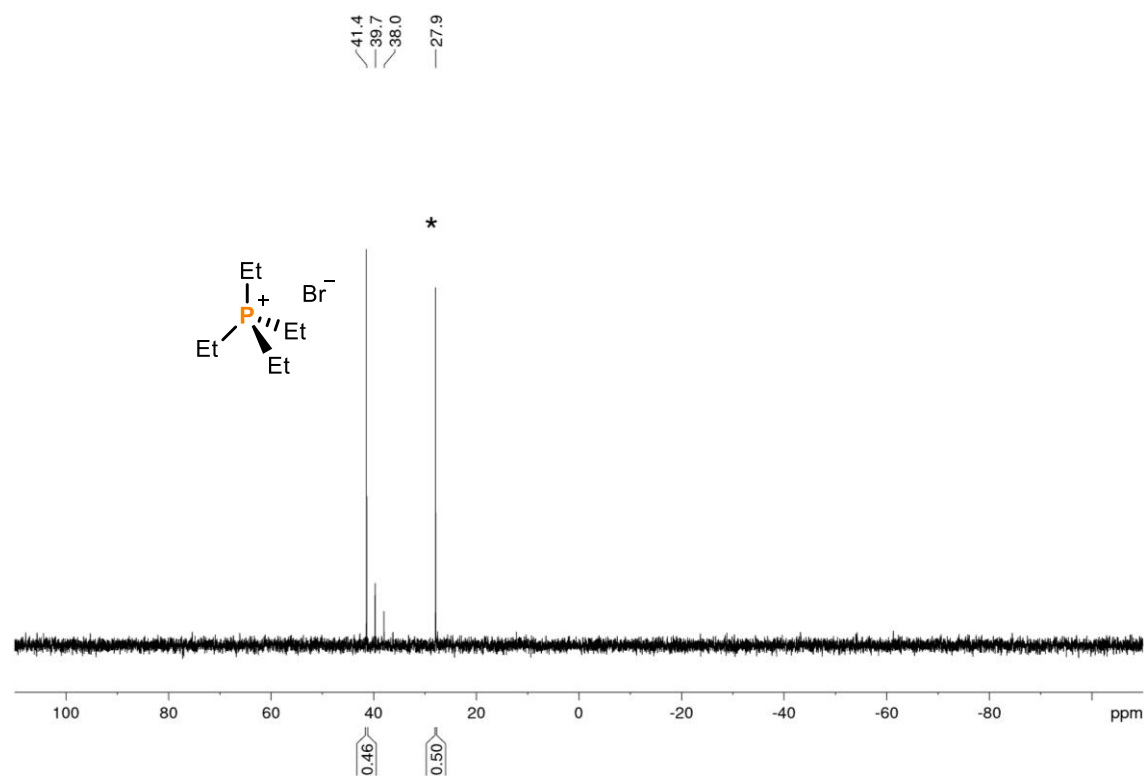
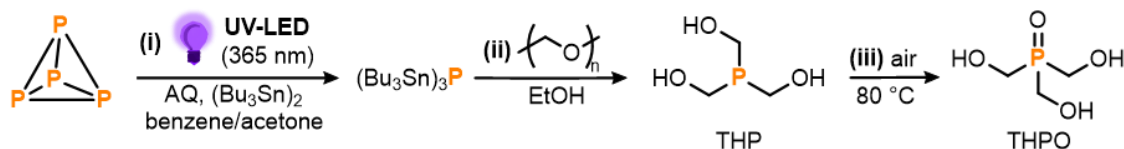


Figure S27. Quantitative $^{31}\text{P}\{^1\text{H}\}$ NMR (zgig) spectrum of [Et₄P]Br generated *via* photocatalytic stannylation of P₄ in benzene/acetone followed by alkylation with benzyl bromide (EtBr, Table S14, Entry 2). * marks the internal standard Ph₃PO (0.02 mmol).

S8.3 Synthesis of THP, THPO and THPC

S8.3.1 Synthesis of THP and oxidation to THPO



To a 10 mL stoppered tube equipped with a stirring bar were added $(Bu_3Sn)_2$ (60.6 μ L, 3 equiv. based on phosphorus atoms, 12 equiv. based on P_4), anthraquinone (AQ) (1.0 mg, 0.5 equiv. based on P_4) and P_4 (0.01 mmol, as a stock solution in 71.3 μ L benzene) in acetone as solvent (429 μ L, in total 0.5 mL PhH/acetone mixture). The tube was sealed, placed in a water-cooled block (to ensure a near-ambient temperature was maintained, Figure S16), and irradiated with UV light (365 nm, 4.3 V, 700 mA, Osram OSOLON SSL 80) for 22 h. The photocatalytically generated P_1 intermediate $(Bu_3Sn)_3P$ was further functionalized by removal of volatiles under vacuum and addition of EtOH (1 mL) and paraformaldehyde (3.6 mg, 0.12 mmol, 12 equiv. based on P_4 , 3 equiv. based on phosphorus atoms). The resulting suspension was stirred at room temperature for 16 h. Ph_3PO (0.02 mmol, stock solution in benzene) was subsequently added to act as an internal standard. The resulting mixture was subjected to $^{31}P\{^1H\}$ NMR analysis and showed 48% conversion of THP (Figure S28).

Afterwards the ‘one-pot’ reaction mixture was stirred at 80 °C under air for 16 h to convert the initially formed product THP into its oxidized form THPO ($^{31}P\{^1H\}$ NMR analysis: 38% conversion to THPO, see Figure S29).

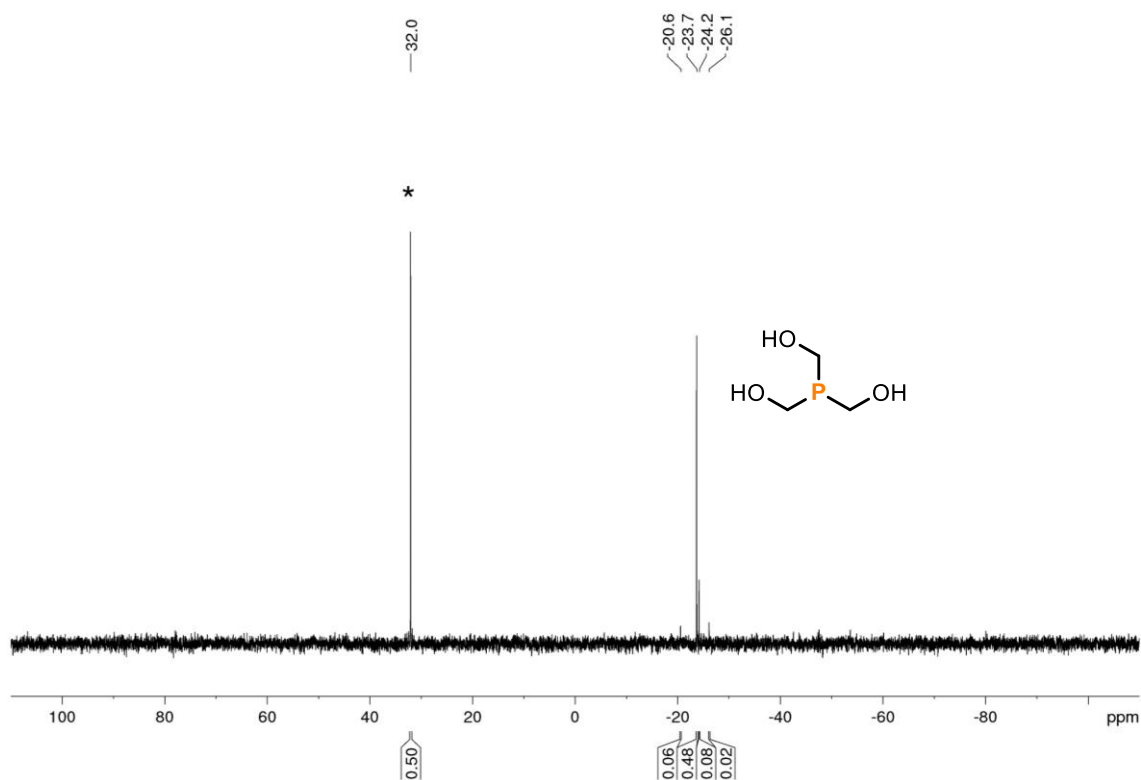


Figure S28. Quantitative $^{31}\text{P}\{^1\text{H}\}$ NMR (zgig) spectrum of THP generated *via* photocatalytic stannylation of P_4 in benzene/acetone followed by addition of paraformaldehyde in EtOH. * marks the internal standard Ph_3PO (0.02 mmol).

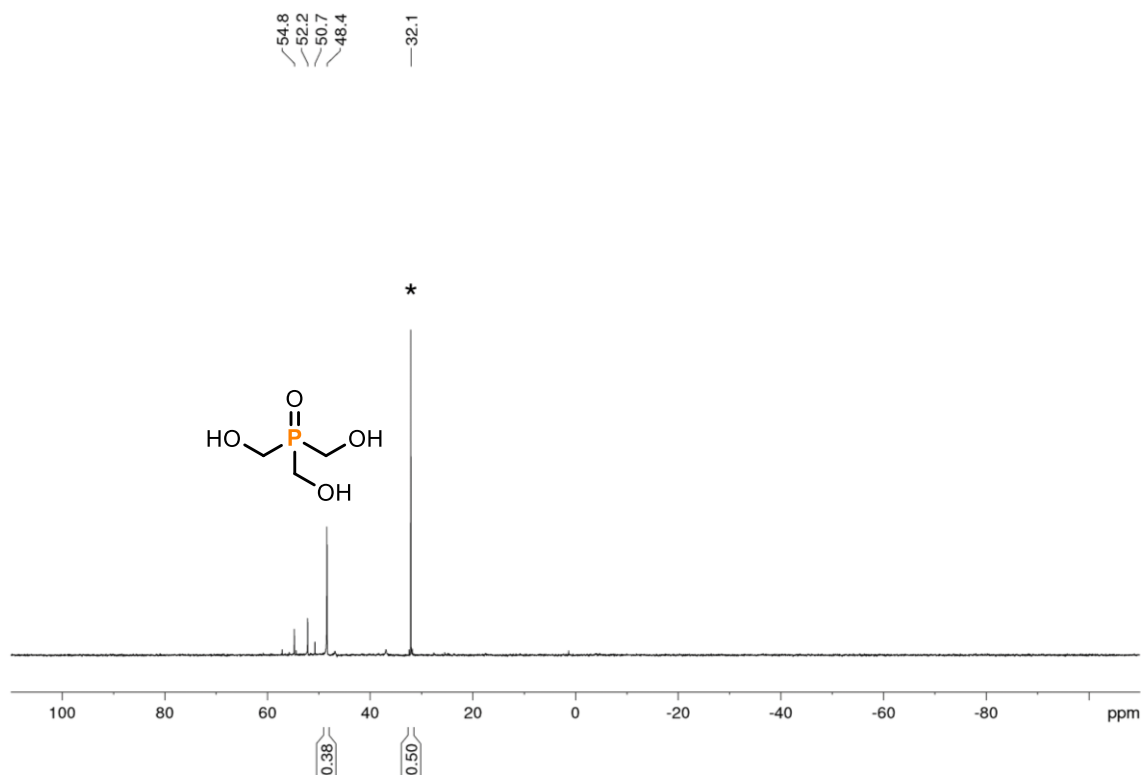
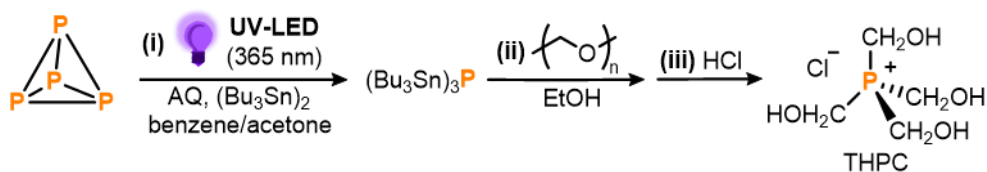


Figure S29. Quantitative $^{31}\text{P}\{^1\text{H}\}$ NMR spectrum of THPO generated *via* photocatalytic stannylation of P_4 in benzene/acetone followed by addition of paraformaldehyde in EtOH and subsequent oxidation in air. * marks the internal standard Ph_3PO (0.02 mmol).

S8.3.2 Synthesis of THPC



To a 10 mL stoppered tube equipped with a stirring bar were added $(\text{Bu}_3\text{Sn})_2$ (60.6 μL , 3 equiv. based on phosphorus atoms, 12 equiv. based on P_4), anthraquinone (**AQ**) (1.0 mg, 0.5 equiv. based on P_4) and P_4 (0.01 mmol, as a stock solution in 71.3 μL benzene) in acetone as solvent (429 μL , in total 0.5 mL PhH/acetone mixture). The tube was sealed, placed in a water-cooled block (to ensure a near-ambient temperature was maintained, Figure S16), and irradiated with UV light (365 nm, 4.3 V, 700 mA, Osram OSOLON SSL 80) for 22 h. The photocatalytically generated P_1 intermediate $(\text{Bu}_3\text{Sn})_3\text{P}$ was further functionalized by removal of volatiles under vacuum and addition of EtOH (1 mL) and paraformaldehyde (15 mg, 0.5 mmol, 20 equiv. based on P_4 , 5 equiv. based on phosphorus atoms). The resulting suspension was stirred at room temperature for 16 h. The mixture was frozen in a liquid-nitrogen bath, and HCl (0.4 M in 1,4-dioxane, 1 mL, 0.4 mmol, 40 equiv. based on P_4 , 10 equiv. based on phosphorus atoms) was added. After thawing, the yellowish reaction mixture was stirred at room temperature for 2 h. Ph_3PO (0.02 mmol, stock solution in benzene) was subsequently added to act as an internal standard. The resulting mixture was subjected to $^{31}\text{P}\{^1\text{H}\}$ NMR analysis and showed 53% conversion of THPC (Figure S30).

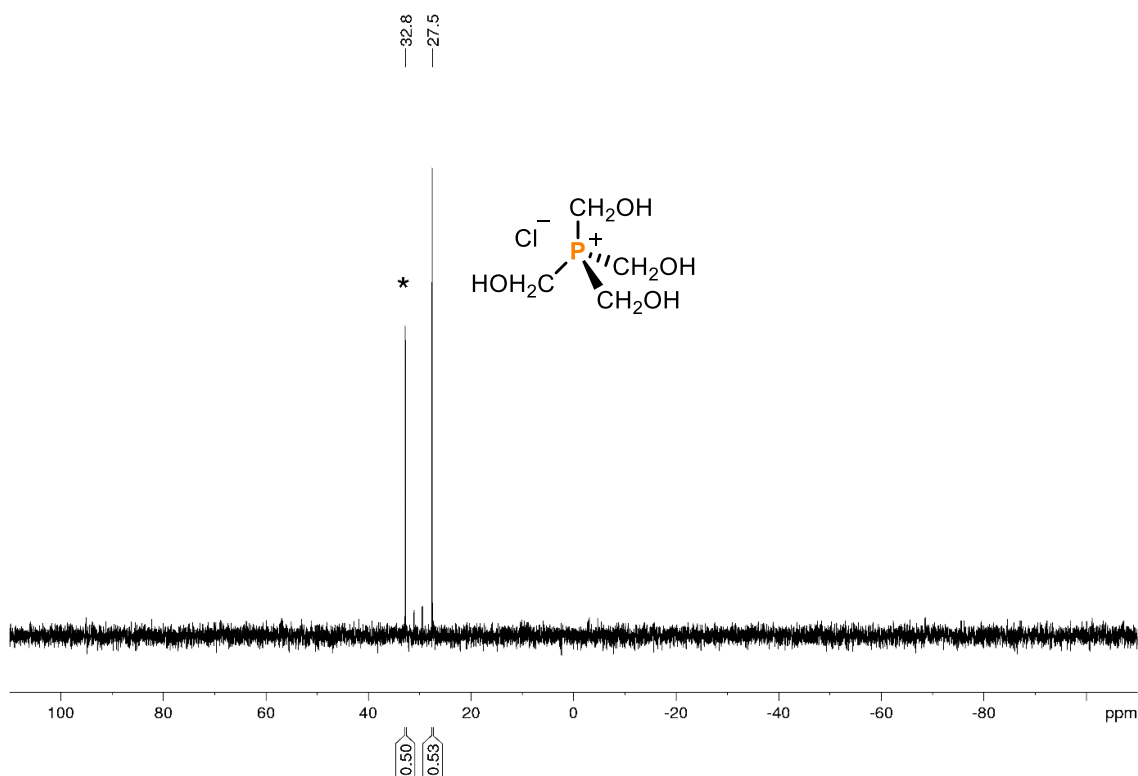


Figure S30. Quantitative $^{31}\text{P}\{^1\text{H}\}$ NMR (zgig) spectrum of THPC generated *via* photocatalytic stannylation of P_4 in benzene/acetone followed by reaction with paraformaldehyde in EtOH and subsequent HCl work-up. * marks the internal standard Ph_3PO (0.02 mmol).

S9. Reactions at 0.8 mmol scale using anthraquinone as a photoinitiator

S9.1 Photocatalytic synthesis of stannylated phosphine $(\text{Bu}_3\text{Sn})_3\text{P}^{[5]}$

To a 100 mL stoppered tube equipped with a stirring bar were added $(\text{Bu}_3\text{Sn})_2$ (1.212 mL, 2.4 mmol, 3 equiv. based on phosphorus atoms, 12 equiv. based on P_4), anthraquinone (AQ) (20.8 mg, 0.1 mmol, 0.5 equiv. based on P_4) and P_4 (0.2 mmol, as a stock solution in 1.426 mL benzene) in acetone as solvent (2.574 mL, in total 4 mL PhH/acetone mixture). The tube was sealed, placed in a water-cooled block (to ensure a near-ambient temperature was maintained, Figure S31), and irradiated with UV light (365 nm, 14 V, 700 mA, Osram OSRON SSL 80) for 48 h. $^{31}\text{P}\{^1\text{H}\}$ NMR spectroscopy (Ph_3PO as internal standard) showed 64% conversion to the stannylated phosphine $(\text{Bu}_3\text{Sn})_3\text{P}$ (see Figure S32).

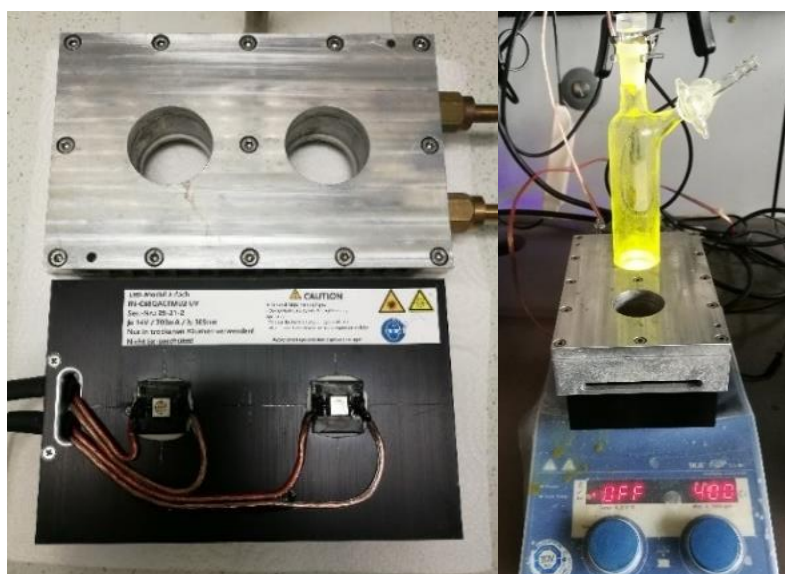


Figure 31. Illustration of the equipment setup used for photocatalytic reactions at 0.8 mmol scale.

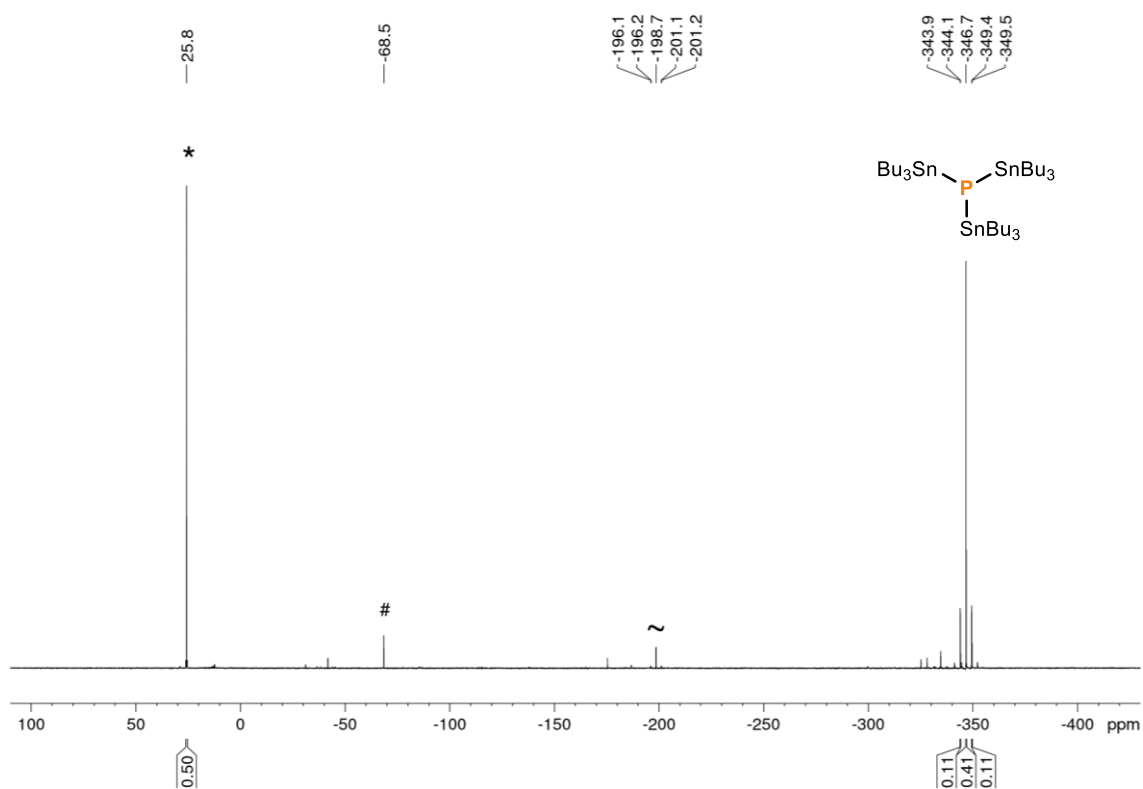


Figure S32. $^{31}\text{P}\{^1\text{H}\}$ NMR spectrum for the **scale-up** (0.8 mmol) photocatalytic stannylation of P_4 using $(\text{Bu}_3\text{Sn})_2$ and photoinitiator anthraquinone (AQ). $*$ marks the internal standard Ph_3PO . \sim marks an unknown Sn-containing side product. $\#$ marks unknown side products.

S9.2 'One-pot' synthesis and purification of (Ph(O)C)₃P

To a 100 mL stoppered tube equipped with a stirring bar were added (Bu₃Sn)₂ (1.212 mL, 2.4 mmol, 3 equiv. based on phosphorus atoms, 12 equiv. based on P₄) anthraquinone (AQ) (20.8 mg, 0.1 mmol, 0.5 equiv. based on P₄) and P₄ (0.2 mmol, as a stock solution in 1.426 mL benzene) in acetone as solvent (2.574 mL, in total 4 mL PhH/acetone mixture). The tube was sealed, placed in a water-cooled block (to ensure a near-ambient temperature was maintained, Figure S31), and irradiated with UV light (365 nm, 14 V, 700 mA, Osram OSOLON SSL 80) for 48 h. Subsequent addition of benzoyl chloride PhC(O)Cl (371 μL, 3.2 mmol, 16 equiv. based on P₄, 4 equiv. based on phosphorus atom) and stirring overnight at room temperature resulted in a color change of the orange reaction mixture to a yellow solution (by internal standard addition to a separate reaction the ³¹P{¹H} NMR showed 62% conversion into (Ph(O)C)₃P, see Figure S33). The volatiles were removed under vacuum and the remaining yellow solid was washed with *n*-hexane (4 x 5 mL). The remaining yellow residue was recrystallized from THF/*n*-hexane at -35 °C. Decanting of the mother liquor and washing with *n*-hexane (2 x 10 mL) afforded the desired product (Ph(O)C)₃P as yellow powder (151.2 mg, 55%).

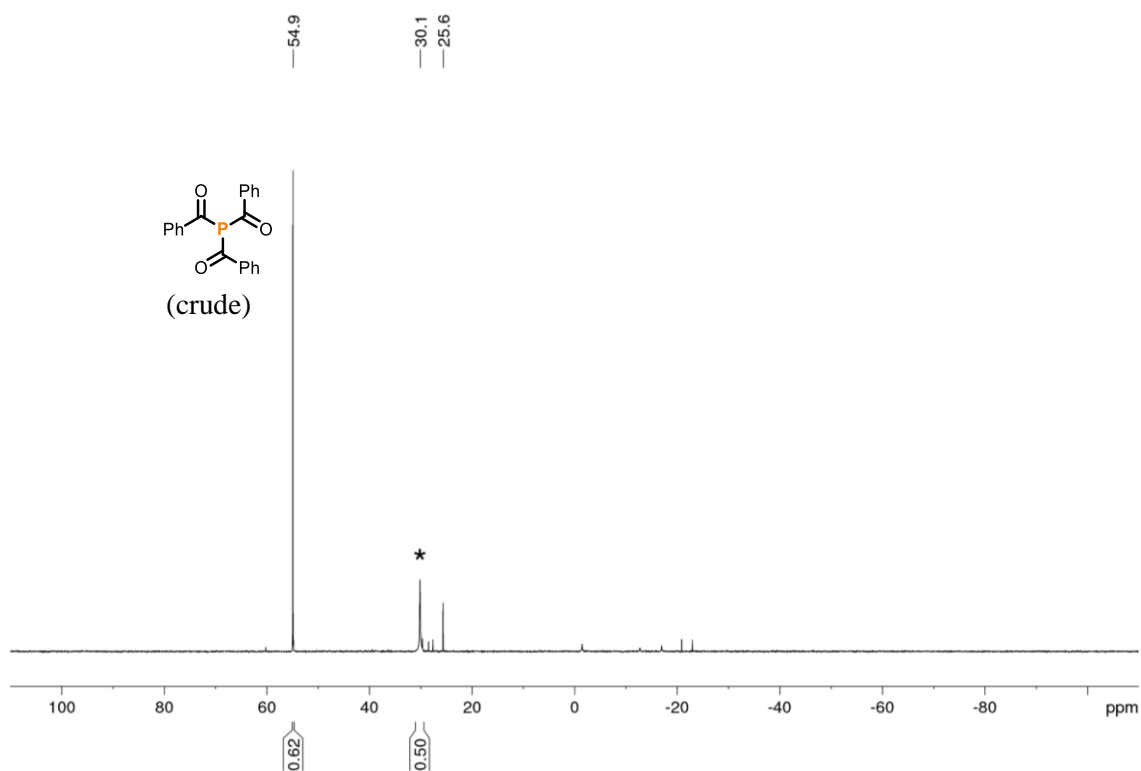


Figure S33. ³¹P{¹H} NMR spectrum of **crude** (Ph(O)C)₃P generated *via* photocatalytic stannylation of P₄ in benzene/acetone (**scale-up** (0.8 mmol)) followed by acylation with benzoyl chloride PhC(O)Cl (**1**). * marks the internal standard Ph₃PO (0.02 mmol)

Spectroscopic data of (Ph(O)C)₃P:

The NMR data are consistent with previous reports.^{[5], [20]}

¹H NMR (400.13 MHz, 300 K, C₆D₆): $\delta = 7.98$ ppm (2H, m), 7.02 ppm (1H, t, $^3J(^1\text{H}-^1\text{H}) = 7.3$ Hz), 6.95 ppm (2H, t, $^3J(^1\text{H}-^1\text{H}) = 7.5$ Hz).

³¹P{¹H} NMR (161.98 MHz, 300 K, C₆D₆): $\delta = 54.3$ ppm (s).

¹³C{¹H} NMR (100.61 MHz, 300 K, C₆D₆): $\delta = 205.3$ ppm (d, $J(^{31}\text{P}-^1\text{H}) = 35.4$ Hz), 140.5 ppm (d, $J(^{31}\text{P}-^1\text{H}) = 35.3$ Hz), 133.5 ppm (d, $J(^{31}\text{P}-^1\text{H}) = 1.2$ Hz), 128.6 ppm (d, $J(^{31}\text{P}-^1\text{H}) = 8.0$ Hz), 128.5 ppm (d, $J(^{31}\text{P}-^1\text{H}) = 0.8$ Hz).

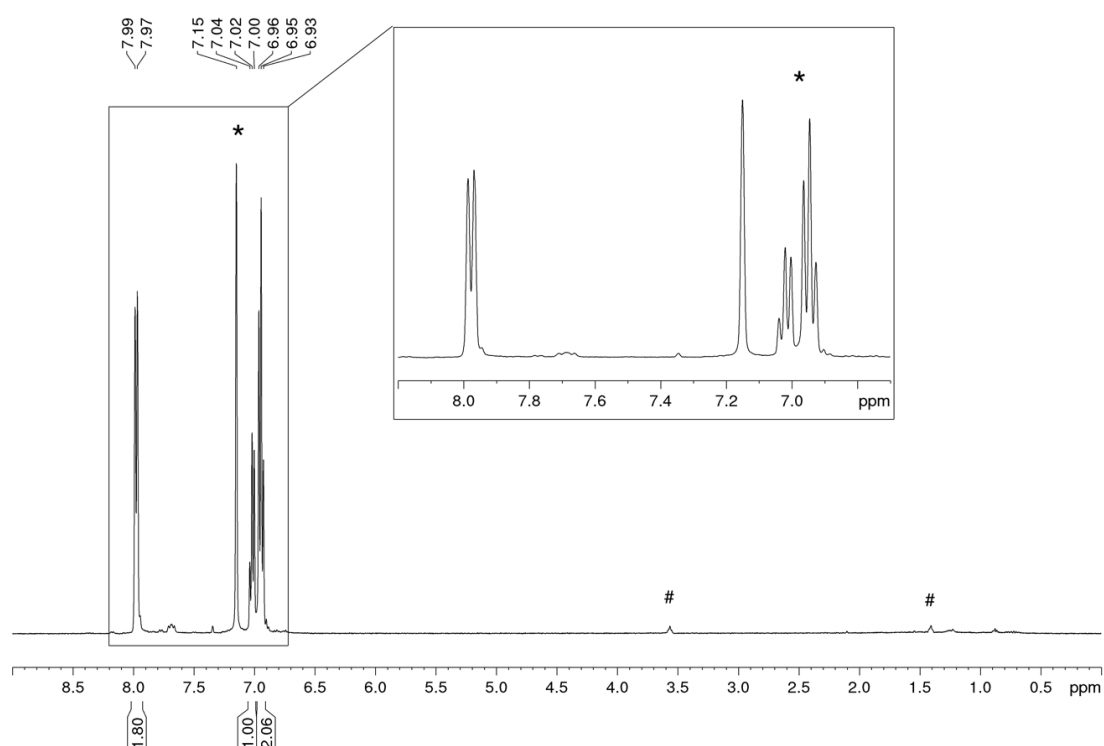


Figure S34. ¹H NMR (400.13 MHz, 300 K, C₆D₆) spectrum of (Ph(O)C)₃P. * marks C₆D₆. # marks minor THF.

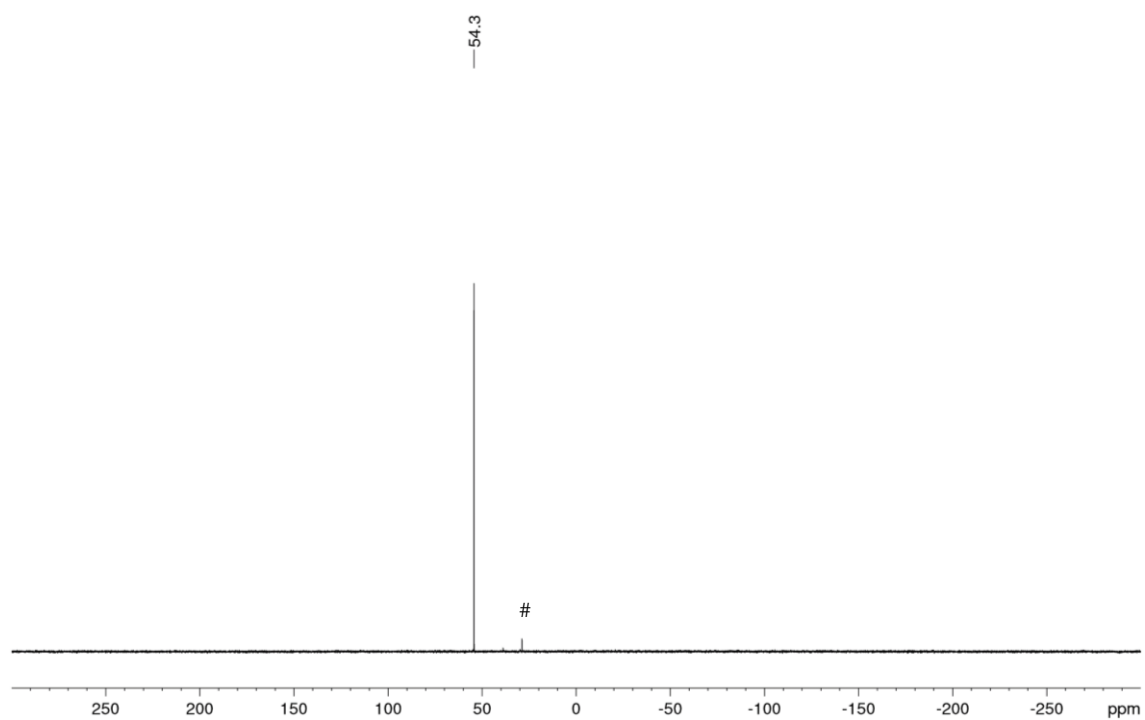


Figure S35. $^{31}\text{P}\{^1\text{H}\}$ NMR (161.98 MHz, 300 K, C_6D_6) spectrum of $(\text{Ph}(\text{O})\text{C})_3\text{P}$. # marks minor unknown impurity.

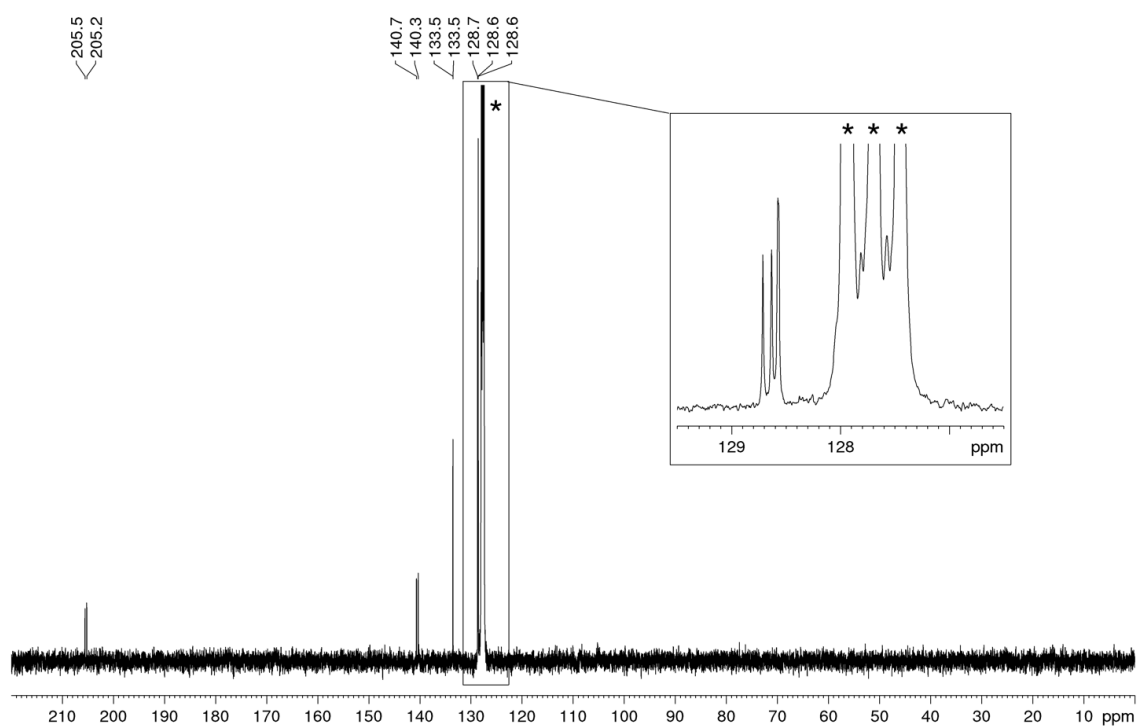


Figure S36. $^{13}\text{C}\{^1\text{H}\}$ NMR (100.61 MHz, 300 K, C_6D_6) spectrum of $(\text{Ph}(\text{O})\text{C})_3\text{P}$. * marks C_6D_6 .

S9.3 ‘One-pot’ synthesis and purification of phosphonium salt [Bn₄P]Br

To a 100 mL stoppered tube equipped with a stirring bar were added (Bu₃Sn)₂ (1.212 mL, 2.4 mmol, 3 equiv. based on phosphorus atoms, 12 equiv. based on P₄) anthraquinone (20.8 mg, 0.1 mmol, 0.5 equiv. based on P₄) and P₄ (0.2 mmol, as a stock solution in 1.426 mL benzene) in acetone as solvent (2.574 mL, in total 4 mL PhH/acetone mixture). The tube was sealed, placed in a water-cooled block (to ensure a near-ambient temperature was maintained, Figure S31), and irradiated with UV light (365 nm, 14 V, 700 mA, Osram OSLON SSL 80) for 48 h. Subsequent addition of benzyl bromide (475 μL, 4 mmol, 20 equiv. based on P₄, 5 equiv. based on phosphorus atoms) and heating overnight at 60 °C resulted in a color change of the orange reaction mixture to a yellow solution (by internal standard addition to a separate reaction the ³¹P{¹H} NMR showed 67% conversion into [Bn₄P]Br, see Figure S37). The volatiles were removed under vacuum. *n*-Hexane was added to the remaining orange oil and the product was precipitated and washed with *n*-hexane (2 x 10 mL). Recrystallization twice from acetone/*n*-hexane afforded the desired product [Bn₄P]Br (212.2 mg, 56%) as an off-white powder.

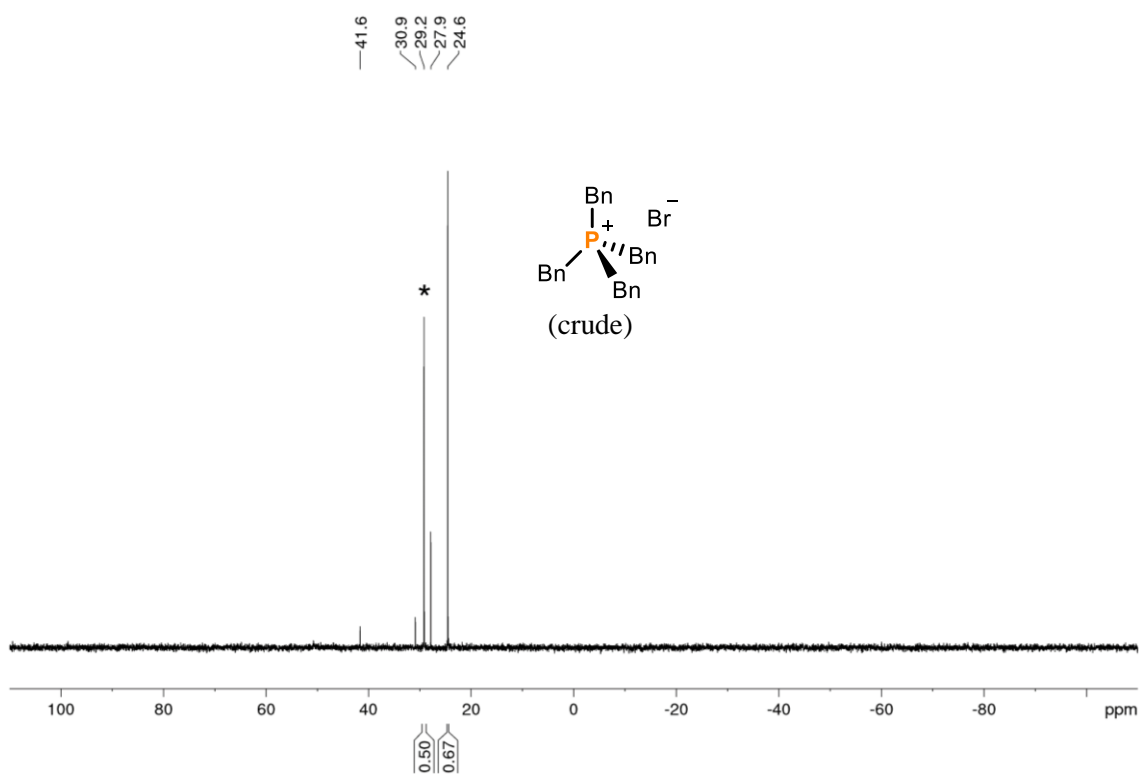


Figure S37. Quantitative ³¹P{¹H} NMR (zgig) spectrum of **crude** [Bn₄P]Br generated *via* photocatalytic stannylation of P₄ in benzene/acetone followed by alkylation with benzyl bromide (BnBr). * marks the internal standard Ph₃PO (0.02 mmol).

Spectroscopic data of [Bn₄P]Br:

The NMR data are consistent with previous reports of both the chloride salt [Bn₄P]Cl^[21] and [Bn₄P]Br.^[5]

¹H NMR (400.13 MHz, 300 K, CDCl₃): δ = 7.32 ppm (3H, m), 7.18 ppm (2H, m), 4.03 ppm (2H, d, ²J(³¹P-¹H) = 14.3 Hz).

³¹P{¹H} NMR (161.98 MHz, 300 K, CDCl₃): δ = 24.7 ppm (s).

³¹P NMR (161.98 MHz, 300 K, CDCl₃): δ = 24.7 ppm (nonet, ²J(³¹P-¹H) = 14.3 Hz).

¹³C{¹H} NMR (100.61 MHz, 300 K, CDCl₃): δ = 130.6 ppm (d, J(³¹P-¹H) = 5.3 Hz), 129.6 ppm (d, J(³¹P-¹H) = 2.9 Hz), 128.7 ppm (d, J(³¹P-¹H) = 3.5 Hz), 127.5 ppm (d, J(³¹P-¹H) = 8.1 Hz), 26.8 ppm (d, J(³¹P-¹H) = 43.2 Hz).

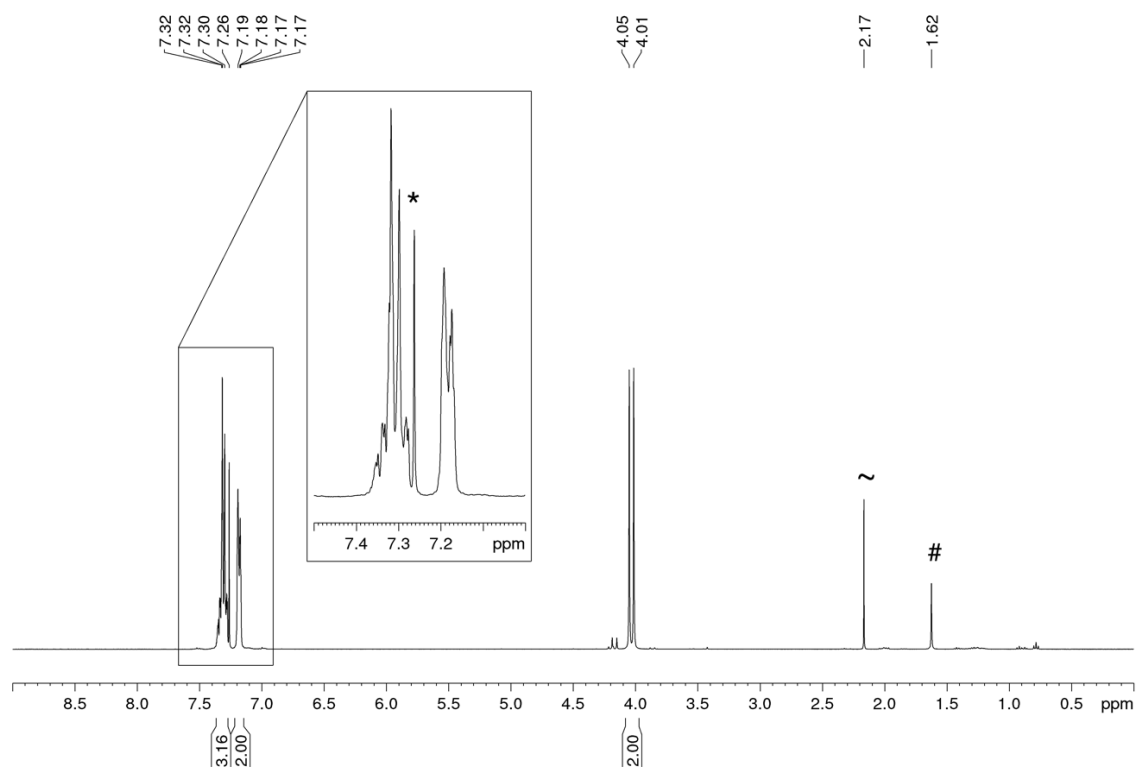


Figure S38. ¹H NMR (400.13 MHz, 300 K, CDCl₃) spectrum of [Bn₄P]Br. * marks CDCl₃. ~ marks residual acetone. # marks water present in the CDCl₃ NMR solvent.

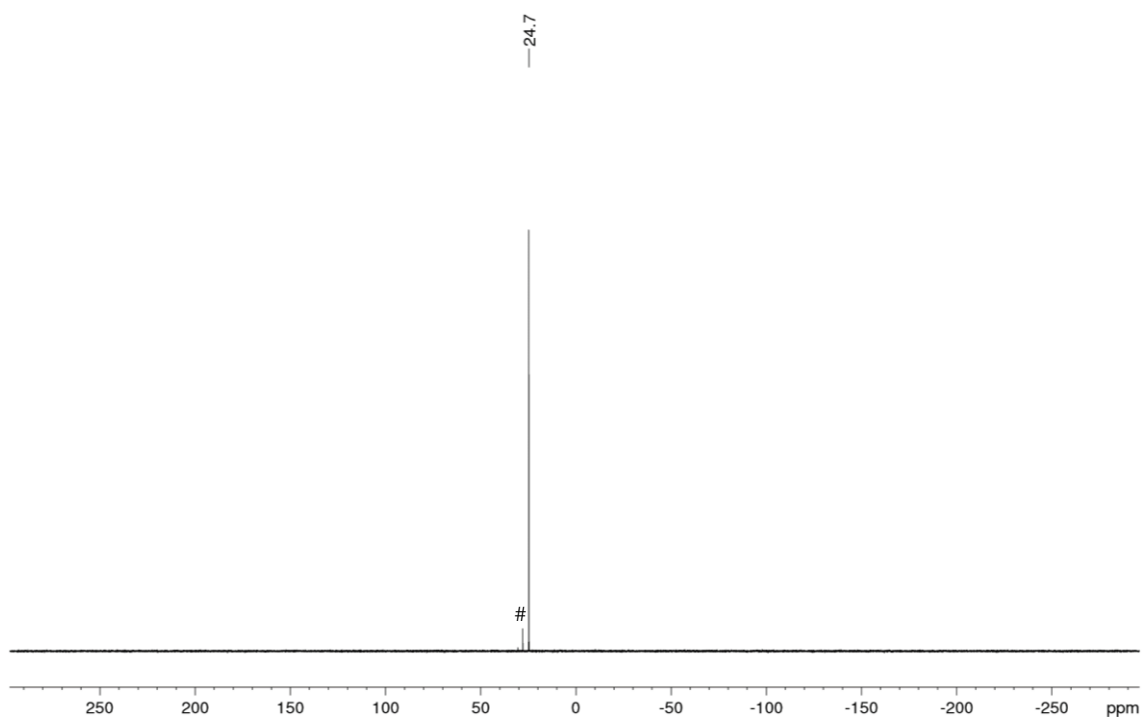


Figure S39. $^{31}\text{P}\{^1\text{H}\}$ NMR (161.98 MHz, 300 K, CDCl_3) spectrum of $[\text{Bn}_4\text{P}]\text{Br}$. # marks minor unknown impurity.

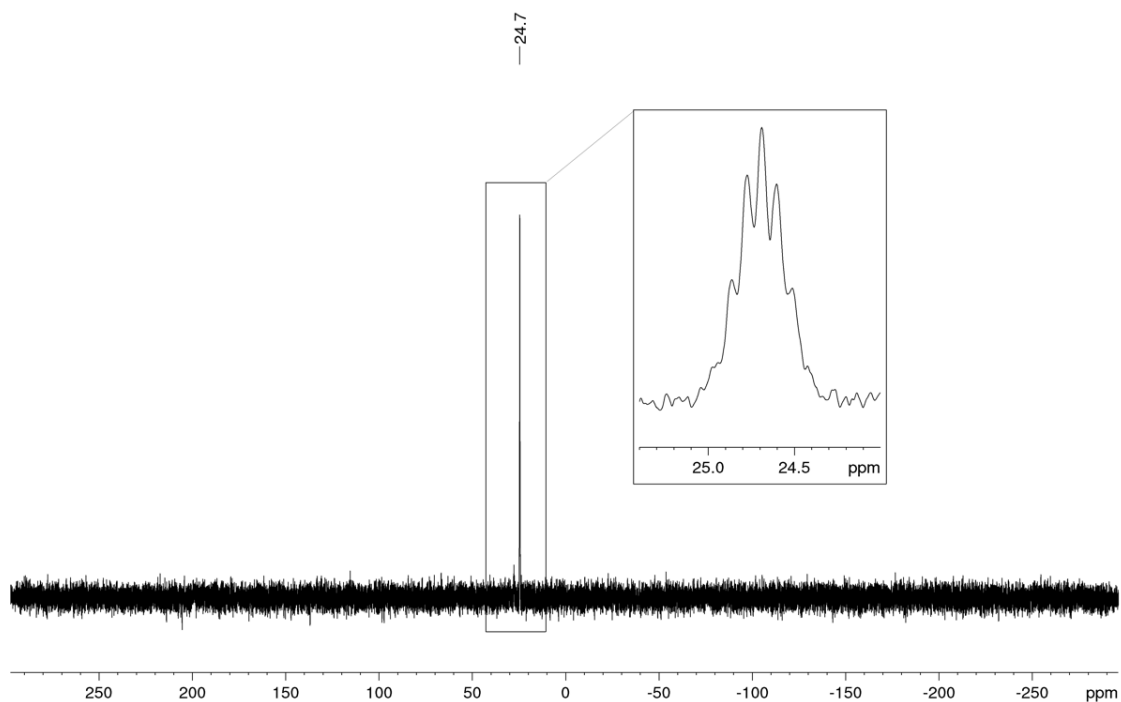


Figure S40. ^{31}P NMR (161.98 MHz, 300 K, CDCl_3) spectrum of $[\text{Bn}_4\text{P}]\text{Br}$.

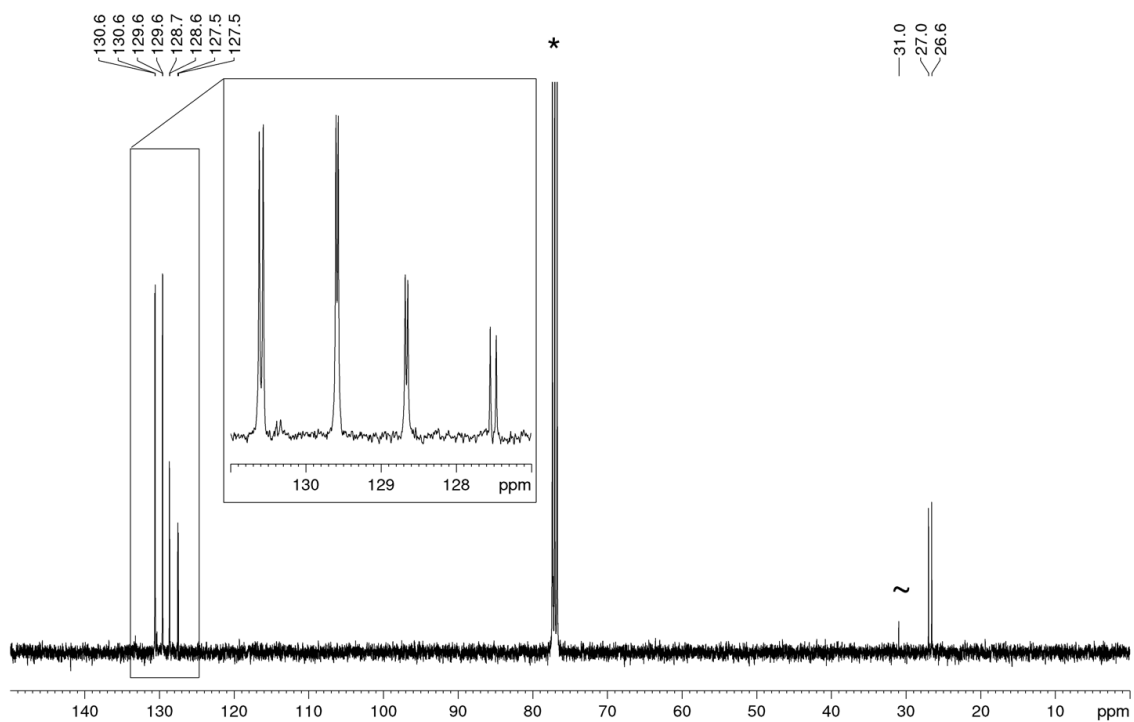


Figure S41. $^{13}\text{C}\{^1\text{H}\}$ NMR (100.61 MHz, 300 K, CDCl_3) spectrum of $[\text{Bn}_4\text{P}]\text{Br}$. * marks C_6D_6 . ~ marks residual acetone.

S9.4 ‘One-pot’ synthesis and purification of THPC and recycling of Bu_3SnCl and $(\text{Bu}_3\text{Sn})_2$

To a 100 mL stoppered tube equipped with a stirring bar were added $(\text{Bu}_3\text{Sn})_2$ (1.212 mL, 2.4 mmol, 3 equiv. based on phosphorus atoms, 12 equiv. based on P_4), anthraquinone (20.8 mg, 0.1 mmol, 0.5 equiv. based on P_4) and P_4 (0.2 mmol, as a stock solution in 1.426 mL benzene) in acetone as solvent (2.574 mL, in total 4 mL PhH/acetone mixture). The tube was sealed, placed in a water-cooled block (to ensure a near-ambient temperature was maintained, Figure S31), and irradiated with UV light (365 nm, 14 V, 700 mA, Osram OSOLON SSL 80) for 48 h. Following removal of volatiles under vacuum, EtOH (5 ml) and paraformaldehyde (300 mg, 10 mmol, 50 equiv. based on P_4 , 12.5 equiv. based on phosphorus atoms) were added, and the resulting suspension was stirred at room temperature for 16 h. The mixture was frozen in a liquid-nitrogen bath, and HCl (4.0 M in 1,4-dioxane, 2 ml, 8 mmol (based on P_4)) was added. After thawing, the yellowish reaction mixture was stirred at room temperature for 2 h and volatiles were removed under vacuum. The remaining orange oily solid residue was washed with Et_2O (3 x 10 ml) to extract the Sn-containing compounds, Bu_3SnCl and $(\text{Bu}_3\text{Sn})_2$. The residue was recrystallized from EtOH/*n*-hexane (4 mL/4 mL) at $-35\text{ }^\circ\text{C}$. Decanting of the mother liquor afforded the desired product THPC as a pale yellow solid (50.3 mg, 33%) after drying under vacuum. The combined Et_2O washes from the above reaction were dried under vacuum to afford a mixture of Bu_3SnCl and $(\text{Bu}_3\text{Sn})_2$ as a yellow oil (1.346 g). ^1H and $^{119}\text{Sn}\{^1\text{H}\}$ NMR indicate a ratio of 1 : 1.3 for the $(\text{Bu}_3\text{Sn})_2$ / Bu_3SnCl mixture (Figure S45 and S46). Overall, 92% of the used $(\text{Bu}_3\text{Sn})_2$ (2.4 mmol) could be recovered as a mixture (1.346 g) of Bu_3SnCl (567.7 mg, 1.74 mmol, 36%) and $(\text{Bu}_3\text{Sn})_2$ (778.3 mg, 1.34 mmol, 56%).

Spectroscopic data of THPC:

The NMR data are consistent with previous reports.^[5]

^1H NMR (400.13 MHz, 300 K, D_2O): $\delta = 4.67$ ppm (d, $^2J(^{31}\text{P}-^1\text{H}) = 1.8$ Hz).

$^{31}\text{P}\{^1\text{H}\}$ NMR (161.98 MHz, 300 K, D_2O): $\delta = 27.1$ ppm (s).

$^{13}\text{C}\{^1\text{H}\}$ NMR (100.61 MHz, 300 K, D_2O): $\delta = 49.1$ ppm (d, $^1J(^{31}\text{P}-^{13}\text{C}) = 51.3$ Hz).

Spectroscopic data of the recycled mixture of Bu_3SnCl and $(\text{Bu}_3\text{Sn})_2$:

The NMR data of Bu_3SnCl ^[22] and $(\text{Bu}_3\text{Sn})_2$ ^[23] are consistent with previous reports. The ^1H NMR and $^{119}\text{Sn}\{^1\text{H}\}$ NMR showed a **1 to 1.3 ratio of $(\text{Bu}_3\text{Sn})_2$ to Bu_3SnCl** .

^1H NMR (400.13 MHz, 300 K, C_6D_6): $\delta = 1.70$ -1.62 (m, 2H, $(\text{Bu}_3\text{Sn})_2$), 1.60-1.53 (m, 1.3H, Bu_3SnCl), 1.46-1.36 (m, 2.1H, $(\text{Bu}_3\text{Sn})_2$), 1.30-1.21 (m, 1.5H, Bu_3SnCl), 1.16-1.12 (m, 2H, $(\text{Bu}_3\text{Sn})_2$), 1.10-1.07 (m, 1.5H, Bu_3SnCl), 0.96 (t, 3H, $(\text{Bu}_3\text{Sn})_2$), $^3J(^1\text{H}-^1\text{H}) = 7.3$ Hz), 0.85 (t, 2H, Bu_3SnCl), $^3J(^1\text{H}-^1\text{H}) = 7.3$ Hz).

$^{119}\text{Sn}\{^1\text{H}\}$ NMR (149.21 MHz, 300 K, C_6D_6): $\delta = -83.2$ ppm (s, 2Sn of $(\text{Bu}_3\text{Sn})_2$, $^1J(^{119}\text{Sn}-^{13}\text{C}) = 240.7$ Hz, $^1J(^{119}\text{Sn}-^{119}\text{Sn}) = 2556.3$ Hz, 146.9 ppm (s, 1.3Sn of Bu_3SnCl).

$^{13}\text{C}\{^1\text{H}\}$ NMR (100.61 MHz, 300 K, C_6D_6): $\delta = 30.8$ (s, $(\text{Bu}_3\text{Sn})_2$), 27.8 (s, Bu_3SnCl), 27.6 (s, $(\text{Bu}_3\text{Sn})_2$), 26.8 (s, Bu_3SnCl), 16.9 (s, Bu_3SnCl), 13.6 (s, $(\text{Bu}_3\text{Sn})_2$), 13.4 (s, Bu_3SnCl), 10.1 (s, $(\text{Bu}_3\text{Sn})_2$).

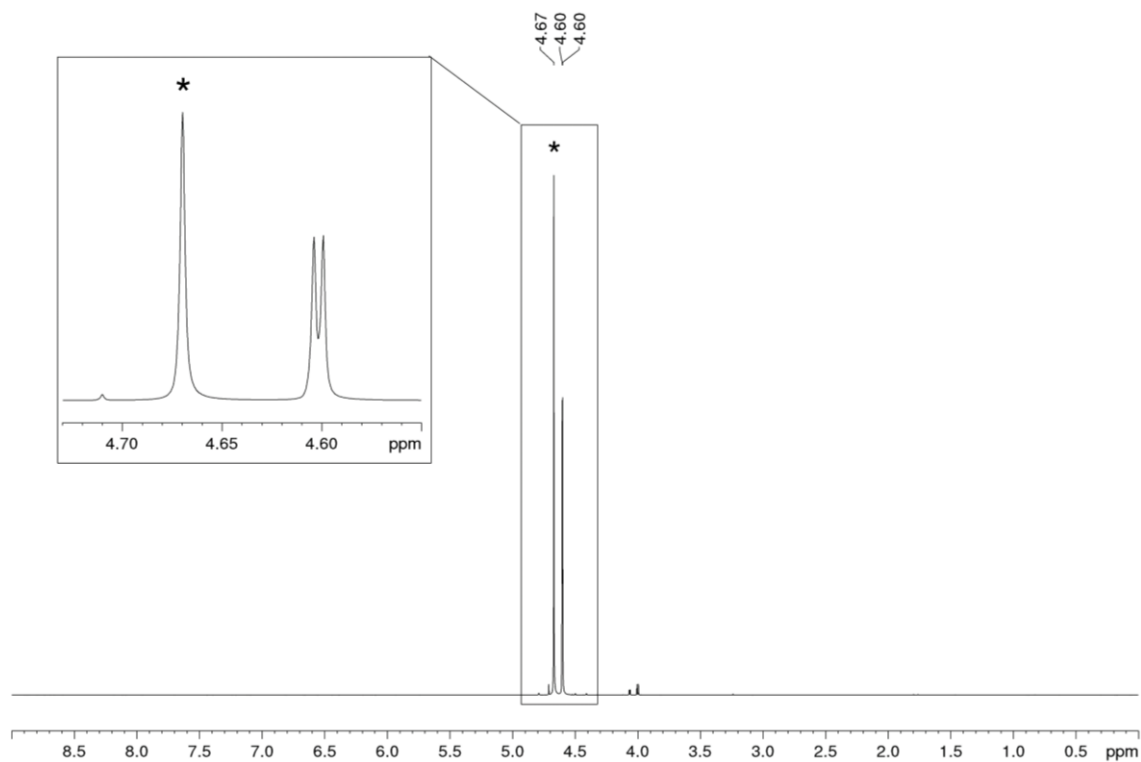


Figure S42. ^1H NMR (400.13 MHz, 300 K, D_2O) spectrum of THPC. * marks D_2O .

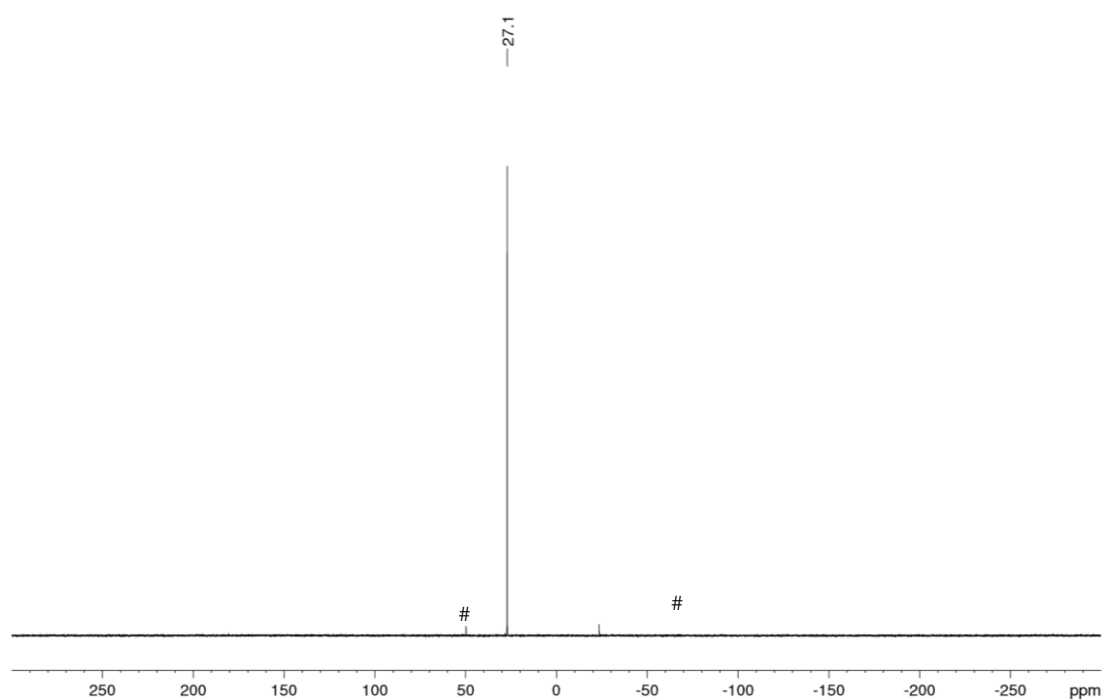


Figure S43. $^{31}\text{P}\{^1\text{H}\}$ NMR (161.98 MHz, 300 K, D_2O) spectrum of THPC. # marks minor unknown impurities.

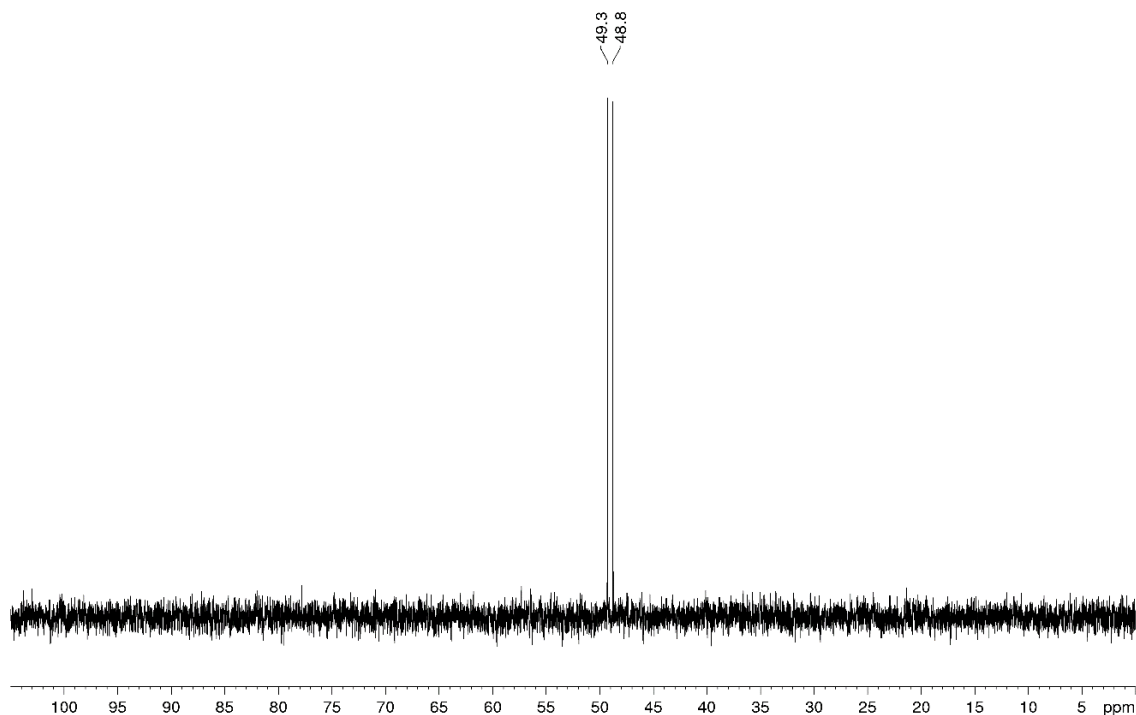


Figure S44. $^{13}\text{C}\{^1\text{H}\}$ NMR (100.61 MHz, 300 K, D_2O) spectrum of THPC.

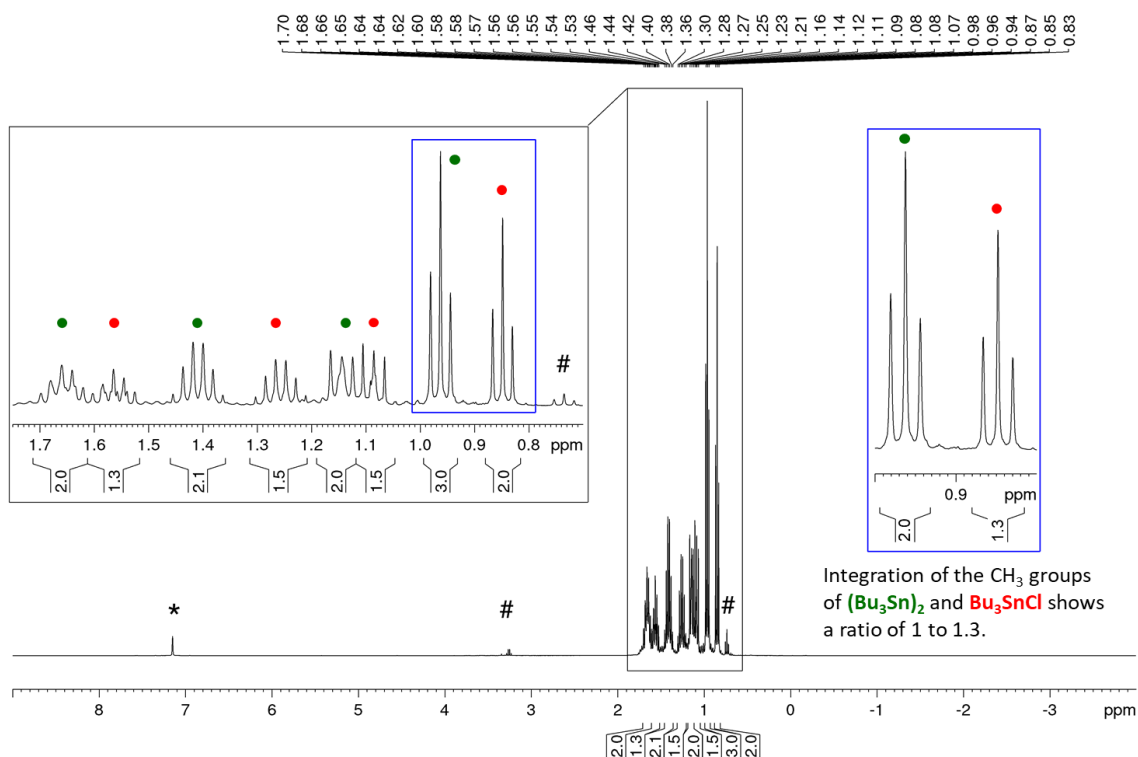


Figure S45. ^1H NMR (400.13 MHz, 300 K, C_6D_6) spectrum of recycled Bu_3SnCl and $(\text{Bu}_3\text{Sn})_2$ mixture. * marks C_6D_6 , # marks minor Et_2O . The blue box shows the integration of the CH_3 groups of $(\text{Bu}_3\text{Sn})_2$ and Bu_3SnCl , which indicates a 1 to 1.3 ratio of the Sn-containing compounds.

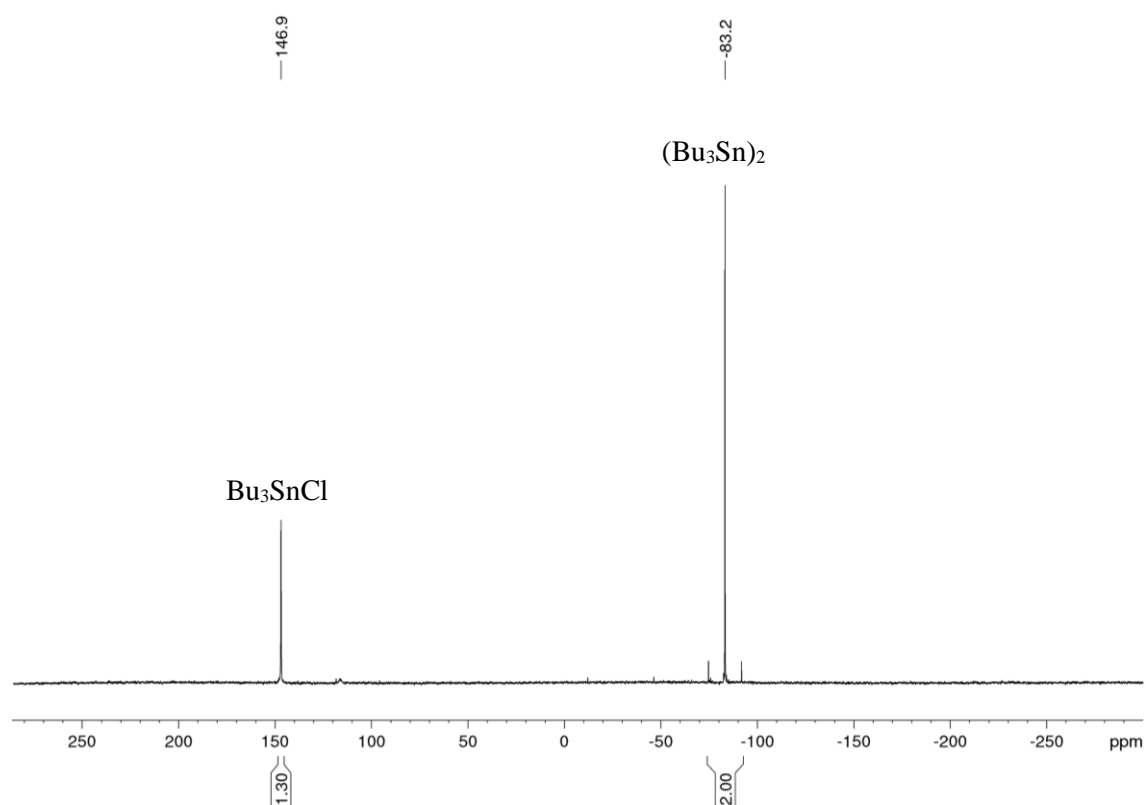


Figure S46. $^{119}\text{Sn}\{^1\text{H}\}$ NMR (149.21 MHz, 300 K, C_6D_6) spectrum of recycled Bu_3SnCl and $(\text{Bu}_3\text{Sn})_2$ mixture (ratio of 1.3 to 1).

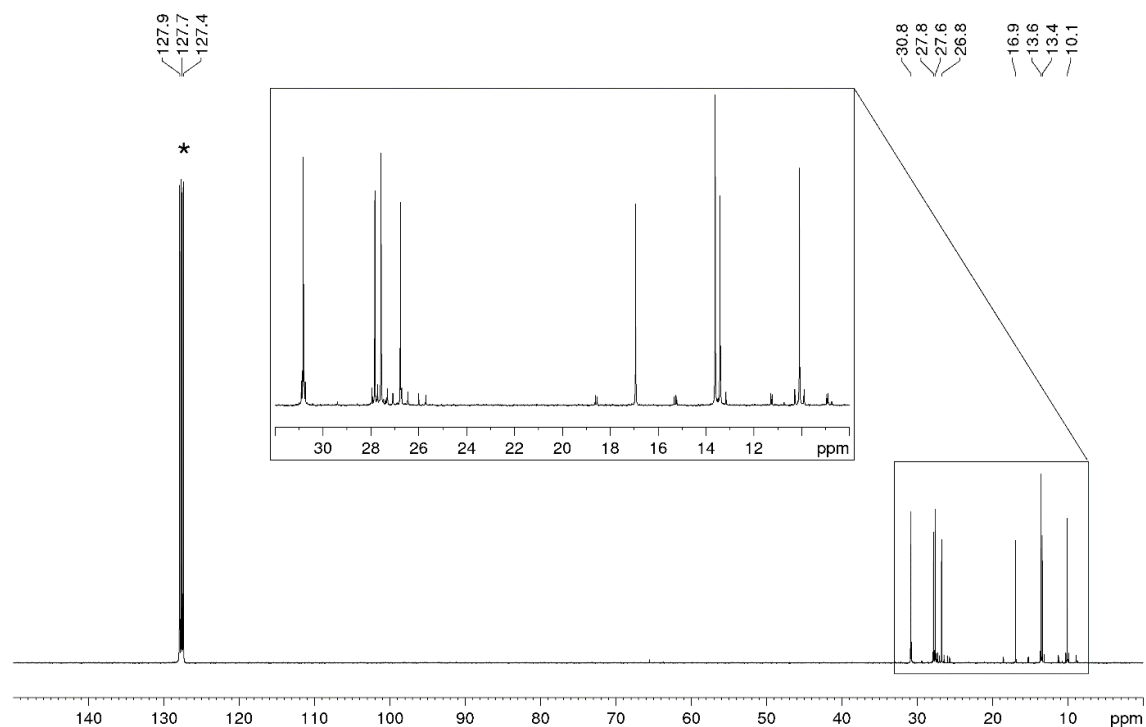


Figure S47. $^{13}\text{C}\{^1\text{H}\}$ NMR (100.61 MHz, 300 K, C_6D_6) spectrum of recycled Bu_3SnCl and $(\text{Bu}_3\text{Sn})_2$ mixture. * marks C_6D_6 .

3.5 References

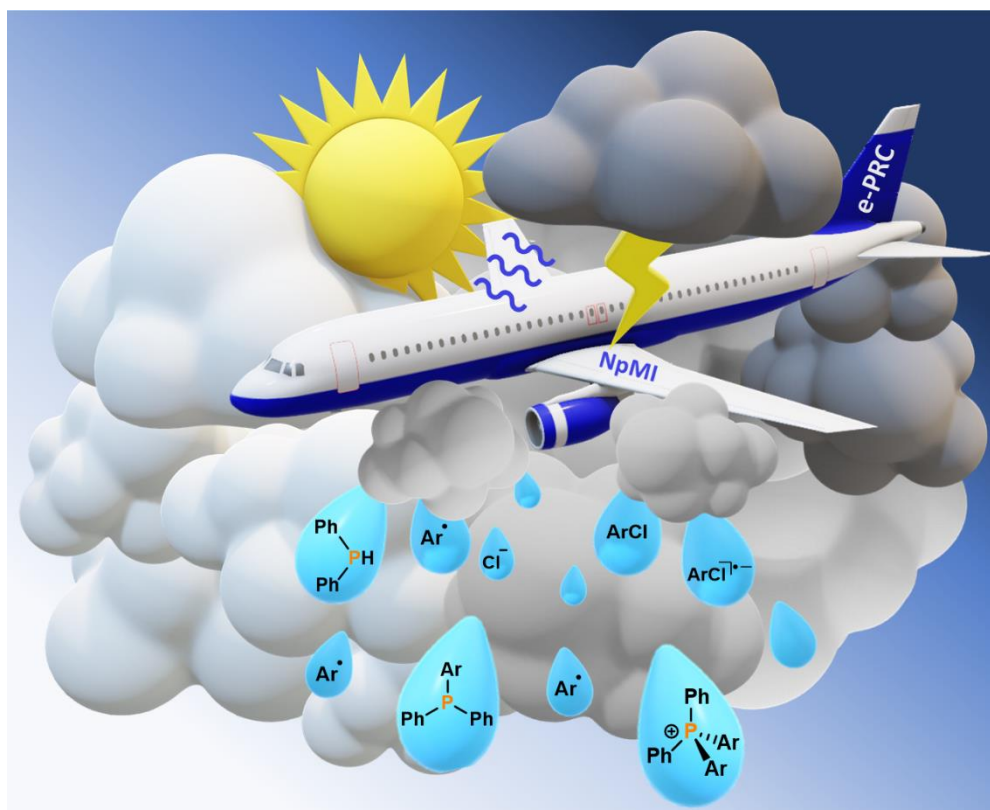
- [1] a) W. Gleason, *JOM*, 2007, **59**, 17-19; b) G. Bettermann, W. Krause, G. Riess and T. Hofmann, *Ullmann's Encyclopedia of Industrial Chemistry* (Wiley), 2000; c) D. E. C. Corbridge, *Phosphorus: Chemistry, Biochemistry, and Technology*, CRC Press, 6th ed., 2013.
- [2] a) B. M. Cossairt, N. A. Piro and C. C. Cummins, *Chem. Rev.*, 2010, **110**, 4164–4177; b) M. Caporali, L. Gonsalvi, A. Rossin and M. Peruzzini, *Chem. Rev.*, 2010, **110**, 4178–4235; c) M. Scheer, G. Balázs and A. Seitz, *Chem. Rev.*, 2010, **110**, 4236–4256; d) C. M. Hoidn, D. J. Scott and R. Wolf, *Chem. Eur. J.*, 2021, **27**, 1886–1902; e) L. Giusti, V. R. Landaeta, M. Vanni, J. A. Kelly, R. Wolf and M. Caporali, *Coord. Chem. Rev.*, 2021, **441**, 2139276–2139375; f) Y. H. Budnikova, T. V. Gryaznova, V. V. Grinenko, Y. B. Dudkina and M. N. Khrizanforov, *Pure Appl. Chem.*, 2017, **89**, 311–330.
- [3] a) S. Reichl, E. Mädl, F. Riedelberger, M. Piesch, G. Balázs, M. Seidl and M. Scheer, *Nat. Commun.*, 2021, **12**, 5774; b) M. Donath, K. Schwedtmann, T. Schneider, F. Hengersdorf, A. Bauzá, A. Frontera and J. J. Weigand, *Nat. Chem.*, 2022, **14**, 384–391; c) Y. Mei, Z. Yan and L. L. Liu, *J. Am. Chem. Soc.*, 2022, **144**, 1517–1522; d) D. H. R. Barton and J. Zhu, *J. Am. Chem. Soc.*, 1993, **115**, 2071–2072; e) D. H. R. Barton and R. A. Vonder Embse, *Tetrahedron*, 1998, **54**, 12475–12496; f) B. M. Cossairt and C. C. Cummins, *New J. Chem.*, 2010, **34**, 1533–1536; g) S. K. Ghosh, C. C. Cummins and J. A. Gladysz, *Org. Chem. Front.*, 2018, **5**, 3421–3429.
- [4] a) D. J. Scott, *Angew. Chem.*, 2022, e202205019, doi.org/10.1002/anie.202205019; b) H. Grützmacher, *Nat. Chem.*, 2022, **14**, 362–364.
- [5] D. J. Scott, J. Cammarata, M. Schimpf and R. Wolf, *Nat. Chem.*, 2021, **13**, 458–464.
- [6] Previous work has shown that $(\text{Bu}_3\text{Sn})_3\text{P}$ can be prepared through stannylation of $(\text{Bu}_3\text{Sn})_x\text{PH}_{3-x}$ with Bu_3SnOMe . However, this requires addition of an extra stoichiometric reagent and results in formation of MeOH as a byproduct which could lead to competing reactivity upon subsequent addition of electrophiles, see ref. [5].
- [7] a) A. Darwish and J. M. Chong, *Syn. Comm.*, 2004, **34**, 1885–1890; b) T. N. Mitchell, *Encyclopedia of Reagents for Organic Synthesis* –

- Hexabutyl-distannane* (Wiley), 2012; c) T. N. Mitchell and G. Walter, *J. Chem. Soc., Perkin Trans.*, 1977, **2**, 1842–1847.
- [8] A. G. Davies, *Organotin Chemistry* (Wiley), 2004.
- [9] For previous examples where photochemical methods have been used to functionalize P₄, see: a) U. Lennert, P. B. Arockiam, V. Streitferdt, D. J. Scott, C. Rödl, R. M. Gschwind and R. Wolf, *Nat. Catal.*, 2019, **2**, 1101–1106; b) P. B. Arockiam, U. Lennert, C. Graf, R. Rothfelder, D. J. Scott, T. G. Fischer, K. Zeitler and R. Wolf, *Chem. Eur. J.*, 2020, **26**, 16374–16382; c) R. Rothfelder, V. Streitferdt, U. Lennert, J. Cammarata, D. J. Scott, K. Zeitler, R. M. Gschwind and R. Wolf, *Angew. Chem. Int. Ed.*, 2021, **60**, 24650–24658; d) M. Till, V. Streitferdt, D. J. Scott, M. Mende, R. M. Gschwind and R. Wolf, *Chem. Commun.*, 2022, **58**, 1100–1103; e) G. Lu, J. Chen, X. Huangfu, X. Li, M. Fang, G. Tang, and Y. Zhao, *Org. Chem. Front.*, 2019, **6**, 190–194; f) D. Tofan and C. C. Cummins, *Angew. Chem. Int. Ed.*, 2010, **49**, 7516–7518; g) L. P. Wang, D. Tofan, J. Chen, T. V. Voorhis and C. C. Cummins, *RSC Adv.*, 2013, **3**, 23166–23171.
- [10] Cleavage of P₄ under photoirradiation (256 nm) can generate highly reactive P₂ (ref. 9f,g). However, this requires very high energy UV light (256 nm) and so seems unlikely to be a major, relevant pathway for the reactivity reported herein, which uses significantly lower energy UV sources (365 nm). Nevertheless, the possibility that this could act as a minor competing pathway, for example leading to minor reaction side-products, cannot yet be fully excluded.
- [11] a) W. P. Neumann, H. Hillgärtner, K. M. Baines, R. Dicke, K. Vorspohl, U. Kobs and U. Nussbeutel, *Tetrahedron*, 1989, **45**, 951–960; b) M. Harendza, J. Junggebauer, K. Leßman, W. P. Neumann and H. Tews, *Synlett*, 1993, **4**, 286–288; c) D. J. Hart, R. Krishnamurthy, L. M. Pook and F. L. Seely, *Tetrahedron Lett.*, 1993, **34**, 7819–7822; d) M. J. Tomaszewski and J. Warkentin, *J. Chem. Soc., Chem. Commun.*, 1993, **18**, 1407–1408.
- [12] a) J. A. Dantas, J. T. M. Correia, M. W. Paixão and A. G. Corrêa, *ChemPhotoChem*, 2019, **3**, 506–520.; b) B. Dinda, *Essentials of Pericyclic and Photochemical Reactions: Photochemistry of Carbonyl Compounds (Chapter 8)*, Springer, 2016; c) B. König, *Chemical Photocatalysis*, de Gruyter, 2013; d) W. A. Green, *Industrial Photoinitiators: A Technical Guide*, CRC Press, 2010; e) J. P. Fouassier and J. Lalevée, *Photoinitiators: Structures, Reactivity and*

- Application in Polymerization*, Wiley, 2021; f) J. Cervantes-González, D. A. Vosburg, S. E. Mora-Rodriguez, M. A. Vázquez, L. G. Zepeda, C. V. Gómez and S. Lagunas-Rivera, *ChemCatChem*, 2020, **12**, 3811–3827.
- [13] Alternative elementary steps such as “outer-sphere” energy transfer between $[R_2CO]^*$ and $(Bu_3Sn)_2$ could also be possible, but would be expected to lead to the same overall outcome. For additional mechanistic discussion, please see ESI, S2.
- [14] Since conversion to $(Bu_3Sn)_3P$ requires activation of 1.5 Sn–Sn bonds per P atom.
- [15] L. Riesel, M. Kant and R. Helbing, *Allg. Chem.*, 1990, **580**, 217–223.
- [16] G. Becker, *Z. Anorg. Allg. Chem.*, 1977, **430**, 66–76.
- [17] H. Schmidbaur, U. Deschler, B. Milewski-Mahrla and B. Zimmer-Gasser, *Chem. Ber.*, 1981, **114**, 608–619.
- [18] a) K. V. Katti, H. Gali, C. J. Smith and D. E. Berning, *Chem. Res.*, 1999, **32**, 9–17; b) M. J. Chen, C. R. Chen, Y. Tan, J. Q. Huang, X.L. Wang, L. Chen and Y. Z. Wang, *Ind. Eng. Chem. Res.*, 2014, **53**, 1160–1171; c) W. J. Vullo, *Ind. Eng. Chem. Proc. Res. Dev.*, 1966, **5**, 346–349; d) W. J. Vullo, *J. Org. Chem.*, 1968, **33**, 3665–3667.
- [19] Yields of isolated materials have not been corrected for the presence of trace impurities observable by $^{31}P\{^1H\}$ NMR spectroscopy. See ESI S9.
- [20] G. D. Macdonnell, A. Radhakrishna, K. D. Berlin, J. Barycki, R. Tyka and P. Mastalerz, *Tetrahedron Lett.*, 1978, **19**, 857–860.
- [21] M. B. Geeson, P. Ríos, W. J. Transue and C. C. Cummins, *J. Am. Chem. Soc.*, 2019, **141**, 6375–6384.
- [22] A. G. Davies, A. Sella and R. Sivasubramaniam, *J. Organomet. Chem.*, 2006, **691**, 3556–3561.
- [23] a) A. Darwish and J. M. Chong, *Syn. Comm.*, 2004, **34**, 1885–1890; b) T. N. Mitchell, *Encyclopedia of Reagents for Organic Synthesis – Hexabutyl-distannane* (Wiley), 2012; c) T. N. Mitchell and G. Walter, *J. Chem. Soc., Perkin Trans.*, 1977, **2**, 1842–1847.

4 Reductive Photoelectrocatalytic Activation of Organic Halides and Diphenylphosphine into Arylphosphines and Phosphonium Salts^[a]

Abstract: Organophosphorus compounds (OPCs) are ubiquitous in industry and academia. Among the various proof-of-principle synthesis procedures toward such products, including photo- and electrochemical activation of P₄ or other P sources, the combined strategy of electrochemically-mediated photoredox catalysis (e-PRC) is almost unexplored. Herein, we describe an electrochemically-mediated photocatalytic functionalization of diphenylphosphine (Ph₂PH) into useful arylphosphines and phosphonium salts using simple organic electrochemically-mediated photoredox catalysts 9,10-dicyanoanthracene (**DCA**) and *N*-2,6-diisopropylphenyl naphthalene monoimide (**NpMI**), and their extraordinary reducing power for the reductive activation of aryl halides and generation of aryl radicals.



^[a] M. Till performed the photoelectrochemical arylation reactions. The photoredox catalysts **DTAC**, **NpMI** and **"BuO-NpMI** were synthesized and provided by the group of J. P. Barham. R. Wolf and J. P. Barham supervised and directed the project. M. Till wrote the manuscript with input from Robert Wolf.

4.1 Introduction

4.1.1 Current functionalization methods with carbon-centered radicals

Tertiary phosphines (R_3P) and the related phosphonium salts ($[R_4P]^+$) are among the notable families of industrially relevant organophosphorus compounds (OPCs).^[1] Despite their extensive application throughout industry and academia, the state-of-the-art method to synthesize these useful OPCs relies on a hazardous and wasteful multistep procedure. As shown in Figure 1a, white phosphorus (P_4) is currently the most important starting material for the preparation of OPCs. The most common method for the preparation of OPCs is based on the transformation of P_4 with toxic chlorine gas into highly reactive phosphorus chlorides, such as PCl_3 and PCl_5 , which are subsequently converted to desirable products with suitable organometallic nucleophiles.^[1]

Since the state-of-the-art synthesis of OPCs is hazardous and wasteful, replacing it by a milder and more efficient strategy is a highly desirable objective. While the activation of P_4 by main group and transition metal compounds has received extensive attention in recent years, such methodology rarely results in the comprehensive breakdown of the P_4 tetrahedron to monophosphorus compounds.^[2] Thus, the development of *efficient, direct* – and, if possible, *catalytic* – transformation of P_4 into useful P_1 products remains a challenging and desirable goal.

In late 2019, Wolf and co-workers reported the first photocatalytic functionalization of P_4 into triarylphosphines and tetraarylphosphonium salts (Figure 1b).^[3] Treatment of P_4 with aryl iodides (ArI) and triethylamine (Et_3N), mediated by an iridium-based photoredox catalyst (PRCat) and irradiation of blue light, yields a variety of valuable OPCs. This transformation of P_4 proceeds through photoredox catalysis (PRC), involving the generation of carbon-centered radicals by single-electron-transfer (SET) of the photo-reduced [Ir]-catalyst and the substrate ArI. These photocatalytically generated aryl radicals break down the P_4 tetrahedron forming, in sequence, phosphine (PH_3), the arylated phosphines, $ArPH_2$, Ar_2PH , and Ar_3P , and in a last step the fully arylated phosphonium salt $[Ar_4P]I$. The Wolf group subsequently reported that the expensive [Ir]-catalyst could be replaced with a much cheaper organic photocatalyst (Figure 1b)^[9] with no impediment to the scope of the reaction. This photoredox-catalytic procedure also provided access to asymmetrical phosphines and phosphonium salts by replacing P_4 with primary and secondary phosphanes, e.g., mono- or diphenylphosphine ($PhPH_2$ or Ph_2PH).^[9]

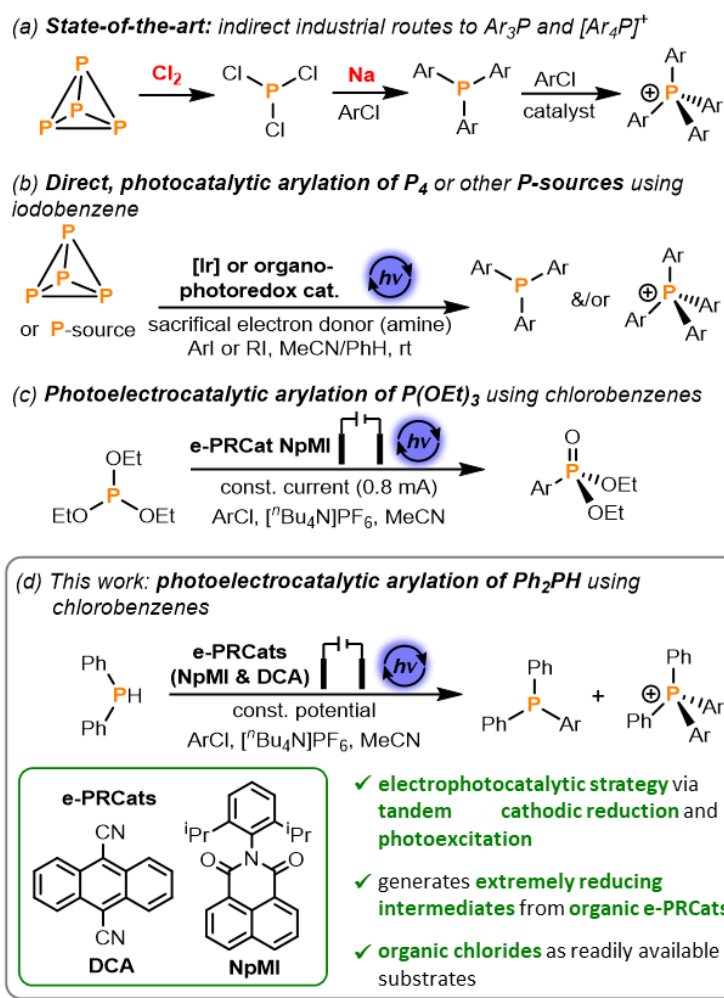


Figure 1. (a) Indirect methods for the synthesis of triarylphosphines Ar_3P and tetraarylphosphonium salts $[\text{Ar}_4\text{P}]^+$ (Ar = aryl substituent) employed industrially.^[1] (b) direct, photocatalytic transformation of P_4 and other P sources into Ar_3P and $[\text{Ar}_4\text{P}]^+$ using an $[\text{Ir}]$ -PRCat,^[3] or an organo-PRCat.^[9] (c) photoelectrocatalytic arylation of $\text{P}(\text{OEt})_3$ generating asymmetrical phosphine oxides.^[15] (d) photoelectrocatalytic arylation of Ph_2PH using **NpMI** or **DCA** as e-PRCats.

In these reports, the generation of aryl radicals was only facilitated by organic bromides and iodides.^{[3],[9]} However, the use of organic chlorides for the preparation of P_1 products would be more economically viable, using cheap and abundant substrates which comprise over two-thirds of commercially available organic halides.^{[14],[6]} Their use as substrates and radical precursors in photocatalytic reactions is a challenging objective due to their chemical inertness caused by a high C–Cl bond strength and the thermodynamically challenging SET.^{[16]-[19]} Previous literature described the use of organic dyes for the dehalogenation of organic chlorides, relying on a consecutive photoinduced electron transfer (con-PET) mechanism (see section 4.1.2).^{[17],[11]} The use of this con-PET strategy provides access to highly reducing excited catalyst species, which are able to generate carbon-centered radicals in a photocatalytic fashion. However, functionalization of P_4 using con-PET activation of chlorobenzenes has yet to be reported.

Among the various proof-of-principle procedures for the photochemical^[3] and electrochemical functionalization of P₄ and other phosphorus compounds,^{[9],[12]–[10]} the combined strategy of electrochemically-mediated photoredox catalysis (e-PRC) for the functionalization of P₄ is surprisingly unexplored. Recently, Wickens and co-workers reported the use of e-PRC for the photoelectrocatalytic arylation of triethyl phosphite (P(OEt)₃) to generate asymmetric phosphonates (Figure 1c).^[15] The reduction of the e-PRCat *N*-2,6-diisopropylphenyl naphthalene monoimide (**NpMI**) is facilitated by electrochemistry instead of the common sacrificial redox additives Et₃N or DIPEA (*N,N*-diisopropylethylamine) (see section 4.1.3)^{[3],[9]} often employed in photocatalytic procedures. With the high reducing power of the reduced and excited e-PRCat **NpMI** it is possible to employ cheap and abundant aryl chlorides for the generation of aryl radicals.^[15]

Herein, we describe a reductive photoelectrocatalytic activation and transformation of organic chlorides and diphenylphosphine (Ph₂PH) into phosphines and phosphonium salts mediated by e-PRCats 9,10-dicyanoanthracene (**DCA**)^[18] and *N*-2,6-diisopropylphenyl naphthalene monoimide (**NpMI**)^[15] (Figure 1d). The motivation of the project is presented in the following summary and comparison of the significant characteristics of the mechanistically related consecutive photoinduced electron transfer (con-PET) strategy and the electrochemically mediated photoredox catalysis (e-PRC) with the help of selected examples.

4.1.2 Definition and selected examples for con-PET

Over the last few decades, the increasing interest in photo(redox)catalysis as a valuable method for organic synthesis has led to some interesting examples of photocatalytic cross-coupling reactions forming new C–H, C–C, or C–E (E = P, S and B) bonds.^{[16],[17]} In order to replace well-established, albeit expensive, redox-active transition metal complexes such as [Ru(bpy)₃]²⁺ or [Ir(ppy)₃], the spectroscopic properties of organic dyes were investigated for their use in photocatalysis.^{[16],[17]} In 2014, König and co-workers introduced the concept of con-PET, reporting a reductive dehalogenation of aryl halides ArX (X = I, Br, Cl) by con-PET in the presence of the organic dye *N,N*-bis(2,6-diisopropylphenyl)perylene-3,4,9,10-bis(dicarboximide) (**PDI**).^[17] In this photocatalytic system two photons are used in one catalytic cycle to generate a highly reactive catalyst species ([**PDI**^{•-}]*), which possesses a sufficient reduction potential to cleave even the C–Cl bond of aryl chlorides to generate carbon-centered radicals (Figure 2).

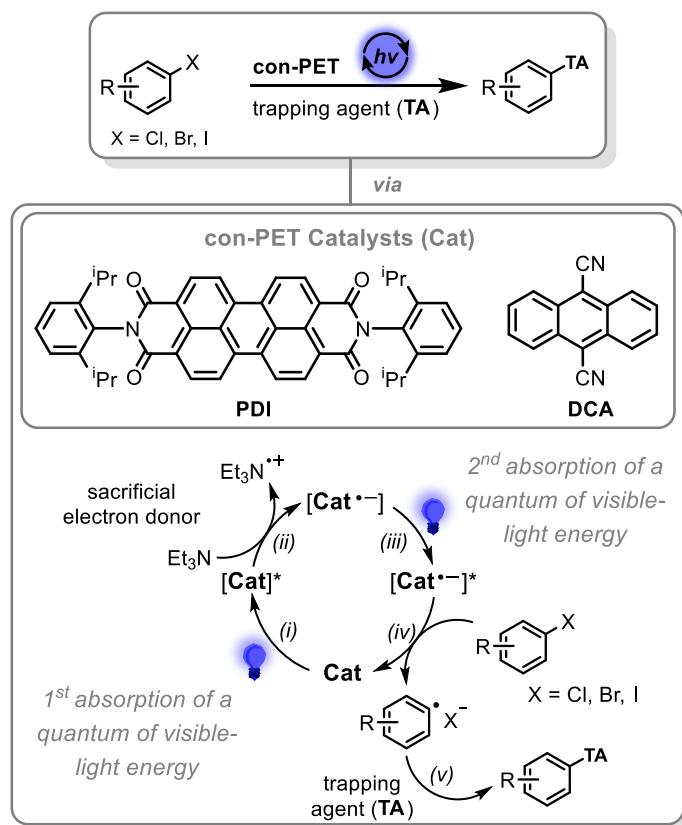


Figure 2. Proposed mechanism for the consecutive photoinduced electron transfer (con-PET) using **PDI**^[17] or **DCA**,^[11] respectively.

Initially, **PDI** is excited by irradiation with blue light and the resulting **[PDI]*** (Figure 2, step i) is reduced by the additive triethylamine (Et_3N) to form **[PDI]^{•-}** (step ii). Upon the second excitation (step iii) the highly reducing species **[PDI]^{•-}*** reduces the aryl halide, forming aryl radicals (step iv) which participate in C–C cross-coupling reactions with various trapping agents (step v). Some years later, Pérez-Ruiz and Jacobi von Wangelin also reported a dichromatic photocatalytic substitution of aryl halides with a simple organic dye.^[11] The commercially available dye 9,10-dicyanoanthracene (**DCA**) performs photocatalytic aromatic substitutions of non-activated aryl halides, such as aryl bromides and chlorides bearing electron-withdrawing substituents. The reaction relies on a dichromatic con-PET mechanism involving a sequential photonic (blue light irradiation), electronic (reduction with DIPEA) and a second photonic activation (green light irradiation) of **DCA** (Figure 2). The resulting highly reducing excited species **[DCA]^{•-}*** is used for the formation of new C–H, C–C, C–P, C–S and C–B bonds.

The concept of con-PET enables the cleavage of C–X bonds (with X = Br, Cl) that could not be split by a single quantum of visible-light energy (e.g., see the photocatalytic functionalization of P_4 via [Ir]-photoredox catalysis).^[18] In both con-PET reactions the organic photocatalyst absorbs one quantum of visible-light energy and is subsequently

reduced by a sacrificial chemical reductant (e.g., Et₃N or DIPEA). The resulting radical anion is excited a second time to form a super-electron donor exhibiting extraordinary reducing power. Nonetheless, this strategy requires an additional reaction component – a sacrificial electron donor for the reduction of the photocatalyst – and the necessary design of photocatalysts that absorb visible light in both their ground state and radical ion state is an undesirable challenge. The use of electrochemically mediated photoredox catalysis (e-PRC) circumvents this photoreduction step and the catalyst radical anion can be accessed from the neutral precursor without the need for a chemical reductant.

4.1.3 Definition and selected examples for e-PRC

Lin and Lambert reported a new photoelectrocatalytic strategy for the dehalogenation of aryl bromides and chlorides mediated by **DCA**^[11] as a photocatalyst (Figure 3).^[18] In contrast to the aforementioned con-PET mechanism of **DCA**,^[11] the first photoinduced excitation and the subsequent reduction step of the reductive photocatalytic procedure are replaced by an electrochemical reduction process (Figure 3, step i). In an H-type divided cell, the cathodic reduction of **DCA** ($E^\circ = -0.82$ V vs. SCE, see Figure 4) to the corresponding radical anion [**DCA**^{•-}] is performed on a porous carbon cathode.

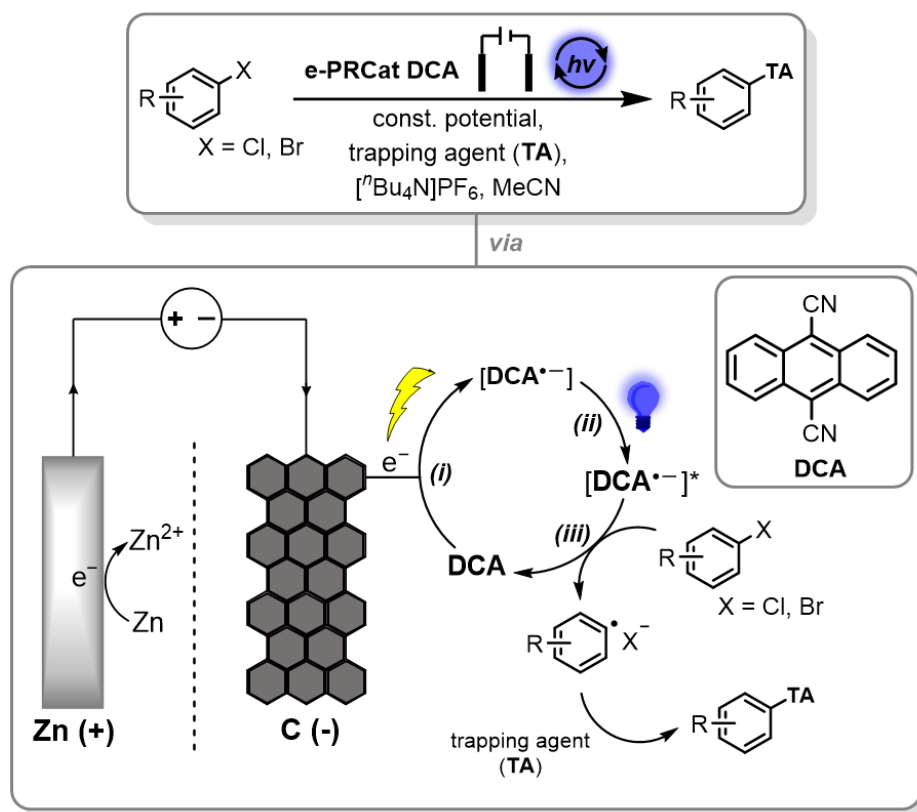


Figure 3. Mechanism for the reductive photoelectrocatalytic functionalization of aryl halides in the presence of e-PRC **DCA**.^[18]

Oxidation of a sacrificial zinc anode serves as the counter reaction in the corresponding anodic cell compartment. The reduced species [**DCA**^{•-}] is itself a weak reductant, but can be transformed into a strong reducing agent by excitation with blue light to form [**DCA**^{•-}]* ($E^\circ = -3.20$ V vs. SCE) (step ii). [**DCA**^{•-}]*, featuring a high reducing potential comparable to that of elemental metals such as lithium ($E^\circ = -3.3$ V vs. SCE), is able to reduce relatively inert substrates, such as aryl chlorides (step iii). This exceptionally high reducing power was proposed to appear from a SOMO–HOMO level inversion featuring a very unstable electronic structure with a half-filled bonding orbital and a filled antibonding orbital, as confirmed by TD-DFT calculations.^{[15],[18]} The tandem electrochemical reduction and photoexcitation provides this highly reducing catalyst in a very low concentration which implicates a controllable reaction outcome.

As already mentioned, Wickens and co-workers reported a new photoredox catalytic strategy to access extremely reducing intermediates *via* tandem electrochemical activation and photochemical amplification.^[15] The organophotoredox catalyst *N*-2,6-diisopropylphenyl naphthalene monoimide (**NpMI**) is used to generate the corresponding excited radical anion [**NpMI**^{•-}]* after cathodic reduction and photoexcitation, which exhibits a remarkable reducing power of -3.7 V (E° vs. SCE) (Figure 4).^{[15],[19]}

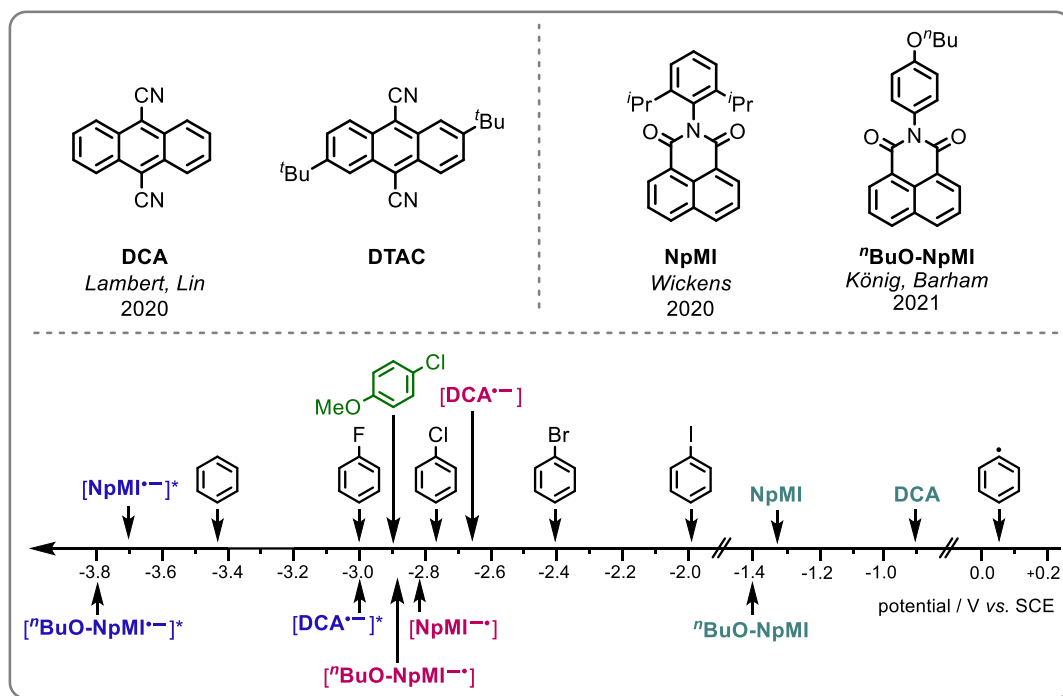


Figure 4. Photocatalysts used for the electrochemically-mediated photoredox catalysis (e-PRC): 9,10-dicyanoanthracene (**DCA**),^[18] 2,6-di-*tert*-butylanthracene-9,10-dicarbonitrile (**DTAC**),^[20] *N*-(2,6-diisopropylphenyl)naphthalene monoimide (**NpMI**)^[15] and *N*-(*para*butoxyphenyl)naphthalene monoimide (**nBuO-NpMI**).^[21] Reducing power of group-state, reduced-state and excited-state of e-PRCats and reduction potentials of used aryl halides (fluoro, chloro,^[21] bromo- and iodobenzene^[25]) and the corresponding aryl radical.^[24]

The e-PRC mechanism of **NpMI** is proposed to proceed *via* the same catalytic cycle as previously described for the reductive photoelectrocatalytic functionalization of aryl halides mediated by e-PRCat **DCA** (see Figure 3, for the **NpMI** system the divided H-cell was equipped with a set of RVC (+) / RVC (-) electrodes). By the use of **NpMI** as a precursor for a highly reducing catalyst, Wickens and co-workers were able to expand the scope of less reactive aryl chlorides (e.g., chlorobenzene ($E^\circ = -2.8$ V vs. SCE) or 4-chloroanisole ($E^\circ = -2.9$ V vs. SCE; see Figure 4) for their phosphorylation reaction. The e-PRCats 9,10-dicyanoanthracene (**DCA**),^[18] 2,6-di-tert-butylanthracene-9,10-dicarbonitrile (**DTAC**),^[20] *N*-2,6-diisopropylphenyl naphthalene monoimide (**NpMI**),^[15] *N*-(*parabutoxyphenyl*)naphthalene monoimide (**"BuO-NpMI**),^[21] and their corresponding excited radical anions show great potential for the dehalogenation of cheap and abundant, but chemically inert chlorobenzenes, which comprise over two-thirds of commercially available aryl halides.^[6] These photoelectrochemically generated carbon-centered radicals could then be used to directly functionalize P_4 into valuable arylphosphines and phosphonium salts.

4.2 Results and Discussion

4.2.1 Photoelectrocatalytic functionalization of white phosphorus with DCA

We were interested in the combination of the extraordinary reducing properties of all aforementioned e-PRCats (Figure 4) to form carbon-centered radicals, and the excellent ability of P₄ to trap these radicals. Initially, the stability of P₄ in the presence of e-PRCat **DCA** and the highly reducing species [DCA^{•-}]* was tested in a stoichiometric photoelectrochemical control reaction to verify these harsh reducing conditions are compatible with P₄. In an H-type divided cell, the cathodic chamber was charged with e-PRCat **DCA**, P₄, electrolyte tetrabutylammonium hexafluoride ([nBu₄N]PF₆ = TBAPF₆), and pencil lead (graphite) was used as a cathode (Figure 5, picture 1). **DCA** exhibits poor solubility in the MeCN/benzene solvent mixture used, resulting in a yellow suspension. The anodic chamber contained the sacrificial zinc anode and TBAPF₆ in a MeCN/benzene solvent mixture. After applying constant potential (2.55 V) and irradiation with blue light (455 nm) to the cathodic chamber of the H-cell for 30 minutes, the formation of [DCA^{•-}]* was identified by a color change to bluish violet (Figure 5, picture 2). After 18 h, a dark violet solution (no orange precipitate, suggestive of polymerized phosphorus species, was observed) was formed in the cathodic chamber which was subjected to ³¹P{¹H} NMR analysis. The resonance for P₄ remained, indicating no significant degradation under these highly reductive electrochemical conditions (Figure 5, picture 3; see also SI S3.1, Figure S80).



Figure 5. Stability test of P₄ in presence of excited radical anion [DCA^{•-}]* as a strong reducing agent. [1] Divided H-cell equipped with Zn (+) / C (-), cathodic chamber: **DCA** & P₄ in MeCN/benzene/electrolyte solution; [2] Irradiation with blue light-LED for 30 minutes; [3] Irradiation with blue light-LED for 18 h.

Having demonstrated the stability of white phosphorus in the presence of the highly reducing radical anion [DCA^{•-}]*, the photoelectrochemical arylation of P₄ was investigated. The cathodic chamber of an H-type divided cell (Zn (+) / C (-)) was equipped with P₄, e-PRCat **DCA** and the substrate 4-chloroanisole (ClC₆H₄-4-OMe). After addition of TBAPF₆ and a solvent mixture of MeCN/benzene in both chambers, the

resulting mixture was irradiated with blue light (455 nm) from beneath the cathodic chamber (Figure 6, picture 2) while a constant potential (1.76 V) was applied across the cell. After 30 minutes a brownish orange solution was obtained, generally attributed to the generated radical anion $[\text{DCA}^{\bullet-}]$ (Figure 6, picture 3).^[18] No bluish violet color change is observed in this reaction, because the excited radical anion $[\text{DCA}^{\bullet-}]^*$ is immediately quenched by the substrate *via* SET. After irradiation and applying constant potential for 21 h, the resulting dark brown reaction mixture was subjected to $^{31}\text{P}\{^1\text{H}\}$ NMR analysis, which showed full consumption of P_4 but no product formation.

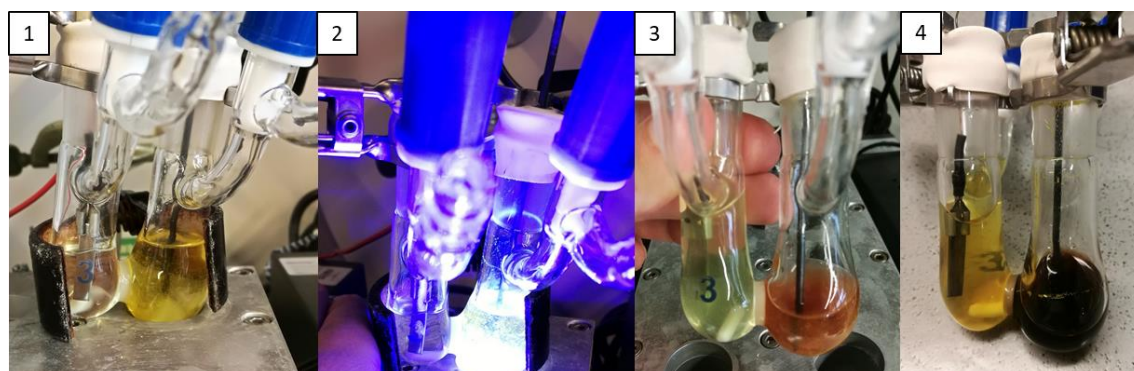


Figure 6. Attempts for the photoelectrocatalytic functionalization of P_4 with 4-chloroanisole mediated by e-PRCat **DCA**. [1] Setup before irradiation and applying potential; [2] Irradiation of the cathodic chamber and applying constant potential of 1.76 V (see SI, Table S10, Entry 2); [3] After 30 minutes of photoelectrochemical reaction (brownish orange solution caused by $[\text{DCA}^{\bullet-}]$); [4] After 21h of irradiation and constant potential (dark brown reaction mixture).

Table 1. Photoelectrocatalytic functionalization of P_4 into $[\text{Ar}_4\text{P}]\text{Cl}$ and Ar_3P using e-PRCats **DCA** and **NpMI**. For all reactions 4-chloroanisole was used as a substrate.

Entry	e-PRCat [mol%]	Potential [V]	Electrodes	Full conv. of P_4 ?	Product formation?
1	DCA (3.3 mol%)	1.76	Zn (+) / C_{foam} (-)	✓	–
2	DCA (3.3 mol%)	1.00	Zn (+) / C_{foam} (-)	✓	–
3	DCA (3.3 mol%)	1.00	Zn (+) / C_{lead} (-)	✗	–
4	NpMI (5 mol%)	1.60	Zn (+) / Fe (-)	✓	–
5	NpMI (5 mol%)	1.60	Zn (+) / C_{foam} (-)	✗	–

Unfortunately, several attempts for the photoelectrocatalytic arylation of P_4 with 4-chloroanisole, using the high reduction power of the corresponding excited radical anions of e-PRCats **DCA** or **NpMI**, yielded no product formation (see Table 1). In most of the reactions an orange precipitate was obtained, which we assume to be polymerized phosphorus species. Potentially, the successful arylation of P_4 is prohibited by the very low concentration of the highly reducing catalysts. By generating an insufficient concentration of aryl radicals, the activated P radical species are prone to polymerize.

4.2.2 Photoelectrochemical functionalization of Ph₂PH using anthracene derivatives

4.2.2.1. Photoelectrochemical functionalization of Ph₂PH mediated by DCA

Despite the unsuccessful P₄ functionalization attempts, we proceeded to investigate the use of diphenylphosphine (Ph₂PH) as a starting material for the photoelectrocatalytic synthesis of phosphines and phosphonium salts. Similarly to the previously described photocatalytic functionalization of different organophosphanes mediated by an [Ir]-catalyst^[3] or an organic photoredox catalyst,^[9] the arylation of Ph₂PH mediated by DCA yields symmetric or asymmetric products depending on the substrate used. 4-Chloroanisole was used as a model substrate, as it possesses a high reduction potential of -2.90 V (E_{red} vs. SCE). The generation of the highly reducing species [DCA^{•-}]* proceeds *via* the e-PRC mechanism of DCA described above (Section 4.1.3), through tandem electrochemical activation and photoexcitation (Figure 7, steps i and ii). Subsequent to the dehalogenation of 4-chloroanisole and the generation of aryl radicals (step iii), Ph₂PH is arylated stepwise to form the asymmetric phosphine Ph₂ArP and the phosphonium salt [Ph₂Ar₂P]Cl (step iv).

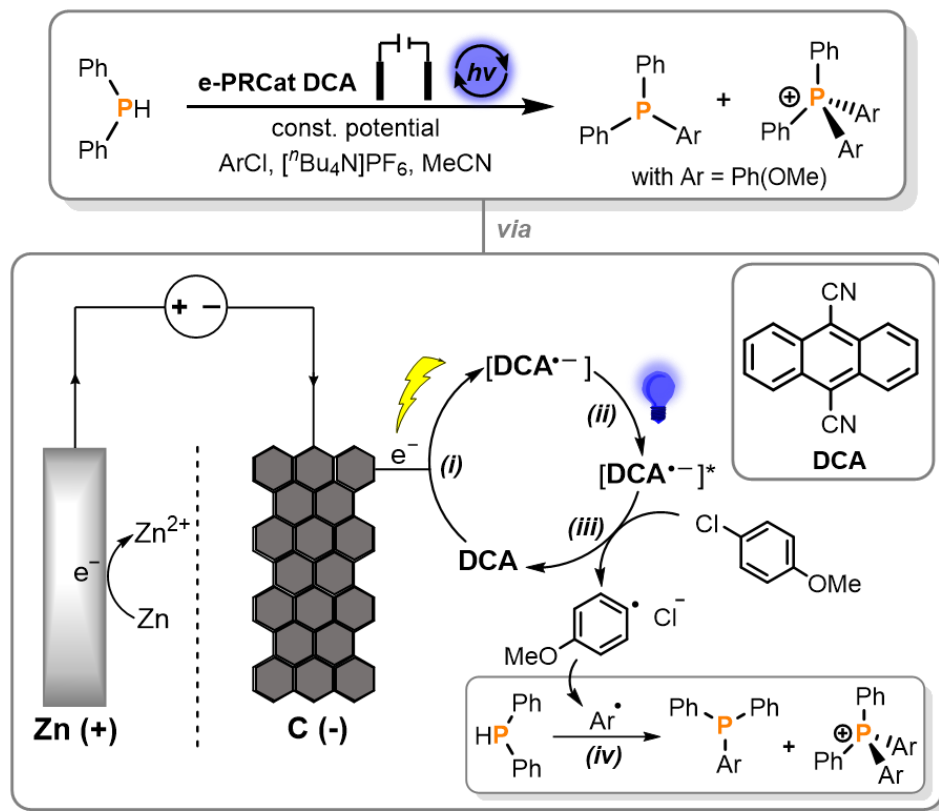


Figure 7. Proposed mechanism for the photoelectrocatalytic arylation of Ph₂PH using aryl chloride in the presence of electrochemically-mediated photoredox catalyst DCA.

The reductive photoelectrochemical functionalization of Ph₂PH was performed in an H-type divided cell equipped with an electrode set of zinc (+) and graphite (-) (pencil lead or carbon foam). The cathodic reduction of **DCA** to the corresponding radical anion [DCA^{•-}] takes place on a porous carbon cathode and oxidation of the sacrificial zinc anode (Zn → Zn²⁺) was chosen as the counter reaction. Unfortunately, the generation of zinc ions excludes triphenylphosphine oxide (Ph₃PO) as a commonly used internal standard for quantification.^{[3],[9],[10]} Ph₃PO precipitates with zinc chloride as the ZnCl₂(Ph₃PO)₂ complex, which disables the phosphine oxide as an suitable internal standard.^[25] For the quantification of the photochemical functionalization using **DCA** as an e-PRCat, the P₁ compound triphenylphosphine (Ph₃P) was tested as an internal standard. A constant potential of 1.6 V was applied to an acetonitrile solution of the substrate, 4-chloroanisole, **DCA** (5 mol%), Ph₂PH and electrolyte (with Zn (+) / C_{foam} (-) electrodes) while irradiating with blue light (455 nm). Subsequent addition of Ph₃P as an internal standard showed 19% NMR yield of Ph₂ArP in the ³¹P{¹H} NMR spectrum (7% of Ph₂PH was left and no phosphonium salt was formed) (see Table 2, Entry 15). For comparison the same reaction was repeated with a pencil lead as the graphite cathode material, which possess much less reactive surface area than the carbon foam electrode. Surprisingly, while using a pencil lead as the cathode (see Table 2, Entry 16) showed comparable conversion to the product (15% Ph₂ArP and 2% [Ph₂Ar₂P]Cl), but much starting material (41%) remained. The carbon foam cathode performs the photoelectrochemical reaction faster, converting most of the starting material because of its high surface area. However, the carbon foam also led to a more inefficient reaction, because similar ³¹P{¹H}-NMR yields were obtained for both cathode materials (Ph₂ArP: 15% (pencil lead) vs. 19% (carbon foam)), but conversion of the starting material diverges drastically (Ph₂PH: 41% (pencil lead) vs. 7% (carbon foam)). Changing the reaction conditions, such as catalyst loading, applied potential, or electrode material always yielded different proportions of the unreacted starting material Ph₂PH, and arylated products Ph₂ArP and [Ph₂Ar₂P]Cl (Table 2, also see SI, S2.1.2 for ³¹P{¹H} NMR spectra). Additionally, some reactions feature small amounts of tetraphenyldiphosphine (Ph₄P₂) as an intermediate of the stepwise arylation, which was already investigated in some of our previous studies.^{[3],[9]} Overall, only moderate conversion was achieved for photoelectrochemical arylation of Ph₂PH with 4-chloroanisole mediated by **DCA**. The experiment performed highlights limitations that require attention, such as the poor solubility of **DCA** in the reaction solution (limited to set-up and efficient light irradiation).

Chapter 4. Reductive Photoelectrocatalytic Activation of Organic Halides and Diphenylphosphine into Arylphosphines and Phosphonium Salts

Table 2. Photoelectrocatalytic functionalization of Ph₂PH into [Ph₂Ar₂P]Cl and Ph₂ArP using 4-chloroanisole (ClC₆H₄-4-OMe) and DCA.

Entry	DCA [mol%]	Potential [V]	Electrodes	Ratio of Ph ₂ PH to Ph ₂ ArP / Ph ₄ P ₂	Ratio of Ph ₂ PH to [Ph ₂ Ar ₂ P]Cl
1	5	1.57	Zn (+) / C _{lead} (-)	1 : 0.35 / 0.31	1 : 0.04
2	10	1.76	Zn (+) / C _{lead} (-)	1 : 0.16 / 0.33	1 : 0.10
3	5	1.76	Zn (+) / C _{foam} (-)	0 : 0.05 / 0.28	0 : 0.09
4	5	1.0	Zn (+) / C _{foam} (-)	1 : 0.31 / 0	1 : 1.62
5	5	1.0	Zn (+) / C _{lead} (-)	1 : 0.27 / 0	1 : 0.80
6	10	1.0	Zn (+) / C _{foam} (-)	1 : 0 / 0	1 : 5.13
7	10	1.0	Zn (+) / C _{lead} (-)	1 : 0.36 / 0	1 : 0.11
8	5	1.6	Zn (+) / C _{foam} (-)	1 : 1.92 / 0	1 : 0.36
9	5	1.6	Zn (+) / C _{lead} (-)	1 : 0.90 / 0.20	1 : 0
10	5	1.6	Zn (+) / C _{felt} (-)	1 : 0.49 / 0.06	1 : 0.02
11 ^[a]	5	1.0	Zn (+) / C _{foam} (-)	–	–
12 ^[a]	5	1.0	Zn (+) / C _{lead} (-)	1 : 1.86 / 0.12	1 : 0.31
13	10	1.6	Zn (+) / C _{foam} (-)	1 : 0.96 / 0	1 : 0.59
14	10	1.6	Zn (+) / C _{lead} (-)	1 : 0.46 / 0	1 : 0.10
15 ^[b]	5	1.6	Zn (+) / C _{foam} (-)	7% Ph₂PH left, 19% Ph₂ArP	0% [Ph₂Ar₂P]Cl
16 ^[b]	5	1.6	Zn (+) / C _{lead} (-)	41% Ph ₂ PH left, 15% Ph ₂ ArP	2% [Ph ₂ Ar ₂ P]Cl

[a] The reaction time was extended from 21h to 3 days. [b] Ph₃P was added as an internal standard (0.05 mmol).

4.2.2.2 Photoelectrochemical functionalization of Ph₂PH mediated by DTAC

The poor solubility of DCA is problematic and severely limits reproducibility. The anthracene derivative 2,6-di-tert-butylanthracene-9,10-dicarbonitrile (DTAC) exhibits better solubility in acetonitrile.^[20] Unfortunately, investigations into the catalytic properties of DTAC in the photoelectrochemical system resulted in an unselective reaction outcome, featuring a lot of unknown compounds in addition to the remaining starting material Ph₂PH and small amounts of the P₁ products [Ph₂Ar₂P]Cl and Ph₂ArP. The comparison of both graphite cathodes also showed higher and more selective product formation for the pencil lead electrode (see SI, S2.2.1, Table S2 and S2.2.2 for ³¹P{¹H} NMR spectra).

4.2.3 Photoelectrochemical functionalization of Ph₂PH using naphthalene-imide derivatives

4.2.3.1 Photoelectrochemical functionalization of Ph₂PH mediated by NpMI

The naphthalene-imide catalyst **NpMI** (Figure 8) reported by Wickens was referred to be an even stronger photoelectron-mediated reducing agent than **DCA**. After electrochemical reduction and irradiation (Figure 8, step i and ii) the corresponding excited radical anion [**NpMI**^{•-}]* (step iii) enabled reduction of chemically inert substrates with potentials as negative as -3.4 V vs SCE.^[15] The generated aryl radicals are trapped by the P source Ph₂PH and the tertiary phosphine and phosphonium salt are produced in sequence (step iv).

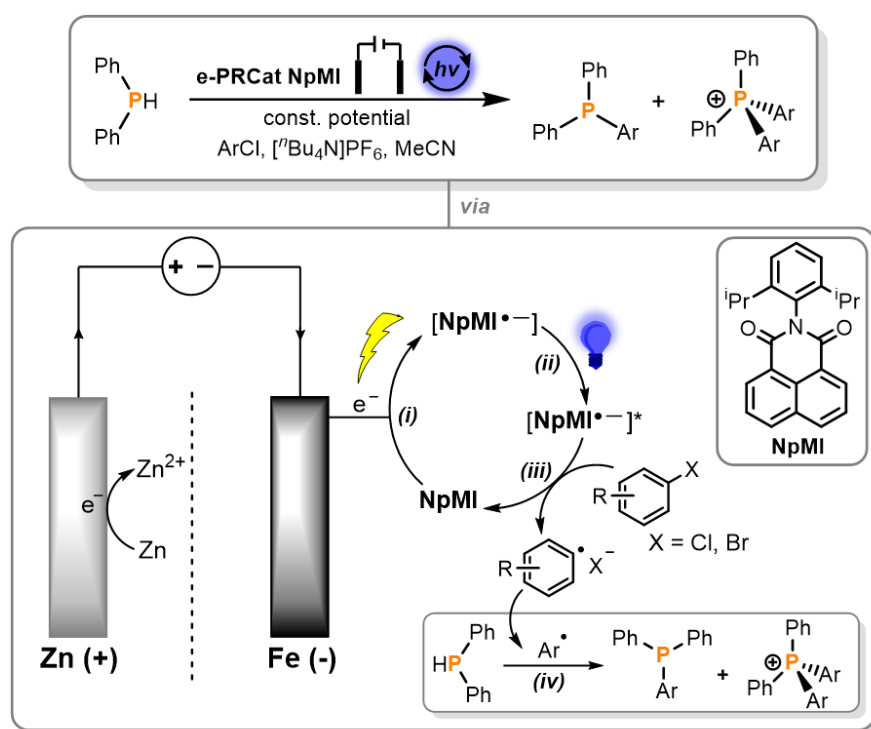


Figure 8. Proposed mechanism for the photoelectrocatalytic arylation of Ph₂PH using aryl chloride in the presence of electrochemically-mediated photoredox catalyst **NpMI**.

In the e-PRC reaction mediated by **NpMI**, a divided H-cell was equipped with a set of Zn (+) / Fe (-) electrodes, thereby precluding the use of the commonly used internal standard Ph₃PO, because of the generated zinc ions (see 4.2.2.1).^[25] After screening different reaction conditions (e.g., modifying the electrolyte, electrode material, and the catalyst loading), the highest conversion of P₄ to ca. 49% asymmetric phosphine and 25% phosphonium salt was obtained using 5 mol% **NpMI**, 1.6 V applied potential and an electrode combination of Zn (+) / Fe(-) (Ph₃P was used as internal standard; 50% Ph₂PH remained unreacted, see SI, S2.3.1, Table S4, Entry 12). Unfortunately, in most cases employing Ph₃P as the internal standard yielded a ³¹P NMR intensity above 100%,

indicating the quantification is unreliable and Ph₃P is not appropriate as an internal standard for these reactions. To solve this issue, bis(triphenylphosphine)iminium chloride ((Ph₃P)₂N]Cl, PPNCl) was investigated as a potentially suitable internal standard for the photoelectrocatalytic arylation. ³¹P{¹H} NMR calibration of PPNCl, the starting material, Ph₂PH, and the product, Ph₃P, showed that PPNCl is an appropriate internal standard for the e-PRC reactions.

Table 3. Reductive photoelectrochemistry with **NpMI** – Quantitative NMR with PPNCl.

Entry	NpMI [mol%]	Substrate	Potential [V]	Electrodes	Full conv. of Ph ₂ PH?	Conv. to Ph ₃ P [%]	Conv. to [Ph ₄ P]Cl [%]
1	5	PhCl	1.6	Zn (+) / Fe (-)	✓	0	0
2	5	PhCl	1.6	Zn (+) / C _{foam} (-)	✗	0	2
3	5	PhBr	1.6	Zn (+) / Fe (-)	✓	0	13
4	5	PhBr	1.6	Zn (+) / C _{foam} (-)	✗	0	2
5	5	PhBr	1.6	Zn (+) / Fe (-)	✓	0	5
6	5	PhBr	1.6	Zn (+) / Fe (-)	✓	0	4
7	5	PhBr	1.3	Zn (+) / Fe (-)	✗	2	6
8	5	PhBr	1.3	Zn (+) / Fe (-)	✗	3	7
9 ^[a]	5	PhBr	1.6	Zn (+) / Fe (-)	✗	11	7

[a] A 1:1 ratio of Ph₂PH and substrate PhBr was used instead of an excess of 10 equiv.

However, repetition of the reaction using PhBr and PhCl as substrates and subsequent addition of the internal standard PPNCl, showed a combined NMR yield of 18% for the tertiary phosphine and the phosphonium salt (Table 3, Entry 9, see SI, S2.3.3.1, Table S8, Entry 9). Overall, all of these quantification attempts reveal a huge loss in phosphorus intensity in the NMR spectra, with no remaining starting material being detected.

Control experiments (see Table 4) confirmed that the arylation of Ph₂PH with the substrate 4-chloroanisole in the presence of **NpMI** represents a photoelectrocatalytic method, as product formation was only observed when all reaction components, applied potential and blue light irradiation were provided.

Chapter 4. Reductive Photoelectrocatalytic Activation of Organic Halides and Diphenylphosphine into Arylphosphines and Phosphonium Salts

Table 4. Photoelectrocatalytic functionalization of Ph₂PH into Ph₂ArP and [Ph₂Ar₂P]Cl using NpMI: screening of **control experiments**.

Entry	Ph ₂ PH	NpMI [mol%]	Sub. ^[a]	Pot. [V]	Electrodes	Electrolyte	Blue LED	Product formation?
1	✓	5	–	1.6	Zn (+) / Fe (–)	TBAPF ₆	✓	X
2	✓	5	✓	1.6	Zn (+) / Fe (–)	TBAPF ₆	–	X
3	✓	5	✓	–	Zn (+) / Fe (–)	TBAPF ₆	✓	X / ✓ ^[b]
4	✓	–	✓	1.6	Zn (+) / Fe (–)	TBAPF ₆	✓	X
5	–	5	✓	1.6	Zn (+) / Fe (–)	TBAPF ₆	✓	X
6	✓	5	✓	1.6	Zn (+) / Fe (–)	–	✓	X
7	✓	5	✓	–	Zn (+) / Fe (–)	TBAPF ₆	–	X
8	✓	5	✓	1.6	Zn (+) / C _{foam} (–)	TBAPF ₆	✓	✓
9	✓	5	✓	3.2	Zn (+) / Fe (–)	TBAPF ₆	–	X

[a] For all control experiments 4-chloroanisole (ClC₆H₄-4-OMe) was used as substrate. [b] After irradiation without potential for 21h shows no product formation in the ³¹P{¹H} NMR spectrum, but subsequent applying of potential yielded Ph₂ArP and [Ph₂Ar₂P]Cl.

4.2.3.2. Photoelectrochemical functionalization of Ph₂PH mediated by ⁿBuO-NpMI

Recently, Barham and König showed that structural variation of the NpMI catalyst, through synthesis of ⁿBuO-NpMI as a novel e-PRCat, improved the yield and selectivity of C(sp³)-O cleavage of a phosphinate (e.g., Ph₂(O)P(OAlkyl)) to give alkyl carbanions.^[21] Therefore, we investigated the photoelectrochemical properties of this slightly modified naphthalene monoimide catalyst in the arylation reaction of Ph₂PH using bromo-, chlorobenzene, and 4-chloroanisole as substrates. When introducing an applied potential of 1.6 V during irradiation of a solution of ⁿBuO-NpMI (5 mol%), 4-chloroanisole and Ph₂PH with blue light, the electrode combination Zn (+) / C_{foam} (-) performed much better than if an Fe (-) cathode was used. Quantification of these reactions with internal standard Ph₃P yielded a product mixture of Ph₂ArP (42%) and [Ph₂Ar₂P]Cl (17%) in good conversion (Table 5, Entry 4, also see SI, S2.4.1, Table S9). For comparison, the reaction with the iron cathode only showed an overall product conversion of 23% (10% Ph₂ArP & 13% [Ph₂Ar₂P]Cl, see Table 5, Entry 1). Moreover, the ³¹P{¹H} NMR spectrum of the photoelectrochemical reduction of PhCl or PhBr showed the phosphonium salt [Ph₄P]Cl as the main product (Table 5, Entry 5 & 6). However, repeating the reactions and determining the conversion of the products by addition of PPnCl as an internal standard, showed either poor conversion or no product formation at all (Table 5, Entry 7 & 8).

Table 5. Photoelectrocatalytic functionalization of Ph₂PH into [Ph₂Ar₂P]Cl and Ph₂ArP using ⁿBuO-NpMI.

Entry	ⁿ BuO-NpMI [mol%]	Substrate	Potential [V]	Electrodes	Ratio of Ph ₂ PH to Ph ₂ ArP	Ratio of Ph ₂ PH to [Ph ₂ Ar ₂ P]Cl
1 ^[a]	5	ClC ₆ H ₄ -4-OMe	1.6	Zn (+) / Fe (-)	19% Ph ₂ PH, 10% Ph ₂ ArP	13% [Ph ₂ Ar ₂]Cl
2	5	PhCl	1.6	Zn (+) / Fe (-)	1 : 1.31	1 : 1.55
3	5	PhBr	1.6	Zn (+) / Fe (-)	1 : 0	1 : 0.37
4 ^[a]	5	ClC ₆ H ₄ -4-OMe	1.6	Zn (+) / C _{foam} (-)	43% Ph₂PH, 42% Ph₂ArP	17% [Ph₂Ar₂]Cl
5	5	PhCl	1.6	Zn (+) / C _{foam} (-)	1 : 2.65	1 : 9.58
6	5	PhBr	1.6	Zn (+) / C _{foam} (-)	1 : 3.62	1 : 6.90
7 ^[b]	5	PhCl	1.6	Zn (+) / C _{foam} (-)	no Ph ₂ PH, 2% Ph ₃ P	no Ph ₂ PH, no product
8 ^[b]	5	PhBr	1.6	Zn (+) / C _{foam} (-)	no Ph ₃ P	8% Ph ₂ PH, 1% [Ph ₄ P]Cl

[a] Ph₃P (0.05 mmol) was added as an internal standard. [b] PPnCl (0.05 mmol) was added as an internal standard.

4.3 Conclusion

The key advantage of electrochemically-mediated photoredox catalysis (e-PRC) is the broadened redox window accessible and the generation of highly reducing photoexcited radical ion catalysts, which are able to reduce more challenging and chemically inert substrates (e.g., organic chlorides) under mild conditions. Moreover, introducing an applied potential in photoredox catalysis is also highly attractive as a replacement for sacrificial redox additives (e.g., amines). The study reported herein demonstrated as a proof-of-principle that photoelectrochemical functionalization of Ph_2PH with aryl chlorides is possible.

Unfortunately, the conversion of starting material and ensuing product yield have remained rather low. Moreover, the reliable quantification of the reaction progress was problematic. Poorly reproducible results were obtained with Ph_3P as an internal standard, yielding a ^{31}P NMR intensity above 100%. Possibly Ph_3P is too reactive and interacts with some active species in the reaction mixture. This would lead to a lower internal standard concentration in solution, presumably causing a falsified phosphorus intensity. However, PPNCl as an internal standard (see SI, section S2.3.3 for calibration) showed very poor product formation with a combined NMR yield of 18%.

The tandem electrochemical activation and photoexcitation provides the photoexcited super-reductants in a very low concentration, which is beneficial for a controllable reaction, but possibly prohibits a successful arylation of P_4 . By generating an insufficient concentration of aryl radicals, the activated P radical species are prone to polymerize. Furthermore, potential decomposition of the e-PRCats **DCA** and **NpMI** during the reaction may lead to issues of conversion and reproducibility.

Overall, the photoelectrochemical functionalization of P_4 or phosphines with organic chlorides is still in its infancy, warranting further study. Intensifying research in this field should seek to develop an efficient system to achieve the highly desirable goal of photoelectrocatalytic functionalization of P_4 with organic chlorides using sustainable energy.

4.4 Supporting Information

S1. General Information and Analytical Techniques

All experiments were performed under an atmosphere of dry N₂ (< 0.1 ppm O₂, H₂O) using standard Schlenk line techniques, an *MBraun* UniLab Glovebox or a *GS* Glovebox (GS117717). All glassware was oven-dried (160 °C) overnight prior to use. Acetonitrile was distilled from CaH₂ and stored over molecular sieves (3 Å). The electrolytes *n*-tetrabutylammonium hexafluorophosphate ([nBu₄N]PF₆, TBAPF₆) and lithium perchlorate (LiClO₄), which were used in all preparative photoelectrochemical reactions, were dried at 100 °C over three days. All other chemicals were purchased from major suppliers (Aldrich, ABCR) and used as received; liquids were purified by Kugelrohr distillation and freeze-pump-thaw degassed three times prior to use; P₄ was purified by sublimation and diphenylphosphine was used as received (Aldrich).

NMR Spectroscopy. Qualitative NMR spectra were recorded at room temperature on *Bruker Avance III HD 400* (400 MHz) spectrometers and were processed using TopSpin 3.2. Chemical shifts δ , are reported in parts per million (ppm); ¹H and ¹³C shifts are reported relative to SiMe₄ and were calibrated internally to residual solvent peaks, while ³¹P shifts were referenced externally to 85 % H₃PO₄ (aq.). The following abbreviations have been used for multiplicities: s = singlet, d = doublet, t = triplet, q = quartet, m = multiplet, dd = doublet of doublet. NMR samples were prepared in the glovebox using NMR tubes fitted with screw caps.

S1.1 Materials and equipment for the photoelectrochemical reactions

Electrode Materials. Faber-Castell 2.0 mm HB pencil lead (purchased from Papier Liebl GmbH); Carbon Felt Electrode purchased from Alfa Aesar (1.27 cm, thick, 99.0%); Glassy Carbon Foam Electrode, thickness: 6.35 mm, porosity: 96.5% (Goodfellow, Product Code: 613-422-20); Fe Cathode was manufactured in house from DC01 CR1 (C 0.12, P 0.045, S 0.045, Mn 0.60, Ti 0.0) by Thyssen Krupp; Zinc Anode purchased from MARAWE (part01-74-00000) (200 x 170 x 0.6 mm).

Glassware. Fabrication of divided H-cells was done in-house by a glassblower. A built-in porous filter disc (Ø 1 cm, max. pore size 16-40µm) was purchased from Duran®.

Power Supply. PeakTech® 6080A digital DC laboratory power supply (output voltage: 0-15 V DC, output current: 0-3A DC).

LEDs. In general, all photoelectrochemical reactions were irradiated with blue light (455 nm, 22V, 0.7A, Osram OSOLON SSL 80). Few reactions were irradiated with high

power LEDs (blue (451 nm), 20.3 V, 350 mA, 7 x LT-3109 Osram SSL 80 royal-blau, Ser.-Nr.:219-20-2).

S1.2 General photoelectrochemical reactions setup

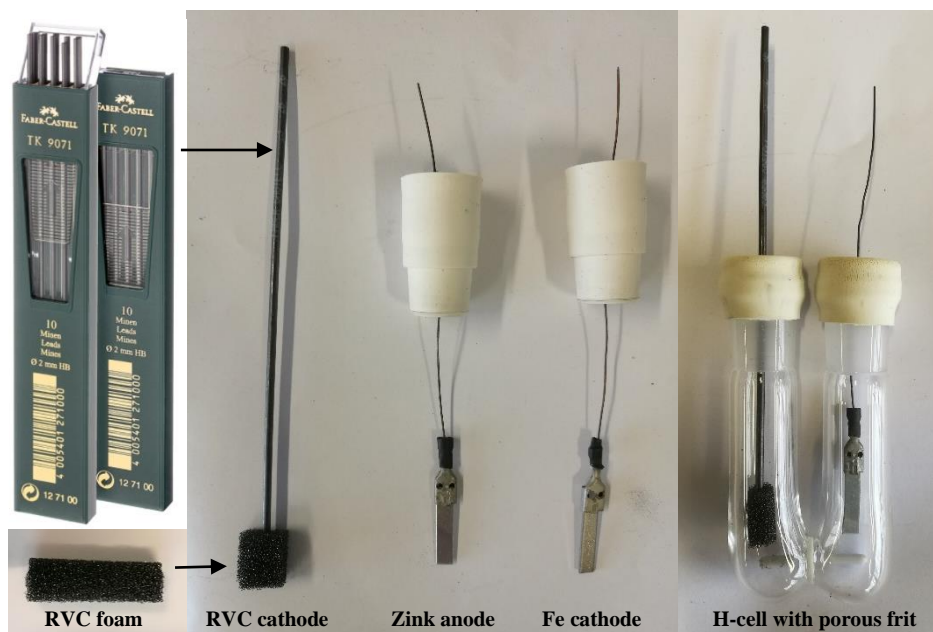


Figure S1. Electrodes and H-cell setup.

Cathode (RVC foam) setup: An HB pencil lead (\varnothing 2 mm) was inserted through a septum with the help of a needle. A small square (around 7 mm x 7 mm) of carbon foam was cut from the carbon foam plate, and the pencil lead was pierced through the resulting foam cube.

Cathode (Fe) setup: A rectangular metal cathode (ca. 20 mm x 4 mm) was inserted into a conductive steel holder. With the help of a needle, the holder was inserted through a septum.

Anode (Zn) setup: A rectangular metal anode (ca. 20 mm x 4 mm) was inserted into a conductive steel holder. With the help of a needle, the holder was inserted through a septum.

H-cell setup: After the H-cell was charged with stirring bars (anodic and cathodic chamber), electrolyte, reactants, catalyst and solvent, the electrodes were added, and the cell was sealed with the septum. The H-cell was connected to the power supply (PeakTech® 6080A; black cable: cathode (-), red cable: anode (+)) and stirred at room temperature above a water-cooled cooling block under irradiation of a 455 nm LED from beneath the cathodic chamber (Figure S2).

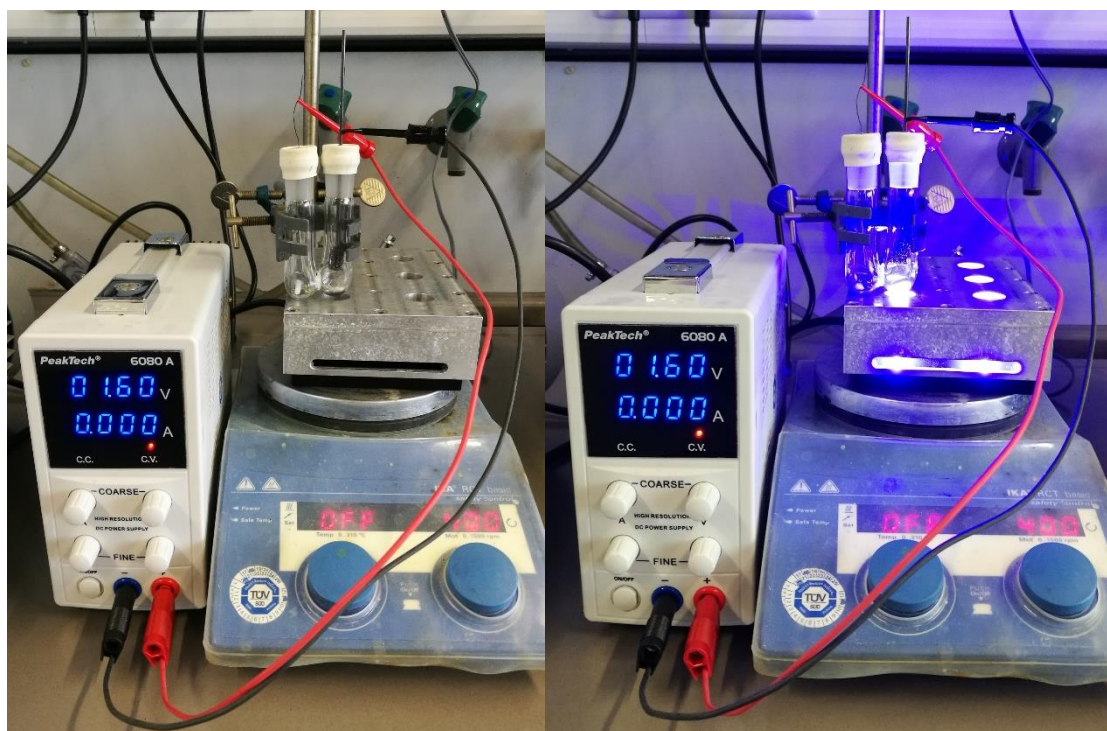


Figure S2. Photoelectrochemical reaction setup. The H-cell is connected to the power supply (PeakTech 6080A, black cable: cathode (-), red cable: anode (+)) The cathodic chamber (RVC-foam electrode, photocatalyst, substrate and trapping agent (Ph_2PH or P_4)) is irradiated with blue light.

S2. Photoelectrochemical functionalization of diphenylphosphine with e-PRC and organic halides

For the photoelectrochemical functionalization of diphenylphosphine (Ph_2PH) the electrochemically mediated photoredox catalysts (e-PRCats) shown in Figure S3 were used. The anthracene derivatives **DCA**^[18] and **DTAC**^[20] and the naphthalene-imide derivatives **NpMI**^[15] and **ⁿBuO-NpMI**^[21] were prepared according to literature procedures. The catalyst loading used in the photoelectrochemical reactions is defined per substrate molecule.

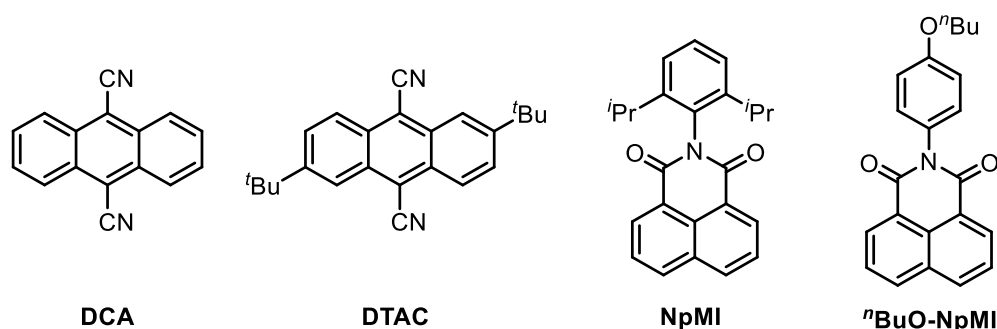
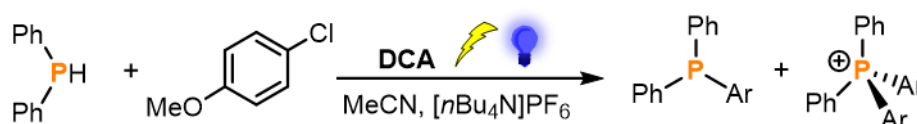


Figure S3. Photocatalysts used for the electrochemically-mediated photoredox catalysis (e-PRC) to functionalize Ph_2PH : 9,10-dicyanoanthracene (**DCA**), 2,6-di-tert-butylanthracene-9,10-dicarbonitrile (**DTAC**), *N*-(2,6-diisopropylphenyl)naphthalene monoimide (**NpMI**) and *N*-(*para*-butoxyphenyl)naphthalene monoimide (**ⁿBuO-NpMI**)

S2.1 Photoelectrochemical functionalization of Ph_2PH mediated by e-PRCat DCA



All preparation steps were carried out in a glovebox under inert gas atmosphere. An oven-dried H-cell was equipped with magnetic stirring bars in both chambers. To the cathodic chamber was added 4-chloroanisole ($\text{ClC}_6\text{H}_4\text{-4-OMe}$, 1.0 mmol, 122 μL), e-PRCat **DCA** (0.05 mmol, 11.4 mg, 5 mol% per substrate molecule), and Ph_2PH (0.1 mmol, 17.4 μL), followed by the additions of $[\text{nBu}_4\text{N}]\text{PF}_6$ (0.1 mmol, 38.74 mg, TBAPF_6) and MeCN (4 mL) in both chambers (resulting in 0.025 M $[\text{nBu}_4\text{N}]\text{PF}_6$ in MeCN as solvent). Both chambers were sealed using rubber septa pierced with wire-connected electrodes (Figure S1). The resulting mixture was stirred at room temperature above a water-cooled block under irradiation of blue LED (455 nm) from beneath the cathodic chamber (Figure S2). A constant potential was applied across the cell. After irradiation for 21h, the mixtures in both chambers were combined and subjected to $^{31}\text{P}\{^1\text{H}\}$ NMR analysis.

For the reactions without additional internal standard a ratio of the starting material Ph₂PH (³¹P{¹H}, integral = 1) and the corresponding products is given. For quantification of selected reactions triphenylphosphine (PPh₃) was added as an internal standard and the determined ³¹P{¹H} NMR yield is shown in Table S1.

S2.1.1 Optimization of reaction conditions

Table S1. Photoelectrocatalytic functionalization of Ph₂PH into [Ph₂Ar₂P]Cl and Ph₂ArP using 4-chloroanisole (ClC₆H₄-4-OMe) and DCA.

Entry	DCA [mol%]	Potential [V]	Electrodes	Ratio of Ph ₂ PH to Ph ₂ ArP / Ph ₄ P ₂	Ratio of Ph ₂ PH to [Ph ₂ Ar ₂ P]Cl
1	5	1.57	Zn (+) / C _{lead} (-)	1 : 0.35 / 0.31	1 : 0.04
2	10	1.76	Zn (+) / C _{lead} (-)	1 : 0.16 / 0.33	1 : 0.10
3	5	1.76	Zn (+) / C _{foam} (-)	0 : 0.05 / 0.28	0 : 0.09
4	5	1.0	Zn (+) / C _{foam} (-)	1 : 0.31 / 0	1 : 1.62
5	5	1.0	Zn (+) / C _{lead} (-)	1 : 0.27 / 0	1 : 0.80
6	10	1.0	Zn (+) / C _{foam} (-)	1 : 0 / 0	1 : 5.13
7	10	1.0	Zn (+) / C _{lead} (-)	1 : 0.36 / 0	1 : 0.11
8	5	1.6	Zn (+) / C _{foam} (-)	1 : 1.92 / 0	1 : 0.36
9	5	1.6	Zn (+) / C _{lead} (-)	1 : 0.90 / 0.20	1 : 0
10	5	1.6	Zn (+) / C _{felt} (-)	1 : 0.49 / 0.06	1 : 0.02
11 ^[a]	5	1.0	Zn (+) / C _{foam} (-)	–	–
12 ^[a]	5	1.0	Zn (+) / C _{lead} (-)	1 : 1.86 / 0.12	1 : 0.31
13	10	1.6	Zn (+) / C _{foam} (-)	1 : 0.96 / 0	1 : 0.59
14	10	1.6	Zn (+) / C _{lead} (-)	1 : 0.46 / 0	1 : 0.10
15 ^[b]	5	1.6	Zn (+) / C _{foam} (-)	7% Ph₂PH left, 19% Ph₂ArP	0% [Ph₂Ar₂P]Cl
16 ^[b]	5	1.6	Zn (+) / C _{lead} (-)	41% Ph ₂ PH left, 15% Ph ₂ ArP	2% [Ph ₂ Ar ₂ P]Cl

[a] The reaction time was extended from 21h to 3 days. [b] Ph₃P was added as an internal standard (0.05 mmol).

S2.1.2 $^{31}\text{P}\{^1\text{H}\}$ NMR spectra of reductive photoelectrochemistry using DCA

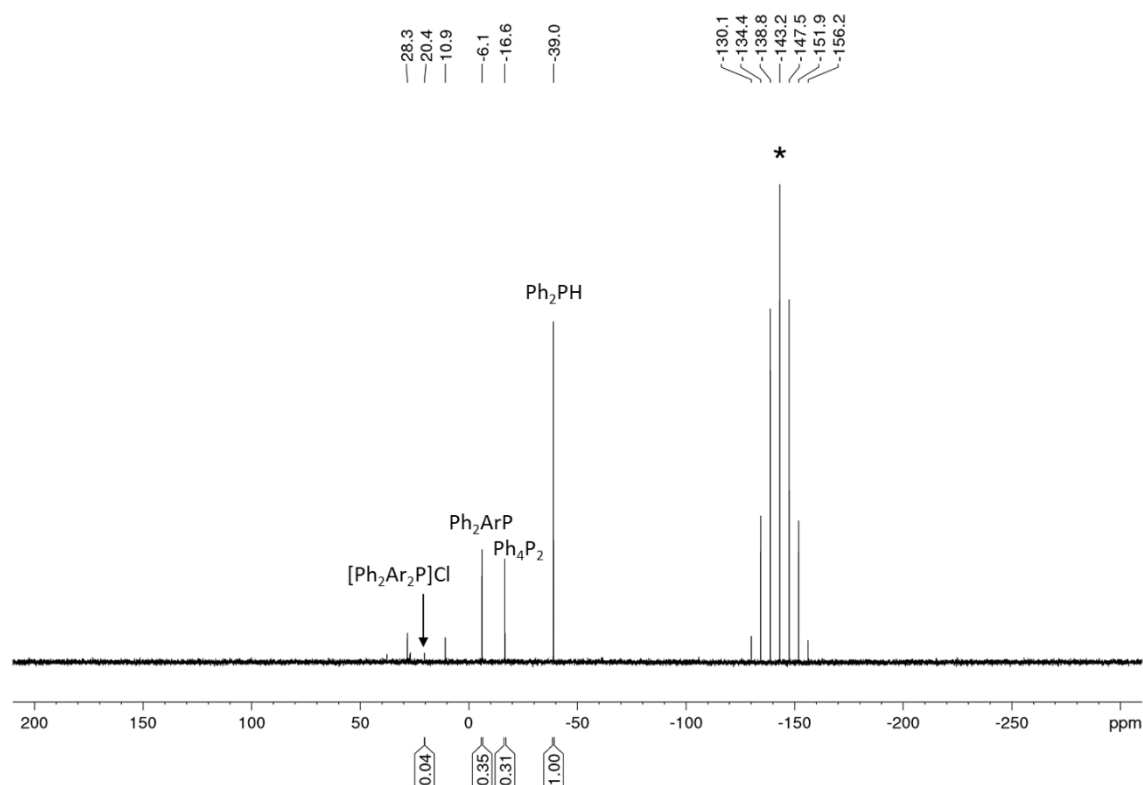


Figure S4. $^{31}\text{P}\{^1\text{H}\}$ NMR spectrum for the photoelectrocatalytic functionalization of Ph_2PH into $[\text{Ph}_2\text{Ar}_2\text{P}]\text{Cl}$ and Ph_2ArP using DCA (Table S1, Entry 1, 5 mol% DCA, $\text{C}_6\text{H}_4\text{-4-OMe}$, blue LED (455 nm), TBAPF_6 (*), 1.57 V, Zn (+) / C_{lead} (-).

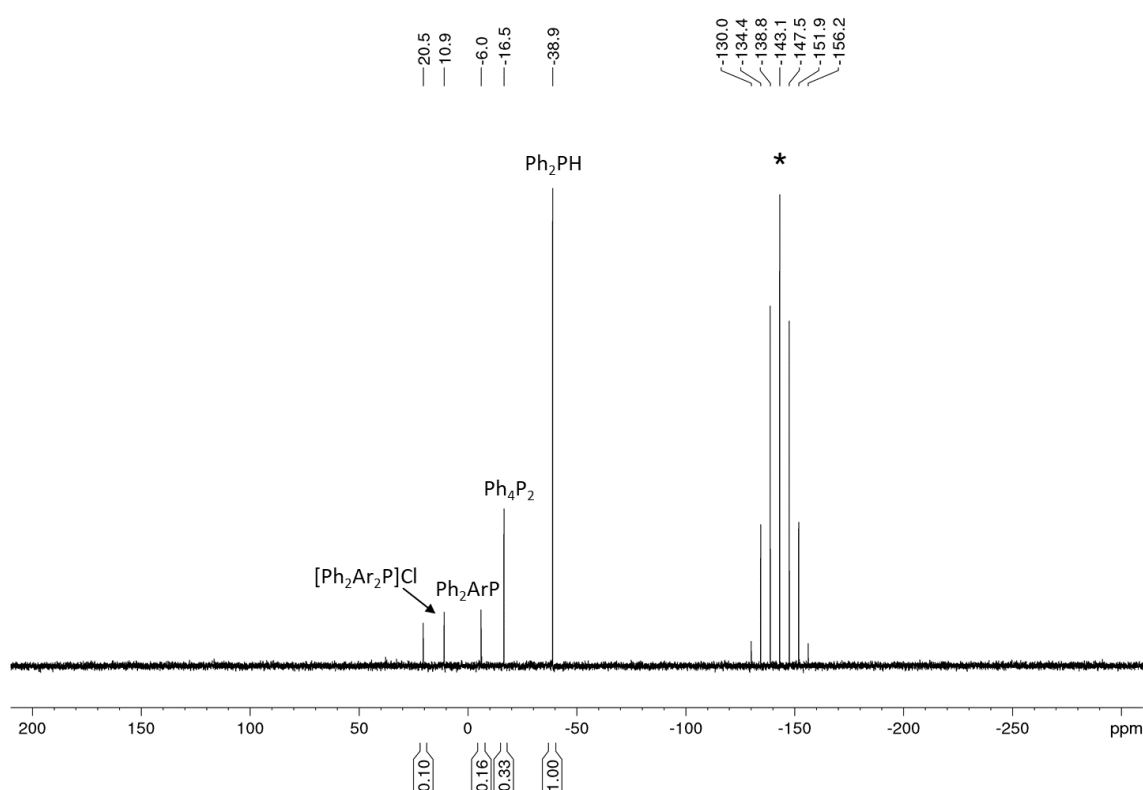


Figure S5. $^{31}\text{P}\{^1\text{H}\}$ NMR spectrum for the photoelectrocatalytic functionalization of Ph_2PH into $[\text{Ph}_2\text{Ar}_2\text{P}]\text{Cl}$ and Ph_2ArP using DCA (Table S1, Entry 2, 10 mol% DCA, $\text{C}_6\text{H}_4\text{-4-OMe}$, blue LED (455 nm), TBAPF_6 (*), 1.76 V, Zn (+) / C_{lead} (-).

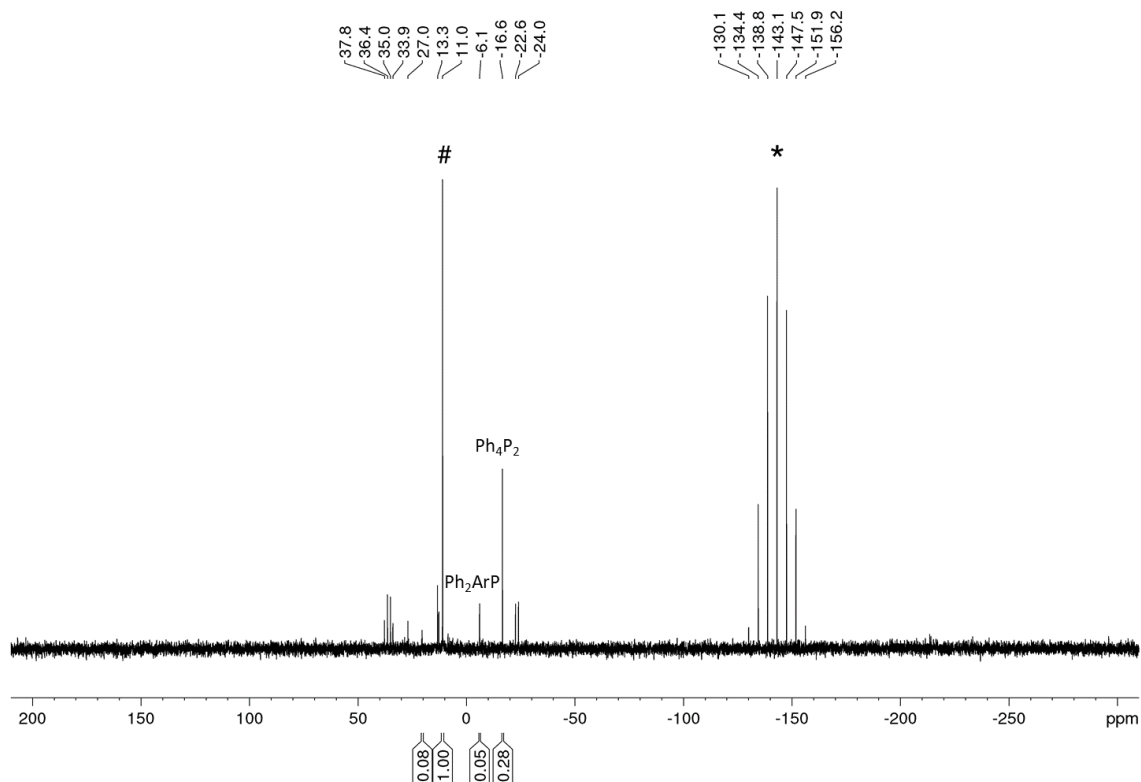


Figure S6. $^{31}\text{P}\{^1\text{H}\}$ NMR spectrum for the photoelectrocatalytic functionalization of Ph_2PH into $[\text{Ph}_2\text{Ar}_2\text{P}]\text{Cl}$ and Ph_2ArP using **DCA** (Table S1, Entry 3, 5 mol% **DCA**, $\text{ClC}_6\text{H}_4\text{-4-OMe}$, blue LED (455 nm), TBAPF_6 (*), 1.76 V, Zn (+) / C_{foam} (-). # marks an unknown species.

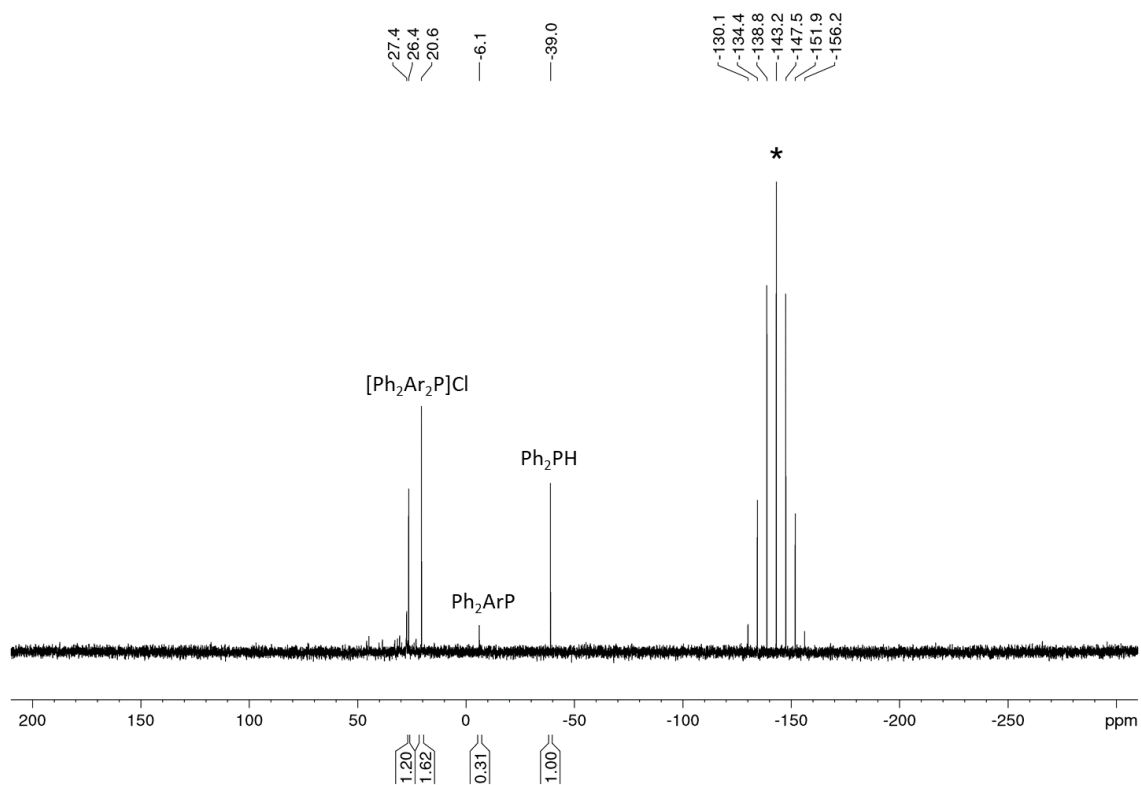


Figure S7. $^{31}\text{P}\{^1\text{H}\}$ NMR spectrum for the photoelectrocatalytic functionalization of Ph_2PH into $[\text{Ph}_2\text{Ar}_2\text{P}]\text{Cl}$ and Ph_2ArP using **DCA** (Table S1, Entry 4, 5 mol% **DCA**, $\text{ClC}_6\text{H}_4\text{-4-OMe}$, blue LED (455 nm), TBAPF_6 (*), 1.00 V, Zn (+) / C_{foam} (-).

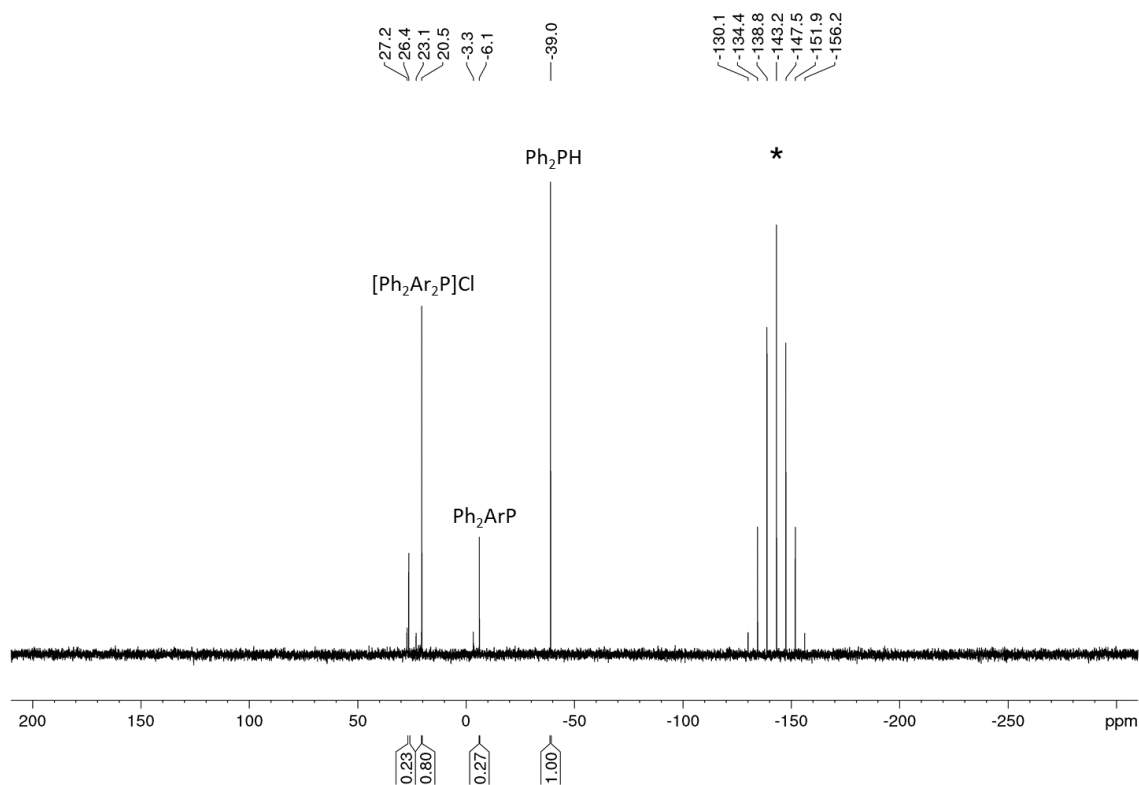


Figure S8. $^{31}\text{P}\{^1\text{H}\}$ NMR spectrum for the photoelectrocatalytic functionalization of Ph_2PH into $[\text{Ph}_2\text{Ar}_2\text{P}]\text{Cl}$ and Ph_2ArP using **DCA** (Table S1, Entry 5, 5 mol% **DCA**, $\text{ClC}_6\text{H}_4\text{-4-OMe}$, blue LED (455 nm), TBAPF_6 (*), 1.00 V, Zn (+) / C_{lead} (-).

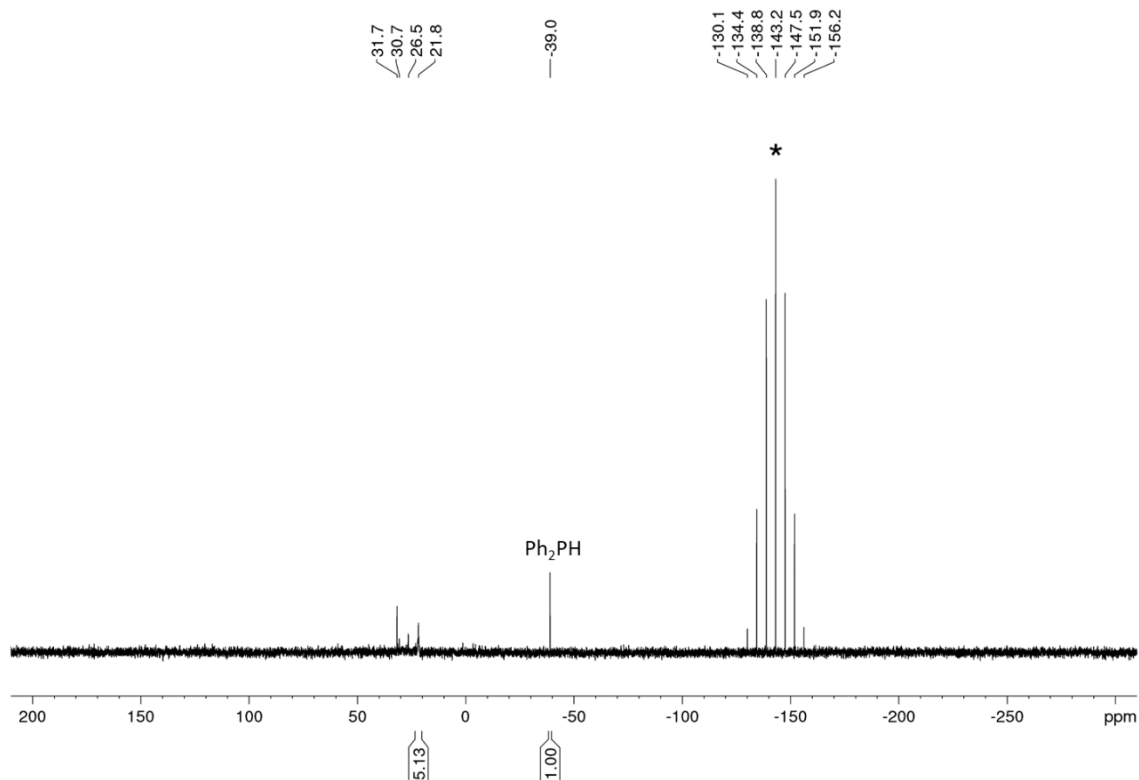


Figure S9. $^{31}\text{P}\{^1\text{H}\}$ NMR spectrum for the photoelectrocatalytic functionalization of Ph_2PH into $[\text{Ph}_2\text{Ar}_2\text{P}]\text{Cl}$ and Ph_2ArP using **DCA** (Table S1, Entry 6, 10 mol% **DCA**, $\text{ClC}_6\text{H}_4\text{-4-OMe}$, blue LED (455 nm), TBAPF_6 (*), 1.00 V, Zn (+) / C_{foam} (-).

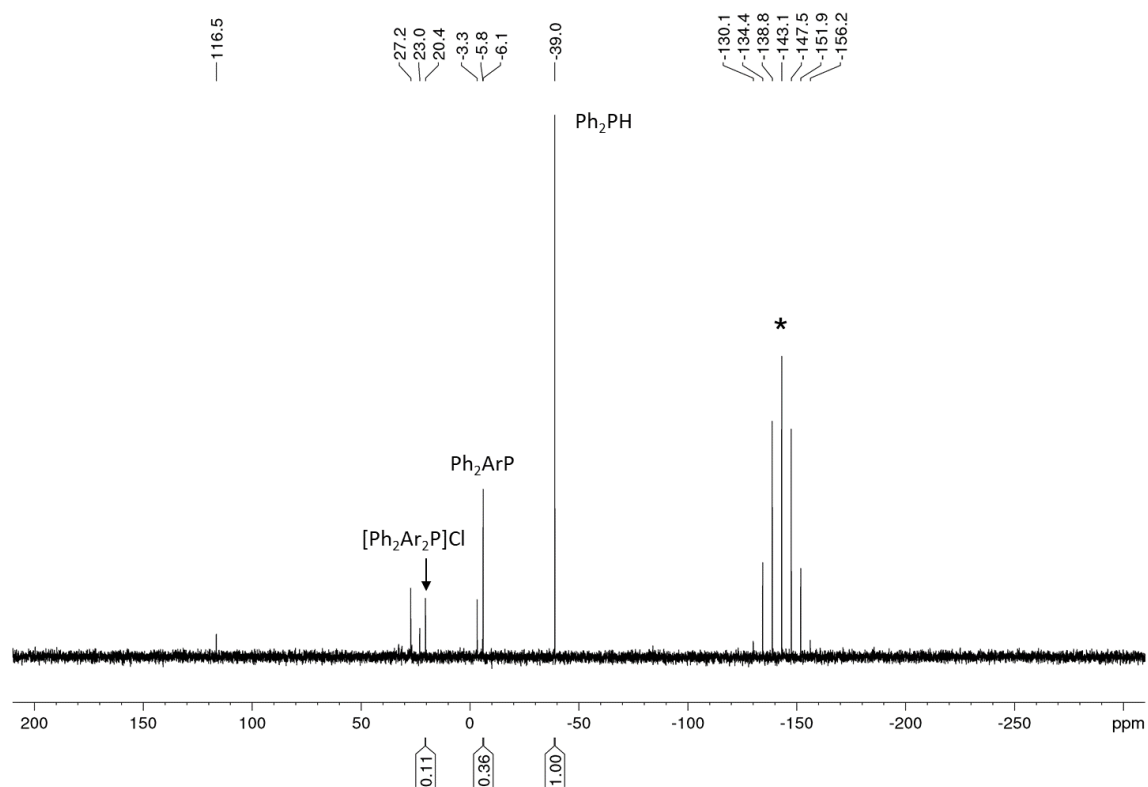


Figure S10. $^{31}\text{P}\{^1\text{H}\}$ NMR spectrum for the photoelectrocatalytic functionalization of Ph_2PH into $[\text{Ph}_2\text{Ar}_2\text{P}]\text{Cl}$ and Ph_2ArP using **DCA** (Table S1, Entry 7, 10 mol% **DCA**, $\text{ClC}_6\text{H}_4\text{-4-OMe}$, blue LED (455 nm), TBAPF_6 (*), 1.00 V, Zn (+) / C_{lead} (-).

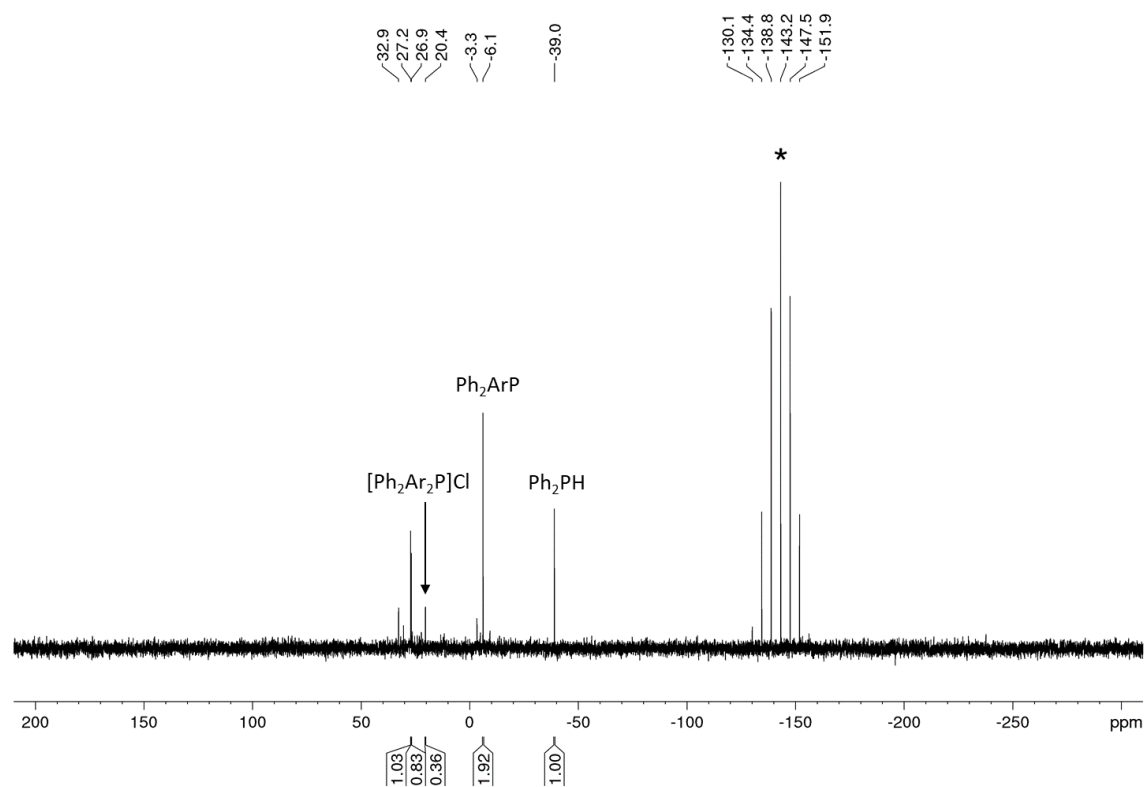


Figure S11. $^{31}\text{P}\{^1\text{H}\}$ NMR spectrum for the photoelectrocatalytic functionalization of Ph_2PH into $[\text{Ph}_2\text{Ar}_2\text{P}]\text{Cl}$ and Ph_2ArP using **DCA** (Table S1, Entry 8, 5 mol% **DCA**, $\text{ClC}_6\text{H}_4\text{-4-OMe}$, blue LED (455 nm), TBAPF_6 (*), 1.60 V, Zn (+) / C_{foam} (-).

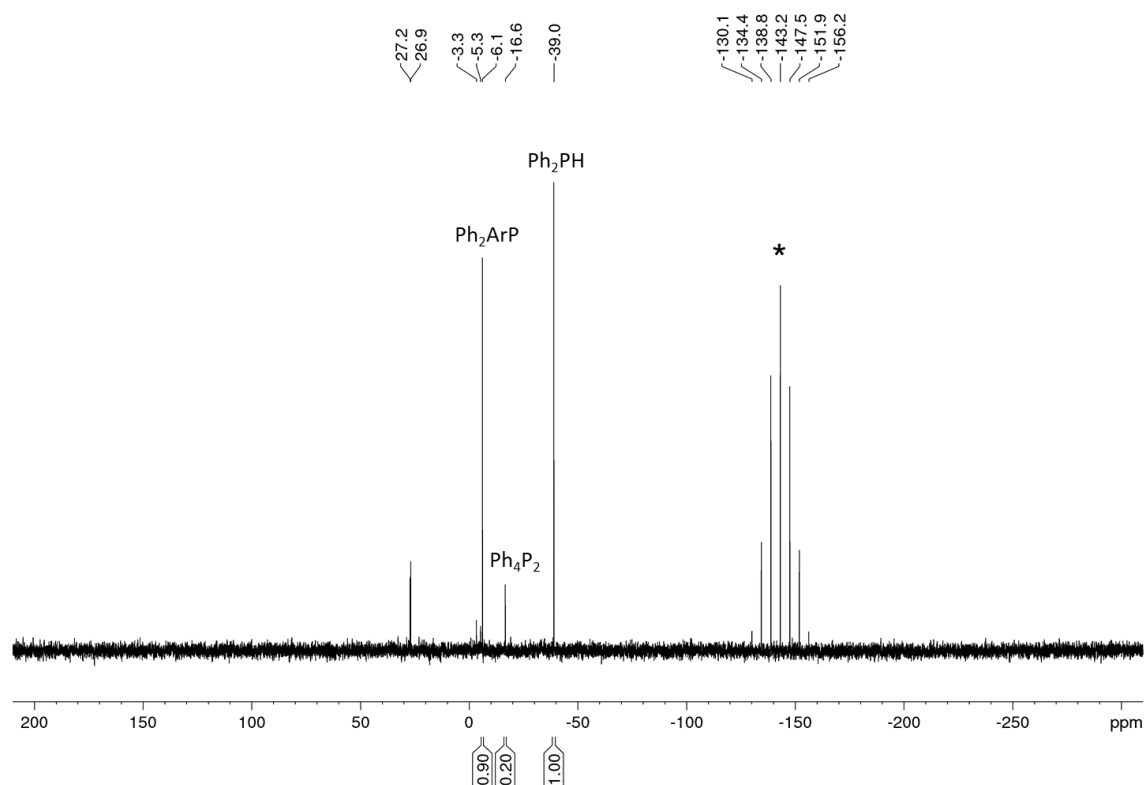


Figure S12. $^{31}\text{P}\{^1\text{H}\}$ NMR spectrum for the photoelectrocatalytic functionalization of Ph_2PH into $[\text{Ph}_2\text{Ar}_2\text{P}]\text{Cl}$ and Ph_2ArP using **DCA** (Table S1, Entry 9, 5 mol% **DCA**, $\text{C}_6\text{H}_4\text{-4-OMe}$, blue LED (455 nm), TBAPF_6 (*), 1.60 V, Zn (+) / C_{lead} (-).

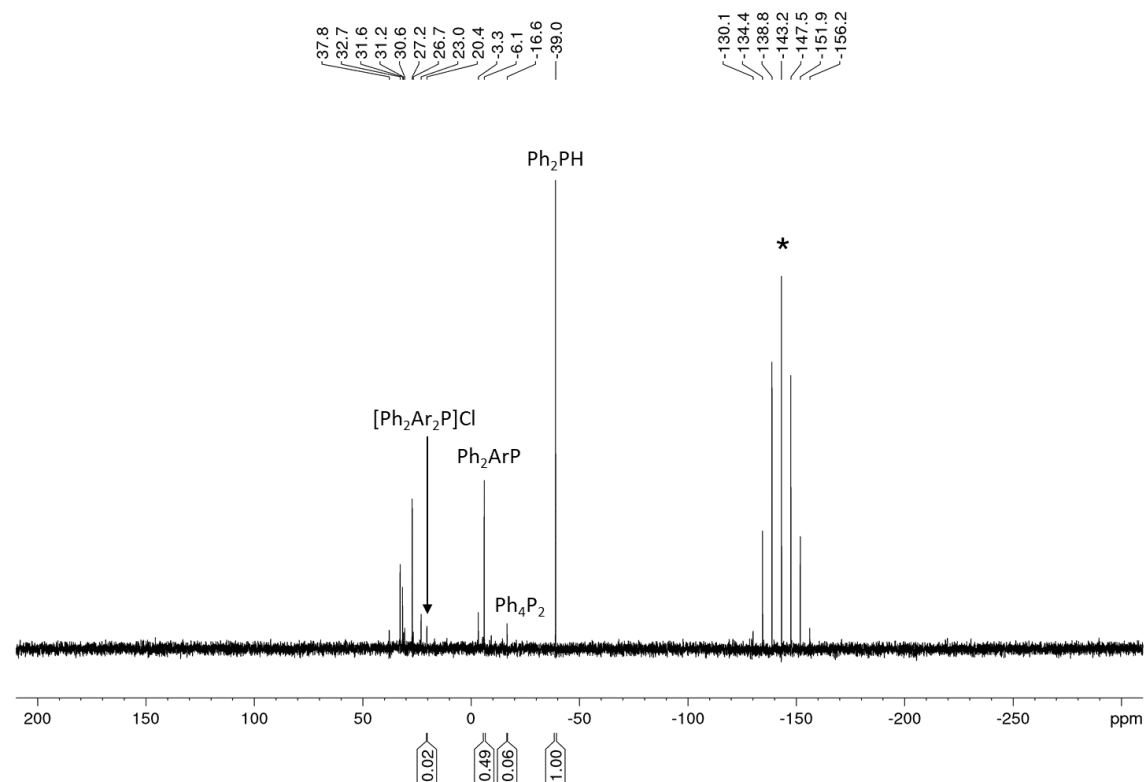


Figure S13. $^{31}\text{P}\{^1\text{H}\}$ NMR spectrum for the photoelectrocatalytic functionalization of Ph_2PH into $[\text{Ph}_2\text{Ar}_2\text{P}]\text{Cl}$ and Ph_2ArP using **DCA** (Table S1, Entry 10, 5 mol% **DCA**, $\text{C}_6\text{H}_4\text{-4-OMe}$, blue LED (455 nm), TBAPF_6 (*), 1.60 V, Zn (+) / C_{felt} (-).

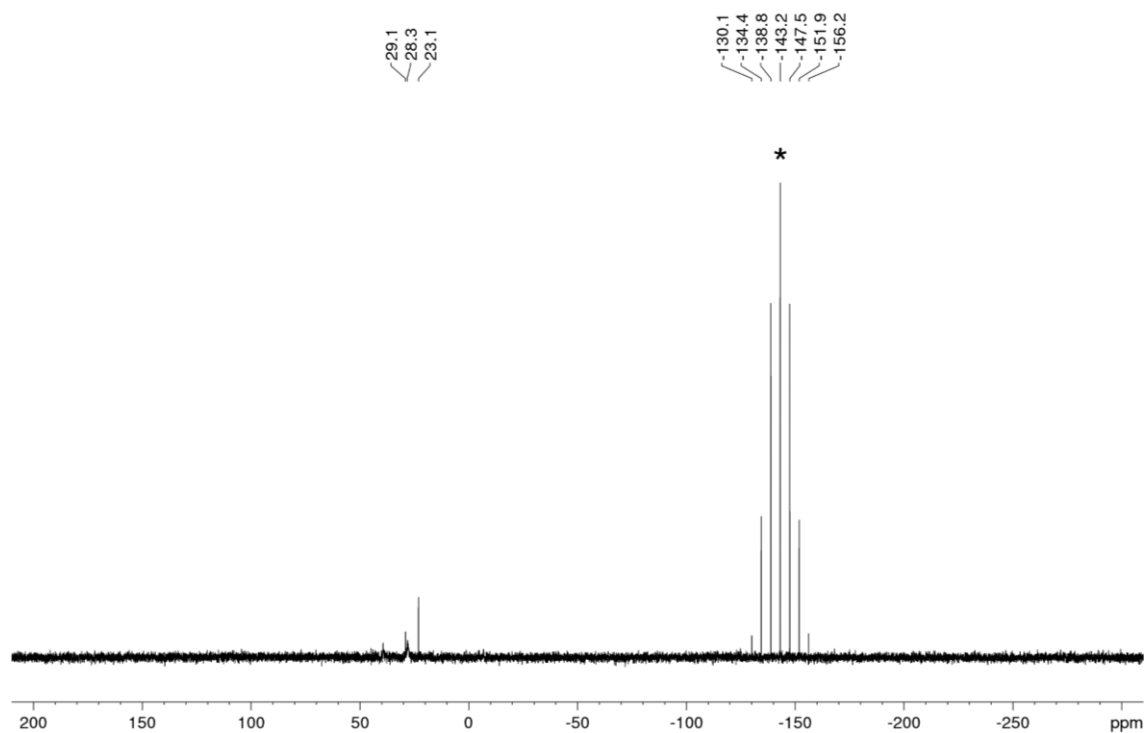


Figure S14. $^{31}\text{P}\{^1\text{H}\}$ NMR spectrum for the photoelectrocatalytic functionalization of Ph_2PH into $[\text{Ph}_2\text{Ar}_2\text{P}]\text{Cl}$ and Ph_2ArP using **DCA** (Table S1, Entry 11, 5 mol% **DCA**, $\text{ClC}_6\text{H}_4\text{-4-OMe}$, blue LED (455 nm), TBAPF_6 (*), 1.00 V, Zn (+) / C_{foam} (-). The reaction time was extended from 21 h to 3 days.

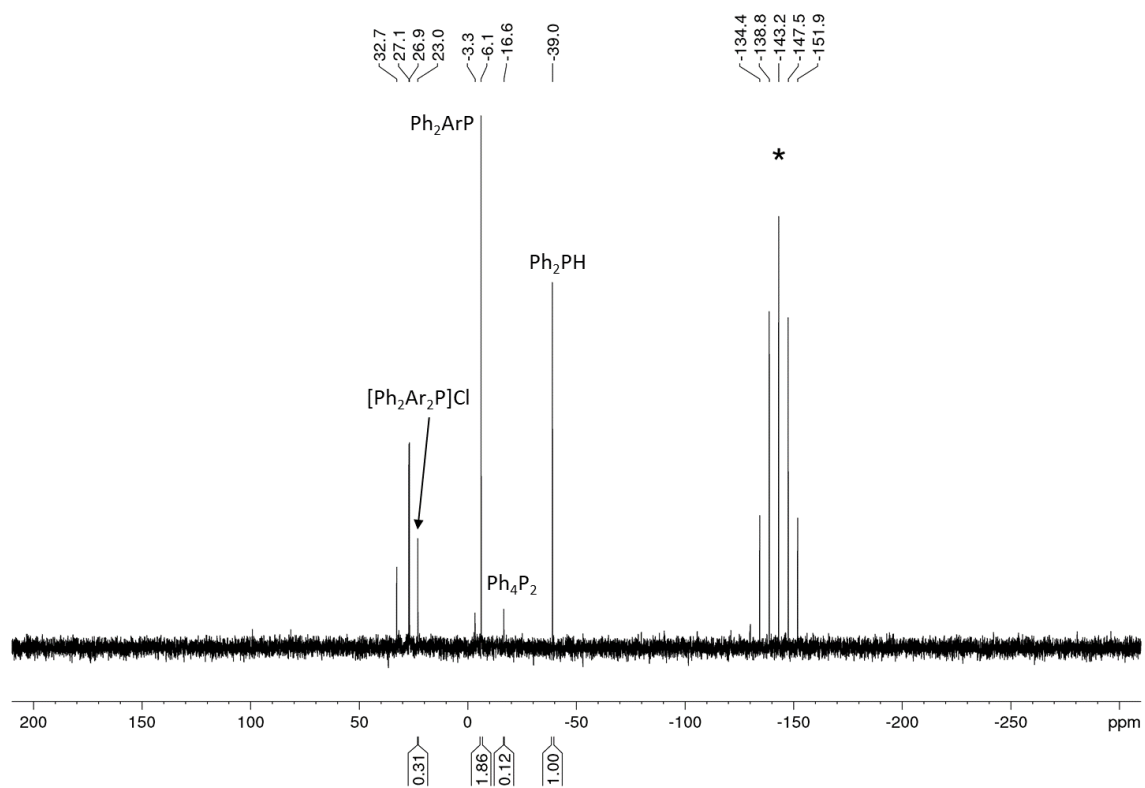


Figure S15. $^{31}\text{P}\{^1\text{H}\}$ NMR spectrum for the photoelectrocatalytic functionalization of Ph_2PH into $[\text{Ph}_2\text{Ar}_2\text{P}]\text{Cl}$ and Ph_2ArP using **DCA** (Table S1, Entry 12, 5 mol% **DCA**, $\text{ClC}_6\text{H}_4\text{-4-OMe}$, blue LED (455 nm), TBAPF_6 (*), 1.00 V, Zn (+) / C_{lead} (-). The reaction time was extended from 21 h to 3 days.

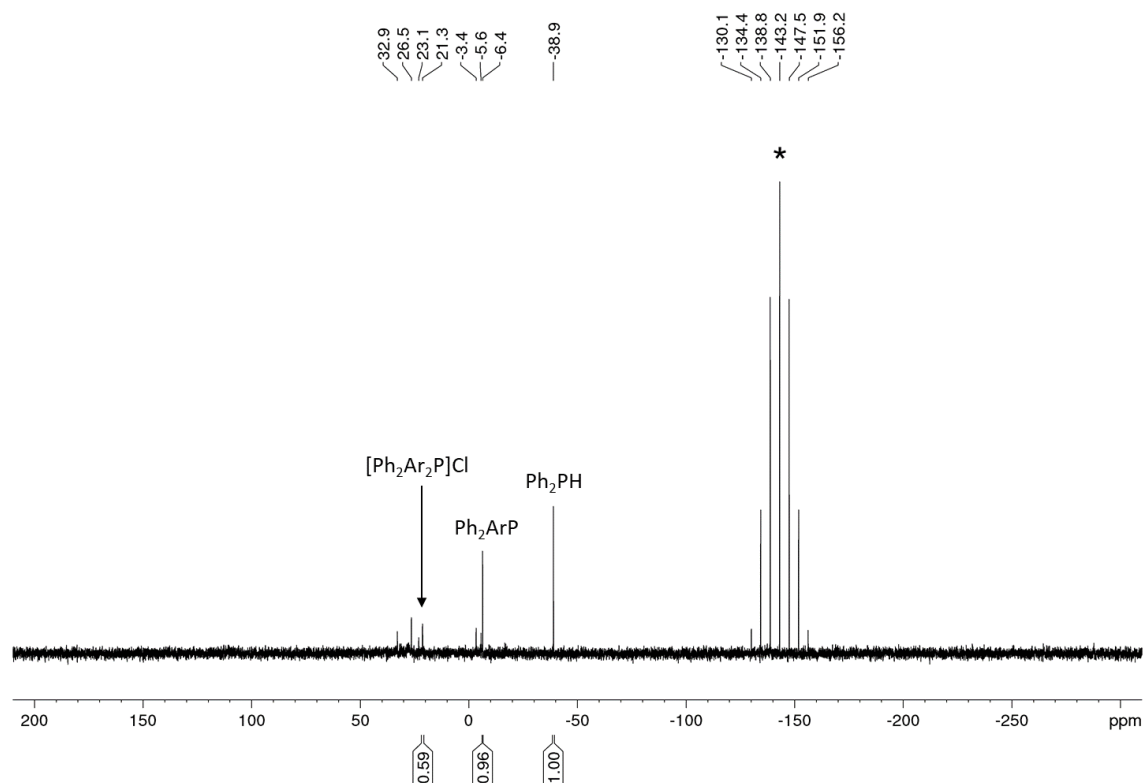


Figure S16. $^{31}\text{P}\{^1\text{H}\}$ NMR spectrum for the photoelectrocatalytic functionalization of Ph_2PH into $[\text{Ph}_2\text{Ar}_2\text{P}]\text{Cl}$ and Ph_2ArP using **DCA** (Table S1, Entry 13, 10 mol% **DCA**, $\text{C}_6\text{H}_4\text{-4-OMe}$, blue LED (455 nm), TBAPF_6 (*), 1.60 V, $\text{Zn (+) / C}_{\text{foam}} (-)$).

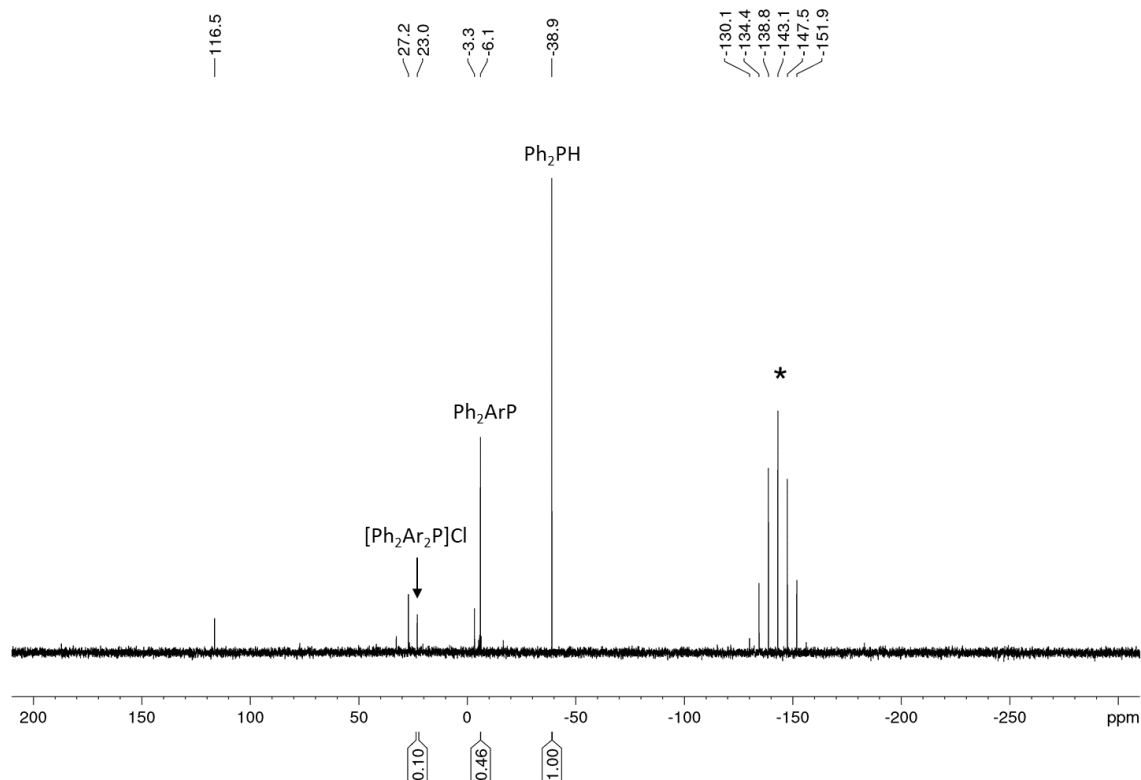


Figure S17. $^{31}\text{P}\{^1\text{H}\}$ NMR spectrum for the photoelectrocatalytic functionalization of Ph_2PH into $[\text{Ph}_2\text{Ar}_2\text{P}]\text{Cl}$ and Ph_2ArP using **DCA** (Table S1, Entry 14, 10 mol% **DCA**, $\text{C}_6\text{H}_4\text{-4-OMe}$, blue LED (455 nm), TBAPF_6 (*), 1.60 V, $\text{Zn (+) / C}_{\text{lead}} (-)$).

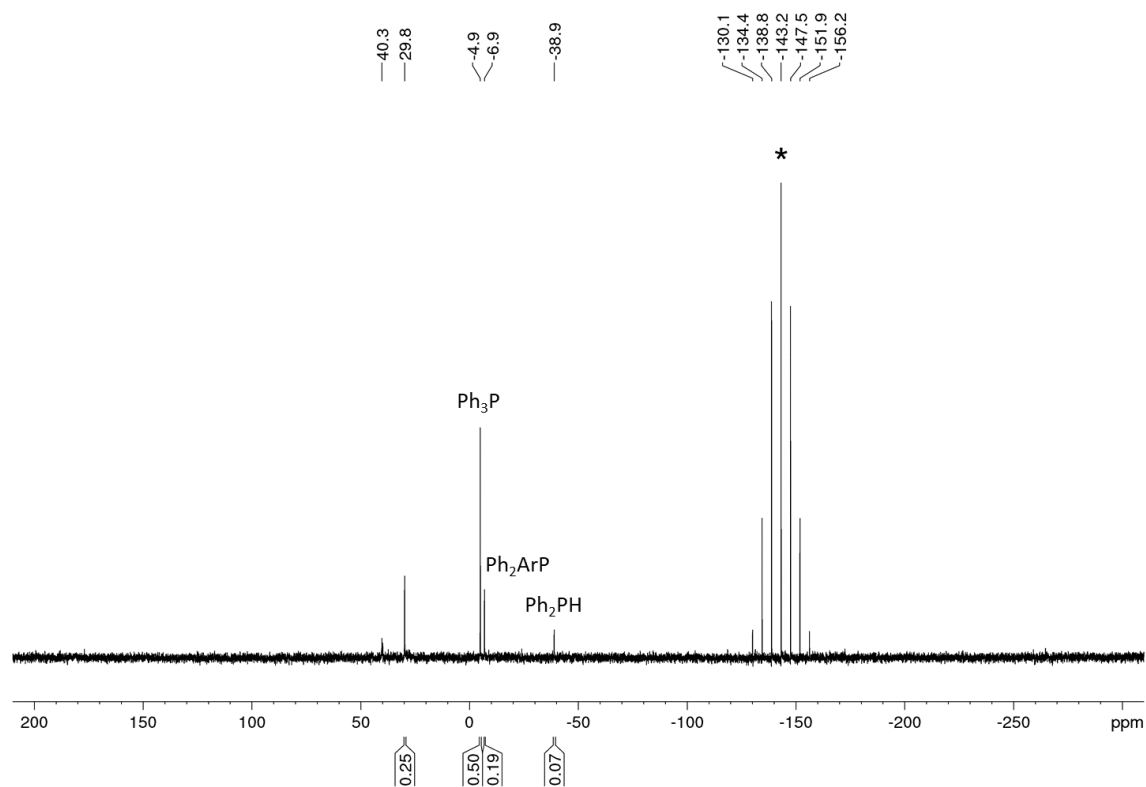


Figure S18. $^{31}\text{P}\{^1\text{H}\}$ NMR spectrum for the photoelectrocatalytic functionalization of Ph_2PH into $[\text{Ph}_2\text{Ar}_2\text{P}]\text{Cl}$ and Ph_2ArP using **DCA** (Table S1, Entry 15, 5 mol% **DCA**, $\text{ClC}_6\text{H}_4\text{-4-OMe}$, blue LED (455 nm), TBAPF_6 (*), 1.60 V, Zn (+) / C_{foam} (-). Ph_3P was added as an internal standard (0.05 mmol).

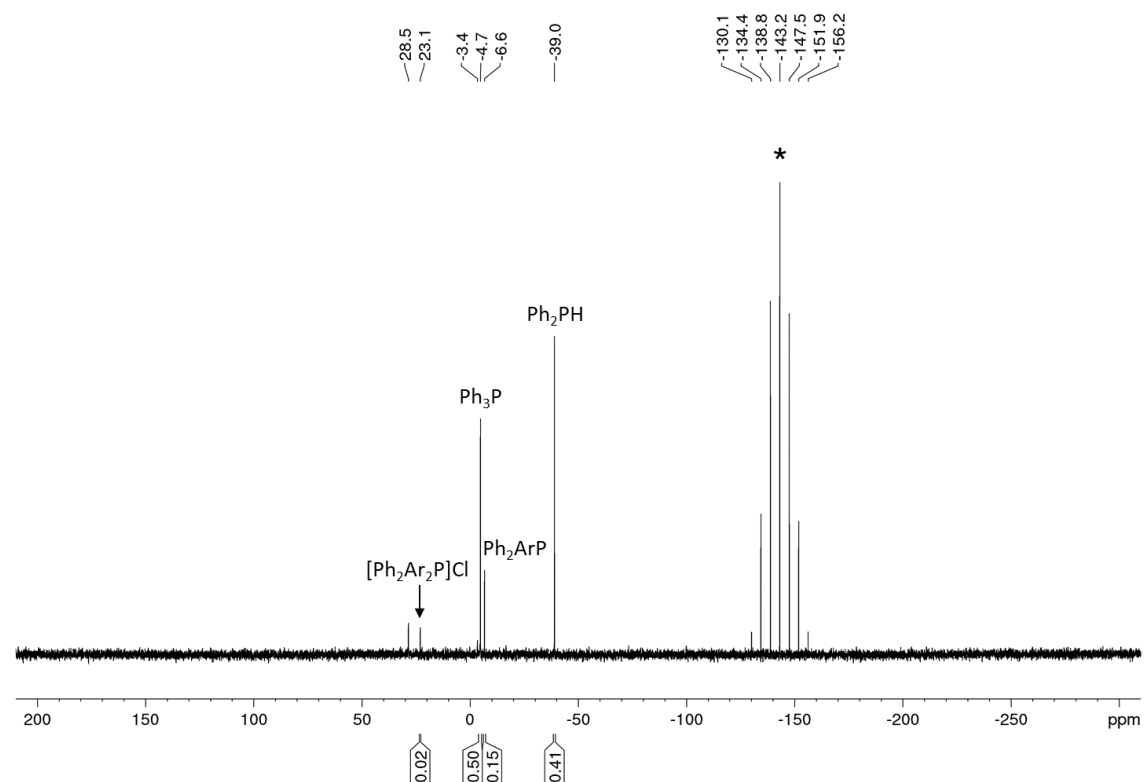
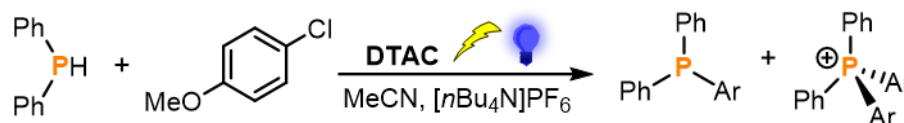


Figure S19. $^{31}\text{P}\{^1\text{H}\}$ NMR spectrum for the photoelectrocatalytic functionalization of Ph_2PH into $[\text{Ph}_2\text{Ar}_2\text{P}]\text{Cl}$ and Ph_2ArP using **DCA** (Table S1, Entry 16, 5 mol% **DCA**, $\text{ClC}_6\text{H}_4\text{-4-OMe}$, blue LED (455 nm), TBAPF_6 (*), 1.60 V, Zn (+) / C_{lead} (-). Ph_3P was added as an internal standard (0.05 mmol).

S2.2 Photoelectrochemical functionalization of Ph₂PH mediated by e-PRCat DTAC



All preparation steps were carried out in a glovebox under inert gas atmosphere. An oven-dried H-cell was equipped with magnetic stirring bars in both chambers. To the cathodic chamber was added 4-chloroanisole (ClC₆H₄-4-OMe, 1.0 mmol, 122 μ L), e-PRCat DTAC (0.05 mmol, 17.0 mg, 5 mol% per substrate molecule), and Ph₂PH (0.1 mmol, 17.4 μ L), followed by the additions of [nBu₄N]PF₆ (0.1 mmol, 38.74 mg, TBAPF₆) and MeCN (4 mL) in both chambers (resulting in 0.025 M [nBu₄N]PF₆ in MeCN as solvent). Both chambers were sealed using rubber septa pierced with wire-connected electrodes (Figure S1). The resulting mixture was stirred at room temperature above a water-cooled cooling block under irradiation of blue LED (455 nm) from beneath the cathodic chamber (Figure S2). A constant potential was applied across the cell (see Table S2). After irradiation for 21h, the mixtures in both chambers were combined and subjected to ³¹P{¹H} NMR analysis. A ratio of the ³¹P{¹H} NMR integrals of the starting material Ph₂PH (³¹P{¹H}, integral = 1) and the corresponding products is given in Table S2.

S2.2.1 Optimization of reaction conditions

Table S2. Photoelectrocatalytic functionalization of Ph₂PH into [Ph₂Ar₂P]Cl and Ph₂ArP using DTAC.

Entry	DTAC [mol%]	Substrate	Potential [V]	Electrodes	Ratio of Ph ₂ PH to Ph ₂ ArP	Ratio of Ph ₂ PH to [Ph ₂ Ar ₂ P]Cl
1	5	ClC ₆ H ₄ -4-OMe	1.6	Zn (+) / C _{foam} (-)	1 : 1.49	1 : 0.52
2	5	ClC ₆ H ₄ -4-OMe	1.6	Zn (+) / C _{lead} (-)	1 : 0.28	1 : 1

S2.2.2 $^{31}\text{P}\{^1\text{H}\}$ NMR spectra of reductive photoelectrochemistry using DTAC

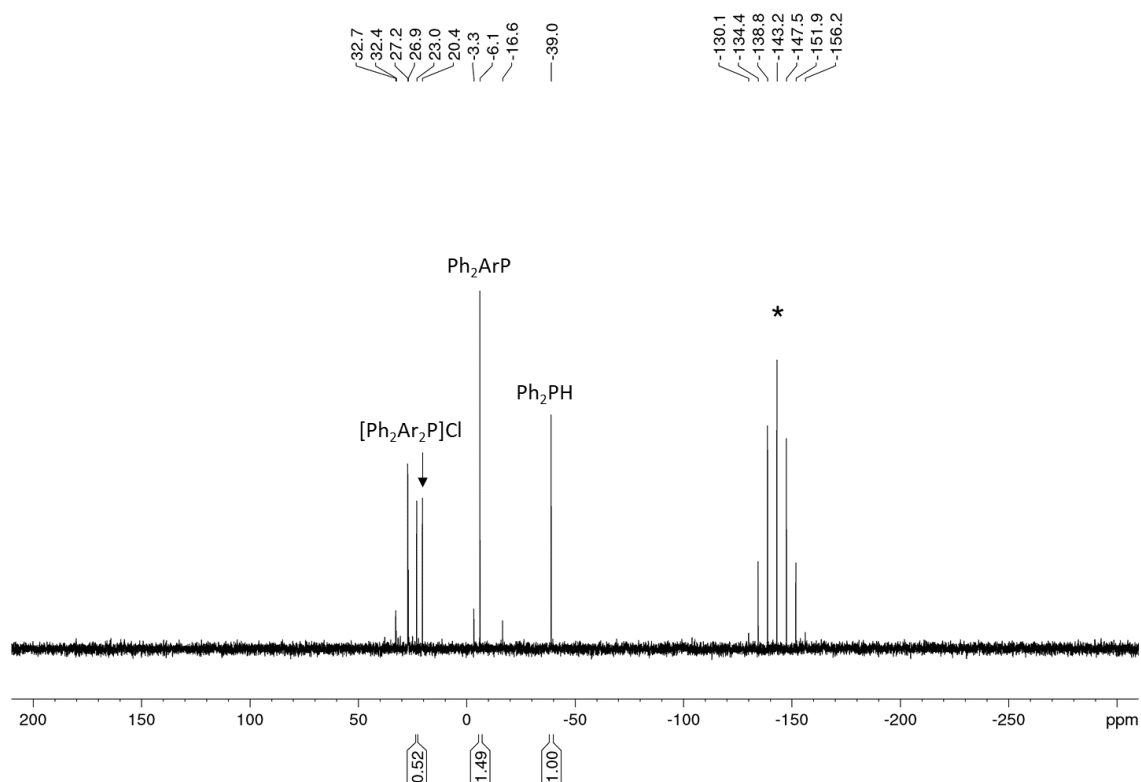


Figure S20. $^{31}\text{P}\{^1\text{H}\}$ NMR spectrum for the photoelectrocatalytic functionalization of Ph_2PH into $[\text{Ph}_2\text{Ar}_2\text{P}]\text{Cl}$ and Ph_2ArP using **DTAC** (Table S2, Entry 1, 5 mol% **DTAC**, ClC_6H_4 -4-OMe, blue LED (455 nm), TBAPF_6 (*), 1.60 V, Zn (+) / C_{foam} (-).

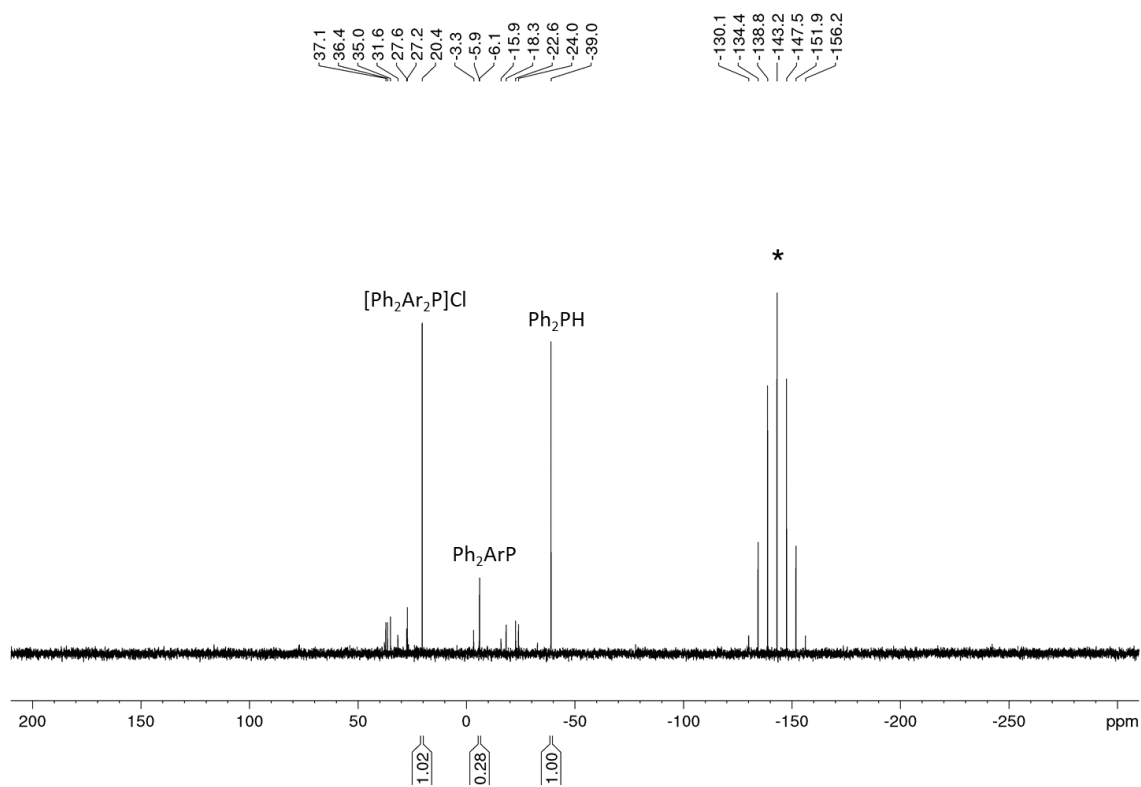
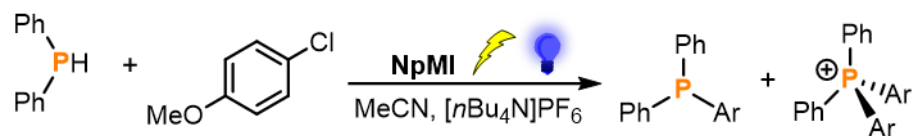


Figure S21. $^{31}\text{P}\{^1\text{H}\}$ NMR spectrum for the photoelectrocatalytic functionalization of Ph_2PH into $[\text{Ph}_2\text{Ar}_2\text{P}]\text{Cl}$ and Ph_2ArP using **DTAC** (Table S2, Entry 2, 5 mol% **DTAC**, ClC_6H_4 -4-OMe, blue LED (455 nm), TBAPF_6 (*), 1.60 V, Zn (+) / C_{lead} (-).

S2.3 Photoelectrochemical functionalization of Ph₂PH mediated by e-PRCat NpMI



All preparation steps were carried out in a glovebox under inert gas atmosphere. An oven-dried H-cell was equipped with magnetic stirring bars in both chambers. To the cathodic chamber was added organic halide (1.0 mmol, ClC₆H₄-4-OMe, PhCl or PhBr), e-PRCat **NpMI** (0.05 mmol, 17.8 mg, 5 mol% per substrate molecule), and Ph₂PH (0.1 mmol, 17.4 μL), followed by the additions of [nBu₄N]PF₆ (0.1 mmol, 38.74 mg, TBAPF₆) and MeCN (4 mL) in both chambers (resulting in 0.025 M [nBu₄N]PF₆ in MeCN as solvent). Both chambers were sealed using rubber septa pierced with wire-connected electrodes (Figure S1). The resulting mixture was stirred at room temperature above a water-cooled cooling block under irradiation of blue LED (455 nm) from beneath the cathodic chamber (Figure S3). A constant potential was applied across the cell (see Table S4). After irradiation for 21h, the mixtures in both chambers were combined and subjected to ³¹P{¹H} NMR analysis. For the reactions without additional internal standard a ratio of the starting material Ph₂PH (³¹P{¹H}, integral = 1) and the corresponding products is given. For quantification of selected reactions triphenylphosphine (PPh₃) was added as an internal standard and the determined ³¹P{¹H} NMR yield is shown in Table S4.

S2.3.1 Optimization of reaction conditions

Table S3. Photoelectrocatalytic functionalization of Ph₂PH into [Ph₂Ar₂P]Cl and Ph₂ArP using substrate 4-chloroanisole (ClC₆H₄-4-OMe) and **NpMI**: screening of **control experiments**.

Entry	Ph ₂ PH	NpMI [mol%]	Substrate	Potential [V]	Electrodes	Electrolyte	Blue LED	Product formation?
1	✓	5	–	1.6	Zn (+) / Fe (–)	TBAPF ₆	✓	X
2	✓	5	✓	1.6	Zn (+) / Fe (–)	TBAPF ₆	–	X
3 ^[a]	✓	5	✓	–	Zn (+) / Fe (–)	TBAPF ₆	✓	X / ✓ ^[a]
4	✓	–	✓	1.6	Zn (+) / Fe (–)	TBAPF ₆	✓	X
5	–	5	✓	1.6	Zn (+) / Fe (–)	TBAPF ₆	✓	X
6	✓	5	✓	1.6	Zn (+) / Fe (–)	–	✓	X
7	✓	5	✓	–	Zn (+) / Fe (–)	TBAPF ₆	–	X
8	✓	5	✓	1.6	Zn (+) / C _{foam} (–)	TBAPF ₆	✓	✓
9	✓	5	✓	3.2	Zn (+) / Fe (–)	TBAPF ₆	–	X

[a] After irradiation without potential for 21h shows no product formation in the ³¹P{¹H} NMR, but subsequent applying of potential yielded Ph₂ArP and [Ph₂Ar₂P]Cl.

Chapter 4. Reductive Photoelectrocatalytic Activation of Organic Halides and Diphenylphosphine into Arylphosphines and Phosphonium Salts

Table S4. Photoelectrocatalytic functionalization of Ph₂PH to [Ph₂Ar₂P]Cl and Ph₂ArP using **NpMI**: screening different conditions.

Entry	NpMI [mol%]	Substrate	Pot. [V]	Electrodes	Electrolyte	Ratio of Ph ₂ PH to Ph ₂ ArP	Ratio of Ph ₂ PH to [Ph ₂ Ar ₂ P]Cl
1	5	ClC ₆ H ₄ -4-OMe	1.6	Zn (+) / Fe (-)	TBAPF ₆	1 : 0.73	1 : 0.60
2	10	ClC ₆ H ₄ -4-OMe	1.6	Zn (+) / Fe (-)	TBAPF ₆	0 : 1.00	–
3 ^[a]	5	ClC ₆ H ₄ -4-OMe	1.6	Zn (+) / Fe (-)	TBAPF ₆	–	–
4 ^[a]	5	ClC ₆ H ₄ -4-OMe	1.6	Zn (+) / C _{foam} (-)	TBAPF ₆	–	–
5 ^[b]	1	ClC ₆ H ₄ -4-OMe	1.6	Zn (+) / C _{foam} (-)	TBAPF ₆	37% Ph ₂ PH left, 20% Ph ₂ ArP	4% [Ph ₂ Ar ₂ P]Cl
6 ^[b]	2.5	ClC ₆ H ₄ -4-OMe	1.6	Zn (+) / C _{foam} (-)	TBAPF ₆	63% Ph ₂ PH left, 10% Ph ₂ ArP	0% [Ph ₂ Ar ₂ P]Cl
7 ^[b]	5	ClC ₆ H ₄ -4-OMe	1.6	Zn (+) / C _{foam} (-)	TBAPF ₆	29% Ph ₂ PH left, 24% Ph ₂ ArP	15% [Ph ₂ Ar ₂ P]Cl
8 ^[b]	5	ClC ₆ H ₄ -4-OMe	1.6	Zn (+) / C _{foam} (-)	LiClO ₄	95% Ph ₂ PH left, 22% Ph ₂ ArP	2% [Ph ₂ Ar ₂ P]Cl
9 ^[b]	5	ClC ₆ H ₄ -4-OMe	1.6	Zn (+) / C _{foam} (-)	TBABF ₄	46% Ph ₂ PH left, 26% Ph ₂ ArP	12% [Ph ₂ Ar ₂ P]Cl
10 ^[b]	1	ClC ₆ H ₄ -4-OMe	1.6	Zn (+) / Fe (-)	TBAPF ₆	39% Ph ₂ PH left, 36% Ph ₂ ArP	13% [Ph ₂ Ar ₂ P]Cl
11 ^[b]	2.5	ClC ₆ H ₄ -4-OMe	1.6	Zn (+) / Fe (-)	TBAPF ₆	63% Ph ₂ PH left, 28% Ph ₂ ArP	35% [Ph ₂ Ar ₂ P]Cl
12 ^[b]	5	ClC ₆ H ₄ -4-OMe	1.6	Zn (+) / Fe (-)	TBAPF ₆	50% Ph₂PH left, 49% Ph₂ArP	25% [Ph₂Ar₂P]Cl
13 ^{[b][c]}	5	ClC ₆ H ₄ -4-OMe	1.6	Zn (+) / Fe (-)	TBAPF ₆	13% Ph ₂ PH left, 20% Ph ₂ ArP	16% [Ph ₂ Ar ₂ P]Cl
14 ^{[b][c]}	5	ClC ₆ H ₄ -4-OMe	1.6	Zn (+) / C _{foam} (-)	TBAPF ₆	29% Ph ₂ PH left, 5% Ph ₂ ArP	0% [Ph ₂ Ar ₂ P]Cl
15	5	PhBr	1.6	Zn (+) / Fe (-)	TBAPF ₆	1 : 7.79	1 : 22.47
16	5	PhBr	1.6	Zn (+) / C _{foam} (-)	TBAPF ₆	1 : 1.42	1 : 4.87
17	5	PhCl	1.6	Zn (+) / Fe (-)	TBAPF ₆	1 : 0.32	1 : 0.95
18 ^[d]	5	PhCl	1.6	Zn (+) / Fe (-)	TBAPF ₆	1 : 0.86	1 : 0.73
19	5	PhBr	1.6	Zn (+) / Fe (-)	TBAPF ₆	0 : 0	0 : 1.00
20 ^[d]	5	PhBr	1.6	Zn (+) / Fe (-)	TBAPF ₆	1 : 1.54	1 : 7.60
21 ^[b]	5	ClC ₆ H ₄ -4-OMe	1.6	Zn (+) / Fe (-)	TBAPF ₆	21% Ph ₂ PH left, 25% Ph ₂ ArP	5% [Ph ₂ Ar ₂ P]Cl
22 ^{[b][d]}	5	ClC ₆ H ₄ -4-OMe	1.6	Zn (+) / Fe (-)	TBAPF ₆	8% Ph₂PH left, 25% Ph₂ArP	38% [Ph₂Ar₂P]Cl

[a] The reaction time was extended from 21h to 3 days. [b] Ph₃P was added as an internal standard (0.05 mmol). [c] The amount of electrolyte TBAPF₆ was increased from 0.1 mmol to 0.4 mmol. [d] The reactions were irradiated with high power LEDs (blue (451 nm), 20.3 V, 350 mA, 7 x LT-3109 Osram SSL 80 royal-blau, Ser.-Nr.:219-20-2).

S2.3.2 $^{31}\text{P}\{^1\text{H}\}$ NMR spectra of reductive photoelectrochemistry using NpMI

S2.3.2.1 $^{31}\text{P}\{^1\text{H}\}$ NMR spectra of control experiments

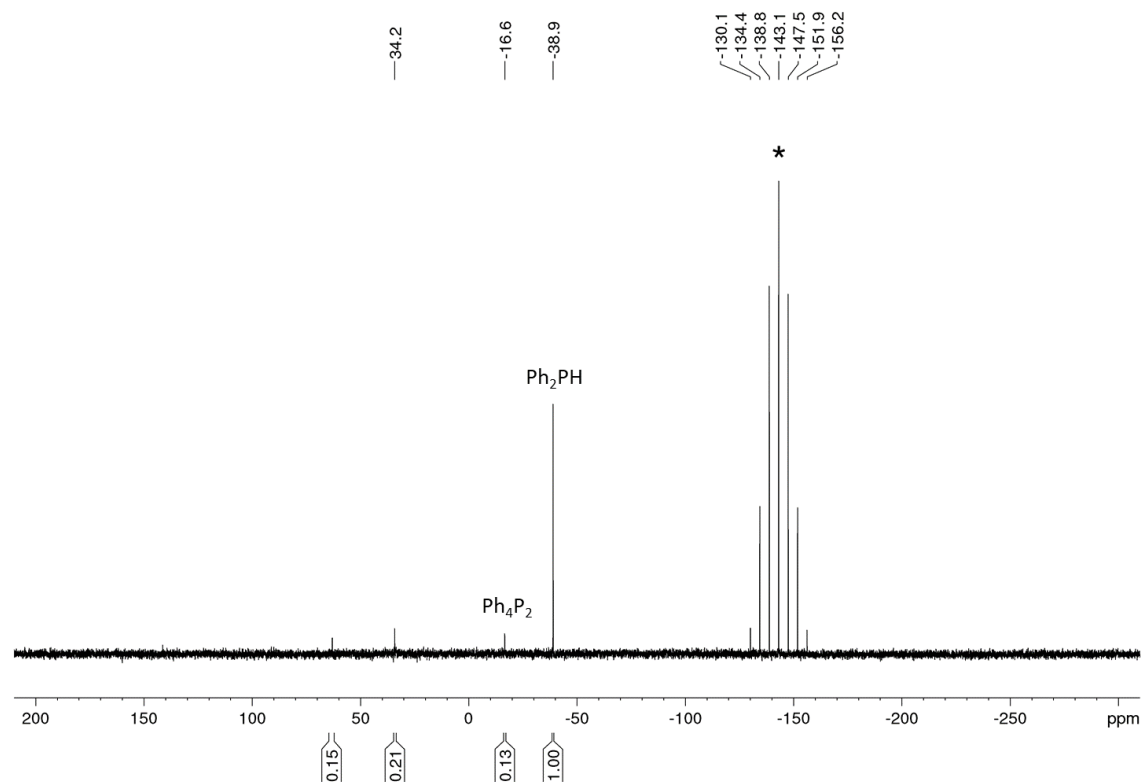


Figure S22. Control experiments for the photoelectrocatalytic functionalization of Ph_2PH into $[\text{Ph}_2\text{Ar}_2\text{P}]\text{Cl}$ and Ph_2ArP using NpMI (Table S3, Entry 1, 5 mol% NpMI, no substrate, blue LED (455 nm), TBAPF_6 (*), 1.60 V, Zn (+) / Fe (-).

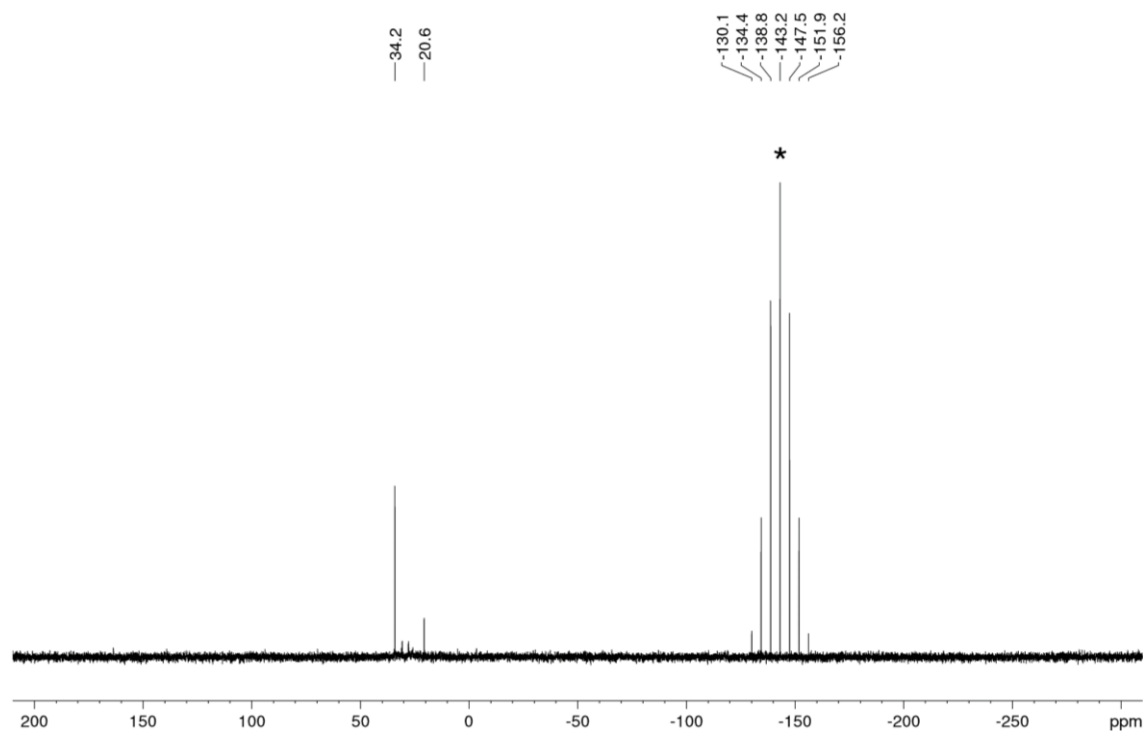


Figure S23. Control experiments for the photoelectrocatalytic functionalization of Ph_2PH into $[\text{Ph}_2\text{Ar}_2\text{P}]\text{Cl}$ and Ph_2ArP using NpMI (Table S3, Entry 2, 5 mol% NpMI, $\text{C}_6\text{H}_4\text{-4-OMe}$, no blue LED (455 nm), TBAPF_6 (*), 1.60 V, Zn (+) / Fe (-).

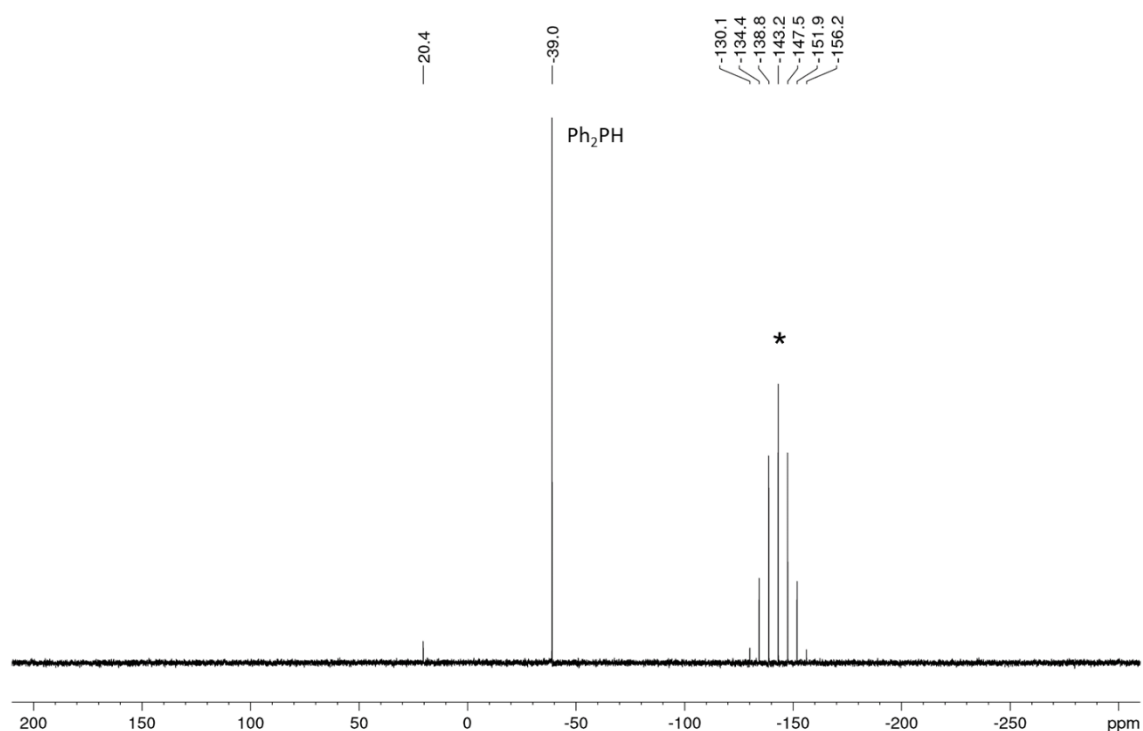


Figure S24. Control experiments for the photoelectrocatalytic functionalization of Ph_2PH into $[\text{Ph}_2\text{Ar}_2\text{P}]\text{Cl}$ and Ph_2ArP using **NpMI** (Table S3, Entry 3, 5 mol% **NpMI**, ClC_6H_4 -4-OMe, blue LED (455 nm), TBAPF_6 (*), **no potential**, Zn (+) / Fe (-).

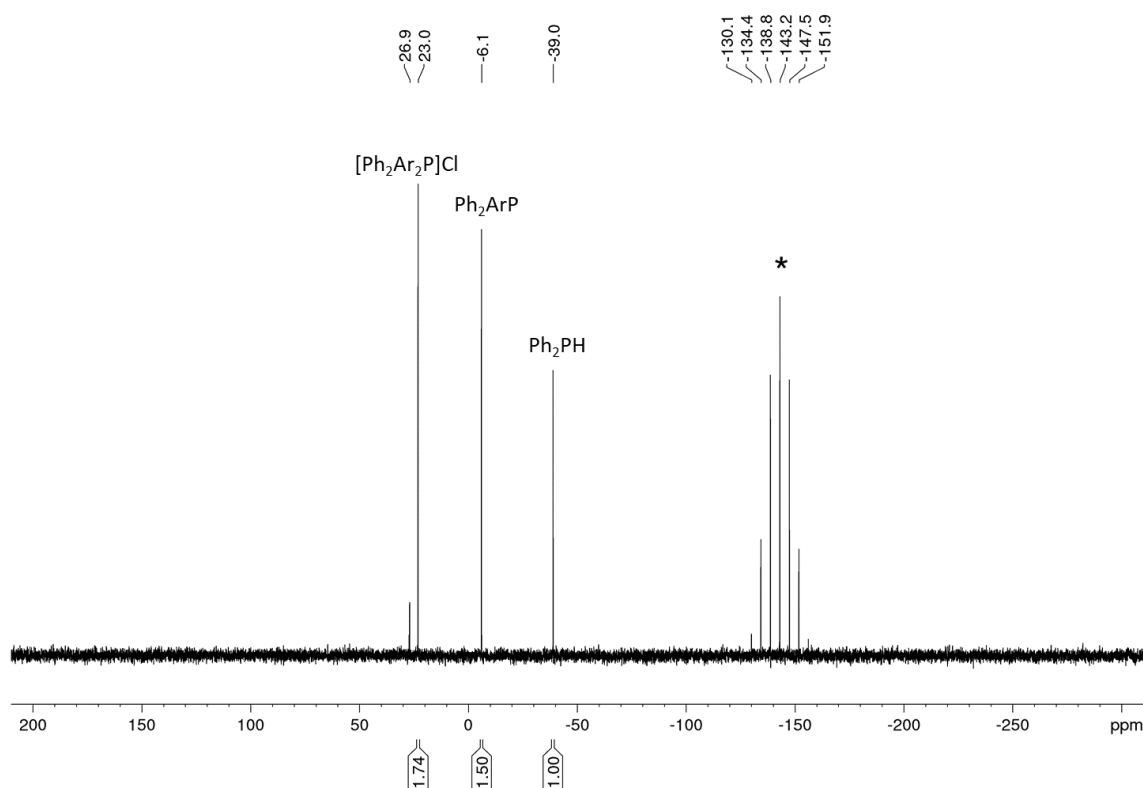


Figure S25. Control experiments for the photoelectrocatalytic functionalization of Ph_2PH into $[\text{Ph}_2\text{Ar}_2\text{P}]\text{Cl}$ and Ph_2ArP using **NpMI** (Table S3, Entry 3, 5 mol% **NpMI**, ClC_6H_4 -4-OMe, blue LED (455 nm), TBAPF_6 (*), **subsequent potential**, 1.60 V, Zn (+) / Fe (-). After irradiation without potential for 21h showed no product formation in the $^{31}\text{P}\{^1\text{H}\}$ NMR (see Figure S24), but subsequent application of potential yielded Ph_2ArP and $[\text{Ph}_2\text{Ar}_2\text{P}]\text{Cl}$

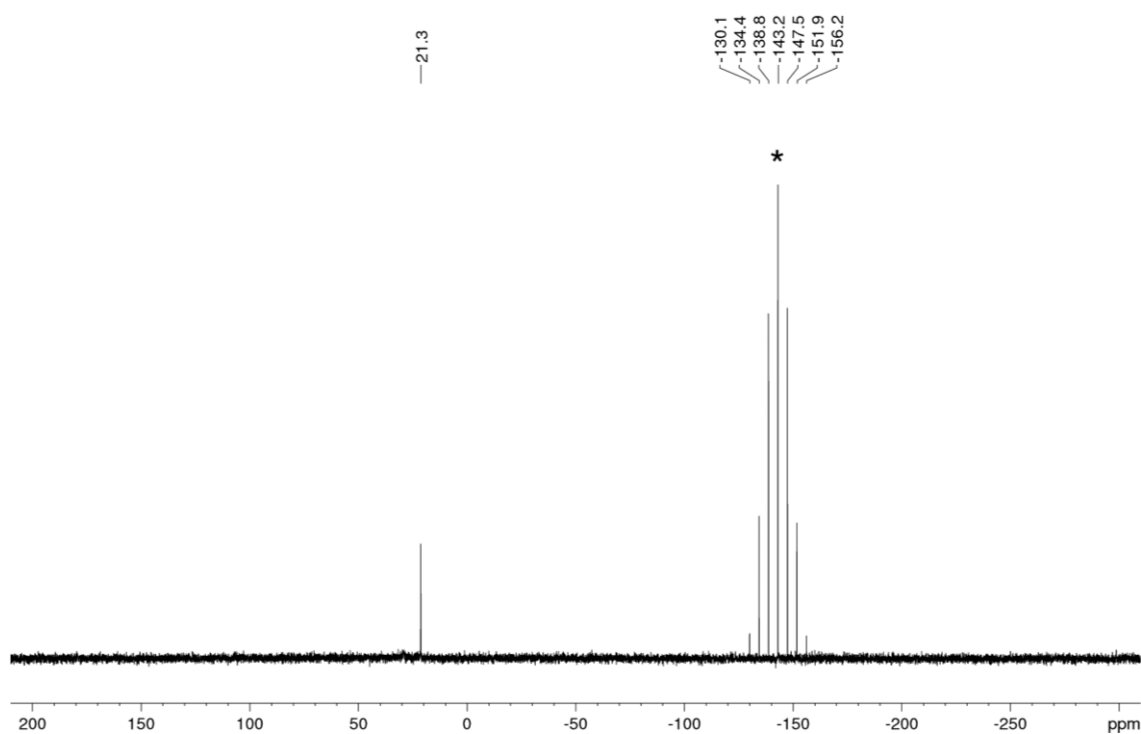


Figure S26. Control experiments for the photoelectrocatalytic functionalization of Ph_2PH into $[\text{Ph}_2\text{Ar}_2\text{P}]\text{Cl}$ and Ph_2ArP using **NpMI** (Table S3, Entry 4, **no e-PRCat**, $\text{ClC}_6\text{H}_4\text{-4-OMe}$, blue LED (455 nm), TBAPF_6 (*), 1.60 V, Zn (+) / Fe (-).

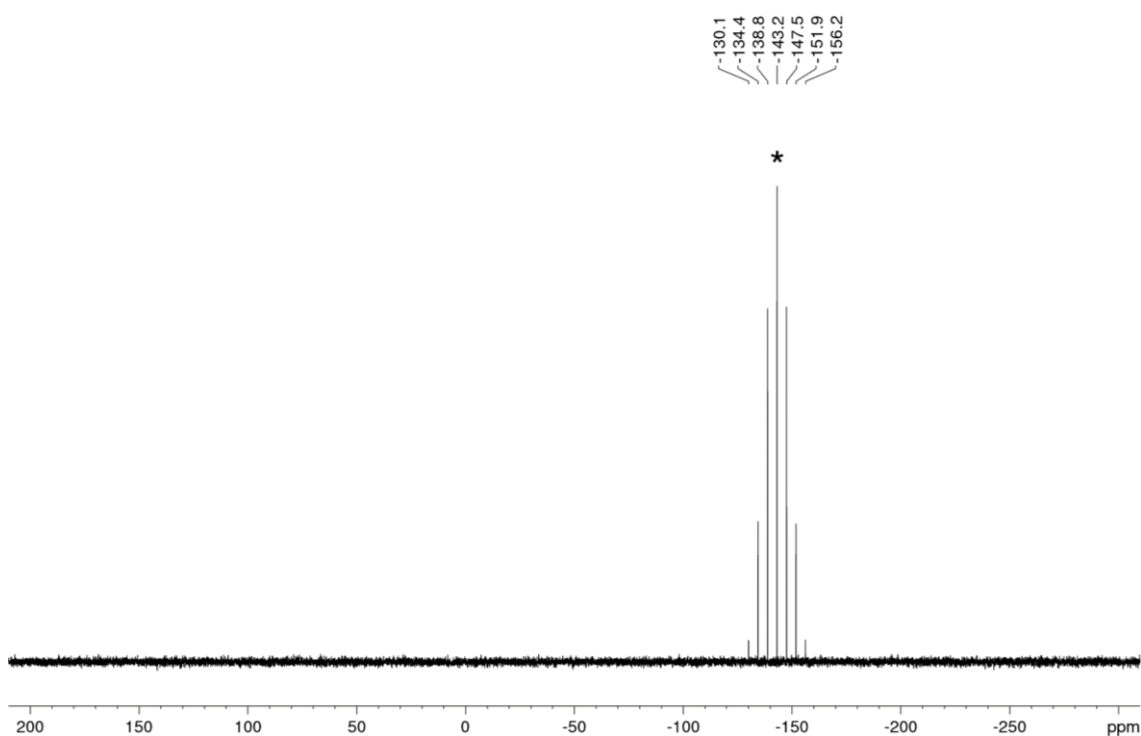


Figure S27. Control experiments for the photoelectrocatalytic functionalization of Ph_2PH into $[\text{Ph}_2\text{Ar}_2\text{P}]\text{Cl}$ and Ph_2ArP using **NpMI** (Table S3, Entry 5, **no Ph₂PH**, 5 mol% **NpMI**, $\text{ClC}_6\text{H}_4\text{-4-OMe}$, blue LED (455 nm), TBAPF_6 (*), 1.60 V, Zn (+) / Fe (-).

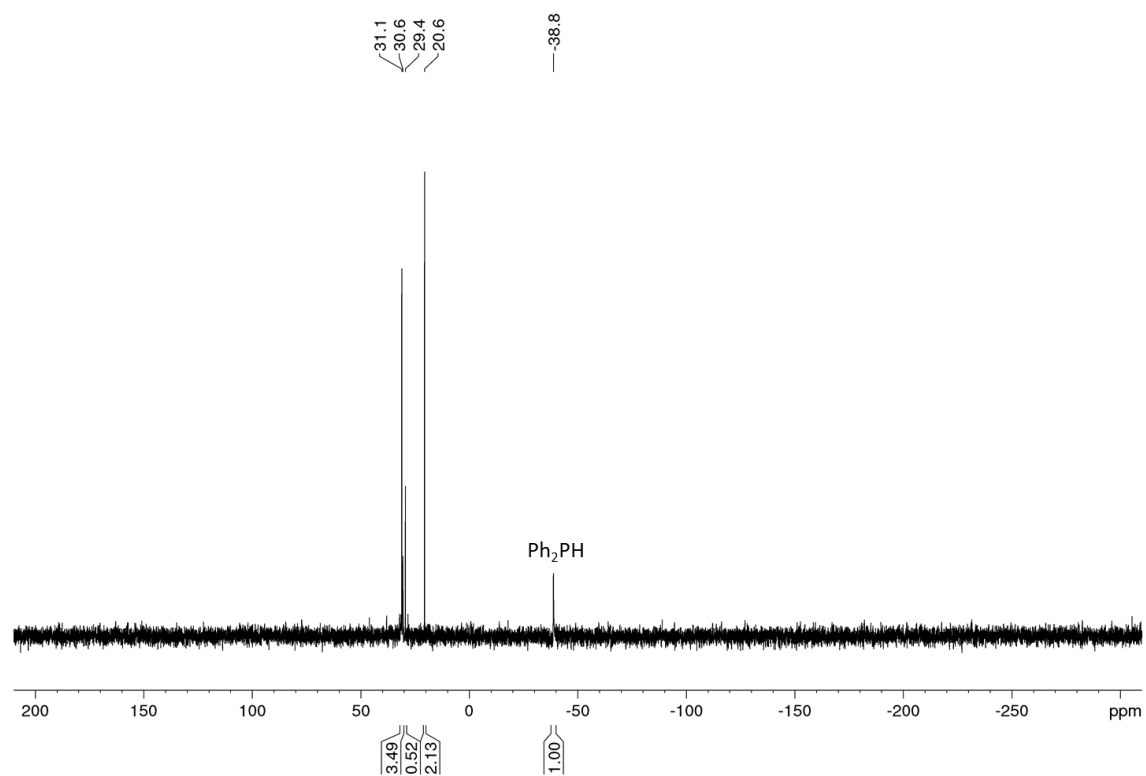


Figure S28. Control experiments for the photoelectrocatalytic functionalization of Ph₂PH into [Ph₂Ar₂P]Cl and Ph₂ArP using **NpMI** (Table S3, Entry 6, 5 mol% **NpMI**, ClC₆H₄-4-OMe, blue LED (455 nm), **no electrolyte**, 1.60 V, Zn (+) / Fe (-).

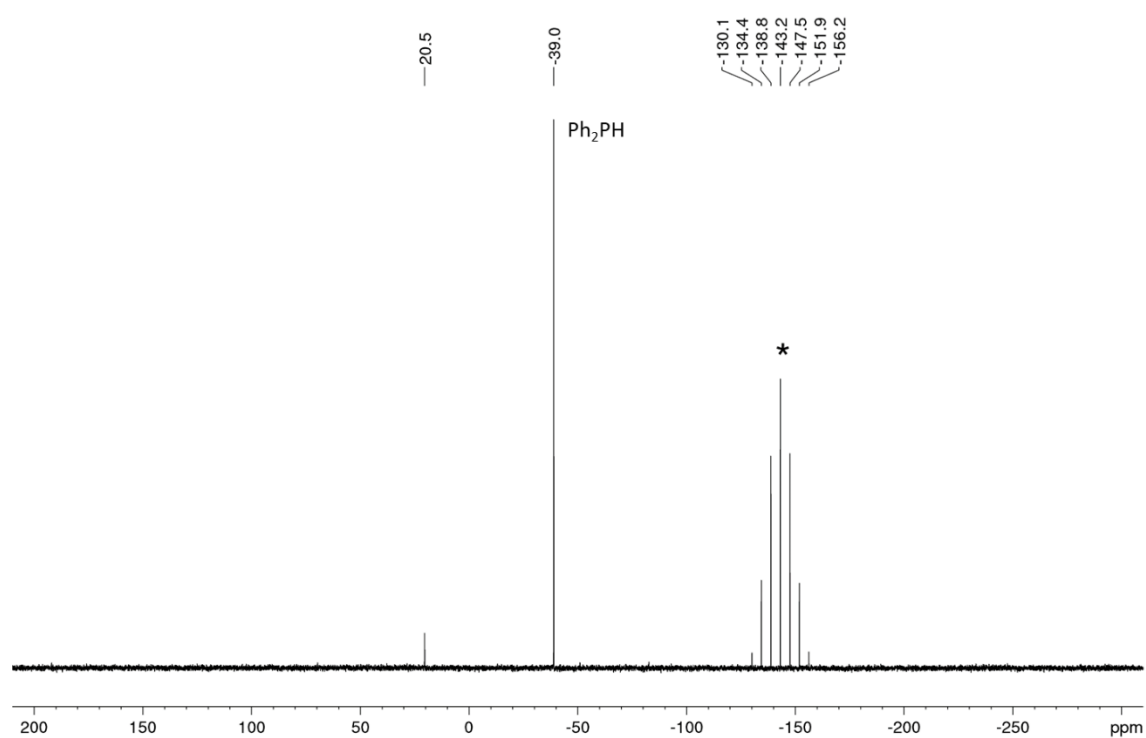


Figure S29. Control experiments for the photoelectrocatalytic functionalization of Ph₂PH into [Ph₂Ar₂P]Cl and Ph₂ArP using **NpMI** (Table S7, Entry 2, 5 mol% **NpMI**, ClC₆H₄-4-OMe, **no blue LED (455 nm)**, TBAPF₆ (*), **no potential**, Zn (+) / Fe (-).

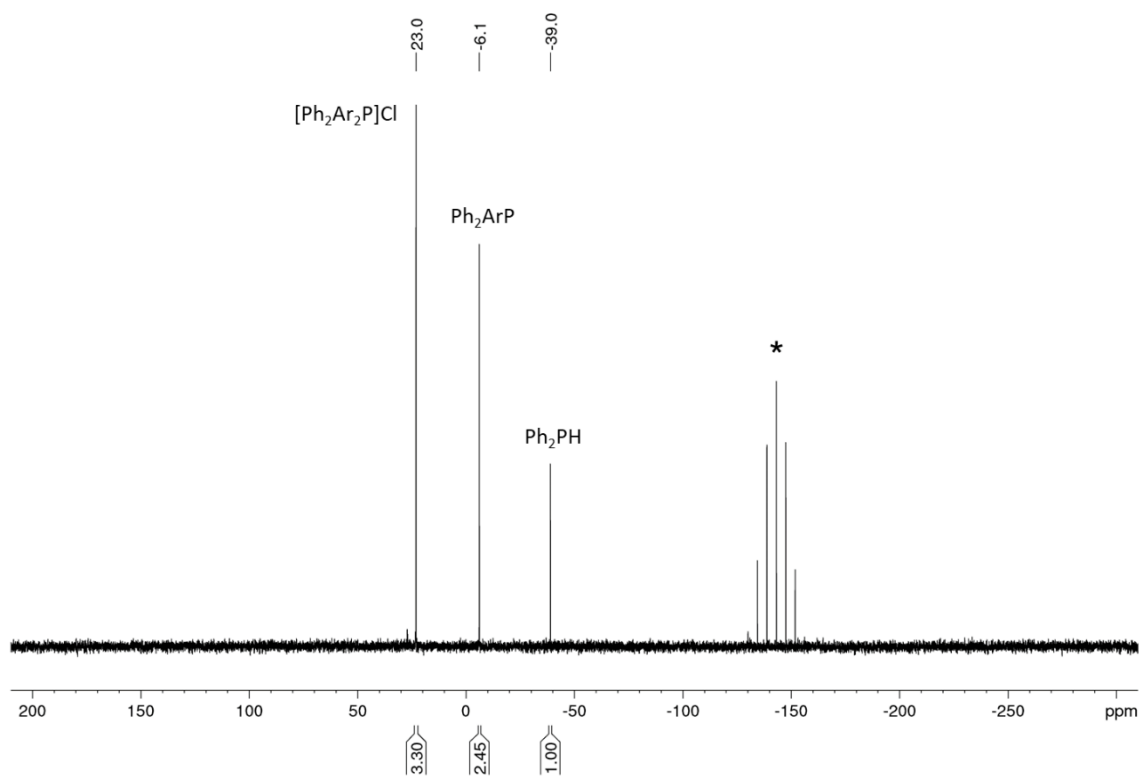


Figure S30. Control experiments for the photoelectrocatalytic functionalization of Ph₂PH into [Ph₂Ar₂P]Cl and Ph₂ArP using **NpMI** (Table S3, Entry 8, 5 mol% **NpMI**, ClC₆H₄-4-OMe, blue LED (455 nm), TBAPF₆ (*), 1.60 V, **Zn** (+) / **C_{foam}** (-).

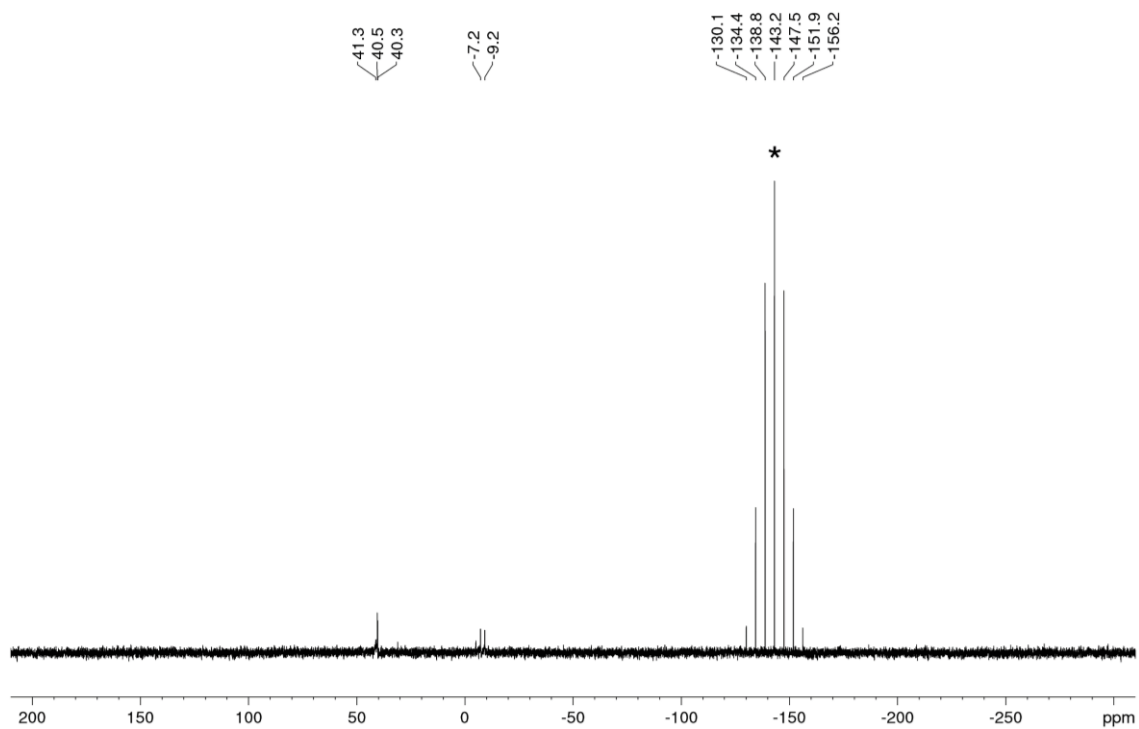


Figure S31. Control experiments for the photoelectrocatalytic functionalization of Ph₂PH into [Ph₂Ar₂P]Cl and Ph₂ArP using **NpMI** (Table S3, Entry 9, 5 mol% **NpMI**, ClC₆H₄-4-OMe, **no blue LED (455 nm)**, TBAPF₆ (*), **overpotential of 3.20 V**, **Zn** (+) / **Fe** (-).

S2.3.2.2 $^{31}\text{P}\{^1\text{H}\}$ NMR spectra of screening different conditions using **NpMI**

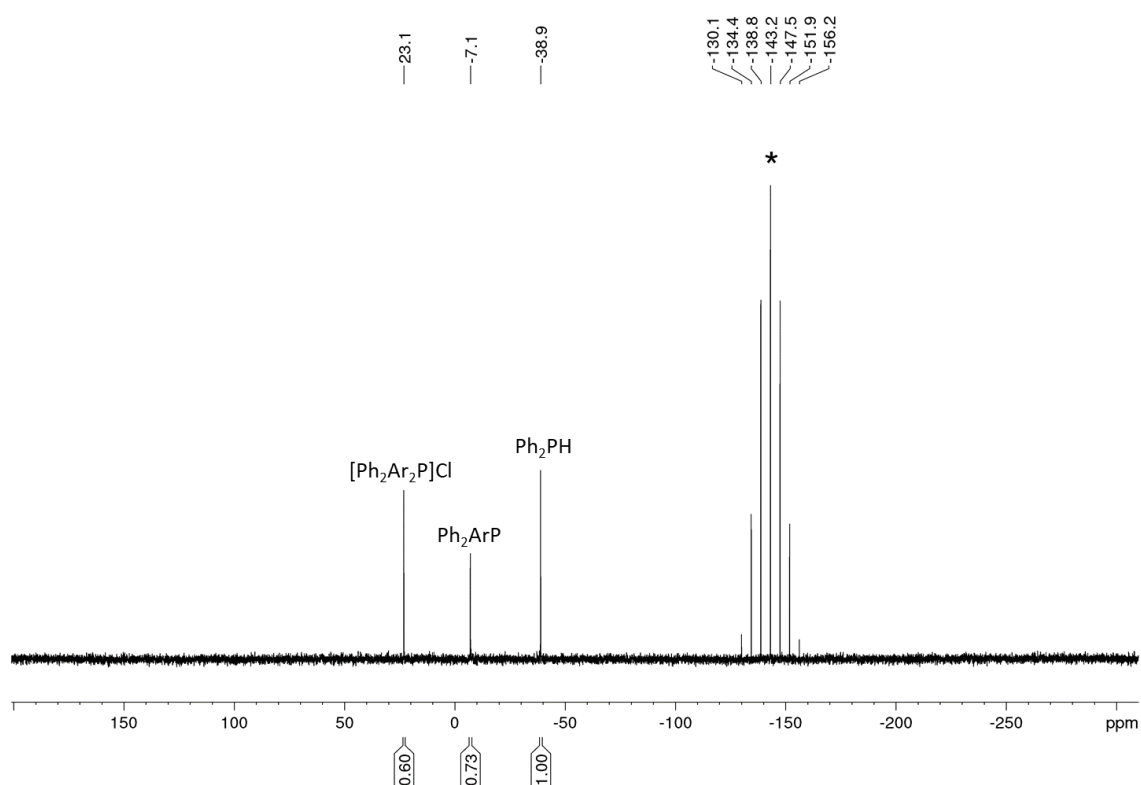


Figure S32. $^{31}\text{P}\{^1\text{H}\}$ NMR spectrum for the photoelectrocatalytic functionalization of Ph_2PH into $[\text{Ph}_2\text{Ar}_2\text{P}]\text{Cl}$ and Ph_2ArP using **NpMI** (Table 4, Entry 1, 5 mol% **NpMI**, $\text{ClC}_6\text{H}_4\text{-4-OMe}$, blue LED (455 nm), TBAPF_6 (*), 1.60 V, Zn (+) / Fe (-).

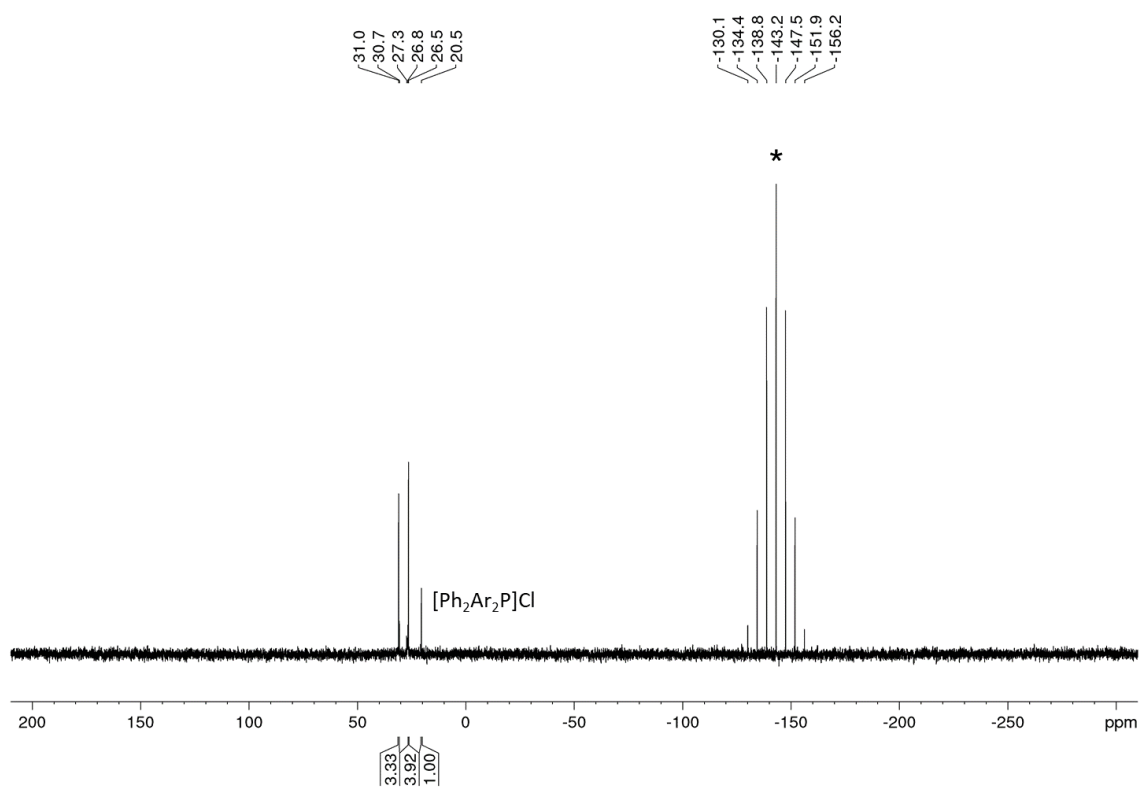


Figure S33. $^{31}\text{P}\{^1\text{H}\}$ NMR spectrum for the photoelectrocatalytic functionalization of Ph_2PH into $[\text{Ph}_2\text{Ar}_2\text{P}]\text{Cl}$ and Ph_2ArP using **NpMI** (Table 4, Entry 2, 10 mol% **NpMI**, $\text{ClC}_6\text{H}_4\text{-4-OMe}$, blue LED (455 nm), TBAPF_6 (*), 1.60 V, Zn (+) / Fe (-).

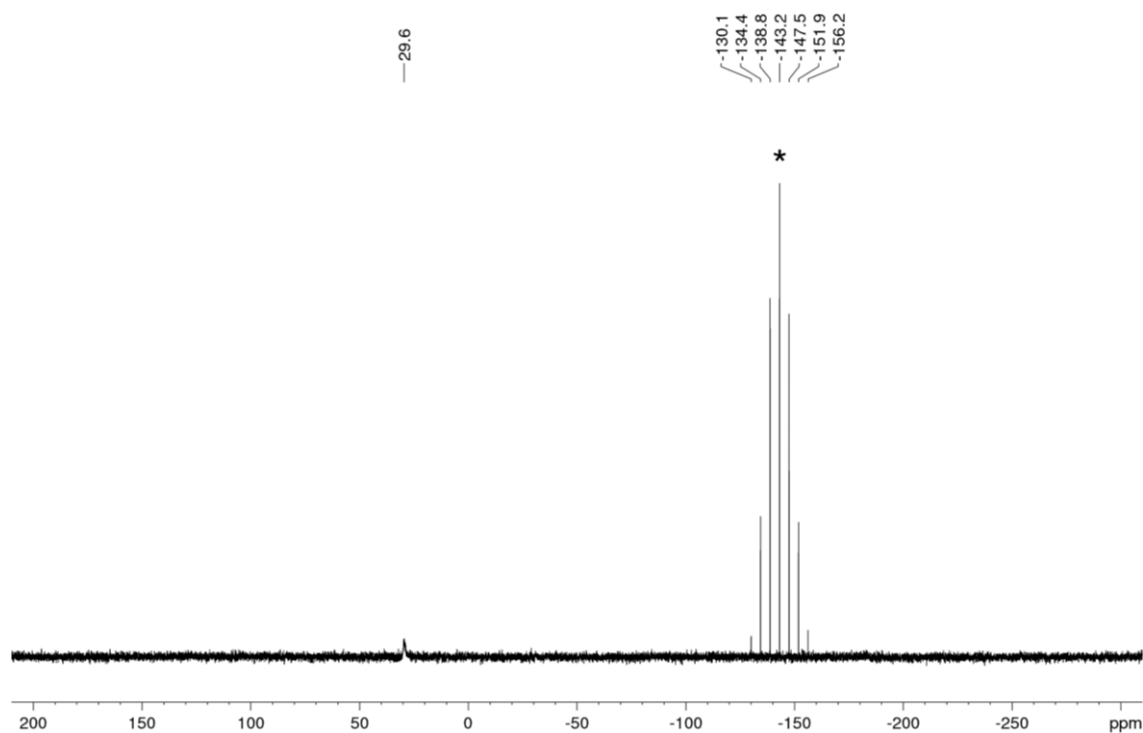


Figure S34. $^{31}\text{P}\{^1\text{H}\}$ NMR spectrum for the photoelectrocatalytic functionalization of Ph_2PH into $[\text{Ph}_2\text{Ar}_2\text{P}]\text{Cl}$ and Ph_2ArP using **NpMI** (Table 4, Entry 3, 5 mol% **NpMI**, $\text{ClC}_6\text{H}_4\text{-4-OMe}$, blue LED (455 nm), TBAPF_6 (*), 1.60 V, Zn (+) / Fe (-). The reaction time was extended from 21h to 3 days.

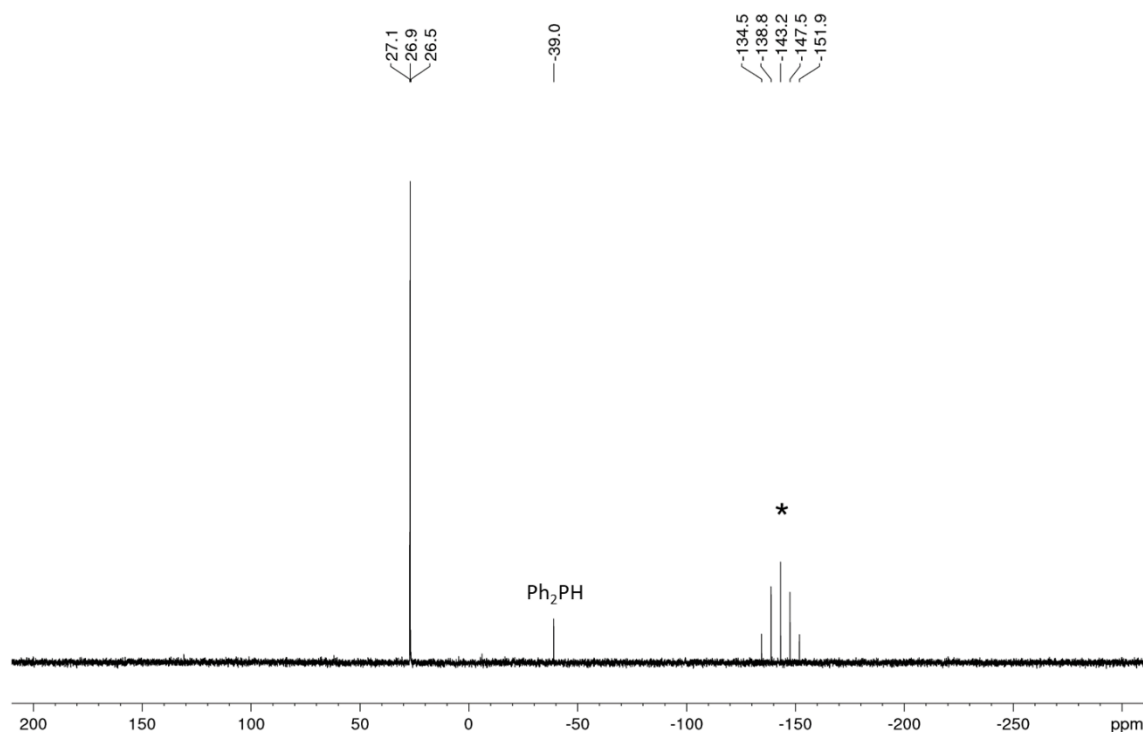


Figure S35. $^{31}\text{P}\{^1\text{H}\}$ NMR spectrum for the photoelectrocatalytic functionalization of Ph_2PH into $[\text{Ph}_2\text{Ar}_2\text{P}]\text{Cl}$ and Ph_2ArP using **NpMI** (Table 4, Entry 4, 5 mol% **NpMI**, $\text{ClC}_6\text{H}_4\text{-4-OMe}$, blue LED (455 nm), TBAPF_6 (*), 1.60 V, Zn (+) / C_{foam} (-). The reaction time was extended from 21h to 3 days.

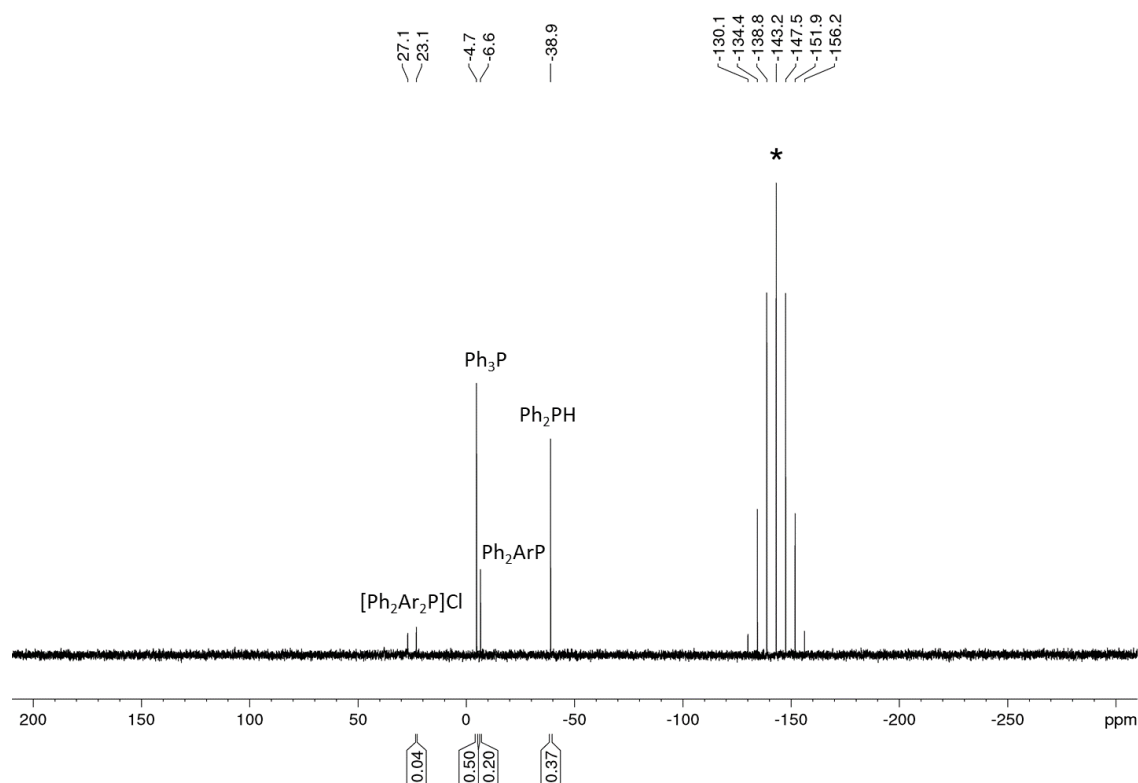


Figure S36. $^{31}\text{P}\{^1\text{H}\}$ NMR spectrum for the photoelectrocatalytic functionalization of Ph_2PH into $[\text{Ph}_2\text{Ar}_2\text{P}]\text{Cl}$ and Ph_2ArP using **NpMI** (Table 4, Entry 5, 1 mol% **NpMI**, $\text{ClC}_6\text{H}_4\text{-4-OMe}$, blue LED (455 nm), TBAPF_6 (*), 1.60 V, Zn (+) / C_{foam} (-). Ph_3P was added as an internal standard (0.05 mmol).

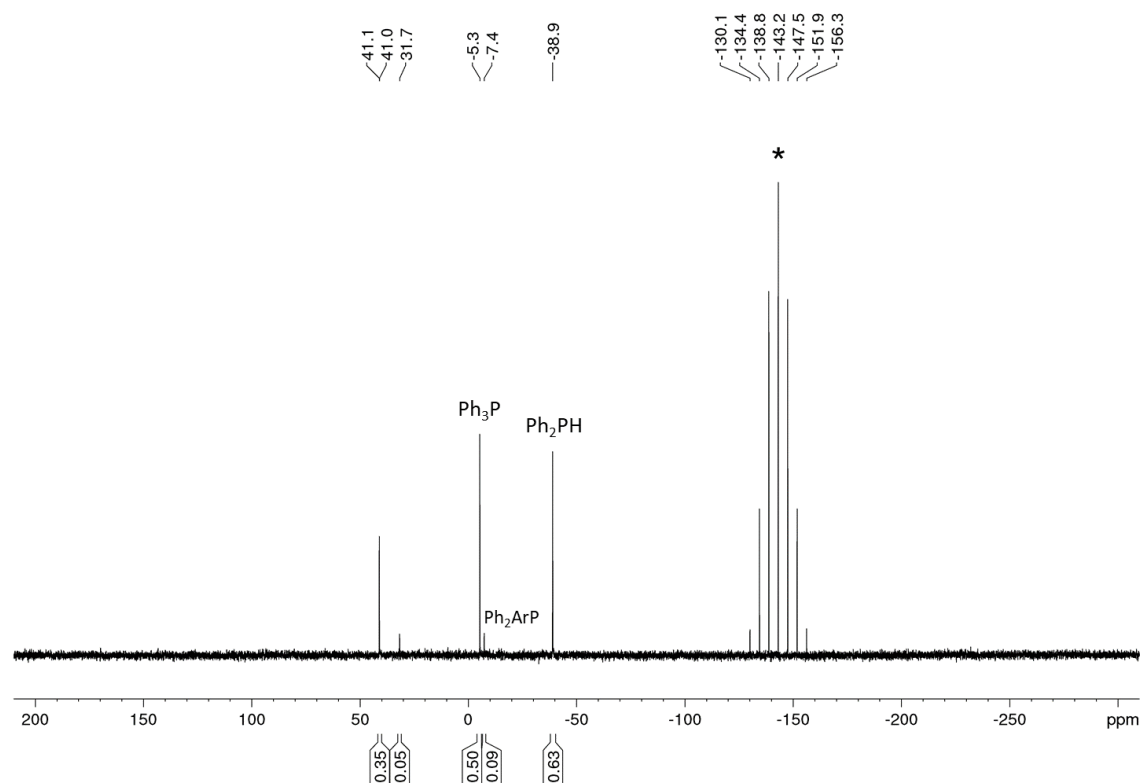


Figure S37. $^{31}\text{P}\{^1\text{H}\}$ NMR spectrum for the photoelectrocatalytic functionalization of Ph_2PH into $[\text{Ph}_2\text{Ar}_2\text{P}]\text{Cl}$ and Ph_2ArP using **NpMI** (Table 4, Entry 6, 2.5 mol% **NpMI**, $\text{ClC}_6\text{H}_4\text{-4-OMe}$, blue LED (455 nm), TBAPF_6 (*), 1.60 V, Zn (+) / C_{foam} (-). Ph_3P was added as an internal standard (0.05 mmol).

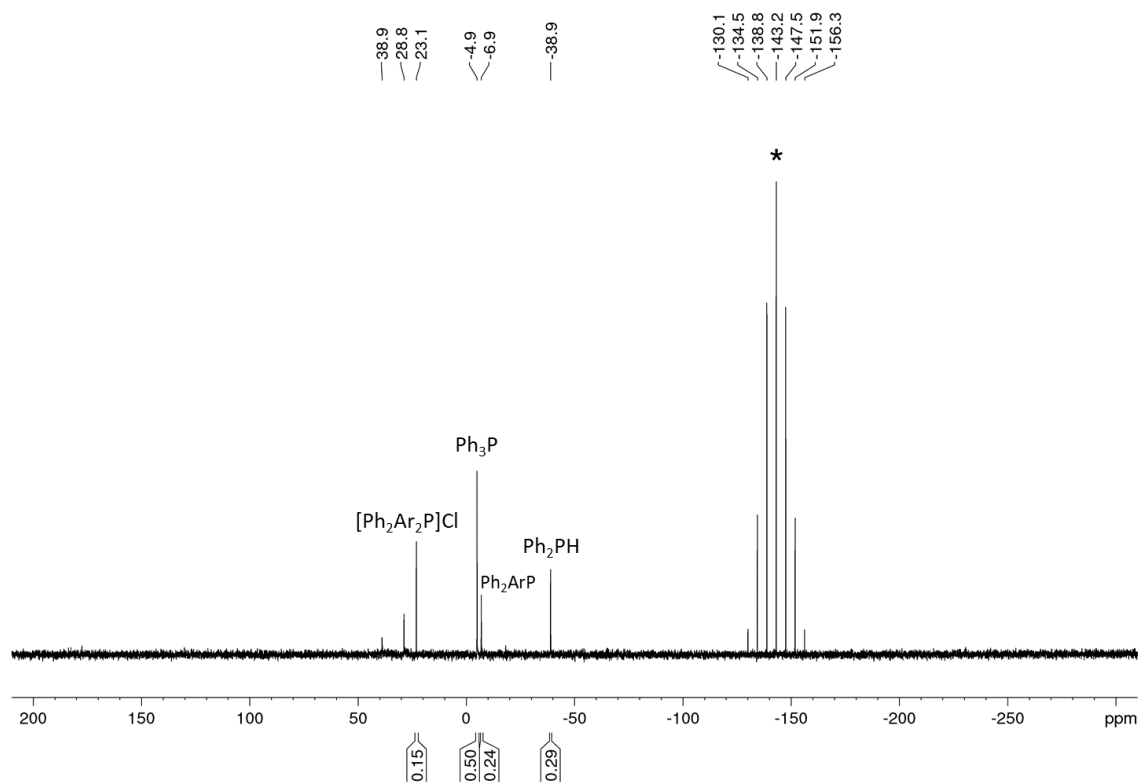


Figure S38. $^{31}\text{P}\{^1\text{H}\}$ NMR spectrum for the photoelectrocatalytic functionalization of Ph_2PH into $[\text{Ph}_2\text{Ar}_2\text{P}]\text{Cl}$ and Ph_2ArP using **NpMI** (Table 4, Entry 7, 5 mol% **NpMI**, $\text{C}_6\text{H}_4\text{-4-OMe}$, blue LED (455 nm), TBAPF_6 (*), 1.60 V, Zn (+) / C_{foam} (-). Ph_3P was added as an internal standard (0.05 mmol).

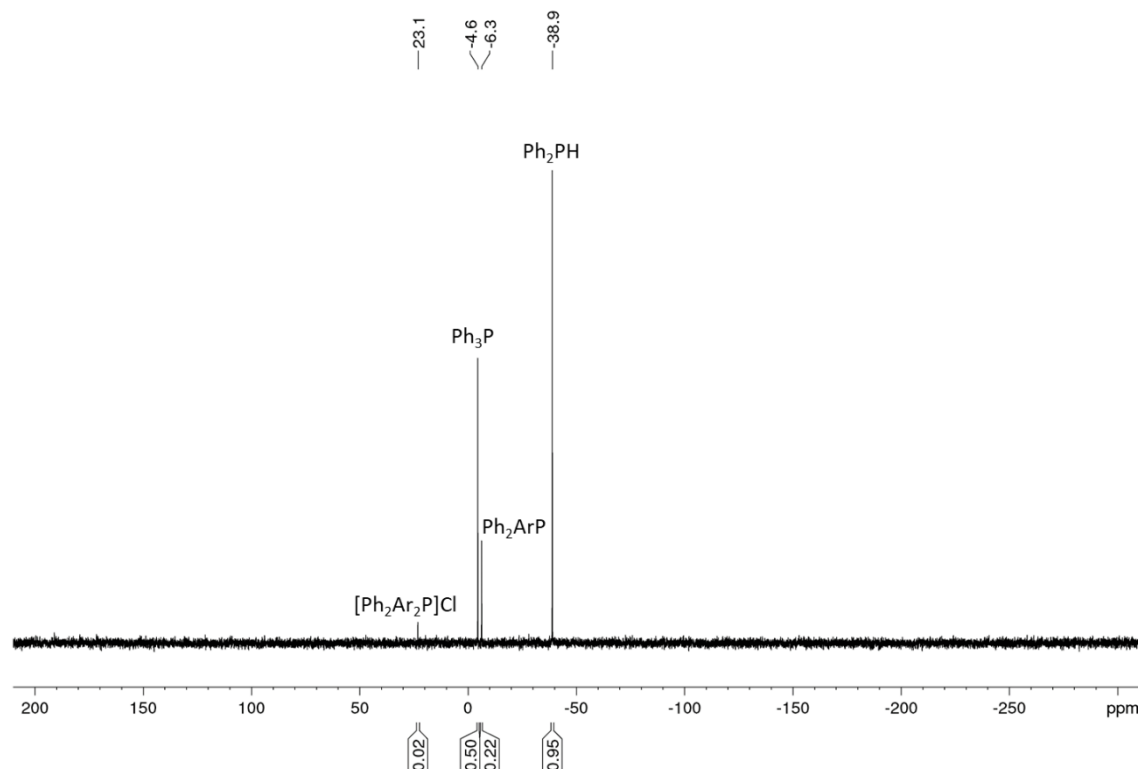


Figure S39. $^{31}\text{P}\{^1\text{H}\}$ NMR spectrum for the photoelectrocatalytic functionalization of Ph_2PH into $[\text{Ph}_2\text{Ar}_2\text{P}]\text{Cl}$ and Ph_2ArP using **NpMI** (Table 4, Entry 8, 5 mol% **NpMI**, $\text{C}_6\text{H}_4\text{-4-OMe}$, blue LED (455 nm), LiClO_4 , 1.60 V, Zn (+) / C_{foam} (-). Ph_3P was added as an internal standard (0.05 mmol).

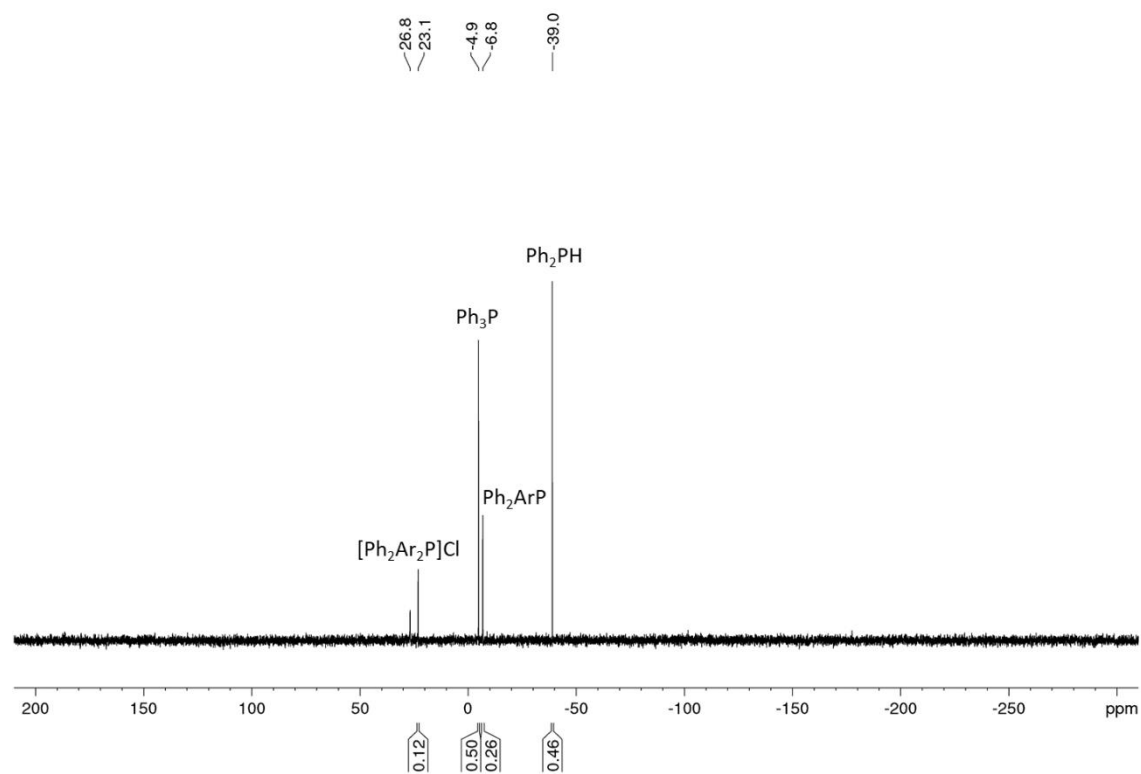


Figure S40. $^{31}\text{P}\{^1\text{H}\}$ NMR spectrum for the photoelectrocatalytic functionalization of Ph_2PH into $[\text{Ph}_2\text{Ar}_2\text{P}]\text{Cl}$ and Ph_2ArP using **NpMI** (Table 4, Entry 9, 5 mol% **NpMI**, ClC_6H_4 -4-OMe, blue LED (455 nm), **TBAPF**₄, 1.60 V, Zn (+) / C_{foam} (-). Ph_3P was added as an internal standard (0.05 mmol).

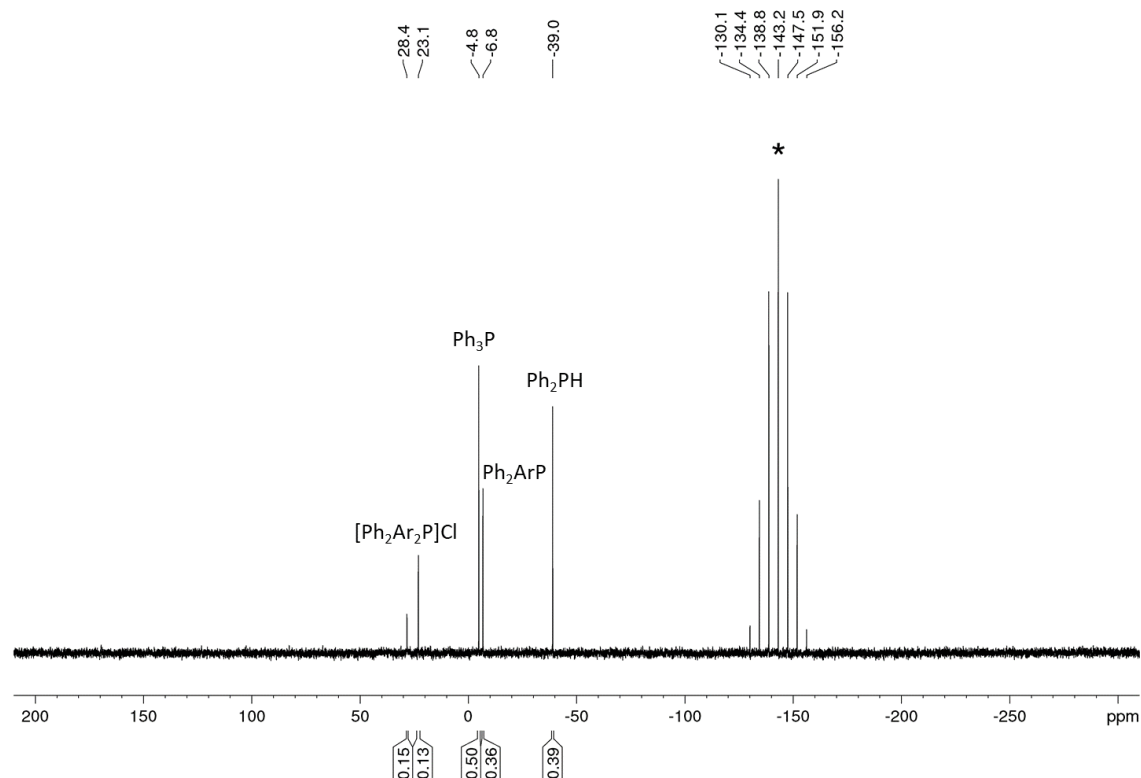


Figure S41. $^{31}\text{P}\{^1\text{H}\}$ NMR spectrum for the photoelectrocatalytic functionalization of Ph_2PH into $[\text{Ph}_2\text{Ar}_2\text{P}]\text{Cl}$ and Ph_2ArP using **NpMI** (Table 4, Entry 10, 1 mol% **NpMI**, ClC_6H_4 -4-OMe, blue LED (455 nm), **TBAPF**₆ (*), 1.60 V, Zn (+) / Fe (-). Ph_3P was added as an internal standard (0.05 mmol).

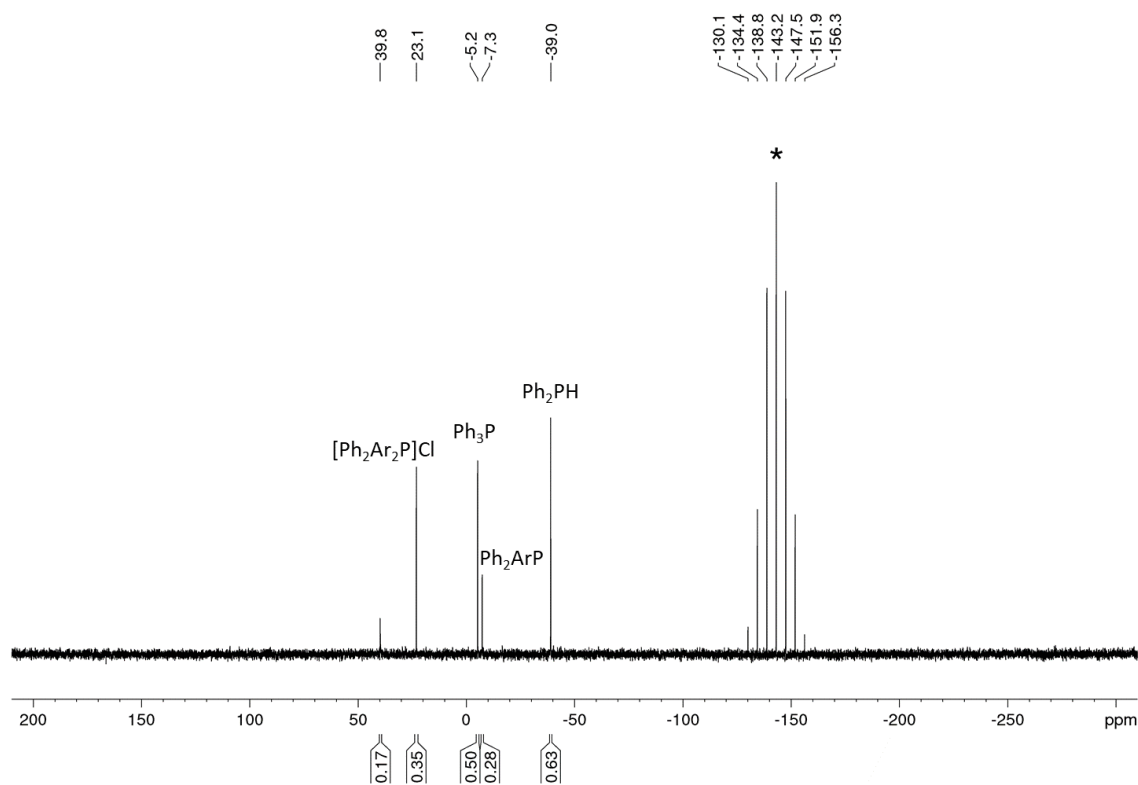


Figure S42. $^{31}\text{P}\{^1\text{H}\}$ NMR spectrum for the photoelectrocatalytic functionalization of Ph_2PH into $[\text{Ph}_2\text{Ar}_2\text{P}]\text{Cl}$ and Ph_2ArP using **NpMI** (Table 4, Entry 11, 2.5 mol% **NpMI**, $\text{ClC}_6\text{H}_4\text{-4-OMe}$, blue LED (455 nm), TBAPF_6 (*), 1.60 V, Zn (+) / Fe (-)). Ph_3P was added as an internal standard (0.05 mmol).

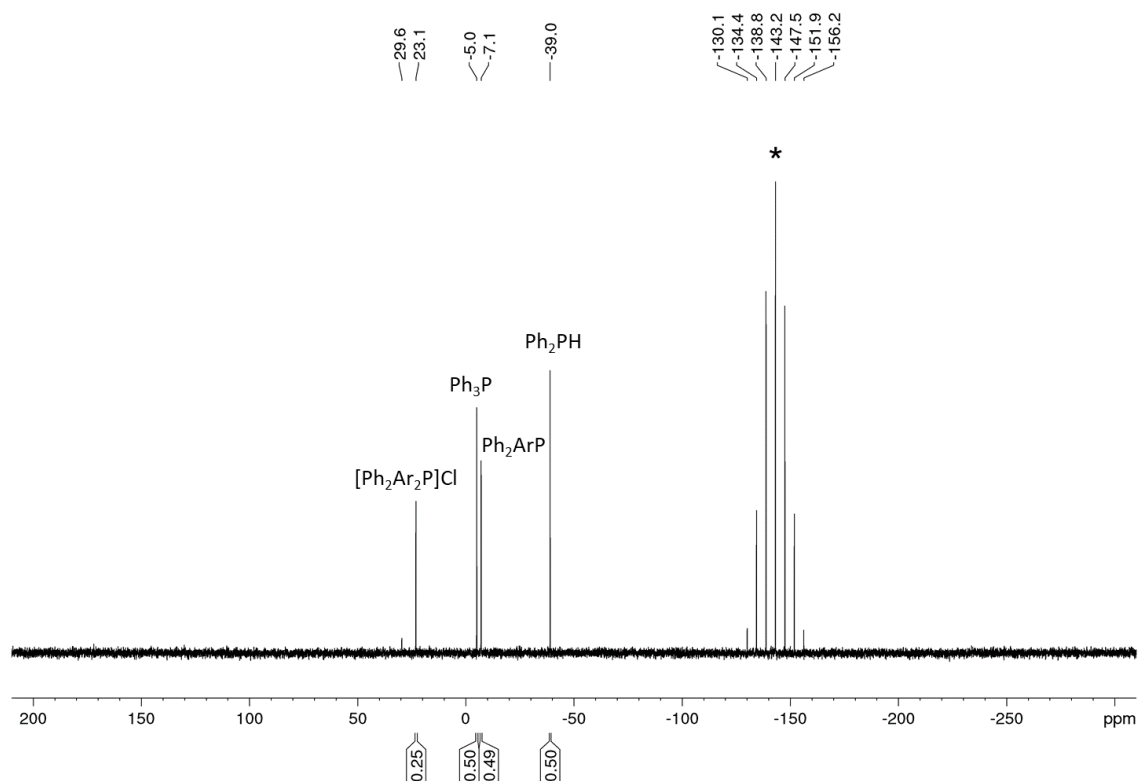


Figure S43. $^{31}\text{P}\{^1\text{H}\}$ NMR spectrum for the photoelectrocatalytic functionalization of Ph_2PH into $[\text{Ph}_2\text{Ar}_2\text{P}]\text{Cl}$ and Ph_2ArP using **NpMI** (Table 4, Entry 12, 5 mol% **NpMI**, $\text{ClC}_6\text{H}_4\text{-4-OMe}$, blue LED (455 nm), TBAPF_6 (*), 1.60 V, Zn (+) / Fe (-)). Ph_3P was added as an internal standard (0.05 mmol).

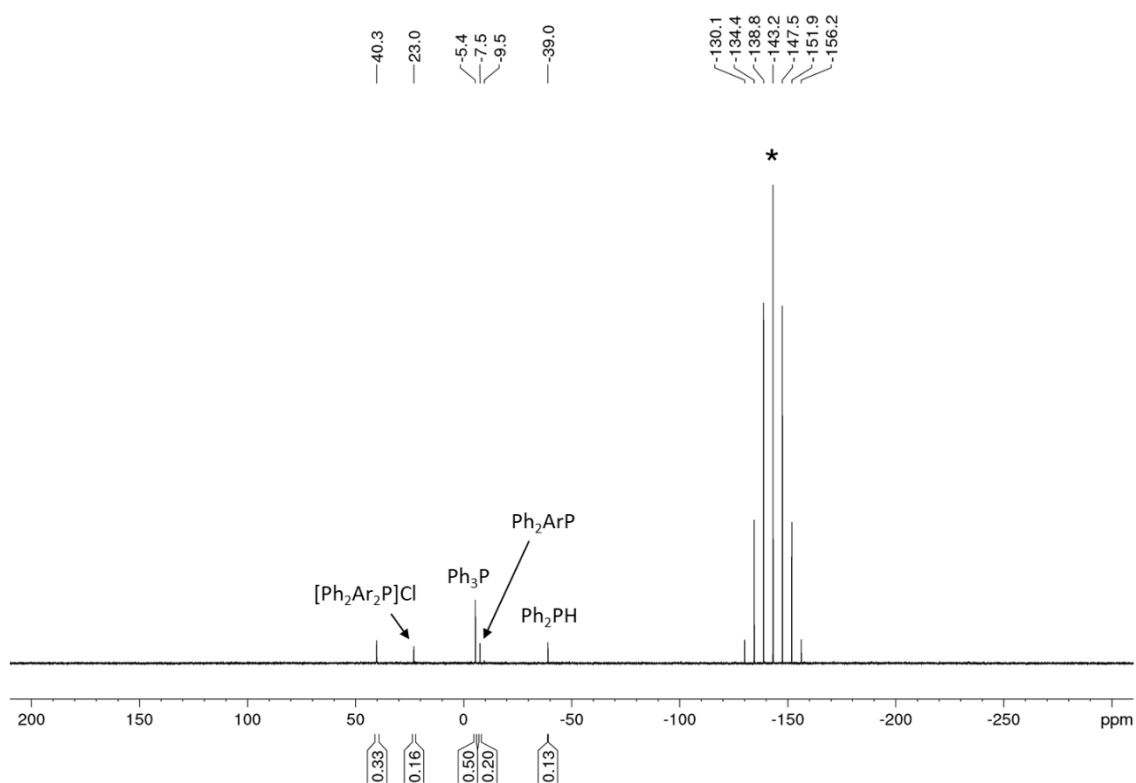


Figure S44. $^{31}\text{P}\{^1\text{H}\}$ NMR spectrum for the photoelectrocatalytic functionalization of Ph_2PH into $[\text{Ph}_2\text{Ar}_2\text{P}]\text{Cl}$ and Ph_2ArP using **NpMI** (Table 4, Entry 13, 5 mol% **NpMI**, $\text{ClC}_6\text{H}_4\text{-4-OMe}$, blue LED (455 nm), TBAPF_6 (*), 1.60 V, Zn (+) / Fe (-). Ph_3P was added as an internal standard (0.05 mmol). The amount of electrolyte TBAPF_6 was increased from 0.1 mmol to 0.4 mmol.

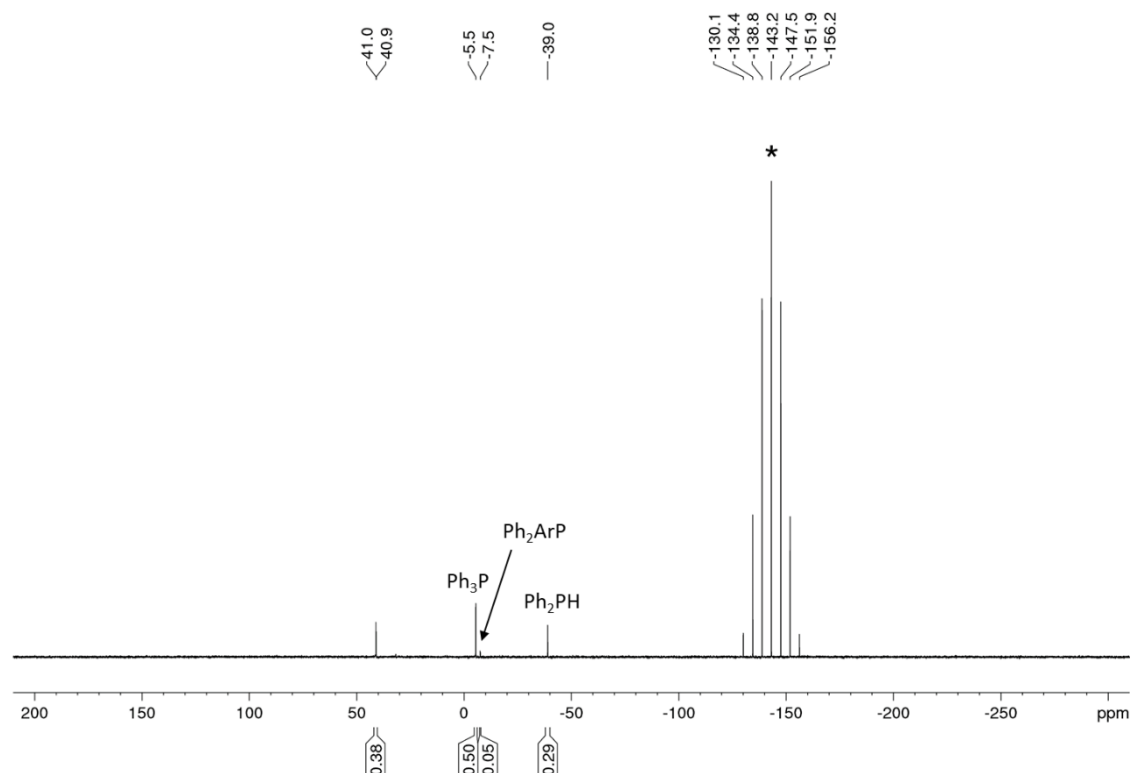


Figure S45. $^{31}\text{P}\{^1\text{H}\}$ NMR spectrum for the photoelectrocatalytic functionalization of Ph_2PH into $[\text{Ph}_2\text{Ar}_2\text{P}]\text{Cl}$ and Ph_2ArP using **NpMI** (Table 4, Entry 14, 5 mol% **NpMI**, $\text{ClC}_6\text{H}_4\text{-4-OMe}$, blue LED (455 nm), TBAPF_6 (*), 1.60 V, Zn (+) / C_{foam} (-). Ph_3P was added as an internal standard (0.05 mmol). The amount of electrolyte TBAPF_6 was increased from 0.1 mmol to 0.4 mmol.

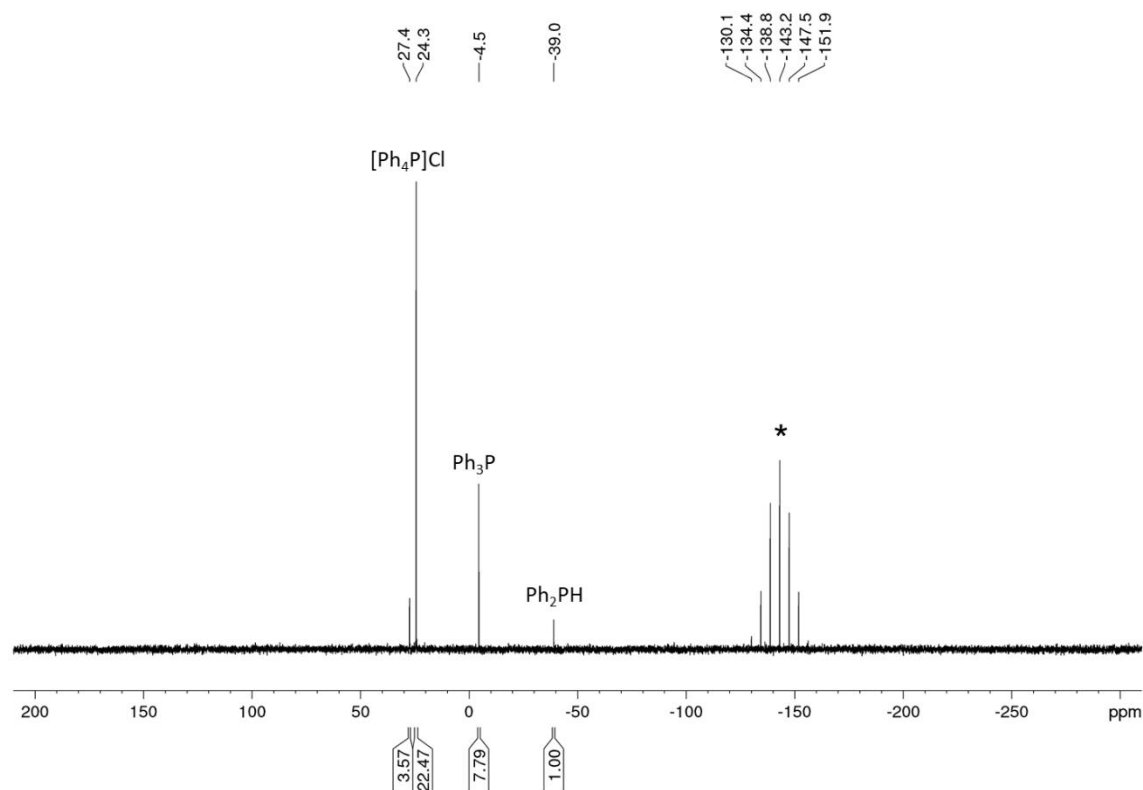


Figure S46. $^{31}\text{P}\{^1\text{H}\}$ NMR spectrum for the photoelectrocatalytic functionalization of Ph_2PH into $[\text{Ph}_2\text{Ar}_2\text{P}]\text{Cl}$ and Ph_2ArP using **NpMI** (Table 4, Entry 15, 5 mol% **NpMI**, PhBr, blue LED (455 nm), TBAPF_6 (*), 1.60 V, Zn (+) / Fe (-).

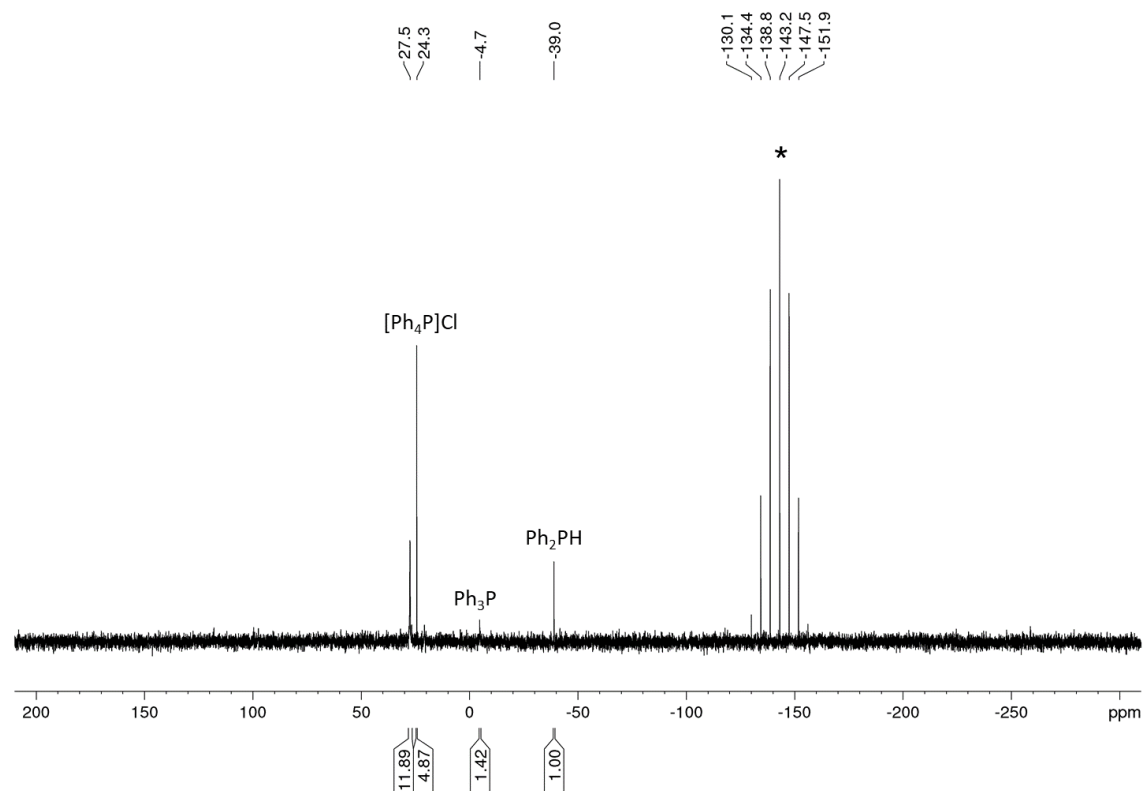


Figure S47. $^{31}\text{P}\{^1\text{H}\}$ NMR spectrum for the photoelectrocatalytic functionalization of Ph_2PH into $[\text{Ph}_2\text{Ar}_2\text{P}]\text{Cl}$ and Ph_2ArP using **NpMI** (Table 4, Entry 16, 5 mol% **NpMI**, PhBr, blue LED (455 nm), TBAPF_6 (*), 1.60 V, Zn (+) / C_{foam} (-).

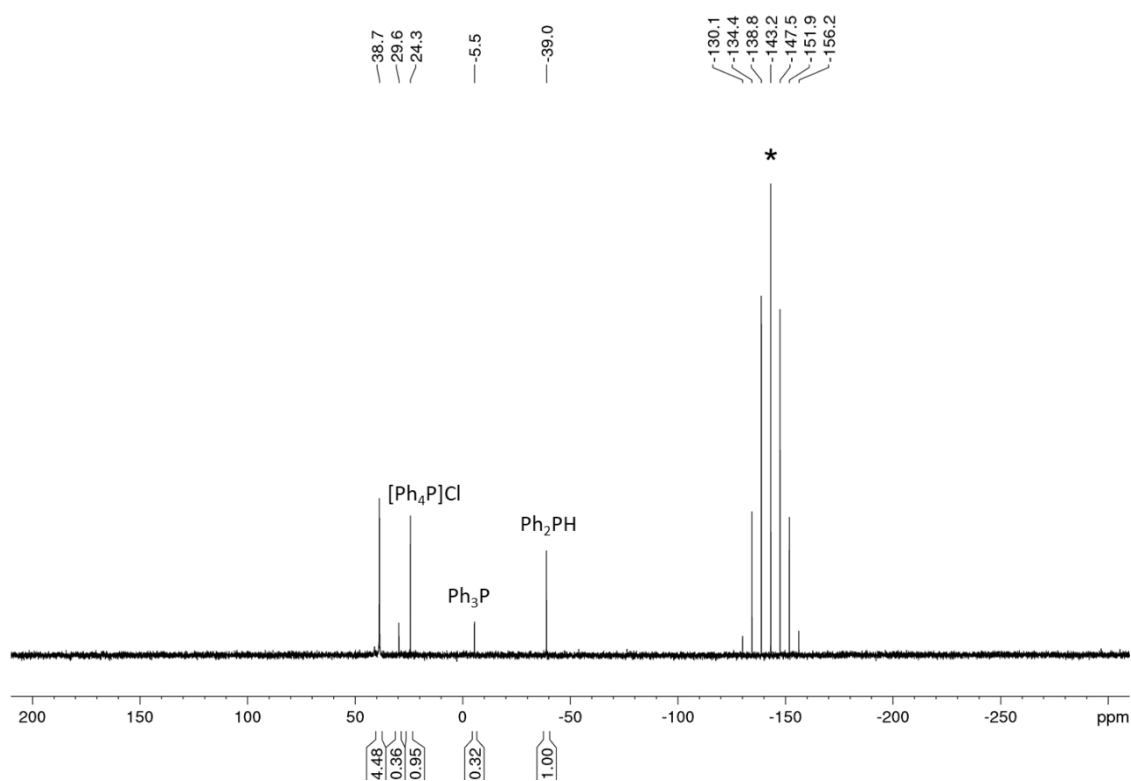


Figure S48. $^{31}\text{P}\{^1\text{H}\}$ NMR spectrum for the photoelectrocatalytic functionalization of Ph_2PH into $[\text{Ph}_2\text{Ar}_2\text{P}]\text{Cl}$ and Ph_2ArP using **NpMI** (Table 4, Entry 17, 5 mol% **NpMI**, PhCl , blue LED (455 nm), TBAPF_6 (*), 1.60 V, Zn (+) / Fe (-).

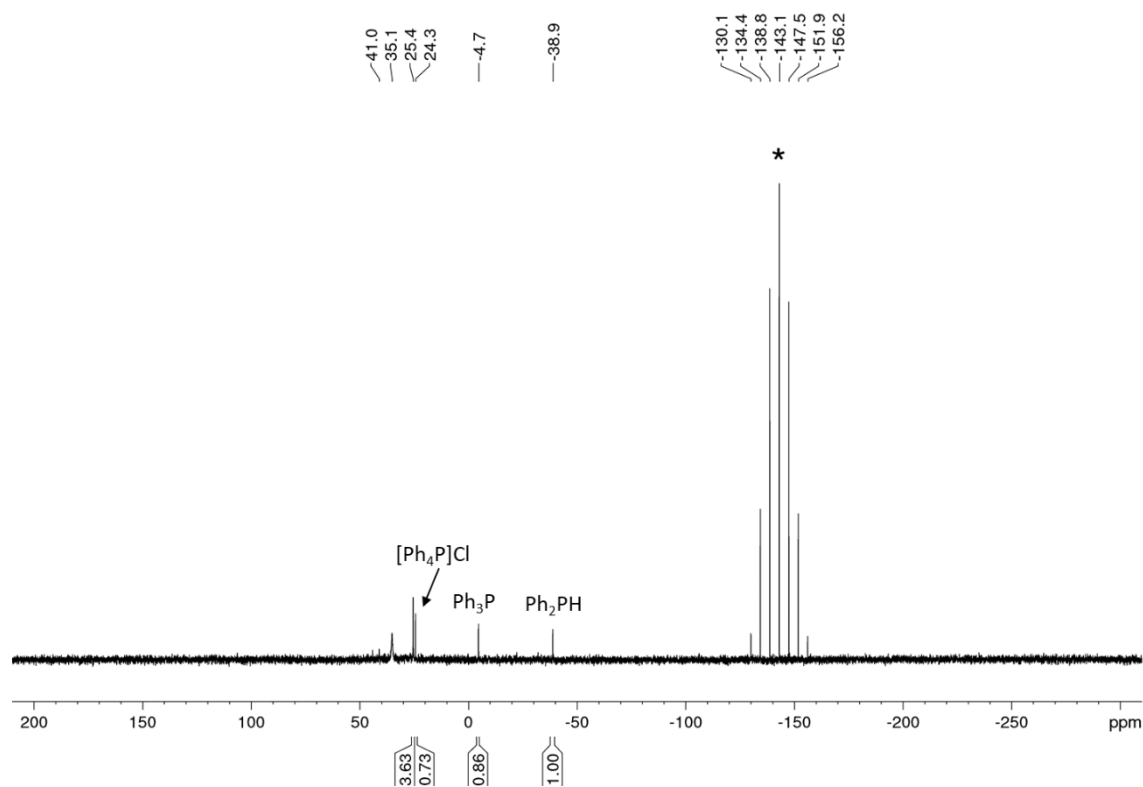


Figure S49. $^{31}\text{P}\{^1\text{H}\}$ NMR spectrum for the photoelectrocatalytic functionalization of Ph_2PH into $[\text{Ph}_2\text{Ar}_2\text{P}]\text{Cl}$ and Ph_2ArP using **NpMI** (Table 4, Entry 18, 5 mol% **NpMI**, PhCl , blue LED (455 nm), TBAPF_6 (*), 1.60 V, Zn (+) / Fe (-). The reaction was irradiated with **high power LEDs** (blue (451 nm), 20.3 V, 350 mA).

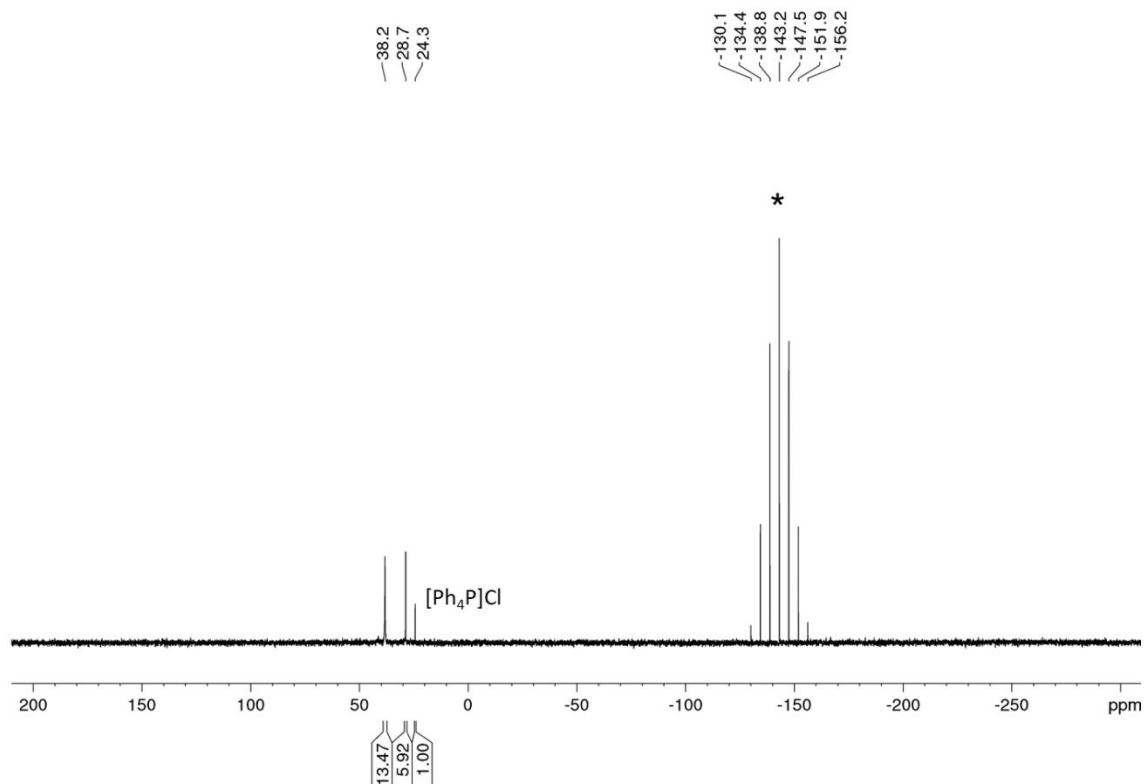


Figure S50. $^{31}\text{P}\{^1\text{H}\}$ NMR spectrum for the photoelectrocatalytic functionalization of Ph_2PH into $[\text{Ph}_2\text{Ar}_2\text{P}]\text{Cl}$ and Ph_2ArP using **NpMI** (Table 4, Entry 19, 5 mol% **NpMI**, PhBr, blue LED (455 nm), TBAPF₆ (*), 1.60 V, Zn (+) / Fe (-).

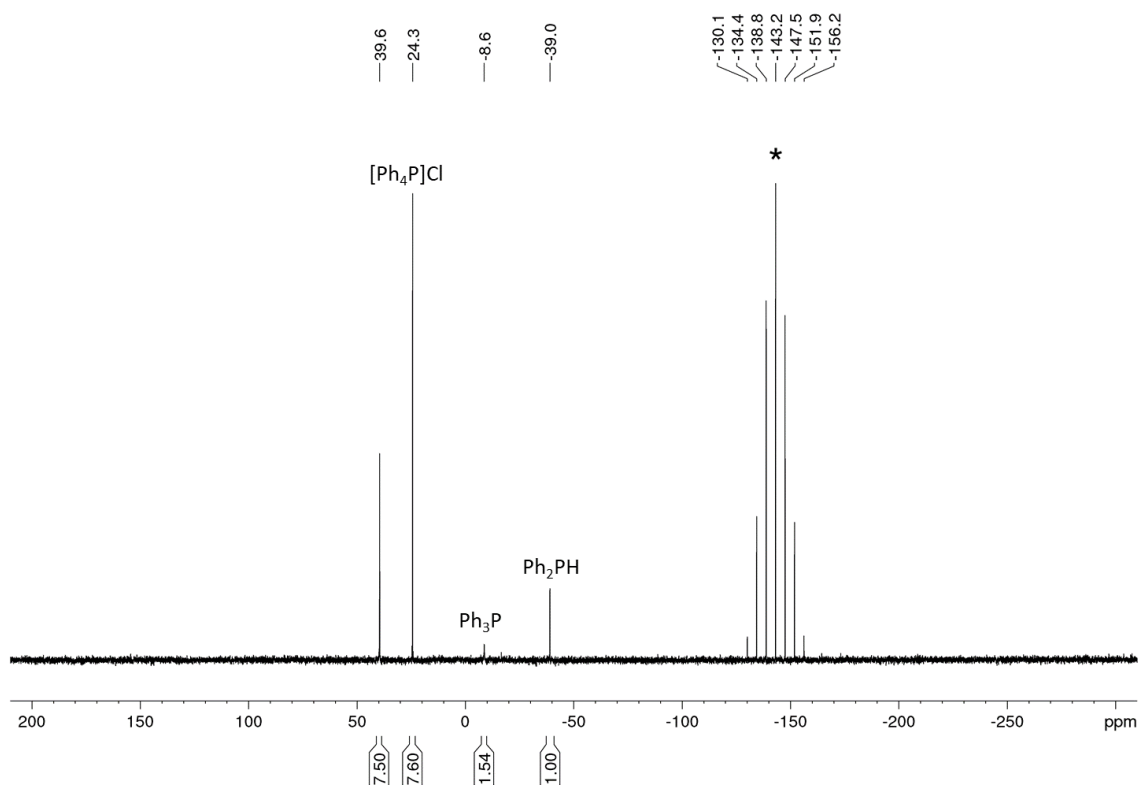


Figure S51. $^{31}\text{P}\{^1\text{H}\}$ NMR spectrum for the photoelectrocatalytic functionalization of Ph_2PH into $[\text{Ph}_2\text{Ar}_2\text{P}]\text{Cl}$ and Ph_2ArP using **NpMI** (Table 4, Entry 20, 5 mol% **NpMI**, PhBr, blue LED (455 nm), TBAPF₆ (*), 1.60 V, Zn (+) / Fe (-). The reaction was irradiated with **high power LEDs** (blue (451 nm), 20.3 V, 350 mA).

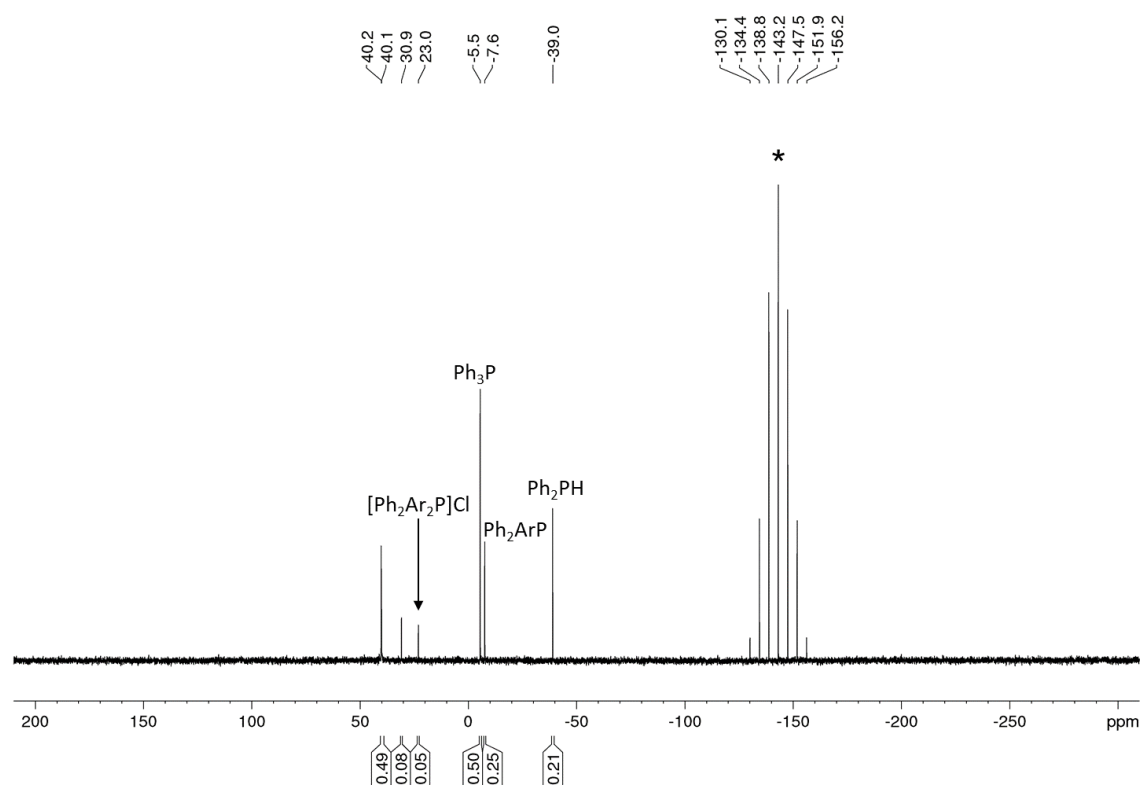


Figure S52. $^{31}\text{P}\{^1\text{H}\}$ NMR spectrum for the photoelectrocatalytic functionalization of Ph_2PH into $[\text{Ph}_2\text{Ar}_2\text{P}]\text{Cl}$ and Ph_2ArP using **NpMI** (Table 4, Entry 21, 5 mol% **NpMI**, $\text{ClC}_6\text{H}_4\text{-4-Ome}$, blue LED (455 nm), TBAPF_6 (*), 1.60 V, Zn (+) / Fe (-). Ph_3P was added as an internal standard (0.05 mmol).

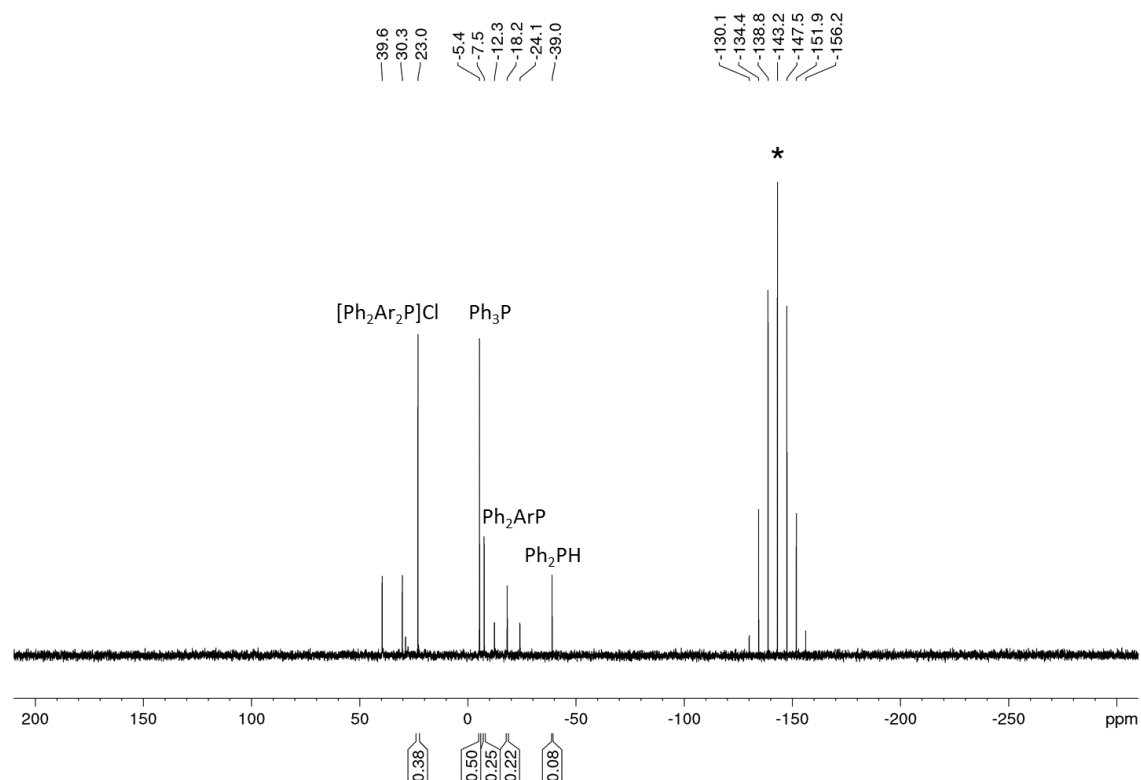
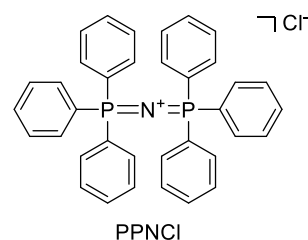


Figure S53. $^{31}\text{P}\{^1\text{H}\}$ NMR spectrum for the photoelectrocatalytic functionalization of Ph_2PH into $[\text{Ph}_2\text{Ar}_2\text{P}]\text{Cl}$ and Ph_2ArP using **NpMI** (Table 4, Entry 22, 5 mol% **NpMI**, $\text{ClC}_6\text{H}_4\text{-4-Ome}$, blue LED (455 nm), TBAPF_6 (*), 1.60 V, Zn (+) / Fe (-). Ph_3P was added as an internal standard (0.05 mmol). The reaction was irradiated with **high power LEDs** (blue (451 nm), 20.3 V, 350 mA).

S2.3.3 Quantification of the photoelectrochemical functionalization of Ph₂PH mediated by e-PRCat NpMI

S2.3.3.1 ³¹P{¹H} NMR calibration of Ph₂PH, Ph₃P and PPNCI

For the quantification of the photoelectrochemical functionalization of Ph₂PH mediated by different e-PRCats, such as DCA and NpMI, a calibration of starting material Ph₂PH, product Ph₃P and internal standard PPNCI was performed.



To demonstrate the different conversion stages of the photoelectrocatalytic arylation reaction of Ph₂PH, different ratios of starting material and product were prepared (Table S5; e.g., Entry 1, Calibr.1: 5% of Ph₂PH are consumed and 5% of product are formed) with a known amount of internal standard PPNCI (0.05 mmol). Imitating the reaction conditions, five calibration solutions were prepared which contained all the reactions components: ZnCl₂ (13.6 mg), **NpMI** (2 mg) and electrolyte TBAPF₆ (38.7 mg). Variable amounts (see Table S5) of starting material Ph₂PH (stock solution of 87 μL in 5 mL MeCN), product Ph₃P (stock solution of 131.15 mg in 5 mL MeCN) and internal standard PPNCI (0.05 mmol, 500 μL, stock solution of 287.02 mg in 5 mL MeCN) were added to the particular calibration solutions. All five calibration solutions were subjected to ³¹P{¹H} NMR analysis. The integral ratios of Ph₂PH / PPNCI and Ph₃P / PPNCI shown in Table S6 and S7, respectively, were determined by ³¹P{¹H} NMR spectra (see Figure S56 – S60, integral of PPNCI was set to 2P). Plotting the integral ratios against the ratio of the molar amounts gave a linear relation of the tested internal standard PPNCI to Ph₂PH and Ph₃P, respectively (see Figures S54 and S55), which demonstrated PPNCI is an appropriate internal standard for the photoelectrochemical system to convert Ph₂PH into Ph₃P.

Table S5. Calibration series of starting material Ph₂PH, product Ph₃P and internal standard PPNCI.

Entry	Consump. of Ph ₂ PH	n(Ph ₂ PH) [mmol]	conv. to Ph ₃ P	n(Ph ₃ P) [mmol]	PPNCI	n(PPNCI) [mmol]
Calibr.1	5%	0.095	5%	0.005	50%	0.05
Calibr.2	25%	0.075	25%	0.025	50%	0.05
Calibr.3	50%	0.05	50%	0.05	50%	0.05
Calibr.4	75%	0.025	75%	0.075	50%	0.05
Calibr.5	95%	0.005	95%	0.095	50%	0.05

Table S6. Quantitative calibration of starting material Ph₂PH and internal standard PPNCI by determination of the ratio/integrals by ³¹P{¹H} NMR. The integral of internal standard PPNCI was set to Int(PPNCI) = 2.

Entry	conv. of Ph ₂ PH	n(Ph ₂ PH) [mmol]	n(PPNCI) [mmol]	n(Ph ₂ PH) / n(PPNCI)	Int(Ph ₂ PH)	Int(Ph ₂ PH) / Int(PPNCI)
1	5%	0.095	0.05	1.9	2.3886	1.1943
2	25%	0.075	0.05	1.5	1.9070	0.9535
3	50%	0.05	0.05	1	1.1896	0.5948
4	75%	0.025	0.05	0.5	0.5766	0.2883
5	95%	0.005	0.05	0.1	0.1017	0.05085

Quantitative Calibration of (Ph₂PH) / PPNCI

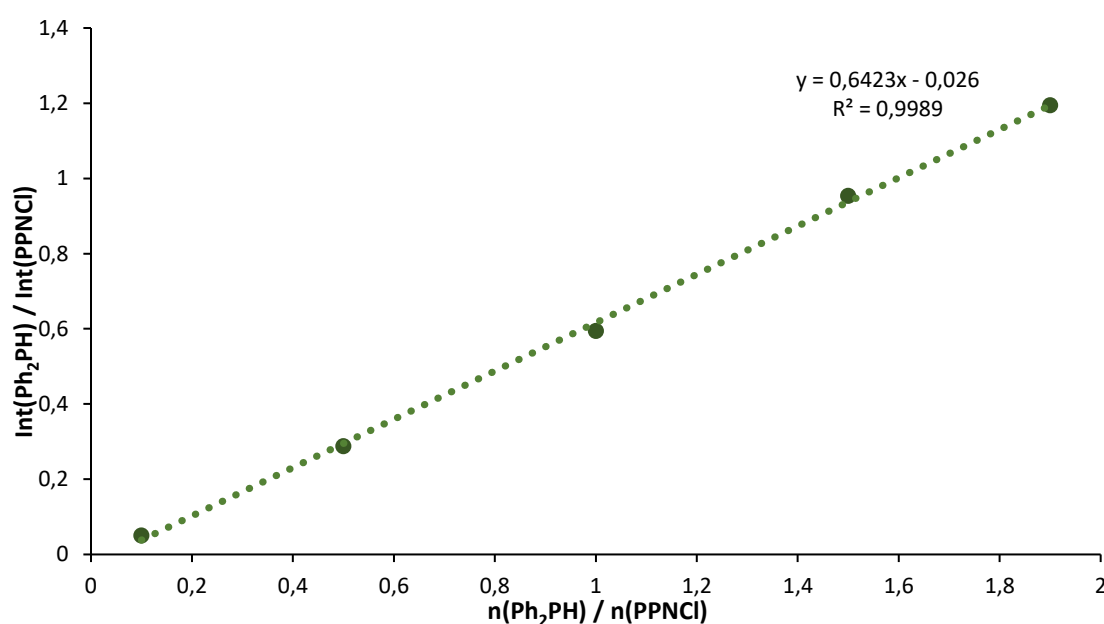


Figure S54. Quantitative calibration of starting material Ph₂PH and internal standard PPNCI. The ratio was determined by ³¹P{¹H} NMR integrals (see Figure S56 – S60).

Table S7. Quantitative calibration of product Ph₃P and internal standard PPNCI by determination of the ratio/integrals by ³¹P{¹H} NMR. The integral of internal standard PPNCI was set to Int(PPNCI) = 2.

Entry	conv. to Ph ₃ P	n(Ph ₃ P) [mmol]	n(PPNCI) [mmol]	n(Ph ₃ P) / n(PPNCI)	Int(Ph ₃ P)	Int(Ph ₃ P) / Int(PPNCI)
1	5%	0.005	0.05	0.1	0.1061	0.05305
2	25%	0.025	0.05	0.5	0.4365	0.21825
3	50%	0.05	0.05	1	0.8720	0.436
4	75%	0.075	0.05	1.5	1.3271	0.66355
5	95%	0.095	0.05	1.9	1.8030	0.9015

Quantitative Calibration of Ph₃P / PPNCI

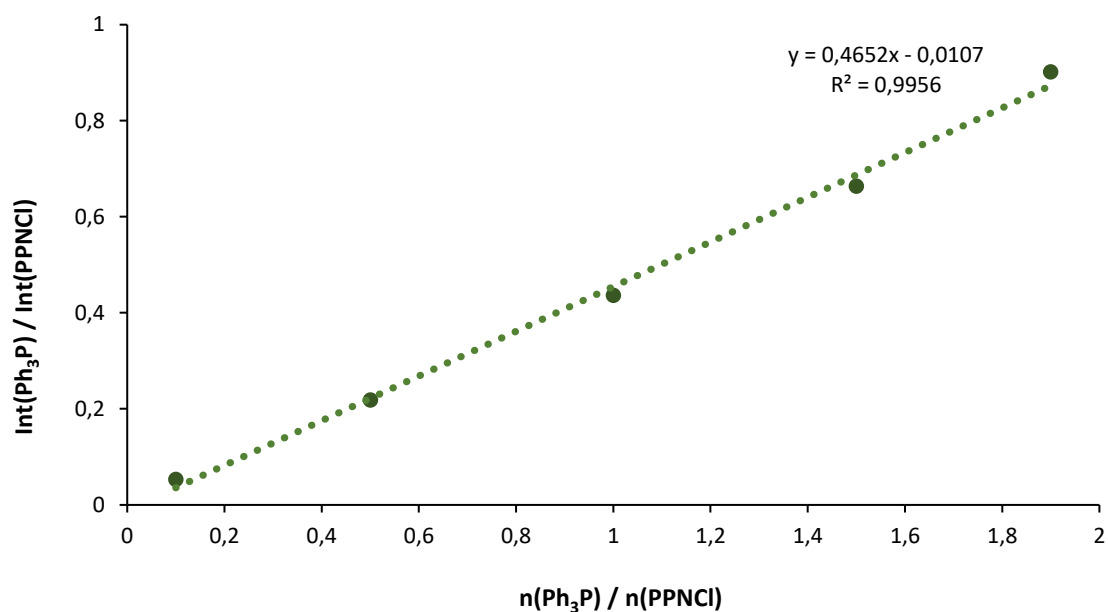


Figure S55. Quantitative calibration of product Ph₃P and internal standard PPNCI. The ratio was determined by ³¹P{¹H} NMR integrals (see Figure S56 – S60).

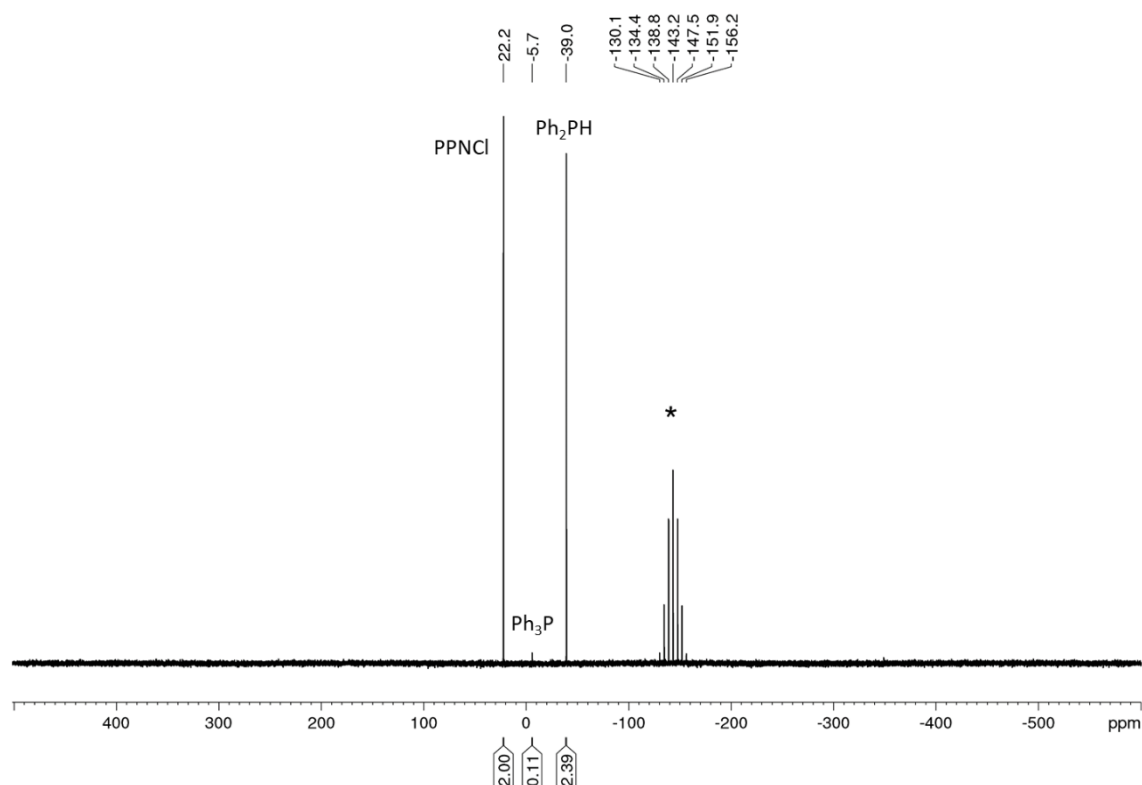


Figure S56. ³¹P{¹H} NMR spectrum of calibration 1 (Table S5, Entry Calibr.1) containing 95% starting material Ph₂PH, 5% product Ph₃P and 50% internal standard PPNCI. * marks electrolyte TBAPF₆.

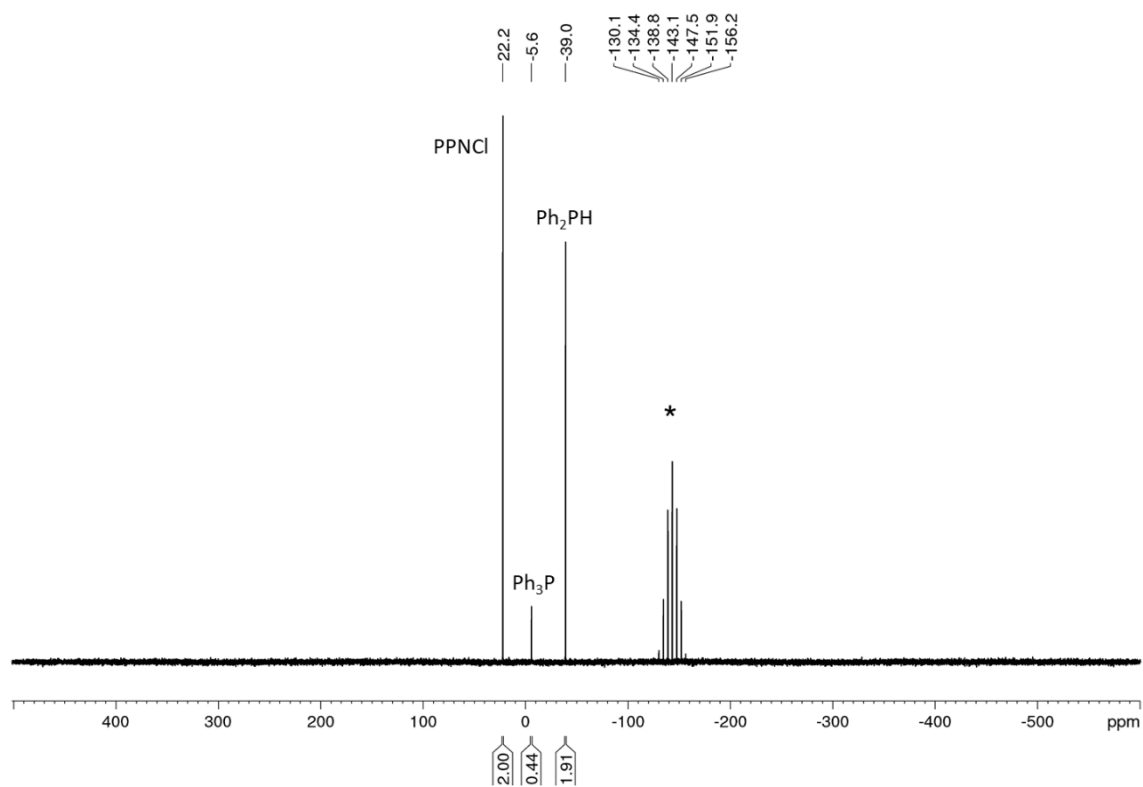


Figure S57. $^{31}\text{P}\{^1\text{H}\}$ NMR spectrum of calibration 2 (Table S5, Entry Calibr.2) containing 75% starting material Ph_2PH , 25% product Ph_3P and 50% internal standard PPNCI. * marks electrolyte TBAPF_6 .

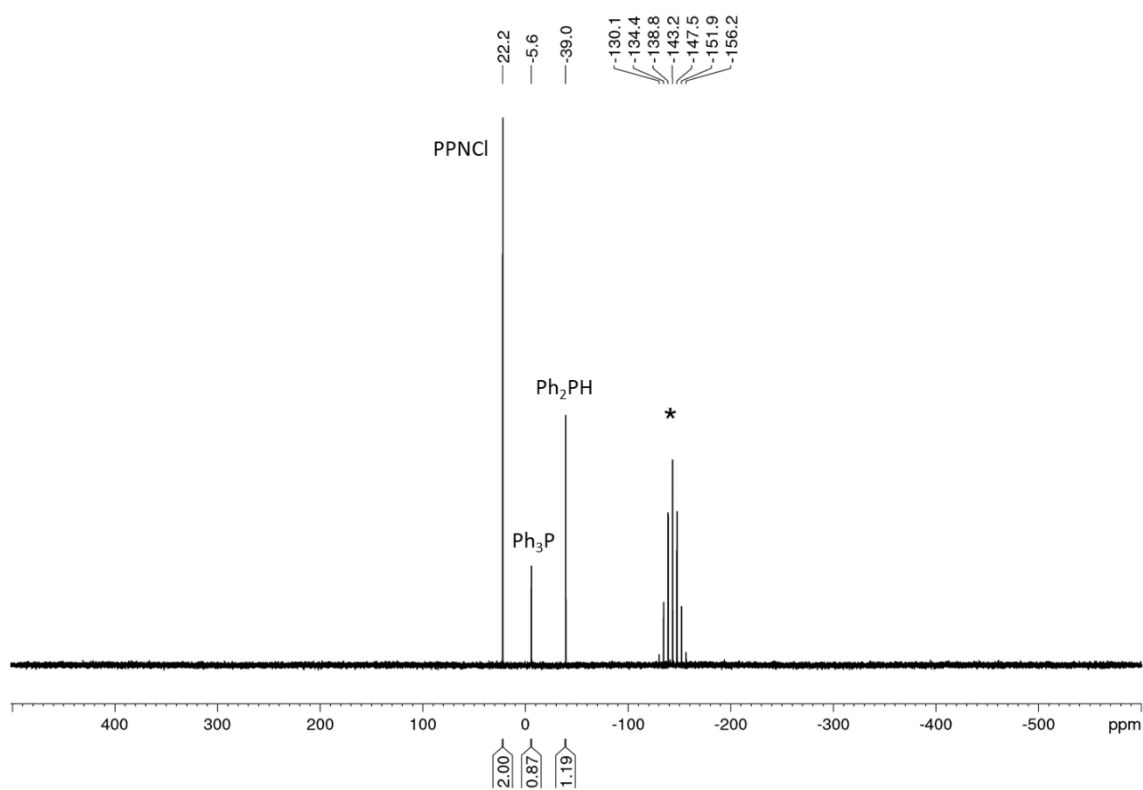


Figure S58. $^{31}\text{P}\{^1\text{H}\}$ NMR spectrum of calibration 3 (Table S5, Entry Calibr.3) containing 50% starting material Ph_2PH , 50% product Ph_3P and 50% internal standard PPNCI. * marks electrolyte TBAPF_6 .

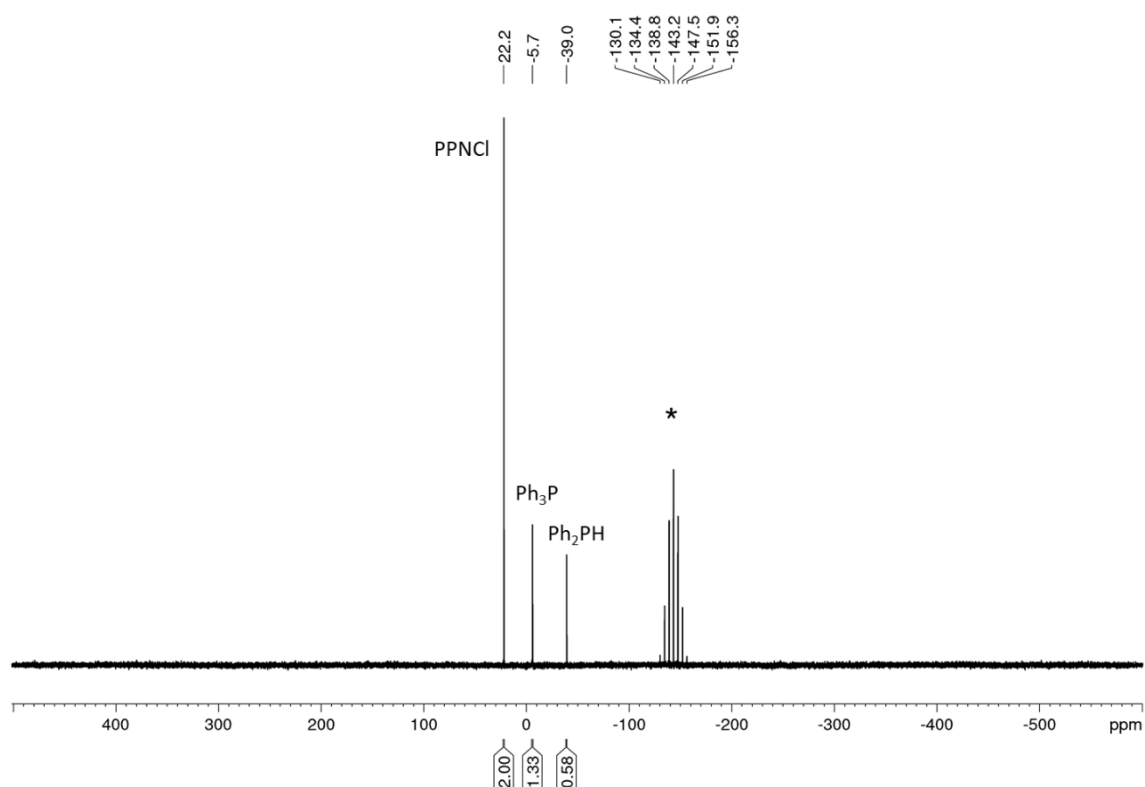


Figure S59. $^{31}\text{P}\{^1\text{H}\}$ NMR spectrum of calibration 4 (Table S5, Entry Calibr.4) containing 25% starting material Ph_2PH , 75% product Ph_3P and 50% internal standard PPNCI. * marks electrolyte TBAPF₆.

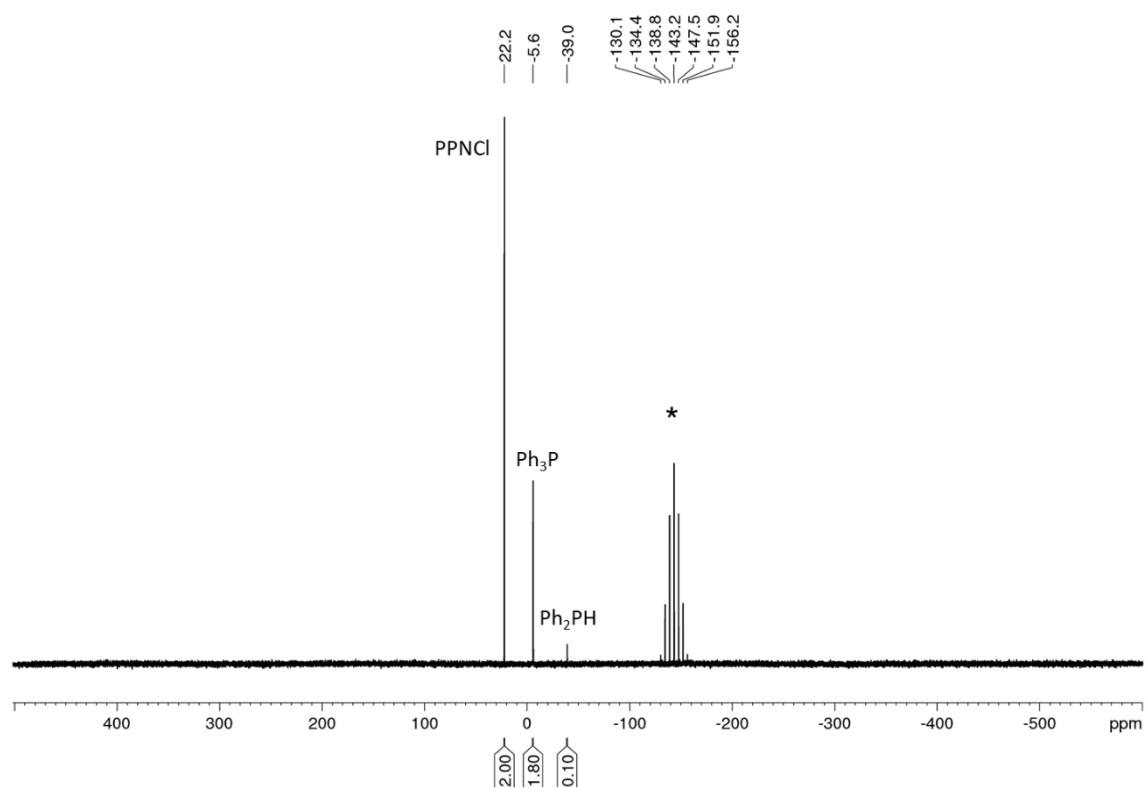
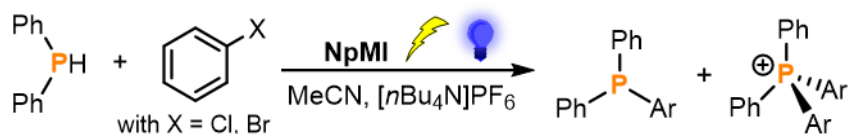


Figure S60. $^{31}\text{P}\{^1\text{H}\}$ NMR spectrum of calibration 5 (Table S5, Entry Calibr.5) containing 5% starting material Ph_2PH , 95% product Ph_3P and 50% internal standard PPNCI. * marks electrolyte TBAPF₆.

S2.3.3.2 Quantification of photoelectrochemical functionalization of Ph₂PH mediated by NpMI



All preparation steps were carried out in a glovebox under inert gas atmosphere. An oven-dried H-cell was equipped with magnetic stirring bars in both chambers. To the cathodic chamber was added organic halide (1.0 mmol, PhCl or PhBr), e-PRCat **NpMI** (0.05 mmol, 17.84 mg, 5 mol% per substrate molecule), and Ph₂PH (0.1 mmol, 17.4 μL), followed by the additions of [nBu₄N]PF₆ (0.1 mmol, 38.74 mg, TBAPF₆) and MeCN (4 mL) in both chambers (resulting in 0.025 M [nBu₄N]PF₆ in MeCN as solvent). Both chambers were sealed using rubber septa pierced with wire-connected electrodes (Figure S1). The resulting mixture was stirred at room temperature above a water-cooled cooling block under irradiation of blue LED (450 nm) from beneath the cathodic chamber (Figure S2). A constant potential was applied across the cell (see Table S8). After irradiation for 21h, the mixtures in both chambers were combined, PPnCl (0.05 mmol, 28.7 mg) was added as an internal standard and the reaction mixture was subjected to ³¹P{¹H} NMR analysis (Table S8).

Table S8. Reductive photoelectrochemistry with **NpMI** – Quantitative NMR with PPnCl.

Entry	NpMI [mol%]	Substrate	Potential [V]	Electrodes	Full conv. of Ph ₂ PH?	Conv. to Ph ₃ P [%]	Conv. to [Ph ₄ P]Cl [%]
1	5	PhCl	1.6	Zn (+) / Fe (-)	✓	0	0
2	5	PhCl	1.6	Zn (+) / C _{foam} (-)	✗	0	2
3	5	PhBr	1.6	Zn (+) / Fe (-)	✓	0	13
4	5	PhBr	1.6	Zn (+) / C _{foam} (-)	✗	0	2
5	5	PhBr	1.6	Zn (+) / Fe (-)	✓	0	5
6	5	PhBr	1.6	Zn (+) / Fe (-)	✓	0	4
7	5	PhBr	1.3	Zn (+) / Fe (-)	✗	2	6
8	5	PhBr	1.3	Zn (+) / Fe (-)	✗	3	7
9 ^[a]	5	PhBr	1.6	Zn (+) / Fe (-)	✗	11	7

[a] A 1:1 ratio of Ph₂PH and substrate PhBr was used instead of an excess of 10 equiv.

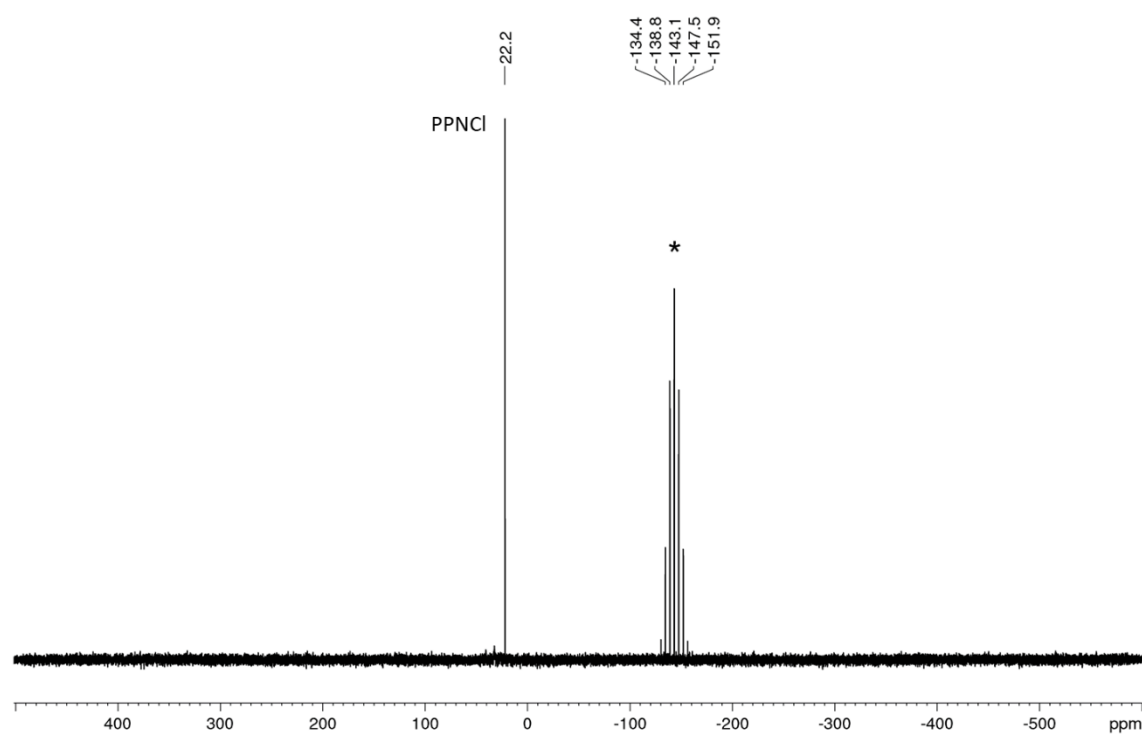


Figure S61. Quantitative $^{31}\text{P}\{^1\text{H}\}$ NMR spectrum for the photoelectrocatalytic functionalization of Ph_2PH into $[\text{Ph}_2\text{Ar}_2\text{P}]\text{Cl}$ and Ph_2ArP using **NpMI** (Table 8, Entry 1, 5 mol% **NpMI**, PhCl , blue LED (455 nm), TBAPF_6 (*), 1.60 V, Zn (+) / Fe (-)). PPNCl was added as an internal standard (0.05 mmol).

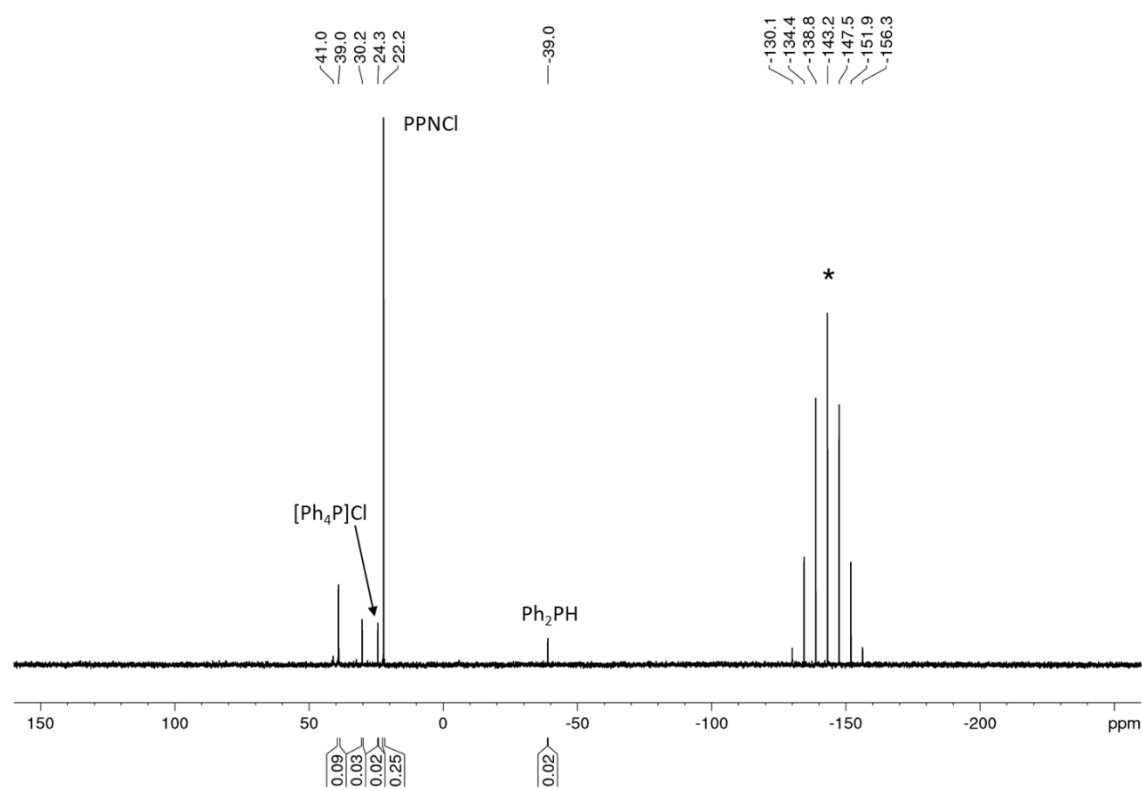


Figure S62. Quantitative $^{31}\text{P}\{^1\text{H}\}$ NMR spectrum for the photoelectrocatalytic functionalization of Ph_2PH into $[\text{Ph}_2\text{Ar}_2\text{P}]\text{Cl}$ and Ph_2ArP using **NpMI** (Table 8, Entry 2, 5 mol% **NpMI**, PhCl , blue LED (455 nm), TBAPF_6 (*), 1.60 V, $\text{Zn (+) / C}_{\text{foam}} (-)$). PPNCl was added as an internal standard (0.05 mmol).

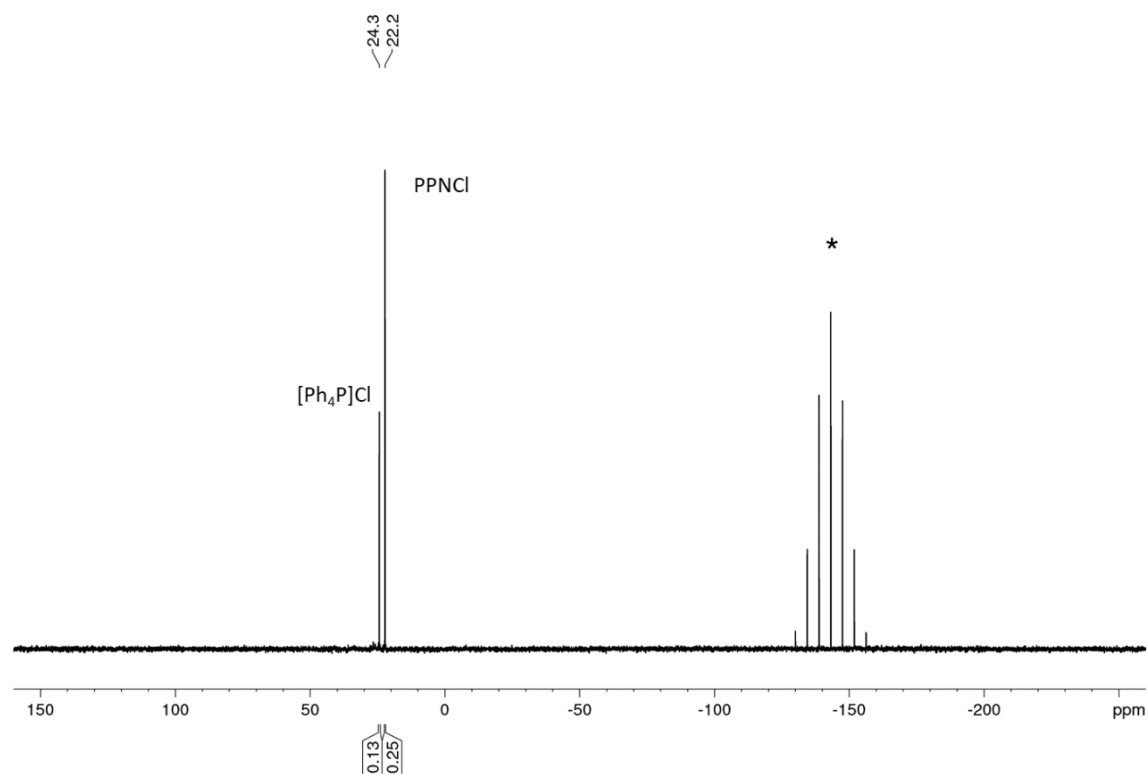


Figure S63. Quantitative $^{31}\text{P}\{^1\text{H}\}$ NMR spectrum for the photoelectrocatalytic functionalization of Ph_2PH into $[\text{Ph}_2\text{Ar}_2\text{P}]\text{Cl}$ and Ph_2ArP using **NpMI** (Table 8, Entry 3, 5 mol% **NpMI**, PhBr , blue LED (455 nm), TBAPF_6 (*), 1.60 V, Zn (+) / Fe (-)). PPNCI was added as an internal standard (0.05 mmol).

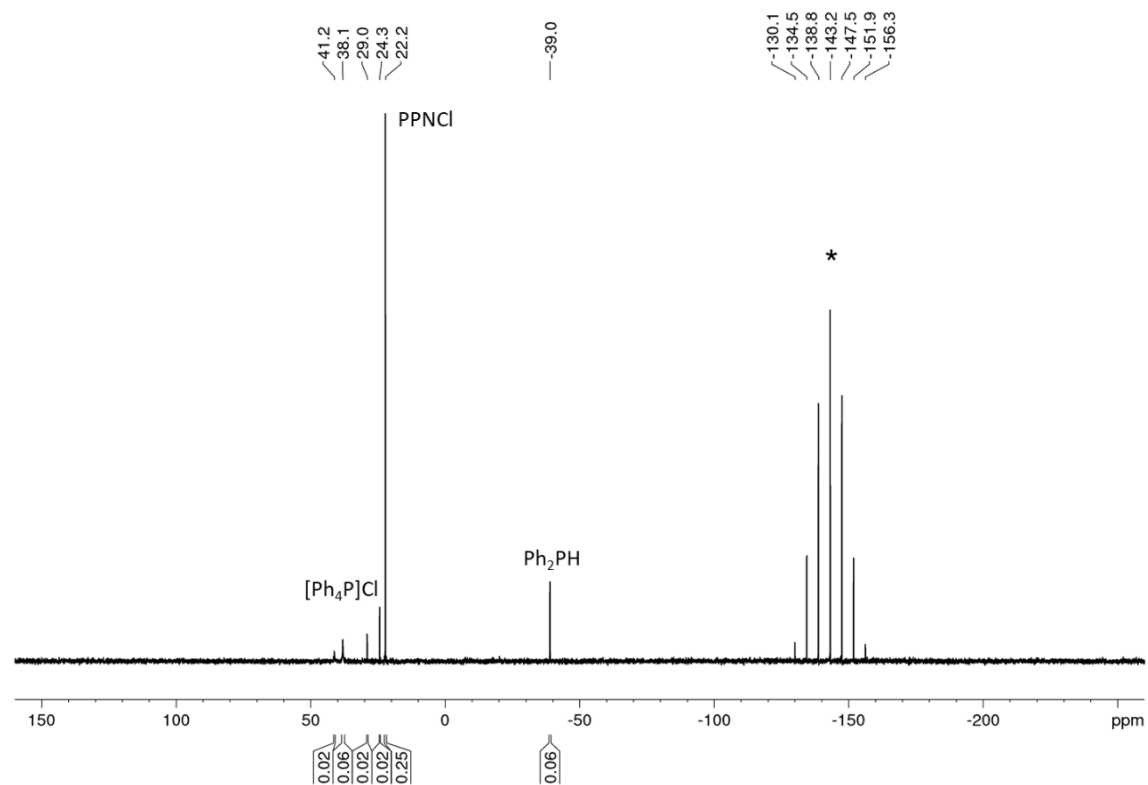


Figure S64. Quantitative $^{31}\text{P}\{^1\text{H}\}$ NMR spectrum for the photoelectrocatalytic functionalization of Ph_2PH into $[\text{Ph}_2\text{Ar}_2\text{P}]\text{Cl}$ and Ph_2ArP using **NpMI** (Table 8, Entry 4, 5 mol% **NpMI**, PhBr , blue LED (455 nm), TBAPF_6 (*), 1.60 V, $\text{Zn (+) / C}_{\text{foam}} (-)$). PPNCI was added as an internal standard (0.05 mmol).

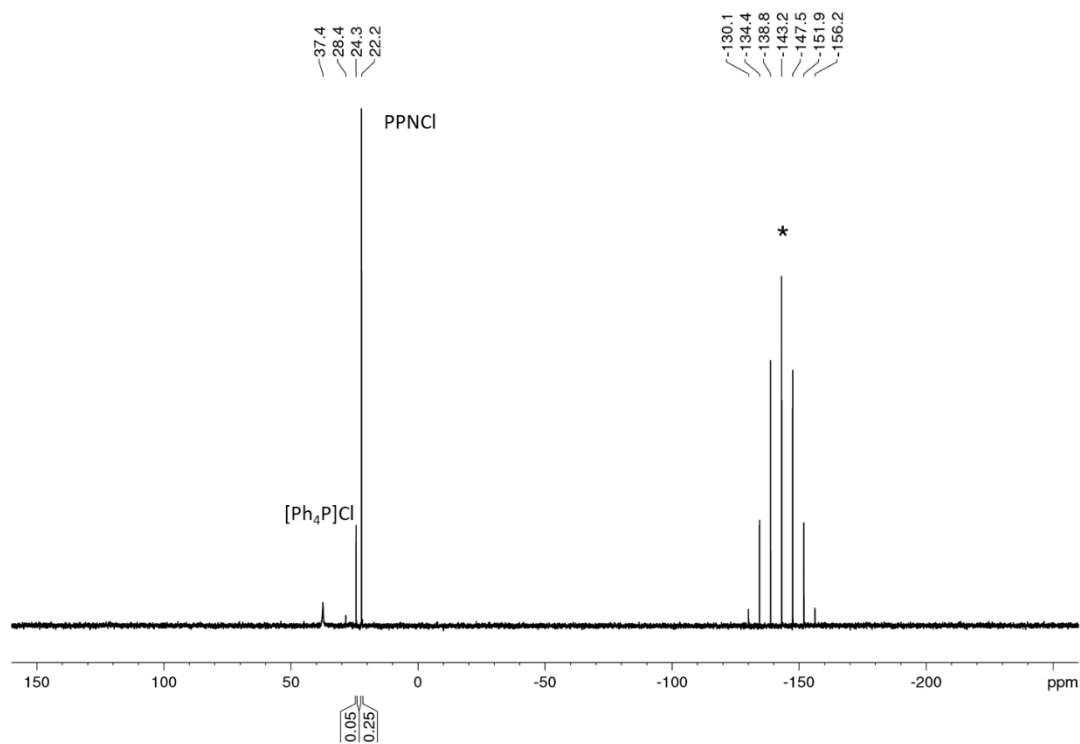


Figure S65. Quantitative $^{31}\text{P}\{^1\text{H}\}$ NMR spectrum for the photoelectrocatalytic functionalization of Ph_2PH into $[\text{Ph}_2\text{Ar}_2\text{P}]\text{Cl}$ and Ph_2ArP using **NpMI** (Table 8, Entry 5, 5 mol% **NpMI**, PhBr, blue LED (455 nm), TBAPF_6 (*), 1.60 V, Zn (+) / Fe (-). PPNCI was added as an internal standard (0.05 mmol).

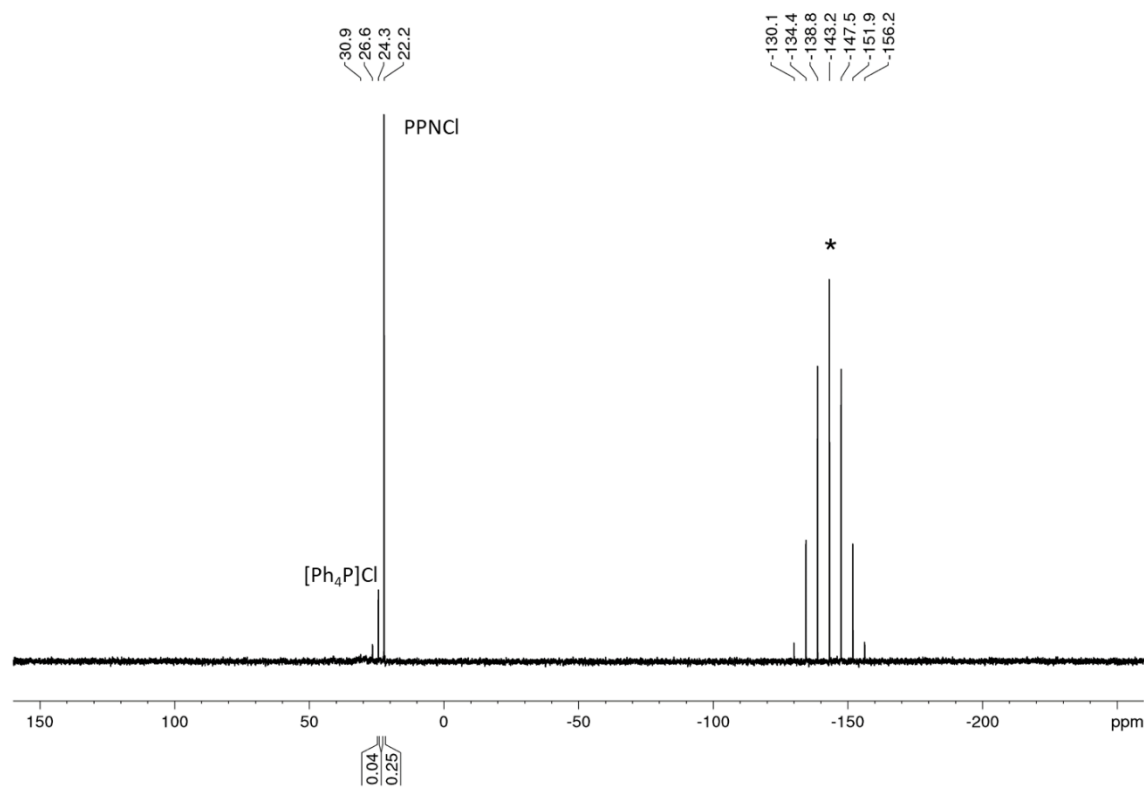


Figure S66. Quantitative $^{31}\text{P}\{^1\text{H}\}$ NMR spectrum for the photoelectrocatalytic functionalization of Ph_2PH into $[\text{Ph}_2\text{Ar}_2\text{P}]\text{Cl}$ and Ph_2ArP using **NpMI** (Table 8, Entry 6, 5 mol% **NpMI**, PhBr, blue LED (455 nm), TBAPF_6 (*), 1.60 V, Zn (+) / Fe (-). PPNCI was added as an internal standard (0.05 mmol).

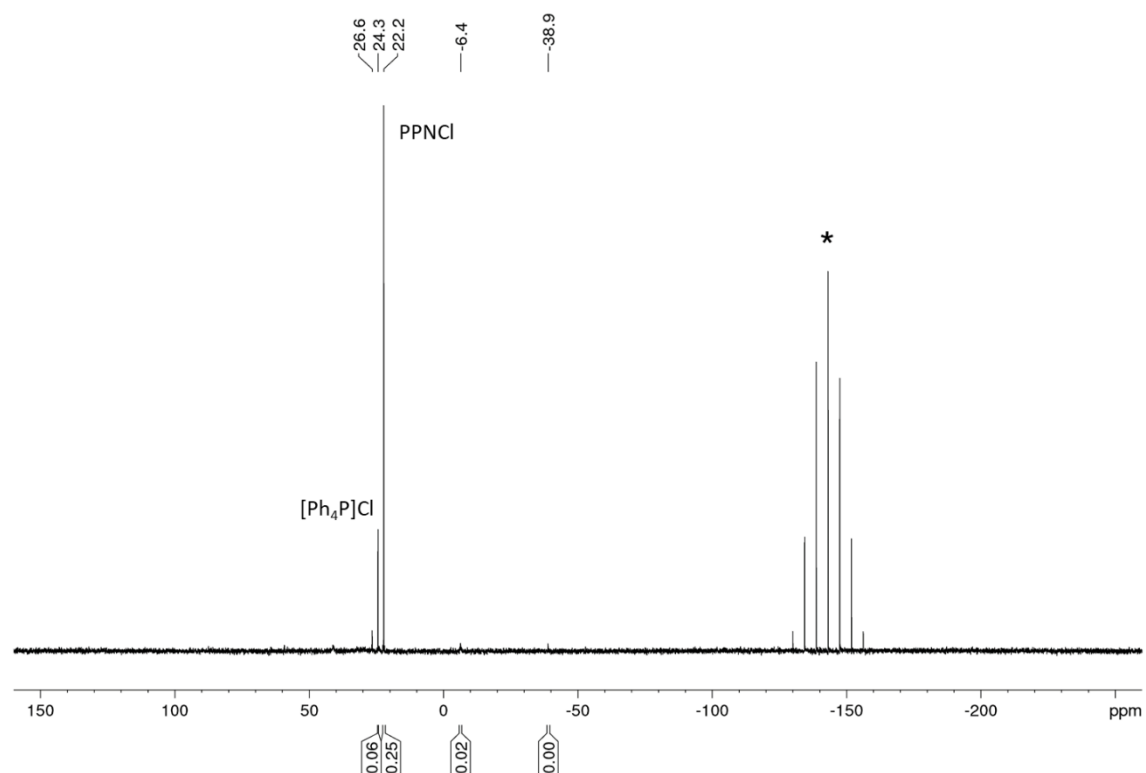


Figure S67. Quantitative $^{31}\text{P}\{^1\text{H}\}$ NMR spectrum for the photoelectrocatalytic functionalization of Ph₂PH into [Ph₂Ar₂P]Cl and Ph₂ArP using **NpMI** (Table 8, Entry 7, 5 mol% **NpMI**, PhBr, blue LED (455 nm), TBAPF₆ (*), 1.30 V, Zn (+) / Fe (-). PPNCI was added as an internal standard (0.05 mmol).

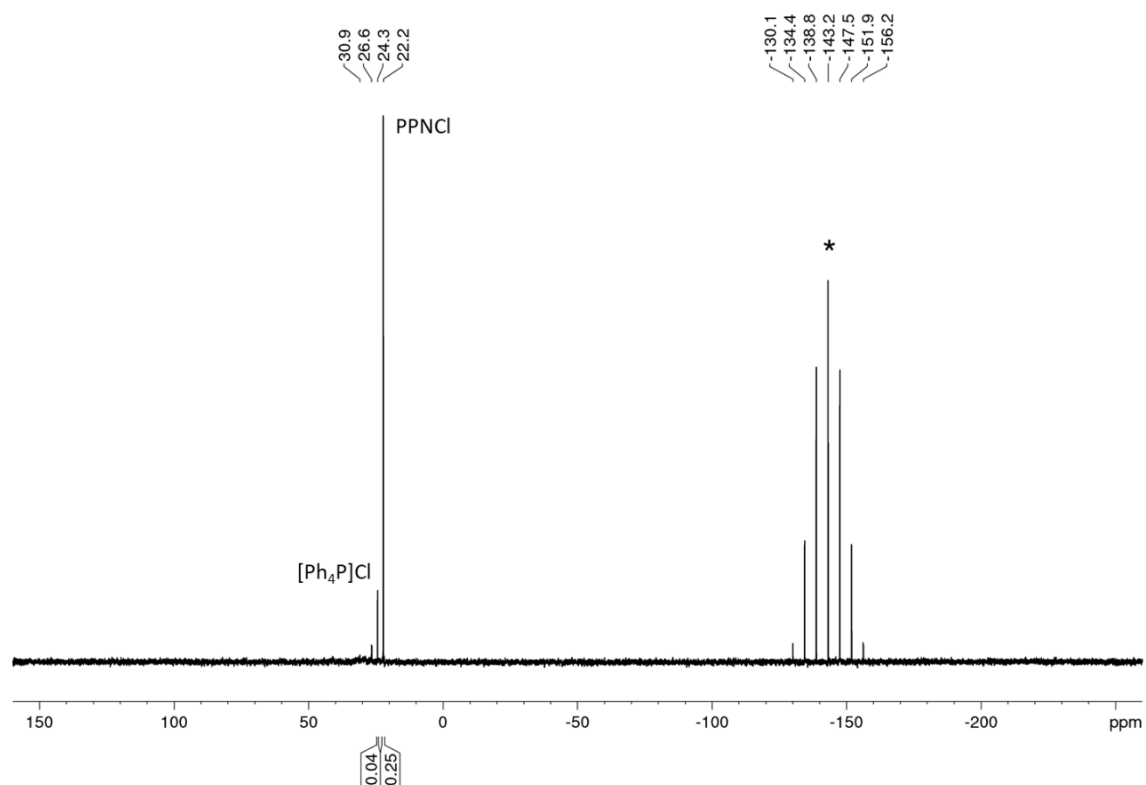


Figure S68. Quantitative $^{31}\text{P}\{^1\text{H}\}$ NMR spectrum for the photoelectrocatalytic functionalization of Ph₂PH into [Ph₂Ar₂P]Cl and Ph₂ArP using **NpMI** (Table 8, Entry 8, 5 mol% **NpMI**, PhBr, blue LED (455 nm), TBAPF₆ (*), 1.30 V, Zn (+) / Fe (-). PPNCI was added as an internal standard (0.05 mmol).

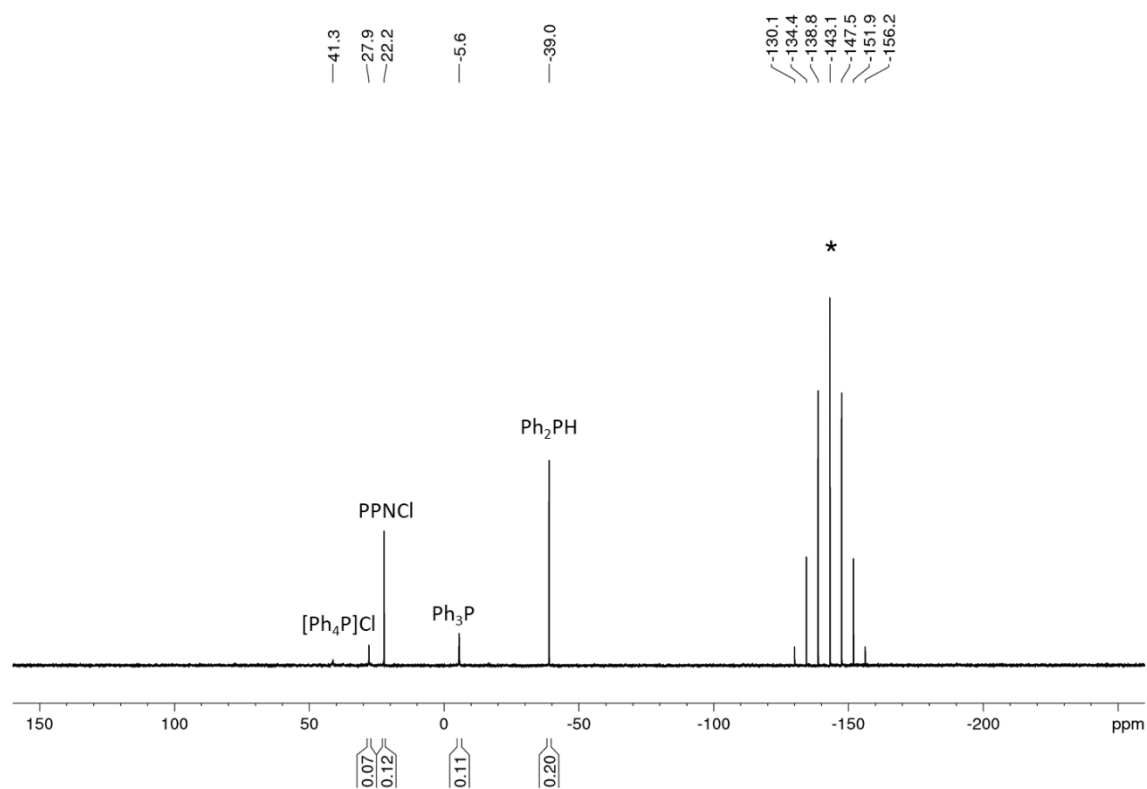
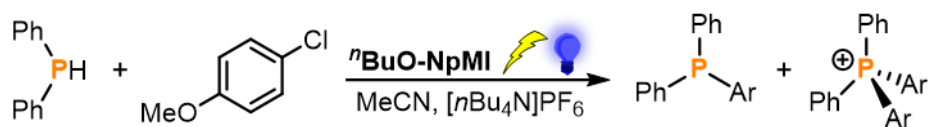


Figure S69. Quantitative $^{31}\text{P}\{^1\text{H}\}$ NMR spectrum for the photoelectrocatalytic functionalization of Ph_2PH into $[\text{Ph}_2\text{Ar}_2\text{P}]\text{Cl}$ and Ph_2ArP using **NpMI** (Table 8, Entry 9, 5 mol% **NpMI**, PhBr, blue LED (455 nm), TBAPF₆ (*), 1.60 V, Zn (+) / Fe (-). PPnCl was added as an internal standard (0.05 mmol). A 1:1 ratio of Ph_2PH and substrate PhBr was used instead of an excess of 10 equiv.

S2.4 Photoelectrochemical functionalization of Ph₂PH mediated by e-PRCat naphthalene-imide derivative ⁿBuO-NpMI



All preparation steps were carried out in a glovebox under inert gas atmosphere. An oven-dried H-cell was equipped with magnetic stirring bars in both chambers. To the cathodic chamber was added organic halide (1.0 mmol, ClC₆H₄-4-OMe, PhCl or PhBr), e-PRCat ⁿBuO-NpMI (0.05 mmol, 17.3 mg, 5 mol% per substrate molecule), and Ph₂PH (0.1 mmol, 17.4 μL), followed by the additions of [nBu₄N]PF₆ (0.1 mmol, 38.74 mg, TBAPF₆) and MeCN (4 mL) in both chambers (resulting in 0.025 M [nBu₄N]PF₆ in MeCN as solvent). Both chambers were sealed using rubber septa pierced with wire-connected electrodes (Figure S1). The resulting mixture was stirred at room temperature above a water-cooled cooling block under irradiation of blue LED (455 nm) from beneath the cathodic chamber (Figure S3). A constant potential was applied across the cell (see Table S9). After irradiation for 21h, the mixtures in both chambers were combined and subjected to ³¹P{¹H} NMR analysis. For the reactions without additional internal standard a ratio of the starting material Ph₂PH (³¹P{¹H}, integral = 1) and the corresponding products is given (Table S9, Entry 1 & 4). For quantification of selected reactions PPh₃ or PPNCl, respectively, was added as internal standard and the determined ³¹P{¹H} NMR yields are shown in Table S9 (Entry 7 & 8).

S2.4.1 Optimization of reaction conditions

Table S9. Photoelectrocatalytic functionalization of Ph₂PH into [Ph₂Ar₂P]Cl and Ph₂ArP using ⁿBuO-NpMI.

Entry	ⁿ BuO-NpMI [mol%]	Substrate	Potential [V]	Electrodes	Ratio of Ph ₂ PH to Ph ₂ ArP	Ratio of Ph ₂ PH to [Ph ₂ Ar ₂ P]Cl
1 ^[a]	5	ClC ₆ H ₄ -4-OMe	1.6	Zn (+) / Fe (-)	19% Ph ₂ PH, 10% Ph ₂ ArP	13% [Ph ₂ Ar ₂]Cl
2	5	PhCl	1.6	Zn (+) / Fe (-)	1 : 1.31	1 : 1.55
3	5	PhBr	1.6	Zn (+) / Fe (-)	1 : 0	1 : 0.37
4 ^[a]	5	ClC ₆ H ₄ -4-OMe	1.6	Zn (+) / C _{foam} (-)	43% Ph ₂ PH, 42% Ph ₂ ArP	17% [Ph ₂ Ar ₂]Cl
5	5	PhCl	1.6	Zn (+) / C _{foam} (-)	1 : 2.65	1 : 9.58
6	5	PhBr	1.6	Zn (+) / C _{foam} (-)	1 : 3.62	1 : 6.90
7 ^[b]	5	PhCl	1.6	Zn (+) / C _{foam} (-)	no Ph ₂ PH, 2% Ph ₃ P	no Ph ₂ PH, no product
8 ^[b]	5	PhBr	1.6	Zn (+) / C _{foam} (-)	no Ph ₃ P	8% Ph ₂ PH, 1% [Ph ₄ P]Cl

[a] Ph₃P (0.05 mmol) was added as an internal standard. [b] PPNCl (0.05 mmol) was added as an internal standard.

S2.4.2 $^{31}\text{P}\{^1\text{H}\}$ NMR spectra of reductive photoelectrochemistry using $^n\text{BuO-NpMI}$

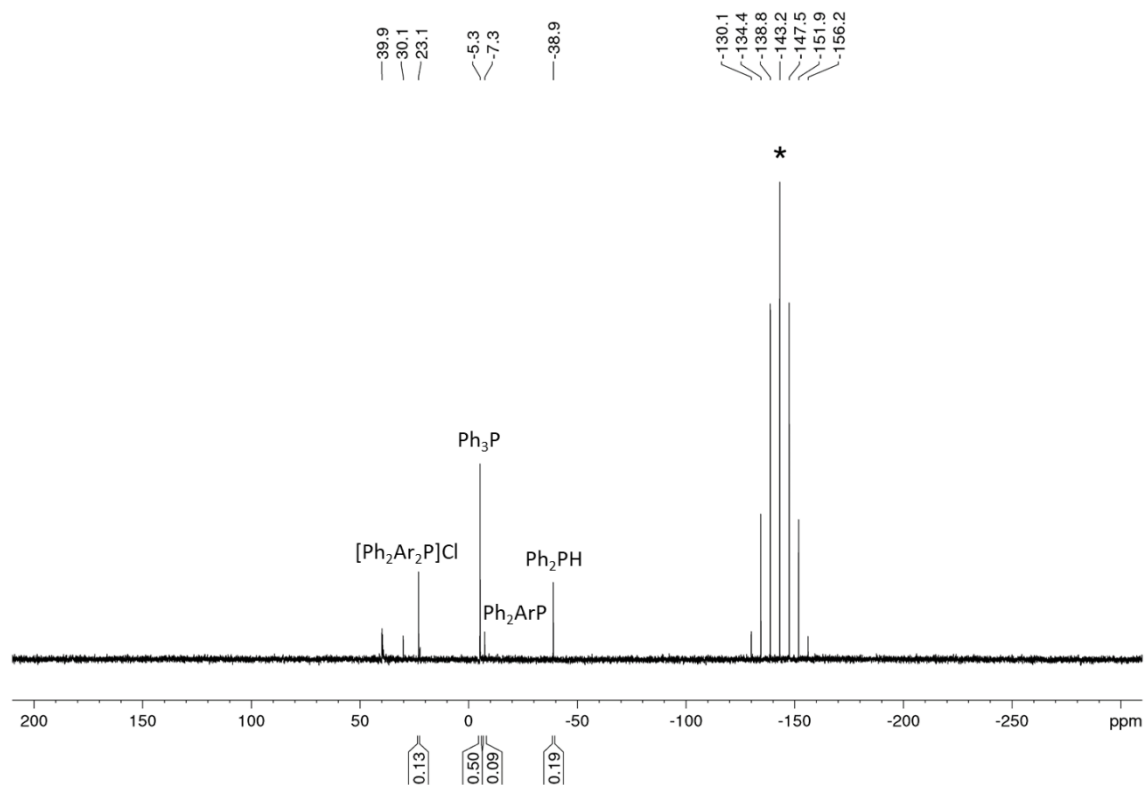


Figure S70. $^{31}\text{P}\{^1\text{H}\}$ NMR spectrum for the photoelectrocatalytic functionalization of Ph_2PH into $[\text{Ph}_2\text{Ar}_2\text{P}]\text{Cl}$ and Ph_2ArP using $^n\text{BuO-NpMI}$ (Table 9, Entry 1, 5 mol% $^n\text{BuO-NpMI}$, $\text{ClC}_6\text{H}_4\text{-4-OMe}$, blue LED (455 nm), TBAPF_6 (*), 1.60 V, Zn (+) / Fe (-). Ph_3P (0.05 mmol) was added as an internal standard.

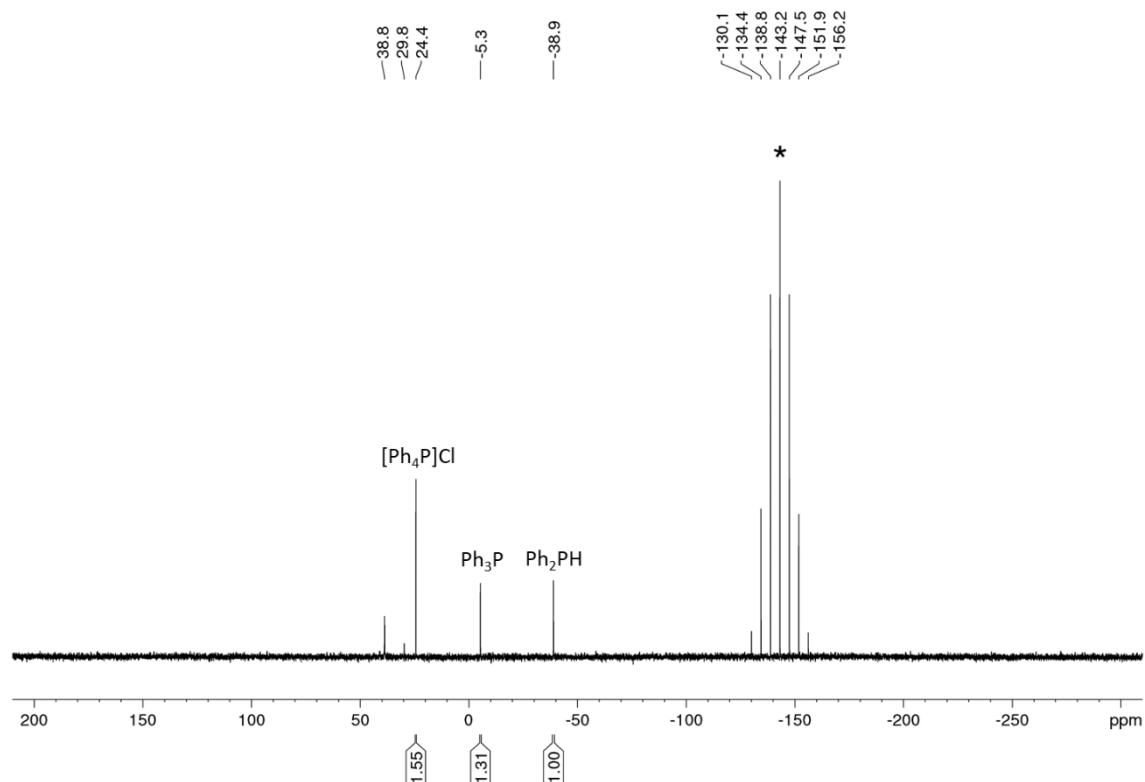


Figure S71. $^{31}\text{P}\{^1\text{H}\}$ NMR spectrum for the photoelectrocatalytic functionalization of Ph_2PH into $[\text{Ph}_2\text{Ar}_2\text{P}]\text{Cl}$ and Ph_2ArP using $^n\text{BuO-NpMI}$ (Table 9, Entry 2, 5 mol% $^n\text{BuO-NpMI}$, PhCl , blue LED (455 nm), TBAPF_6 (*), 1.60 V, Zn (+) / Fe (-).

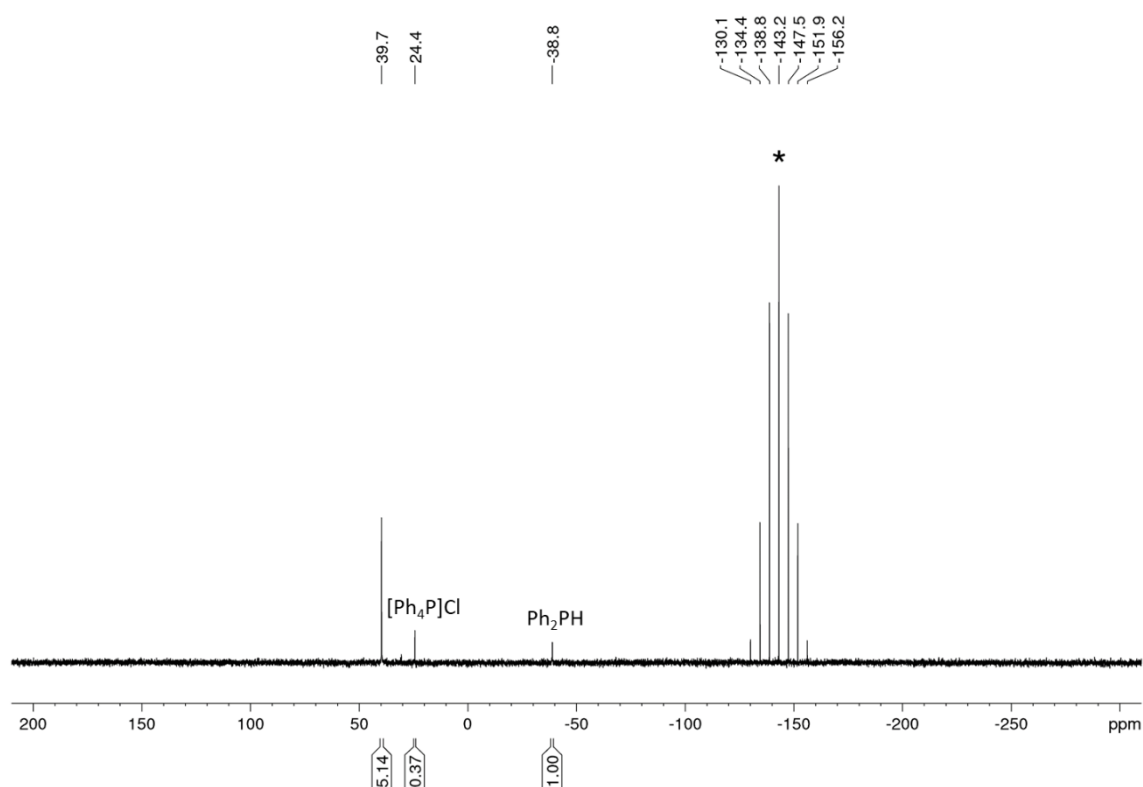


Figure S72. $^{31}\text{P}\{^1\text{H}\}$ NMR spectrum for the photoelectrocatalytic functionalization of Ph_2PH into $[\text{Ph}_2\text{Ar}_2\text{P}]\text{Cl}$ and Ph_2ArP using ***t*BuO-NpMI** (Table 9, Entry 3, 5 mol% ***t*BuO-NpMI**, PhBr, blue LED (455 nm), TBAPF₆ (*), 1.60 V, Zn (+) / Fe (-).

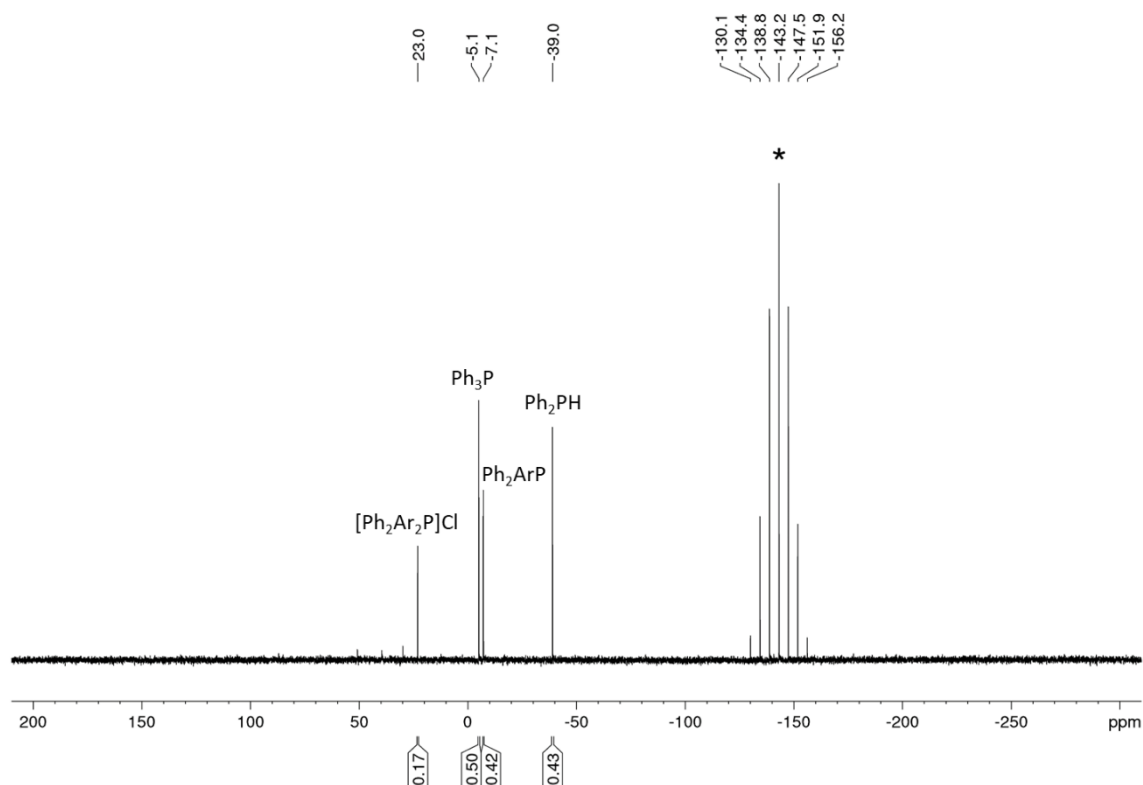


Figure S73. $^{31}\text{P}\{^1\text{H}\}$ NMR spectrum for the photoelectrocatalytic functionalization of Ph_2PH into $[\text{Ph}_2\text{Ar}_2\text{P}]\text{Cl}$ and Ph_2ArP using ***t*BuO-NpMI** (Table 9, Entry 4, 5 mol% ***t*BuO-NpMI**, $\text{ClC}_6\text{H}_4\text{-4-OMe}$, blue LED (455 nm), TBAPF₆ (*), 1.60 V, Zn (+) / C_{foam} (-). Ph_3P (0.05 mmol) was added as an internal standard.

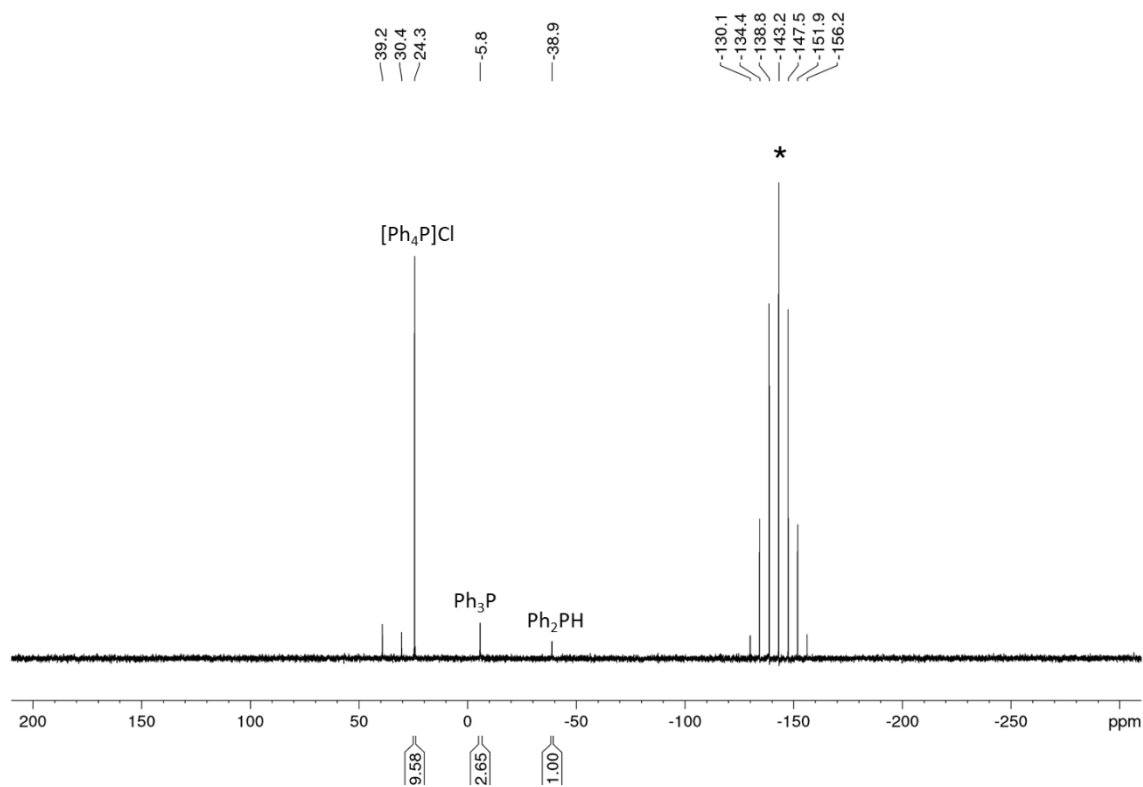


Figure S74. $^{31}\text{P}\{^1\text{H}\}$ NMR spectrum for the photoelectrocatalytic functionalization of Ph_2PH into $[\text{Ph}_2\text{Ar}_2\text{P}]\text{Cl}$ and Ph_2ArP using $^n\text{BuO-NpMI}$ (Table 9, Entry 5, 5 mol% $^n\text{BuO-NpMI}$, PhCl , blue LED (455 nm), TBAPF_6 (*), 1.60 V, $\text{Zn (+) / C}_{\text{foam}} (-)$.

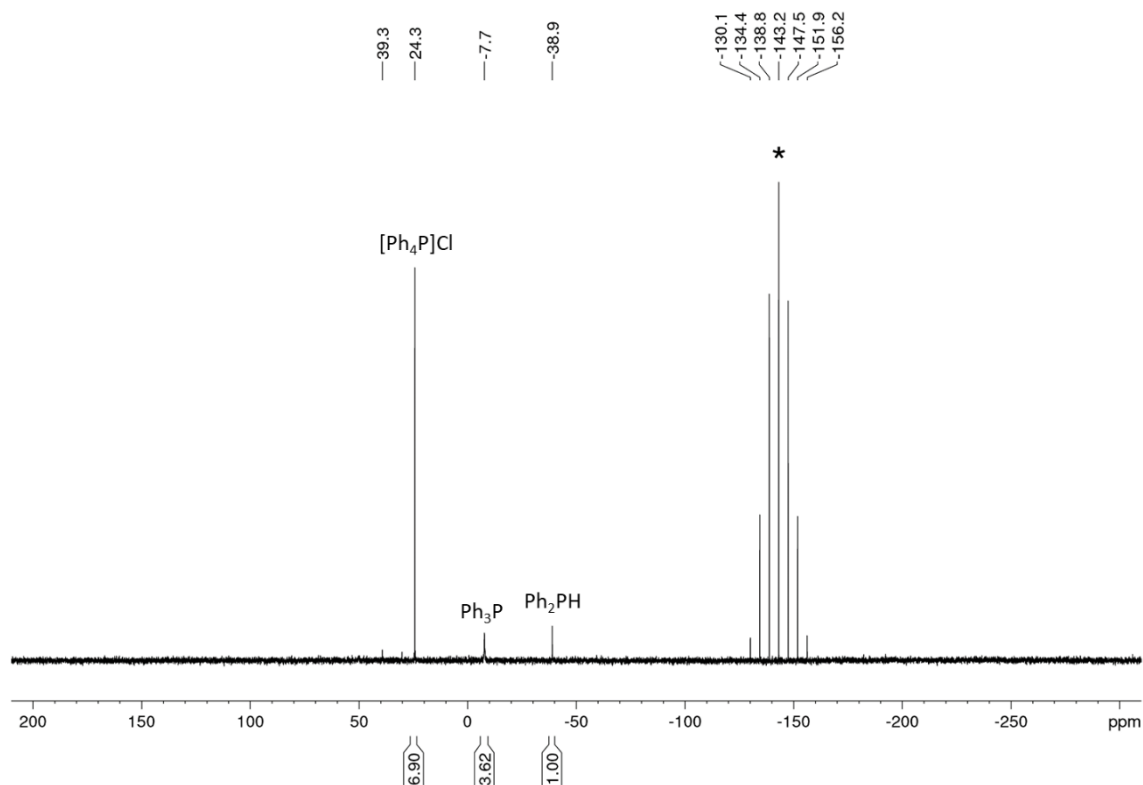


Figure S75. $^{31}\text{P}\{^1\text{H}\}$ NMR spectrum for the photoelectrocatalytic functionalization of Ph_2PH into $[\text{Ph}_2\text{Ar}_2\text{P}]\text{Cl}$ and Ph_2ArP using $^n\text{BuO-NpMI}$ (Table 9, Entry 6, 5 mol% $^n\text{BuO-NpMI}$, PhBr , blue LED (455 nm), TBAPF_6 (*), 1.60 V, $\text{Zn (+) / C}_{\text{foam}} (-)$.

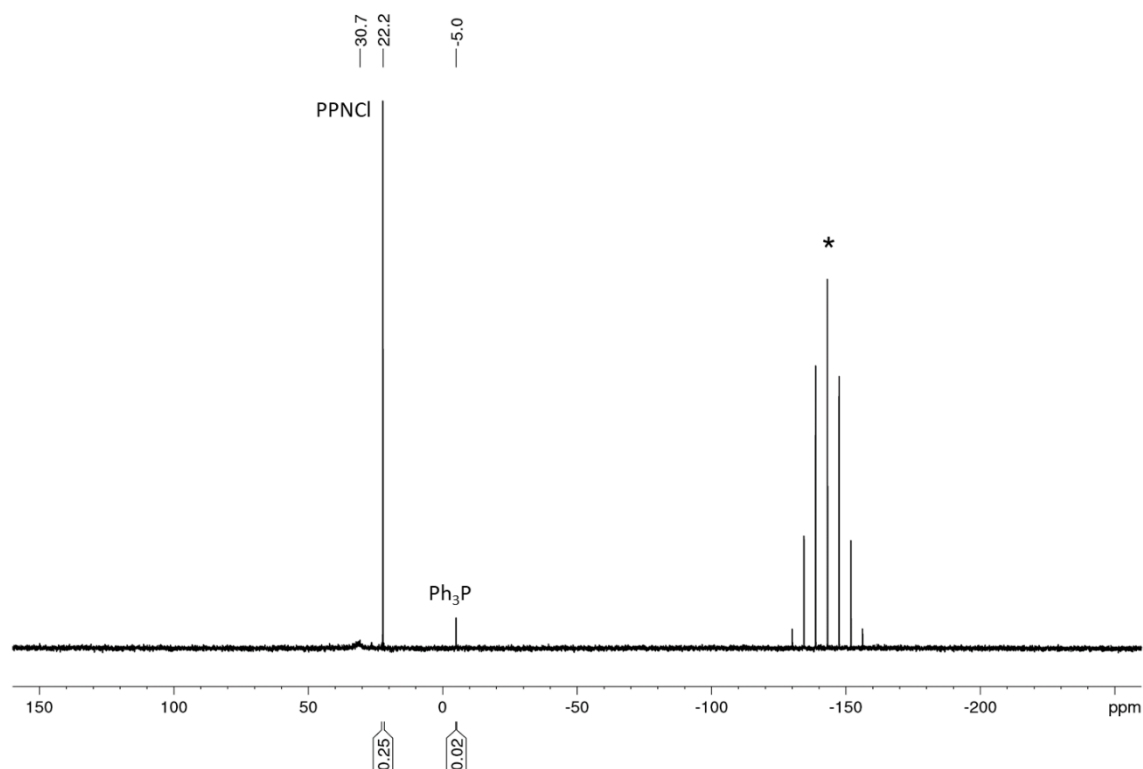


Figure S76. $^{31}\text{P}\{^1\text{H}\}$ NMR spectrum for the photoelectrocatalytic functionalization of Ph_2PH into $[\text{Ph}_2\text{Ar}_2\text{P}]\text{Cl}$ and Ph_2ArP using **BuO-NpMI** (Table 9, Entry 7, 5 mol% **BuO-NpMI**, PhCl , blue LED (455 nm), TBAPF_6 (*), 1.60 V, Zn (+) / C_{foam} (-). PPNCI (0.05 mmol) was added as an internal standard.

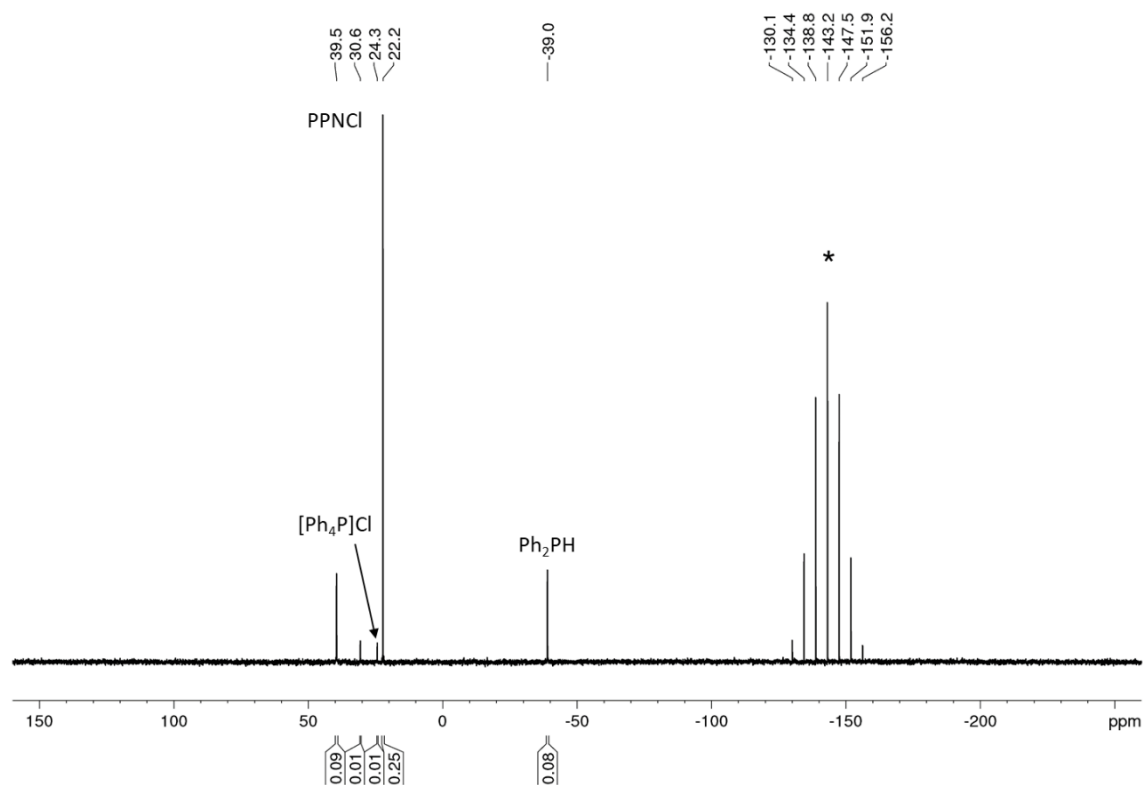
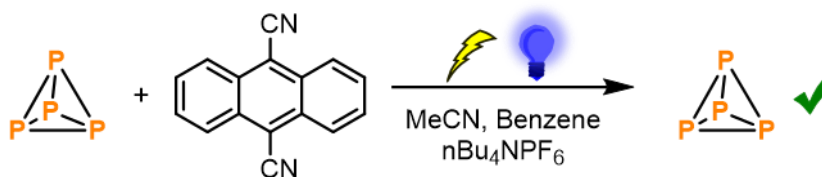


Figure S77. $^{31}\text{P}\{^1\text{H}\}$ NMR spectrum for the photoelectrocatalytic functionalization of Ph_2PH into $[\text{Ph}_2\text{Ar}_2\text{P}]\text{Cl}$ and Ph_2ArP using **BuO-NpMI** (Table 9, Entry 8, 5 mol% **BuO-NpMI**, PhBr , blue LED (455 nm), TBAPF_6 (*), 1.60 V, Zn (+) / C_{foam} (-). PPNCI (0.05 mmol) was added as an internal standard.

S3. Attempted arylation of white phosphorus via reductive photoelectrochemical activation of 4-chloroanisole

S3.1 Stability of P₄ in the presence of excited DCA radical anion ([DCA^{•-}])*



The stability of P₄ in the presence of e-PRCat **DCA**, and especially its strong reducing form of the excited radical anion [DCA^{•-}]*, was investigated by a stoichiometric photoelectrochemical reaction. All preparation steps were carried out in a glovebox under inert gas atmosphere. An oven-dried H-cell was equipped with magnetic stirring bars in both chambers. To the cathodic chamber was added e-PRCat **DCA** (0.04 mmol, 9.1 mg), and P₄ (0.04 mmol, 4.96 mg), followed by the additions of [nBu₄N]PF₆ (0.04 mmol, 15.5 mg) and a solvent mixture of MeCN (3 mL) and benzene (1 mL) in both chambers (resulting in 0.01 M [nBu₄N]PF₆ in MeCN/benzene). Both chambers were sealed using rubber septa pierced with electrodes (Figure S78, Zn (+) / C_{lead} (-)). The resulting yellow suspension was stirred at room temperature above a water-cooled cooling block under irradiation of blue LED (455 nm) from beneath the cathodic chamber (Figure S78 [1]). A constant potential of 2.55 V was applied across the cell (see Table S10, Entry 1). After irradiation and applying potential for 30 minutes the color of the cathodic chamber changed from yellow to violet (still undissolved yellow solid of **DCA**) (Figure S78 [2]) which indicates the formation of excited radical anion [DCA^{•-}]*. The photoelectrochemical reaction showed a dark violet solution after 18 h (Figure S78 [3]). ³¹P{¹H} NMR analysis showed P₄ has not degraded in the presence of the strong reducing agent [DCA^{•-}]* (Figure S80).

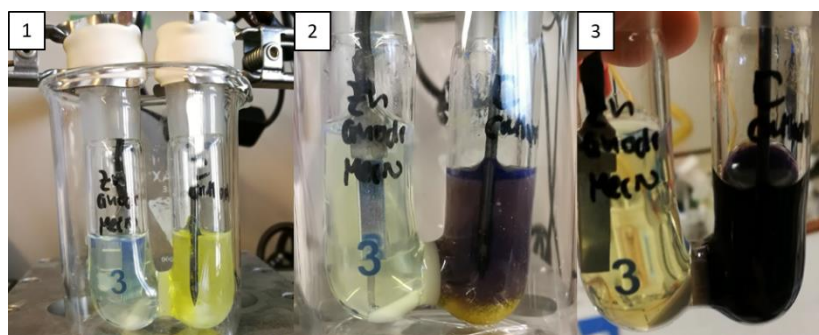
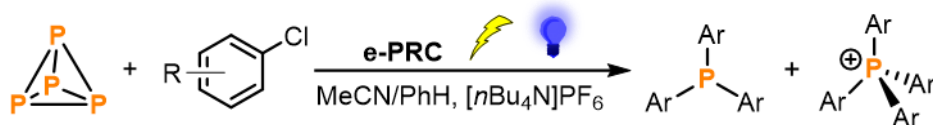


Figure S78. Stability test of P₄ in presence of excited **DCA** radical anion [DCA^{•-}]* as a strong reducing agent. [1] The cathodic chamber containing e-PRCat **DCA**, P₄, electrolyte TBAPF₆ and pencil lead as an electrode shows a yellow MeCN/benzene suspension (bad solubility of **DCA**). [2] Applying constant potential (2.55 V) and irradiation with blue light (455 nm) of the cathodic chamber of the H-cell for 30 minutes the formation of [DCA^{•-}]* was identified by color change to violet. [3] The photoelectrochemical test reaction showed a dark violet solution after 18 h and the ³¹P{¹H} NMR spectrum shows the stability of P₄ under these conditions.

S3.2 Photoelectrochemical arylation of P₄ mediated by e-PRCats



All preparation steps were carried out in a glovebox under inert gas atmosphere. An oven-dried H-cell was equipped with magnetic stirring bars in both chambers. To the cathodic chamber was added 4-chloroanisole (ClC₆H₄-4-OMe, 1.0 mmol, 122 μ L), e-PRC catalyst (0.05 mmol, 3.3 mol% **DCA** (see Figure S79) or 5 mol% **NpMI** per substrate molecule), and P₄ (0.04 mmol, 4.96 mg), followed by the additions of [nBu₄N]PF₆ (0.1 mmol, 38.74 mg) and a solvent mixture of MeCN (4 mL) and benzene (1 mL) in both chambers (resulting in 0.02 M [nBu₄N]PF₆ in MeCN/benzene). Both chambers were sealed using rubber septa pierced with wire-connected electrodes (Figure S1). The resulting mixture was stirred at room temperature above a water-cooled cooling block under irradiation of blue LED (455 nm) from beneath the cathodic chamber (Figure S3). A constant potential was applied across the cell (see Table S8). After irradiation for 21h, the mixtures in both chambers were combined and subjected to ³¹P{¹H} NMR analysis.

Table S10. Photoelectrocatalytic functionalization of P₄ into [Ar₄P]Cl and Ar₃P using e-PRCats **DCA** and **NpMI**.

Entry	e-PRCat [mol%]	Substrate	Potential [V]	Electrodes	Full conv. of P ₄ ?	Product formation?
1	DCA (stoich.)	–	2.55	Zn (+) / C _{lead} (–)	X	–
2	DCA (3.3 mol%)	ClC ₆ H ₄ -4-OMe	1.76	Zn (+) / C _{foam} (–)	✓	–
3	DCA (3.3 mol%)	ClC ₆ H ₄ -4-OMe	1.00	Zn (+) / C _{foam} (–)	✓	–
4	DCA (3.3 mol%)	ClC ₆ H ₄ -4-OMe	1.00	Zn (+) / C _{lead} (–)	X	–
5	NpMI (5 mol%)	ClC ₆ H ₄ -4-OMe	1.60	Zn (+) / Fe (–)	✓	–
6	NpMI (5 mol%)	ClC ₆ H ₄ -4-OMe	1.60	Zn (+) / C _{foam} (–)	X	–

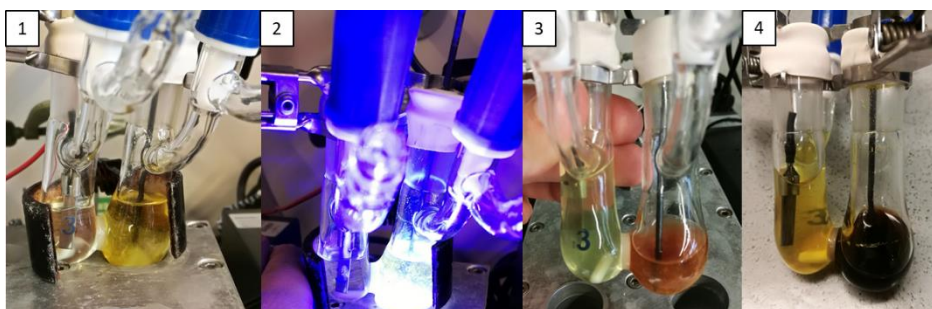


Figure S79. Photoelectrochemical arylation of P₄ with 4-chloroanisole mediated by e-PRCat **DCA**. [1] Setup before irradiation and applied potential. [2] Irradiation of the cathodic chamber and applying constant potential of 1.76 V (see Table 10, Entry 2). [3] Color change to orange brownish solution after 30 minutes of photoelectrochemical reaction, which is caused by generated [DCA^{•-}]. [4] After 21h of irradiation and constant potential the dark brown reaction mixture showed full conversion of P₄ but no product formation.

S3.3 $^{31}\text{P}\{^1\text{H}\}$ NMR spectra of functionalization of P_4 via reductive photoelectrochemical activation of 4-chloroanisole

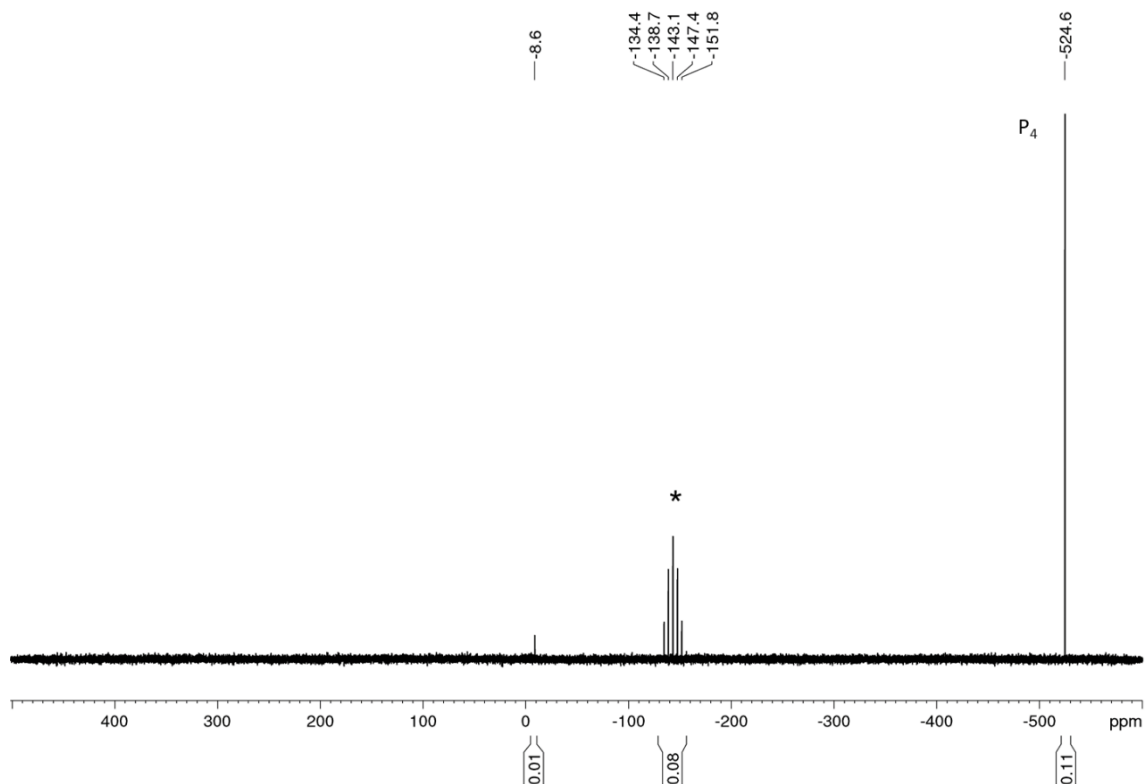


Figure S80. $^{31}\text{P}\{^1\text{H}\}$ NMR spectrum for the control experiment of the photoelectrocatalytic functionalization of P_4 (0.04 mmol) into $[\text{Ph}_2\text{Ar}_2\text{P}]\text{Cl}$ and Ph_2ArP using e-PRCats (Table 10, Entry 1, **DCA (stoichiometric)**, no substrate, blue LED (455 nm), TBAPF_6 (*), 2.55 V, $\text{Zn (+) / C}_{\text{lead}} (-)$.

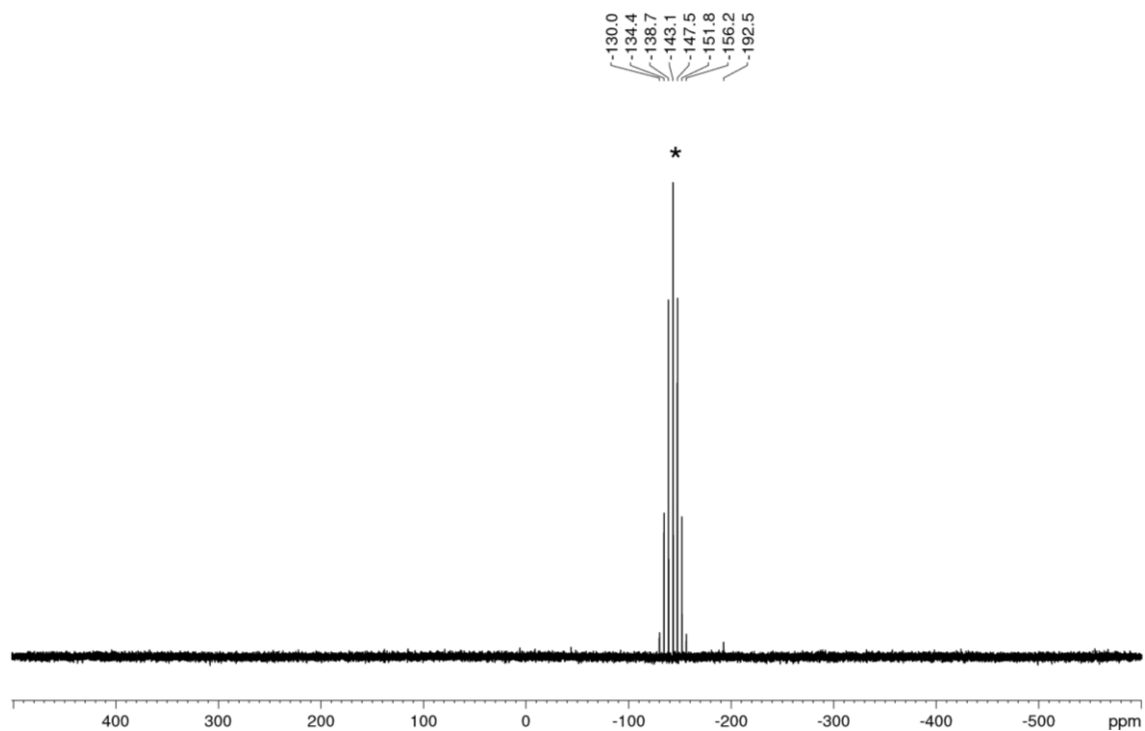


Figure S81. $^{31}\text{P}\{^1\text{H}\}$ NMR spectrum for the photoelectrocatalytic functionalization of P_4 (0.04 mmol) into $[\text{Ph}_2\text{Ar}_2\text{P}]\text{Cl}$ and Ph_2ArP using e-PRCats (Table 10, Entry 2, 3.3 mol% **DCA**, $\text{ClC}_6\text{H}_4\text{-4-OMe}$, blue LED (455 nm), TBAPF_6 (*), 1.76 V, $\text{Zn (+) / C}_{\text{foam}} (-)$.

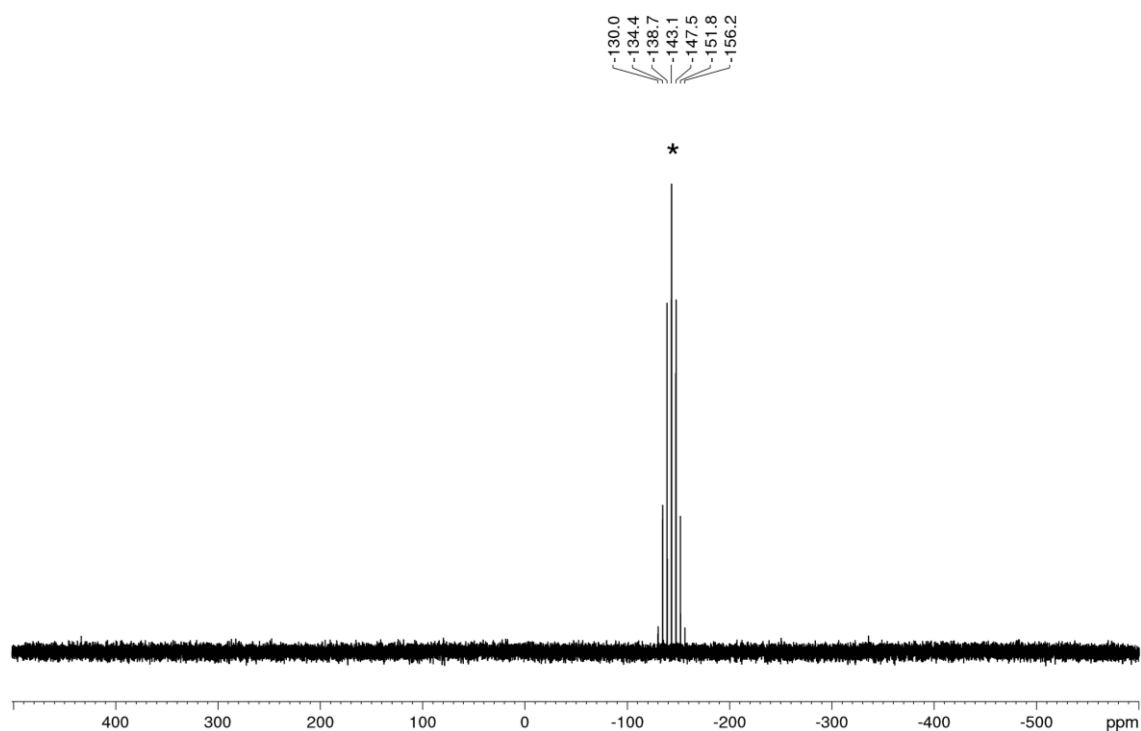


Figure S82. $^{31}\text{P}\{^1\text{H}\}$ NMR spectrum for the photoelectrocatalytic functionalization of P_4 (0.04 mmol) into $[\text{Ph}_2\text{Ar}_2\text{P}]\text{Cl}$ and Ph_2ArP using e-PRCats (Table 10, Entry 3, 3.3 mol% **DCA**, ClC_6H_4 -4-OMe, blue LED (455 nm), TBAPF_6 (*), 1.00 V, Zn (+) / C_{foam} (-).

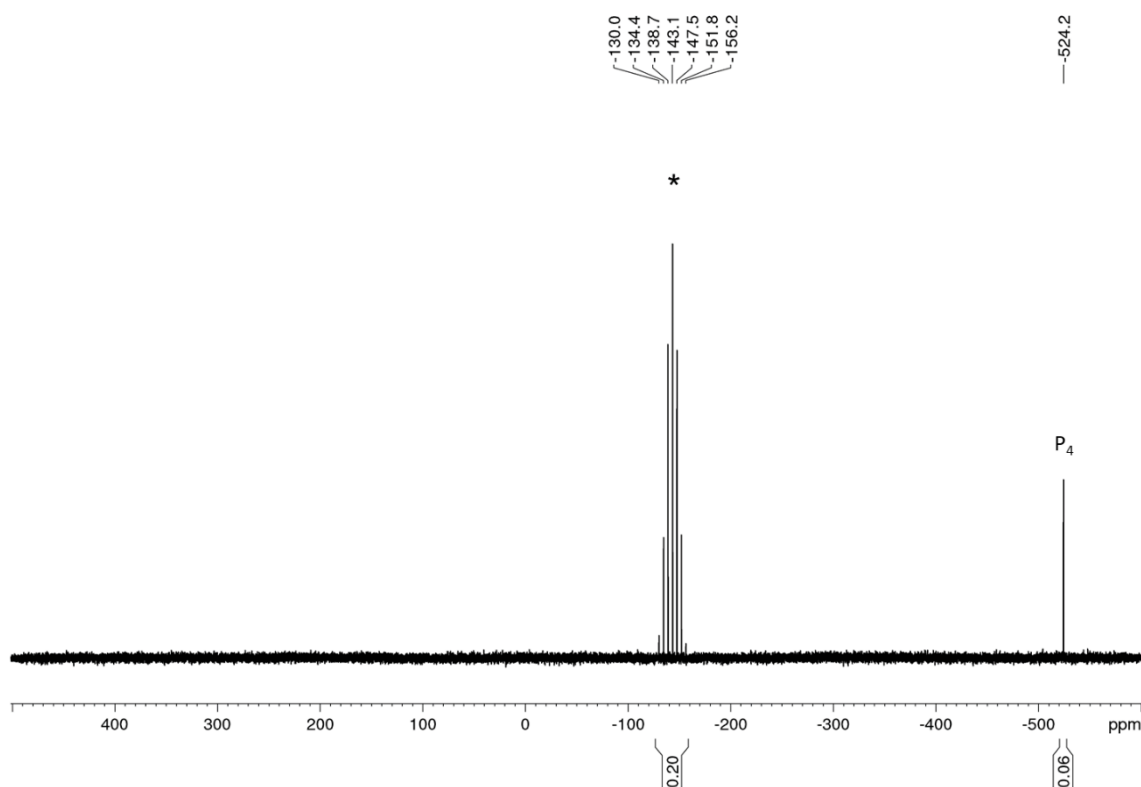


Figure S83. $^{31}\text{P}\{^1\text{H}\}$ NMR spectrum for the photoelectrocatalytic functionalization of P_4 (0.04 mmol) into $[\text{Ph}_2\text{Ar}_2\text{P}]\text{Cl}$ and Ph_2ArP using e-PRCats (Table 10, Entry 4, 3.3 mol% **DCA**, ClC_6H_4 -4-OMe, blue LED (455 nm), TBAPF_6 (*), 1.76 V, Zn (+) / C_{lead} (-).

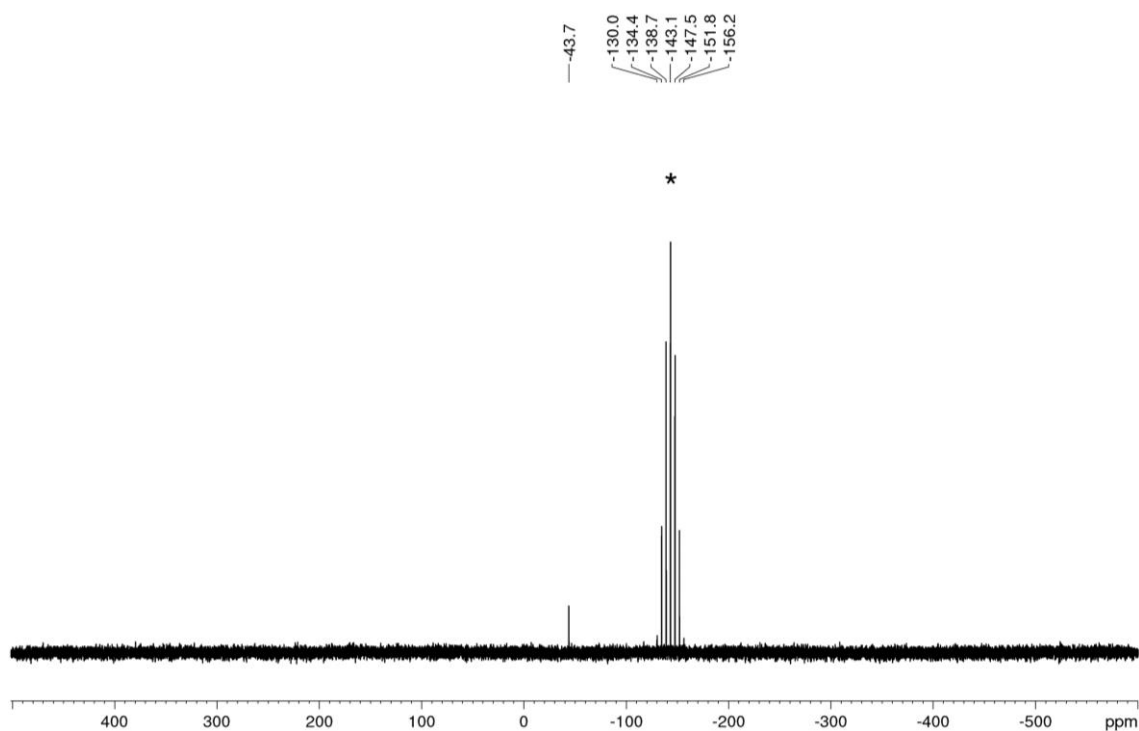


Figure S84. $^{31}\text{P}\{^1\text{H}\}$ NMR spectrum for the photoelectrocatalytic functionalization of P_4 (0.04 mmol) into $[\text{Ph}_2\text{Ar}_2\text{P}]\text{Cl}$ and Ph_2ArP using e-PRCats (Table 10, Entry 5, 5 mol% **NpMI**, ClC_6H_4 -4-OMe, blue LED (455 nm), TBAPF_6 (*), 1.60 V, Zn (+) / Fe (-).

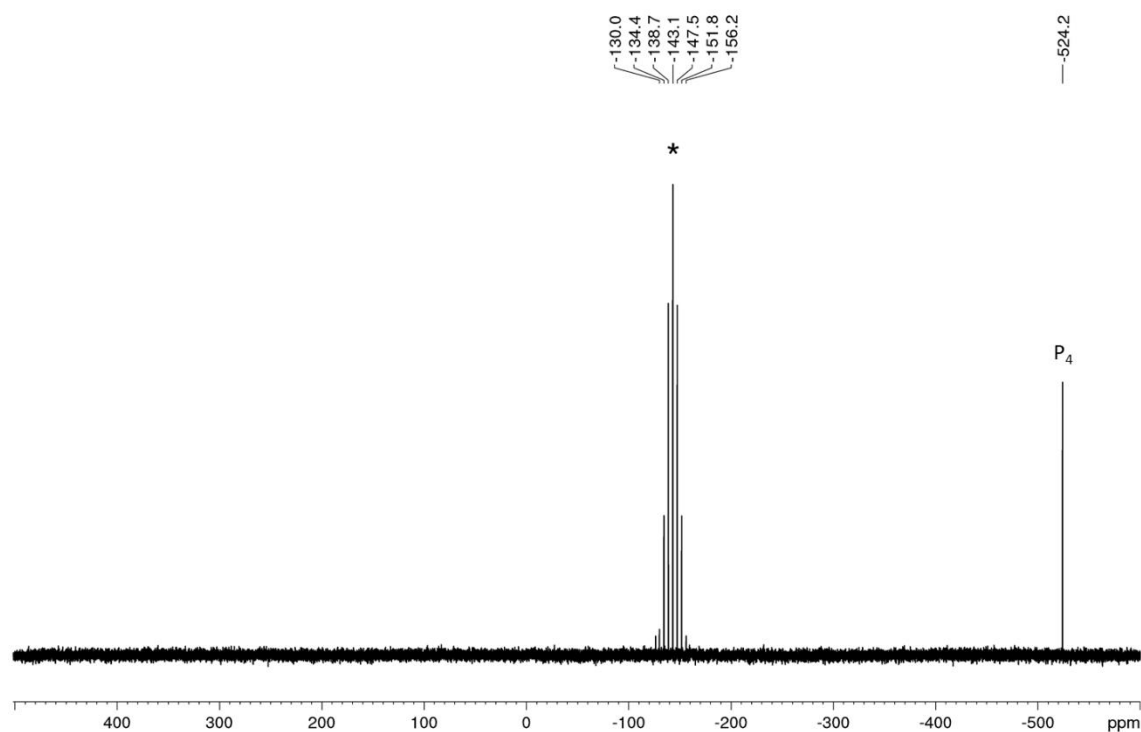


Figure S85. $^{31}\text{P}\{^1\text{H}\}$ NMR spectrum for the photoelectrocatalytic functionalization of P_4 (0.04 mmol) into $[\text{Ph}_2\text{Ar}_2\text{P}]\text{Cl}$ and Ph_2ArP using e-PRCats (Table 10, Entry 6, 5 mol% **NpMI**, ClC_6H_4 -4-OMe, blue LED (455 nm), TBAPF_6 (*), 1.60 V, Zn (+) / C_{foam} (-).

S4 List and assignment of photoelectrochemical reactions (PEC)

Table S1. Reductive photoelectrochemistry with substrate 4-chloroanisole (ClC₆H₄-4-OMe) and DCA.

Reaction	Entry	DCA [mol%]	Potential [V]	Electrodes	Ratio of Ph ₂ PH to Ph ₂ ArP / Ph ₄ P ₂	Ratio of Ph ₂ PH to [Ph ₂ Ar ₂ P]Cl
PEC50	1	5	1.57	Zn (+) / C _{lead} (-)	1 : 0.35 / 0.31	1 : 0.04
PEC51	2	10	1.76	Zn (+) / C _{lead} (-)	1 : 0.16 / 0.33	1 : 0.10
PEC52	3	5	1.76	Zn (+) / C _{foam} (-)	0 : 0.05 / 0.28	0 : 0.09
PEC53_A	4	5	1.0	Zn (+) / C _{foam} (-)	1 : 0.31 / 0	1 : 1.62
PEC53_B	5	5	1.0	Zn (+) / C _{lead} (-)	1 : 0.27 / 0	1 : 0.80
PEC55_A	6	10	1.0	Zn (+) / C _{foam} (-)	1 : 0 / 0	1 : 5.13
PEC55_B	7	10	1.0	Zn (+) / C _{lead} (-)	1 : 0.36 / 0	1 : 0.11
PEC56_A	8	5	1.6	Zn (+) / C _{foam} (-)	1 : 1.92 / 0	1 : 0.36
PEC56_B	9	5	1.6	Zn (+) / C _{lead} (-)	1 : 0.90 / 0.20	1 : 0
PEC56_C	10	5	1.6	Zn (+) / C _{felt} (-)	1 : 0.49 / 0.06	1 : 0.02
PEC57_A ^[a]	11	5	1.0	Zn (+) / C _{foam} (-)	–	–
PEC57_B ^[a]	12	5	1.0	Zn (+) / C _{lead} (-)	1 : 1.86 / 0.12	1 : 0.31
PEC58_A	13	10	1.6	Zn (+) / C _{foam} (-)	1 : 0.96 / 0	1 : 0.59
PEC58_B	14	10	1.6	Zn (+) / C _{lead} (-)	1 : 0.46 / 0	1 : 0.10
PEC60_A ^[b]	15	5	1.6	Zn (+) / C _{foam} (-)	7% Ph ₂ PH left, 19% Ph ₂ ArP	0% [Ph ₂ Ar ₂ P]Cl
PEC60_B ^[b]	16	5	1.6	Zn (+) / C _{lead} (-)	41% Ph ₂ PH left, 15% Ph ₂ ArP	2% [Ph ₂ Ar ₂ P]Cl

[a] The reaction time was extended from 21h to 3 days. [b] Ph₃P was added as an internal standard (0.05 mmol).

Table S2. Reductive photoelectrochemistry with DTAC.

Reaction	Entry	DTAC [mol%]	Substrate	Pot. [V]	Electrodes	Ratio of Ph ₂ PH to Ph ₂ ArP	Ratio of Ph ₂ PH to [Ph ₂ Ar ₂ P]Cl
PEC69_A	1	5	ClC ₆ H ₄ -4-OMe	1.6	Zn (+) / C _{foam} (-)	1 : 1.49	1 : 0.52
PEC69_B	2	5	ClC ₆ H ₄ -4-OMe	1.6	Zn (+) / C _{lead} (-)	1 : 0.28	1 : 1

Table S3. Reductive Photoelectrochemistry with substrate 4-chloroanisole (ClC₆H₄-4-OMe) and NpMI – Control experiments.

Reaction	Entry	Ph ₂ PH	NpMI [mol%]	Substrate	Pot. [V]	Electrodes	Electrolyte	Blue LED	Product formation?
PEC62	1	✓	5	–	1.6	Zn (+) / Fe (-)	TBAPF ₆	✓	X
PEC64_A	2	✓	5	✓	1.6	Zn (+) / Fe (-)	TBAPF ₆	–	X
PEC64_B ^[a]	3	✓	5	✓	–	Zn (+) / Fe (-)	TBAPF ₆	✓	X / ✓ ^[a]
PEC64_C	4	✓	–	✓	1.6	Zn (+) / Fe (-)	TBAPF ₆	✓	X
PEC65_A	5	–	5	✓	1.6	Zn (+) / Fe (-)	TBAPF ₆	✓	X
PEC65_B	6	✓	5	✓	1.6	Zn (+) / Fe (-)	–	✓	X
PEC66_A	7	✓	5	✓	–	Zn (+) / Fe (-)	TBAPF ₆	–	X
PEC66_B	8	✓	5	✓	1.6	Zn (+) / C _{foam} (-)	TBAPF ₆	✓	✓
PEC67	9	✓	5	✓	3.2	Zn (+) / Fe (-)	TBAPF ₆	–	X

[a] After irradiation without potential for 21h shows no product formation in the ³¹P{¹H} NMR, but subsequent applying of potential yielded Ph₂ArP and [Ph₂Ar₂P]Cl.

Chapter 4. Reductive Photoelectrocatalytic Activation of Organic Halides and Diphenylphosphine into Arylphosphines and Phosphonium Salts

Table S4. Reductive photoelectrochemistry with **NpMI** – Screening conditions. (A potential of 1.6 V was applied to all reactions.)

Reaction	Entry	NpMI [mol%]	Substrate	Electrodes	Electrolyte	Ratio of Ph ₂ PH to Ph ₂ ArP	Ratio of Ph ₂ PH to [Ph ₂ Ar ₂ P]Cl
PEC59_A	1	5	ClC ₆ H ₄ -4-OMe	Zn (+) / Fe (-)	TBAPF ₆	1 : 0.73	1 : 0.60
PEC59_B	2	10	ClC ₆ H ₄ -4-OMe	Zn (+) / Fe (-)	TBAPF ₆	0 : 1.00	–
PEC68_A ^[a]	3	5	ClC ₆ H ₄ -4-OMe	Zn (+) / Fe (-)	TBAPF ₆	–	–
PEC68_B ^[a]	4	5	ClC ₆ H ₄ -4-OMe	Zn (+) / C _{foam} (-)	TBAPF ₆	–	–
PEC70_A ^[b]	5	1	ClC ₆ H ₄ -4-OMe	Zn (+) / C _{foam} (-)	TBAPF ₆	37% Ph ₂ PH left, 20% Ph ₂ ArP	4% [Ph ₂ Ar ₂ P]Cl
PEC70_B ^[b]	6	2.5	ClC ₆ H ₄ -4-OMe	Zn (+) / C _{foam} (-)	TBAPF ₆	63% Ph ₂ PH left, 10% Ph ₂ ArP	0% [Ph ₂ Ar ₂ P]Cl
PEC70_C ^[b]	7	5	ClC ₆ H ₄ -4-OMe	Zn (+) / C _{foam} (-)	TBAPF ₆	29% Ph ₂ PH left, 24% Ph ₂ ArP	15% [Ph ₂ Ar ₂ P]Cl
PEC71_A ^[b]	8	5	ClC ₆ H ₄ -4-OMe	Zn (+) / C _{foam} (-)	LiClO ₄	95% Ph ₂ PH left, 22% Ph ₂ ArP	2% [Ph ₂ Ar ₂ P]Cl
PEC71_B ^[b]	9	5	ClC ₆ H ₄ -4-OMe	Zn (+) / C _{foam} (-)	TBABF ₄	46% Ph ₂ PH left, 26% Ph ₂ ArP	12% [Ph ₂ Ar ₂ P]Cl
PEC72_A ^[b]	10	1	ClC ₆ H ₄ -4-OMe	Zn (+) / Fe (-)	TBAPF ₆	39% Ph ₂ PH left, 36% Ph ₂ ArP	13% [Ph ₂ Ar ₂ P]Cl
PEC72_B ^[b]	11	2.5	ClC ₆ H ₄ -4-OMe	Zn (+) / Fe (-)	TBAPF ₆	63% Ph ₂ PH left, 28% Ph ₂ ArP	35% [Ph ₂ Ar ₂ P]Cl
PEC72_C ^[b]	12	5	ClC ₆ H ₄ -4-OMe	Zn (+) / Fe (-)	TBAPF ₆	50% Ph ₂ PH left, 49% Ph ₂ ArP	25% [Ph ₂ Ar ₂ P]Cl
PEC73_A ^{[b][c]}	13	5	ClC ₆ H ₄ -4-OMe	Zn (+) / Fe (-)	TBAPF ₆	13% Ph ₂ PH left, 20% Ph ₂ ArP	16% [Ph ₂ Ar ₂ P]Cl
PEC73_B ^{[b][c]}	14	5	ClC ₆ H ₄ -4-OMe	Zn (+) / C _{foam} (-)	TBAPF ₆	29% Ph ₂ PH left, 5% Ph ₂ ArP	0% [Ph ₂ Ar ₂ P]Cl
PEC74_A	15	5	PhBr	Zn (+) / Fe (-)	TBAPF ₆	1 : 7.79	1 : 22.47
PEC74_B	16	5	PhBr	Zn (+) / C _{foam} (-)	TBAPF ₆	1 : 1.42	1 : 4.87
PEC76_A	17	5	PhCl	Zn (+) / Fe (-)	TBAPF ₆	1 : 0.32	1 : 0.95
PEC76_B ^[d]	18	5	PhCl	Zn (+) / Fe (-)	TBAPF ₆	1 : 0.86	1 : 0.73
PEC77_A	19	5	PhBr	Zn (+) / Fe (-)	TBAPF ₆	0 : 0	0 : 1.00
PEC77_B ^[d]	20	5	PhBr	Zn (+) / Fe (-)	TBAPF ₆	1 : 1.54	1 : 7.60
PEC78_A ^[b]	21	5	ClC ₆ H ₄ -4-OMe	Zn (+) / Fe (-)	TBAPF ₆	21% Ph ₂ PH left, 25% Ph ₂ ArP	5% [Ph ₂ Ar ₂ P]Cl
PEC78_B ^{[b][d]}	22	5	ClC ₆ H ₄ -4-OMe	Zn (+) / Fe (-)	TBAPF ₆	8% Ph ₂ PH left, 25% Ph ₂ ArP	38% [Ph ₂ Ar ₂ P]Cl

[a] The reaction time was extended from 21h to 3 days. [b] Ph₃P was added as an internal standard (0.05 mmol). [c] The amount of electrolyte TBAPF₆ was increased from 0.1 mmol to 0.4 mmol. [d] The reactions were irradiated with high power LEDs (blue (451 nm), 20.3 V, 350 mA, 7 x LT-3109 Osram SSL 80 royal-blau, Ser.-Nr.:219-20-2).

Table S5. Calibration series of starting material Ph₂PH, product Ph₃P and internal standard PPNCI.

Entry	Consump. of Ph ₂ PH	n(Ph ₂ PH) [mmol]	conv. to Ph ₃ P	n(Ph ₃ P) [mmol]	PPNCI	n(PPNCI) [mmol]
PEC_Cal.1	5%	0.095	5%	0.005	50%	0.05
PEC_Cal.2	25%	0.075	25%	0.025	50%	0.05
PEC_Cal.3	50%	0.05	50%	0.05	50%	0.05
PEC_Cal.4	75%	0.025	75%	0.075	50%	0.05
PEC_Cal.5	95%	0.005	95%	0.095	50%	0.05

Chapter 4. Reductive Photoelectrocatalytic Activation of Organic Halides and Diphenylphosphine into Arylphosphines and Phosphonium Salts

Table S8. Reductive photoelectrochemistry with **NpMI** – Quantitative $^{31}\text{P}\{^1\text{H}\}$ NMR with PPNCI.

Reaction	Entry	NpMI [mol%]	Substrate	Potential [V]	Electrodes	Full conv. of Ph ₂ PH?	Conv. to Ph ₃ P [%]	Conv. to [Ph ₄ P]Cl [%]
PEC81_A	1	5	PhCl	1.6	Zn (+) / Fe (-)	✓	0	0
PEC81_B	2	5	PhCl	1.6	Zn (+) / C _{foam} (-)	✗	0	2
PEC82_A	3	5	PhBr	1.6	Zn (+) / Fe (-)	✓	0	13
PEC82_B	4	5	PhBr	1.6	Zn (+) / C _{foam} (-)	✗	0	2
PEC83_A_1.6	5	5	PhBr	1.6	Zn (+) / Fe (-)	✓	0	5
PEC83_B_1.6	6	5	PhBr	1.6	Zn (+) / Fe (-)	✓	0	4
PEC83_A_1.3	7	5	PhBr	1.3	Zn (+) / Fe (-)	✗	2	6
PEC83_B_1.3	8	5	PhBr	1.3	Zn (+) / Fe (-)	✗	3	7
PEC84 ^[a]	9	5	PhBr	1.6	Zn (+) / Fe (-)	✗	11	7

[a] A 1:1 ratio of Ph₂PH and substrate PhBr was used instead of an excess of 10 equiv.

Table S9. Reductive photoelectrochemistry with **ⁿBuO-NpMI**.

Reaction	Entry	ⁿ BuO-NpMI [mol%]	Substrate	Potential [V]	Electrodes	Ratio of Ph ₂ PH to Ph ₂ ArP	Ratio of Ph ₂ PH to [Ph ₂ Ar ₂]Cl
PEC79_A ^[a]	1	5	ClC ₆ H ₄ -4-OMe	1.6	Zn (+) / Fe (-)	19% Ph ₂ PH, 10% Ph ₂ ArP	13% [Ph ₂ Ar ₂]Cl
PEC79_B	2	5	PhCl	1.6	Zn (+) / Fe (-)	1 : 1.31	1 : 1.55
PEC79_C	3	5	PhBr	1.6	Zn (+) / Fe (-)	1 : 0	1 : 0.37
PEC80_A ^[a]	4	5	ClC ₆ H ₄ -4-OMe	1.6	Zn (+) / C _{foam} (-)	43% Ph ₂ PH, 42% Ph ₂ ArP	17% [Ph ₂ Ar ₂]Cl
PEC80_B	5	5	PhCl	1.6	Zn (+) / C _{foam} (-)	1 : 2.65	1 : 9.58
PEC80_C	6	5	PhBr	1.6	Zn (+) / C _{foam} (-)	1 : 3.62	1 : 6.90
PEC81_C ^[b]	7	5	PhCl	1.6	Zn (+) / C _{foam} (-)	no Ph ₂ PH, 2% Ph ₃ P	no Ph ₂ PH, no product
PEC82_C ^[b]	8	5	PhBr	1.6	Zn (+) / C _{foam} (-)	no Ph ₃ P	8% Ph ₂ PH, 1% [Ph ₄ P]Cl

[a] Ph₃P (0.05 mmol) was added as internal standard. [b] PPNCI (0.05 mmol) was added as an internal standard.

Table S10. Reductive photoelectrochemistry with e-PRCats and P₄.

Reaction	Entry	e-PRCat [mol%]	Substrate	Potential [V]	Electrodes	Full conv. of P ₄ ?	Product formation?
PEC48	1	DCA (stoichiometric.)	–	2.55	Zn (+) / C _{lead} (-)	✗	–
PEC49	2	DCA (3.3 mol%)	ClC ₆ H ₄ -4-OMe	1.76	Zn (+) / C _{foam} (-)	✓	–
PEC54_A	3	DCA (3.3 mol%)	ClC ₆ H ₄ -4-OMe	1.00	Zn (+) / C _{foam} (-)	✓	–
PEC54_B	4	DCA (3.3 mol%)	ClC ₆ H ₄ -4-OMe	1.00	Zn (+) / C _{lead} (-)	✗	–
PEC75_A	5	NpMI (5 mol%)	ClC ₆ H ₄ -4-OMe	1.60	Zn (+) / Fe (-)	✓	–
PEC75_B	6	NpMI (5 mol%)	ClC ₆ H ₄ -4-OMe	1.60	Zn (+) / C _{foam} (-)	✗	–

4.5 References

- [1] a) W. Gleason, *JOM*, 2007, **59**, 17-19; b) G. Bettermann, W. Krause, G. Riess and T. Hofmann, *Ullmann's Encyclopedia of Industrial Chemistry* (Wiley), 2000; c) D. E. C. Corbridge, *Chemistry, Biochemistry and Technology* (Elsevier), 2000.
- [2] a) B. M. Cossairt, N. A. Piro and C. C. Cummins, *Chem. Rev.*, 2010, **110**, 4164–4177; b) M. Caporali, L. Gonsalvi, A. Rossin and M. Peruzzini, *Chem. Rev.*, 2010, **110**, 4178–4235; c) M. Scheer, G. Balázs and A. Seitz, *Chem. Rev.*, 2010, **110**, 4236–4256; d) C. M. Hoidn, D. J. Scott and R. Wolf, *Chem. Eur. J.*, 2021, **27**, 1886–1902; e) L. Giusti, V. R. Landaeta, M. Vanni, J. A. Kelly, R. Wolf and M. Caporali, *Coord. Chem. Rev.*, 2021, **441**, 2139276–2139375; f) Y. H. Budnikova, T. V. Gryaznova, V. V. Grinenko, Y. B. Dudkina and M. N. Khrizanforov, *Pure Appl. Chem.*, 2017, **89**, 311–330.
- [3] U. Lennert, P. B. Arockiam, V. Streitferdt, D. J. Scott, C. Rödl, R. M. Gschwind and R. Wolf, *Nat. Catal.*, 2019, **2**, 1101–1106.
- [4] P. B. Arockiam, U. Lennert, C. Graf, R. Rothfelder, D. J. Scott, T. G. Fischer, K. Zeitler and R. Wolf, *Chem. Eur. J.*, 2020, **26**, 16374–16382.
- [5] L. Huang, L. K. G. Ackerman, K. Kang, A. M. Parsons and D. J. Weix, *J. Am. Chem. Soc.*, 2019, **141**, 10978–10983.
- [6] A. F. Chmiel, O. P. Williams, C. P. Chernowsky, C. S. Yeung and Z. K. Wickens, *J. Am. Chem. Soc.*, 2021, **143**, 10882–10889.
- [7] M. Cybularczyk-Cecotka, J. Szczepanik and M. Giedyk, *Nat. Catal.*, 2020, **3**, 872–886.
- [8] I. Ghosh, T. Ghosh, J. I. Bardagi and B. König, *Science*, 2014, **346**, 725–728.
- [9] H. Kim, H. Kim, T. H. Lambert and S. Lin, *J. Am. Chem. Soc.*, 2020, **142**, 2087–2092.
- [10] N. Kvasovs and V. Gevorgyan, *Chem. Soc. Rev.*, 2021, **50**, 2244–2259.
- [11] M. Neumeier, D. Sampedro, M. Májek, V. A. de la Peña O'Shea, A. Jacobi von Wangelin and R. Pérez-Ruiz, *Chem. Eur. J.*, 2018, **24**, 105–108.
- [12] a) D. G. Yakhvarov, Y. H. Budnikova, D. I. Tazeev and O. G. Sinyashin, *Russ. Chem. Bull.*, 2002, **51**, 2059–2064; b) D. G. Yakhvarov, Y. G. Budnikova and O. G. Sinyashin, *Russ. J. Electrochem.*, 2003, **39**, 1261–1270; c) Y. H. Budnikova, D. G. Yakhvarov and O. G. Sinyashin, *J. Organomet. Chem.* 2005, **690**, 2416–2425; d) Y. G. Budnikova, D. I. Tazeev, A. G. Kafiyatullina, D. G. Yakhvarov, V. I. Morozov, N. K. Gusarova, B. A. Trofimov and O. G. Sinyashin, *Russ. Chem. Bull.*, 2005, **54**, 942–947; e) Y. H. Budnikova, T. V. Gryaznova, V. V. Grinenko, Y. B. Dudkina and M. N. Khrizanforov, *Pure Appl. Chem.*, 2017, **89**, 311–330.

- [13] Y. Mei, Z. Yan and L. L. Liu, *J. Am. Chem. Soc.*, 2022, **144**, 1517–1522.
- [14] R. Rothfelder, V. Streitferdt, U. Lennert, J. Cammarata, D. J. Scott, K. Zeitler, R. M. Gschwind and R. Wolf, *Angew. Chem. Int. Ed.*, 2021, **60**, 24650–24658.
- [15] N. G. W. Cowper, C. P. Chernowsky, O. P. Williams and Z. K. Wickens, *J. Am. Chem. Soc.*, 2020, **142**, 2093–2099.
- [16] For selected reviews of visible-light photoredox catalysis, see: a) C. K. Prier, D. A. Rankic and D. W. C. MacMillan, *Chem. Rev.*, 2013, **113**, 5322–5363; b) M. H. Shaw, J. Twilton and D. W.C. MacMillan, *J. Org. Chem.*, 2016, **81**, 6898–6926; c) N. A. Romero and D. A. Nicewicz, *Chem. Rev.*, 2016, **116**, 10075–10166; d) K. L. Skubi, T. R. Blum and T. P. Yoon, *Chem. Rev.*, 2016, **116**, 10035–10074; e) D. A. DiRocco, K. Dykstra, S. Krska, P. Vachal, D. V. Conway and M. Tudge, *Angew. Chem. Int. Ed.*, 2014, **53**, 4802–4806; f) J. M. R. Narayanam and C. R. Stephenson, *Chem. Soc. Rev.*, 2011, **40**, 102–113.
- [17] For a special issue on photoredox catalysis in organic chemistry, see: Accounts of Chemical Research 2016, Vol. **49**, Issue 10.
- [18] J. P. Barham and B. König, *Angew. Chem. Int. Ed.*, 2020, **59**, 11732–11747.
- [19] S. Wu, J. Kaur, T. A. Karl, X. Tian, and J. P. Barham, *Angew. Chem. Int. Ed.*, 2022, **61**, e202107811.
- [20] a) M. A. Reddy, A. Thomas, K. Srinivas, V. J. Rao, K. Bhanuprakash, B. Sridhar, A. Kumar, M. N. Kamalasanan and R. Srivastava, *J. Mater. Chem.*, 2009, **19**, 6172–6184; b) E. Alfonzo and A. B. Beeler, *Chem. Sci.*, 2019, **10**, 7746–7754.
- [21] X. Tian, T. A. Karl, S. Reiter, S. Yakubov, R. de Vivie-Riedle, B. König and J. P. Barham, *Angew. Chem. Int. Ed.*, 2021, **60**, 20817–20825.
- [22] L. Pause, M. Robert and J. M. Savéant, *J. Am. Chem. Soc.*, 1999, **121**, 7158–7159.
- [23] C. J. Zeman, IV, S. Kim, F. Zhang and K. S. Schanze, *J. Am. Chem. Soc.*, 2020, **142**, 2204–2207.
- [24] C. P. Andrieux and J. Pinson, *J. Am. Chem. Soc.*, 2003, **125**, 14801–14806.
- [25] D. C. Batesky, M. J. Goldfogel and D. J. Weix, *J. Org. Chem.*, 2017, **82**, 9931–9936.

5 Synthesis and Characterization of Bidentate Isonitrile Iron Complexes^[a]

Abstract: The divalent iron complexes *trans*-[FeBr₂(BINC)₂], [Cp*FeCl(BINC)] (Cp* = Me₅C₅) and [FeBr₂(CNAr₃NC)₂] with the chelating bis(isonitrile) ligands BINC (bis(2-isocyanophenyl)phenylphosphonate) and CNAr₃NC (2,2''-diisocyano-3,5,5''-tetramethyl-1,1':3',1''-terphenyl) have been prepared and characterized. Their subsequent reduction yields the di- and trinuclear compounds [Fe₃(BINC)₆], [Cp*Fe(BINC)]₂, [Fe(CNAr₃NC)₂]₂ and [K(Et₂O)]₂[Fe(CNAr₃NC)₂]₂. The molecular structures of all new species were determined by X-ray crystallography and compared to those of related iron carbonyl complexes, demonstrating that the bidentate isonitrile ligands are capable surrogates for two CO ligands with only minimal distortion of the tetrahedral or octahedral geometry of the parent complexes. The complexes were further characterized by NMR and IR spectroscopy, and the electrochemical properties of selected compounds were analyzed by UV-vis-NIR spectroelectrochemistry.



Reproduced with permission from: M. Till, J. A. Kelly, C. G. P. Ziegler, T. Guo, M. R. Ringenberg, E. Lutsker, O. Reiser and R. Wolf, *Organometallics*, **2021**, *40*, 1042–1052.

^[a] M. Till performed the reactions and the characterization of all compounds. E. Lutsker initially provided isonitrile ligands and gave advice on ligand synthesis. C. G. P. Ziegler performed DFT calculations of compound **6**. T. Guo and M. R. Ringenberg performed the UV-Vis spectroelectrochemistry of compound **2** and **4**. R. Wolf and O. Reiser supervised and directed the project. M. Till wrote the manuscript with input from R. Wolf.

5.1 Introduction

With the discovery of isocyanides by Lieke^[1] in 1859 came a new and emerging field within organometallic chemistry.^[2] Isonitriles show stronger σ -donating character and weaker π -acceptor properties in comparison to carbon monoxide. However, they feature similar behavior when they coordinate to metals both as terminal and bridging ligands.^{[3],[4]} Isonitriles can be electronically and sterically tuned through modification of their organic substituents, which makes them versatile ligands for metal catalysis.^[5] Chelating bis(isonitriles) confer rigidity to metal complexes, which has been proven to be especially valuable for the design of 3d-metal complexes with sufficient excited-state lifetimes to efficiently initiate single-electron-transfer (SET) processes. This approach has been successful for copper^[6], molybdenum^[7], and rhenium^[8], providing alternatives to established but scarce ruthenium- and iridium-based photocatalysts.^[9]

Extending this concept to iron holds the promise of making this metal broadly available for photocatalysis. This is especially challenging, given that excited-state lifetimes of iron complexes are often in the picosecond range and have been reported at best in the low nanosecond range.^[10] However, there are only limited data available on coordination complexes of iron with bidentate isocyanides,^{[20]–[23]} in contrast with monodentate isocyanide iron complexes, which have attracted considerable attention due to the high prevalence of iron carbonyl complexes.^[11] For example, dinuclear iron complexes such as $[\text{CpFe}(\text{CNPh})_2]$ ^[12] (**A**, Ph = C₆H₅) and $[\text{Fe}_2(\text{CNPh})_9]$ ^[13] (**B**) feature terminal and bridging isocyanide ligands (Figure 1).

The trinuclear compound $[\text{Fe}_3(\text{CO})_{10}(\text{CNPh})_2]$ (**C**)^[14] possesses both CO and monodentate isocyanide ligands, having replaced two of the axial CO ligands in $[\text{Fe}_3(\text{CO})_{12}]$. Iron isocyanide analogues of $[\text{Fe}(\text{CO})_4]^{2-}$, $[\text{Fe}(\text{CNXyl})_4]^{2-}$ (Xyl = 2,6-Me₂C₆H₃)^[15] and $[\text{Fe}(\text{CNAr}^{\text{Mes}2})_4]^{2-}$ (Ar^{Mes2} = 2,6-(2,4,6-Me₃C₆H₂)₂C₆H₃)^[16] further demonstrate the propensity of monodentate isocyanides to act as surrogates for CO. In comparison to monodentate isocyanide ligands, the reactivity and coordination chemistry of bidentate isocyanides has been generally unexplored.^[5] Given the linear structure of the isocyanide unit, such ligands need to form much larger chelates relative to the typical *N,N*- or *P,P*-ligands that are commonly found in 5- and 6-membered rings. The minimal ring size in a bidentate isocyanide-metal complex was found to be 12^[19]. With this design concept, a number of iron(II) complexes with bidentate isocyanide ligands were realized; representative examples are **D–G** (Figure 1).^{[5],[20]–[23]}

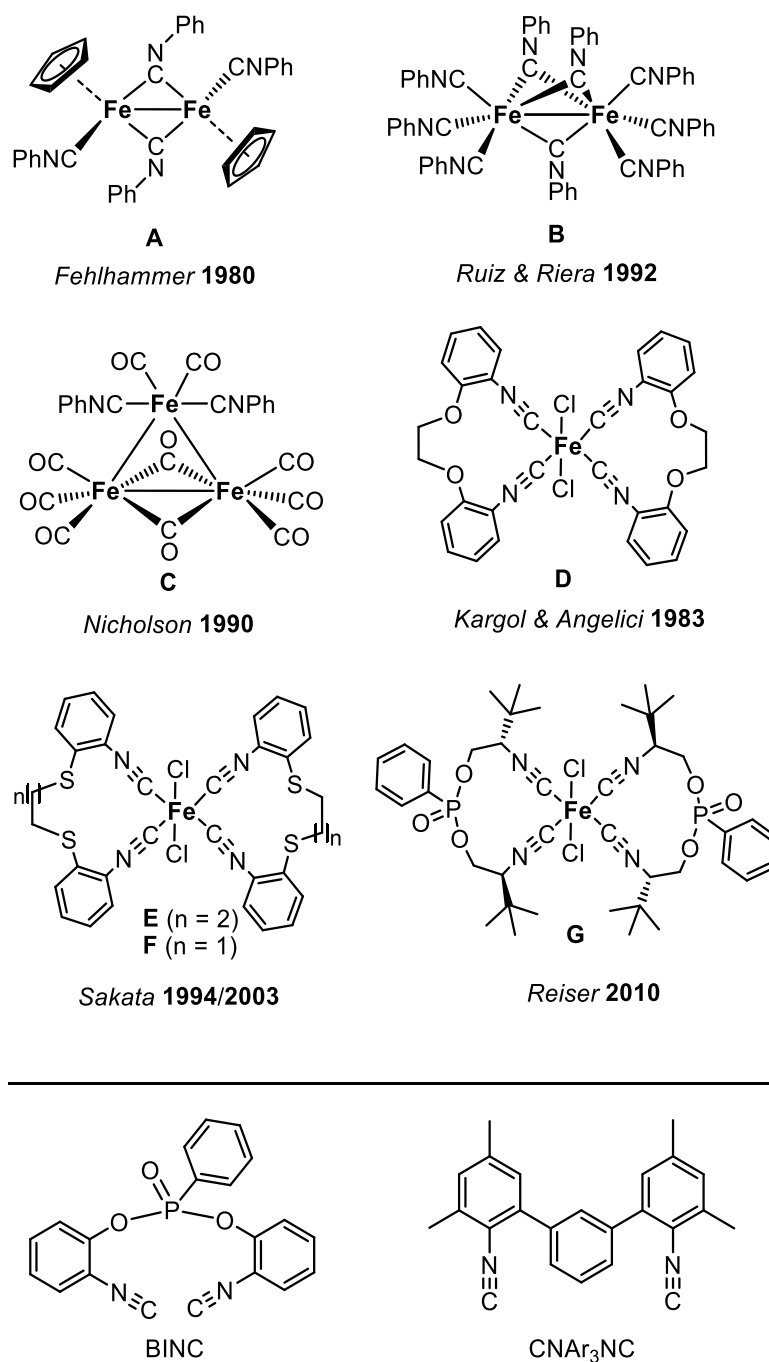


Figure 1. Selected examples of di- and trinuclear iron isonitrile complexes.

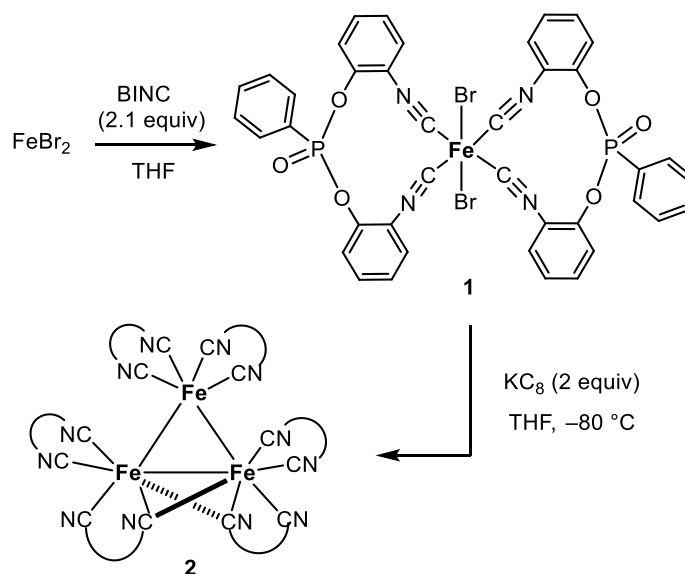
Our research group has previously been interested in the synthesis and reactivity of low-oxidation-state polyarene and alkene ferrates.^[24] Such complexes have been used for various applications, including the activation of small molecules (e.g., P₄ and CO₂) and as catalysts for hydrogenation and hydroboration reactions.^[25] Taking advantage of the well-known ability of isocyanides to stabilize low-oxidation-state transition metal complexes,^{[15]–[18],[26]} in combination with imposing rigidity, we were interested in exploring the potential of the aforementioned chelating isocyanide ligands in the stabilization of highly-reduced iron complexes. We particularly questioned if polynuclear

iron complexes with chelating bis(isonitrile) ligands can still be formed, for which to the best of our knowledge, no previous examples have been described in the literature. Here, we report the synthesis and characterization of new iron complexes with the ligands BINC (bis(2-isocyanophenyl)phenylphosphonate) and CNAr_3NC (2,2''-diisocyano-3,5,3'',5''-tetramethyl-1,1':3',1''-terphenyl), demonstrating that indeed di- and trinuclear structures can be realized.

5.2 Results and Discussion

Treating anhydrous FeBr_2 with two equivalents of BINC resulted in the formation of *trans*- $[\text{FeBr}_2(\text{BINC})_2]$ (**1**) as a blue solid in 33% isolated yield (Scheme 1). Compound **1** displays structural and spectroscopic features similar to those of compounds **D-G** (see Figure S34 in the SI for a graphical representation of the structure).

Reduction of **1** with an excess of KC_8 in THF afforded an orange-brown solution from which brown crystals of $[\text{Fe}_3(\text{BINC})_6]$ (**2**) were isolated in a yield of 26% by slow diffusion of *n*-hexane into the reaction mixture.



Scheme 1. Synthesis of $[\text{FeBr}_2(\text{BINC})_2]$ (**1**) and $[\text{Fe}_3(\text{BINC})_6]$ (**2**).

Single-crystal X-ray diffraction (XRD, Figure 2) revealed that **2** crystallizes in the space group $\text{P}\bar{1}$ with two molecules in the unit cell. At first glance, the structure of **2** resembles that of $[\text{Fe}_3(\text{CO})_{12}]$ (**H**) with respect to the Fe1–Fe2–Fe3-core (Table 1), showing that the BINC ligand can displace the carbonyl groups without imposing constraints due to its chelating structure.

Table 1. Selected bond lengths [Å] and angles [°] of **2** and [Fe₃(CO)₁₂] (**H**). The data for **2** were collected at 123 K, while the data for **H** were collected at room temperature.^[27]

	2	[Fe ₃ (CO) ₁₂]
Fe1–Fe2	2.682(6)	2.677(2)
Fe2–Fe3	2.495(6)	2.558(1)
Fe3–Fe1	2.685(6)	2.683(1)
Fe1–Fe2–Fe3	62.37(2)	61.6(2)
Fe2–Fe3–Fe1	62.23(2)	61.2(2)
Fe3–Fe1–Fe2	55.41(2)	57.2(2)

Each atom in the triiron core is coordinated by two BINC ligands, displaying one shorter and two longer Fe–Fe bonds (Fe2–Fe3 2.495(6) Å vs. Fe1–Fe2 2.682(6) Å and Fe1–Fe3 2.685(6) Å) resembling an isosceles triangle. The shorter Fe2–Fe3 bond features two bridging isonitrile donor moieties, similar to the case of **H** which possesses ten terminal and two bridging carbonyl ligands.^[27] Nevertheless, due to the chelate ring in the bis(isonitrile) ligand the triiron core of **2** shows a slightly widened bond angles of 62.37° and 62.23° for Fe1–Fe2–Fe3 and Fe2–Fe3–Fe1, respectively, and a more acute angle of 55.41° for Fe2–Fe1–Fe3 in comparison with **H** (61.6°, 61.2° and 57.2°, respectively).

The ³¹P{¹H} NMR spectrum of **2** shows only one singlet at δ 13.2 ppm in THF-d₈, indicating a fluxional behavior by fast exchange of the bridging C≡N units in solution. In agreement with this analysis, only one ¹³C{¹H} NMR signal is observed for the isonitrile carbon atoms at δ 218.7 ppm, which is shifted downfield in comparison to the corresponding signal of the free BINC ligand (δ = 172.4 ppm). The solid-state infrared spectrum of **2** features a broad band centered at 2035 cm⁻¹ assignable to the isonitrile ν[CN] stretch, shifted to lower wave numbers compared to the isonitrile ν[CN] stretch in **1** (2122 cm⁻¹). The ν[CN] stretching frequencies for the divalent complex **1** is similar to that of the free BINC (2126 cm⁻¹), as the isonitrile functions essentially as a pure donor ligand. In contrast, compound **2**, with an iron center in the formally zerovalent oxidation state, shows ν[CN] stretching frequencies shifted to lower energies, shortened Fe–C bond lengths (1.81(1) Å vs. 1.87(4) Å in **1** (average values of terminal CN)), and slightly more bent Fe–C–N angles (173.5(9)° vs. 175.2(4)° in **1** (average values of terminal CN)). When they are taken together, these data indicate substantial M(dπ)→π* back-bonding in compound **2**.^[28]

The electrochemical behavior of **2** (see SI, Figure S41) was analyzed with UV-vis-NIR spectroelectrochemistry (SEC) in an optically transparent thin-layered electrode

(OTTLE) cell.^[29] The cyclic voltammogram showed a single partially reversible oxidation at $E_{pa} = -0.6$ V versus $[\text{FeCp}_2]^{0/+}$, which was used as the internal standard for all potentials reported herein unless otherwise noted. The neutral complex could be regenerated at $E_{pc} = -1.35$ V. The SEC for the oxidation process showed that the bands at 350 and 715 nm were consumed and replaced by a band at 475 nm with a shoulder at 580 nm. The spectrum of **2** could be regenerated after a cathodic potential of <1.5 V was reached. The electrochemical behavior of $[\text{Fe}_3(\text{CO})_{12}]$ in THF was reported to show only irreversible processes.^[30]

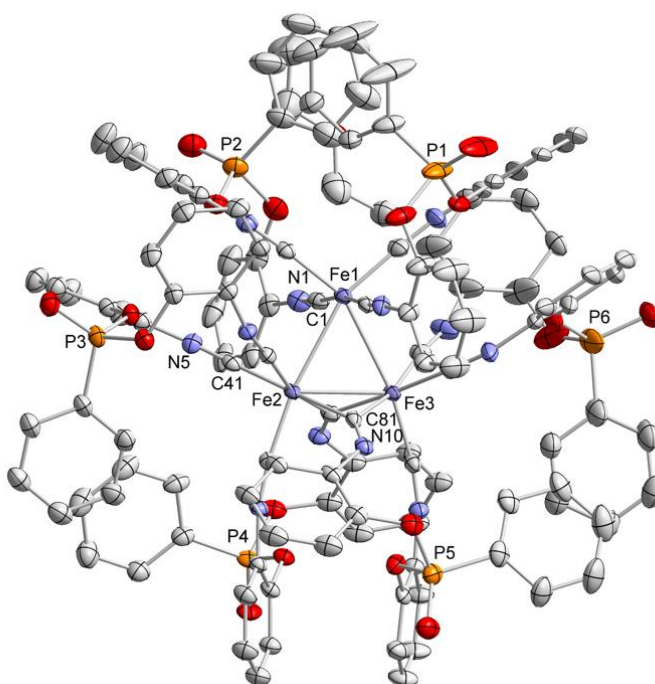
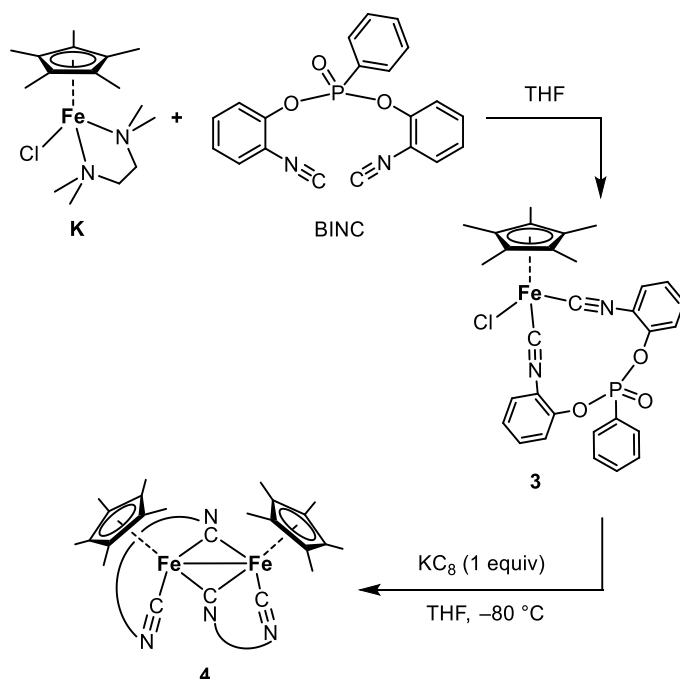


Figure 2. Solid-state molecular structure of complex $[\text{Fe}_3(\text{BINC})_6]$ (**2**). Ellipsoids are drawn at the 40% probability level. H atoms and disorder in the phenyl groups are omitted for clarity. Selected bond lengths [\AA] and angles [$^\circ$]: Fe1–C1 1.839(3), C1–N1 1.176(4), Fe2–C81 2.014(3), Fe3–C81 1.945(3), C81–N10 1.235(4), Fe2–C41 1.853(3), C41–N5 1.168(4); Fe2–C81–Fe3 78.10(1), Fe1–Fe2–C81 89.64(8), C81–Fe3–Fe1 91.04(8); Fe–Fe distances and Fe–Fe–Fe angles are given in Table 1.

Other prominent motifs for iron(II) complexes are mononuclear and dinuclear iron carbonyl species such as $[\text{CpFeCl}(\text{CO})_2]$ (**I**), which was first synthesized by Hubbard^[31], and $[\text{CpFe}(\text{CO})_2]_2$ (**J**).^[32] In the case of **J** it was demonstrated that the CO ligands could be substituted with monodentate isonitrile ligands, resulting in **A** (Figure 1). Again, we questioned if substitution by bidentate isonitrile ligand BINC is also tolerated.

With $[\text{Cp}^*\text{FeCl}(\text{tmeda})]$ ^[33] (Scheme 2; **K**, tmeda = tetramethylethylene-1,2-diamine) as the starting material, the mononuclear $[\text{Cp}^*\text{FeCl}(\text{BINC})]$ (**3**, $\text{Cp}^* = \text{Me}_5\text{C}_5$) could be readily synthesized in 82% yield and fully characterized by NMR/IR spectroscopy and XRD (see the Supporting Information, Figure S35). The iron atom shows a distorted

tetrahedral geometry, being η^5 -coordinated by the Cp* ligand, the two isonitrile moieties of the BINC ligand, and a chloride ligand. The carbon monoxide analogue **1** shows a similar distorted tetrahedral geometry in which the chloride and the two CO ligands are sterically repelled by the η^5 -coordinated cyclopentadienyl ligand and possess C–Fe–C angles of $95.6(2)^\circ$ and C–Fe–Cl angles of $90.4(2)^\circ$ (vs. angles in **3**: C1–Fe–C20 $88.4(7)^\circ$, C1–Fe–Cl $94.3(6)^\circ$; C20–Fe–Cl $91.4(6)^\circ$).^[34] The $^{31}\text{P}\{^1\text{H}\}$ NMR spectrum of **3** gives rise to a sharp singlet at $\delta = 15.2$ ppm. The IR spectrum shows two broad bands at 2084 and 2023 cm^{-1} , which are assigned to the symmetrical and asymmetrical CN stretching vibrations.



Scheme 2. Synthesis of [Cp*FeCl(BINC)] (**3**) and [Cp*Fe(BINC)]₂ (**4**).

The reduction of **3** in THF at low temperatures with one equivalent KC₈ affords green crystals of **4** in a yield of 18% after workup and crystallization from THF/*n*-hexane (Scheme 2). Single-crystal XRD revealed that **4** crystallizes as the *cis*-isomer, in which the Cp*-groups are both coordinated above the Fe–Fe bond (Figure 3). One C≡N unit of the BINC ligands links terminally to iron, while the other bridges the iron–iron bond. As a result of the double bridging isonitrile units there is a Fe–Fe bond of 2.575 Å. The iron bound bridging isonitrile groups result in an almost planar butterfly motif (Fe1–C20–Fe2–C40) with a torsion angle of 7.82° .

The structure of **4** is related to that of the phenyl-isonitrile complex *trans*-[CpFe(CNPh)₂]₂ (**A**, see Figure 1), which was already reported by Fehlhammer in 1980.^[12] In contrast to **4**, compound **A** crystallizes in a *trans/anti*-configuration with a strictly planar Fe₂C₂ core.

The Fe–Fe bond in **A** is 2.523(1) Å, which is shorter than in complex **4** (2.575(3) Å). In both complexes the aryl groups of the bridging isonitrile units show an *anti*-conformation.

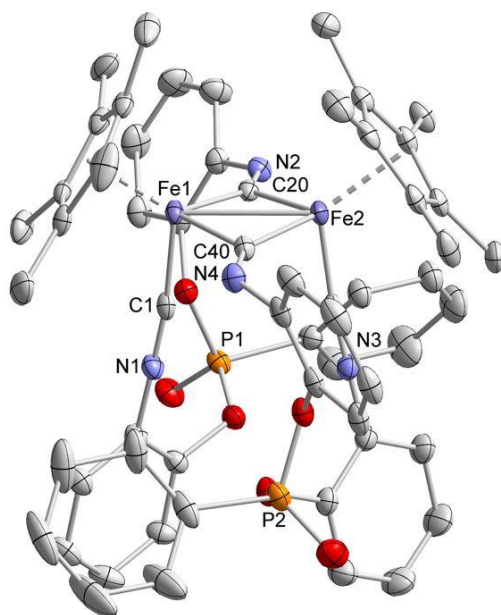


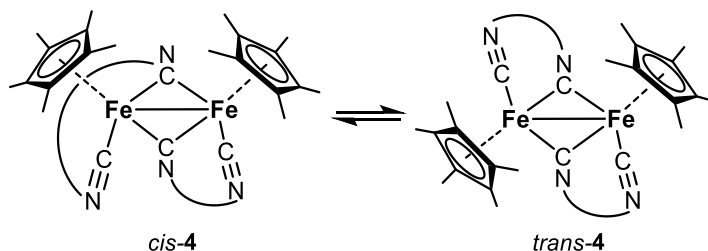
Figure 3. Solid-state molecular structure of complex $[\text{Cp}^*\text{Fe}(\text{BINC})]_2$ (**4**). Ellipsoids are drawn at the 40% probability level. H atoms, solvent molecules and disorder in the Cp* groups are omitted for clarity. Selected bond lengths [Å] and angles [°]: Fe1–Fe2 2.575(3), Fe1–C20 1.914(2), Fe2–C20 1.956(2), C20–N2 1.242(2), C21–N3 1.178(2), Fe1–C1 1.787(2), Fe2–C21 1.795(2), C1–N1 1.176(2), Fe1–C40 1.936(2), Fe2–C40 1.919(2), C40–N4 1.246(2); C1–Fe1–Fe2 95.48(3), C1–Fe1–C20 89.88(5), C21–Fe2–Fe1 96.85(5), Fe1–C1–N1 173.08(1), Fe2–C21–N3 173.93(1), C20–Fe1–C40 96.26(7), Fe1–C20–Fe2 83.43(7).

Table 2. Comparison of selected bond lengths [Å] and angles [°] of compound **4**, *cis*- $[\text{CpFe}(\text{CO})_2]_2$ (**J**),^[36] *trans*- $[\text{Cp}^*\text{Fe}(\text{CO})_2]_2$ (**L**),^[39] and $[\text{CpFe}(\text{CNPh})_2]_2$ (**A**).^[12]

	4	J	L	A
Fe1–Fe2	2.575(3)	2.531(2)	2.560(1)	2.523(1)
Fe1–C _{terminal}	1.787(2)	1.730(7)	1.753(3)	1.775(6)
C _{terminal} –N/O	1.176(2)	1.159(9)	1.154(3)	1.161(8)
Fe1–C _{bridged}	1.914(2)	1.918(7)	1.936(2)	1.934(6)
Fe2–C _{bridged}	1.956(2)	1.908(7)	1.936(2)	1.905(6)
C _{bridged} –N/O	1.242(2)	1.178(9)	1.172(3)	1.242(8)
C _{terminal} –Fe1–C _{bridged}	89.88(5)	92.3(3)	95.2(1)	–
Fe1–C _{terminal} –N/O	173.08(1)	176.5(8)	175(8)	178.4(4)

The NMR spectroscopic measurements indicate **4** is in a *cis*-/*trans*-isomer equilibrium in THF-*d*₈ (Scheme 3) which is not affected by temperature changes (see Figure S16). The ratio of the isomers depends on the isolated form of **4**; the crystalline product gives rise

to the *cis*-isomer as the main component, while for an amorphous powder the *trans*-isomer predominates (see the Supporting Information for spectra).



Scheme 3. *cis*-/*trans*-isomer equilibrium of compound **4** in solution.

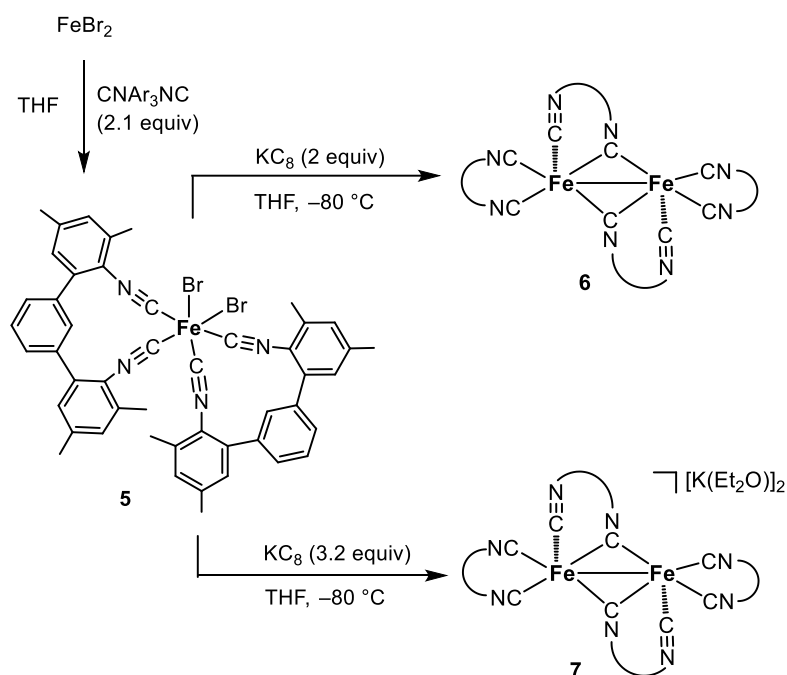
The occurrence of *cis*- and *trans*-isomers observed for **4** is also found in the dinuclear carbonyl analogue $[\text{CpFe}(\text{CO})_2]_2$ (**J**).^[35] X-ray crystal structures for both *trans*-**J**^[32] and *cis*-**J**^{[36],[37]} were obtained. The structure of the *cis*-isomer contains a shortened iron–iron bond (2.531(2) Å vs. compound **4**; Fe1–Fe2 2.575(3) Å; Table 2) due to the smaller ligands coordinated to the iron centers.^[36] It is noteworthy that the sterically more hindered permethylated derivative $[\text{Cp}^*\text{Fe}(\text{CO})_2]_2$ ^[38] (**L**) appears to exist exclusively as the *trans*-isomer, although the *cis*-configuration has been observed as a short-lived, photogenerated species.^[37] In contrast, **4** exists both as the *cis*- and *trans*-isomer in solution. Nevertheless, the structural parameters of **A**, **J**, **L** and **4** are similar. This shows that the exchange of the ancillary ligands (Cp vs. Cp*, and CO vs. CNPh and BINC) influences the solution behavior, but it does not strongly affect Fe–C and C–N bond lengths and Fe–C–N angles.

The electrochemical behavior of **4** in 0.1 M $\text{nBu}_4\text{NPF}_6/\text{THF}$ showed a partially reversible oxidation wave at $E_{\text{pa}} = -0.7$ V versus $[\text{FeCp}_2]^{+/0}$ and two irreversible processes at $E_{\text{pa}} = -0.35$ and 0.05 V. SEC of **4** showed that the bands at 600 and 390 nm decreased upon oxidation, and the process was irreversible (SI, Figure S42). In contrast, the CV of compound **4** in CH_2Cl_2 (SI, Figure S43) showed more resolved redox transitions at -0.7 V, -0.15 V, 0.3 V and 0.65 V. No reduction signal was observed. These transitions were partially reversible according to the UV–vis SEC spectrum, which showed the absorption bands at 310 nm and 370 nm were consumed and a band at 290 nm appeared. Upon further oxidation the band at 600 nm was consumed and the band at 290 nm coalesced.

In hopes of isolating isonitrile ferrate complexes with greater kinetic shielding, BINC was substituted for the bulkier bidentate chelating isonitrile, CNAr_3NC .^[7] The addition of two equivalents of CNAr_3NC to a solution of anhydrous FeBr_2 in THF affords an orange suspension, from which $[\text{FeBr}_2(\text{CNAr}_3\text{NC})_2]$ (**5**) can be isolated as orange crystals in 55%

yield after crystallization from $\text{CH}_2\text{Cl}_2/n\text{-hexane}$ (Scheme 4). The solid-state molecular structure of **5** shows a distorted octahedral geometry at the iron center with a *cis*-configuration of the bromido ligands (Br1-Fe1-Br2 $92.12(2)^\circ$, see the SI for a graphical representation of the structure and further characterization details).

Reduction of **5** in THF at low temperature with two equivalents of KC_8 (Scheme 4) results in an orange red solution from which dark red crystals of $[\text{Fe}(\text{CNAr}_3\text{NC})_2]_2$ (**6**) were isolated in a yield of 12%. ^1H NMR spectra and two-dimensional experiments (^1H , ^1H -NOESY) show that compound **6** is isolated in an equilibrium with one main isomer (*cis*-isomer, see solid-state molecular structure, Figure 4) and two other species (presumably isomers) with minor population (see the Supporting Information for spectra).



Scheme 4. Synthesis of $[\text{FeBr}_2(\text{CNAr}_3\text{NC})_2]$ (**5**), $[\text{Fe}(\text{CNAr}_3\text{NC})_2]_2$ (**6**) and $[\text{K}(\text{Et}_2\text{O})]_2[\text{Fe}(\text{CNAr}_3\text{NC})_2]_2$ (**7**).

Single-crystal XRD of **6** confirms the formation of a dimeric iron complex with four CNAr_3NC isonitrile ligands two of which are bridging the iron-iron bond. Compound **6** features a relatively short metal–metal bond ($2.434(6)$ Å) because of the bridging isonitrile ligands and assumes a butterfly structural motif. The Fe1-C25-Fe2-C49 torsion angle is 17.9° which indicates the Fe-C-Fe-C moiety is nearly planar.

A structural arrangement comparable to that of **6** is the structure of the unsaturated dinuclear iron carbonyl complex $[\text{Fe}_2(\text{CO})_8]$ (**M**), which was first observed in 1971 by Poliakoff and Turner as one of the main products from the low temperature photolysis of $[\text{Fe}_2(\text{CO})_9]$ conducted in CO matrixes.^{[39],[41]} On the basis of infrared spectroscopic

measurements the CO-bridged and unbridged isomers of **M** were proposed.^[39] The calculated iron–iron bond length (2.482 Å, Table 3, BP86/TZVP) of the singlet state of **M** with a C_s symmetry (global minimum) matches with the symmetry (two bridged CO units) and bond lengths of the solid-state molecular structure of **6** (Fe1–Fe2 2.434(6) Å).

Table 3. Comparison of selected bond lengths [Å] and angles [°] (average values) of **6** and [Fe₂(CO)₈] (**M**) (optimized singlet geometry in C_s symmetry (BP86/TZVP)).^[39]

	6	M
Fe–Fe	2.434(6)	2.482
Fe–C _{bridged}	1.939	1.982
C _{bridged} –N/O	1.240	1.177
Fe–C _{terminal}	1.848	1.802
C _{terminal} –N/O	1.171	1.154
Fe–C _{terminal} –N/O	174.88	178.00

The heightened stability and analogous nature of **6** compared to **M** allows for the latter's structural realization, something not possible previously due to its inherent instability. As expected for CN-bridged **6** with C_s symmetry, an analysis of the DFT calculated CN stretching frequencies determined six IR-active modes (for a comparison of the calculated IR spectra of **M** and **6**, see the Supporting Information). The solid-state IR spectrum of **6** features two ν [CN] specific bands at 2070 cm⁻¹ and 2022 cm⁻¹ (broad bands) for the terminally and bridged coordinated isonitrile units. These data are in good agreement with the DFT calculated values (see the SI for further details).

It was previously reported that when monodentate isonitrile ligands were used it was not possible to isolate a dinuclear iron complex bearing eight ligands. An example is [Fe₂(CNPh)₉] (**B**, Fe–Fe 2.458(1) Å, see Figure 1) which is synthesized in a manner comparable to that of **6** except partial decomposition must occur to provide an extra isonitrile ligand.^[13] This result shows that the use of the sterically demanding bidentate ligand CNAr₃NC is key to the successful stabilization of **6**, allowing for the isolation of a dinuclear iron complex with a lower coordination number.

When the reduction of **5** is repeated with three equivalents of finely ground KC₈ instead of two in THF at –80 °C, a brownish orange solution forms from which [K(Et₂O)]₂[Fe(CNAr₃NC)₂]₂ (**7**) can be isolated as a black solid in 46% yield by crystallization from Et₂O (Scheme 4). The solid-state molecular structure of **7** shows a similar motif as for complex **6**. The iron-iron bond is bridged by two isonitrile units and

the other ligands coordinate terminally to the iron centers. In the solid state, **7** is a contact-pair with significant interactions between the potassium and bridging isonitrile units (see Figure 4).

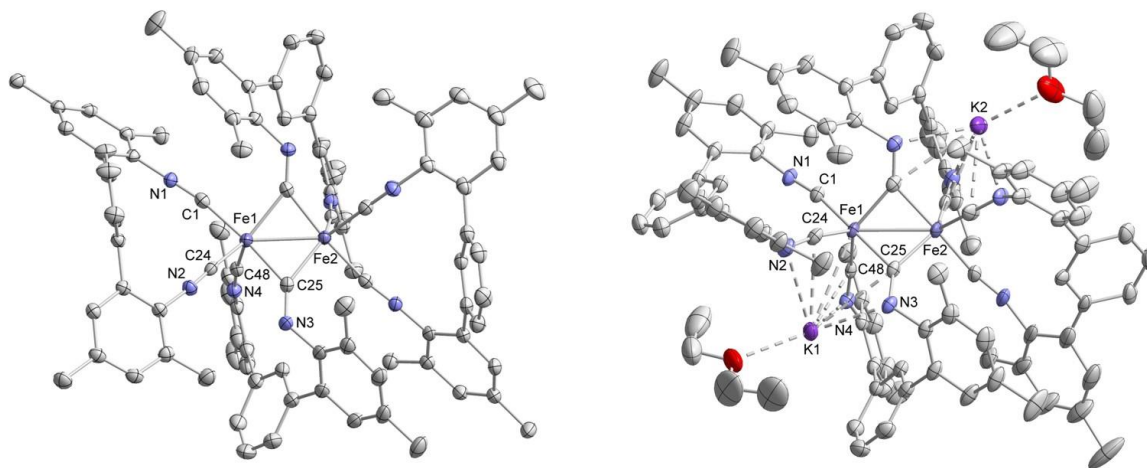


Figure 4. Solid-state molecular structures of $[\text{Fe}(\text{CNAr}_3\text{NC})_2]_2$ (**6**, on the left) and $[\text{K}(\text{Et}_2\text{O})_2][\text{Fe}(\text{CNAr}_3\text{NC})_2]_2$ (**7**, on the right). Ellipsoids are drawn at the 40% probability level. H atoms and solvent molecules are omitted for clarity. Selected bond lengths [\AA] and angles [$^\circ$] of **6**: Fe1–Fe2 2.434(6), Fe1–C1 1.835(3), C1–N1 1.165(4), Fe1–C25 1.977(3), Fe2–C25 1.900(3), C25–N3 1.244(4), Fe1–C24 1.860(3), C24–N2 1.176(4), Fe2–C48 1.800(3), C48–N4 1.186(4); Fe1–C25–Fe2 77.73(1), C1–Fe1–C24 87.39(1), Fe1–C1–N1 178.3(3). Selected bond lengths [\AA] and angles [$^\circ$] of **7**: Fe1–Fe2 2.552(8), Fe1–C1 1.747(5), Fe1–C24 1.838(5), Fe1–C25 1.951(4), Fe2–C25 1.963(4), Fe2–C48 1.789(4), Fe1–K1 3.439(1), Fe2–K2 3.410(1), C1–N1 1.214(9), C24–N2 1.176(6), C25–N3 1.266(5), C48–N4 1.206(5), Fe1–C25–Fe2 81.38(2), Fe1–C1–N1 146.0(6), Fe1–C24–N2 170.7(4), Fe1–C25–N3 142.9(3), Fe2–C25–N3 135.2(3).

The dinuclear dianionic complex, $[\text{Fe}_2(\text{CO})_8]^{2-}$ (**N**), which was first reported by Hieber and Brendel,^[42] is the carbon monoxide analogue of compound **7**. The solid-state structures of **N** feature different coordination modes depending on the counter ion used. Single-crystal XRD of $[\text{Na}(\text{DMF})_3]_2[\text{Fe}_2(\text{CO})_8]$ (**Na-N**) shows no bridging CO ligands, explaining why the Fe–Fe bond is significantly longer (2.804(1) \AA) than the metal–metal bond in **7** (Fe–Fe 2.552(8) \AA).^[43] The solid-state structure of $[\text{Li}(\text{THF})_3]_2[\text{Fe}_2(\text{CO})_8]$ (**Li-N**)^[44], in which the lithium atoms are bonded to the oxygen atoms of bridging CO groups, shows the same symmetry (C_{2v}) and coordination motif as compound **7** which results in similar bond lengths (Table 4, 2.551(1) \AA vs. 2.552(8) \AA for **7**). Because of the bridging CO/isonitrile ligands, both complexes **Li-N** and **7** assume a butterfly structural motif and show similar Fe–C–Fe–C torsion angles of 40.6(3) $^\circ$ for **Li-N** and 38.5(2) $^\circ$ for **7**.

Table 4. Comparison of selected bond lengths [Å] and angles [°] of **7** and [Li(THF)₃]₂[Fe₂(CO)₈] (Li-N)^[44] and [Na(DMF)₃]₂[Fe₂(CO)₈] (Na-N)^[43].

	7	[Li-N]	[Na-N]
Fe–Fe	2.552(8)	2.551(1)	2.804(1)
Fe–C _{bridged}	1.951(4)	1.929(8)	-
C _{bridged} –N/O	1.266(6)	1.216(9)	-
Fe–C _{terminal}	1.838(5)	1.765(8)	1.781(2)
C _{terminal} –N/O	1.176(6)	1.164(1)	1.158(2)
Fe–C _{terminal} –N/O	170.7(4)	177.5(7)	176.8(2)

5.3 Conclusion

We have reported the synthesis and characterization of isonitrile analogues of the classic tri- and dinuclear iron carbonyl complexes. The reduction of the iron(II) precursors *trans*-[FeBr₂(BINC)₂] (**1**), [Cp*FeCl(BINC)] (**3**) and [FeBr₂(CNAr₃NC)₂] (**5**) led to oligonuclear iron compounds with chelating bidentate isonitrile ligands. [Fe₃(BINC)₆] (**2**) possesses a triangular iron arrangement which is comparable to the structure motif of [Fe₃CO₁₂] and has been shown to have fluxional behavior with the bridging and terminal coordinated isonitrile units in solution. The reduction of compound **3** resulted in the dimeric heteroleptic complex [Cp*Fe(BINC)]₂ (**4**) as a *cis*-/*trans*-isomer mixture. The reduction of **5** bearing the bulkier isonitrile ligand results in [Fe(CNAr₃NC)₂]₂ (**6**) and [K(Et₂O)]₂[Fe(CNAr₃NC)₂]₂ (**7**), both possessing a butterfly arrangement. Contrary to its CO analogue [Fe₂(CO)₈], compound **6** is stable and isolable at room temperature. A detailed comparison of the spectroscopic and structural parameters of complexes **4**, **5**, **6** and **7** to mono(isonitrile) and CO analogues shows that replacing these monodentate ligands with bidentate isonitrile molecules, such as BINC and CNAr₃NC, does not dramatically affect the molecular or electronic structures. Thus, future investigations will be aimed at the synthesis of further highly reduced ferrate complexes and their utilization for electro- or photocatalysis, where the stable coordination of bidentate (chelating) isonitrile ligands might be beneficial.

5.4 Supporting Information

S1. General Information

General Procedure. All experiments were performed under an atmosphere of dry Argon (Argon 4.6, Linde) using standard Schlenk line techniques, a *MBraun* UniLab Glovebox or a *GS* Glovebox (GS117717). Solvents were dried and degassed with a *MBraun* SPS800 solvent-purification system. THF, diethyl ether and DCM were stored over molecular sieves (3 Å). *n*-Hexane was stored over a potassium mirror. Deuterated tetrahydrofuran was purchased from Sigma Aldrich and used as received. Elemental analyses were determined by the analytical department of the University of Regensburg with a Micro Vario Cube (Elementar).

General Analytical Techniques

NMR Spectroscopy. NMR spectra were recorded on *Bruker Avance 300* (300 MHz) and *Bruker Avance 400* (400 MHz) spectrometers at 300 K if not stated otherwise. ^1H and $^{13}\text{C}\{^1\text{H}\}$ spectra were referenced internally to residual solvent resonances, while $^{31}\text{P}\{^1\text{H}\}$ spectra were referenced externally to 85% $\text{H}_3\text{PO}_4(\text{aq.})$. The assignment of ^1H and ^{13}C NMR signals was confirmed by two-dimensional ($^1\text{H},^1\text{H}$ -COSY, $^1\text{H},^1\text{H}$ -NOESY, $^1\text{H},^{13}\text{C}$ -HSQC, $^1\text{H},^{13}\text{C}$ -HMBC) experiments. The following abbreviations have been used for multiplicities: s = singlet, d = doublet, t = triplet, q = quartet, m = multiplet, dd = doublet of doublet.

IR Spectroscopy. IR spectra were recorded using a Bruker ALPHA spectrometer equipped with a diamond ATR unit. The following abbreviations were used for the intensities and characteristics of important IR absorption bands: vs = very strong, s = strong, m = medium, w = weak, br. = broad.

Electrochemistry and UV-vis-NIR Spectroelectrochemistry.

UV-vis-NIR absorption spectra were recorded on J&M TIDAS spectrophotometer. Cyclic voltammetry was carried out in 0.1 M $\text{Bu}_4\text{NPF}_6/\text{THF}$ solutions using a three-electrode configuration (Pt working, Pt wire counter, and Ag quasi-reference electrodes) and was performed on a Metrohm Autolab potentiostat. THF was distilled from Na/K amalgam and degassed directly before use in the electrochemistry.

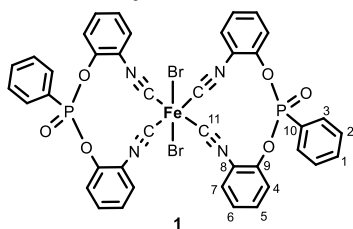
X-ray Crystallography. Single-crystal X-ray diffraction data were recorded on an Agilent Technologies SuperNova diffractometer with Cu-K_α radiation ($\lambda = 1.54184 \text{ \AA}$). Crystals were selected under mineral oil, mounted on MicroMount loops and quenched-cooled using an Oxford Cryo-system open flow N_2 cooling device. Either semiempirical

multiscan absorption corrections^[45] or analytical corrections^[46] were applied to the data. Using Olex2^[47], the structures were solved with SHELXT^[48] structure solution program using Intrinsic Phasing and refined with SHELXL^[49] refinement package using Least Squares refinements on F^2 .^[50] The hydrogen atoms were located in idealized positions and refined isotropically with a riding model. Crystallographic data for the structures in this paper have been deposited with the Cambridge Crystallographic Data Centre, CCDC, 12 Union Road, Cambridge CB21EZ, UK. Copies of the data can be obtained free of charge on quoting the depository numbers: 2056040 (for **1**), 2056041 (for **2**), 2056042 (for **3**), 2056043 (for **4**), 2056044 (for **5**), 2056046 (for **6**) and 2056045 (for **7**).

S2. Synthesis of Compounds

Starting materials. The chelating bidentate isonitrile ligands bis(2-isocyanophenyl)-phenylphosphonate (BINC)^[6] and 2,2''-diisocyano-3,5,3'',5''-tetramethyl-1,1':3',1''-terphenyl (CNAr₃NC)^[7] and [Cp*FeCl(tmeda)]^[33] were prepared according to reported procedures.

S2.1 Synthesis of *trans*-[FeBr₂(BINC)₂] (**1**)

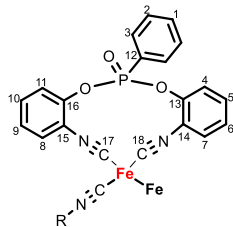
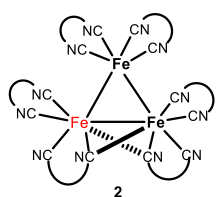


A solution of BINC (0.350 g, 0.970 mmol) in THF (10 mL) was added to a solution of FeBr₂ (0.100 g, 0.460 mmol) in THF (60 mL) at ambient temperature. The orange brownish reaction mixture turned into a grayish suspension after 30

minutes. After stirring overnight, product **1** could be isolated as blue solid after decanting off the supernatant solution, washing with THF (3 x 10 mL) and drying *in vacuo*. Recrystallisation by slow diffusion of *n*-hexane into a DCM solution resulted in blue crystals of **1**. Yield: 154 mg, 33% (the calculated yield assumes the presence of 8% FeBr₂ in the sample, vide infra). Elemental analysis calcd. for C₄₀H₂₆Br₂FeN₄O₆P₂ (Mw = 936.27 g/mol) C 51.31; H 2.80; N 5.98, found C 50.27; H 2.87; N 5.77. Elemental analyses consistently gave low carbon and nitrogen, which indicated the presence of a persistent impurity. The impurity could not be removed by extraction or crystallization. We presume the impurity to be unreacted FeBr₂. A calculated C, H, N analysis for **1** · 0.08 FeBr₂ (C 50.39; H 2.75; N 5.88) fits well to the found values (C 50.27; H 2.87; N 5.77). ¹H-NMR (400.13 MHz, 300 K, CD₂Cl₂): δ[ppm] 8.31-8.37 (m, 4H, H₂), 7.71 (d, ³J_{HH} = 8.5 Hz, 4H, H₄), 7.65 (d, ³J_{HH} = 7.9 Hz, 4H, H₇), 7.6 (dt, ³J_{HH} = 1.4 Hz, ³J_{HH} = 7.5 Hz, 2H, H₁), 7.46-7.50 (m, 2H, H₃), 7.40 (dt, ³J_{HH} = 1.6 Hz, ³J_{HH} = 7.7 Hz, 4H, H₅), 7.28 (t, ³J_{HH} = 7.7 Hz, 4H, H₆). ¹³C{¹H}-NMR (100.61 MHz, 300 K, CD₂Cl₂): δ[ppm]

147.4 (d, $J = 7.0$ Hz, C₉), 134.6 (d, $J = 2.6$ Hz, C₁), 133.9 (d, $J = 11.5$ Hz, C₂), 130.8 (s, C₅), 129.4 (d, $J = 16.4$ Hz, C₃), 127.6 (s, C₇), 126.1 (s, C₆), 123.8 (d, $J = 190$ Hz, C₁₀), 121.9 (d, $J = 2.7$ Hz, C₄), 121.2 (d, $J = 5.1$ Hz, C₈), (C₁₁≡N) signals were not detected. ³¹P{¹H}-NMR (161.98 MHz, 300 K, CD₂Cl₂): δ[ppm] 15.5 (s, 2P). IR: ν[cm⁻¹] 2122 (ν[C≡N], vs), 1585 (w), 1486 (s), 1486 (m), 1439 (m), 1288 (m), 1239 (m), 1130 (s), 1100 (s), 1031 (m), 916 (br. s), 799 (s), 755 (s), 713 (m), 596 (s), 563 (s), 531 (vs).

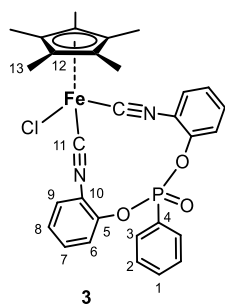
S2.2 Synthesis of [Fe₃(BINC)₆] (2)



KC₈ (coarse, 144 mg, 1.068 mmol) was added in portions to a suspension of **1** (500 mg, 0.534 mmol) in THF (30 mL) at -80 °C. After stirring overnight and warming up to room temperature, a brownish yellow solution was formed. The solution was filtered, concentrated *in vacuo* (ca. 15 mL) and layered with *n*-hexane (20 mL). Product **2** could be isolated as brown crystals after decanting off the supernatant solution and drying under vacuum.

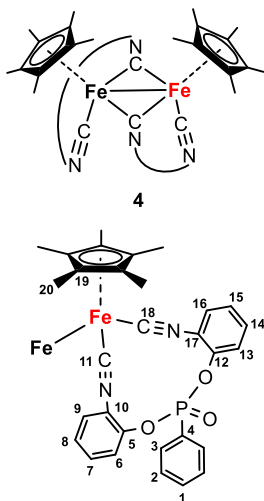
Yield: 107 mg, 26%. Elemental analysis calcd. for

C₁₂₀H₇₈Fe₃O₁₈N₁₂P₆ (Mw = 2329.39 g/mol) C 61.88; H 3.38; N 7.22, found C 61.47; H 3.42; N 6.95. ¹H-NMR (400,13 MHz, 300 K, THF-*d*₈): δ[ppm] 8.50 (dd, ⁴J_{HH} = 1.1 Hz, ³J_{HH} = 8.1 Hz, 1H, H₇), 8.29 (m, 2H, H₂), 7.56 (d, ³J_{HH} = 8.1 Hz, 1H, H₄), 7.14-7.16 (m, 1H, H₅), 7.13 (d, ³J_{HH} = 8.0 Hz, 1H, H₁₁), 6.94 (t, ³J_{HH} = 8.1 Hz, 1H, H₆), 6.83 (t, ³J_{HH} = 7.4 Hz, 1H, H₁), 6.68-6.75 (m, 2H, H₃), 6.68-6.75 (m, 1H, H₁₀), 6.53-6.57 (dt, ³J_{HH} = 1.0 Hz, ³J_{HH} = 7.8 Hz, 1H, H₉), 5.48 (d, ³J_{HH} = 7.8 Hz, 1H, H₈). ¹³C{¹H}-NMR (100.61 MHz, 300 K, THF-*d*₈): δ[ppm] 218.7 (s, C₁₈), 188.1 (s, C₁₇), 146.4 (d, $J = 5.0$ Hz, C₁₆), 144.9 (d, $J = 10.1$ Hz, C₁₃), 134.0 (d, $J = 10.7$ Hz, C₂), 133.9 (d, $J = 2.8$ Hz, C₁), 130.7 (d, $J = 4.2$ Hz, C₁₄), 128.9 (d, $J = 15.7$ Hz, C₃), 127.4 (s, C₇), 126.9 (d, C₅), 126.7 (s, C₆), 126.6 (s, C₁₀), 126.5 (d, $J = 188.9$ Hz, C₁₂), 125.2 (s, C₉), 124.9 (s, C₈), 123.4 (d, $J = 2.1$ Hz, C₄), 123.3 (d, $J = 7.2$ Hz, C₁₅), 120.2 (s, C₁₁). ³¹P{¹H}-NMR (161.98 MHz, 300, THF-*d*₈): δ[ppm] 13.2 (s). IR: ν[cm⁻¹] 2035 (ν[C≡N], br. m), 1643 (m), 1581 (s), 1485 (s), 1451 (m), 1440 (m), 1282 (m), 1265 (s), 1247 (s), 1200 (w), 1130 (s), 1101 (s), 927 (vs), 809 (s), 753 (vs). 516 (s).

S2.3 Synthesis of $[\text{Cp}^*\text{FeCl}(\text{BINC})]$ (**3**)

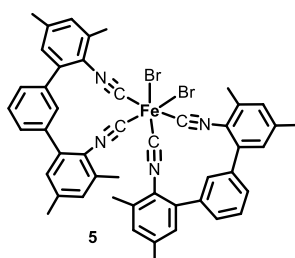
A solution of BINC (420 mg, 1.17 mmol) in THF (5 mL) was added to a yellow solution of $[\text{Cp}^*\text{FeCl}(\text{tmeda})]^{[33]}$ (400 mg, 1.17 mmol) in THF (15 mL). An immediate color change to dark red was obtained. After stirring the reaction mixture overnight, a red/brown suspension was formed. After removing the solvent under reduced pressure, the brown solid was dried *in vacuo*. Recrystallization by

slow diffusion of *n*-hexane into a DCM solution resulted in red/black crystals of **3**. Yield: 560 mg, 82%. Elemental analysis calcd. for $\text{C}_{30}\text{H}_{28}\text{ClFeN}_2\text{O}_3\text{P}$ ($M_w = 586.83$ g/mol) C 61.40; H 4.81; N 4.77, found C 60.78; H 4.81; N 4.70. The elemental analysis consistently indicates the presence of persistent impurities in samples of **3** prepared in the above manner. The unknown impurities could not be removed by washing or recrystallization of compound **3**. $^1\text{H-NMR}$ (400.13 MHz, 300 K, CDCl_3): δ [ppm] 8.17-8.11 (m, 2H, H_2), 8.12 (d, $^3J_{\text{HH}} = 7.4$ Hz, 1H, H_3 or H_3'), 7.56 (d, $^3J_{\text{HH}} = 8.1$ Hz, 2H, H_6), 7.48-7.42 (m, 3H, H_1/H_3), 7.27 (d, $^3J_{\text{HH}} = 7.6$ Hz, 2H, H_9), 7.15 (t, $^3J_{\text{HH}} = 7.6$ Hz, 2H, H_7), 7.08 (t, $^3J_{\text{HH}} = 7.6$ Hz, 2H, H_8), 1.75 (s, 15H, H-Cp*). $^{13}\text{C}\{^1\text{H}\}$ -NMR (100.61 MHz, 300 K, CDCl_3): δ [ppm] 188.7 (s, C_{11}), 146.1 (d, $J = 6.6$ Hz, C_5), 133.9 (d, $J = 3.2$ Hz, C_1), 133.5 (d, $J = 11.5$ Hz, C_2), 128.9 (d, $J = 16.5$ Hz, C_3), 127.7 (d, $J = 1.1$ Hz, C_7), 125.6 (s, C_9), 125.4 (d, $J = 1.0$ Hz, C_8), 123.4 (d, $J = 189.9$ Hz, C_4), 123.2 (d, $J = 6.2$ Hz, C_{10}), 121.4 (d, $J = 2.8$ Hz, C_6), 93.1 (s, C_{12}), 9.9 (s, C_{13}). $^{31}\text{P}\{^1\text{H}\}$ -NMR (161.98 MHz, 300 K, CDCl_3): δ [ppm] 15.2 (s, 1P). IR: ν [cm^{-1}] 2908 (w), 2084 (ν [$\text{C}\equiv\text{N}$], s), 2023 (ν [$\text{C}\equiv\text{N}$], s), 2011 (ν [$\text{C}\equiv\text{N}$], s), 1489 (s), 1439 (m), 1265 (m), 1244 (m), 1102 (s), 944 (vs), 923 (vs), 763 (vs), 573 (s).

S2.4 Synthesis of $[\text{Cp}^*\text{Fe}(\text{BINC})]_2$ (**4**)

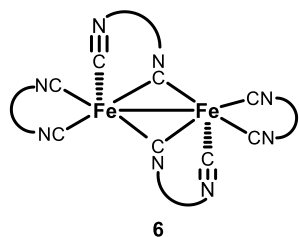
KC_8 (coarse, 138 mg, 1.023 mmol) was added to a red suspension of **3** (600 mg, 1.023 mmol) in THF (30 mL) at -80 °C. The green reaction solution obtained was stirred and warmed up to room temperature overnight. After filtration and concentration in vacuum the green solution was layered with *n*-hexane. After decanting off the supernatant solution and drying under vacuum **4** was isolated as green crystals. Yield: 100 mg, 18%. Elemental analysis calcd. for $\text{C}_{60}\text{H}_{56}\text{Fe}_2\text{N}_4\text{O}_6\text{P}_2$ ($M_w = 1102.77$ g/mol) C 65.35; H 5.12; N 5.08, found C 65.06; H 5.33; N 4.84. $^1\text{H-NMR}$

(400.13 MHz, 300 K, THF- d_8): δ [ppm] 8.14-8.09 (m, 4H, H₂, *cis*), 8.10-8.05 (m, 1.3H, H₂, *trans*), 7.77-7.72 (m, 1.3H, H₂, *trans*), 7.66-7.63 (m, 2.3H, H₁, *cis* (overlapping with *trans*)), 7.60-7.55 (m, 4.7H, H₃, *cis*), 7.53-7.48 (m, 1.4H, H₃, *trans*), 7.44 (d, $^3J = 7.6$ Hz, 0.8H, H_{Ar}, *trans*), 7.40-7.38 (m, 2.8H, H₆, *cis*), 7.34-7.32 (m, 2.8H, H₉, *cis* (overlapping with *trans*)), 7.29-7.22 (m, 2.6H, H_{Ar}, *trans*), 7.11-7.08 (m, 1H, H_{Ar}, *trans*), 7.05-7.02 (t, $^3J = 7.6$ Hz, 2.3H, H₈, *cis*), 7.01-6.95 (m, 2.0H, *trans*), 6.88 (t, $^3J = 7.6$ Hz, 1H, H_{Ar}, *trans*), 6.70 (t, $^3J = 7.6$ Hz, 2.0H, H₁₄, *cis*), 6.64 (t, $^3J = 7.6$ Hz, 2.8H, H₇, *cis*), 6.54 (t, $^3J = 7.6$ Hz, 1H, H_{Ar}, *trans*), 6.48-6.44 (m, 1.3H, H_{Ar}, *trans*), 6.45-6.37 (m, 4H, H₁₃ and H₁₅, *cis* (overlapping with *trans*)), 6.32 (t, $^3J = 7.6$ Hz, 0.8H, H_{Ar}, *trans*), 6.27 (d, $^3J = 7.6$ Hz, 0.6H, H₁₆, *trans*), 6.18 (d, $^3J = 7.6$ Hz, 2H, H₁₆, *cis*), 6.14 (d, $^3J = 7.6$ Hz, 0.6H, H₁₆, *trans*), 1.87 (s, 8.4H, H₂₀, *trans*-Cp*), 1.74 (s, 30H, H₂₀, *cis*-Cp*), 1.63 (s, 8.2H, H₂₀, *trans*-Cp*). $^{13}\text{C}\{^1\text{H}\}$ -NMR (100.61 MHz, 300 K, THF- d_8): δ [ppm] 265.1 (s, C₁₁, *cis*), 262.6 (s, C₁₁, *trans*), 259.9 (s, C₁₁, *trans*), 189.9 (s, C₁₈, *trans*), 183.7 (s, C₁₈, *cis*), 182.7 (s, C₁₈, *trans*), 143.9 (d, $J = 10.7$ Hz, C₁₂, *cis*), 144.0 (d, $J = 10.4$ Hz, C₁₂, *trans*), 146.0 (m, C₁₂, *trans*), 138.9 (d, $J = 5.0$ Hz, C₅, *cis*), 138.6 (d, $J = 5.0$ Hz, C₅, *trans*), 138.3 (d, $J = 5.0$ Hz, C₅, *trans*), 137.4 (d, $J = 6.3$ Hz, C₁₀, *cis*), 137.0 (d, $J = 4.5$ Hz, C₁₀, *trans*), 137.8 (d, $J = 6.0$ Hz, C₁₀, *trans*), 133.0 (d, $J = 10.3$ Hz, C₂, *trans*), 132.9 (d, $J = 11.3$ Hz, C₂, *cis*), 132.8 (d, $J = 10.5$ Hz, C₂, *trans*), 132.6 (m, C₁, *cis*), 128.2 (d, $J = 15.8$ Hz, C₃, *cis*), 127.9 (d, $J = 15.8$ Hz, C₃, *trans*), 127.7 (d, $J = 15.5$ Hz, C₃, *trans*), 127.6 (s, C_{Ar}), 126.7 (d, $J = 1.7$ Hz, C₁₆), 125.7 (s, C_{Ar}), 125.6 (dd, $J = 1.8$ Hz, $J = 6.3$ Hz, C_{Ar}), 125.1 (d, $J = 1.7$ Hz, C₁₄), 124.8 (s, C_{Ar}), 124.6 (s, C_{Ar}, *trans*), 124.5 (s, C₈, *cis*), 124.0 (d, $J = 3.4$ Hz, C₁₇, *cis*), 123.6 (d, $J = 190$ Hz, C₄, *cis*), 123.3 (d, $J = 3.4$ Hz, C₁₃ and C₁₅, *cis*), 123.8 (d, $J = 3.4$ Hz, C_{Ar}), 122.8 (s, C₉, *trans*), 122.7 (s, C₉, *cis*), 122.5 (s, C₉, *trans*), 119.9 (d, $J = 2.8$ Hz, C_{Ar}), 119.7 (s, C₆, *cis*), 119.6 (d, $J = 2.8$ Hz, C₇, *cis*), 119.4 (s, C_{Ar}), 118.9 (d, $J = 1.4$ Hz, C_{Ar}), 118.7 (d, $J = 2.5$ Hz, C_{Ar}), 96.7 (s, C₁₉, *trans*), 96.3 (s, C₁₉, *cis*), 95.7 (s, C₁₉, *trans*), 10.8 (s, C₂₀, *trans*), 10.0 (s, C₂₀, *cis*), 9.3 (s, C₂₀, *trans*). $^{31}\text{P}\{^1\text{H}\}$ -NMR (161.98 MHz, 300 K, THF- d_8): δ [ppm] 14.5 (s, 2P, *cis*), 14.3 (s, 0.6P, *trans*), 12.1 (s, 0.6P, *trans*). IR: ν [cm⁻¹] 3057 (w), 2899 (w), 2853 (w), 2053 (ν [C \equiv N], br. s), 2028 (ν [C \equiv N], br. s), 1656 (s), 1580 (s), 1478 (s), 1440 (m), 1256 (s), 1129 (s), 1098 (s), 924 (vs), 750 (vs), 645 (s), 580 (s), 533 (s), 501 (s).

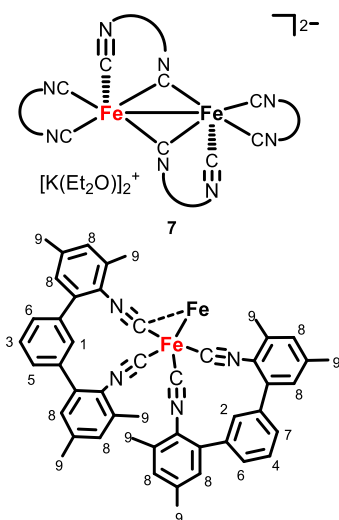
S2.5 Synthesis of $[\text{FeBr}_2(\text{CNAr}_3\text{NC})_2]$ (**5**)

A solution of CNAr_3NC (98.3 mg, 0.292 mmol) in THF (15 mL) was added to a solution of FeBr_2 (30 mg, 0.139 mmol) in THF (15 mL). After stirring overnight, the orange suspension was filtrated and the remaining orange residue was washed with THF (2×5 mL) and dried *in vacuo*.

Recrystallization by slow diffusion of *n*-hexane into a DCM solution resulted in orange crystals of **5**. Yield: 73.6 mg, 55% (the calculated yield assumes the presence of 8% FeBr_2 in the sample, *vide infra*). Elemental analysis calcd. for $\text{C}_{48}\text{H}_{40}\text{Br}_2\text{FeN}_4$ ($M = 888.53$ g/mol) C 64.89, H 4.54, N 6.3, found C 63.58; H 4.80; N 5.93. Elemental analyses consistently gave low carbon and nitrogen values, which indicated the presence of a persistent impurity. The impurity could not be removed by extraction or crystallization. We presume the impurity to be unreacted FeBr_2 . A calculated C, H, N analysis for $\mathbf{5} \cdot 0.08 \text{ FeBr}_2$ (C 63.65; H 4.48; N 6.19) fits well to the found values (C 63.58; H 4.80; N 5.93). $^1\text{H-NMR}$ (400,13 MHz, 213 K, CD_2Cl_2): δ [ppm] 8.08 (ps. t, 1H, H_{Ar}), 7.77 (ps. t, 1H, H_{Ar}), 7.66 (t, $^3J_{\text{HH}} = 7.7$ Hz, 1H, H_{Ar}), 7.63 (t, $^3J_{\text{HH}} = 7.7$ Hz, 1H, H_{Ar}), 7.50 (d, $^3J_{\text{HH}} = 7.8$ Hz, 1H, H_{Ar}), 7.46(d, $^3J_{\text{HH}} = 7.8$ Hz, 1H, H_{Ar}), 7.42 (d, $^3J_{\text{HH}} = 7.8$ Hz, 1H, H_{Ar}), 7.35 (d, $^3J_{\text{HH}} = 7.8$ Hz, 1H, H_{Ar}), 7.18 (s, 1H, H_{Ar}), 7.14 (s, 1H, H_{Ar}), 7.12 (s, 1H, H_{Ar}), 7.09 (br. s, 2H, H_{Ar}), 7.05 (s, 1H, H_{Ar}), 6.94 (s, 1H, H_{Ar}), 6.91 (s, 1H, H_{Ar}), 2.64 (s, 3H, H_{Methyl}), 2.55 (s, 3H, H_{Methyl}), 2.53 (s, 3H, H_{Methyl}), 2.37 (s, 6H, H_{Methyl}), 2.33 (s, 3H, H_{Methyl}), 2.26 (s, 3H, H_{Methyl}), 1.53 (s, 3H, H_{Methyl}). $^{13}\text{C}\{^1\text{H}\}$ -NMR (100.61 MHz, 213 K, CD_2Cl_2): δ [ppm] 167.3 (s, C_{CN}), 166.8 (s, C_{CN}), 164.6 (s, C_{CN}), 164.4 (s, C_{CN}), 139.4 (s, C_{Ar}), 138.9 (s, C_{Ar}), 138.6 (s, C_{Ar}), 138.3 (s, C_{Ar}), 137.8 (s, C_{Ar}), 137.7 (s, C_{Ar}), 137.1 (s, C_{Ar}), 137.1 (s, C_{Ar}), 136.9 (s, C_{Ar}), 136.8 (s, C_{Ar}), 136.5 (s, C_{Ar}), 136.1 (s, C_{Ar}), 135.4 (s, C_{Ar}), 135.2 (s, C_{Ar}), 130.1 (s, C_{Ar}), 130.0 (s, C_{Ar}), 129.9 (s, C_{Ar}), 129.9 (s, C_{Ar}), 129.6 (s, C_{Ar}), 129.1 (s, C_{Ar}), 129.0 (s, C_{Ar}), 128.9 (s, C_{Ar}), 128.9 (s, C_{Ar}), 128.8 (s, C_{Ar}), 128.6 (s, C_{Ar}), 128.5 (s, C_{Ar}), 128.5 (s, C_{Ar}), 123.1 (s, C_{Ar}), 122.8 (s, C_{Ar}), 122.2 (s, C_{Ar}), 122.2 (s, C_{Ar}), 21.1 (s, C_{Methyl}), 21.0 (s, C_{Methyl}), 20.9 (s, C_{Methyl}), 18.7 (s, C_{Methyl}), 18.7s (s, C_{Methyl}), 18.6 (s, C_{Methyl}), 18.0 (s, C_{Methyl}). Characterization by NMR spectroscopy at 300 K showed broadened signals in the $^1\text{H-NMR}$ spectra. Variable temperature NMR confirmed the assumption of a *cis/trans*-isomer mixture. The NMR characterization of compound **5** at 213 K (-60 °C) identified the multiplet as a 1:1-isomeric mixture. IR: ν [cm^{-1}] 2158 (w), 2144 (ν [$\text{C}\equiv\text{N}$], vs), 2126 (ν [$\text{C}\equiv\text{N}$], vs), 1594 (w), 1462 (m), 860 (m), 805 (s), 733 (m), 705 (s), 607 (m), 567 (m).

S2.6 Synthesis of $[\text{Fe}(\text{CNAr}_3\text{NC})_2]_2$ (**6**)

KC_8 (coarse, 30.4 mg, 0.225 mmol) was added in portions to a suspension of **5** (100.0 mg, 0.113 mmol) in THF (15 mL) at -80°C . After 30 minutes a dark orange/red reaction solution was formed. The solution was stirred overnight and warmed up to room temperature. The dark red reaction mixture was filtered, concentrated *in vacuo* (ca. 5 mL) and **6** was crystallized by slow diffusion of *n*-hexane into a THF solution. Compound **6** was isolated as red/brown crystals. Yield: 10 mg, 12%. Elemental analysis calcd. for $\text{C}_{96}\text{H}_{80}\text{Fe}_2\text{N}_8$ (Mw = 1457.44 g/mol) C 79.12; H 5.53; N 7.69, found C 79.27; H 5.89; N 6.92. ^1H -NMR (400.13 MHz, 300 K, THF- d_8): δ [ppm] 8.53 (s, 1H, H_{Ar}), 8.13 (s, 1H, H_{Ar}), 8.10 (s, 1H, H_{Ar}), 7.66 (s, 1H, H_{Ar}), 7.49 (s, 1H, H_{Ar}), 7.48 (t, $^3J = 7.7$ Hz 1H, H_{Ar}), 7.39 (t, $^3J = 7.4$ Hz 1H, H_{Ar}), 7.35 (m, 1H, H_{Ar}), 7.32 (m, 1H, H_{Ar}), 7.26 (t, $^3J = 7.6$ Hz 1H, H_{Ar}), 7.15 (d, $^3J = 8.0$ Hz 1H, H_{Ar}), 7.10 (d, $^3J = 8.0$ Hz 1H, H_{Ar}), 7.05 (m, 3H, H_{Ar}), 7.00 (m, 2H, H_{Ar}), 6.97 (m, 3H, H_{Ar}), 6.89 (m, 3H, H_{Ar}), 6.73 (m, 2H, H_{Ar}), 6.67 (m, 2H, H_{Ar}), 6.62 (m, 2H, H_{Ar}), 6.59 (m, 2H, H_{Ar}), 6.55 (m, 1H, H_{Ar}), 6.44 (d, $^3J = 7.6$ Hz, 1H, H_{Ar}), 6.40 (dd, $^3J = 7.8$ Hz, $^3J = 1.5$ Hz, 1H, H_{Ar}), 6.22 (s, 1H, H_{Ar}), 6.18 (d, $^3J = 7.3$ Hz, 1H, H_{Ar}), 6.05 (s, 1H, H_{Ar}), 5.40 (s, 1H, H_{Ar}), 5.36 (s, 1H, H_{Ar}), 2.62 (s, 3H, H_{Methyl}), 2.54 (s, 3H, H_{Methyl}), 2.46 (s, 6H, H_{Methyl}), 2.34 (s, 3H, H_{Methyl}), 2.28 (m, 6H, H_{Methyl}), 2.18 (m, 9H, H_{Methyl}), 2.10 (s, 3H, H_{Methyl}), 1.83 (s, 3H, H_{Methyl}), 1.75 (s, 3H, H_{Methyl}), 1.70 (s, 3H, H_{Methyl}), 1.65 (s, 3H, H_{Methyl}), 1.23 (s, 3H, H_{Methyl}), 1.13 (s, 3H, H_{Methyl}), 0.53 (s, 3H, H_{Methyl}). $^{13}\text{C}\{^1\text{H}\}$ -NMR (150.88 MHz, 300 K, THF- d_8): δ [ppm] 244.2 (s, C_{CN}), 235.5 (s, C_{CN}), 208.7 (s, C_{CN}), 191.1 (s, C_{CN}), 142.2 (s, C_{Ar}), 140.9 (s, C_{Ar}), 140.5 (s, C_{Ar}), 139.5 (s, C_{Ar}), 138.3 (s, C_{Ar}), 138.1 (s, C_{Ar}), 137.9 (s, C_{Ar}), 137.4 (s, C_{Ar}), 136.4 (s, C_{Ar}), 136.2 (s, C_{Ar}), 135.8 (s, C_{Ar}), 135.6 (s, C_{Ar}), 135.5 (s, C_{Ar}), 134.9 (s, C_{Ar}), 134.7 (s, C_{Ar}), 134.1 (s, C_{Ar}), 134.0 (s, C_{Ar}), 132.9 (s, C_{Ar}), 132.8 (s, C_{Ar}), 129.6 (s, C_{Ar}), 129.5 (s, C_{Ar}), 129.4 (s, C_{Ar}), 129.2 (s, C_{Ar}), 128.7 (s, C_{Ar}), 128.4 (s, C_{Ar}), 127.9 (s, C_{Ar}), 127.8 (s, C_{Ar}), 126.1 (s, C_{Ar}), 125.1 (s, C_{Ar}), 29.6 (s, C_{Methyl}), 27.0 (s, C_{Methyl}), 25.4 (s, C_{Methyl}), 22.0 (s, C_{Methyl}), 20.8 (s, C_{Methyl}), 20.5 (s, C_{Methyl}), 20.2 (s, C_{Methyl}), 20.1 (s, C_{Methyl}), 20.0 (s, C_{Methyl}), 19.9 (s, C_{Methyl}), 19.8 (s, C_{Methyl}), 19.7 (s, C_{Methyl}), 18.8 (s, C_{Methyl}), 18.5 (s, C_{Methyl}), 18.4 (s, C_{Methyl}), 17.8 (s, C_{Methyl}), 17.5 (s, C_{Methyl}), 17.1 (s, C_{Methyl}). On the basis of the ^1H , ^1H -NOESY of **6** showing three different sets of methyl groups (eight in each set) it can be concluded that compound **6** can be isolated as a mixture of three isomers. IR: ν [cm^{-1}] 2914 (w), 2852 (w), 2070 (ν [$\text{C}\equiv\text{N}$], s), 2022 (ν [$\text{C}\equiv\text{N}$], s), 1676 (m), 1593 (m), 1460 (m), 1370 (s), 855 (vs), 733 (vs).

S2.7 Synthesis of $[\text{K}(\text{Et}_2\text{O})]_2[\text{Fe}(\text{CNAr}_3\text{NC})_2]_2$ (**7**)

Kc_8 (finely ground, 104.9 mg, 0.776 mmol) was added to a suspension of **5** (215.5 mg, 0.243 mmol) in THF (25 mL) at -80°C . After 30 minutes a dark orange/brown reaction solution was formed. The red solution was stirred overnight and warmed up to room temperature. The solvent was removed under reduced pressure and the brown/red residue was extracted with Et_2O (50 mL). After filtration the solution was concentrated *in vacuo* (ca. 20 mL) and stored at -30°C . Compound **7** was isolated as black crystals.

Yield: 98.8 mg, 46%. Elemental analysis calcd. for

$\text{C}_{104}\text{H}_{100}\text{Fe}_2\text{N}_8\text{O}_2\text{K}_2$ ($M_w = 1683.88$ g/mol) C 74.18; H 5.99; N 6.65, found C 74.20; H 6.17; N 6.78. $^1\text{H-NMR}$ (400.13 MHz, 300 K, THF- d_8): δ [ppm] 8.96 (s, 1H, H_1 or H_2), 8.31 (s, 1H, H_1 or H_2), 7.40 (t, $^3J = 7.5$ Hz, 1H, H_3 or H_4), 7.32 (t, $^3J = 7.6$ Hz, 1H, H_3 or H_4), 7.26 (d, $^3J = 7.6$ Hz, 1H, H_5 or H_7), 7.17 (d, $^3J = 7.5$ Hz, 2H, H_6), 7.13 (d, $^3J = 7.5$ Hz, 1H, H_5 or H_7), 6.86 (s, 2H, H_8), 6.81 (s, 1H, H_8), 6.76 (s, 1H, H_8), 6.65 (s, 1H, H_8), 6.55 (s, 2H, H_8), 6.43 (s, 1H, H_8), 2.27 (s, 3H, H_9), 2.24 (s, 3H, H_9), 2.22 (s, 3H, H_9), 2.19 (s, 6H, H_9), 1.72 (s, 9H, H_9 , overlapping with THF- d_8). $^{13}\text{C}\{^1\text{H}\}$ -NMR (100.61 MHz, 300 K, THF- d_8): δ [ppm] 297.6 (m, C_{CN}), 209.5 (m, C_{CN}), 203.2 (m, C_{CN}), 147.0 (m, C_{Ar}), 142.5 (m, C_{Ar}), 140.7 (m, C_{Ar}), 138.8 (m, C_{Ar}), 138.6 (d, $J = 3.5$ Hz, C_{Ar}), 134.5 (d, $J = 12.3$ Hz, C_1 or C_2), 133.7 (s, C_{Ar}), 133.4 (s, C_{Ar}), 133.0 (s, C_{Ar}), 131.5 (m, C_8), 131.0 (s, C_{Ar}), 129.9 (s, C_{Ar}), 129.4 (d, $J = 15.9$ Hz, C_8), 129.5 (m, C_{Ar}), 128.9 (m, C_8), 128.8 (m, C_8), 128.6 (s, C_1 or C_2), 128.1 (s, C_{Ar}), 127.8 (d, $J = 7.0$ Hz, C_8), 127.5 (d, $J = 6.0$ Hz, C_6), 127.2 (s, C_3 or C_4), 126.8 (s, C_5 or C_7), 126.5 (s, C_5 or C_7), 125.6 (s, C_6), 20.2 (m, C_9), 20.0 (m, C_9), 19.7 (m, C_9), 18.8 (m, C_9). IR: ν [cm^{-1}] 2968 (w), 2912 (w), 2853 (w), 1982 (ν [$\text{C}\equiv\text{N}$], w), 1961 (ν [$\text{C}\equiv\text{N}$], w), 1765 (br. m), 1602 (w), 1514 (m), 1456 (m), 1381 (m), 1210 (m), 855 (vs), 744 (vs), 534 (vs).

S3. NMR Spectra

S3.1 NMR spectra of 1

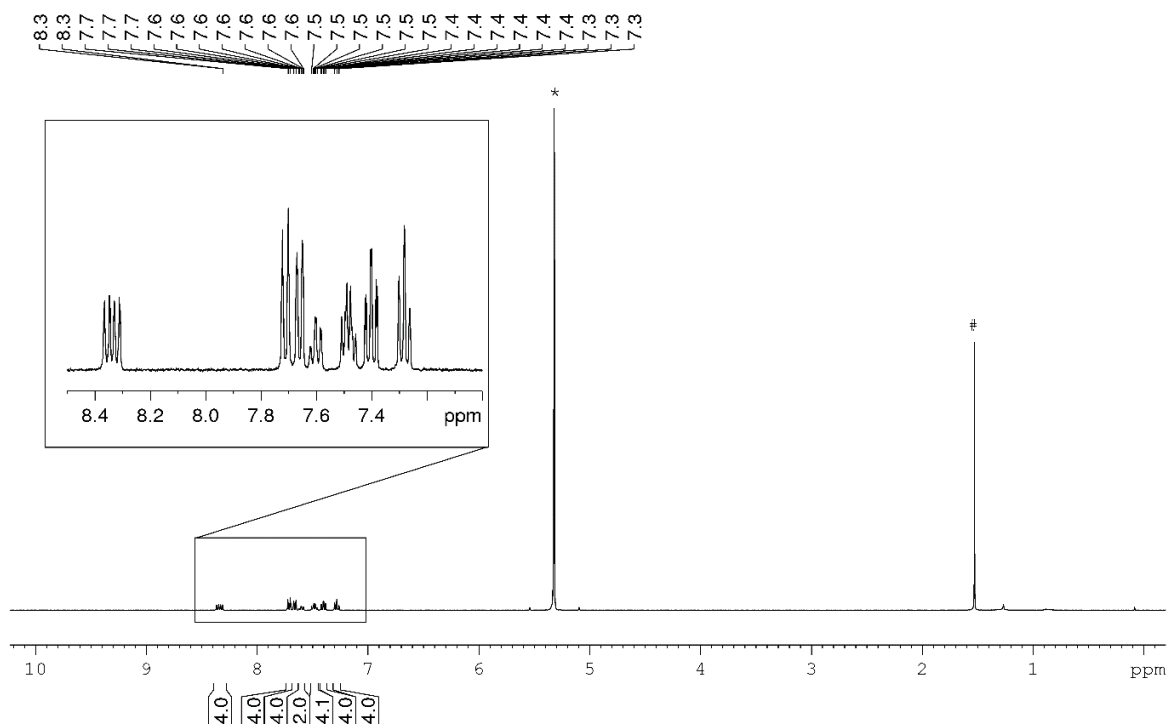


Figure S1. ^1H NMR spectrum (400.13 MHz, 300 K, CD_2Cl_2) of **1**; * CD_2Cl_2 , # H_2O in CD_2Cl_2 .

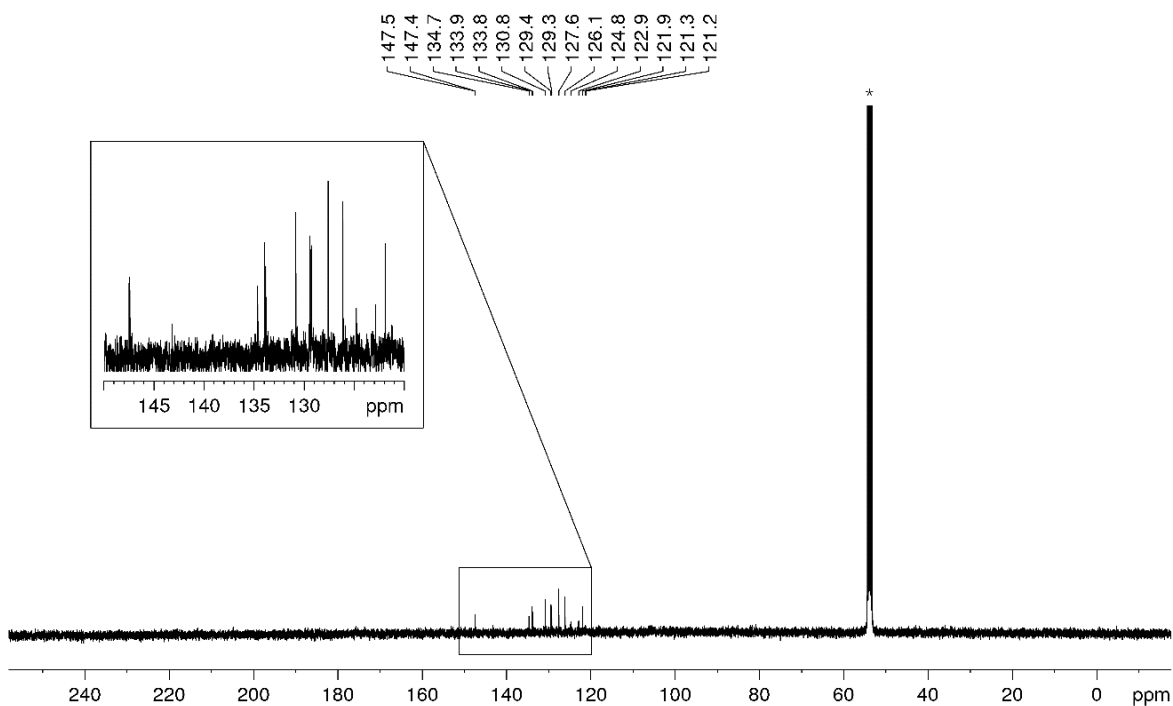


Figure S2. $^{13}\text{C}\{^1\text{H}\}$ NMR spectrum (100.61 MHz, 300 K, CD_2Cl_2) of **1**; * CD_2Cl_2 .

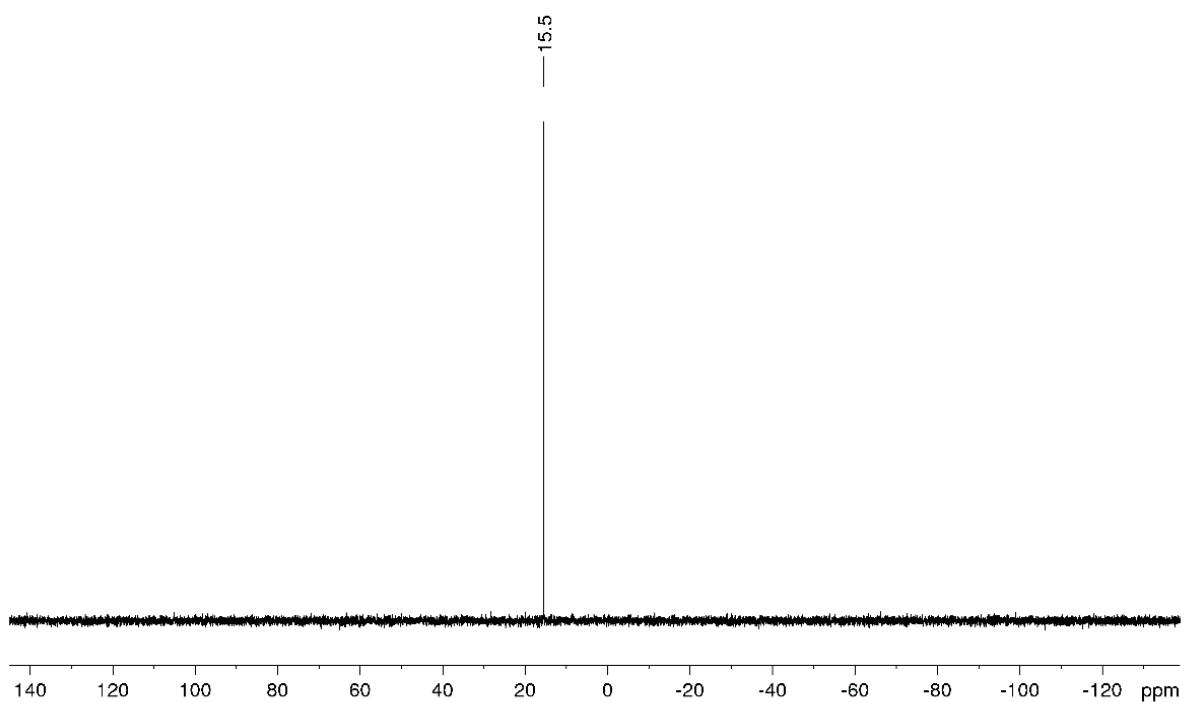


Figure S3. $^{31}\text{P}\{^1\text{H}\}$ NMR spectrum (161.98 MHz, 300 K, CD_2Cl_2) of **1**.

S3.2 NMR spectra of **2**

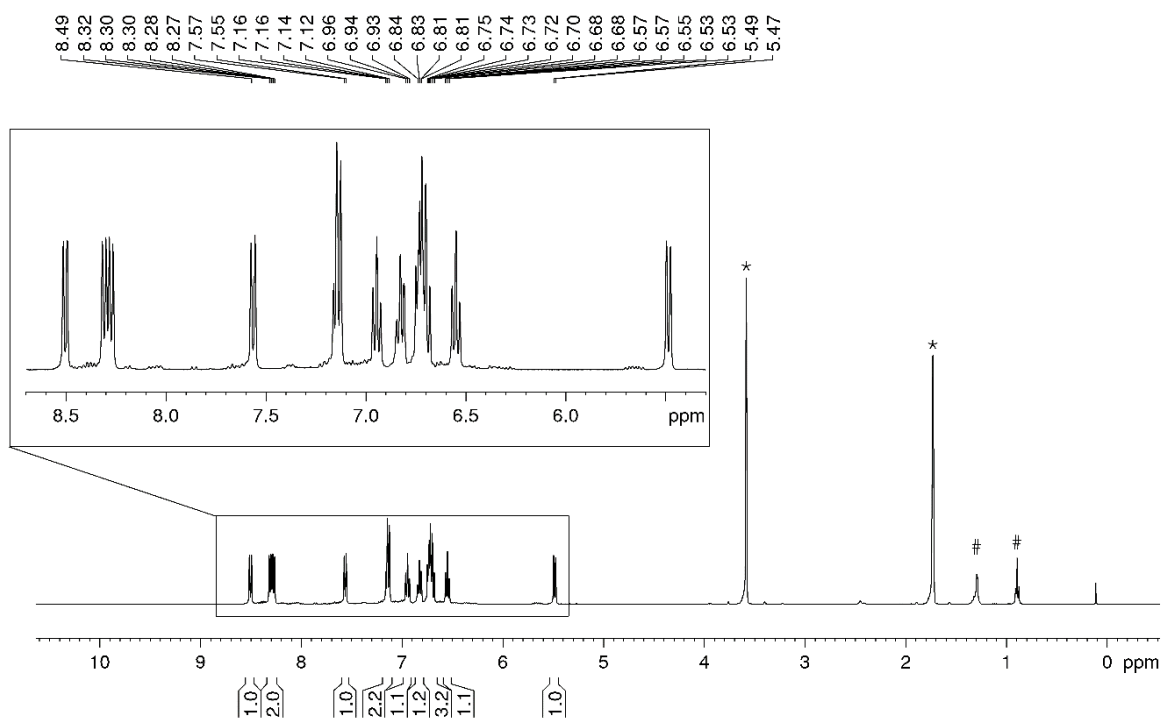


Figure S4. ^1H NMR spectrum (400.13 MHz, 300 K, THF-d_8) of **2**; * THF-d_8 , #*n*-hexane.

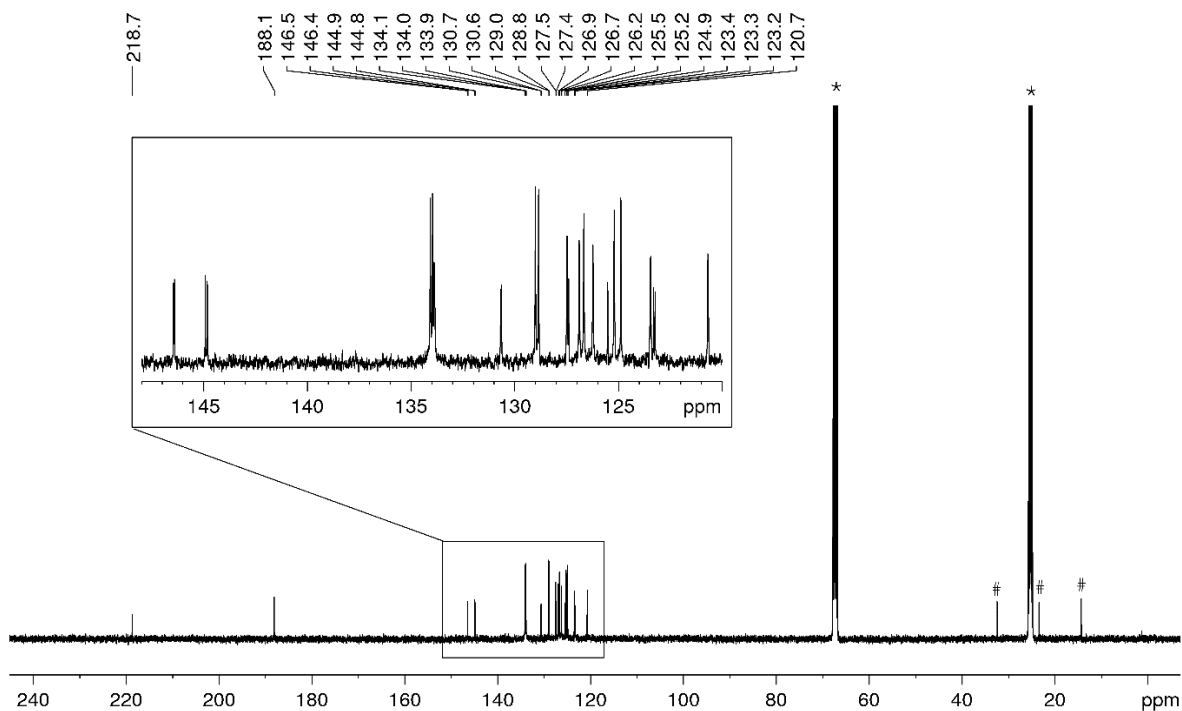


Figure S5. $^{13}\text{C}\{^1\text{H}\}$ NMR spectrum (100.61 MHz, 300 K, THF-d_8) of **2**; * THF-d_8 , #*n*-hexane.

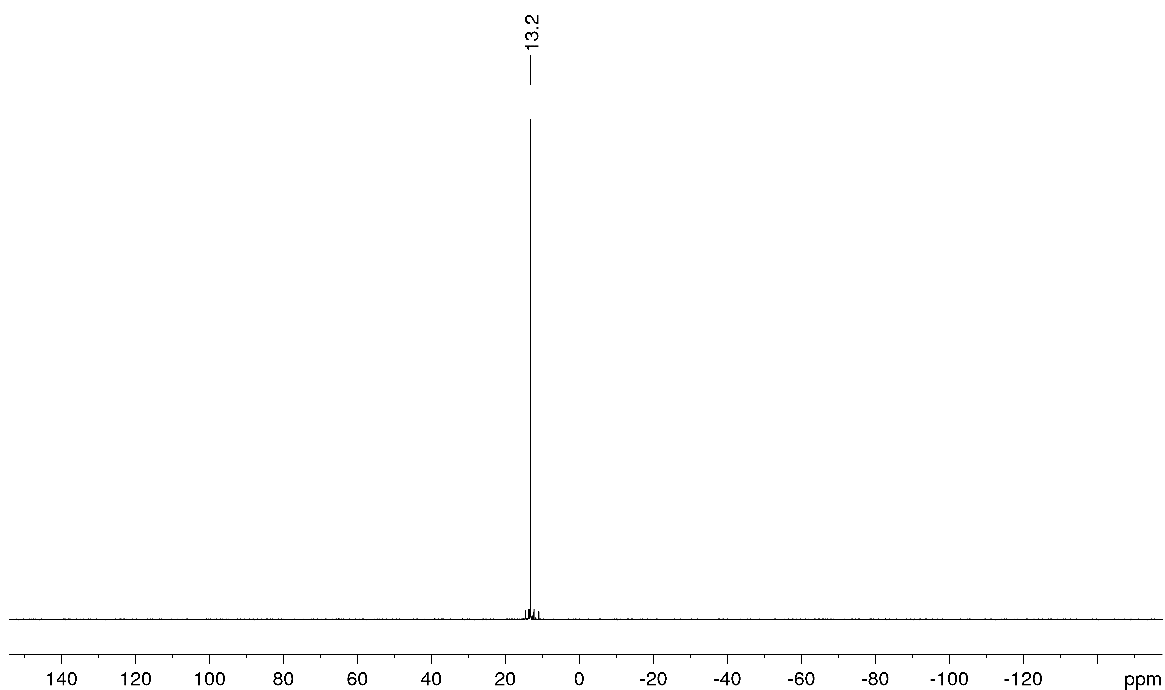


Figure S6. $^{31}\text{P}\{^1\text{H}\}$ NMR spectrum (161.98 MHz, 300 K, THF-d_8) of **2**.

S3.3 NMR Spectra of 3

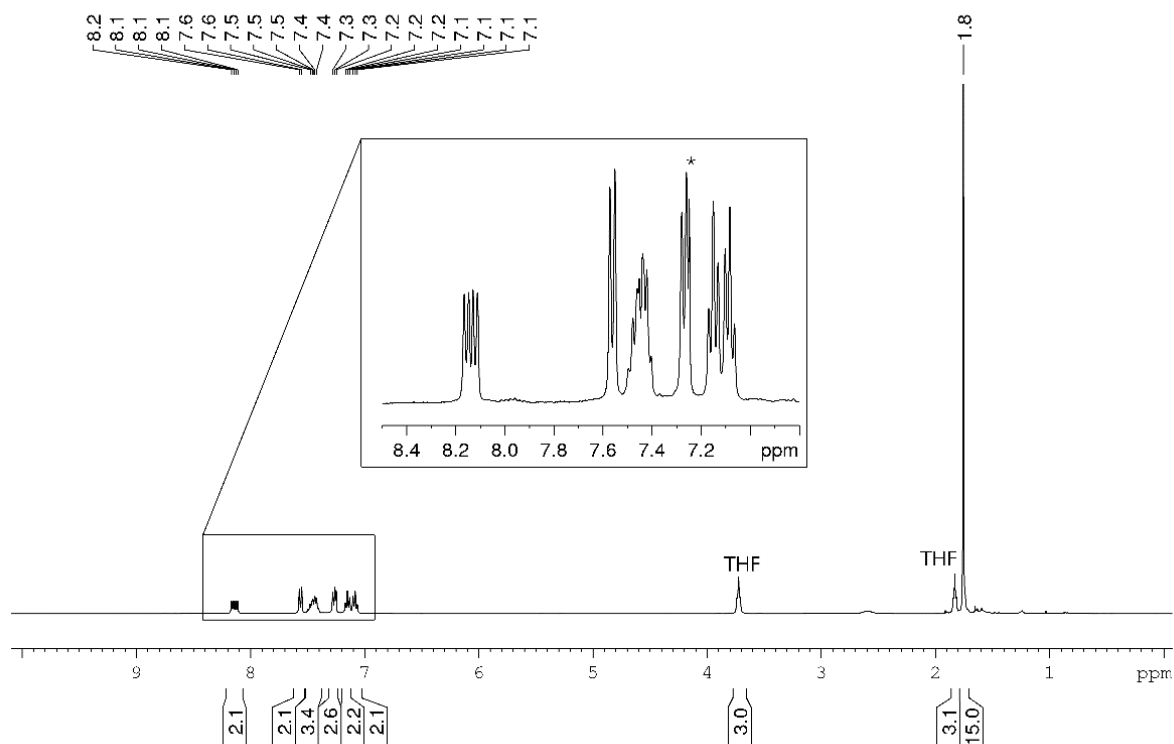


Figure S7. ^1H NMR spectrum (400.13 MHz, 300 K, CDCl_3) of 3; $^*\text{CDCl}_3$.

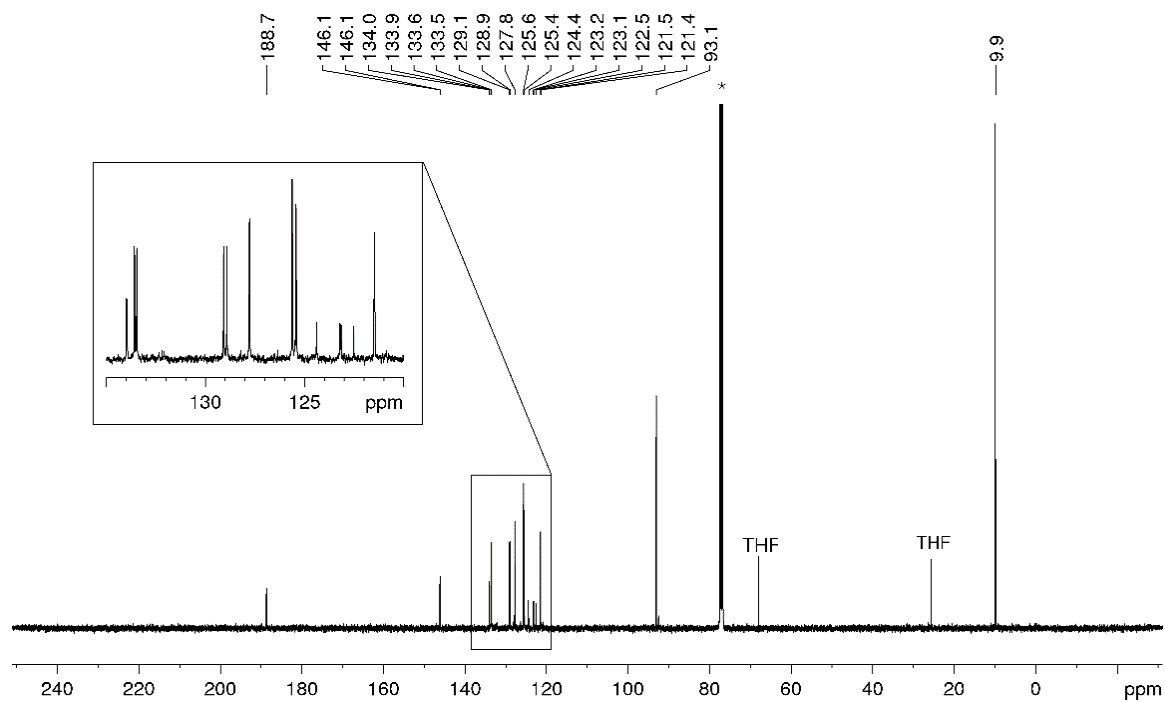


Figure S8. $^{13}\text{C}\{^1\text{H}\}$ NMR spectrum (100.61 MHz, 300 K, CDCl_3) of 3; $^*\text{CDCl}_3$.

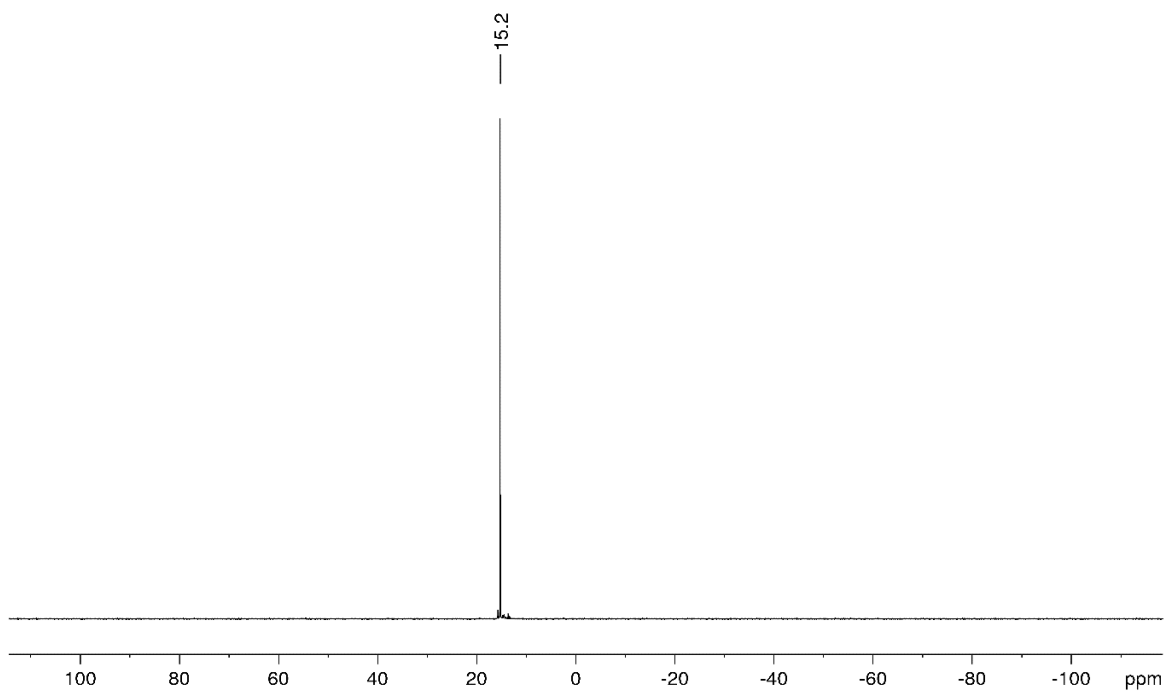


Figure S9. $^{31}\text{P}\{^1\text{H}\}$ NMR spectrum (161.98 MHz, 300 K, CDCl_3) of **3**; $^*\text{CDCl}_3$.

S3.4 NMR Spectra of **4**

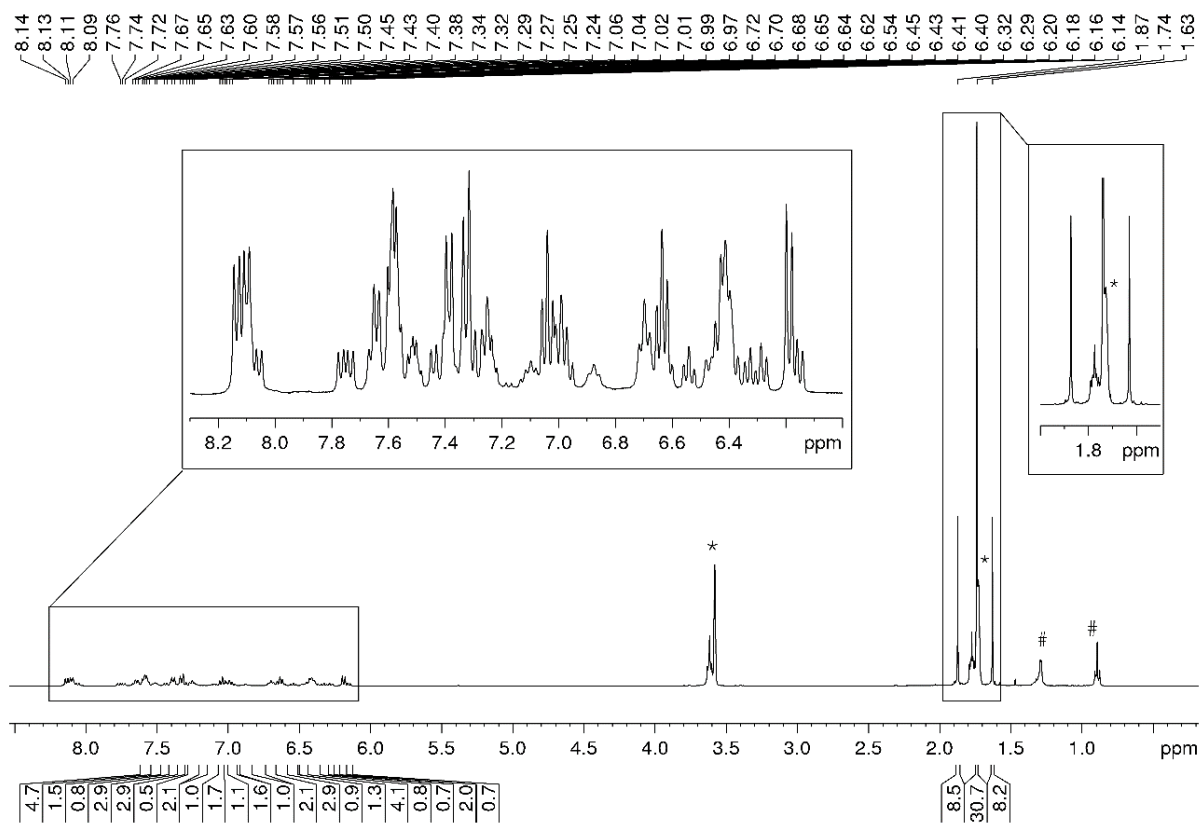


Figure S10. ^1H NMR spectrum (400.13 MHz, 300 K, THF-d_8) of **4**; $^*\text{THF-d}_8$, $\#n$ -hexane.

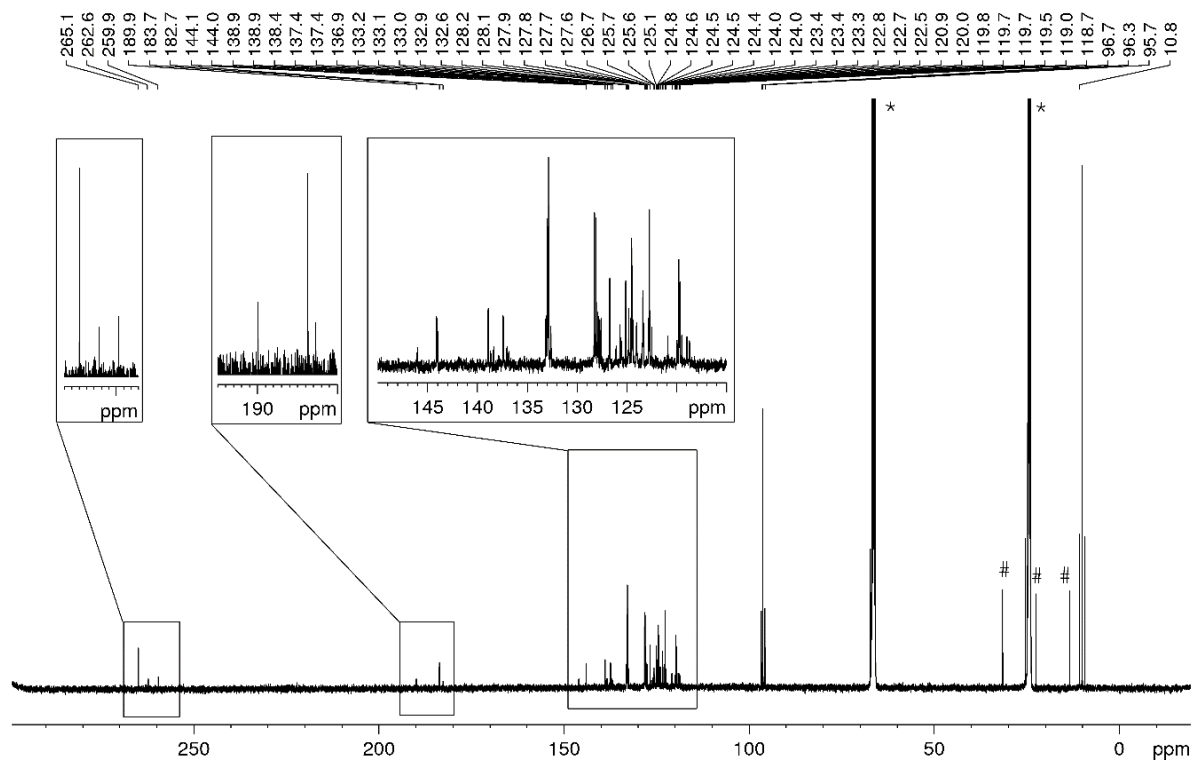


Figure S11. $^{13}\text{C}\{^1\text{H}\}$ NMR spectrum (100.61 MHz, 300 K, THF-d_8) of **4**; * THF-d_8 , #*n*-hexane.

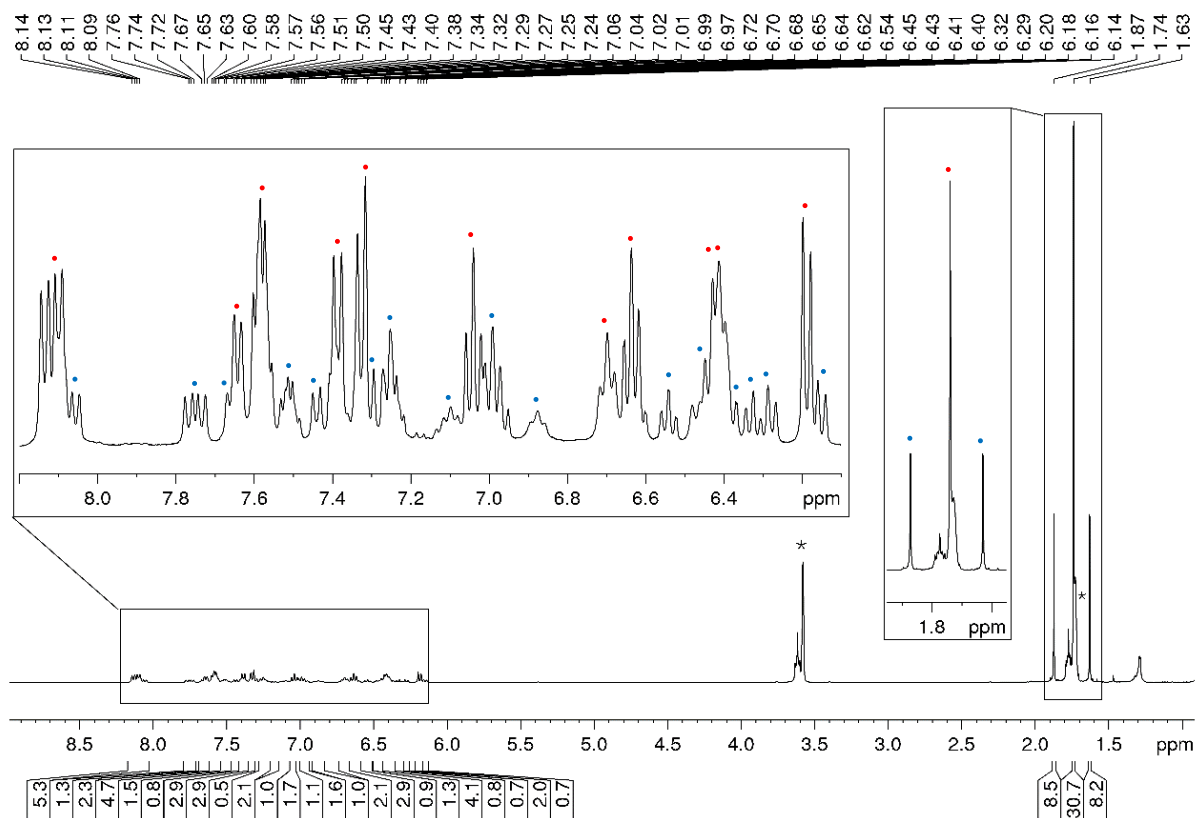


Figure S12. ^1H NMR spectrum (400.13 MHz, 300 K, THF-d_8) of **4**; * THF-d_8 , *cis*-isomer: red, *trans*-isomer: blue.

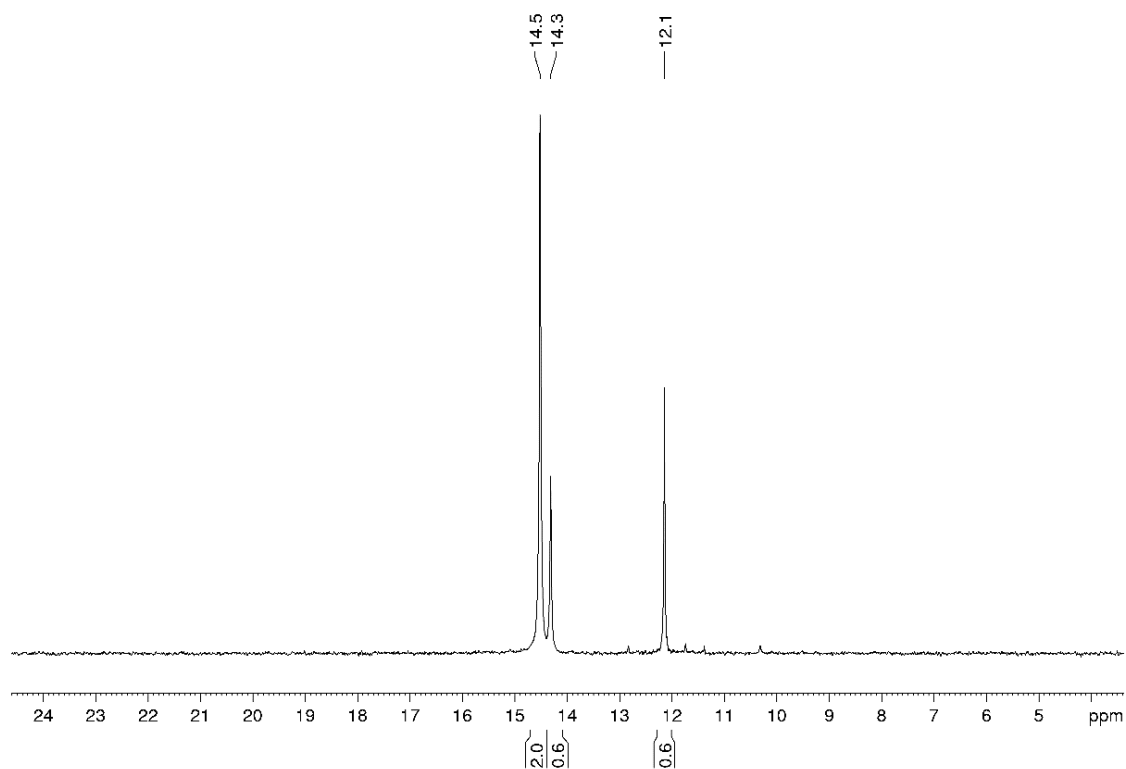


Figure S13. $^{31}\text{P}\{^1\text{H}\}$ NMR spectrum (161.98 MHz, 300 K, THF-d_8) of **4**.

The ratio of the isomers depends on the isolated form of compound **4**; crystalline product mainly gives rise to the *cis*-isomer as the main component (Figure S14) and when **4** is isolated as an amorphous powder the *trans*-isomer predominates (Figure S15).

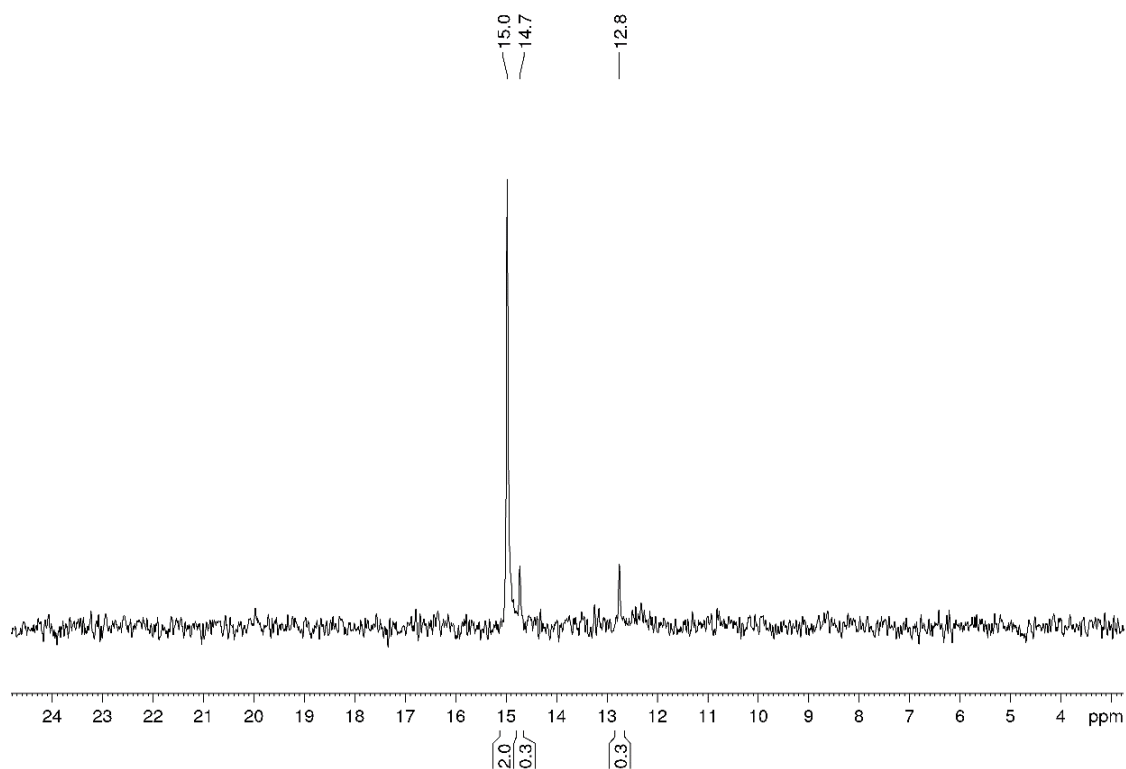


Figure S14. $^{31}\text{P}\{^1\text{H}\}$ NMR spectrum (161.98 MHz, 300 K, C_6D_6) of crystals of **4**.

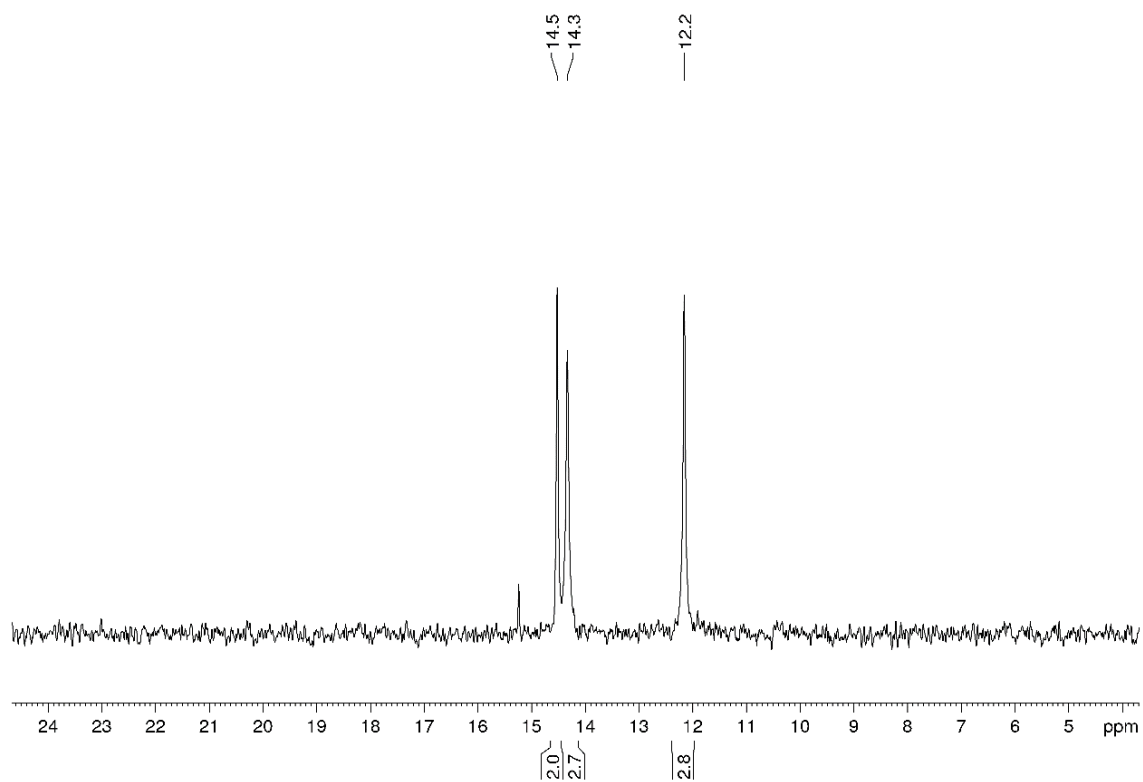


Figure S15. $^{31}\text{P}\{^1\text{H}\}$ NMR spectrum (161.98 MHz, 300 K, THF-d_8) of amorphous powder of **4**.

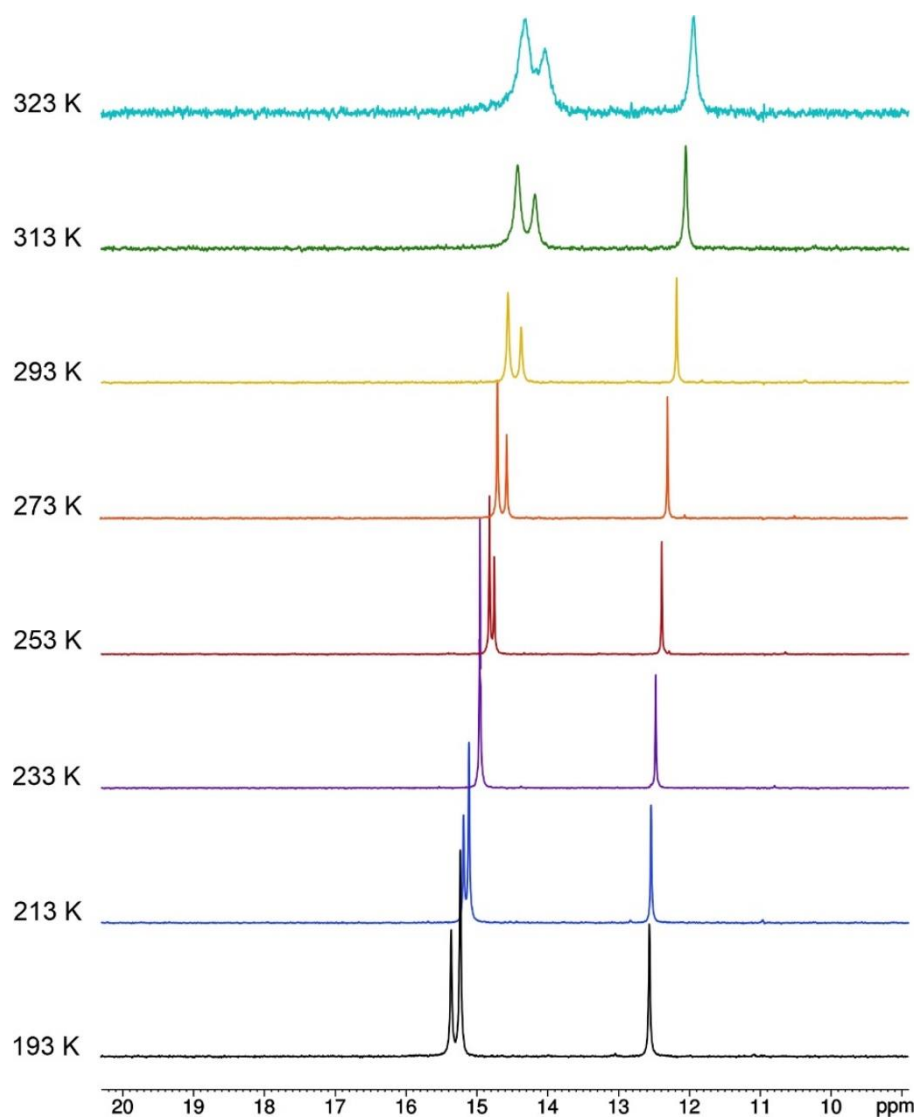


Figure S16. Variable temperature $^{31}\text{P}\{^1\text{H}\}$ NMR spectrum (161.98 MHz, 193 K–323 K, THF-d_8) of **4**.

Variable temperature $^{31}\text{P}\{^1\text{H}\}$ NMR experiments showed no partial isomerization into one of the two isomers (no change in the *cis*-/*trans*-isomer ratio). One of the signals of the *trans*-isomers is slightly shifting depending on the temperature. At higher temperatures (313 K–323 K) compound **4** features broadened signals in the $^{31}\text{P}\{^1\text{H}\}$ NMR.

S3.5 NMR spectra of **5**

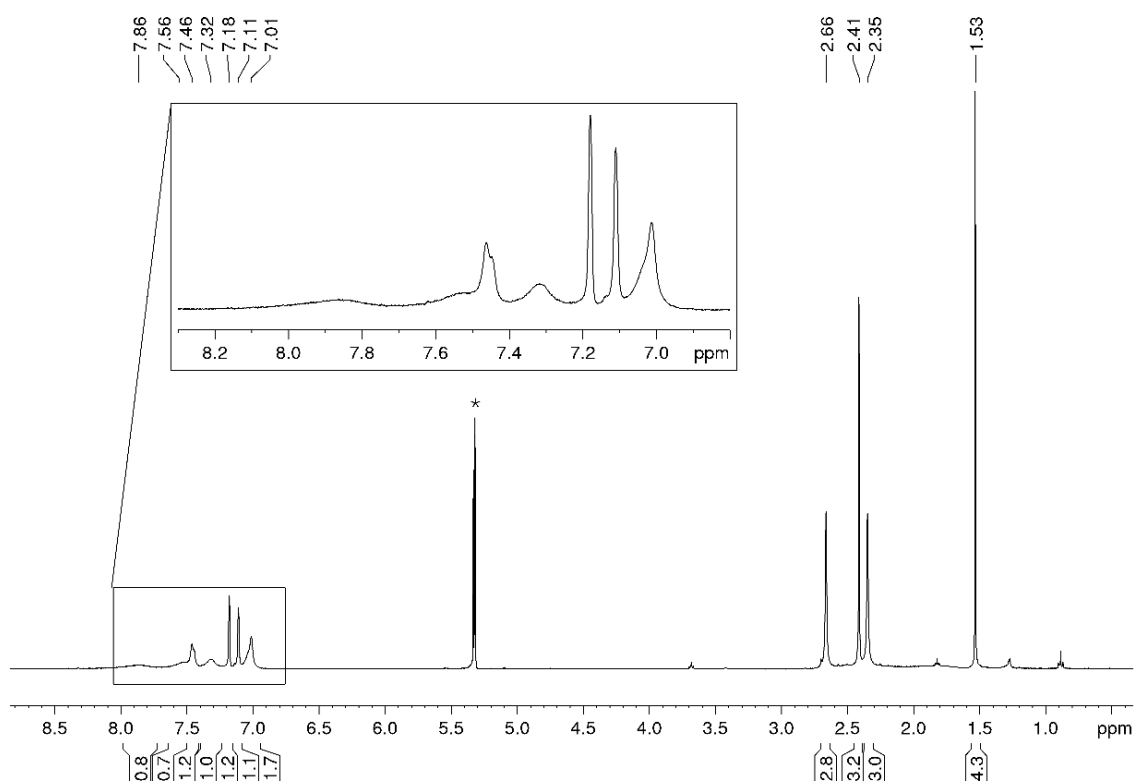


Figure S17. ^1H NMR spectrum (400.13 MHz, 300 K, CD_2Cl_2) of **5** at room temperature; * CD_2Cl_2 .

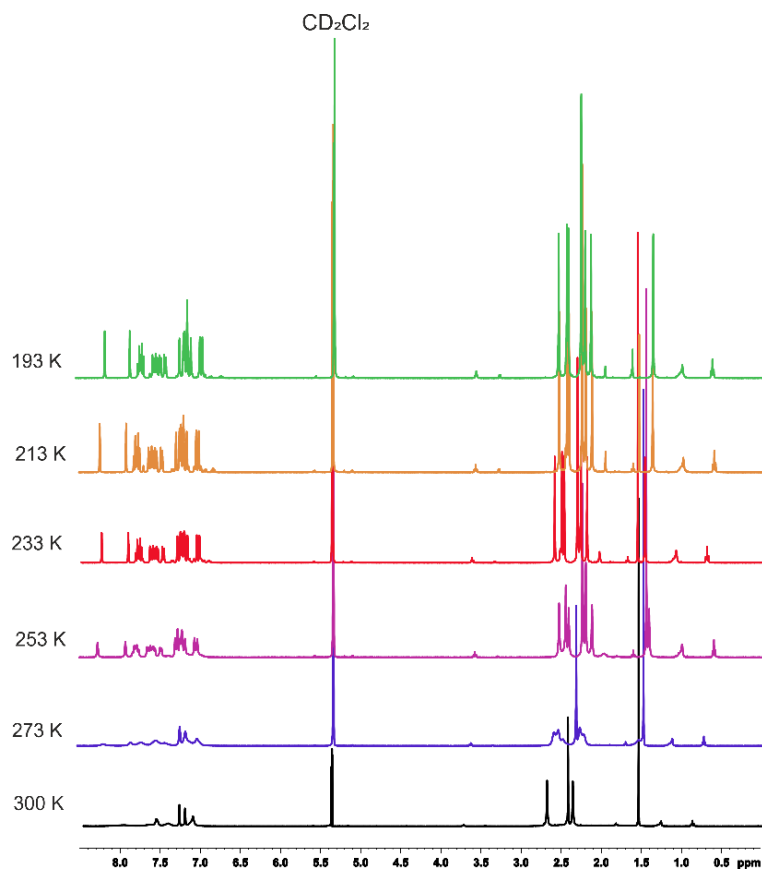


Figure S18. Variable temperature ^1H NMR spectrum (400.13 MHz, 300 K–193 K, CD_2Cl_2) of **5**.

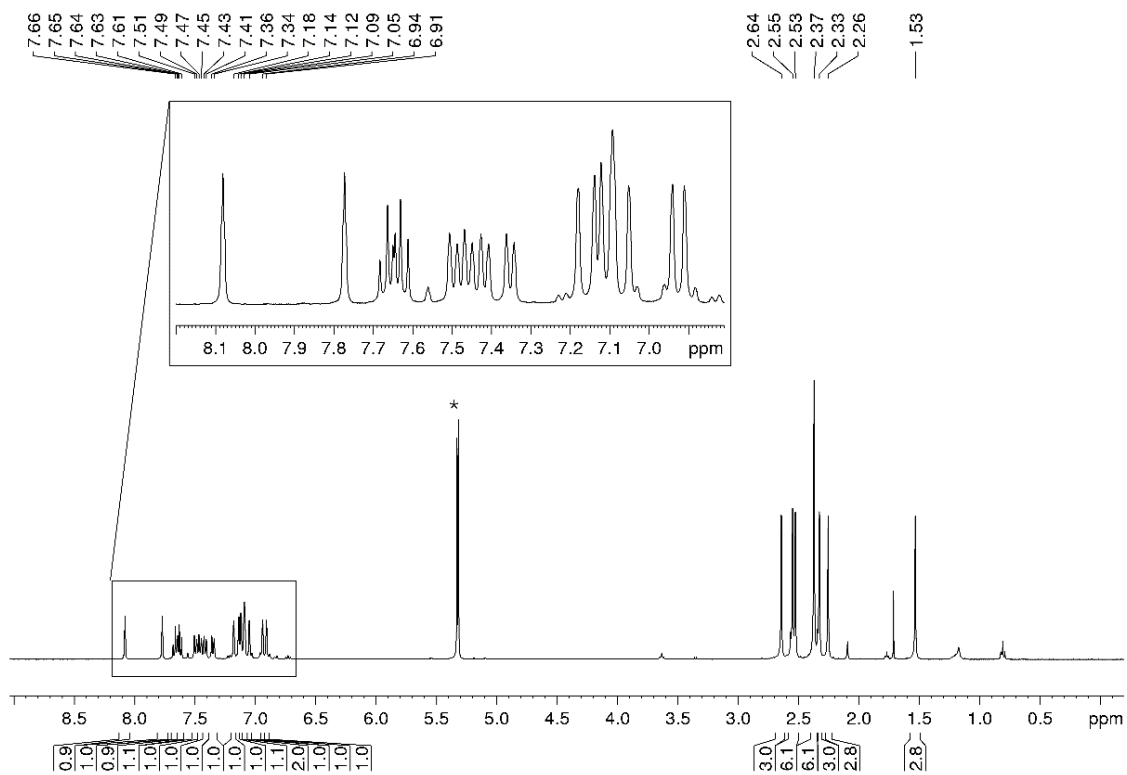


Figure S19. ^1H NMR spectrum (400.13 MHz, 213 K, CD_2Cl_2) of **5** at $-60\text{ }^\circ\text{C}$; $^*\text{CD}_2\text{Cl}_2$.

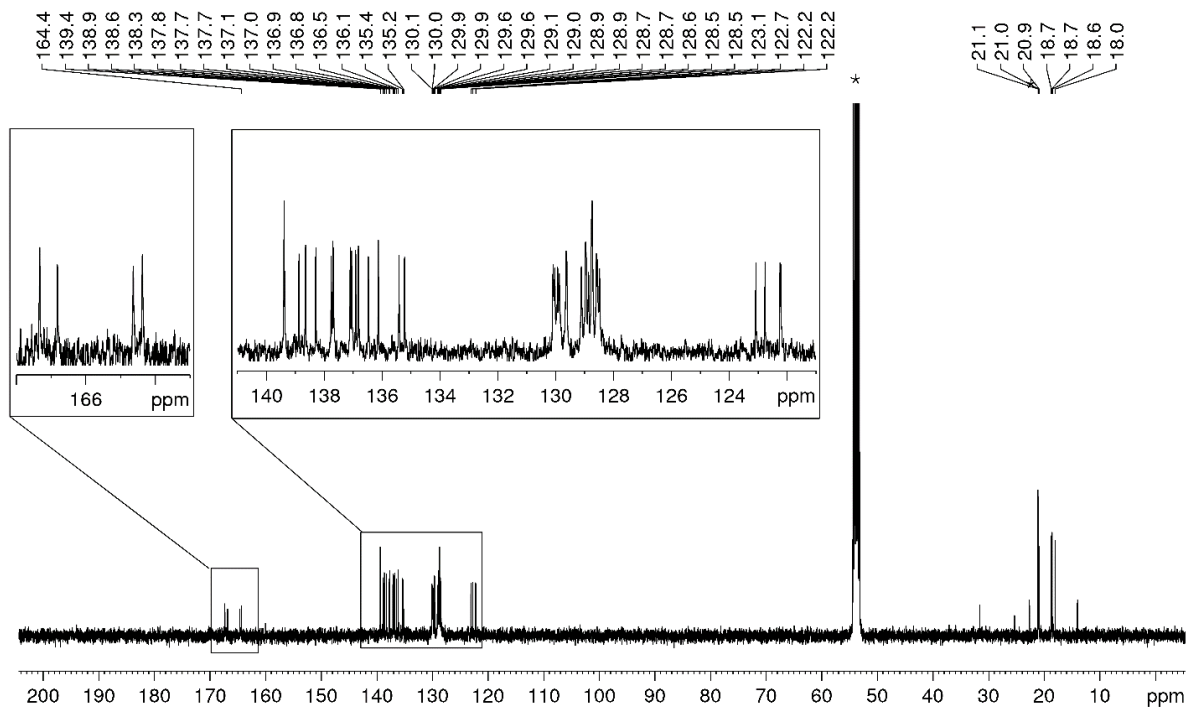


Figure S20. $^{13}\text{C}\{^1\text{H}\}$ NMR spectrum (100.61 MHz, 213 K, CD_2Cl_2) of **5** at $-60\text{ }^\circ\text{C}$; $^*\text{CD}_2\text{Cl}_2$.

S3.6 NMR Spectra of 6

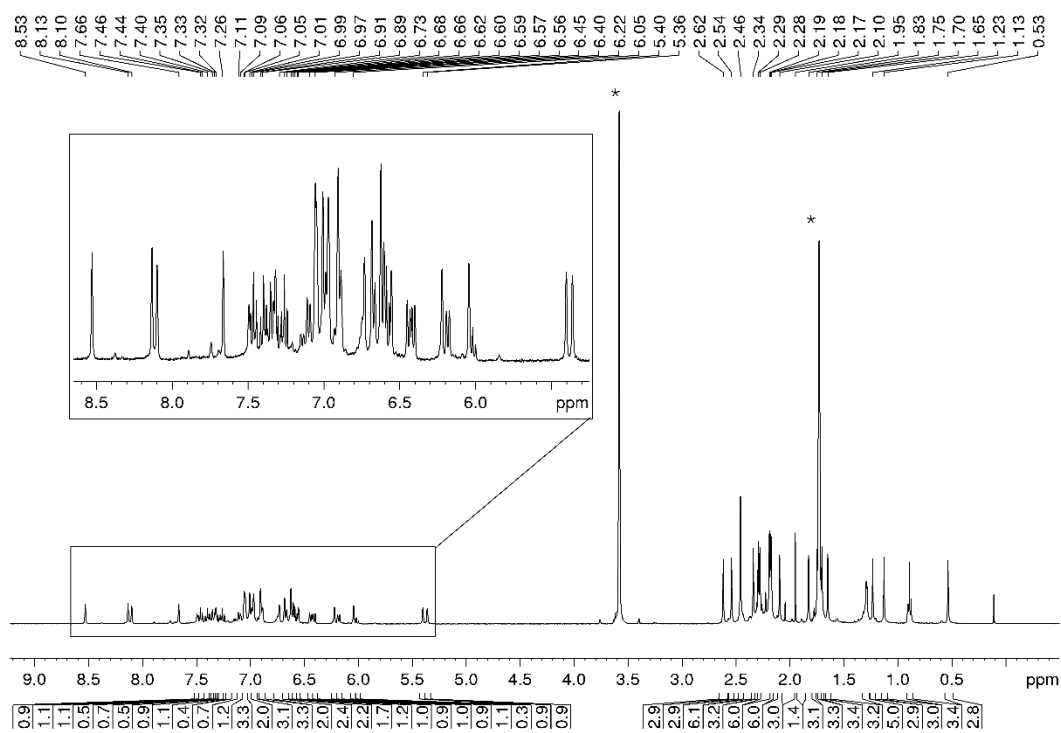


Figure S21. ^1H NMR spectrum (400.13 MHz, 300 K, THF-d_8) of **6**; * THF-d_8 .

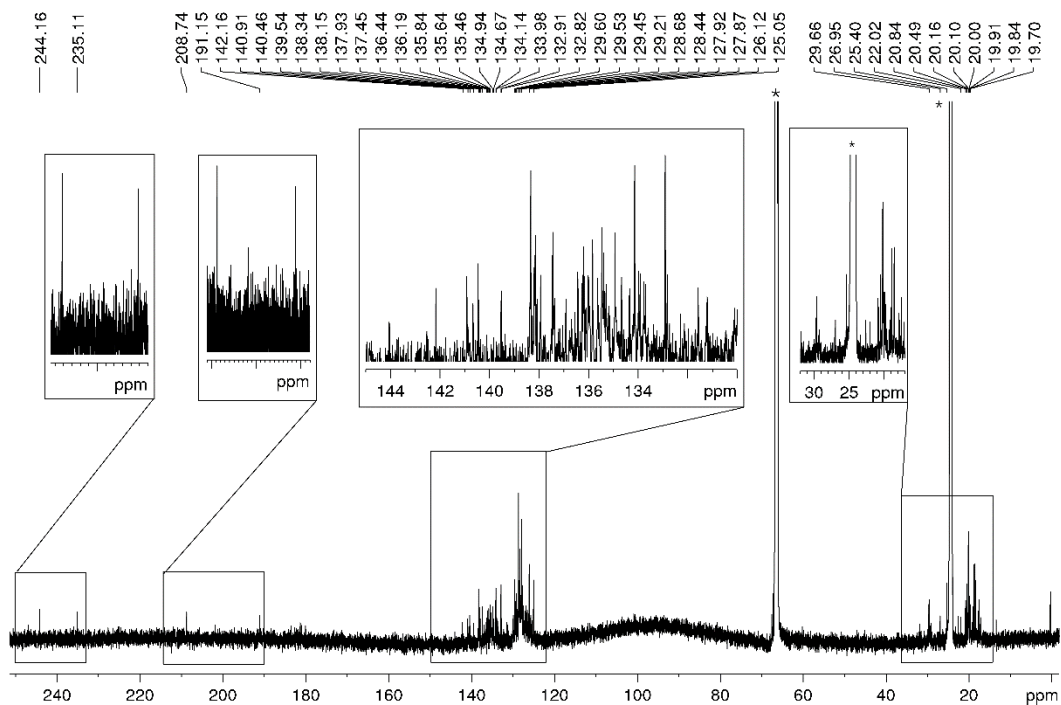


Figure S22. $^{13}\text{C}\{^1\text{H}\}$ NMR spectrum (100.61 MHz, 300 K, THF-d_8) of **6**; * THF-d_8 .

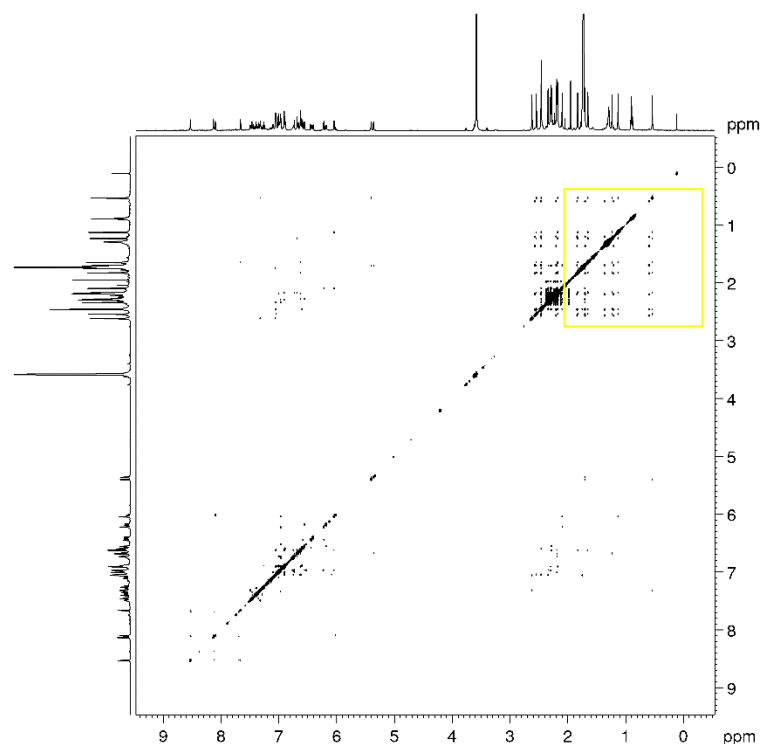


Figure S23. $^1\text{H},^1\text{H}$ -NOESY (600.03 MHz, 300 K, THF- d_8) of **6**.

On basis of the $^1\text{H},^1\text{H}$ -NOESY of **6** showing three different sets of methyl groups (eight in each set; Figure S24, red, green and blue) it can be concluded that compound **6** can be isolated in a mixture of three isomers.

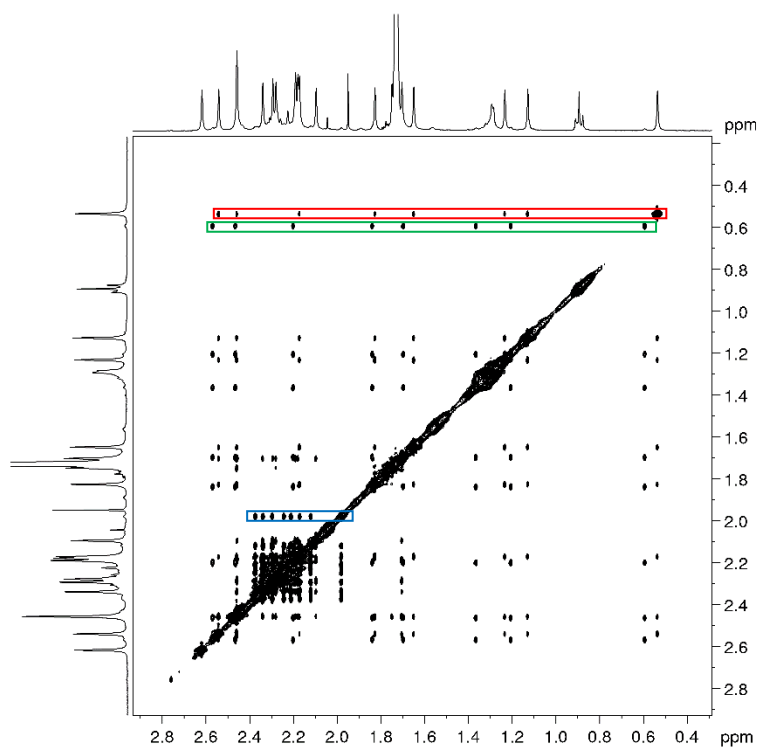
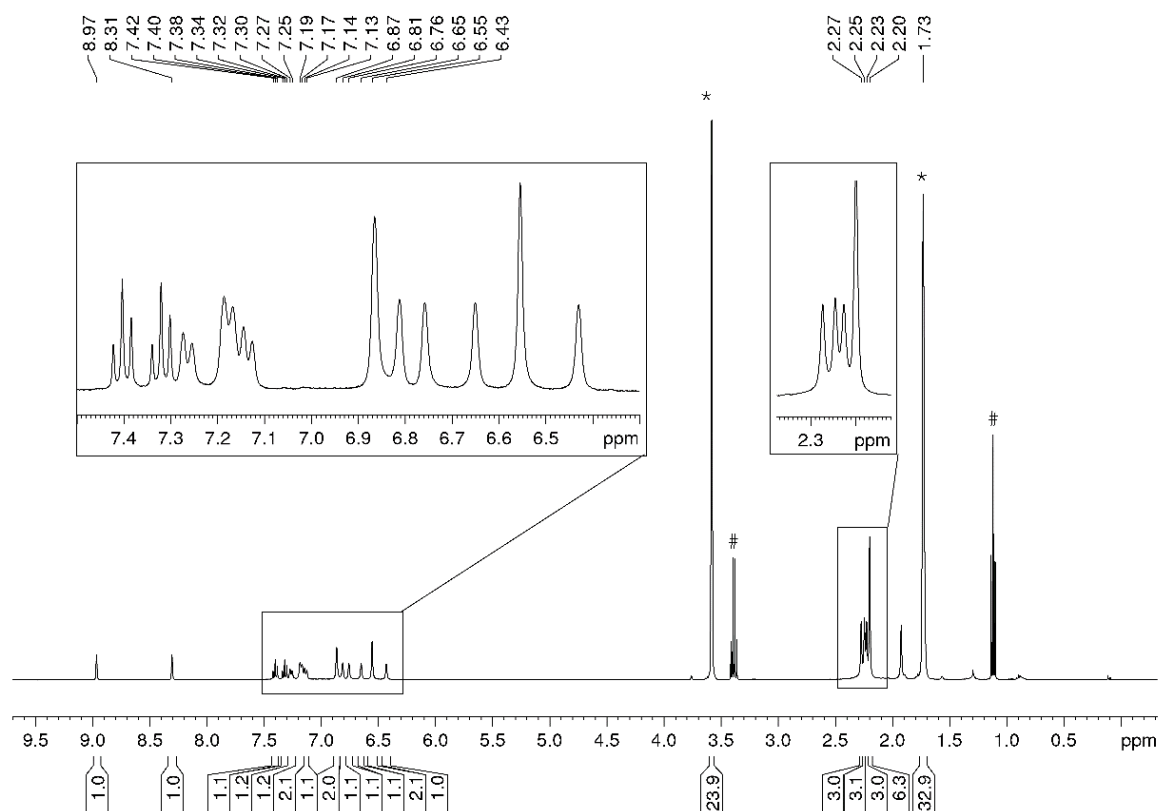
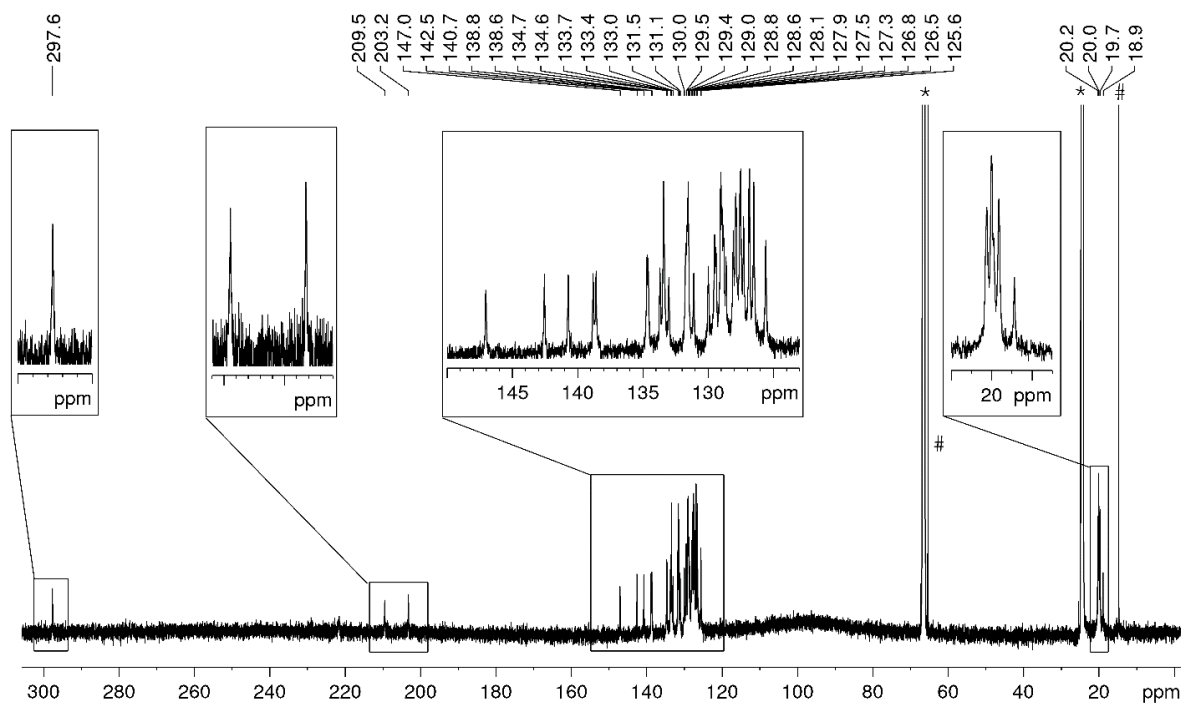


Figure S24. $^1\text{H},^1\text{H}$ -NOESY (600.03 MHz, 300 K, THF- d_8) of **6** (cutout of methyl groups; yellow sector in Figure S22).

S3.7 NMR Spectra of 7

Figure S25. ^1H NMR spectrum (400.13 MHz, 300 K, THF-d_8) of 7; * THF-d_8 , #diethyl ether.Figure S26. $^{13}\text{C}\{^1\text{H}\}$ NMR spectrum (150.88 MHz, 300 K, THF-d_8) of 7; * THF-d_8 , #diethyl ether.

S4. IR spectra

S4.1 IR spectrum of 1

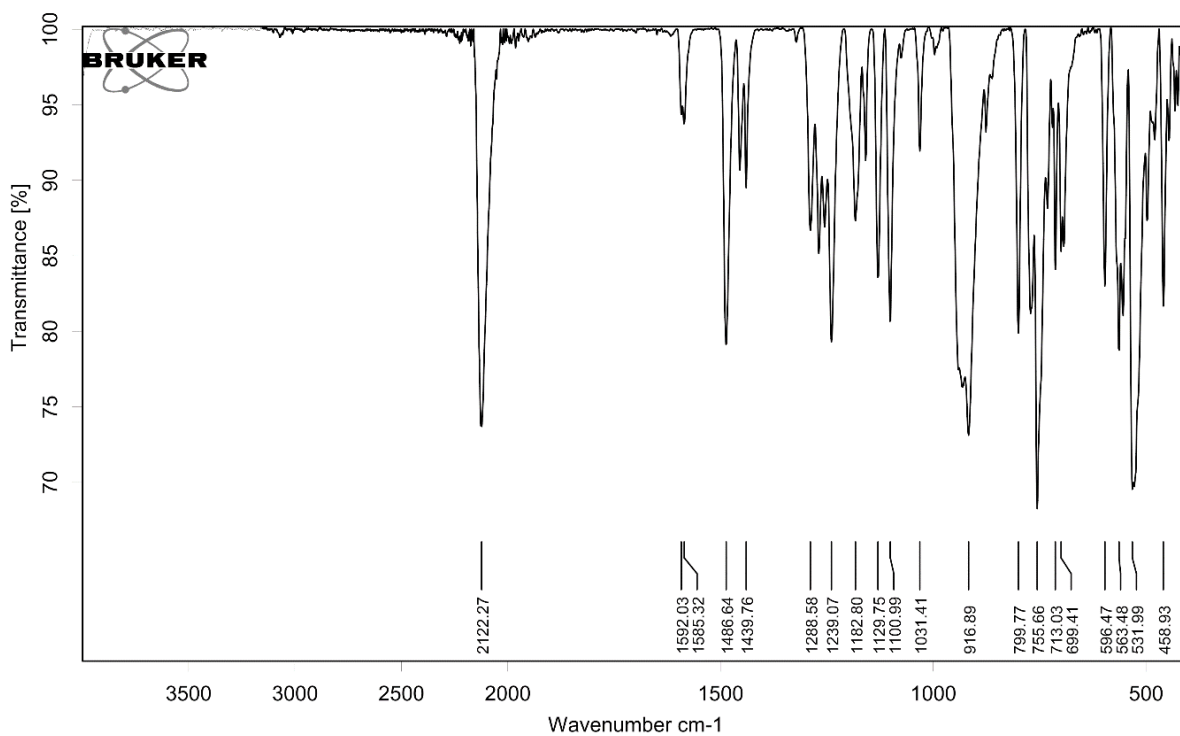


Figure S27. Solid state IR spectrum of 1.

S4.2 IR spectrum of 2

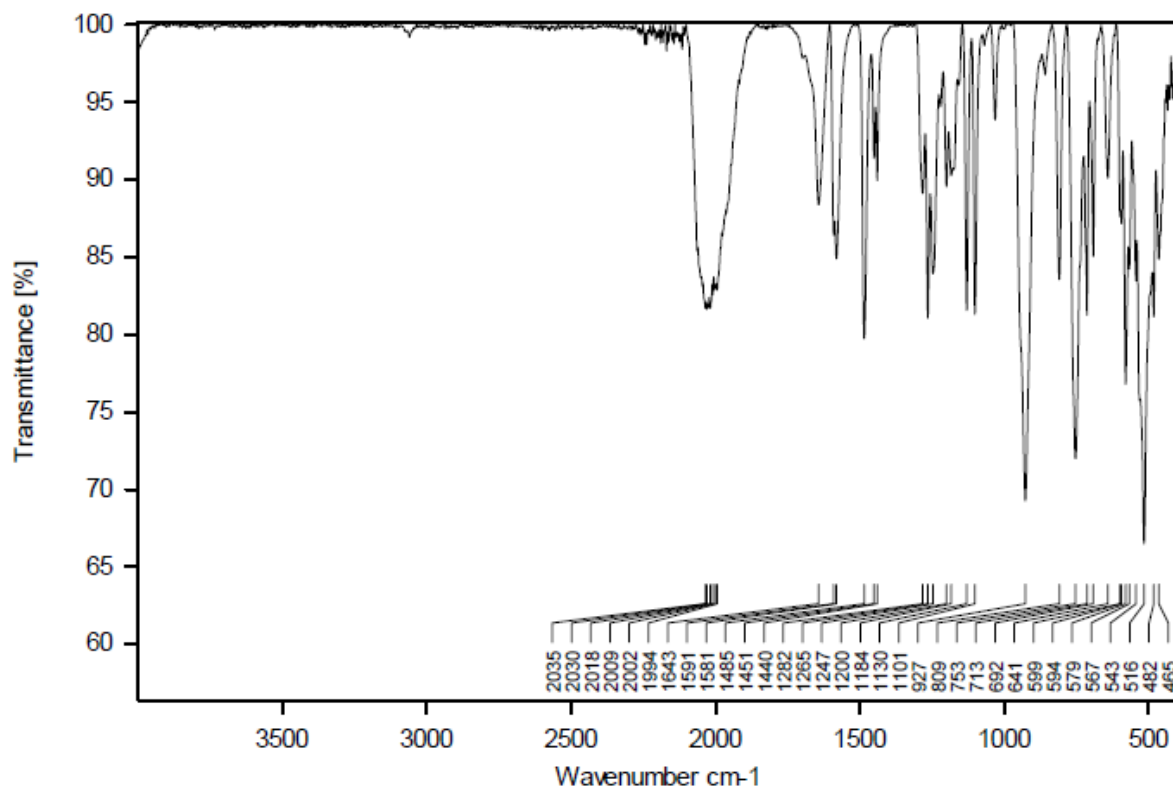


Figure S28. Solid state IR spectrum of 2.

S4.3 IR spectrum of 3

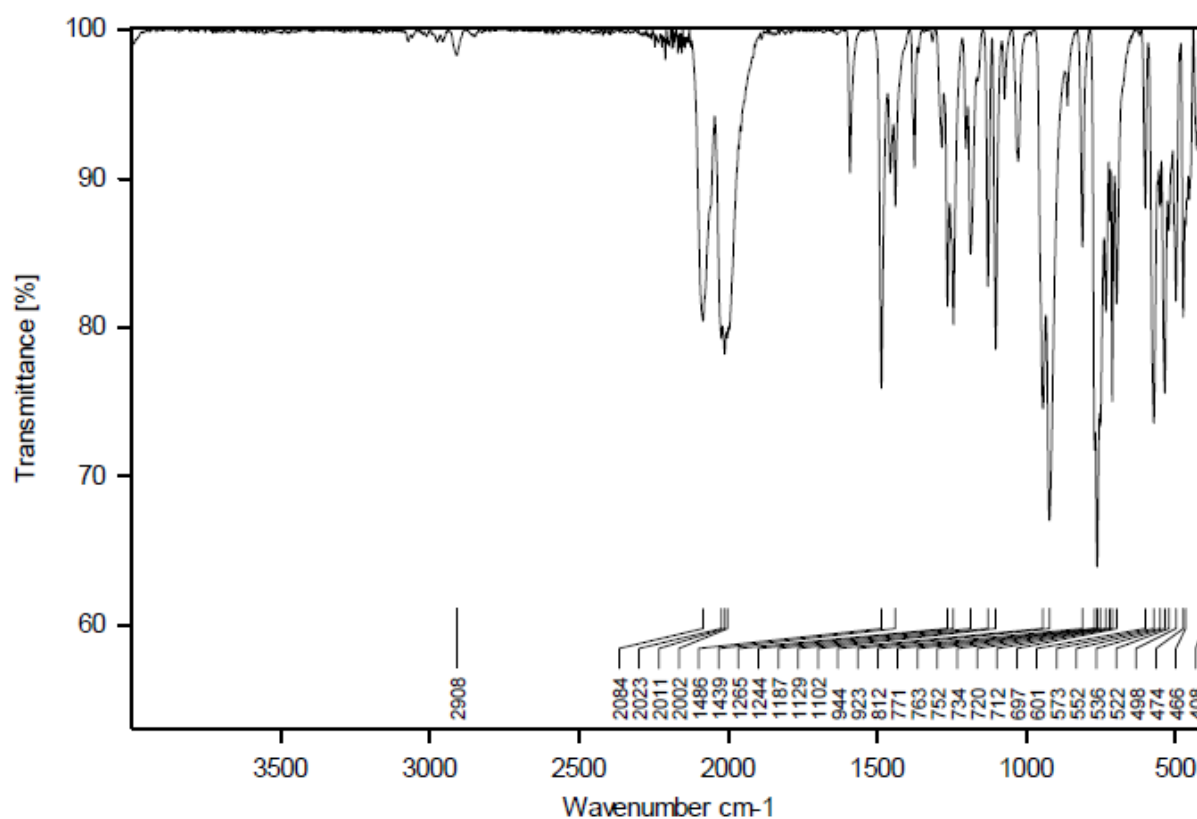


Figure S29. Solid state IR spectrum of 3

S4.4 IR spectrum of 4

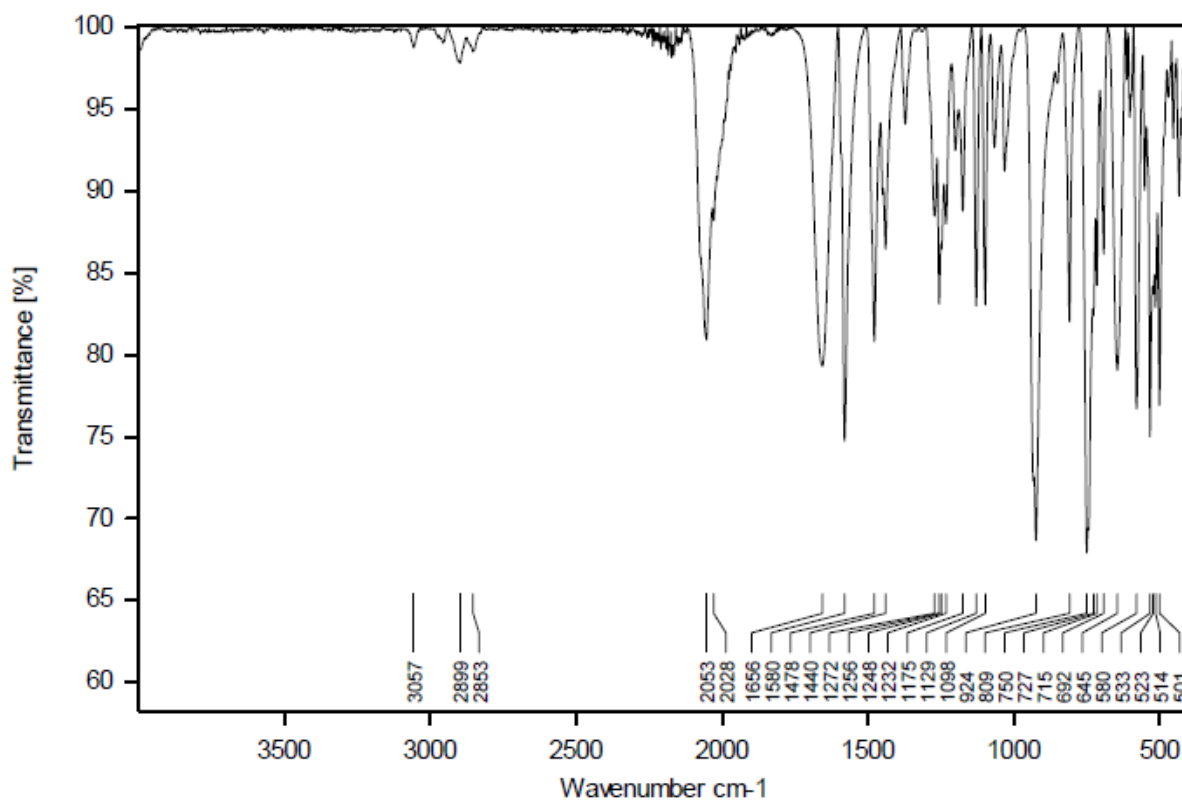


Figure S30. Solid state IR spectrum of 4.

S4.5 IR spectrum of 5

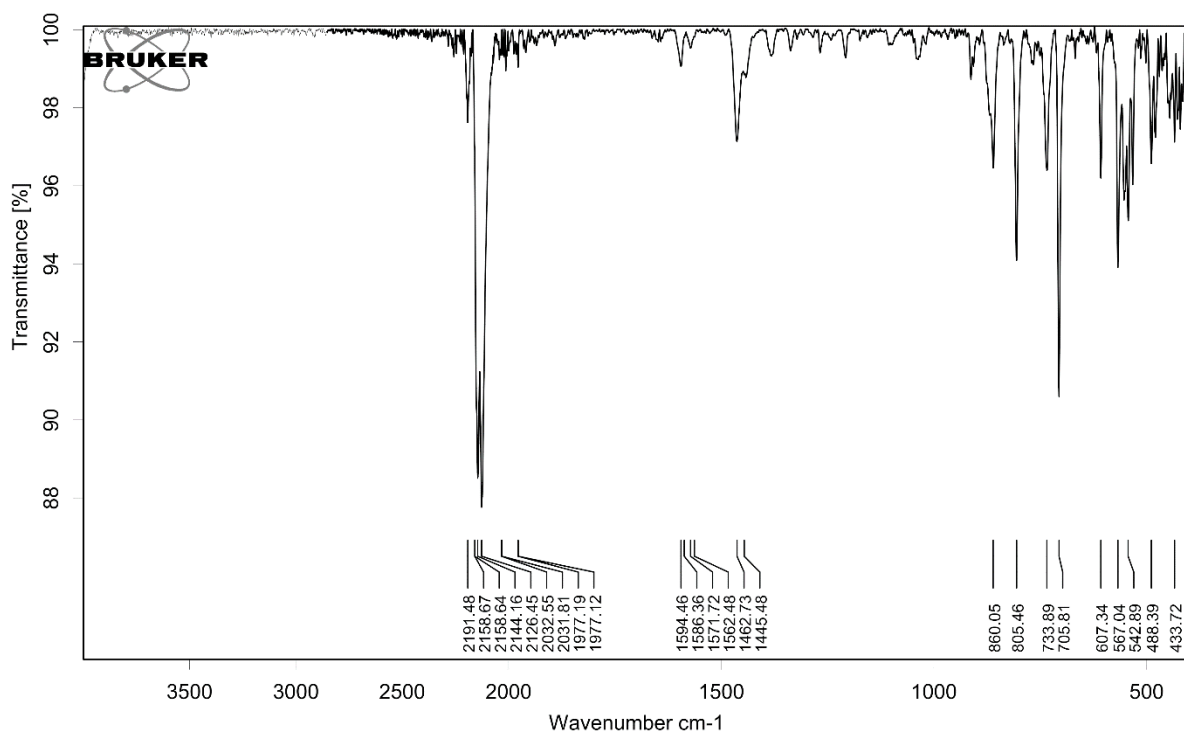


Figure S31. Solid state IR spectrum of 5.

S4.6 IR spectrum of 6

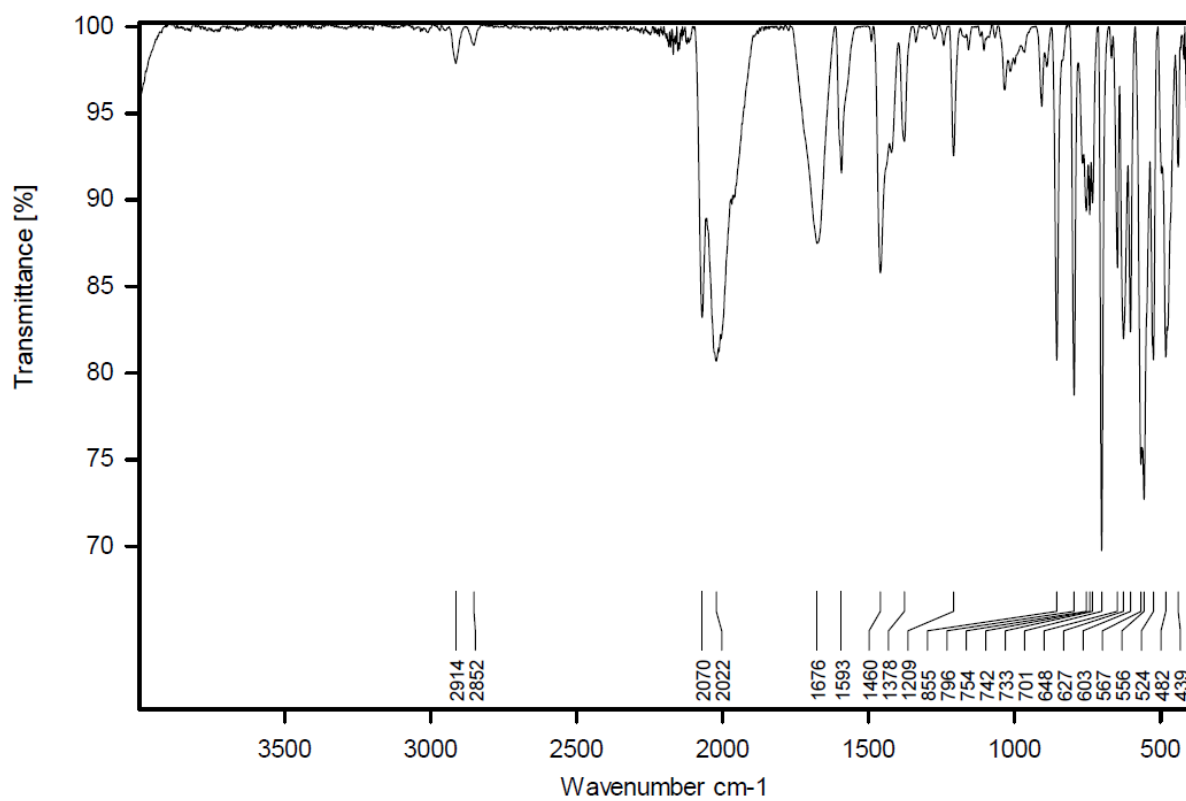


Figure S32. Solid state IR spectrum of 6.

S4.7 IR spectrum of 7

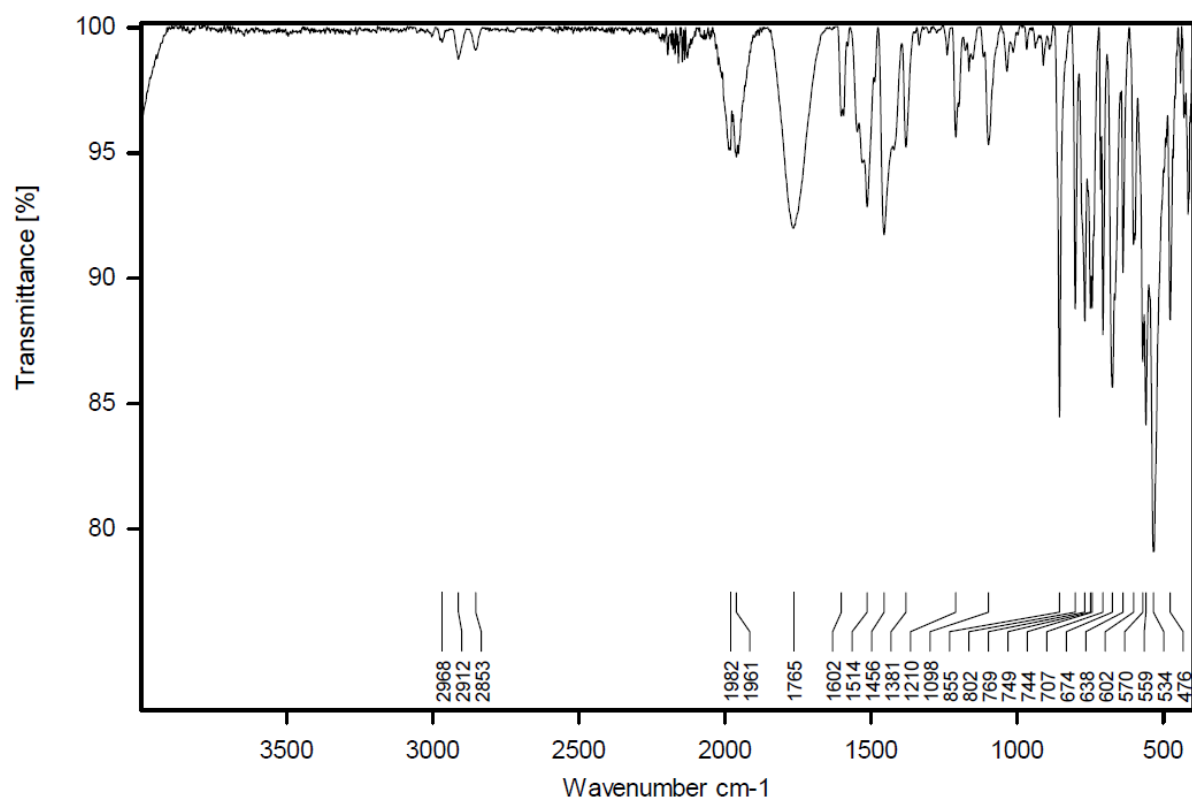


Figure S33. Solid state IR spectrum of 7.

S5. X-ray Crystallographic Data**S5.1 X-ray Crystallographic Data of compounds 1, 3 and 5****Table S1.** Crystallographic data and structure refinement of **1**, **3** and **5**.

	1	3	5
CCDC	2056040	2056042	2056044
Empirical formula	C ₄₆ H ₃₈ Br ₂ FeN ₄ O _{7.5} P ₂	C ₃₄ H ₃₆ ClFeN ₂ O ₄ P	C ₅₀ H ₄₄ Br ₂ Cl ₄ FeN ₄
Formula weight	1044.41	658.92	1058.36
Temperature/K	123.01(10)	123.01(10)	123.00(10)
Crystal system	triclinic	triclinic	triclinic
Space group	P-1	P-1	P-1
a/Å	12.4026(3)	9.4890(3)	10.6425(3)
b/Å	12.9001(3)	13.2660(5)	11.4204(4)
c/Å	15.7254(4)	13.4334(5)	19.2624(7)
α/°	71.183(2)	73.941(3)	80.133(3)
β/°	71.992(2)	72.163(3)	88.486(3)
γ/°	74.248(2)	80.848(3)	83.575(3)
Volume/Å ³	2223.24(10)	1541.80(10)	2292.00(13)
Z	2	2	2
ρ _{calc} /cm ³	1.560	1.419	1.534
μ/mm ⁻¹	5.982	5.547	7.136
F(000)	1056.0	688.0	1072.0
Crystal size/mm ³	0.212 × 0.18 × 0.138	0.59 × 0.213 × 0.175	0.272 × 0.232 × 0.136
Radiation	CuKα (λ = 1.54184)	Cu Kα (λ = 1.54184)	CuKα (λ = 1.54184)
2θ range for data collection/°	7.376 to 148.586	6.956 to 148.482	7.904 to 147.27
Index ranges	-14 ≤ h ≤ 15, -16 ≤ k ≤ 16, -19 ≤ l ≤ 19	-11 ≤ h ≤ 11, -16 ≤ k ≤ 16	-13 ≤ h ≤ 10, -14 ≤ k ≤ 13
Reflections collected	25664	12978	17140
Independent reflections	8775 [R _{int} = 0.0211, R _{sigma} = 0.0199]	6017 [R _{int} = 0.0311, R _{sigma} = 0.0362]	9002 [R _{int} = 0.0438, R _{sigma} = 0.0483]
Data/restraints/parameters	8775/0/577	6017/0/413	9002/0/558
Goodness-of-fit on F ²	1.043	1.028	1.033
Final R indexes [I ≥ 2σ (I)]	R ₁ = 0.0260, wR ₂ = 0.0669	R ₁ = 0.0297, wR ₂ = 0.0745	R ₁ = 0.0518, wR ₂ = 0.1395
Final R indexes [all data]	R ₁ = 0.0270, wR ₂ = 0.0675	R ₁ = 0.0315, wR ₂ = 0.0760	R ₁ = 0.0551, wR ₂ = 0.1440
Largest diff. peak/hole / e Å ⁻³	0.80/-0.38	0.33/-0.28	1.26/-0.84
Diffractometer	SuperNova	SuperNova	SuperNova

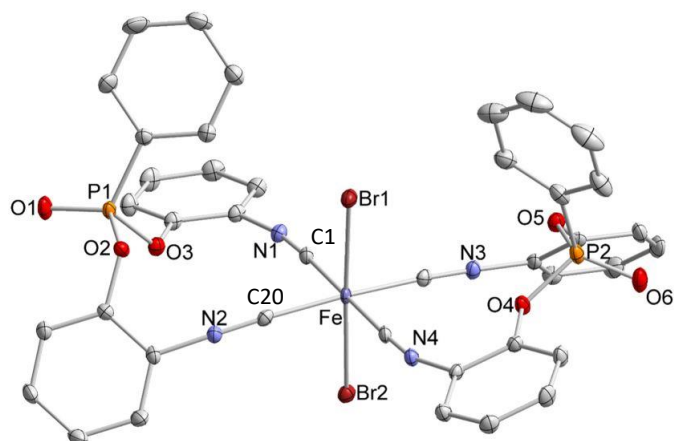


Figure S34. Solid-state molecular structure of complex *trans*-[FeBr₂(BINC)₂] (**1**). Ellipsoids are drawn at the 40% probability level. H atom and solvent molecules (2.5 x THF) are omitted for clarity.

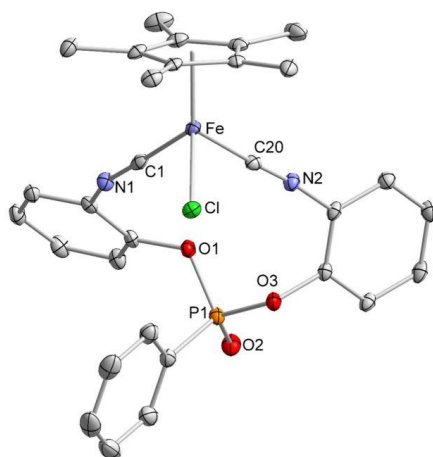


Figure S35. Solid-state molecular structure of complex [Cp*FeCl(BINC)] (**3**). Ellipsoids are drawn at the 40% probability level. H atoms and solvent molecules (disordered THF) are omitted for clarity.

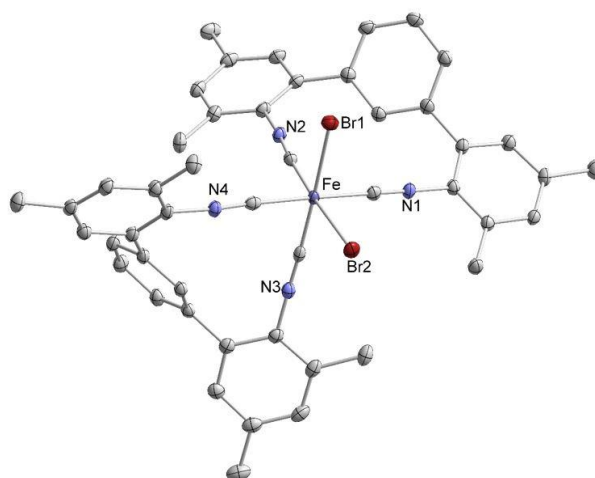


Figure S36. Solid-state molecular structure of complex *cis*-[FeBr₂(CNAr₃NC)₂] (**5**). Ellipsoids are drawn at the 40% probability level. H atoms and solvent molecules (2 x DCM) are omitted for clarity.

S5.2 X-ray Crystallographic Data of compounds 2, 4, 6 and 7

Table S2. Crystallographic data and structure refinement of 2, 4, 6 and 7.

	2	4	6	7
CCDC	2056041	2056043	2056046	2056045
Empirical formula	C ₁₂₄ H ₈₈ Fe ₃ N ₁₂ O ₁₉ P ₆	C ₆₀ H ₅₆ Fe ₂ N ₄ O ₆ P ₂	C ₁₀₄ H ₁₀₀ Fe ₂ N ₈ O ₂	C ₁₀₆ H ₁₀₅ Fe ₂ K ₂ N ₈ O _{2.5}
Formula weight	2403.43	1102.72	1605.61	1720.87
Temperature/K	123.00(10)	123.00(10)	123.00(10)	122.96(11)
Crystal system	triclinic	monoclinic	monoclinic	monoclinic
Space group	P-1	P2 ₁ /n	P2 ₁ /c	P2 ₁ /c
a/Å	12.9811(3)	12.4034(2)	20.2707(4)	21.9888(5)
b/Å	18.2483(5)	31.8679(3)	14.4768(3)	19.9138(4)
c/Å	25.1393(7)	16.1915(2)	28.9951(7)	23.0414(8)
α/°	89.394(2)	90	90	90
β/°	84.002(2)	111.1680(10)	95.741(2)	112.275(3)
γ/°	71.137(2)	90	90	90
Volume/Å ³	5602.7(3)	5968.18(14)	8466.1(3)	9336.5(5)
Z	2	4	4	4
ρ _{calc} /cm ³	1.425	1.227	1.260	1.224
μ/mm ⁻¹	4.510	4.806	3.185	3.708
F(000)	2472.0	2296.0	3392.0	3628.0
Crystal size/mm ³	0.349 × 0.219 × 0.119	0.286 × 0.149 × 0.094	0.204 × 0.144 × 0.114	0.543 × 0.433 × 0.247
Radiation	CuKα (λ = 1.54184)	Cu Kα (λ = 1.54184)	CuKα (λ = 1.54184)	Cu Kα (λ = 1.54184)
2θ range for data collection/°	7.074 to 147.308	7.77 to 147.83	7.168 to 152.99	7.768 to 148.178
Index ranges	-12 ≤ h ≤ 16, -20 ≤ k ≤ 22, -31 ≤ l ≤ 31	-15 ≤ h ≤ 15, -35 ≤ k ≤ 39, -20 ≤ l ≤ 20	-25 ≤ h ≤ 25, -18 ≤ k ≤ 14, -36 ≤ l ≤ 36	-25 ≤ h ≤ 27, -24 ≤ k ≤ 23, -28 ≤ l ≤ 20
Reflections collected	44591	45509	100589	54638
Independent reflections	22002 [R _{int} = 0.0406, R _{sigma} = 0.0556]	11884 [R _{int} = 0.0276, R _{sigma} = 0.0226]	17434 [R _{int} = 0.0693, R _{sigma} = 0.0492]	18531 [R _{int} = 0.0380, R _{sigma} = 0.0358]
Data/restraints/parameters	22002/295/1716	11884/120/773	17434/36/1085	18531/426/1271
Goodness-of-fit on F ²	1.025	1.034	1.057	1.073
Final R indexes [I ≥ 2σ (I)]	R ₁ = 0.0573, wR ₂ = 0.1461	R ₁ = 0.0334, wR ₂ = 0.0850	R ₁ = 0.0638, wR ₂ = 0.1598	R ₁ = 0.0865, wR ₂ = 0.2349
Final R indexes [all data]	R ₁ = 0.0653, wR ₂ = 0.1531	R ₁ = 0.0364, wR ₂ = 0.0869	R ₁ = 0.0868, wR ₂ = 0.1736	R ₁ = 0.0999, wR ₂ = 0.2451
Largest diff. peak/hole / e Å ⁻³	0.93/-1.50	0.45/-0.34	0.51/-0.75	1.24/-0.60
Diffractometer	SuperNova	SuperNova	SuperNova	SuperNova

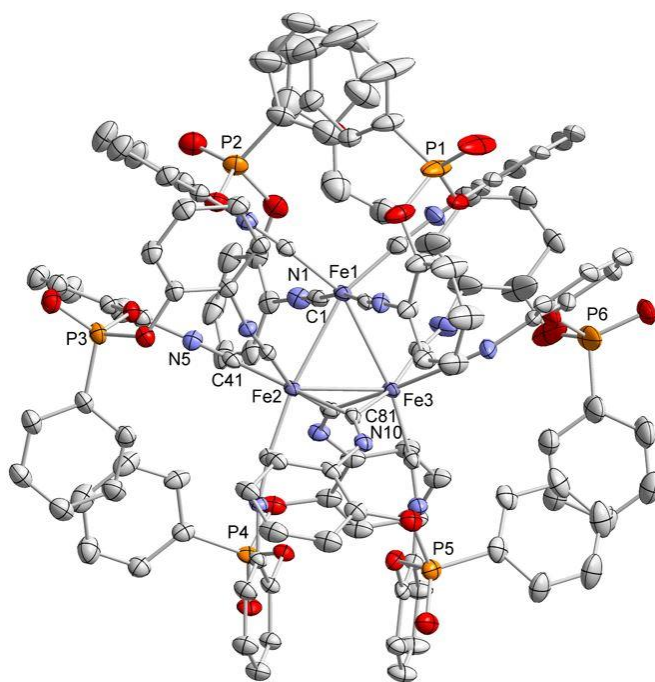


Figure S37. Solid-state molecular structure of complex $[\text{Fe}_3(\text{BINC})_6]$ (**2**). Ellipsoids are drawn at the 40% probability level. H atoms, solvent molecules (one disordered Et_2O molecule) and disorder in the phenyl groups are omitted for clarity.

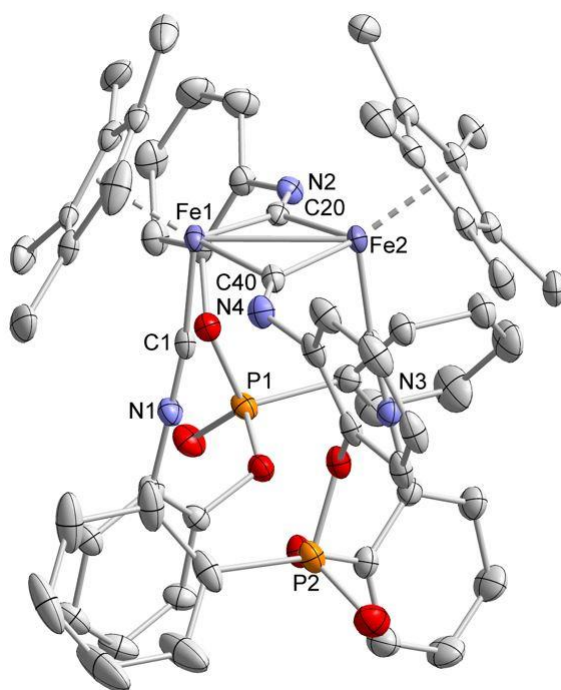


Figure S38. Solid-state molecular structures of complex $[\text{Cp}^*\text{Fe}(\text{BINC})]_2$ (**4**). Ellipsoids are drawn at the 40% probability level. H atoms, solvent molecules (2 x Et_2O , solvent mask) and disorder in the Cp^* groups are omitted for clarity.

The crystal of **4** contained disordered molecules of diethyl ether which were refined by using the solvent mask command. A solvent mask was calculated, and 286.0 electrons were found in a volume of 1262.0 \AA^3 in one void per unit cell. This is consistent with the presence of one diethyl ether per asymmetric unit which account for 336.0 electrons

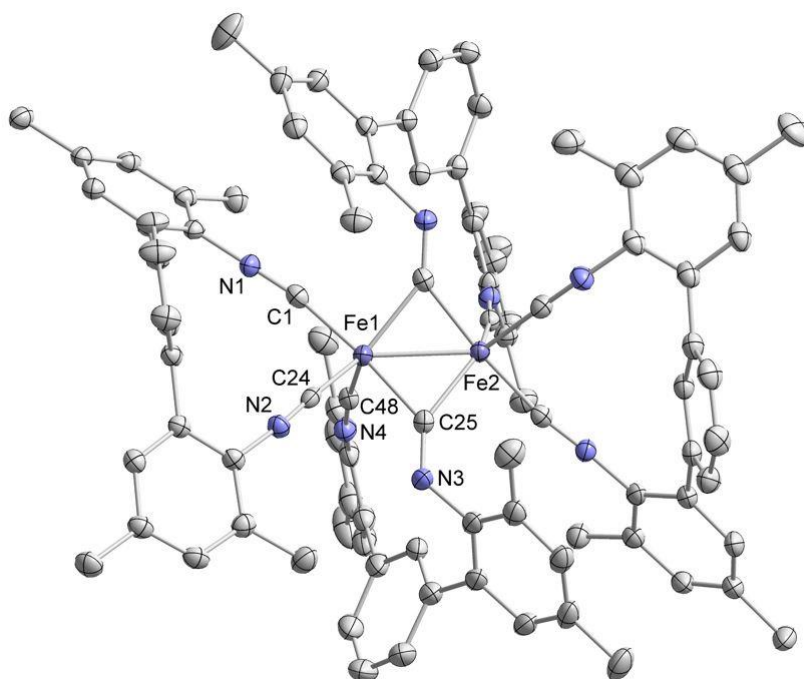


Figure S39. Solid-state molecular structures of complex $[\text{Fe}(\text{CNAr}_3\text{NC})_2]_2$ (**6**). Ellipsoids are drawn at the 40% probability level. H atoms and solvent molecules (two Et_2O molecules (one disordered)) are omitted for clarity.

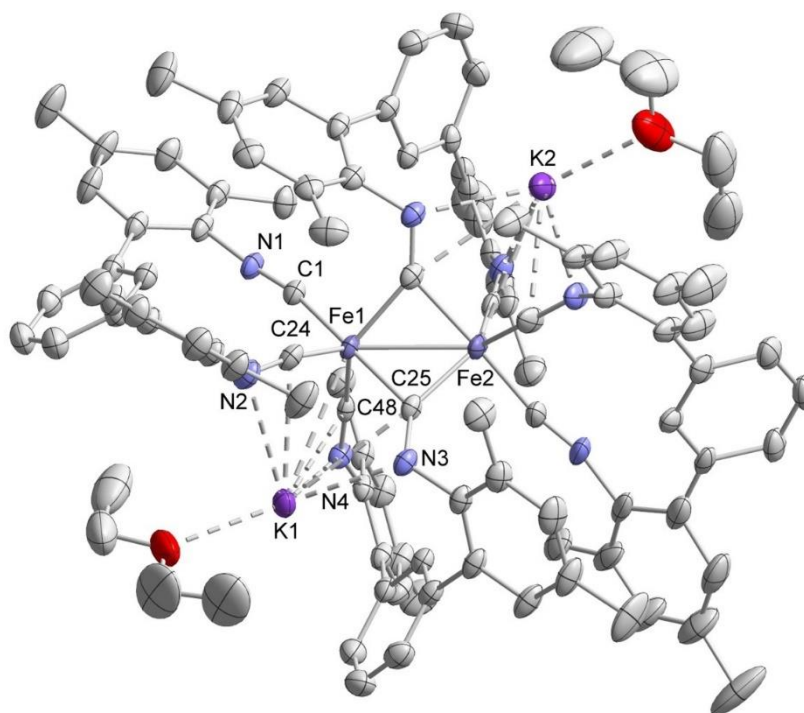


Figure S40. Solid-state molecular structures of complex $[\text{K}(\text{Et}_2\text{O})_2][\text{Fe}(\text{CNAr}_3\text{NC})_2]_2$ (**7**). Ellipsoids are drawn at the 40% probability level. H atoms and solvent molecules (one not coordinated Et_2O) are omitted for clarity.

S6. UV-vis-NIR Spectroelectrochemistry

S6.1 Spectroelectrochemistry of compound 2

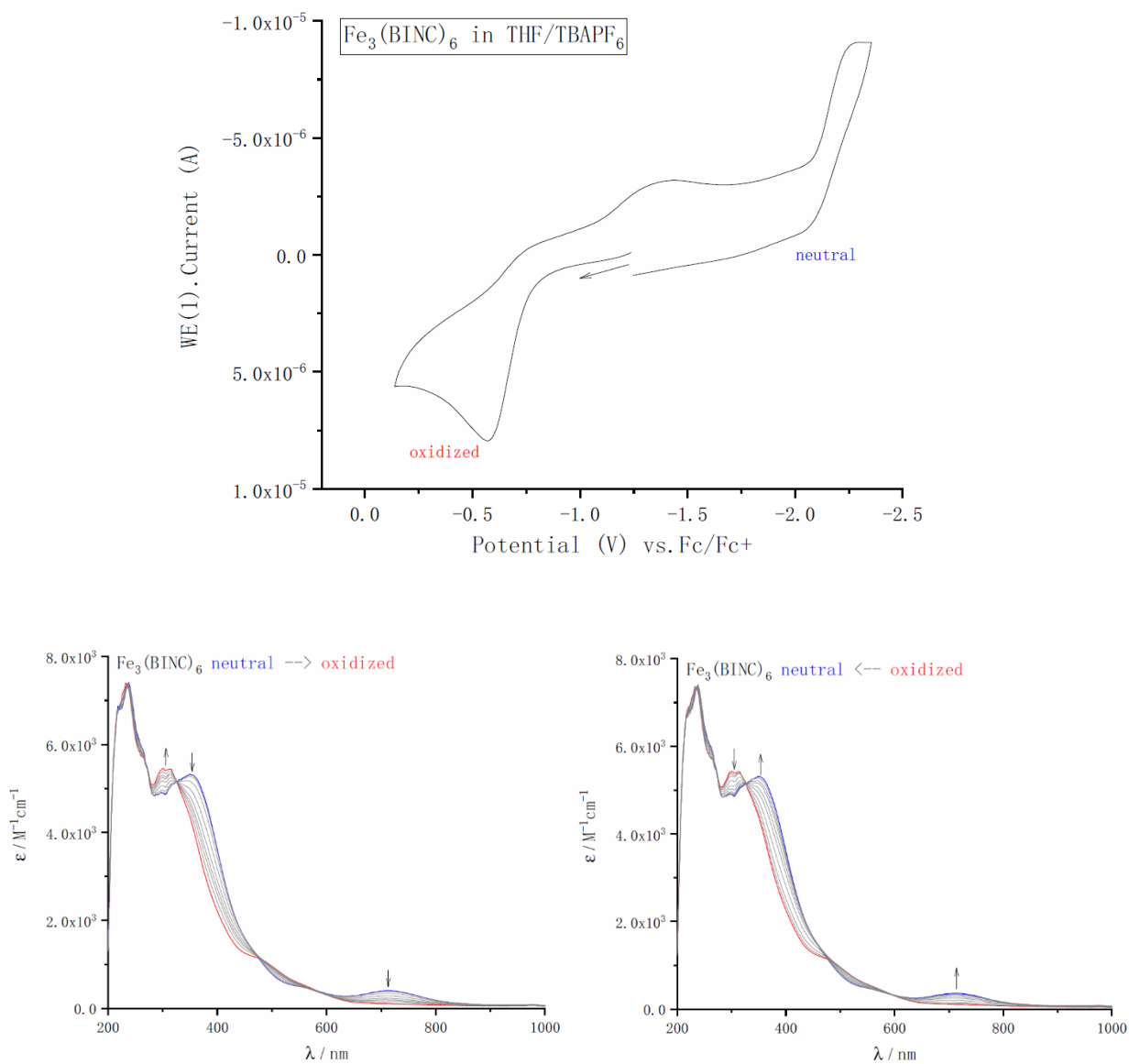


Figure S41. Spectroelectrochemistry of compound 2 in 0.1 M n-Bu₄NPF₆/THF, scan rate 100 mV/s, neutral (blue) → oxidized (red).

S6.2 Spectroelectrochemistry of compound 4

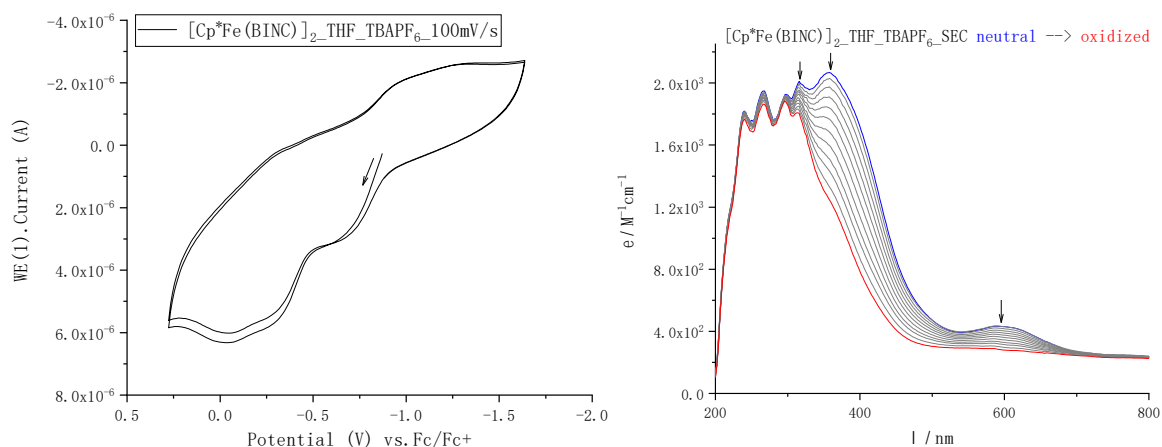


Figure S42. Spectroelectrochemistry of compound 4 in 0.1 M n-Bu₄NPF₆/THF, scan rate 100 mV/s, neutral (blue) → oxidized (red).

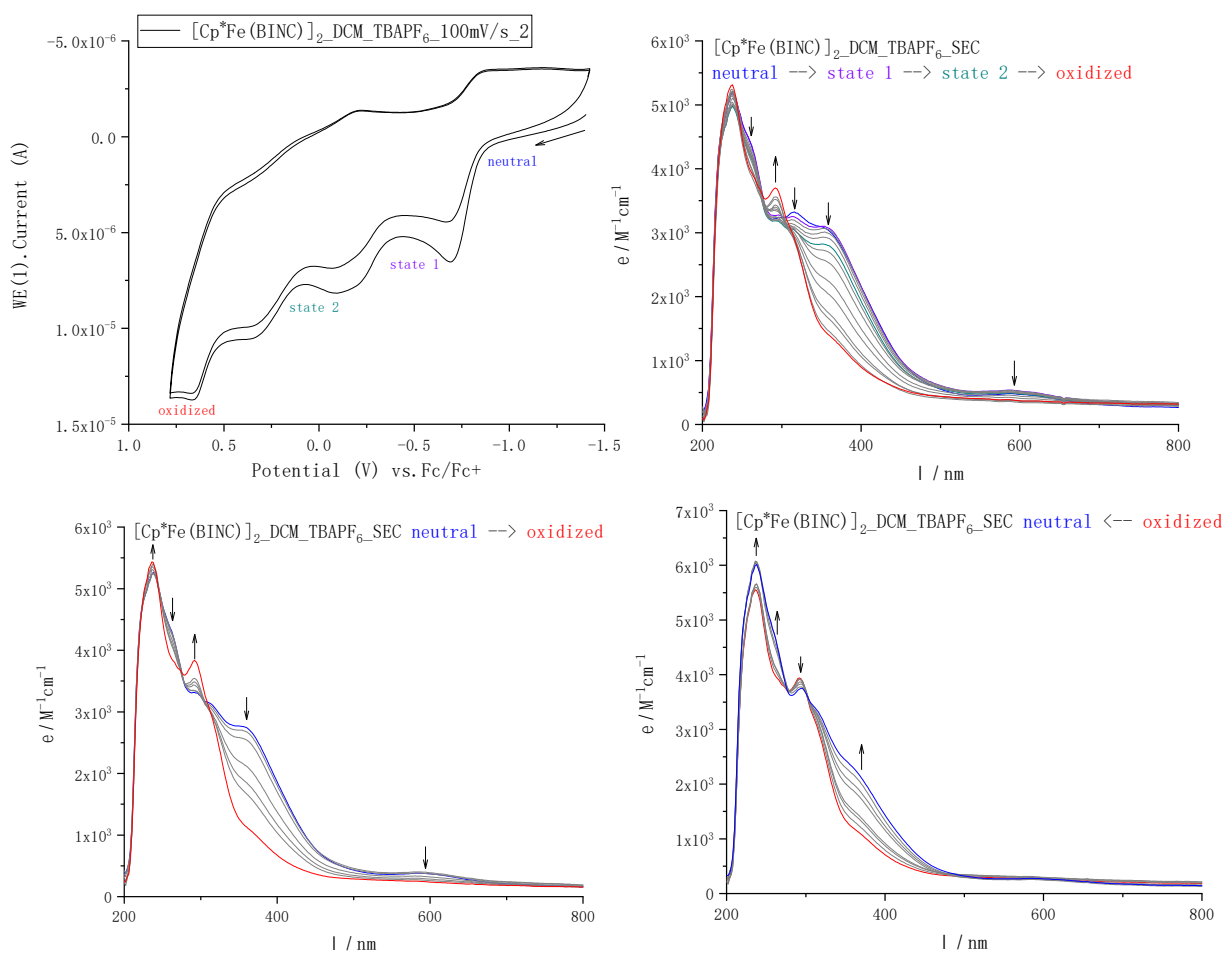


Figure S43. Spectroelectrochemistry of compound 4 in 0.1 M n-Bu₄NPF₆/CD₂Cl₂, scan rate 100 mV/s, neutral (blue) → state 1 → state 2 → oxidized (red).

S6.3 Cyclic Voltammetry and UV/Vis of compound 7

Cyclic voltammetry experiments were performed in a single-compartment cell inside a nitrogen-filled glovebox using a CH Instruments CHI600E potentiostat. The cell was equipped with a platinum disc working electrode (2 mm diameter) polished with 0.05 μm alumina paste, a platinum wire counter electrode and a silver/silver nitrate reference electrode. The supporting electrolyte, tetra-n-butylammonium hexafluorophosphate $[(n\text{Bu}_4\text{N})\text{PF}_6]$, was dried in vacuo at 110 $^\circ\text{C}$ for three days. All redox potentials are reported versus the ferrocene/ferrocenium (Fc/Fc $^+$) couple. The scan rate is $v = 100 \text{ mV s}^{-1}$ unless stated otherwise.

UV-Vis spectra were recorded on an Ocean Optics Flame Spectrometer. High resolution mass spectra were recorded by the analytical department at the University of Regensburg using a Jeol AccuTOF GCX.

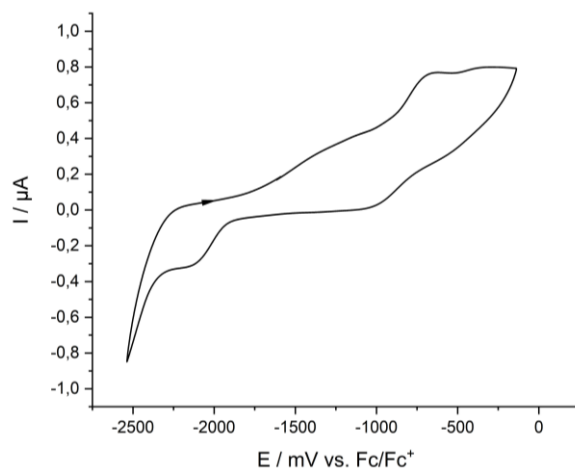


Figure S44. Cyclic voltammogram of compound 7 recorded in THF/ $[(n\text{Bu}_4\text{N})\text{PF}_6]$.

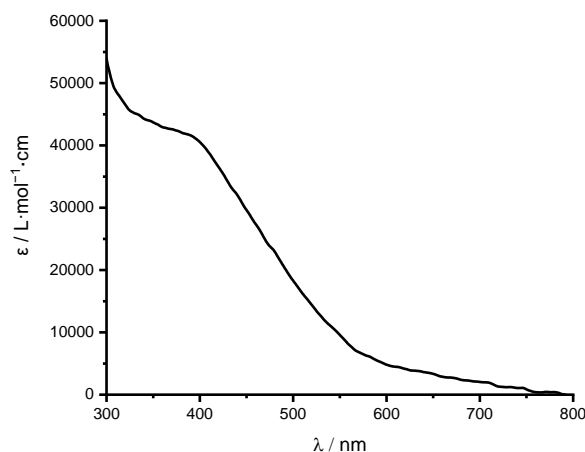


Figure S45. UV/Vis of compound 7 recorded in THF.

S7. DFT Calculations and Cartesian coordinates of compound **6** (Optimized Structures)

All calculations were performed with the ORCA program package.^[51] Geometry optimisations have been carried out at the BP86-D3BJ/def2-SVP^[52] level of theory. Calculated IR spectra were rendered with the software Avogadro.^[53]

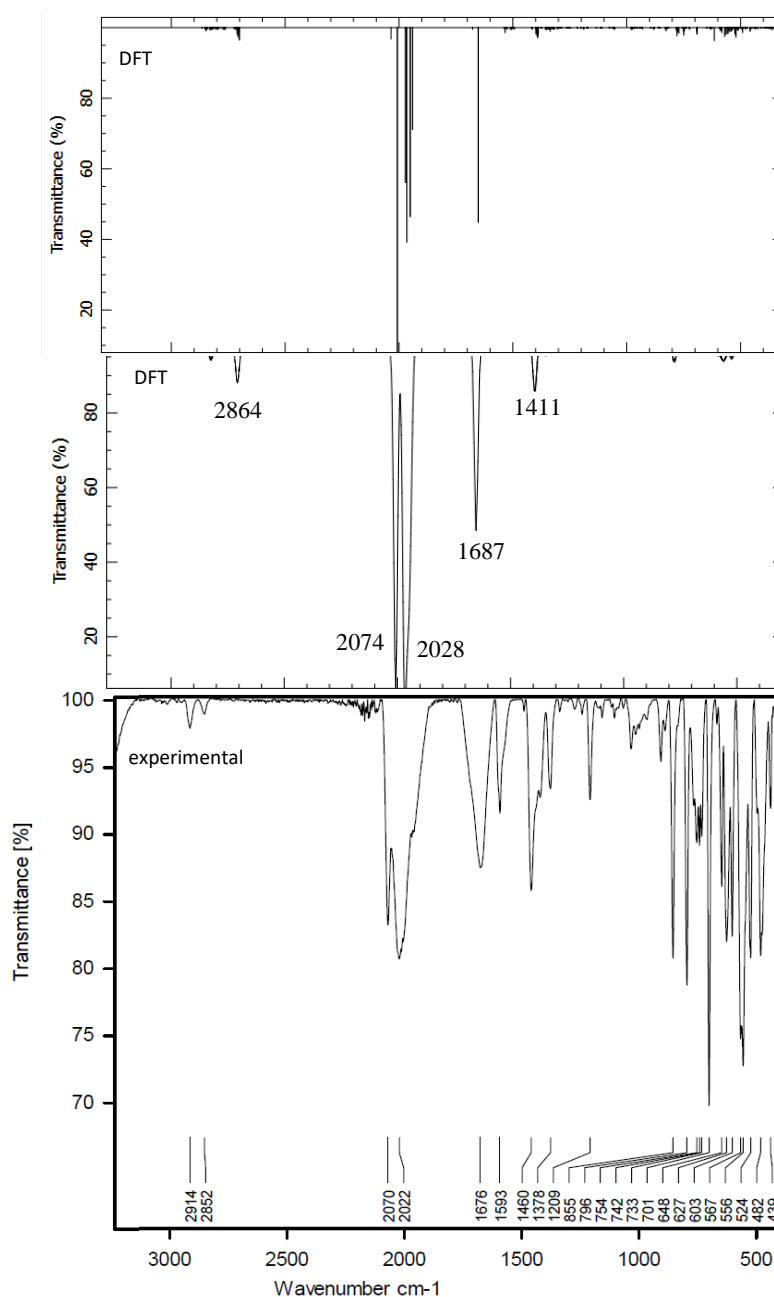


Figure S46. Comparison of DFT calculated (BP86-D3BJ/def2-SVP, *top/middle*) and experimental (*bottom*) IR spectra of compound **6**. DFT calculated IR spectra without peak broadening (*top*): scaling type: linear, line shape: gaussian, scale factor: 0.97, peak width: 0.0, points per peak 10. DFT calculated IR spectra settings (*middle*): scaling type: linear, line shape: gaussian, scale factor: 0.97, peak width: 25.0, points per peak 10.

Table S3. Comparison of DFT calculated IR spectra (different modes of C_s symmetry) of $[\text{Fe}_2(\text{CO})_8]$ ^[39] and **6** (see Figure S46). ^a CO stretching frequencies in cm^{-1} ; IR intensities in $\text{km}\cdot\text{mol}^{-1}$; ^b CN stretching frequencies in cm^{-1} ; IR intensities in $\text{km}\cdot\text{mol}^{-1}$.

modes	1C_s	BP86 ^a of $[\text{Fe}_2(\text{CO})_8]$	BP86 ^b of 6
VCO1/CN1	a''	1849 (739)	2001 (1096)
VCO2/CN2	a'	1872 (240)	2012 (2036)
VCO3/CN3	a'	1990 (297)	2028 (2311)
VCO4/CN4	a'	2015 (1012)	2035 (1669)
VCO5/CN5	a''	2022 (1090)	2074 (3806)
VCO6/CN6	a'	2041 (2103)	2105 (119)

Optimized Coordinates of compound 6

Fe	5.72008653071447	7.30172336312875	10.61052451108407
Fe	3.63783887202780	7.01654069684813	9.41701409435489
N	7.17713179111246	5.84230357179250	12.78978263466850
N	2.04720446674053	8.61925564416819	7.44117054105589
N	5.44286746658315	9.33761216647204	8.49036711258423
N	1.82649489340481	7.25519074835482	11.74209459867973
N	4.95173742696437	9.71885243613527	12.13042132579248
N	2.49179960264802	4.68245030812948	7.97671237091544
N	8.45615875026180	7.98867421213783	9.67256037866579
N	4.27777153473304	4.60448036937161	10.99469480360202
C	4.94561401977673	9.97080305115822	7.36516098694028
C	4.49049763110335	5.73733170164599	10.52792444798738
C	2.74242300737528	8.07759215290583	8.23793872649691
C	1.98118079157450	3.63361655464044	7.26724717854375
C	1.67507809679955	6.26315201915896	5.52878919945396
H	1.04171362863819	6.35127520272984	6.41058027115141
C	6.51002840758350	6.35251851772732	11.94942124939653
C	0.36261313949413	11.29971243717674	5.62295326203162
H	-0.05047123227855	12.29048603133452	5.82738592534527
C	4.49902452161659	11.31306705227711	7.44376754729044
C	3.71397776413620	11.76848066343964	12.44370993024912
C	7.36640079417153	7.70135041295303	10.03717599245808
C	7.88703353393616	5.05412093258218	13.65627549406336
C	1.41785345683591	8.74618436090804	5.10952283380890
C	9.07178880669013	4.40622337233515	13.23193136770651
C	0.85880805252600	9.52489060833043	4.08599173993455
H	0.81506533424892	9.10133550711127	3.08086491309161
C	5.10791562786675	8.33151181518518	9.13996615998797
C	1.78243314170212	3.75778805938269	5.87297238589844
C	0.90227976799345	10.57323299713169	6.68262370635746
C	4.51121989112807	12.08270462768028	8.71034650293702
C	2.13170929496435	4.99470901467375	5.13265966193561
C	1.20970051937637	1.35593030936729	7.21631431812279
H	0.99036885203019	0.42048714352721	7.73719365678936
C	1.44531996961077	9.29591332941443	6.41358891958109
C	2.47343366259095	7.19537563025546	10.74158472718255
C	4.91745440521078	13.42992506071096	8.67720233797559
H	5.26057166290419	13.85620945552211	7.73383932191471
C	4.16062125546176	10.51522672478117	12.92092162344326
C	2.96315286975946	5.61291951364815	8.53810946734611
C	4.52285770339580	13.65315048506273	11.04917301029679
H	4.55800755613251	14.25066326284049	11.96099887434162
C	4.11807790467895	12.30816994178921	11.12280345305624

C	9.83556000248359	5.82971961367402	11.28329076453166
H	9.52067760975070	6.72404925457036	11.81946607450991
C	0.98953006478281	1.44036221878212	5.83275407742958
C	0.33733313917696	10.79990817941186	4.31458619947135
C	3.84410399511164	10.06380712983101	14.22406157551588
C	5.33295987585931	8.72118126041338	11.59902872619484
C	7.37643857816554	4.86812054583445	14.96143141682316
C	4.98047476348726	9.30279031815159	6.11435138091721
C	2.90685018246659	12.53631859284149	13.29754136667711
H	2.52692840273530	13.49130790521768	12.92917732129611
C	4.11691361272582	11.53706110966102	9.94679345469938
H	3.78076226170623	10.50344559492250	9.98343796602873
C	1.28652087948690	2.64247668908502	5.18387283734845
H	1.11559167549727	2.73044419642782	4.10912132631887
C	4.05206045951640	11.93985579256773	6.26781191289778
H	3.65028370380668	12.95292227247602	6.33961799599714
C	4.55490831458778	9.98832046987736	4.97715270404756
H	4.58587296783929	9.46739452208565	4.01757324392925
C	10.47443471992374	5.96180311717606	10.03882849695817
C	9.65339016481272	4.57114960354334	11.87878513944872
C	0.78897243482083	9.11627187559911	12.83250718330133
C	1.96563684498052	7.41067786011080	4.77343947063452
C	1.70360062022227	2.42932559673288	7.95635152267767
C	1.31193304077959	7.80275498183654	12.89117748652223
C	4.91976778651518	14.20647303045609	9.83361078701259
H	5.25491072373296	15.24410816013477	9.79196144168269
C	9.72606176583693	8.25134299221101	9.24531964834066
C	5.02119742066964	3.71669047799815	11.75200785035156
C	10.74114121053609	7.28270799752850	9.41911882425780
C	2.91881702565026	4.88929815897763	3.97357009427797
H	3.30076851216642	3.91164941218189	3.67690516647668
C	4.07471683027121	11.30368262068340	5.02727844137328
C	-0.21596869383788	11.62435992547720	3.18316461506346
H	-1.08236336681709	12.21921855798481	3.50436054194594
H	-0.52477850615119	10.99240607471944	2.33976026529062
H	0.54267152138270	12.32989205532231	2.80663392413582
C	6.19300595409795	3.13792845700517	11.20067491520213
C	9.97443080069981	9.48467449289529	8.59759169342768
C	0.92468586244926	11.12207317507011	8.07747843786705
H	1.95057418857084	11.18997948125435	8.46397351012947
H	0.36783764635371	10.47064783838390	8.76653335550552
H	0.47994170134141	12.12416499395871	8.11052129426670
C	4.55993286891321	3.31196731688280	13.02911120929450
C	8.05191666300311	4.00213499487947	15.81919903727158
H	7.65485721657645	3.85123206642792	16.82599456227529
C	2.57103936807699	12.11702301455460	14.58719545237487
C	6.13026782019387	5.58220925750007	15.39073054780249
H	5.27451762202780	5.30453534484819	14.76031814536845
H	6.24918501879353	6.67167168584012	15.30297564273726
H	5.88021954906822	5.34140223555591	16.43120486436669
C	4.36139784200009	8.73977204203060	14.70053154195751
H	4.08167554179927	7.93027445530845	14.01243151709113
H	3.96550158547988	8.49657261577901	15.69345840633505
H	5.46169510619888	8.74207022397980	14.74759451886734
C	10.90777091468121	4.80282252000897	9.37311801002699
H	11.37805873588601	4.89635179560068	8.39343588382622

C	9.21422468114335	3.32464181549921	15.42889516588917
C	9.70712382400703	3.54895549641194	14.14178723764446
H	10.63210390409365	3.06001138322482	13.83042114836766
C	12.02079424586507	7.58596069775834	8.93405555533458
H	12.81650717329881	6.85173352843975	9.07473758848916
C	3.06328764663816	10.88356779142981	15.03469891375673
H	2.81294652691572	10.53624081944931	16.03954894078029
C	5.31523002526191	2.36762219772832	13.74543218887042
H	4.99280708156373	2.10220674720572	14.75463940773383
C	2.91470582053908	5.17866380634424	13.54920724092324
H	3.56628777280644	5.88762042649013	13.04373336636395
C	1.72403025579440	5.63279390718543	14.14399912829998
C	1.27831413399359	7.04598463416365	14.08441574860945
C	5.46446834133145	7.88287323585972	6.02967945542514
H	6.43597274919970	7.76215770163964	6.53216628307332
H	5.55766351976408	7.56450660533980	4.98407392535227
H	4.77091055637781	7.19293513367350	6.53551952772378
C	11.26823198385025	9.72931697931894	8.13937977376750
H	11.47303489156455	10.67879542404393	7.63835665648962
C	10.72023311735159	3.54644629652021	9.94661319871103
H	11.04746138718104	2.65106734468837	9.41615696693097
C	0.42559785800881	0.26807193578615	5.07307335104328
H	0.93196783118526	-0.66830411591008	5.34903553741664
H	0.52869660367140	0.40723453407404	3.98889699042783
H	-0.64566211972917	0.13329057748334	5.29169868511409
C	10.10765798235475	3.43144617849866	11.19169207349048
H	9.95919387065220	2.44871148741968	11.63879572716101
C	3.30236861887648	3.82713770528242	13.62066266381672
C	6.88194572551080	2.18175580593794	11.94603413581937
H	7.78315245169001	1.74060473680004	11.51436817331677
C	2.74708016603548	7.27011941655076	3.61283355436143
H	2.98968698237123	8.15631385587382	3.02675516889177
C	1.95040868710841	2.34104164811069	9.43504588663245
H	2.98012769038732	2.62905918274669	9.69314186152357
H	1.76121578884487	1.32558873071696	9.80393158564221
H	1.30375624438731	3.03930112245165	9.98816864892939
C	0.22319897644035	8.95802816392551	15.20382291641959
C	6.47171310480702	1.78687803503513	13.22622968484102
C	3.22657014103148	6.02248799845304	3.22275795550151
H	3.84994623979723	5.93308423059188	2.33193027746579
C	12.30642186981341	8.79852986338840	8.29975107297670
C	8.85774803081479	10.47285191358973	8.41941229823836
H	9.19070104825224	11.33918550809580	7.83492770364459
H	8.48464782670369	10.83024419489634	9.39138372598716
H	7.98850429038801	10.01849724596520	7.92152589398909
C	0.82137613297228	9.87452947279360	11.53958004626987
H	1.84123811488040	9.92988757272092	11.13475466587543
H	0.45104280929225	10.89758043059508	11.67387287248465
H	0.20943868158257	9.37260024111259	10.77381820453073
C	6.67541602507365	3.55788162403529	9.84105829200783
H	5.86371112207298	3.51534404347619	9.09934128307910
H	7.50274516834743	2.91989493662207	9.50667920969961
H	7.02991350465680	4.60059730163589	9.84660352985469
C	9.89953927362091	2.36433024848690	16.36385225268690
H	9.85122833703744	2.71217655340547	17.40515351314870
H	10.95527350155567	2.22642325873328	16.09463083553186

H	9.41764780125720	1.37356691848192	16.32810380153375
C	0.91238232676081	4.70745360189252	14.82459028185919
H	-0.02882968620844	5.04320528088568	15.26171331501485
C	0.24368100345483	9.66146285299525	13.99182642396019
H	-0.15675602297287	10.67688176642563	13.95153619300614
C	2.46058176139711	2.92897699173832	14.30325060767156
H	2.72901686694634	1.87243409764111	14.33550662488858
C	0.74204037375150	7.66112945852687	15.22644108678538
H	0.74084696110932	7.10033257252543	16.16321198234793
C	7.24817746796340	0.75873741265933	14.00632288371224
H	8.32821185153470	0.85827197352677	13.82856102206946
H	6.95925638641726	-0.26645688338434	13.72208614393852
H	7.07203644537883	0.86503907537601	15.08561079731718
C	1.66951056013526	12.94698460182405	15.46223797941823
H	1.65104054040751	13.99661509591907	15.13985709896029
H	1.99005993600046	12.91523453168514	16.51326949825176
H	0.63304445847553	12.57302335209229	15.42936327007226
C	3.61253830966832	12.00777142421682	3.77861074679764
H	2.91444712218428	12.82152745581125	4.01861625691002
H	3.10076983180985	11.31296625240800	3.09785411933334
H	4.45907104535894	12.44822435699253	3.22666127316682
C	1.28088775270812	3.36594134012192	14.90126791277848
H	0.63194213676194	2.65194895593752	15.41099670914557
C	13.69873386272404	9.11225053055456	7.81764020369132
H	14.33143031456670	8.21499007317817	7.81179340132098
H	14.18367591264944	9.85835862641074	8.46699682137302
H	13.68510141752368	9.52965179285000	6.80027731568989
C	-0.30830628084931	9.60282066843773	16.45646038532306
H	0.43948297192129	10.28012767368750	16.90051855485867
H	-0.56610596544988	8.85310217297830	17.21632489438521
H	-1.20446340754108	10.20477072561257	16.24884934316233

5.5 References

- [1] Lieke, W. Ueber das Cyanallyl. *Justus Liebigs Ann. Chem.* **1859**, *112*, 316–321.
- [2] a) Meyer, E. Neue Versuche mit Cyansilber. *J. Prakt. Chem.* **1866**, *67*, 147–153; b) Gautier, A. Ueber die Einwirkung des Chlorwasserstoffs ua auf das Aethyl- und Methylcyanür. *Justus Liebigs Ann. Chem.* **1867**, *142*, 289–294; c) Hofmann, A. W. Ueber eine neue Reihe von Homologen der Cyanwasserstoffsäure. *Justus Liebigs Ann. Chem.* **1867**, *144*, 114–120; d) Gautier, A. Ueber eine neue Reihe von Verbindungen, welche mit den Cyanwasserstoffsäure-Aethern isomer sind. *Justus Liebigs Ann. Chem.* **1868**, *146*, 119–124; e) Ugi, I.; Meyr, R. Neue Darstellungsmethode für Isonitrile. *Angew. Chem.* **1958**, *70*, 702–703; f) Ugi, I. *Isonitrile Chemistry*, Academic Press, **1971**.
- [3] Malatesta, L. Isocyanide Complexes of Metals. *Prog. Inorg. Chem.*, Wiley-Blackwell, **2007**, 283–379.
- [4] Elschenbroich, C. *Organometallchemie*, Teubner, **2008**.
- [5] Knorn, M.; Lutsker, E.; Reiser, O. Isonitriles as supporting and non-innocent ligands in metal catalysis. *Chem. Soc. Rev.* **2020**, *49*, 7730–7752.
- [6] Knorn, M.; Rawner, T.; Czerwieńec, R.; Reiser, O. [Copper(phenanthroline)(bisisonitrile)]⁺-Complexes for the Visible-Light-Mediated Atom Transfer Radical Addition and Allylation Reactions. *ACS Catal.* **2015**, *5*, 5186–5193.
- [7] Büldt, L. A.; Guo, X.; Prescimone, A.; Wenger, O. S. A Molybdenum(0) Isocyanide Analogue of Ru(2,2'-Bipyridine)₃²⁺: A Strong Reductant for Photoredox Catalysis. *Angew. Chem. Int. Ed.* **2016**, *55*, 11247–11250.
- [8] Larsen, C. B.; Wenger, O. S. Photophysics and Photoredox Catalysis of a Homoleptic Rhenium(I) Tris(diisocyanide) Complex. *Inorg. Chem.*, **2018**, *57*, 2965–2968.
- [9] Wenger, O. S. Photoactive Complexes with Earth-Abundant Metals. *J. Am. Chem. Soc.*, **2018**, *140*, 13522–13533.
- [10] Zhou, W. J.; Wu, X. D.; Miao, M.; Wang, Z. H.; Chen, L.; Shan, S. Y.; Cao, G. M.; Yu, D. G. Light Runs Across Iron Catalysts in Organic Transformations. *Chem. Eur. J.* **2020**, *26*, 15052–15064.
- [11] Duncan Lyngdoh, R. H.; Schaefer, III, H. F.; Bruce King, R. Metal-metal (MM) bond distances and bond orders in binuclear metal complexes of the first-row transition metals titanium through zinc. *Chem. Rev.* **2018**, *118*, 11626–11706.
- [12] a) Fehlhammer, W. P.; Mayr, A.; Kehr, W. Isocyanide- und Heteroallen-verbrückte Metallkomplexe. *J. Organomet. Chem.* **1980**, *197*, 327–334; b) Coville, N. J.; Albers, M. O.; Singleton, E. An Investigation of the Reaction Between [$\{\text{Fe}(\eta^5\text{-C}_5\text{H}_5)(\text{CO})_2\}_2$] and Aryl Isonitriles. *J. Chem. Soc., Dalton Trans.* **1982**, 1389–1391.
- [13] Ruiz, R.; Riera, V.; Vivanco, M.; Garcia-Granda, S.; Pertierra, P. A Homoleptic (Aryl Isocyanide)Iron(0) Dimer. X-ray Structure Determination of Nonakis(phenyl isocyanide)diiron. *Organometallics* **1992**, *11*, 2734–2736.
- [14] a) Murray, J. B.; Nicholson, B. K.; Whitton, A. J. Multi-substituted isonitrile and mixed ligand derivatives of Fe₃(CO)₁₂; the crystal structure of Fe₃(CO)₁₀(CNBu^t)₂. *J. Organomet. Chem.* **1990**, *385*, 91–100; b) Decker, C.; Henderson, W.; Nicholson,

- B. K. Reactions of isonitriles with $[\text{Fe}_3(\text{CO})_{12}]$ and $[\text{Ru}_3(\text{CO})_{12}]$ monitored by electrospray mass spectrometry; structural characterization of $[\text{Fe}_3(\text{CO})_{10}(\text{CNPh})_2]$ and $[\text{Ru}_4(\text{CO})_{11}(\mu_3\text{-}\eta^2\text{-CNPh})]$. *J. Organomet. Chem.* **2004**, 689, 1691–1701.
- [15] Brennessel, W. W.; Ellis, J. E. $[\text{Fe}(\text{CNXyl})_4]^{2-}$: An Isolable and Structurally Characterized Homoleptic Isocyanide-metalate Dianion. *Angew. Chem. Int. Ed.* **2007**, 46, 598–600.
- [16] Mokhtarzadeh, C. C.; Margulieux, G. W.; Carpenter, A. E.; Weidemann, N.; Moore, C. E.; Rheingold, A. L.; Figueroa, J. S. Synthesis and Protonation of an Encumbered Iron Tetra-isocyanide Dianion. *Inorg. Chem.* **2015**, 54, 5579–5587.
- [17] Drance, M. J.; Sears, J. D.; Mrse, A. M.; Moore, C. E.; Rheingold, A. L.; Neidig, M. L.; Figueroa, J. S. Terminal coordination of diatomic boron monofluoride to iron. *Science*, **2019**, 363, 1203–1205.
- [18] Barybin, M. V.; Meyers, J. J., Jr.; Neal, B. M. Renaissance of Isocyanoarenes as Ligands in Low-Valent Organometallics. In *Isocyanide Chemistry – Applications in Synthesis and Material Science*; Nenajdenko, V., Ed.; Wiley-VCH: Weinheim, Germany, **2012**, 493–529.
- [19] Hahn, F. E. The Coordination Chemistry of Multidentate Isocyanide Ligands. *Angew. Chem. Int. Ed. Engl.* **1993**, 32, 650–665.
- [20] a) Angelici, R. J.; Quick, M. H.; Kraus, G. A.; Plummer, D. T. Synthesis of Chelating Bidentate Isocyano and Cyano Ligands and Their Metal Complexes *Inorg. Chem.* **1982**, 21, 2178–2184; b) Kargol, J. A.; Angelici, R. J. Iron(II) Complexes with the Chelating Bidentate Isonitrile Ligand DiNC. *Inorg. Chim. Acta* **1983**, 68, 127–130.
- [21] Sakata, K.; Fujitsu, T.; Tajiri, H.; Masatsugu, M.; Hashimoto, M. Syntheses and Characterization of Iron(II), Copper(I) and Rhodium(I) Complexes with a Chelating Bidentate Isonitrile Ligand. *Synth. React. Inorg. Met.-Org. Chem.* **1994**, 24, 1509–1522.
- [22] Sakata, K.; Urabe, K.; Hashimoto, M.; Yanagi, T.; Tsuge, A.; Angelici, R. J. Synthesis and Spectral Properties of Iron(II), Copper(I), Silver(I), and Palladium(II) Complexes of a Bidentate Diisonitrile. *Synth. React. Inorg. Met.-Org. Chem.* **2003**, 33, 11–22.
- [23] Naik, A.; Maji, T.; Reiser, O. Iron(II)-bis(isonitrile) complexes: novel catalysts in asymmetric transfer hydrogenations of aromatic and heteroaromatic ketones. *Chem. Commun.* **2010**, 46, 4475–4477.
- [24] Selected examples: a) Wolf, R.; Ghavtadze, N.; Weber, K.; Schnöckelborg, E.-M.; de Bruin, B.; Ehlers, A. W.; Lammertsma, K. P-C dichotomy: divergent iron (-I)-mediated alkyne and phosphalkyne cyclooligomerisations. *Dalton Trans.* **2010**, 39, 1453–1456; b) Wolf, R.; Schnöckelborg, E.-M. A reactive iron naphthalene complex provides convenient access to the Cp^*Fe^- synthon ($\text{Cp}^* = \text{C}_5\text{H}_5$). *Chem. Commun.* **2010**, 46, 2832–2834; c) Schnöckelborg, E.-M.; Khusniyarov, M. M.; de Bruin, B.; Hartl, F.; Langer, T.; Eul, M.; Schulz, S.; Pöttgen, R.; Wolf, R. Unraveling the Electronic Structures of Low-Valent Naphthalene and Anthracene Iron Complexes: X-ray, Spectroscopic, and Density Functional Theory Studies. *Inorg. Chem.* **2012**, 51, 6719–6730; d) Maier, T. M.; Gawron, M.; Coburger, P.; Bodensteiner, M.; Wolf, R.; van Leest, N. P.; de Bruin, B.; Demeshko, S.; Meyer,

- F. Low-Valence Anionic α -Diimine Iron Complexes: Synthesis, Characterization, and Catalytic Hydroboration Studies. *Inorg. Chem.* **2020**, *59*, 16035–16052.
- [25] Selected examples: a) Rezaei Rad, B.; Herrmann, D.; Lescop, C.; Wolf, R. A tetradentate metalloligand: synthesis and coordination behaviour of a 2-pyridyl-substituted cyclobutadiene iron complex. *Dalton Trans.* **2014**, *43*, 4247–4250; b) Rezaei Rad, B.; Chakraborty, U.; Mühldorf, B.; Bodensteiner, M.; Sklorz, J. A. W.; Müller, C.; Wolf, R. Synthesis, Structure, and Reactivity of Pentamethylcyclopentadienyl 2,4,6-Triphenylphosphinine Iron Complexes. *Organometallics* **2015**, *34*, 622–635; c) Büschelberger, P.; Gärtner, D.; Reyes-Rodriguez, E.; Kreyenschmidt, F.; Koszinowski, K.; Jacobi von Wangelin, A.; Wolf, R. Alkene Metalates as Hydrogenation Catalysts. *Chem. Eur. J.* **2017**, *23*, 3139–3151; d) Chakraborty, U.; Leitl, J.; Mühldorf, B.; Bodensteiner, M.; Pelties, S.; Wolf, R. Mono- and dinuclear tetraphosphabutadiene ferrate anions. *Dalton Trans.* **2018**, *47*, 3693–3697 e) Leitl, J.; Marquardt, M.; Coburger, P.; Scott, D. J.; Streitferdt, V.; Gschwind, R. M.; Müller, C.; Wolf, R. Facile C=O Bond Splitting of Carbon Dioxide Induced by Metal-Ligand Cooperativity in a Phosphinine Iron(0) Complex. *Angew. Chem. Int. Ed.* **2019**, *58*, 15407–15411.
- [26] Warnock, G. F.; Cooper, N. J. The first transition-metal isonitrilate: synthesis and characterization of cobalt complex $K[Co(2,6-Me_2C_6H_3NC)_4]$. *Organometallics* **1989**, *8*, 1826–1827.
- [27] a) Brill, R. *Z. Krist.* **1931**, *72*, 36; b) Sheline, R. K. The Spectra and Structure of Iron Carbonyl. II. Iron Tetracarbonyl. *J. Am. Chem. Soc.* **1951**, *73*, 1615; c) Dahl, L. F.; Rundle, R. E. Polynuclear Metal Carbonyl. III. Infrared Analysis of Iron Tetracarbonyl. *J. Chem. Phys.* **1957**, *27*, 323–324; d) Dahl, L. F.; Blount, J. F. The Probable Structure of $Fe_3(CO)_{12}$ as Obtained from the Structure of $HFe_3(CO)_{11}^-$. *Inorg. Chem.* **1965**, *4*, 1373–1375; e) Wei, C. H.; Dahl, L. F. Molecular Structure of Triiron Dodecacarbonyl and Tetracobalt Dodecacarbonyl. *J. Am. Chem. Soc.* **1966**, *88*, 1821–182; f) Wei, C. H.; Dahl, L. F. Triiron Dodecacarbonyl: An Analysis of Its Stereochemistry. *J. Am. Chem. Soc.* **1969**, *91*, 1351–1361; g) Cotton, F. A.; Troup, J. M. Further Refinement of the Molecular Structure of Triiron Dodecacarbonyl. *J. Am. Chem. Soc.* **1974**, *96*, 4155–4159; h) Braga, D.; Farrugia, L.; Grepioni, F.; Johnson, B. F. G. On the molecular structure of $[Fe_3(CO)_{12}]$ in the solid state. *J. Organomet. Chem.* **1994**, *464*, C39–C41; i) Braga, D.; Grepioni, F.; Tedesco, E.; José Calhorda, M.; Lopes, P. E. M. Molecular Structure and Crystal Structure Generation for $[Fe_3(CO)_{12}]$. *J. Chem. Soc., Dalton Trans.* **1995**, 3297–3306; j) Hunstock, E.; Mealli, C.; Calhorda, M. J.; Reinhold, J. Molecular Structures of $M_2(CO)_9$ and $M_3(CO)_{12}$ (M = Fe, Ru, Os): New Theoretical Insights. *Inorg. Chem.* **1999**, *38*, 5053–5060.
- [28] Brennessel, W. W.; Kucera, B. E.; Young Jr, V. G.; Ellis, J. E. Crystal structure and spectroscopic characterization of $MBr_2(CNXyl)_n$ (M = Fe and Co, n = 4; M = Ni, n = 2; Xyl = 2,6-dimethylphenyl), and of formally zero-valent iron as a cocrystal of $Fe(CNXyl)_5$ and $Fe_2(CNXyl)_9$. *Acta Cryst.* **2019**, *C75*, 1118–1127.
- [29] Krejcik, M.; Danek, M.; Hartl, F. Simple construction of an infrared optically transparent thin layer electrochemical cell. Applications to the redox reactions of

- ferrocene, $\text{Mn}_2(\text{CO})_{10}$ and $\text{Mn}(\text{CO})_3(3,5\text{-di-}t\text{-butyl-catecholate})^-$. *J. Electroanal. Chem. Interfacial Electrochem.* **1991**, 317, 179-187.
- [30] Murr, N. E.; Chaloyard, A. Redox properties of iron carbonyl complexes. *Inorg. Chem.* **1982**, 21, 2206-2208.
- [31] Hubbard, J. L.; McVicar, W. K. Facile conversion of $(\eta^5\text{-C}_5\text{R}_5)\text{M}(\text{CO})_2$ -halide complexes to halomethyl, alkoxymethyl, and cyanomethyl derivatives (R = H, CH₃; M = Fe, Ru; halide = Cl, Br, I). *J. Organomet. Chem.* **1992**, 429, 369-378.
- [32] a) Mills, O. S. Studies of some carbon compounds of the transition metals. I. The crystal structure of dicyclopentadienyldiiron tetracarbonyl. *Acta Cryst* **1958**, 11, 620–623; b) Mills, O. S.; Nice, J. P. Carbon compounds of the transition metals: V. The structure of bis(cyclopentadienyldicarbonyl-ruthenium). *J. Organomet. Chem.* **1967**, 9, 339.
- [33] Jonas, K.; Klusmann, P.; Goddard, R. Pentamethylcyclopentadienylbis(ethen)eisen – ein 17 e-Halbsandwichkomplex mit leicht verdrängbaren Ethenliganden. *Z. Naturforsch., Teil B* **1995**, 50, 394.
- [34] Torubaev, Y. V.; Skabitskiy, I. V.; Rusina, P.; Pasynskii, A. A.; Rai, D. K.; Singh, A. Organometallic halogen bond acceptors: directionality, hybrid cocrystals precipitation, and blueshifted CO ligand vibrational band. *CrystEngComm* **2018**, 20, 2258-2266.
- [35] Hallam, B. F.; Mills, O. S.; Pauson, P. L. Dicyclopentadienyldiiron tetracarbonyl. *J. Inorg. Nucl. Chem.* **1955**, 1, 313–316.
- [36] Bryan, R. F.; Greene, P. T.; Newlands, M. J.; Field, D. S. Metal-Metal Bonding in Coordination Complexes. Part X. Preparation, Spectroscopic Properties, and Crystal Structure of the *cis*-Isomer of Di- μ -carbonyl-dicarbonyldi- π -cyclopentadienyldi-iron (Fe-Fe). *J. Chem. Soc. Inorg. Phys. Theor.* **1970**, 3068–3074.
- [37] a) Bullitt, J. G.; Cotton, F. A.; Marks, T. J. Structural and Dynamic Properties of the Pentahaptocyclopentadienylmetal Dicarbonyl Dimers. *Inorg. Chem.* **1972**, 11, 671–676; b) Vitale, M.; Lee, K. K.; Hemann, C. F.; Hille, R.; Gustafson, T. L.; Bursten, B. E. Resonance Raman Studies of $[\text{CpFe}(\text{CO})_2]_2$ and $[\text{Cp}^*\text{Fe}(\text{CO})_2]_2$: A Probe of Photoreactive States and Intermedites. *J. Am. Chem. Soc.* **1995**, 117, 2286–2296; c) Anna, J. M.; King, J. T.; Kubarych, K. J. Multiple Structures and Dynamics of $[\text{CpRu}(\text{CO})_2]_2$ and $[\text{CpFe}(\text{CO})_2]_2$ in Solution Revealed with Two-Dimensional Infrared Spectroscopy. *Inorg. Chem.* **2011**, 50, 9273–9283.
- [38] King, R. B.; Bisnette, M. B. Organometallic Chemistry of the Transition Metals XXI. Some π -Pentamethylcyclopentadienyl Derivates of various Transition Metals. *J. Organomet. Chem.* **1967**, 8, 287–297.
- [39] Teller, R. G.; Williams, J. M. Crystals and molecular structure of bis[dicarbonyl(π -pentamethylcyclopentadienyl) iron], $(\eta^5\text{-C}_5\text{Me}_5)_2\text{Fe}_2(\text{CO})_4$, and structural comparisons with the nonmethylated analog. *Inorg. Chem.* **1980**, 19, 2770-2773.
- [40] (a) Poliakoff, M.; Turner, J. J. Infrared Spectrum and Photochemistry of Di-iron Enneacarbonyl in Matrices at 20K: Evidence for the Formation of $\text{Fe}_2(\text{CO})_8$. *J. Chem. Soc. A* **1971**, 2403-2410. (b) Bertini, L.; Bruschi, M.; De Gioia, L.; Fantucci, P. Structure and Energetics of $\text{Fe}_2(\text{CO})_8$ Singlet and Triplet Electronic States. *J. Phys. Chem. A* **2007**, 111, 12152–12162.

- [41] Safa, M.; Dong, Z.; Song, Y.; Huang, Y. Examining the structural changes in $\text{Fe}_2(\text{CO})_9$ under high external pressures by Raman spectroscopy. *Can. J. Chem.* **2007**, *85*, 866–872.
- [42] Hieber, W.; Brendel, G. Entstehung mehrkerniger Carbonylferrate aus mehrkernigen Eisencarbonylen. *Z. anorg. allg. Chem.* **1957**, *289*, 324–337.
- [43] Chen, X.; Lingam, H. K.; Meyers, E. A.; Shore, S. G. Structures of DMF potassium and sodium salts of $[\text{Fe}(\text{CO})_4]^{2-}$ and $[\text{M}_2(\text{CO})_8]^{2-}$ (M = Fe, Ru). *J. Organomet. Chem.* **2012**, *721-722*, 137-143.
- [44] Neumüller, B.; Petz, W. Reactions of $\text{Fe}_2(\text{CO})_9$ with Lithium: Preparation and Structures of Compounds with Strong Ion Pairing. *Organometallics* **2001**, *20*, 163-170.
- [45] a) Sheldrick, G. M. SADABS, Bruker AXS, Madison, USA **2007**; b) CrysAlisPro, Scale3 Abspack, Rigaku Oxford Diffraction **2019**.
- [46] Clark, R. C.; Reid, J. S. The analytical calculation of absorption in multifaceted crystals. *Acta Crystallogr. A* **1995**, *51*, 887–897.
- [47] Dolomanov, O. V.; Bourhis, L. J.; Gildea, R. J.; Howard, J. A. K.; Puschmann, H. Complete Structure Solution, Refinement and Analysis Program. *J. Appl. Crystallogr.* **2009**, *42*, 339–341.
- [48] Sheldrick, G. M. Crystal structure refinement with SHELXL. *Acta Crystallogr. A* **2015**, *71*, 3–8.
- [49] Sheldrick, G. M. SHELXT-Integrated space-group and crystal-structure determination. *Acta Crystallogr. Section C, Structural chemistry* **2015**, *71*, 3–8.
- [50] Sheldrick, G. M. A short history of SHELX. *Acta Crystallogr. A* **2008**, *64*, 112–122.
- [51] a) Kendall, R. A.; Früchtl, H. A. The impact of the resolution of the identity approximate integral method on modern ab initio algorithm development. *Theor. Chem. Acc.* **1997**, *97*, 158–163; b) Neese, F. The ORCA program system. *Wiley Interdiscip. Rev. Comput. Mol. Sci.* **2012**, *2*, 73–78; c) Neese, F. Software update: the Orca program system, version 4.0. *Wiley Interdiscip. Rev. Comput. Mol. Sci.* **2018**, *8*, DOI 10.1002/wcms.1327.
- [52] a) Weigend, F.; Ahlrichs, R. Balanced basis sets of split valence, triple zeta valence and quadruple zeta valence quality for H to Rn: Design and assessment of accuracy. *Phys. Chem. Chem. Phys.* **2005**, *7*, 3297–3305; b) Grimme, S.; Antony, J.; Ehrlich, S.; Krieg, H. A consistent and accurate *ab initio* parametrization of density functional dispersion correction (DFT-D) for the 94 elements H-Pu. *J. Chem. Phys.* **2010**, *132*, 154104; c) Grimme, S.; Ehrlich, S.; Goerigk, L. Effect of the damping function in dispersion corrected density functional theory. *J. Comput. Chem.* **2011**, *32*, 1456–1465; d) Perdew, J. P. Density-functional approximation for the correlation energy of the inhomogeneous electron gas. *Phys. Rev. B* **1986**, *33*, 8822–8824; e) Becke, A. D. Density-functional exchange-energy approximation with correct asymptotic behavior. *Physical Rev. A* **1988**, *38*, 3098–3100.
- [53] Hanwell, M. D.; Curtis, D. E.; Lonie, D. C.; Vandermeersch, T.; Zurek, E.; Hutchison, G. R. Avogadro: an advanced semantic chemical editor, visualization, and analysis platform. *J. Cheminformatics* **2012**, *4*, 17.

6 Summary and Outlook

This doctoral thesis has primarily focused on the synthesis of valuable organophosphorus compounds (OPCs) by developing chlorine-free functionalization procedures. An introduction into this topic gives a summary of the state of the art of the research field (*Chapter 1*) and the subsequent experimental chapters describe how different mechanistic strategies can be harnessed for the functionalization of white phosphorus (P_4) and diphenylphosphine (Ph_2PH). These concepts include photo-electron transfer of strongly reducing organic photosensitizers (*Chapter 2* and *Chapter 3*) and electron-primed photoredox catalysis (e-PRC, *Chapter 4*). In a distinct project focused on fundamental investigations in organometallic chemistry, the final chapter of this thesis describes the synthesis of new low-oxidation state iron complexes with bidentate isonitrile ligands (*Chapter 5*). The content of this thesis can be summarized as follows:

Chapter 1. Recent Developments in the Organofunctionalization of Inorganic Phosphorus Compounds

The introductory chapter of this thesis reviewed the social and industrial significance of OPCs, illustrating their numerous applications in daily life and academia, e.g., as flame retardants, herbi-/pesticides, pharmaceuticals, photoinitiators and as reagents in organic synthesis and catalysis. A brief description of the industrial state-of-the-art functionalization procedure for the synthesis of OPCs, using P_4 as a starting material, highlights that this method, relying on toxic, chlorinated intermediates, should be avoided. This review was subdivided into the organofunctionalization of P_4 and other phosphorus compounds, such as phosphites and H-phosphonates. Mechanistically diverse routes for the synthesis of monophosphorus compounds studied and reported over the last few decades, including stoichiometric radical reactions, photocatalysis, hydrostannylation, (photo)electrochemistry, oxidative onioation and metal complex-mediated functionalization are described. Unfortunately, all of these transformations remain only proof-of-principle and cannot replace the industrial state-of-the-art procedure for the synthesis of OPCs. Efficient and direct functionalization protocols are rare and the development of new methods avoiding chlorinated P intermediates by directly converting P_4 into OPCs is a challenging yet highly desirable objective. The need for the development of chlorine-free syntheses of OPCs directly from P_4 or other P-containing sources provided the main motivation for the investigations described in this thesis.

Chapter 2. Photochemical Transformation of Chlorobenzenes and White Phosphorus into Arylphosphines and Phosphonium Salts

Chlorobenzenes are important starting materials for the preparation of commercially valuable triarylphosphines and tetraarylphosphonium salts, but their use in the direct arylation of elemental phosphorus has proved elusive. Chapter 2 describes the photochemical synthesis of arylated phosphines and phosphonium salts directly from P_4 and chlorobenzene (PhCl) in presence of organic super-photoreductant tetrakis(dimethylamino)ethylene (TDAE) with UV-light irradiation (Figure 1).

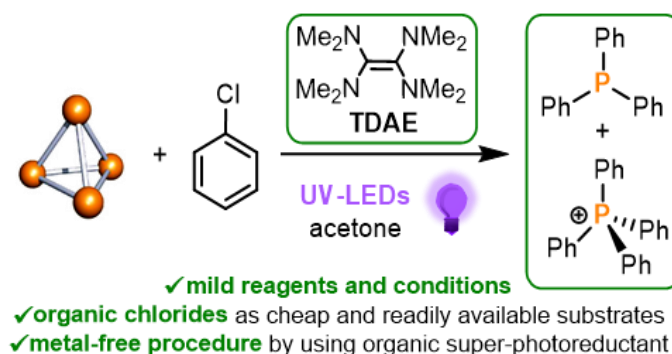


Figure 1. A simple photochemical procedure for the arylation of white phosphorus with aryl chlorides, using the strong photoreductant tetrakis(dimethylamino)ethylene (TDAE) and UV light irradiation.

To overcome the relative inertness of chlorobenzene, which possesses a high energetic barrier for C–Cl bond activation, a strong (photo)reductant is needed. As a single-electron reducing agent, TDAE is insufficiently strong to homolytically cleave a chloride anion from chlorobenzene to generate aryl radicals, but the photoactive excited state of TDAE ($*TDAE$) offers an extraordinary reducing power (-3.4 V vs. SCE). Irradiation (365 nm) of a solution of P_4 , PhCl and TDAE in acetone for 20 hours yielded the phosphonium salt $[Ph_4P]Cl$ (53%) and tertiary phosphine Ph_3P (9%). To our knowledge, this represents the first example of an aryl chloride successfully being reacted with P_4 to provide these products in a direct manner. Investigation of the substrate scope shows that the method works well for chlorobenzenes bearing electron-donating (Me, OMe) groups. Use of alkyl radicals also led to product formation. Time-resolved $^{31}P\{^1H\}$ NMR spectroscopic investigation showed rapid consumption of P_4 and the formation of Ph_3P , $[Ph_4P]Cl$ and an intermediate (**Int1** = TDAE skeleton coordinated to a Ph_2P moiety *via* one of its methyl groups). Furthermore, to validate their intermediacy, the different arylated phosphorus compounds $PhPH_2$, Ph_2PH , Ph_4P_2 and Ph_3P were investigated as starting materials for the photochemical phenylation with chlorobenzene. $[TDAE]Cl_2$, the insoluble side product of the photochemical reaction, could be recovered from the

reaction mixture and used for the recycling of TDAE, facilitating use of the organic photoreductant as part of a closed synthetic loop. This chapter represents an important proof-of-principle as the first example of employing chlorobenzenes for the direct functionalization of P_4 , even though the photochemical method still suffers from several practical disadvantages. Motivated by this unique photochemical P_4 functionalization method, further studies of the activation of chloro- and bromobenzenes for the catalytic P_4 transformation using highly reducing catalysts are ongoing in the Wolf group.

Chapter 3. Photocatalytic Stannylation of White Phosphorus

The third chapter described the photocatalytic stannylation of P_4 , as a follow up study to a recently reported P_4 hydrostannylation method for the synthesis of OPCs. In the hydrostannylation procedure the radical reagent nBu_3SnH was used for the reductive activation of P_4 , yielding a mixture of hydrostannylated phosphines $(Bu_3Sn)_xPH_{3-x}$ ($x = 0-3$) which can be converted into a number of OPCs by reaction with electrophiles. Building on this method, we sought to simplify the intermediates generated during activation from a mixture to a single species. Chapter 3 reviewed a photocatalytic method for the atom-precise stannylation of P_4 by a commercially available distannane, $(Bu_3Sn)_2$, using anthraquinone (AQ) as a photocatalyst under UV-LED irradiation, to exclusively yield $(Bu_3Sn)_3P$ (Figure 2).

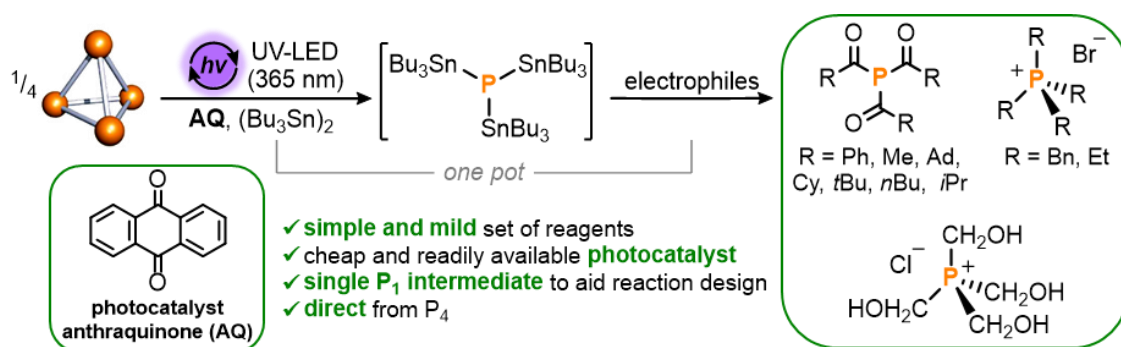


Figure 2. A simple photochemical procedure for the efficient, direct, catalytic stannylation of P_4 and ‘one pot’ transformation into valuable monophosphorus compounds.

For the Sn–Sn homolysis of $(Bu_3Sn)_2$ simple ketones can be used as photocatalysts to furnish Bu_3Sn^\bullet radicals, which our previous work has shown to be capable of breaking down the P_4 tetrahedron to generate stannylated phosphines. As a proof-of-principle, benzophenone (BP) was chosen as a photocatalyst, due to both its simplicity and the fact that its photoreactivity towards hexaalkyldistannanes has been studied previously. In

order to improve the reaction outcome, a broader range of benzophenone derivatives was investigated. Best results were obtained using anthraquinone (**AQ**), and after optimization 79% conversion to $(\text{Bu}_3\text{Sn})_3\text{P}$ could be achieved using significantly reduced loadings of both **AQ** (12.5 mol%) and $(\text{Bu}_3\text{Sn})_2$ (3 equiv.). ‘One-pot’ transformation of the intermediate, $(\text{Bu}_3\text{Sn})_3\text{P}$, with electrophiles provided direct access to valuable OPCs, such as triacylphosphines $(\text{R}(\text{O})\text{C})_3\text{P}$ ($\text{R} = \text{Ph}, \text{Cy}, \text{Ad}, i\text{Bu}, i\text{Pr}, n\text{Bu}, \text{Me}$) and tetrakis(alkyl)phosphonium salts $[\text{R}_4\text{P}]\text{Br}$ ($\text{R} = \text{Bn}, \text{Et}$). Moreover, hydroxymethyl-substituted phosphine derivatives were targeted, as they constitute another industrially important class of P_1 products. Bu_3SnCl , the Sn-containing byproduct of these transformations, was successfully recovered from the reaction mixture in an excellent overall yield of 92%. The results reported in this chapter expand the currently very limited range of strategies that are available for the direct functionalization of P_4 .

Chapter 4. Reductive Photoelectrocatalytic Activation of Organic Halides and Diphenylphosphine into Arylphosphines and Phosphonium Salts

Chapter 2 investigated the photochemical functionalization of P_4 with chemically inert chlorobenzenes in the presence of the organic photoreductant TDAE, yielding valuable triarylphosphines and tetraarylphosphonium salts. For the generation of such highly reducing species, chapter 4 of this thesis examined the use of the photoredox catalysts 9,10-dicyanoanthracene (**DCA**) and *N*-2,6-diisopropylphenyl naphthalene monoimide (**NpMI**) in electrochemically mediated photoredox catalysis (e-PRC) for the dehalogenation of chlorobenzenes. Previous literature reports revealed that a tandem electrochemical reduction and photoexcitation (blue LED, 455 nm) of these two simple organic precursors provide highly reducing species, $[\text{DCA}^{\bullet-}]^*$ or $[\text{NpMI}^{\bullet-}]^*$, respectively. The high reducing power of these catalysts led to reductive activation of organic chlorides and the generation of aryl radicals. Unfortunately, the photoelectrocatalytic arylation of P_4 with chlorobenzene in presence of the presented catalysts showed no product formation. Switching from P_4 to the more easily functionalized diphenylphosphine (Ph_2PH), photoelectrochemical activation of chlorobenzenes yielded a mixture of arylphosphines and phosphonium salts, although the conversions remain rather low (Figure 3).

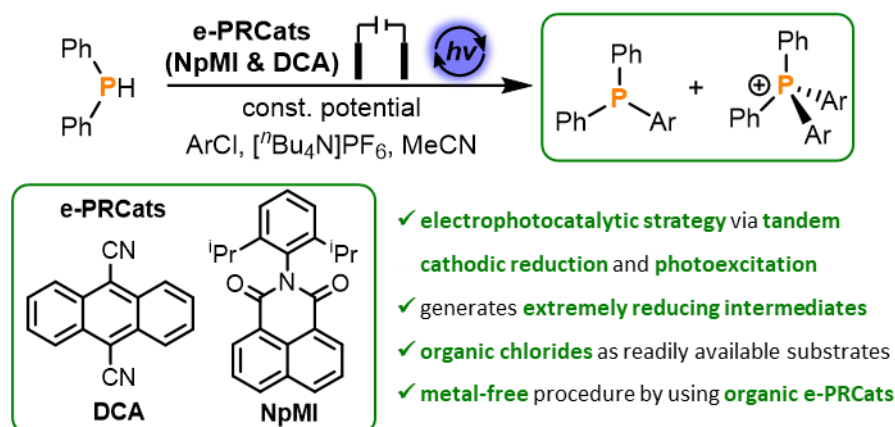


Figure 3. Electrochemically mediated photoredox catalytic (e-PRC) functionalization of Ph_2PH using e-PRCats **DCA** and **NpMI** or the dehalogenation of chlorobenzenes.

Overall, this photoelectrocatalytic method is an interesting new approach for the synthesis of valuable organophosphorus compounds but needs further development to overcome limitations. Going forward, the principal aim will be to achieve photoelectrocatalytic functionalization of P_4 with organic chlorides.

Chapter 5. Synthesis and Characterization of Bidentate Isonitrile Iron Complexes

Finally, chapter 5 of this thesis covered a distinct project describing the synthesis and characterization of novel bidentate isonitrile iron complexes. The reduction of the divalent iron precursors *trans*-[FeBr₂(BINC)₂] (**1**), [Cp*FeCl(BINC)] (**3**) (Cp* = Me₅C₅) and [FeBr₂(CNAr₃NC)₂] (**5**), featuring chelating bis(isonitrile) ligands BINC (bis(2-isocyanophenyl)phenylphosphonate) and CNAr₃NC (2,2''-diisocyanophenyl-1,1':3',1''-terphenyl), led to oligonuclear iron compounds. These di- and trinuclear compounds [Fe₃(BINC)₆] (**2**), [Cp*Fe(BINC)]₂ (**4**), [Fe(CNAr₃NC)₂]₂ (**6**) and [K(Et₂O)]₂[Fe(CNAr₃NC)₂]₂ (**7**) (Figure 4) represent the isonitrile analogues of the corresponding classic iron carbonyl complexes, demonstrating that the bidentate isonitrile ligands are capable surrogates for two CO ligands.

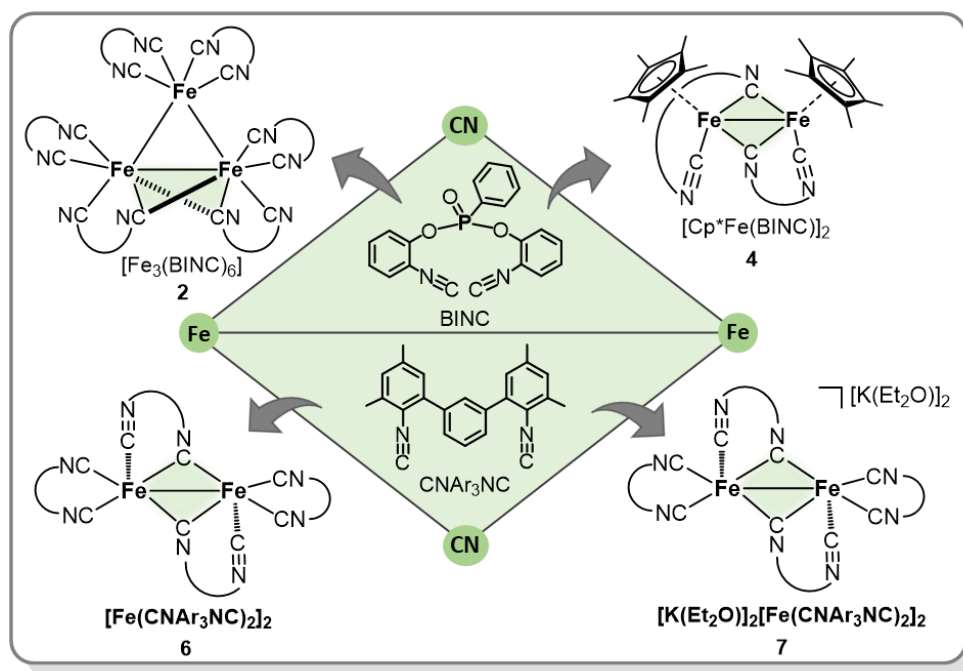


Figure 4. Di- and trinuclear compounds [Fe₃(BINC)₆] (**2**), [Cp*Fe(BINC)]₂ (**4**), [Fe(CNAr₃NC)₂]₂ (**6**) and [K(Et₂O)]₂[Fe(CNAr₃NC)₂]₂ (**7**) with chelating bis(isonitrile) ligands BINC and CNAr₃NC.

Outlook

Due to the importance of organophosphorus compounds in daily life of society, the development of new direct and chlorine-free functionalization protocols for their synthesis is a highly desirable objective. The work reported in this thesis has broadened the spectrum of methods available for the direct functionalization of P₄. Nevertheless, all of these procedures for the synthesis of OPCs remain proof-of-principle and further research is required to replace the industrial state-of-the-art routes with more efficient and sustainable synthetic methodology. In considering the development of green chemistry protocols, some important challenges and opportunities for phosphorus chemistry should be targeted by academia and industry.

The most promising strategies are direct, catalytic P₄ functionalization processes, which persist in being exceedingly rare to date. In particular, research into the establishment of greener strategies, such as a reliable (photo)electrocatalytic approach for the synthesis of a broad range of OPCs using electricity, as this work has sought to initiate, will undoubtedly receive increasing attention through studies in the coming years. Waste-recycling management is also a key aspect to consider in the future development of phosphorus chemistry. In any given synthesis of OPCs, the chemical reagents should ideally be used in a closed loop.

The final part of this thesis is distinct from the topics discuss above and concerns the development on organometallic isonitrile compounds. A detailed comparison of the spectroscopic and structural parameters of bidentate isonitrile complexes with mono(isonitrile) and CO analogues showed that replacing these monodentate ligands with does not dramatically affect the molecular or electronic structures. Thus, future investigations will aim at the synthesis of further highly reduced ferrate complexes and their utilization in electro- or photocatalysis, where the stable coordination of bidentate (chelating) isonitrile ligands might be beneficial.

7 Acknowledgements

Ganz besonderer Dank gilt meinem Doktorvater Prof. Dr. Robert Wolf für die Betreuung in den letzten Jahren, die interessante Aufgabenstellung, die anregenden Diskussionen, die exzellenten Arbeitsbedingungen und die große Freiheit bei meiner Forschung.

Prof. Dr. Manfred Scheer (Zweitgutachter), Prof. Dr. Ruth Gschwind (Drittprüferin) und Prof. Dr. Rainer Müller (Vorsitz) möchte ich für die Mitwirkung in der Prüfungskommission danken.

Weiter möchte ich mich auch bei den Mitarbeitern der zentralen Analytik und Werkstätten für ihre jahrelange Unterstützung bedanken, insbesondere bei Sabine Stempfhuber und Birgit Hischa (Röntgenstrukturanalyse), Annette Schramm, Georgine Stühler, Veronica Scheidler, Fritz Kastner, Tuan Anh Nguyen und Ilya Shenderovich (NMR-Abteilung), Barbara Baumann und Helmut Schüller (Elementaranalyse), Markus Lindner, Helena Ackermann (Glasbläserei), Peter Fuchs und Andreas Gruber (Elektronikwerkstatt).

Für Unterstützung im Labor bedanke ich mich bei Sarah Koschabek, Maximilian Widmann, Michael Mende und Nicholas Sammy für ihre Mitwirkung an den Projekten in Form von Bachelorarbeiten und Forschungspraktika.

A special thanks to Dr. Daniel Scott, Dr. John Kelly and Dr. Thomas Horsley-Downie for proofreading my papers and PhD thesis. Thank you very much for your support!

Außerdem möchte ich mich bei Dr. Christoph Ziegler für die Durchführung und Unterstützung bei quantenchemischen Rechnungen und die Beantwortung sämtlicher Fragen bedanken.

Des Weiteren bedanke ich mich bei den aktuellen und früheren Arbeitskreismitgliedern: Dirk, Stefan, Bernd, Philipp, Christian R., Anup, Christian H., Uli, Thomas M., Julia L., Christoph, Gabi, Julia M., Matthew, Daniel, John, Percia, Miguel, Rafael, Vanessa, Peter, Felix, Sebastian, Jose, Karo, Robin, Maxi, Martin, Maria, Franzi, Ajdin, Thomas H.-D., Zahra, Michael, Riccardo, Benjamin, Marco, Alex, David und Joan für die einmalige Stimmung im Arbeitskreis, die entspannte Arbeits-Atmosphäre, die lustigen und unterhaltsamen Mittags-/Kaffeepausen, spontanen Aperol-Feierabende, die Medien-

Kompetenz-Seminare, die Lasertag-Besuche, die vielen lustigen AK-Partys und auch schönen (Spiele)-Abende außerhalb der Uni.

Ein besonderer Dank dabei an Gabi, Julia M. und Maria, die immer etwas Zeit für Klatsch und Tratsch hatten, um die neusten interessanten News auszutauschen.

Ein riesiges Dankeschön geht an meine Studienkollegin und beste Freundin Susi, die immer ein offenes Ohr für mich hat und dieses Studium und die PhD-Zeit durch spontane Shopping-Touren, Flohmarkt-Besuche oder Glühwein-Abende auch an schlechten Tagen aufgeheitert hat.

Von ganzem Herzen möchte ich mich bei meinen Eltern, Johanna und Kurt, und meiner Schwester Tatjana bedanken. Sie haben mir mein ganzes Leben lang bedingungslosen Rückhalt gegeben und mich auf meinem Weg immer uneingeschränkt unterstützt. Ohne Euch wäre dies alles nicht möglich gewesen.

Zuletzt möchte ich mich bei meinem Partner Willi für die Geduld und den Rückhalt während unserem gemeinsamen Chemie Studiums und unsrer Promotionszeit bedanken. Danke, dass du mich in schwierigen Phasen unterstützt hast und dass wir diese vergangenen Jahre tagtäglich zusammen gemeistert haben. Ich freue mich darauf einen neuen spannenden Lebensabschnitt mit dir zu beginnen. ♥

8 Curriculum Vitae

EDUCATION

- Since 11/2018 **Ph.D.** in the group of Prof. Dr. R. Wolf, Institute of Inorganic Chemistry, University of Regensburg, theme: “*Light-Driven Syntheses of Monophosphorus Compounds*”
- 10/2016 – 09/2018 **Master of Science in Chemistry** at the University of Regensburg with focus on Inorganic, Physical and Sustainable Chemistry and Nanoscience
Master’s Thesis in the group of Prof. Dr. R. Wolf (Institute of Inorganic Chemistry): “*Neue Übergangsmetall-Isocyanid-Komplexe*”
- 10/2013 – 09/2016 **Bachelor of Science in Chemistry** at the University of Regensburg
Bachelor’s Thesis in the group of Prof. Dr. R. Wolf (Institute of Inorganic Chemistry): “*Synthese und Untersuchung der Reaktivität eines Bis(1,3-diphosphacyclo-butadien)-Komplexes*”
- 09/2005 – 05/2013 **Abitur** in the natural scientific–technical and linguistic secondary school in Dingolfing; Abitur Subjects: German, English, Mathematics, Chemistry and Religion

OCCUPATIONAL CAREER

- Since 11/2018 **Scientific Assistant** in the group of Prof. Dr. R. Wolf, Institute of Inorganic Chemistry, University of Regensburg
- Student / Scientific Assistant**
- 10/2016 – 03/2017 Tutorials for first year bachelor students:
and Allgemeine Chemie – Analytischer und Anorganischer Teil:
10/2017 – 03/2018 Vertiefungsseminar (Dr. S. Gärtner, WS2016/17 and WS2017/18)
03/2018 Supervision of lab courses, elective module: Nanoscience (Prof. Dr. R. Wolf)

CONFERENCES AND PRESENTATIONS

24. – 29.07.2022 Poster – 16th International Symposium on Inorganic Ring Systems (IRIS) 2022, Graz, Austria
29. – 30.09.2020 Poster – Online-Vortragstagung für Anorganische Chemie der Fachgruppen Wöhler-Vereinigung, Festkörperchemie & Materialforschung
01. – 03.03.2020 Poster – 16. Koordinationschemie-Treffen (KCT) 2020, Freiburg, Germany
06. – 09.10.2019 Poster – ICASEC Summer School on Electrochemical Approaches to Chemical Synthesis, Göttingen, Germany
25. - 30.08.2019 Talk – Wissenschaftliches Kolloquium von Arbeitsgruppen der Anorganische Chemie 2019, Hirschegg, Austria

9 List of Publications

- 1) M. Till, J. Cammarata, R. Wolf and D. J. Scott, "Photocatalytic Stannylation of White Phosphorus", *Chem. Commun.*, 2022, **58**, 8986–8989.

- 2) M. Till, V. Streitferdt, D. J. Scott, M. Mende, R. M. Gschwind and R. Wolf, "Photochemical transformation of chlorobenzenes and white phosphorus into arylphosphines and phosphonium salts", *Chem. Commun.*, 2022, **58**, 1100-1103.
(Front cover)

- 3) M. Till, J. A. Kelly, C. G. P. Ziegler, R. Wolf, T. Guo, M. R. Ringenber, E. Lutsker and O. Reiser, "Synthesis and Characterization of Bidentate Isonitrile Iron Complexes", *Organometallics*, 2021, **40**, 1042–1052.

10 Eidesstattliche Erklärung

Ich erkläre hiermit an Eides statt, dass ich die vorliegende Arbeit ohne unzulässige Hilfe Dritter und ohne Benutzung anderer als der angegebenen Hilfsmittel angefertigt habe; die aus anderen Quellen direkt oder indirekt übernommenen Daten und Konzepte sind unter Angabe des Literaturzitats gekennzeichnet. Die Arbeit wurde bisher weder im In- noch im Ausland in gleicher oder ähnlicher Form einer anderen Prüfungsbehörde vorgelegt.

Marion Till